

Dissertation zur Erlangung des Doktorgrades
der Fakultät für Chemie und Pharmazie
der Ludwig-Maximilians-Universität München

**Synthesis and Characterization of
Energetic Oxetane Derivatives
and
Nitrogen-rich Energetic Materials**

Michael Voggenreiter
aus Freising, Deutschland

2022

Erklärung

Diese Dissertation wurde im Sinne von § 7 der Promotionsordnung vom 28. November 2011 von Herrn Prof. Dr. Thomas M. Klapötke betreut.

Eidesstattliche Versicherung

Diese Dissertation wurde eigenständig und ohne unerlaubte Hilfsmittel erarbeitet.

München, den 16.05.2022

Michael Voggenreiter

Dissertation eingereicht am	19.05.2022
1. Gutachter:	Prof. Dr. Thomas M. Klapötke
2. Gutachter:	Prof. Dr. Konstantin Karaghiosoff
Mündliche Prüfung am	19.07.2022

*„Man braucht nichts im Leben zu fürchten,
man muss nur alles verstehen.“*

Marie Curie (1867–1934)
Physikerin und Chemikerin

Danksagung

Zu Beginn dieser Danksagung möchte ich mich bei meinem Doktorvater Herrn Prof. Dr. Thomas M. Klapötke bedanken, der es mir ermöglichte in seinem Arbeitskreis über sehr spannende Themen und Fragestellungen zu promovieren. Auch für die finanzielle Unterstützung und die Freiheiten beim Forschen, seien es neue Moleküle oder Kooperationen, möchte ich Danke sagen.

Herrn Prof. Dr. Konstantin Karaghiosoff danke ich für die Übernahme des Zweitgutachtens dieser Dissertation, sowie für das Bekanntmachen mit der Welt der Kristallographie und die ausführlichen Diskussionen über Strukturen.

Ich danke den folgenden Professoren für ihre Zeit und die Bildung der Prüfungskommission: Herr Prof. Dr. Thomas M. Klapötke, Herr Prof. Dr. Konstantin Karaghiosoff, Herr Prof. Dr. Achim Hartschuh, Herr Prof. Dr. Andreas Kornath, Herr Prof. Dr. Hans-Christian Böttcher und Frau Prof. Dr. Silvija Markic.

Herrn Dr. Burkhard Krumm und Frau Brigitte Breitenstein danke ich für das Messen zahlloser NMRs und auch für den zeitlichen Mehraufwand, wenn ich wieder mit schwierigen Proben vorbeikam, welche nicht lange existent waren.

Mein Dank gilt auch Herrn Dr. Jörg Stierstorfer, der mir immer wieder Tipps und Syntheseideen mit auf den Weg gab, als auch die zahlreichen Diskussionen über Synthese und diverse Strukturen. Ebenso für das Korrekturlesen diverser Manuskripte und das Heraussuchen und Diskutieren der neuesten Literatur möchte ich mich bedanken.

Frau Irene Scheckenbach möchte ich für ihren unglaublichen Durchblick bei dem Formularetschungel und bei allen bürokratischen Angelegenheiten danken. Durch ihre immer gut gelaunte Art läuft es in diesem Arbeitskreis wie in keinem Anderen.

Ich möchte mich auch bei allen aktuellen und ehemaligen Mitgliedern dieses Arbeitskreises bedanken, die ich kennenlernen konnte. Allen voran bei dem besten Labor, D3.110, in dem aus Kollegen Freunde wurden: Alexander Harter, der immer für eine (nicht) chemische

Diskussion zu begeistern war und der für die Weiterbildung in Sachen Astronomie und Astrophysik (Astro-Nachmittag) sorgte. Jelena „Jelly“ Reinhardt, für die gute Musikauswahl, ihre unverwechselbare Art und die Mitbringsel des Beauty-Freitages. Jan Wilhelm „Willy“ Cremers, für die Erläuterungen über den Schmelzofen. Veronika „Vroni“ Fuchs, die mir bei meinen Synthesen zur Seite gestanden hat. Ebenfalls möchte ich mich bei den Teilnehmern der Schafkopfrunden bedanken (Alex S., Alex G., Vroni, Maxi, Tobi, Dodo, Marco). Maximilian Benz möchte ich für die gute Zusammenarbeit, das unfassbare Wissen über die energetische Literatur, die Gespräche über die abgefahrensten Moleküle und die Synthese dieser danken.

Stefan Huber möchte ich für das Messen von teils extrem empfindlichen Substanzen danken, sowie zahlreiche Diskussionen und diverse Geschichten. Du hattest immer ein offenes Ohr.

Ein besonderer Dank geht an Alexander Schweiger und Veronika Fuchs, für die Einladungen zum Kochen und das unermüdliche Finden eines Sauna-Termines.

Außerhalb der Uni möchte ich mich bei meiner Handballmannschaft bedanken, durch die ich immer wieder gefordert wurde, an meine physische Leistungsgrenze zu gehen. Das war ein perfekter Ausgleich zur Laborarbeit. Ebenfalls möchte ich mich bei meinen Freunden bedanken, im Speziellen bei Sophie und Patrick. Mit euch war und wird es nie langweilig, sei es beim Spieleabend, beim Bergsteigen oder beim Musical.

Ein ganz besonderer Dank geht an meine zukünftige Frau Jana, die mich immer mit ihrer Liebe unterstützt hat und mich durch die Promotion begleitet hat. Auch für das Aushalten und das Verständnis, wenn ich daheim wieder über Chemie gesprochen und nicht mehr aufgehört habe.

Meiner gesamten Familie, die mich immer unterstützt und dies alles erst ermöglicht hat, gilt ebenfalls ein besonderer Dank. Danke Petra und Jürgen, für eure liebevolle elterliche Unterstützung.

Vielen Dank!

Table of Contents

I Introduction	1
1 Classification of Energetic Materials	1
1.1 Primary Explosives	2
1.2 Secondary Explosives	2
1.3 Propellants	3
1.4 Pyrotechnics	4
1.5 References	5
2 Objectives	6
2.1 New Energetic Oxetanes	6
2.2 Nitrogen-rich Energetic Materials	7
2.3 References	8
II Summary and Conclusion	11
III Results and Discussion	23
1 Oxygen-Rich Oxetanes	25
1.1 Abstract	26
1.2 Introduction	26
1.3 Results and Discussion	27
1.4 Conclusion	32
1.5 Supporting Information	32
1.5.1 Experimental Part and General Methods	32
1.5.2 NMR Spectra	35
1.5.3 X-Ray Diffraction and Hirshfeld Analysis	39
1.5.4 Heat of formation calculation	42
1.5.5 Thermal Analysis	42
1.6 References	43
2 Oxetanes based on LLM-116	47
2.1 Abstract	48
2.2 Introduction	48
2.3 Results and Discussion	50
2.3.1 Synthetic Procedures	50
2.3.2 Crystallography	52
2.3.3 Hirshfeld Analysis	56
2.3.4 Thermal Analysis	58
2.3.5 Small-scale Shock Reactivity and Initiation Test	59
2.3.6 Energetic Properties	62
2.4 Conclusion	62

2.5 Supporting Information	64
2.5.1 Experimental part and general methods.....	64
2.5.2 NMR Spectra	71
2.5.3 Crystallography and Hirshfeld Analysis	84
2.5.4. Heat of Formation Calculation	90
2.5.5 Thermal Analysis	91
2.5.6 Performance Calculation for State-of-the-art Monomers (Comparison)	91
2.5.7 Pratical Tests	94
2.6 References	97
3 Spiro Oxetanes	101
3.1 Abstract.....	102
3.2 Introduction	102
3.3 Results and Discussion	104
3.3.1 Synthetic Procedures	104
3.3.2 Crystallography	105
3.3.3 Spectroscopic Analysis	109
3.3.4 Physicochemical Properties	110
3.4 Conclusion.....	110
3.5 Supporting Information	112
3.5.1 Experimental Part and General Methods.....	112
3.5.2 NMR Discussion and Spectra.....	115
3.5.3 X-ray Diffraction	124
3.5.4 Thermal analysis.....	133
3.5.5 Heat of Formation Calculation	133
3.6 References	135
4 Geminal Diazides	139
4.1 Abstract.....	140
4.2 Introduction	140
4.3 Results and Discussion	142
4.3.1 Synthesis	142
4.3.2 Crystal Structures	143
4.3.3 Physicochemical Properties	148
4.3.4 Toxicity Assessment	150
4.4 Conclusion.....	151
4.5 Supporting Information	151
4.5.1 Experimental Section	151
4.5.2 X-ray Diffraction	155
4.5.3 Heat of Formation Calculation and Thermal Analysis	158
4.6 References	158
5 Carbonylazides	163
5.1 Abstract.....	164
5.2 Introduction	164
5.3 Results and Discussion	165

5.4 Conclusion	172
5.5 Supporting Information.....	172
5.5.1 Experimental Procedures.....	172
5.5.2 NMR Discussion and Spectra	176
5.5.3 IR Spectroscopy of Carbamoyl azide (2).....	185
5.5.4 X-ray Diffraction and Hirshfeld Analysis.....	186
5.5.5 Thermal Analysis	196
5.5.6 Computation	197
5.6 References	199
6 Hydrazonyl-Propandihydrazide	203
6.1 Abstract.....	204
6.2 Introduction	204
6.3 Results and Discussion	206
6.3.1 Synthesis	206
6.3.2 Crystal Structures.....	206
6.3.3 NMR and Vibrational Spectroscopy	210
6.3.4 Physicochemical Properties	211
6.3.4 Toxicity Assessment	214
6.4 Conclusion	214
6.5 Supporting Information.....	215
6.5.1 Experimental Procedures.....	215
6.5.2 X-ray Diffraction.....	220
6.5.3 Heat of Formation Calculation	224
6.6 References	225
7 Binary 2,2'-Azobis-5-Azidotetrazole.....	229
7.1 Abstract.....	230
7.2 Introduction	230
7.3 Results and Discussion	232
7.4 Conclusion	237
7.5 Supporting Information.....	237
7.5.1 Experimental Procedures.....	237
7.5.2. X-ray Diffraction and Hirshfeld Analysis.....	240
7.5.3 Computations and Heat of Formation Calculation.....	244
7.5.4 Spectroscopy.....	249
7.5.5 Thermal Analysis	251
7.6 References	252
8 1-Amino-5-nitriminotetrazole	257
8.1 Abstract.....	258
8.2 Introduction	258
8.3 Results and Discussion	259
8.4 Conclusion	265
8.5 Supporting Information.....	265

8.5.1 Experimental Procedures	265
8.5.2 Crystallographic Detail	269
8.5.3 Computational Details.....	274
8.6 References	275

I Introduction

1 Classification of Energetic Materials

The general definition of an energetic material is not that entirely easy, because there are several different approaches. An energetic material can be characterized as a compound or mixture of substances which contains a fuel and an oxidizer and reacts with the release of energy and gas.^[1,2] According to *Klapötke*, an “energetic materials derive their energy from a chemical reaction (in contrast to a nuclear reaction)”.^[1] But there are many other ways to look at energetic materials, in particular laws are crucial. So is the German Explosives Act, *Sprengstoffgesetz*, which states energetic materials as solid or liquid compounds and formulations, “which could detonate due to a not extraordinary thermal, mechanical or other stress” and “show explosive behavior during test methods such as thermal sensitivity and mechanical sensitivity with respect to either shock or friction”.^[3] Another view of energetic materials is the chemical way: energetic materials are characterized by a number of explosophoric groups, such as nitro, azido or nitrato, on carbon backbones.

This whole world of energetic materials needs to be classified and categorized, but there are also a lot of approaches. One of the most important is the classification by their use according to *Klapötke*.^[1] An energetic material can be used as a high explosive for civil or military purposes, as a primary explosive, as a pyrotechnic formulation, or as a propellant for gun charges or rocket propellants. (Figure 1) The individual categories are discussed in more detail in the following sections, using specific examples of molecules and applications.

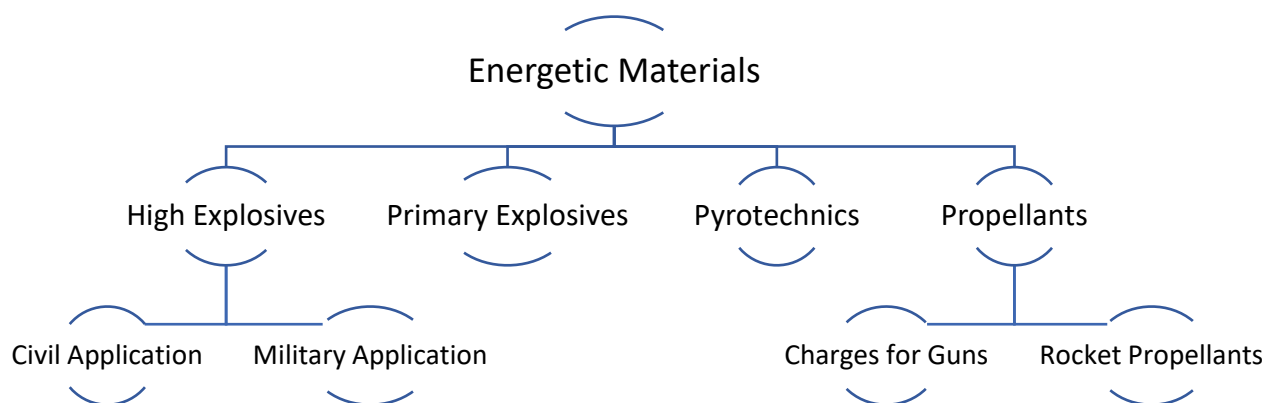


Figure 1. Classification based on their use according to *Klapötke*.^[1]

1.1 Primary Explosives

Primary explosives can be further classified as molecules that are highly sensitive towards external stimuli, tend to explode easily and undergo a fast transition from deflagration to detonation.^[4] When subjected to heat, friction or impact, they produce a shockwave which can initiate low sensitive secondary explosives.^[1] In general, the performance is significantly lower than typical secondary explosives, but primary explosives are mostly used to detonate the main charge.^[1] The basic properties of primary explosives are as follows: ≤ 4 J for impact, ≤ 10 N for friction and ≤ 20 mJ for electrostatic discharge.^[1, 4, 5] Over the years, requirements have changed and the trend has gone from heavy metal containing primary explosives (lead azide **LA**, lead styphnate **LS**, mercury fulminate **MF**), which are extremely negative for humans and the environment, to metal containing primary explosives (**K₂DNABT**, **DBX-1**) to metal free primary explosives (**DDNP**, **Tetrazene**, **CTA**).^[1, 4, 6] The formulas of these primary explosives are shown in **Figure 2**. All of the depicted ones have (partially) made it into application but the search for primary explosives with even better properties is ongoing.

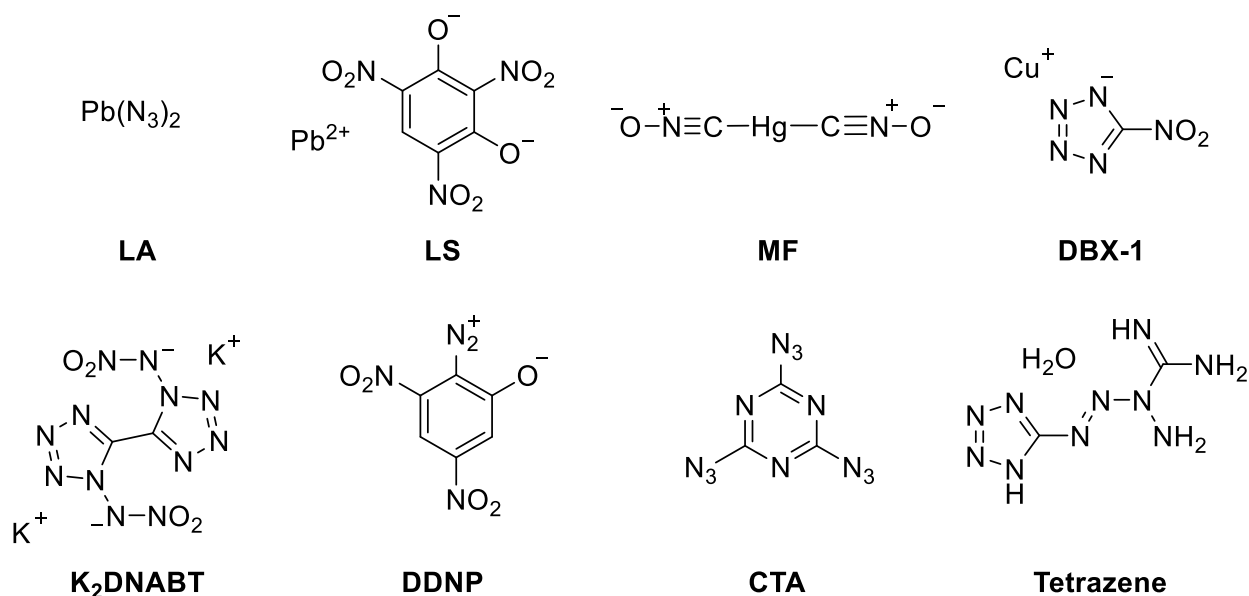


Figure 2. Structural formula of selected primary explosives: lead azide **LA**, lead styphnate **LS**, mercury fulminate **MF**, copper(I) 5-nitrotetrazolate **DBX-1**, dipotassium 1,1'-dinitramino-5,5'-bistetrazolate **K₂DNABT**, diazodinitrophenol **DDNP**, cyanuric triazide **CTA**, tetrazolyl-guanyl-tetrazene-hydrate **Tetrazene**.

1.2 Secondary Explosives

Secondary explosives are higher performing explosives than primary explosives. They cannot be easily detonated as primary explosives due to higher physical stabilities such as thermal stability

1 Classification of Energetic Materials

and mechanical stability. The main properties are: ≥ 4 J for impact and ≥ 80 N for friction.^[1] An ideal secondary explosive should have the highest possible heat of explosion, detonation velocity, and pressure, be insensitive to impact and friction, and have thermal stability above 250°C.^[1] The trend has gone from carbon-based six rings (**TNT**) to carrying less and less carbon that needs to be oxidized, thereby increasing the explosive power. For example, **RDX** and **HMX** offered significantly higher performance with a similar framework but less carbon. More recent developments then went to **FOX-7** and **TKX-50**, which have incredible performance with moderate sensitivities and very good thermal stability.^[1,7] By far the strongest non-nuclear explosives are **ONC** and **CL-20** which feature a cage structure, again increasing the detonation velocity to about 10 000 m s⁻¹. The main disadvantage of the latter is the high synthetic effort and the associated high cost.^[1, 8, 9]

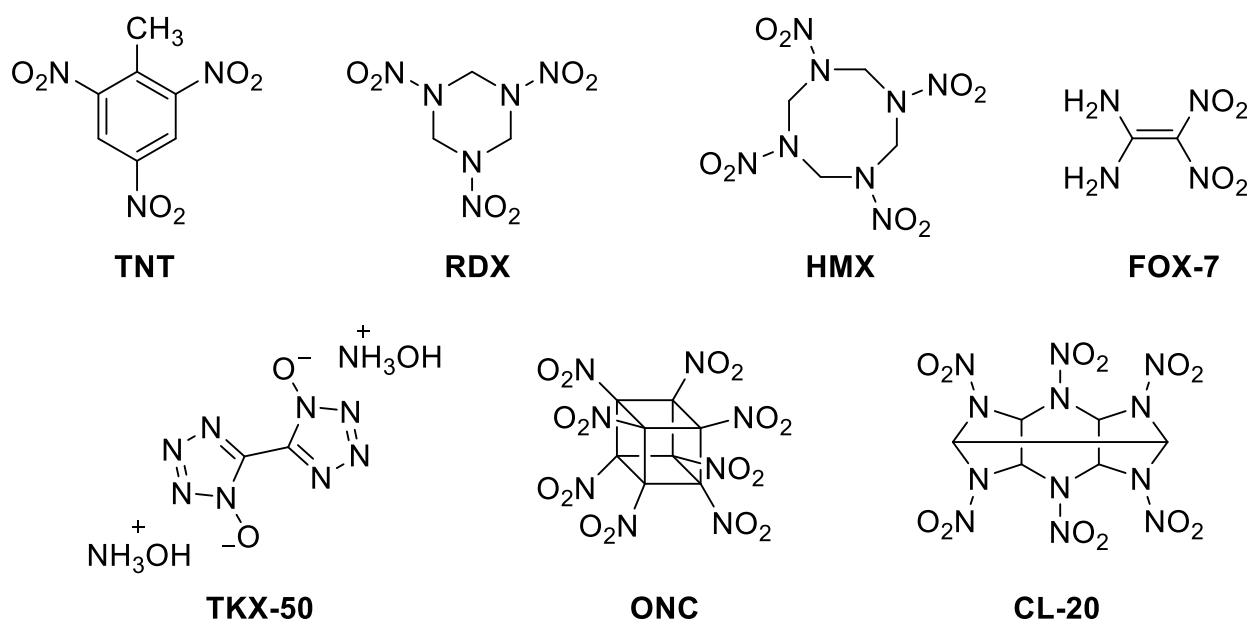


Figure 3. Structural formula of selected secondary explosives: 2,4,6-trinitrotoluol **TNT**, hexogen **RDX**, octogen **HMX**, 1,1-diamino-2,2-dinitroethylene **FOX-7**, dihydroxylammonium 5,5'-bitetrazole-1,1'-dioxide **TKX-50**, octanitrocubane **ONC**, hexanitro hexaazaisowurtzitane **CL-20**.

1.3 Propellants

Propellants in general do not tend to explode, they produce a large amount of hot gas and consist of a fuel and an oxidizer.^[1] This class can be subdivided into gun propellants and rocket propellants. Gun propellants should not have a high combustion temperature due to the erosion of the barrel but a fast burning rate to eject and transport the projectile in the desired way. A main criterion is the oxygen balance that should be ideally zero, so no external oxygen is needed

1 Classification of Energetic Materials

for complete combustion.^[10] One of the simplest and oldest is nitrocellulose **NC** which is synthesized by nitration of cotton and it is still in use today. Recent developments are smokeless single, double or triple base propellants consisting of various compositions of nitrocellulose, nitroguanidine **NQ** and nitroglycerine **NG**.^[1] Recent developments focus on the erosion of the gun barrel and mixture with bis triaminoguanidinium azotetrazolate **TAGzT** that have a low combustion temperature were investigated.^[1] The most important property for rocket propellants is the specific impulse (I_{sp}), which is used to calculate the maximum payload of the rocket.^[1] Here, solid mixture with ammonium perchlorate **AP** have made it into application due to the good properties. Drawback is the release of chlorinated species after combustion which have negative impact on the environment.^[1] Liquid propellants are also currently in use for example with monomethylhydrazine **MMH** and nitric acid or N_2O_4 which reacts hypergolic after mixing and thrust is generated.^[1]

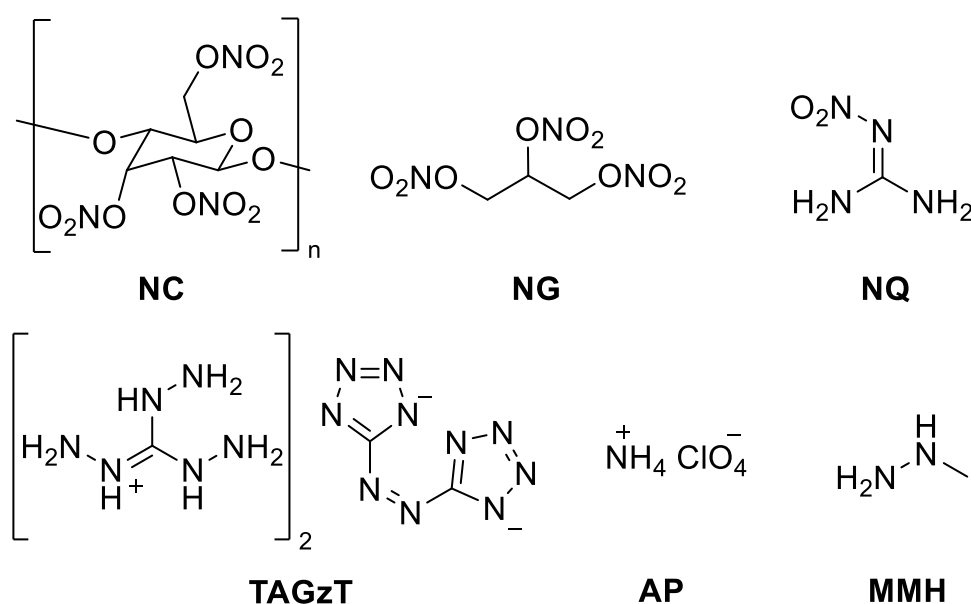


Figure 4. Structural formula of selected molecules used for propellants: nitrocellulose **NC**, nitroglycerine **NG**, nitroguanidine **NQ**, bis triaminoguanidinium 5,5'-azotetrazolate **TAGzT**, ammonium perchlorate **AP**, monomethylhydrazine **MMH**.

1.4 Pyrotechnics

Pyrotechnics is a mixture or formulation that produces a distinct color impression, heat, sound or smoke.^[1] Civil application of pyrotechnics is the widely known firework at the end of a year, whereas in military it is used for signal flares, smoke clouds for coverage and decoy bodies.^[11-14] Pyrotechnical compositions consist mainly of an oxidizer (e. g. nitrates or perchlorates) and metal as fuel (magnesium or aluminum). For formulation that give a color impression, a coloring agent

1 Classification of Energetic Materials

is added like strontium or lithium.^[1] Perchlorates as mentioned in the previous section, have a negative environmental impact due to the release polychlorinated species. Recently, Glück removed the chlorine source and establish are red-burning pyrotechnical formulation that meets the requirements.^[15]

1.5 References

- [1] T. M. Klapötke, *Chemistry of High-Energy Materials*, 5th ed., Berlin, Boston: De Gruyter, **2019**.
- [2] J. P. Agrawal, R. D. Hodgson, *Organic Chemistry of Explosives*, 1st ed., New York: John Wiley, **2007**.
- [3] C. Papsthart, *Waffenrecht, Waffengesetz, Beschussgesetz, Sprengstoffgesetz, Gesetz über die Kontrolle von Kriegswaffen und Durchführungsvorschriften; Textausgabe mit Sachverzeichnis und einer Einführung*, 16., überarb. Aufl., Dt. Taschenbuch-Verl., München, **2012**.
- [4] R. Matyáš, J. Pachman, *Primary Explosives*, Heidelberg: Springer, **2013**.
- [5] M. Neha, O. Karl, C. Gattung, S. Akash, M. John, Y. Kin, *Z. Anorg. Allg. Chem.* **2014**, *640*, 1309–1313.
- [6] T. M. Klapötke, N. Mehta, *Propellants Explos. Pyrotech.* **2014**, *39*, 7–8.
- [7] N. Fischer, D. Fischer, T. M. Klapötke, D. G. Piercey, J. Stierstorfer, *J. Mater. Chem.* **2012**, *22*, 20418–20422
- [8] P. Eaton, M.-X. Zhang, R. Gilardi, N. Gelber, S. Iyer, R. Surapaneni, *Propellants, Explosives, Pyrotechnics* **2002**, *27*, 1–6.
- [9] U. R. Nair, R. Sivabalan, G. M. Gore, M. Geetha, S. N. Asthana, H. Singh, *Combustion, Explosion and Shock Waves*, **2005**, *41(2)*, 121–132.
- [10] J. Stierstorfer, *Dissertation*, Ludwig-Maximilians-Universität München, **2009**.
- [11] U. S. Army Material Command, *Engineering Design Handbook: Theory and Application, Military Pyrotechnics Series, Part One*, Washington, DC, USA, **1967**.
- [12] H. Ellern, *Military and civilian pyrotechnics*, Chemical Pub. Co, New York, **1968**.
- [13] M. Russell, *The Chemistry of Fireworks*, The Royal Society of Chemistry, Cambridge, UK, **2009**
- [14] J. A. Conkling, C. Mocella, *Chemistry of Pyrotechnics: Basic Principles and Theory*, CRC Press, Boca Raton, **2010**.
- [15] J. Glück, I. Gospodinov, T. M. Klapötke, J. Stierstorfer, *Z. Anorg. Allg. Chem.* **2019**, *645*, 370–376.

2 Objectives

Goals and motivation for this thesis can be divided into two parts, first the synthesis of new energetic oxetanes which are suitable for ring-opening polymerization. So only 3-mono and 3,3-di-substituted oxetane are considered. The second part addresses the goal of synthesizing new high-energy nitrogenous materials, in particular the chemistry of azides and tetrazoles.

2.1 New Energetic Oxetanes

One objective of this thesis was to synthesize and investigate new energetic oxetanes that can be suitable for possible ring-opening polymerization. Oxetanes are generally strained four-membered heterocycles containing an oxygen atom. The ring tension is minimized by a nearly planar configuration of the ring shown by *Luger*.^[1] In the 1980s several energetic oxetanes were developed such as **AMMO**, **NIMMO** and **BAMO** which are used in formulations.^[2-6] (**Figure 5**) *Baum* et al. also synthesized energetic oxetane such as 3,3-dinitrooxetane **DNO** and 3-azidooxetane **3AO** but they did not make it into application due to several difficulties with the

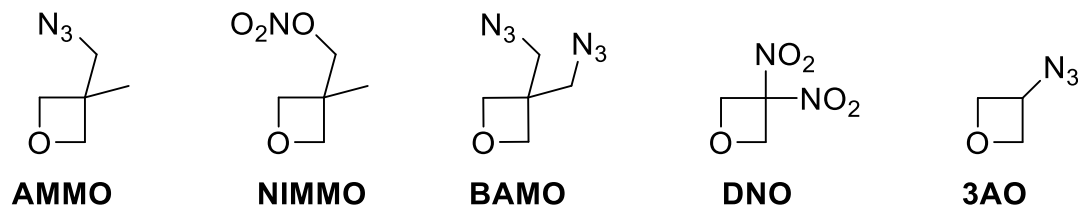


Figure 5. Selected energetic oxetane derivatives: 3-azidomethyl-3-methyloxetane **AMMO**, 3-nitratomethyl-3-methyloxetane **NIMMO**, 3,3-bis(azidomethyl)oxetane **BAMO**, 3,3-dinitrooxetane **DNO**, 3-azidooxetane **3AO**.

synthesis.^[7] Since then, almost no new energetic oxetanes have been synthesized and discovered, probably also due to the high price. Recently, however, the pharmaceutical industry has become interested in oxetanes, and so prices have dropped and oxetanes have become commercially available. In this work, oxetan-3-ol, oxetan-3-one and 3-bromomethyl-3-hydroxymethyloxetane were chosen as starting materials due to their commercial availability and, in the case of 3-bromomethyl-3-hydroxymethyloxetane, due to its good synthetic accessibility. Various energetic groups and molecules were introduced into the oxetane compounds to obtain as energetic as possible 3-substituted oxetane monomers.

2.2 Nitrogen-rich Energetic Materials

A main strategy for the synthesis of nitrogen-rich energetic materials is mainly the introduction of azido groups to the molecule. Azides contribute about +300 kJ/mol to the heat of formation of a molecule.^[1] For even higher nitrogen content and heat of formation, heterocyclic azoles are used, mainly tetrazoles, because they best combine the relevant properties (heat of formation, thermal stability, sensitivity and detonation speed). The chemistry of such nitrogen-rich materials is quite exciting and challenging due to the mostly not long stable molecules and the extremely high sensitivities. For example, carbonyl azides undergo *Curtius* rearrangement reactions, even at room temperatures, to form a reactive isocyanate which can react with moist air. (Figure 6)

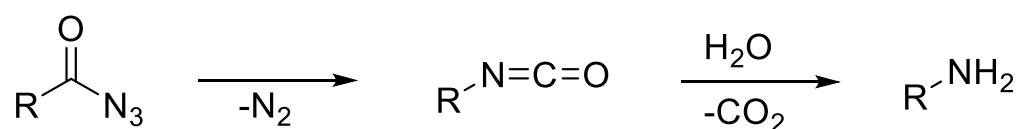


Figure 6. *Curtius* rearrangement and subsequent reaction with water to form an amine.

In general, the more azides in a molecule and the closer they are together, the more unstable it becomes. For example, geminal azides are really sensitive towards external stimuli. The molecules become even more unstable when azides are combined with tetrazoles. The nitrogen content is then very high, as with 5-azidotetrazoles (88.3%).^[8] Several energetic and sensitive nitrogen-rich materials are depicted in Figure 7.^[3, 8-11] Nitrogen-rich energetic materials tend to

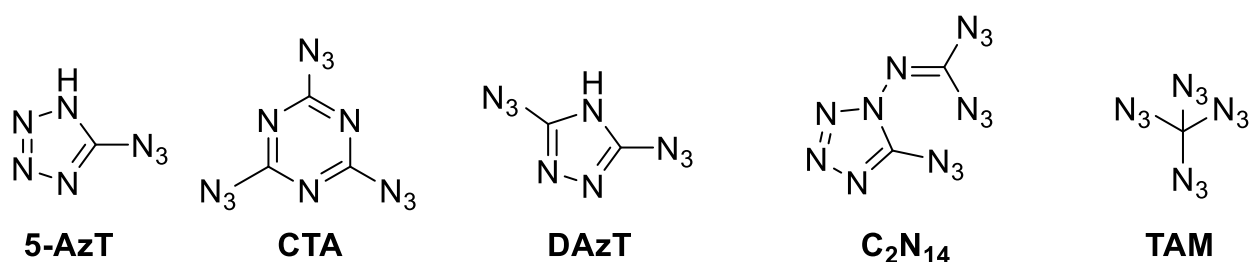


Figure 7. Selected nitrogen-rich energetic materials: 5-azidotetrazole **5-AzT**, cyanuric triazide **CTA**, 3,5-diazido-1,2,4-triazole **DAzT**, (5-azido-1H-tetrazol-1-yl)carbonimidoyl diazide **C₂N₁₄**, tetraazidomethane **TAM**.

Be used as primary explosive due to the high sensitivities. However, the scope of this thesis was to develop high performing and stable nitrogen rich materials, probably for use in primary explosives. The characterization of these materials, in particular the X-ray structure

2 Objectives

determination, was the main focus, since usually little amounts of them are synthesized. With the X-ray structure it is possible to estimate the sensitivities by Hirshfeld analysis before more material is synthesized for practical testing.^[12]

2.3 References

- [1] P. Luger, J. Buschmann, *J. Am. Chem. Soc.* **1984**, *106*(23), 7118–7121.
- [2] H. G. Ang, S. Pisharath, *Energetic Polymers - Binders and Plasticisers for Enhancing Performance*, 1st ed.; Wiley-VCH: Weinheim, **2012**.
- [3] T. M. Klapötke, *Chemistry of High-Energy Materials*, 5th ed., Berlin, Boston: De Gruyter, **2019**.
- [4] G. E. Manser, A. A. Malik, T. G. Archibald, *Polymer and Copolymers from 3-azidomethyl-3-nitratomethyloxetane*. Patent US 5463019, **1995**.
- [5] A. Provatas, *Energetic Polymers and Plasticisers for Explosive Formulations - A Review of Recent Advances*; DSTO Aeronautical and Maritime Research Laboratory, **2000**.
- [6] T. G. Archibald, A. A. Malik, G. E. Manser, US Patent 5489700, Aerojet-General Corporation **1996**.
- [7] K. Baum, P. T. Berkowitz, V. Grakauskas, T. G. Archibald, *J. Org. Chem.* **1983**, *48*, 2953–2956.
- [8] T. M. Klapötke, J. Stierstorfer, *J. Am. Chem. Soc.* **2009**, *131*, 1122–1134.
- [9] N. Fischer, T. M. Klapötke, J. Stierstorfer, E. N. Wiedemann, *Proceedings of the 14th seminar on, New trends in research of energetic materials*, Czech Republic, **2011**, 637-645.
- [10] T. M. Klapötke, F. A. Martin, J. Stierstorfer, *Angew. Chem. Int. Ed.* **2011**, *50*, 4227–4229.
- [11] K. Banert, Y.-H. Joo, T. Rüffer, B. Walfort, H. Lang, *Angew. Chem. Int. Ed.* **2007**, *46*, 1168–1171.
- [12] D. E. Dosch, M. Reichel, M. Born, T. M. Klapötke, K. Karaghiosoff, *Cryst. Growth Des.* **2021**, *21*(1), 243–248.

II Summary and Conclusion

One aim of this thesis was to synthesize and characterize new energetic oxetanes which can be possibly ring-opened to form energetic polymers. The second goal was to synthesize and characterize new highly energetic nitrogen-rich materials. During this thesis, overall 47 new compounds were synthesized and characterized. It was possible to crystallize 42 of them and the structures were obtained by low temperature X-ray diffraction. 18 (38%) new oxetanes and 29 (62%) nitrogen-rich materials were synthesized. They can be classified according to their sensitivities for potential use: 13 (28%) primary explosives, 24 (51%) secondary explosives and 10 (21%) others. The group of other can be described as intermediates, non-energetic compounds, characterized decomposition products or compounds with other applications.

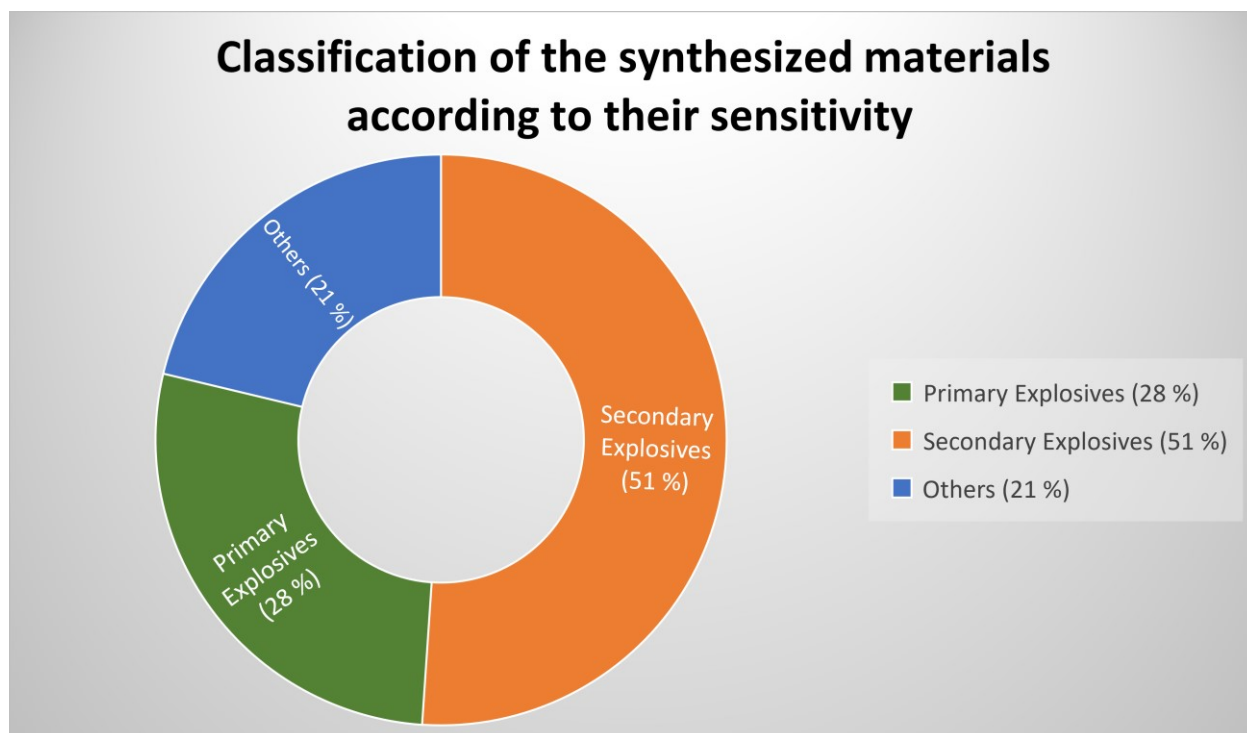


Figure 1. Classification of the investigated compounds

Chapters 1–3 deal with the synthesis of new energetic oxetanes and chapters 4–7 are about highly energetic nitrogen-rich materials which were synthesized and characterized.

Chapter 1 starts with oxygen-rich oxetane compounds based on nitrate esters. In particular, the addition of dinitrogen pentoxide to the double bond of oxetan-3-one is a powerful synthetic route to obtain geminal dinitrates. Solid 3,3-dinitratooxetane (**DNO**) is a promising candidate as solid-state oxidizer because of the positive oxygen balance with respect to CO. The

Summary and Conclusion

major drawbacks are the low thermal stability (93°C), the very high sensitivities towards impact (1 J) and friction (1 N) and general instability with decomposition over time at room temperature. The other two synthesized compounds by nitration of the respective alcohol, namely 3-nitratooxetane (**3NO**) and 3-nitrato-3-methyloxetane (**3N3MO**), are liquids with moderate thermal stabilities (153°C and 145°C, respectively) and performance but they are insensitive towards impact and friction.

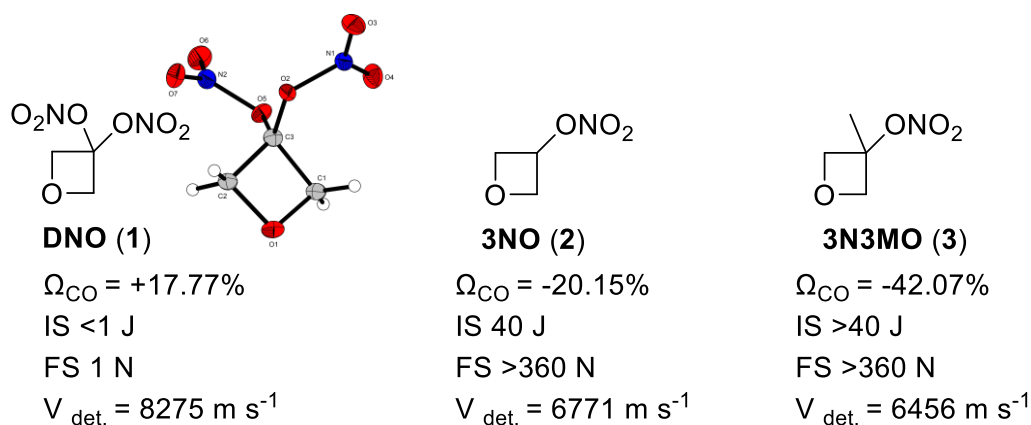


Figure 2. Formula of 3,3-dinitratooxetane (**DNO**) and the corresponding crystal structure, and the formulas of 3-nitratooxetane (**3NO**) and 3-nitrato-3-methyloxetane (**3N3MO**).

In chapter 2, energetic oxetanes based on the secondary explosive, 4-amino-3,5-dinitropyrazole (LLM116), were synthesized and characterized. The synthetic route started from cheap 3-bromomethyl-3-hydroxyoxetane with subsequent nucleophilic substitution reaction by the potassium salt of LLM116. The residual hydroxy position was further functionalized by nitration to obtain the nitrate ester. A side reaction was observed and (3-((4-diazo-3-nitro-5-oxo-4,5-dihydro-1H-pyrazol-1-yl)methyl)oxetan-3-yl)methyl nitrate was obtained. The hydroxy function was converted into a leaving group which allowed further functionalization with azide, LLM116 and 1H-tetrazole. The obtained compounds are depicted in **Figure 3**. All compounds were

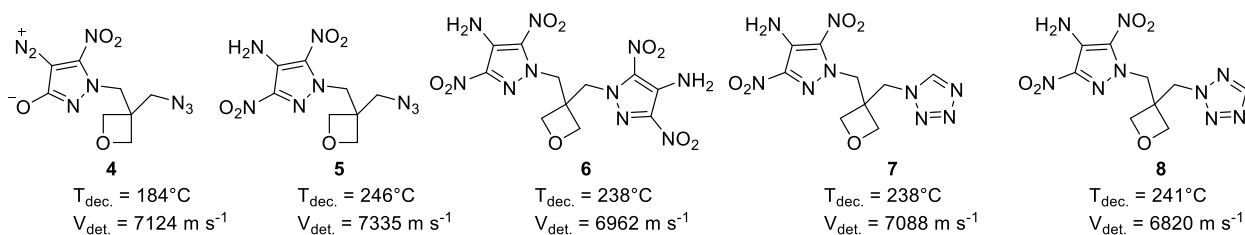


Figure 3. Structures of the energetic synthesized compounds **4–8**.

Summary and Conclusion

characterized by low temperature X-ray diffraction and the thermal stabilities of the compounds are sufficient for possible practical application. The energetic compounds were tested for practical use in SSRT and initiation test. In SSRT, the compounds **4–7** have significant smaller dents as the reference TNT (343 mm³) (**Table 1**). Only **5** is almost as powerful as TNT having a dent volume of 298 mm³. The dent volume was measured with a 3D profilometer to have accurate values (**Figure 4**). Initiation test showed that all compounds expect **4** are too insensitive to be affected by lead azide. With the use of a booster explosive such as PETN, it was possible to initiate **4–8**.

Table 1. Mass of explosive versus dent size in the SSRT

Compound	4	5	6	7	TNT
m_e (mg)	426	459	424	428	445
V_{dent} (mm ³)	160	298	34	162	343

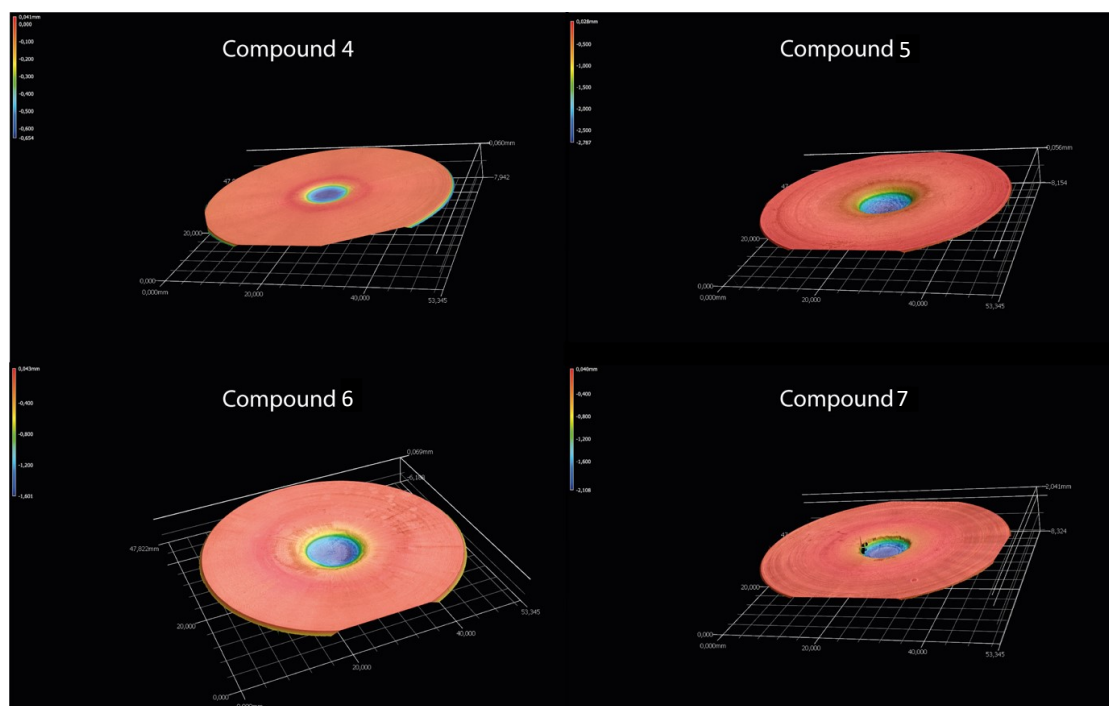


Figure 4. Dent volume determination with a 3D profilometer.

Chapter 3 is about condensation reaction of oxetan-3-one with different energetic hydrazinic compounds to form Schiff bases. Those Schiff bases undergo hydrazinolysis at elevated temperatures really fast to form *spiro*-tetrahydrotetrazines which are quite rare in the literature. (**Figure 5**) The structures of compounds **8–15** except **11** (liquid) were obtained. The performance was calculated using the EXPLO5 code. Compound **13** has a detonation velocity of nearly 8000 m s⁻¹ and is insensitive towards external stimuli which is quite promising for application.

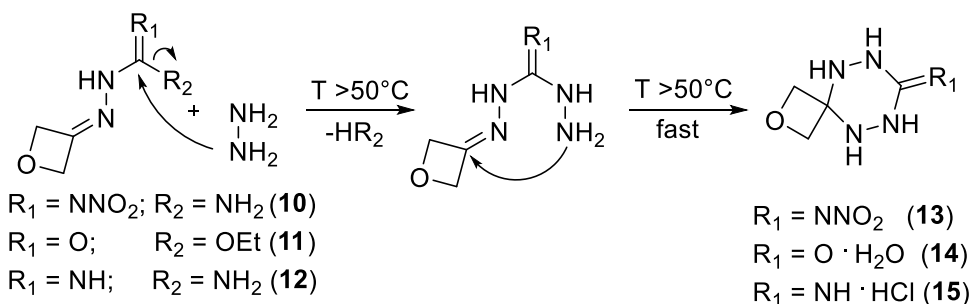


Figure 5. Hydrazinolysis of compound **10–12** to form the tetrahydrotetrazine derivatives **13–15** with the open form as possible intermediate.

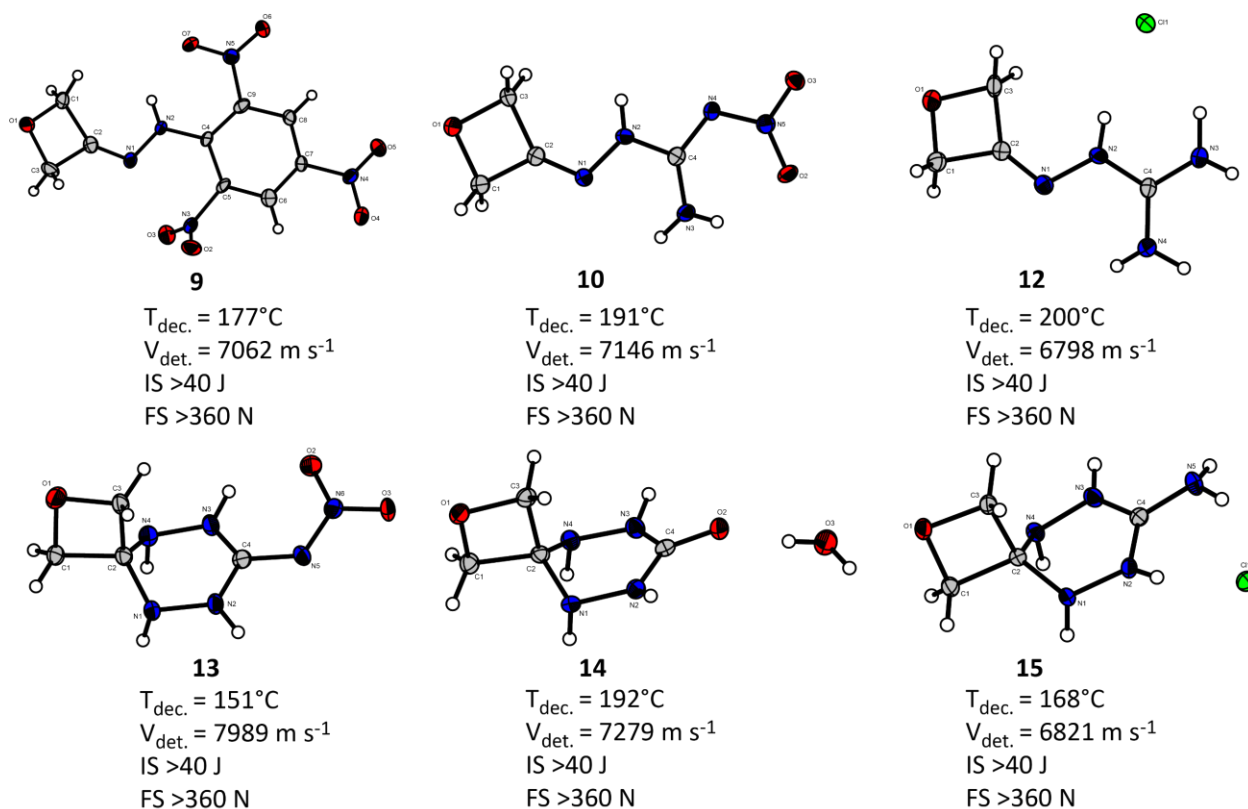


Figure 6. Crystal structures of compound **9, 10** and **12–15** and the respective energetic parameter comprising of decomposition temperature, detonation velocity and impact and friction sensitivity.

Summary and Conclusion

In chapter 4, the geminal diazide, 2,2-diazidomalonic acid, and salts thereof were synthesized and characterized (**Figure 7**). The neutral compound is very sensitive towards impact and friction with sensitivities of 1 J impact and 1 N friction. The salts are quite insensitive but the energetic properties were quite disappointing with detonation velocities of around 7000 m s^{-1} . The potassium salt can eventually be used as a TNT substitute, as it is a bit more powerful and non-toxic.

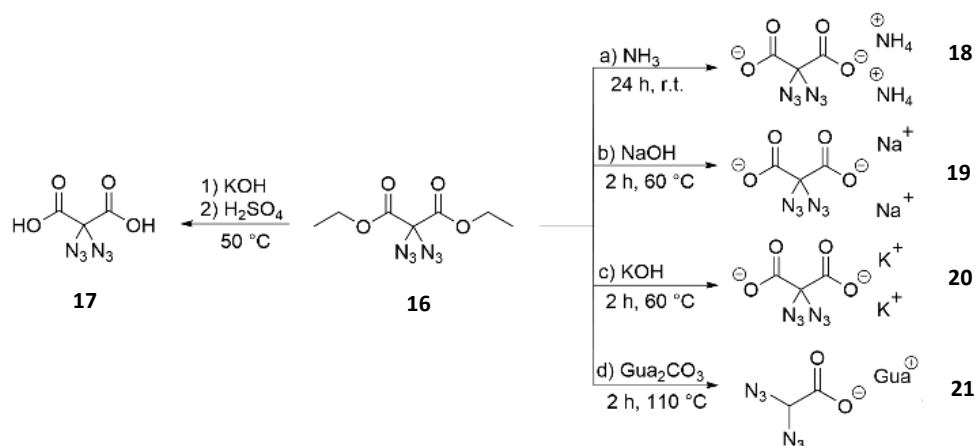


Figure 7. Synthesis of 2,2-diazidomalonic acid and salts thereof.

Chapter 5 deals with the synthesis of small carbonyl azides such as oxalyl diazide, carbamoyl azide and N,N'-bis(azidocarbonyl)hydrazine. All three compounds were obtained by diazotation of the corresponding hydrazo precursor (**Figure 8**). The crystal structures were elucidated by X-ray diffraction and the instable oxalyl diazide was converted in a *Curtius* degradation to a reactive isocyanatocarbonyl azide which undergoes trapping reaction with hydroxy and amine functional groups to form carbamate-like or acetamide-like carbonyl azide derivatives. The trapping products were also crystallized and the structure was obtained. Carbamoyl azide **24** was intensively spectroscopically characterized by different IR methods (ATR solid, gas 0.1 mbar, Ne-matrix 3 K) and Raman and the values were compared and discussed. **24** and **25** have a surprisingly high thermal stabilities of 133°C and 154°C which is really high for carbonyl azides, probably because of the hindered *Curtius* degradation. Oxalyl diazide **23** is incredible sensitive with sensitivities below the limit of the test setups. **23** and **25** are very powerful with detonation velocities of about 8000 m s^{-1} but they are too sensitive for application. Oxalyl diazide **23** can further be functionalized because of the good handling in solution to access new compounds with a carbonyl azide function.

Summary and Conclusion

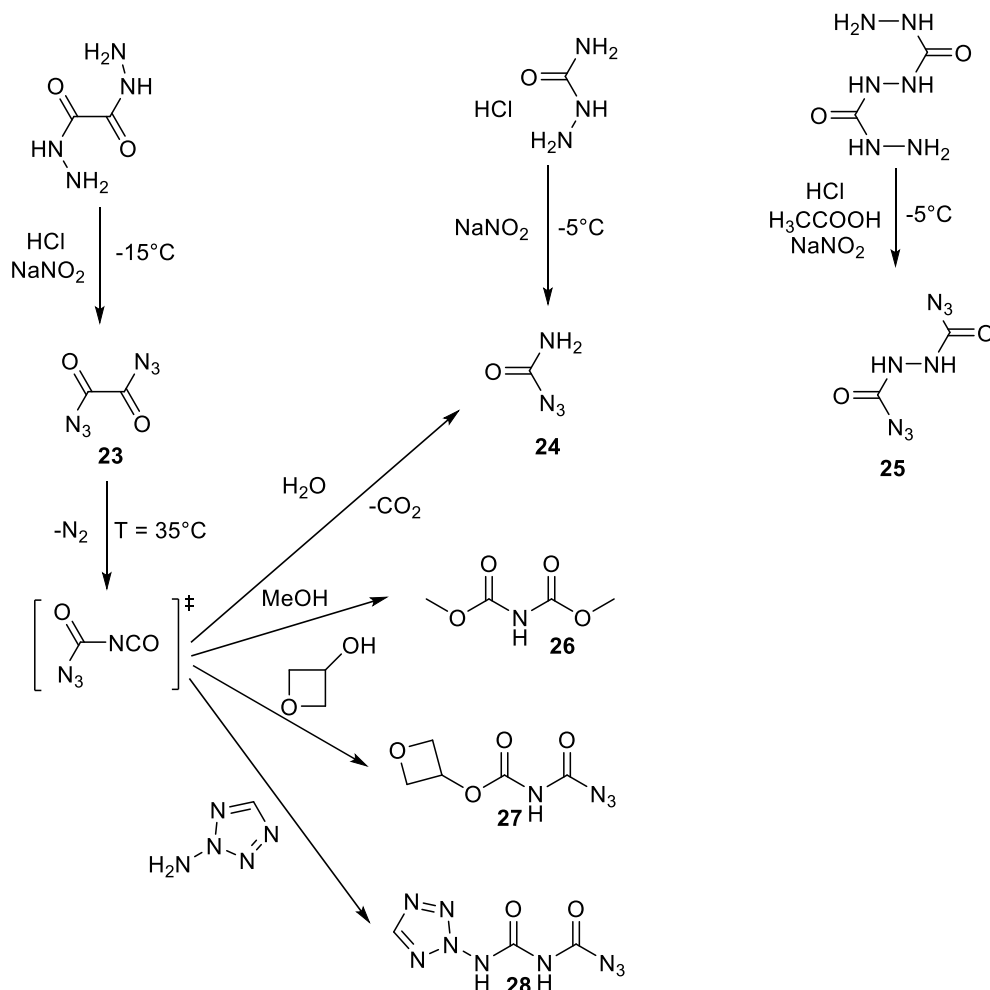


Figure 8. Diazotation reaction to form compound **23–25** and different trapping reaction of the reactive isocyanatcarbonylazide to **26–28**.

In chapter 6, a versatile precursor, namely 2-hydrazonyl-propandihydrazide **30**, was synthesized and investigated for the synthesis of high-energy materials. The perchlorate salt as well as the nitrate salt are high energy materials with detonation velocities of about 9000 m s^{-1} . Further the reaction with N-methyl-N-nitroso-N'-nitroguanidine to form an open product with subsequent ring closure reaction to a triazole gives also highly energetic compounds with detonation velocities of 8228 m s^{-1} and 8654 m s^{-1} . It was shown that the starting material has a great versatility to develop new high-energy materials. Further the investigated compounds are quite insensitive which could lead them into application. Also remarkable is the non-toxicity of the precursor which is quite valuable for other synthetic procedures, also for pharmaceutical uses.

Summary and Conclusion

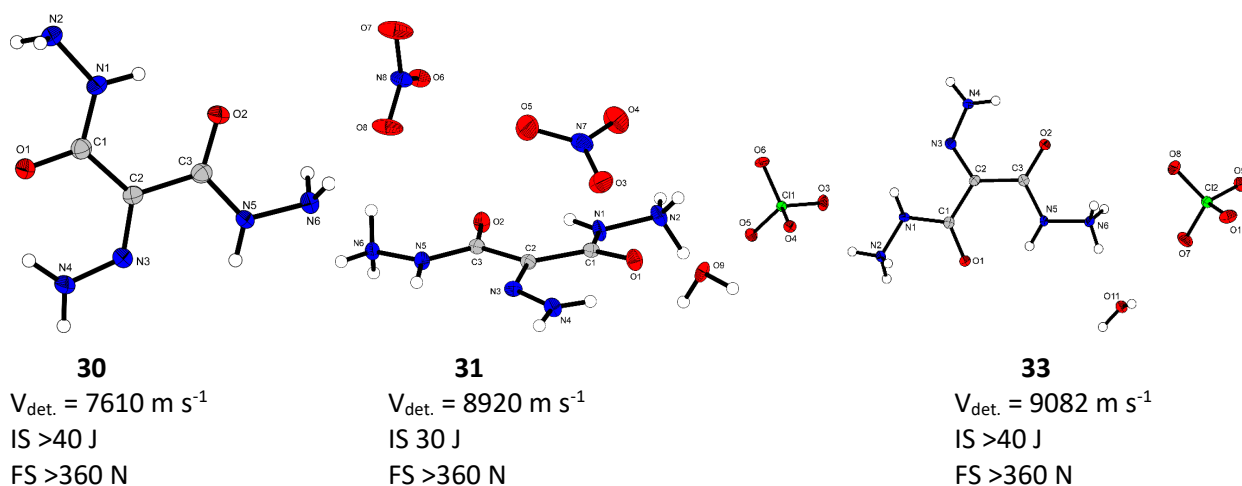


Figure 9. Crystal structures of **30**, **31** and **33** and the respective properties depicted underneath.

Chapter 7 is about the binary and extremely sensitive 2,2'-azobis-5-azidotetrazole also known as C_2N_{16} which has a higher nitrogen to carbon ratio than C_2N_{14} . Compound **39** is synthesized via amination with TOSA. It has also the capabilities of being a primary explosive with sensitivities of <1 J impact and 2 N friction. The thermal stability is 142°C which is comparably

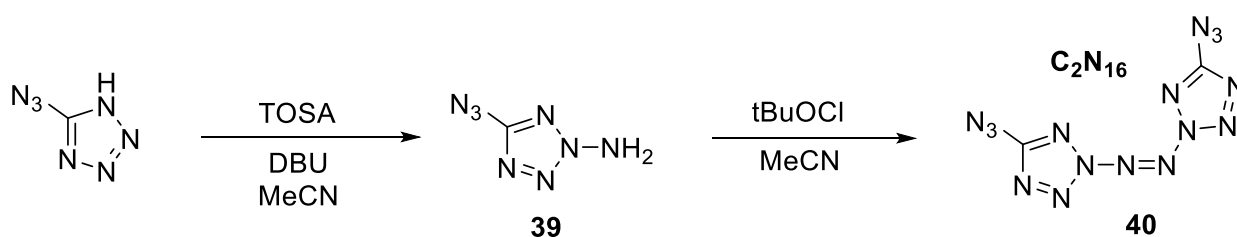


Figure 10. Synthesis of 2,2'-azobis-5-azidotetrazole, C_2N_{16} , **40**.

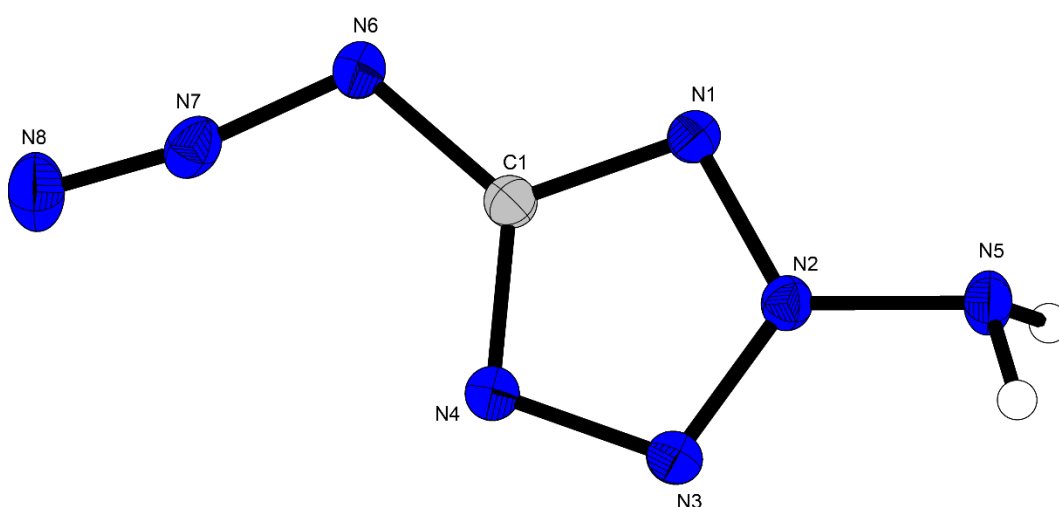


Figure 11. Crystal structure of 2-amino-5-azidotetrazole **39**

Summary and Conclusion

high. **40** is synthesized via oxidative azo-coupling using tBuOCl which has the advantage that nothing precipitates during the reaction. This is important because of spontaneous detonation of C_2N_{16} . Compound **40** is extremely sensitive towards external stimuli, a detonation occurring at the smallest possible values and also during standing without any obvious source of stimulus. But it was possible to get single crystals and the low temperature crystal structure was elucidated. (Figure 12) Both compounds have detonation velocities of about 9500 m s^{-1} . Remarkable is the endothermic heat of formation of C_2N_{16} which is 1700.7 kJ/mol and one of the highest ever reported. The values are summarized in Table 2.

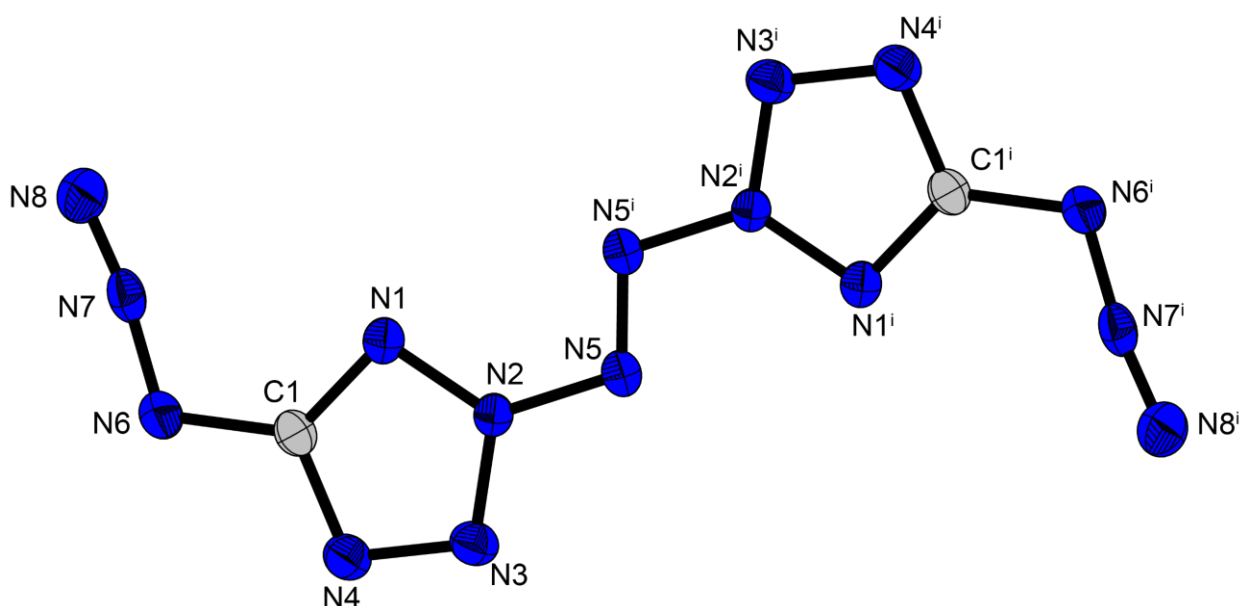


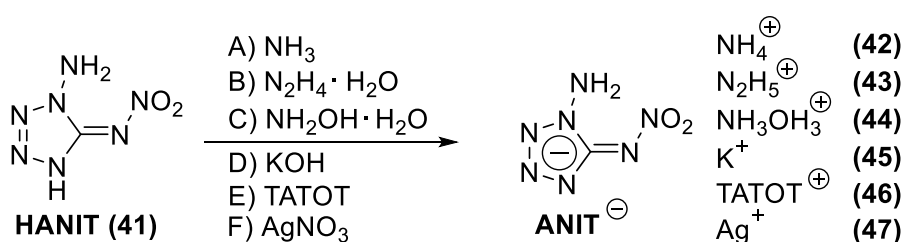
Figure 12. Crystal structure of 2,2'-azobis-5-azidotetrazole, C_2N_{16} (**40**).

Table 2. Physico-chemical properties of **39** and **40** as well as for C_2N_{14} (1-diazidocarbamoyl-5-azidotetrazole).

	39	40	$C_2N_{14}^1$
Formula	CH_2N_8	C_2N_{16}	C_2N_{14}
IS [J]	<1	$\lll 0.25$	<0.25
FS [N]	2	$\lll 0.1$	<5
ρ [g cm^{-3}]	1.736	1.803	1.679
N [%]	88.9	90.3	89.1
$T_{\text{melt}}/T_{\text{dec}}$	62/142	-/114	78/124
$\Delta_f H^\circ$ [kJ mol^{-1}]	703.7	1700.7	1495.0
$-\Delta_{\text{Ex}} U^\circ$ [kJ kg^{-1}] ¹	5672	6705	6632
P_{CJ} [kbar]	343	366	300
V_{det} [ms^{-1}]	9472	9515	8853

Summary and Conclusion

The last chapter 8 is about 1-amino-5-nitriminotetrazole and its salts which are quite high-performing energetic materials with moderate sensitivities. The synthetic procedure is quite simple: protection of 1,5-diaminotetrazole with acetone, aprotic nitration with dinitrogen pentoxide and deprotection by acid, which proceeds in the same step during quenching. Quick extraction is necessary due to the water solubility of **41**. The salt formation proceeds in high yields and quite fast. (Figure 13) All compounds are solids of which a crystal structure was obtained.



TATOT = 3,6,7-triamino-[1,2,4]triazole[4,3-b][1,2,4]triazole

Figure 13. Salt formation of HANIT **41** with different molecules to form compounds **42–47**.

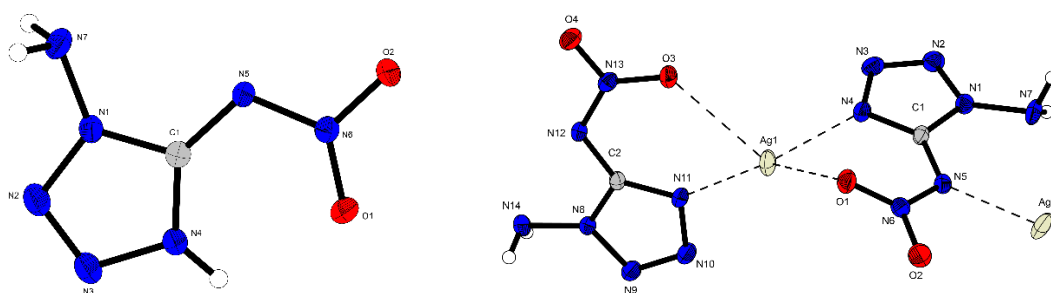


Figure 14. Crystal structures of **41** and **47**.

The materials except the potassium salt **45** have detonation velocities of higher than 9000 m s^{-1} . **43** and **44** even have detonation velocities of 9850 m s^{-1} and 9915 m s^{-1} respectively, which is really high. A drawback is the sensitivity of those compounds of 2 J impact and 15 to 20 N friction. The thermal stability is acceptable (**43**: 175°C ; **44**: 170°C) for compounds with such a high performance. The synthesized compounds compete with the most powerful non-nuclear explosives such as CL-20 and TKX-50 and they easily beat RDX. Compound **46** is nearly insensitive towards impact (20 J) and friction (240 N) and is one of the most promising compounds for application. The decomposition temperature is 215°C and the detonation velocity is 9312 m s^{-1} which is in the range of TKX-50.

The following table summarizes the relevant properties of the most promising compound of each chapter and compares them with RDX and TKX-50.

Summary and Conclusion

Table 3. Comparison of the most promising compound of each chapter with RDX and TKX-50.

	1	5	13	20	25	33	40	44	RDX	TKX-50
Formula	$C_3H_4N_2O_7$	$C_{11}H_{12}N_{10}O_9$	$C_4H_8N_6O_3$	$C_3N_6O_4K_2$	$C_2H_2N_8O_2$	$C_3H_{12}N_6O_{11}Cl_2$	C_2N_{16}	$CH_6N_8O_3$	$C_3H_6N_6O_6$	$C_2H_8N_{10}O_4$
IS [J]	<1	>40	>40	5	1–2	>40	<<<0.25	2	7.5	20
FS [N]	1	>360	>360	288	0.1	>360	<<<0.1	20	120	120
$N+O$ [%]	77.75	64.4	70.2	56.44	84.69	68.60	90.3	89.86	81.06	86.41
$T_{dec.}$ [°C]	93	246	151	105	154	124	114	170	210	221
$\Delta_f H^\circ$ [kJ mol ⁻¹]	-302.6	105.2	223.1	-455.0	309.3	-239.2	1700.7	436.1	86.3	446.6
$V_{det.}$ [m s ⁻¹]	8275	7335	7989	7275	7907	9082	9515	9915	8983	9698
P_{Cl} [GPa]	29.7	20.9	23.2	19.0	23.7	36.9	36.6	40.2	38.0	42.4

Summary and Conclusion

A total of 13 compounds have been synthesized and characterized that have a detonation velocity of more than 8000 m s⁻¹. Furthermore, 8 of them even have a detonation velocity of more than 9000 m s⁻¹. The insensitive perchlorate salt **33** is capable of outperforming RDX in almost every category, but its low thermal stability of only 124°C prevents it from entering the application. Among the oxetane compounds, **5** and **13** could make it to application. **5** could serve as an insensitive TNT substitute or, if polymerized, as an energetic, thermally stable binder. **13**, on the other hand, could be very well suited, if polymerized, as binder with high performance. Unfortunately, **1** cannot be considered for possible applications due to overall instability (decomposition at room temperature). The same applies for C₂N₁₆ **40**, which detonates already without obvious source of stimulus at room temperatures and is also way too sensitive for application. Compound **44** is so powerful that it may find an application where thermal stability of 170°C is sufficient and where the sensitivities of 2 J impact and 20 N friction are not a problem. Further, the TATOT salt **46** is quite insensitive (20 J impact, 240 N friction), has a significantly higher detonation velocity and thermal stability (215°C) than RDX, so it may find its application as (partially) RDX-replacement.

III Results and Discussion

The following chapters contain the full manuscripts including the respective supporting information which were published within the course of this dissertation in peer reviewed journals. They have been reproduced and reprinted with permission of the corresponding journal. The list of publications can be viewed beneath this paragraph.

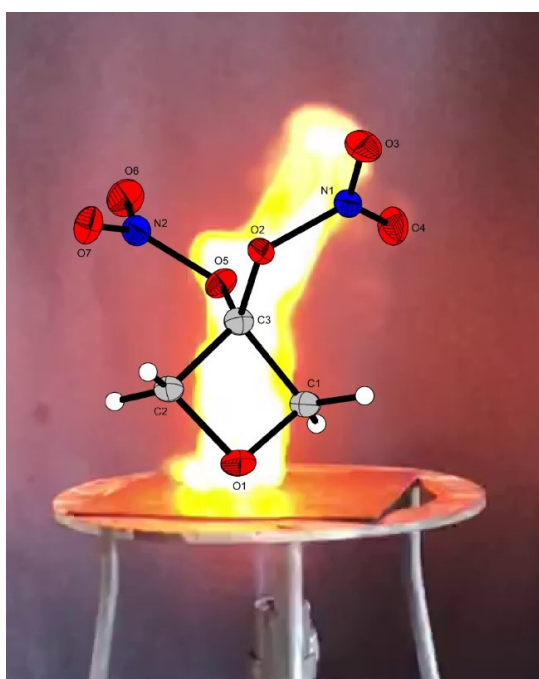
1. M. Born, T. C. Fessard, L. Göttemann, T. M. Klapötke, J. Stierstorfer, M. Voggenreiter, 3,3-Dinitratoxetane – an important leap towards energetic oxygen-rich monomers and polymer, *Chem. Commun.* **2021**, 57, 2804–2807.
2. M. Born, K. Karaghiosoff, T. M. Klapötke, M. Voggenreiter, Highly energetic, insensitive and thermostable oxetane monomers based on the powerful explosive LLM-116, *ChemPlusChem* **2022**, 87, e202200049.
3. T. C. Fessard, I. Gospodinov, T. M. Klapötke, J. Stierstorfer, M. Voggenreiter, Energetic but insensitive spiro-tetrahydrotetrazines based on oxetane-3-one, *Journal of Heterocyclic Chemistry* **2022**, accepted author manuscript.
4. A. G. Harter, T. M. Klapötke, C. Riedelsheimer, J. Stierstorfer, M. Voggenreiter, Synthesis and Characterization of Geminal Diazido Derivatives Based on Diethyl Malonate, *Eur. J. Inorg. Chem.* **2021**, 23, 2241–2247.
5. T. Klapötke, A. G. Harter, J. Stierstorfer, M. Voggenreiter, X. Zeng, Synthesis, Characterization and Energetic Performance of Oxalyl Diazide, Carbamoyl Azide, and N,N'-Bis(azidocarbonyl)hydrazine, *ChemPlusChem* **2021**, 86(6), 870–874.
6. A. G. Harter, T. M. Klapötke, C. Riedelsheimer, J. Stierstorfer, S. M. Strobel, M. Voggenreiter, 2-Hydrazonyl-Propandihydrazide – A Versatile Precursor for High-Energy Materials, *Eur. J. Inorg. Chem.* **2022**, e202200100.
7. M. Benz, T. M. Klapötke, J. Stierstorfer, M. Voggenreiter, Synthesis and Characterization of Binary, Highly Endothermic, and Extremely Sensitive 2,2'-Azobis(5-azidotetrazole), *J. Am. Chem. Soc.* **2022**, 144(14), 6143–6147.
8. M. Benz, T. M. Klapötke, J. Stierstorfer, M. Voggenreiter, 1-Amino-5-nitriminotetrazolate: High Performing Energetic Anion, unpublished manuscript.

1 Oxygen-Rich Oxetanes

3,3-Dinitratooxetane - An Important Leap Towards Energetic Oxygen-Rich Monomers and Polymer

Max Born, Thomas C. Fessard, Lucas Göttemann, Thomas M. Klapötke, Jörg Stierstofer and Michael Voggenreiter

As published in *Chemical Communications* **2021**, 57, 2804–2807; DOI: 10.1039/D1CC00466B



1.1 Abstract

3-Substituted oxetanes are valuable monomers for modern ring-opening polymerizations. A new solid-state oxidizer, 3,3-dinitratooxetane ($C_3H_4N_2O_7$), which has an oxygen content of 62.2% was synthesized by the addition of N_2O_5 to oxetan-3-one. Monoclinic single crystals suitable for X-ray diffraction (ρ 1.80 g cm^{-3}) were obtained by recrystallization from dichloromethane. In addition, 3-nitratooxetane was prepared by an improved method and 3-nitrato-3-methyloxetane was synthesized for the first time. Theoretical calculations were computed by the EXPLO5 software and additionally sensitivities towards impact and friction were determined.

1.2 Introduction

Since the synthesis of oxetane by *Reboul* in 1878, oxetanes have long remained a niche structural motif.^[1] However, this changed drastically in the last two decades due to the use of the oxetane motif in the field of medicinal chemistry.^[1,2] Here it is employed as a bioisoster for geminal methyl groups or carbonyl groups. Due to this development, an increasing number of oxetane derivatives are becoming commercially available.^[3] This concern, for example, oxetan-3-one, which rich chemistry has become known in the literature.^[4] The field of energetic polymers is largely defined by 3,3-bis-(azidomethyl)oxetane (BAMO), 3-azidomethyl-3-methyloxetane (AMMO) and 3-nitratomethyl-3-methyloxetane (NIMMO), all of which have a very poor oxygen balance in common.^[5,6] Especially oxygen-rich monomers and polymers has been very limited so far. *Baum et al.* succeeded in a first step by preparing the oxygen-rich 3,3-dinitrooxetane and the corresponding polymer. However, its preparation is a six-step synthesis starting from oxetan-3-ol with an accordingly low overall yield.^[7] The state of the is mainly dominated by the

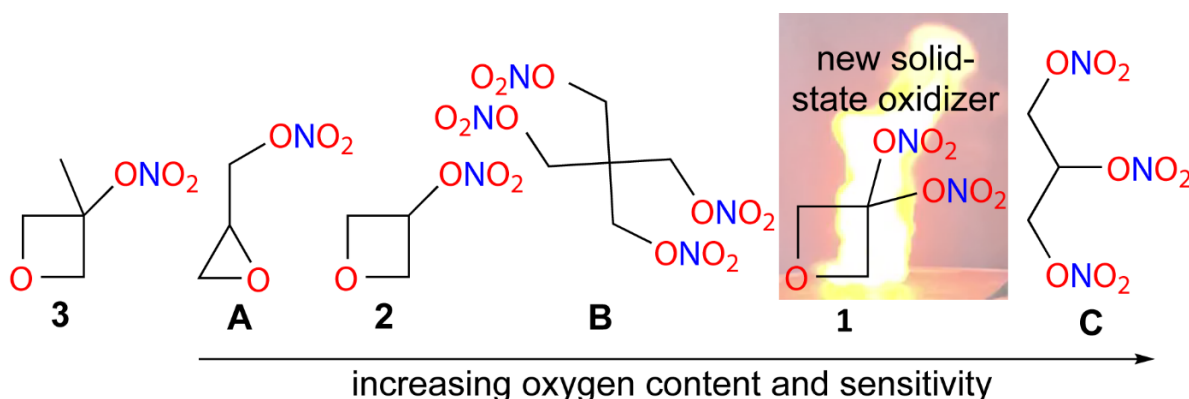


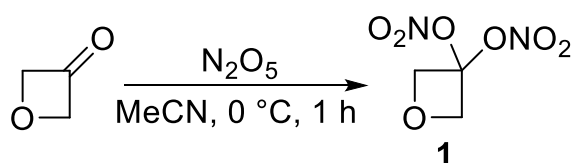
Figure 1. Structural formula of 3-nitrato-3-methyloxetane (**3**), glycidyl nitrate (**A**), 3-nitratooxetane (**2**), pentaerythritol tetranitrate (**B**), the new solid-state oxidizer 3,3-dinitratooxetane (**1**) and nitroglycerine (**C**) in the ascending order of oxygen content and sensitivities.

1 Oxygen-Rich Oxetanes

constitutional isomers glycidyl nitrate (**A**) and 3-nitratooxetane (**2**) which lead to useful binders after cationic ring-opening polymerization.^[6,8,9] Nitrate ester as energetic structural motifs are also used as in common explosives. Although accidents happen every year due to its high impact sensitivity, still nitroglycerine (**C**) is widespread and used in double or triple base propellants. For today's application as booster, pentaerythritol tetranitrate (PETN) (**B**) is preferred. The compounds **A–C** have the nitrate moiety in common. The use of this structural motif is one of the most promising ways to synthesize molecules with positive oxygen balance. This is the ability to form O₂ besides N₂, H₂O and CO/CO₂ during combustion. In literature, there are only a few examples of molecules having a carbon bonded dinitrato moiety. In 1938, *Travagli* reported on the synthesis of the simplest and first geminal C-nitrato compound, dinitratomethane, which he obtained by nitration of 1,3,5-trioxane in mixed acid.^[10] The synthesis of dinitratomethane was improved by *Reichel et al.* in 2019 by the reaction of silver nitrate with diiodomethane in acetonitrile.^[11] Dinitrogen pentoxide can be added to the double bond of aldehydes to obtain the dinitrato compound. This was done by *Kacmarek et al.* in 1975 in which he added dinitrogen pentoxide to acetaldehyde to obtain 1,1-dinitratoethane.^[12] In 2016, *Fischer et al.* impressively demonstrated the power of this synthetic route: he added dinitrogen pentoxide to monomeric glyoxal and obtained tetranitratoethane in quantitative yield.^[13]

1.3 Results and Discussion

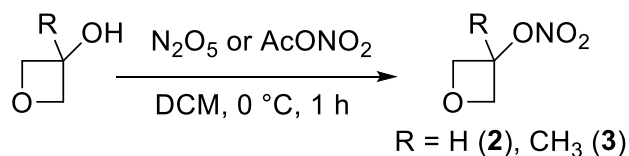
The synthetic pathway was used for the reaction according to **Scheme 1** in order to synthesize the title compound. Oxetan-3-one was added to a solution of dinitrogen pentoxide in acetonitrile at 0 °C. After one hour, the reaction mixture was poured into ice-water and extracted with ethyl acetate. After washing with bicarbonate solution to remove residues of acid, the solvent was removed to obtain crude **1** as colorless solid which was purified by recrystallization from dichloromethane. The crystals obtained were suitable for X-ray diffraction and were dried under high vacuum. The purified material is stable at –20 °C under a dry atmosphere. At ambient temperatures 3,3-dinitratooxetane slowly decomposes forming NO_x radicals. In air the product



Scheme 1. Synthesis of **1** via the addition of N₂O₅ to oxetan-3-one.

1 Oxygen-Rich Oxetanes

hydrolyses to form nitric acid and oxetan-3-one again as indicated by a singlet resonance of low intensity (5.37 ppm) next to the signal of the target compound which is also a singlet (5.11 ppm) due to its A₄ spin system. However, the hydrolysis is slow enough to allow quenching of the reaction with ice water. 3-Nitratooxetane (**2**) was prepared by modified literature procedures



Scheme 2. Preparation of 3-nitratooxetane (**2**) and 3-nitrato-3-methyloxetane (**3**).

using acetyl nitrate as mild and cost-efficient nitrating agent.^[8] Since the crude product is usually contaminated with acetyl nitrate, this was quantitatively removed by selective hydrolysis with hydrogen carbonate solution without decomposing the ester. This allows subsequent purification by distillation without the risk of explosion induced by acetyl nitrate. ¹H NMR spectroscopy showed an AA'BB'X spin system of higher order. Two multiplet signals were obtained for both methylene groups (4.68, 4.93 ppm) while the coupling of the methine-proton with the AB-part caused a triplet of triplets. Similar to compound **1**, liquid 3-nitrato-3-methyloxetane (**3**) was obtained by nitration of the corresponding alcohol with N₂O₅. Despite the highest basicity of the oxetane oxygen in the series of reactants used, ring opening was so avoided and the product obtained in high purity and yield as yellow liquid. The corresponding ¹H NMR spectrum was of high purity, showed duplet signals for the methylene groups (4.52, 4.78 ppm) and a singlet for the methyl group following the A₂B₂X₃ spin system. Regarding vibrational spectroscopy (IR, Raman), the characteristic asymmetric (1629–1687 cm⁻¹) and symmetric stretching vibrations (1275–1306 cm⁻¹) of the nitrate-groups were found for all compounds. Beyond, the well-known ring-breathing motion of the oxetane-moiety was observed as strong absorption band in all IR-spectra (977–1042 cm⁻¹). Being the only solid in the series, compound **1** crystallizes in the monoclinic space group *P2₁/c* with 4 molecules in the unit cell and a density of 1.80 g cm⁻³ at 107 K. The angles in the oxetane motif vary between 86.9(3)° at C1–C3–C2 to 92.3(3)° at C2–O1–C1 and thus provide insight into the high ring strain. The oxetane ring shows a puckering of 5.4(3)° while both nitrate-groups are planar. The view along the *a*-axis reveals that the oxetane moieties form corridors and nitrate-groups spaced away from each other as possible. Hirshfeld analysis showed a high percentage of repulsive O...O contacts (31.6 %) which cause strong repulsive

1 Oxygen-Rich Oxetanes

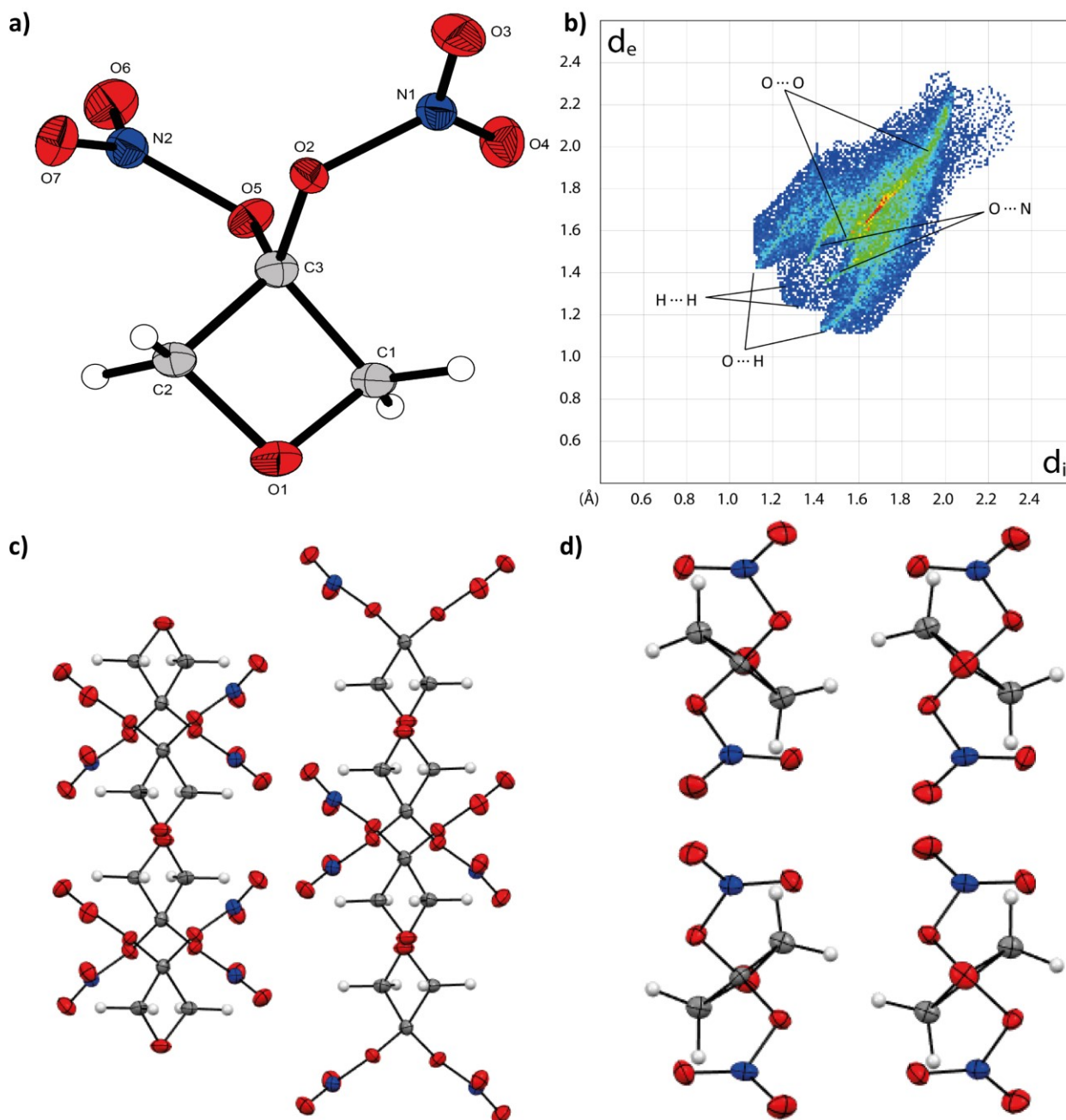


Figure 2. a) Molecular structure of compound 1. Thermal ellipsoids are drawn at the 50% probability level. b) Two dimensional Hirshfeld fingerprint plot. c) View along the a -axis. d) View in the direction of the c -axis.

interactions upon lattice deformation by mechanic stimuli and therefore indicate a high sensitivity.^[14–16] Accordingly, the view (a -axis) also reveals pairwise layers of nitro-groups directed to each other causing this particular oxygen-oxygen repulsion. A large population of normally stabilizing O...H interactions (54.4 %) was found, but they are weak due to their large distance (>2.5 Å) and thus cannot contribute significantly to the stabilization of 3,3-dinitratoxetane. Another possible stabilizing effect is N...O interaction, but the extent is low (7.5 %) and also weak due to the large distance.^[17] In total, the O...O interaction is hardly

1 Oxygen-Rich Oxetanes

counterbalanced by stabilizing effects and high sensitivity and low thermal stability must be assumed. This is in excellent agreement with measured values. DTA analysis of **1** shows a melting point at 69 °C, followed by another endo-peak at 88 °C which is associated with the cleavage of a nitrate-group. The exothermic decomposition is observed directly afterwards at 93 °C. 3,3-Dinitratooxetane is extremely sensitive towards impact (<1 J) which is comparable to the impact sensitivity of nitroglycerine and way more sensitive than PETN (**Table 1**). Compound **1** is also very sensitive to friction with a sensitivity of 1 N. These high sensitivities are a result of the nitrate groups arranged in the crystal (**Figure 2c**), which are in spatial vicinity to each other. If these layers are moved against each other by mechanical stimuli, the distance between these groups decreases and the repulsion between the groups increases which then causes explosion. Also, the electronegative nitrate groups on side of the molecule and the electropositive oxetane ring on the other side which is an uneven distribution and makes the molecule more sensitive. In contrast, the liquid 3-nitratooxetane (**2**), which has only one nitrate moiety shows drastically higher decomposition temperature of 153 °C as assessed by DSC. Furthermore, only one nitrate-group causes the compound to be completely insensitive towards impact and friction while the sensitivity of **1** already falls in the range of primary explosives. Unexpectedly, 3-nitrato-3-methyloxetane (**3**) has an even lower decomposition temperature of 141 °C (DSC) and was found to be insensitive towards impact according to expectation. Despite, it is slightly sensitive towards friction with a value of 160 N. This might be explained by the heat generally caused by friction which can obviously be sufficient to cause thermal initiation. 3,3-Dinitratooxetane features an outstanding oxygen content that is even higher than the content of pentaerythritol tetranitrate but slightly lower than the content of nitroglycerine. With ease it surpasses the oxygen balance of commonly known energetic monomers such as GLYN and 3-NO (**Table 1**). The Gaussian16 program package was used to calculate room temperature enthalpy of formation on the CBS-4M level of theory using the atomization method for all investigated compounds. The EXPLO5 code was used to calculate the energetic properties of compounds **1–3**. Here, DNO shows the highest performance with a detonation velocity of almost 8300 m s⁻¹ and a specific impulse of 264 s as pure substance and 267 s as a mixture with aluminum, whereby these values considerably exceed the specific impulse for ammonium perchlorate. To the best of our knowledge, this resembles the highest performance known in the field of energetic oxetanes.

1 Oxygen-Rich Oxetanes

Table 1. Physicochemical values of 3,3-dinitratooxetane (**DNO**, **1**), 3-nitratooxetane (**3-NO**, **2**), 3-nitrato-3-methyloxetane (**3N3MO**, **3**), ammonium perchlorate (**AP**), nitroglycerine (**NG**), pentaerythritol tetranitrate (**PETN**), glycidyl nitrate (**GLYN**), and 3-nitratooxetane (**3-NO**).

	DNO (1)	3-NO (2)	3N3MO (3)	AP [18]	NG [18–20]	PETN [18–20]	GLYN [9, 19, 20]
Formula	C ₃ H ₄ N ₂ O ₇	C ₃ H ₅ NO ₄	C ₄ H ₇ NO ₄	NH ₄ ClO ₄	C ₃ H ₅ N ₃ O ₉	C ₅ H ₈ N ₄ O ₁₂	C ₃ H ₅ NO ₄
FW [g·mol ⁻¹]	180.07	119.08	133.10	117.49	227.09	316.14	119.08
IS ^[a] [J]	<1	40	>40	20	0.2 – 1	3	2 – 4
FS ^[b] [N]	1	>360	>160	>360	>360	60	>360
N, O ^[c] [%]	15.56, 62.19	11.76, 53.74	10.52, 48.08	11.92, 54.47	18.5, 63.41	17.72, 60.73	11.76, 53.74
Ω _{CO} , Ω _{CO₂} ^[d] [%]	+17.77, -8.89	-20.15, -60.46	-42.07, -90.20	+34.04, +34.04	+24.66, +3.50	+15.18, -10.12	-20.15, -60.46
T _m ^[e] / T _{dec.} ^[f] [°C]	69/93	-/153	-/141	-/240	13/185	141/202	-/195
ρ ^[g] [g·cm ⁻³]	1.74	1.34	1.33	1.95	1.60	1.77	1.33
ΔH _f ^[h] [kJ·mol ⁻¹]	-302.6	-168.0	-245.8	-295.8	-311.3	-479.7	-199.3
EXPLO5 V6.04^[10]							
-Δ _E U ^[i] [kJ·kg ⁻¹]	6176	5089	4356	1419	6305	6165	4852
D _{C-J} ^[k] [m·s ⁻¹]	8275	6771	6456	6903	7823	8369	6664
ρ _{C-J} [GPa]	29.7	16.6	13.9	18.6	23.7	30.5	15.8
I _{sp} ^[l] [s]	264	235	204	157	275	267	228
I _{sp} ^[m] [s] (15% Al)	267	265	245	236	267	270	261

[a] Impact sensitivity (BAM drophammer, method 1 of 6); [b] friction sensitivity (BAM drophammer, method 1 of 6); [c] Nitrogen and oxygen content; [d] Oxygen balance toward carbon monoxide ($\Omega_{CO} = (nO - xC - yH/2)(1600/FW)$) and carbon dioxide ($\Omega_{CO_2} = (nO - 2xC - yH/2)(1600/FW)$); [e] melting point (DTA, $\beta = 5 \text{ }^\circ\text{C}\cdot\text{min}^{-1}$); [f] temperature of decomposition (DTA, $\beta = 5 \text{ }^\circ\text{C}\cdot\text{min}^{-1}$); [g] density at 298 K; [h] standard molar enthalpy of formation; [i] detonation energy; [j] detonation temperature; [k] detonation velocity; [l] Specific impulse of neat compound (70.0 bar chamber pressure, isobaric combustion conditions (1 bar), equilibrium expansion); [m] Specific impulse for compositions with 85 % compound and 15 % aluminum (70.0bar chamber pressure, isobaric combustion conditions (1 bar), equilibrium expansion).

1.4 Conclusion

Both 3,3-Dinitratooxetane (**1**) and 3-nitrato-3-methyloxetane (**3**) were prepared by the versatile use of dinitrogen pentoxide and investigated by multinuclear spectroscopy. Summarizing the physicochemical properties of compound **1**, especially the low thermal stability, the decomposition at room temperature and the high sensitivities will probably exclude it from application. Possibly **1** could be much safer and more stable when the polymer is formed, and our investigation are ongoing. Offering both the highest oxygen content and performance ever obtained in the field of oxetanes, 3,3-dinitratooxetane represents an important step towards especially oxygen-rich and high-performing oxetane compounds. Its synthesis is anticipated to trigger more intensive research with regard to oxetane-based polynitro- and polynitrato compounds and is likely to accelerate the development in this field.

Financial support of this work by the Ludwig-Maximilian University of Munich (LMU), the Office of Naval Research (ONR) under grant no. ONR N00014-19-1-2078 and the Strategic Environmental Research and Development Program (SERDP) under contract no. WP19-1287 is gratefully acknowledged. There are no conflicts to declare.

1.5 Supporting Information

1.5.1 Experimental Part and General Methods

Caution! 3,3-Dinitratooxetane is a powerful energetic material with high sensitivities towards shock and friction. Therefore, proper security precautions (safety glass, face shield, earthened equipment and shoes, Kevlar gloves and ear plugs) have to be applied while synthesizing and handling the described compounds.

Chemicals and solvents were employed as received (Sigma-Aldrich, Acros, TCI, Spirochem AG). ^1H , ^{13}C and ^{14}N spectra were recorded using a Bruker AMX 400 instrument. The chemical shifts quoted in ppm refer to tetramethylsilane (^1H , ^{13}C) and nitromethane (^{14}N). Decomposition temperatures were determined on a Mettler Toledo DSC822e at a heating rate of $5\text{ }^\circ\text{C min}^{-1}$ using $40\text{ }\mu\text{L}$ aluminum crucibles and nitrogen purge gas at a flow rate of 30 mL min^{-1} . Evaluations of thermal behavior were performed using the STARe Software Version 16.20. Infrared (IR) spectra were recorded using a Perkin-Elmer Spektrum One FT-IR instrument. Raman spectra were obtained using a Bruker MultiRam FT Raman spectrometer and a neodymium-doped yttrium aluminum garnet (Nd:YAG) laser ($\lambda = 1064\text{ nm}$, 1074 mW). Elemental analyses were performed

1 Oxygen-Rich Oxetanes

with an Elementar Vario el by pyrolysis of the sample and subsequent analysis of formed gases (standard deviation liquids: +/- 0.5 %). The sensitivity data were collected using a BAM (Bundesanstalt für Materialforschung) drophammer^[21] according to STANAG 4489^[22] modified instruction^[23] and a BAM friction tester^[21] according to STANAG 4487^[24] modified instruction.^[25] The classification of the tested compounds results from the 'UN Recommendations on the Transport of Dangerous Goods'.^[26]

3,3-Dinitratooxetane

Oxetan-3-one (0.50 g, 6.94 mmol, 1.0 eq.) was dissolved in acetonitrile (5 mL) and added to a solution of dinitrogen pentoxide (2.25 g, 20.8 mmol, 3.0 eq.) in acetonitrile (10 mL) which was cooled to 0 °C. The mixture was stirred for 1 hour at 0 °C and then let come to ambient temperature over 30 minutes. The solution was poured into ice-water (70 mL) and was extracted with ethyl acetate (3x 25 mL). The organic layer was washed with saturated bicarbonate solution (2x 30 mL) prior to drying over sodium sulfate. The solvent was removed, and the product was dried under high vacuum to give 0.51 g of 3,3-dinitratooxetane (2.83 mmol, 41 %) as colorless solid. The product has to be stored at -20°C under dry atmosphere to prevent decomposition. **DSC** (T_{onset} , 5 °C min⁻¹): 69.4 °C (mp.), 93.3 °C (dec.); **FT-IR** (ATR): $\tilde{\nu}$ = 2962 (w), 1687 (m), 1655 (s), 1445 (w), 1305 (s), 1286 (m), 1180 (m), 1158 (s), 1113 (m), 982 (s), 961 (m), 935 (w), 884 (m), 842 (m), 791 (s), 739 (s), 669 (s), 591 (m), 438 (m) cm⁻¹; **¹H NMR** (400 MHz, Acetone-d₆, 25 °C): δ = 5.11 (s, 4H) ppm; **¹³C NMR**{¹H} (101 MHz, Acetone-d₆, 25 °C): δ = 77.5, 103.8 ppm; **¹⁴N NMR** (27 MHz, Acetone-d₆, 25 °C): δ = -56.3 ppm; **EA** (C₃H₄N₂O₇) calcd.: C 20.01, H 2.24, N 15.56; found: C 20.25, H 2.52, N 15.29; **BAM drophammer** < 1 J (> 500 μ m); **Friction test** 1 N (> 500 μ m).

3-Nitratooxetane

Acetic anhydride (6.00 g, 58.8 mmol) was dissolved in dry dichloromethane (5.00 mL) and white fuming nitric acid (100 %, 3.90 g, 61.9 mmol) was added at -10 °C using an ice bath with sodium chloride. The mixture was stirred for one hour prior to the addition of oxetan-3-ol (3.00 g, 40.5 mmol) in dry dichloromethane (5.00 mL). The solution was stirred for one hour and then poured onto ice (15.0 g). Dichloromethane (10.0 mL) was added and the layers were separated. The organic layer was washed with saturated sodium bicarbonate solution (3x 20 mL) and separated. The solvent was then removed by rotary evaporation to give a slightly yellowish liquid and sodium bicarbonate solution (10%, 20.0 mL) was added. The resulting emulsion was heavily

1 Oxygen-Rich Oxetanes

stirred for 30 minutes (to remove any traces of acetyl nitrate) and the target compound subsequently extracted with dichloromethane (3x 30 mL). After drying over sodium sulfate, the solvent was removed to give 2.78 g (23.3 mmol, 58%) of 3-nitratooxetane as slightly yellowish liquid. The product may be further purified by distillation (27 mbar, 65 °C) to give colorless 3-nitratooxetane suitable for polymerization reactions.

DSC (T_{onset} , 5 °C min⁻¹): 152.8 °C (dec.); **FT-IR** (ATR): $\tilde{\nu}$ = 3112 (w), 2961 (m), 2887 (w), 2803 (w), 1629 (vs), 1373 (m), 1327 (m), 1275 (vs), 1175 (m), 1069 (m), 975 (s), 928 (w), 881 (s), 846 (s), 754 (m), 690 (m), 556 (w), 404 (w) cm⁻¹. **Raman** (1064 nm, 1074 mW): $\tilde{\nu}$ = 2975 (100), 2932 (78), 2892 (88), 1642 (14), 1480 (36), 1374 (32), 1328 (22), 1279 (63), 1177 (36), 1116 (20), 1071 (47), 1042 (27), 977 (15), 932 (32), 853 (75), 693 (25), 558 (41), 406 (19) cm⁻¹; **¹H NMR** (400 MHz, Acetone-d₆, 25 °C): δ = 4.68 (ddd, 2H, CH₂, J = 8.2, 4.9, 1.1 Hz), 4.93 (ddd, 2H, CH₂, J = 8.3, 6.2, 1.2 Hz), 5.68 (tt, 1H, CH, J = 6.2, 4.9 Hz) ppm; **¹³C NMR{¹H}** (101 MHz, Acetone-d₆, 25 °C): δ = 74.8, 75.3 ppm; **¹⁴N NMR** (27 MHz, Acetone-d₆, 25 °C): δ = -45.6 ppm; **EA** (C₃H₄N₂O₇) calcd.: C 30.26, H 4.23, N 11.76; found: C 29.76, H 3.73, N 11.49; **BAM drophammer** > 40 J; **Friction test** > 160 N.

3-Nitrato-3-methyloxetane

3-Hydroxy-3-methyloxetane (0.50 g, 5.67 mmol) was added to a solution of dinitrogen pentoxide (674 mg, 6.24 mmol, 1.1 eq.) in dry dichloromethane (15 mL) at 0 °C using an ice-bath. The resulting solution was stirred for 1 h at the initial temperature and subsequently poured into ice-water (50 mL). Additional dichloromethane (20 mL) was added and the phases were separated. The organic phase was washed again with water (30 mL) and finally with saturated sodium bicarbonate solution (25 mL) prior to drying over sodium sulfate. The solvent was removed by rotary evaporation to give 0.74 g (3.92 mmol, 69%) as yellow liquid.

DSC (5 °C min⁻¹): 141.0 °C (dec.); **FT-IR** (ATR): $\tilde{\nu}$ = 3113 (m), 2962 (m), 2887 (m), 2803 (m), 1754 (w), 1628 (s), 1447 (m), 1385 (s), 1304 (vs), 1254 (m), 1178 (s), 1138 (m), 977 (s), 925 (m), 850 (s), 755 (m), 691 (m) cm⁻¹. **Raman** (1064 nm, 1074 mW): $\tilde{\nu}$ = 2977 (69), 2942 (100), 2888 (70), 2751 (7), 1636 (11), 1480 (24), 1461 (19), 1349 (8), 1306 (47), 1254 (11), 1191 (12), 1139 (13), 992 (31), 982 (35), 855 (37), 736 (12), 693 (13), 506 (35), 433 (19) cm⁻¹; **¹H-NMR** (400 MHz, CDCl₃, 25 °C): δ = 1.81 (s, 3H, CH₃), 4.52 (d, 2H, CH₂, J = 8.6 Hz), 4.78 (d, 2H, CH₂, J = 8.6 Hz) ppm; **¹³C-NMR{¹H}** (101 MHz, CDCl₃, 25 °C): δ = 20.6, 79.8, 83.4 ppm; **¹⁴N NMR** (27 MHz CDCl₃, 25 °C): δ = -46.2 ppm; **EA** (C₃H₄N₂O₇) calcd.: C 36.10, H 5.30, N 10.52; found: C 36.37, H 5.17, N 10.26; **BAM drophammer** > 40 J; **Friction test** > 160 N.

1.5.2 NMR Spectra

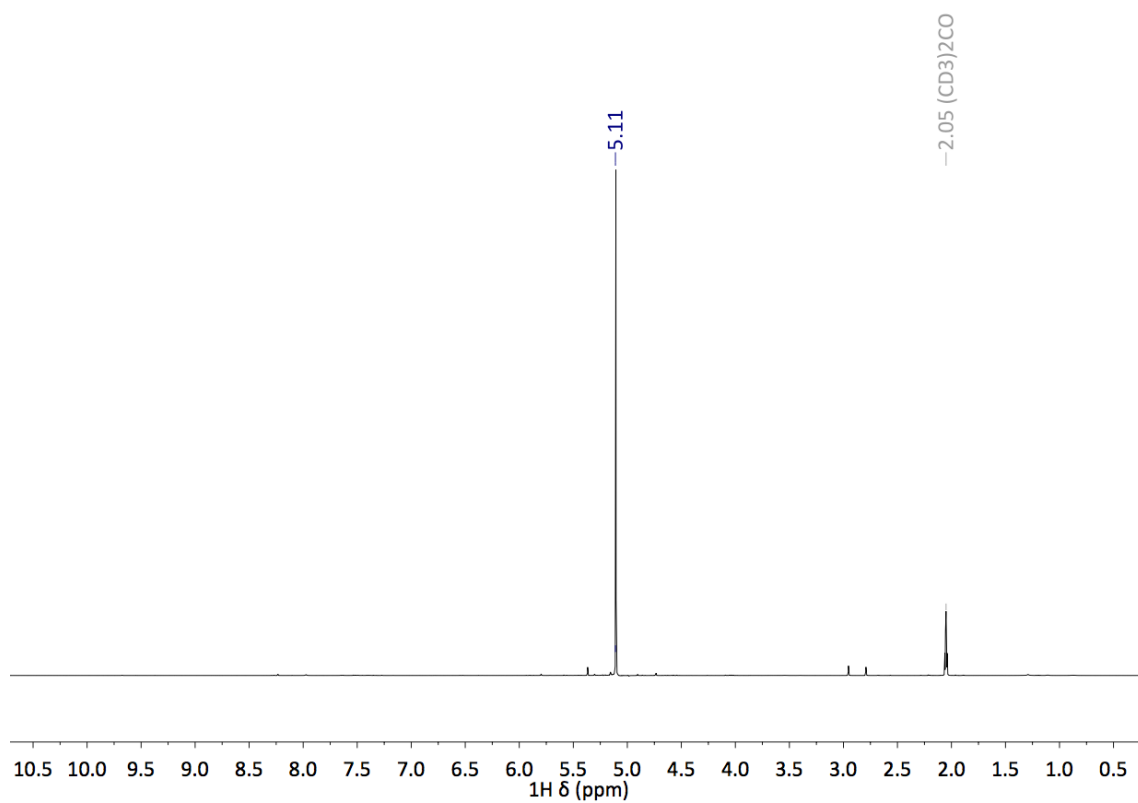


Figure 3. ^1H NMR spectrum of 3,3-dinitratooxetane.

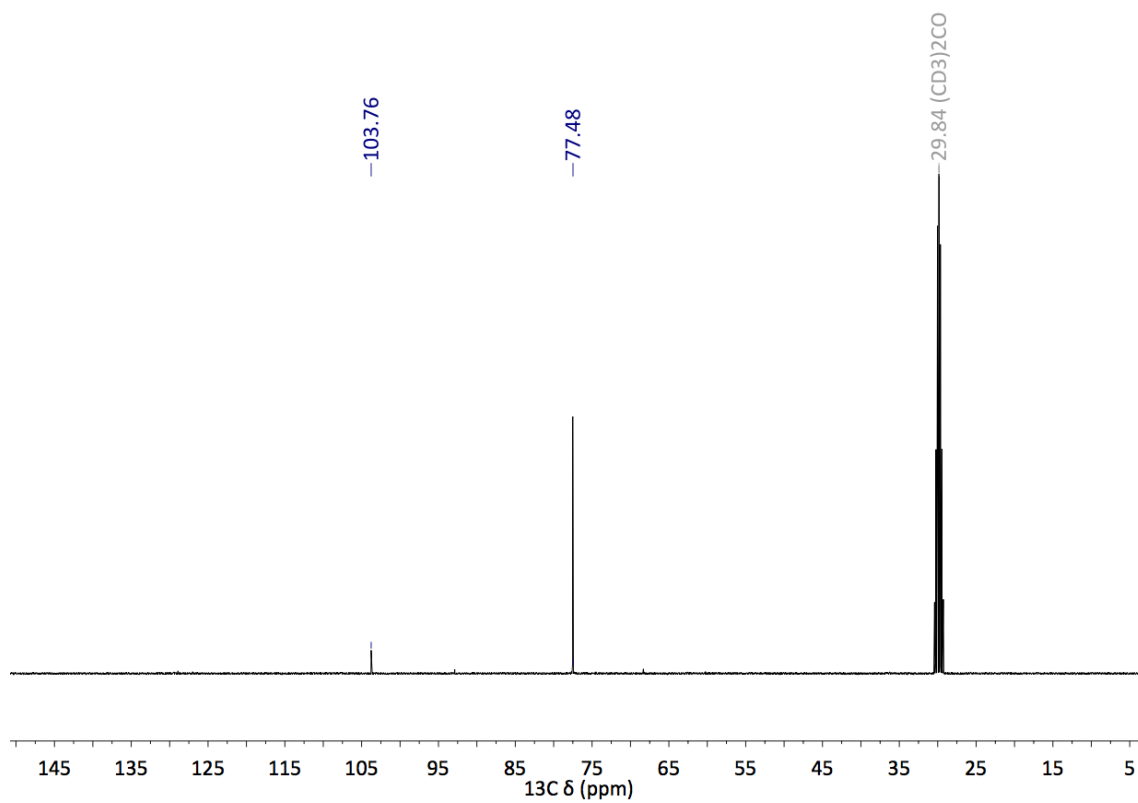


Figure 4. ^{13}C NMR spectrum of 3,3-dinitratooxetane.

1 Oxygen-Rich Oxetanes

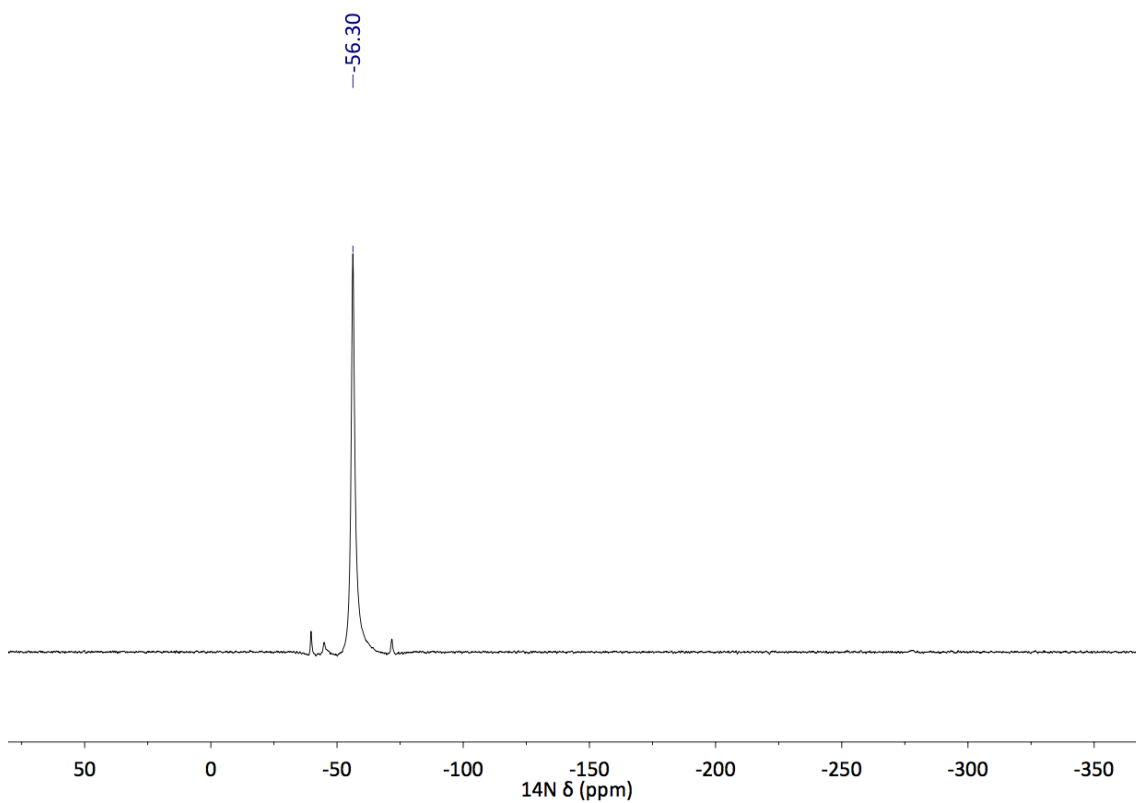


Figure 5. ^{14}N NMR spectrum of 3,3-dinitrooxetane.

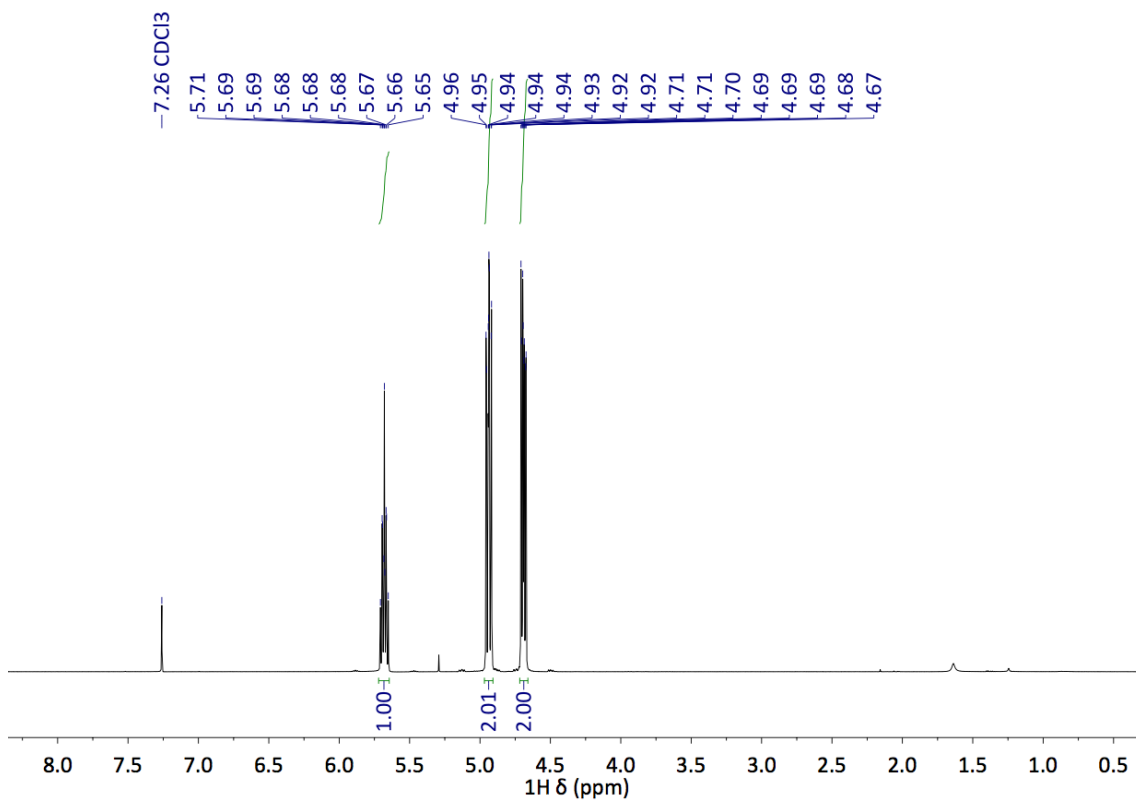


Figure 6. ^1H NMR spectrum of 3-nitrooxetane.

1 Oxygen-Rich Oxetanes

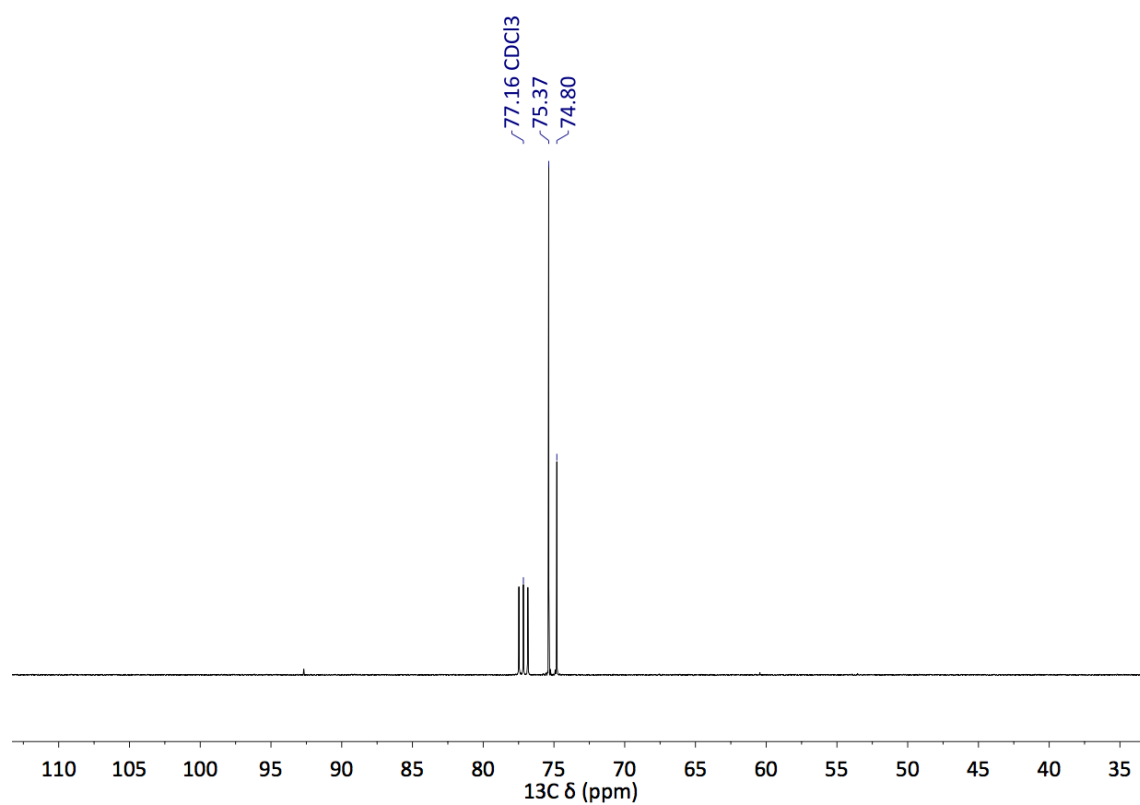


Figure 7. Carbon spectrum (^{13}C) of 3-nitrooxetane.

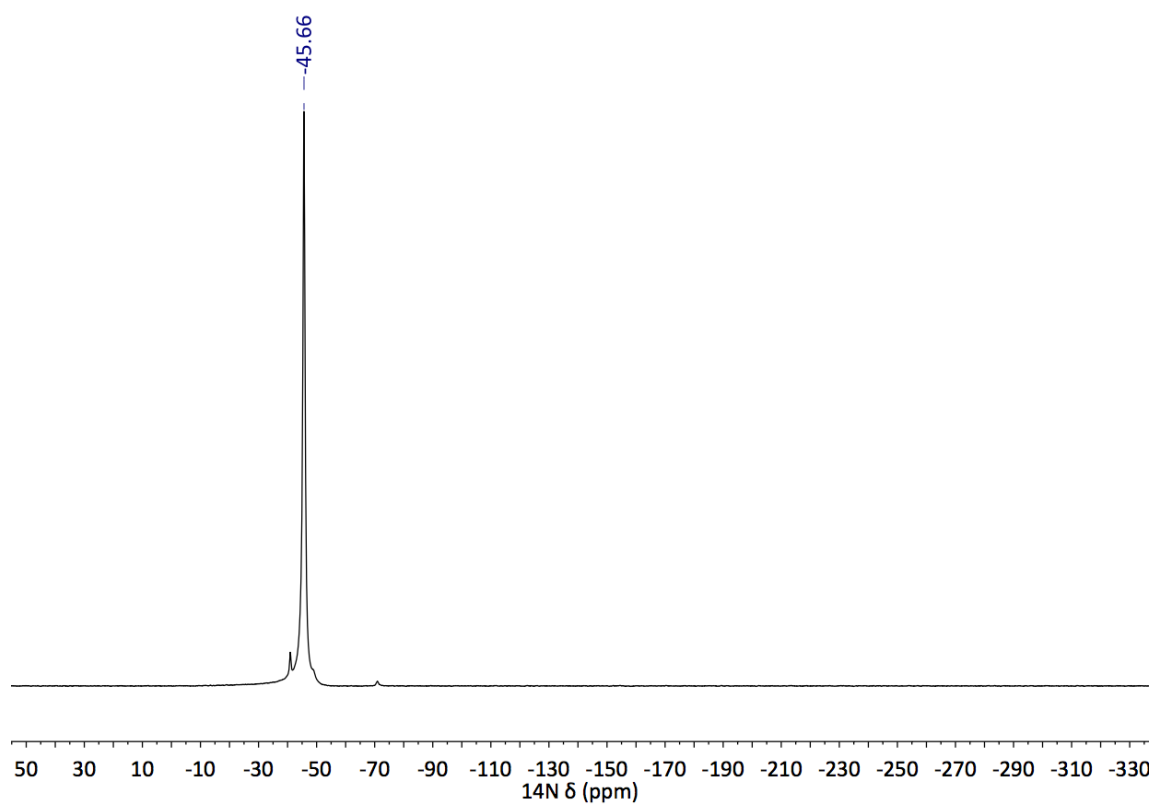


Figure 8. Nitrogen spectrum (^{14}N) of 3-nitrooxetane.

1 Oxygen-Rich Oxetanes

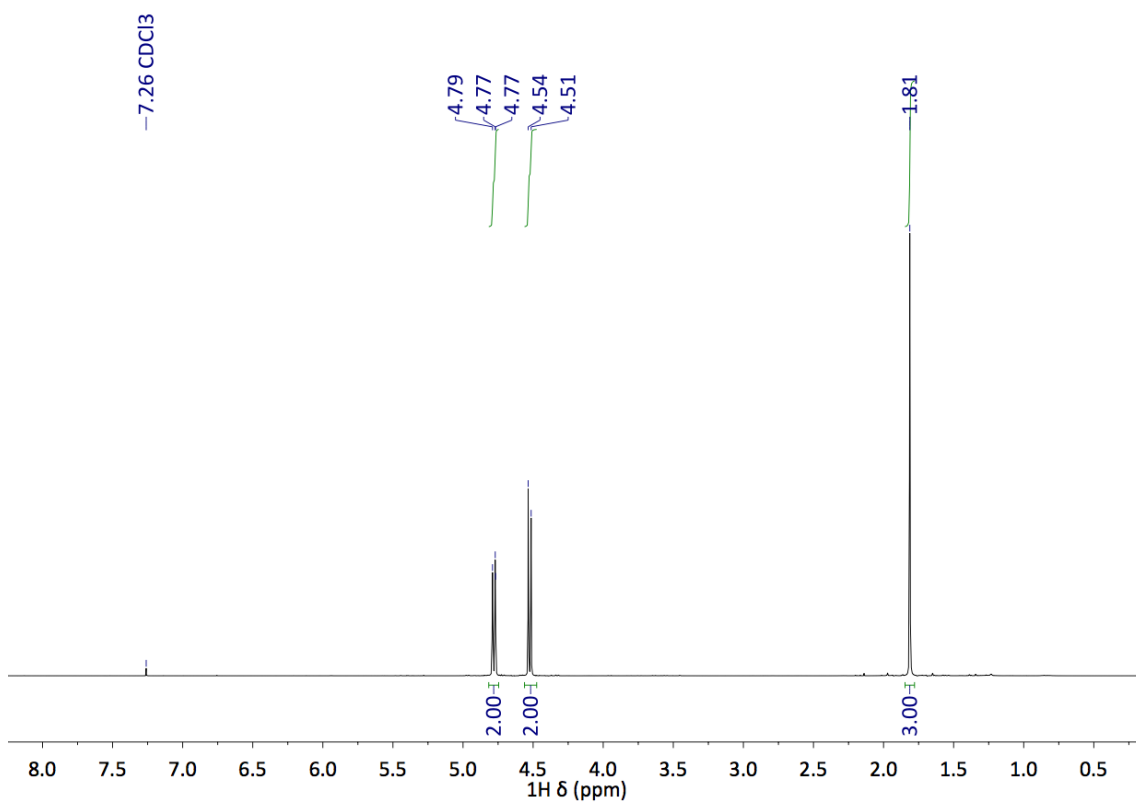


Figure 9. Proton spectrum (^1H) of 3-nitrato-3-methyloxetane.

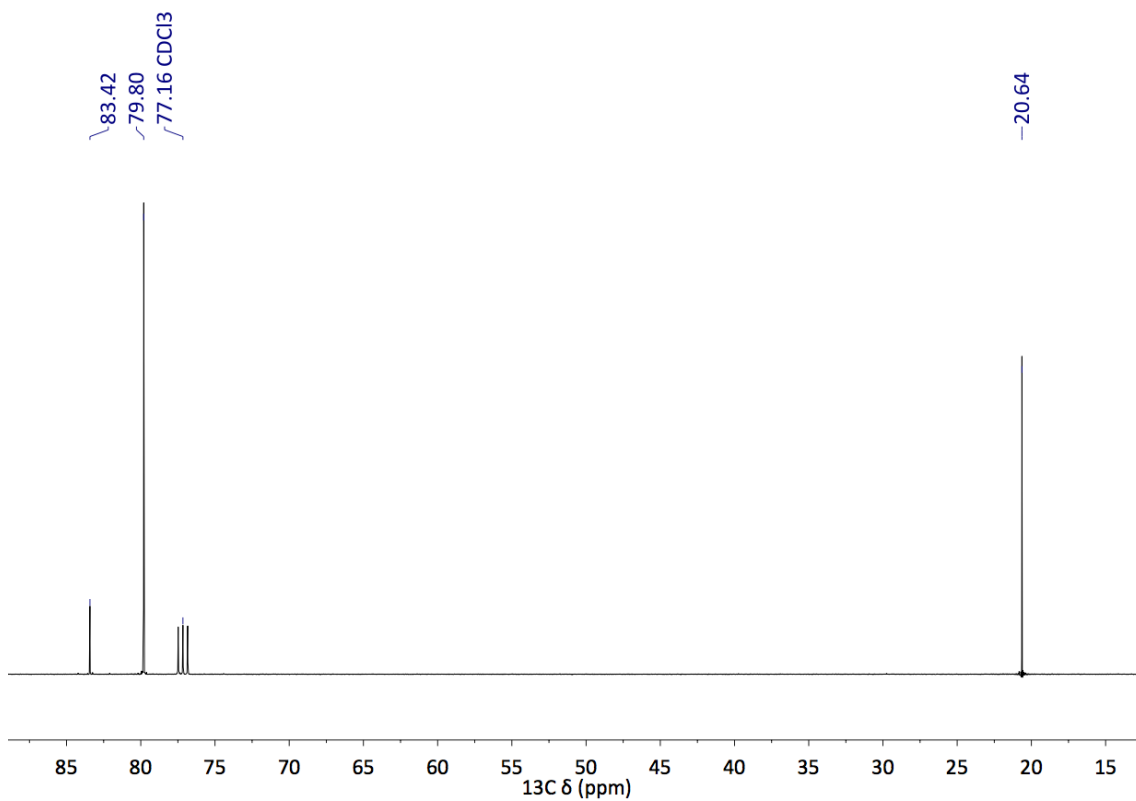


Figure 10. Carbon spectrum (^{13}C) of 3-nitrato-3-methyloxetane.

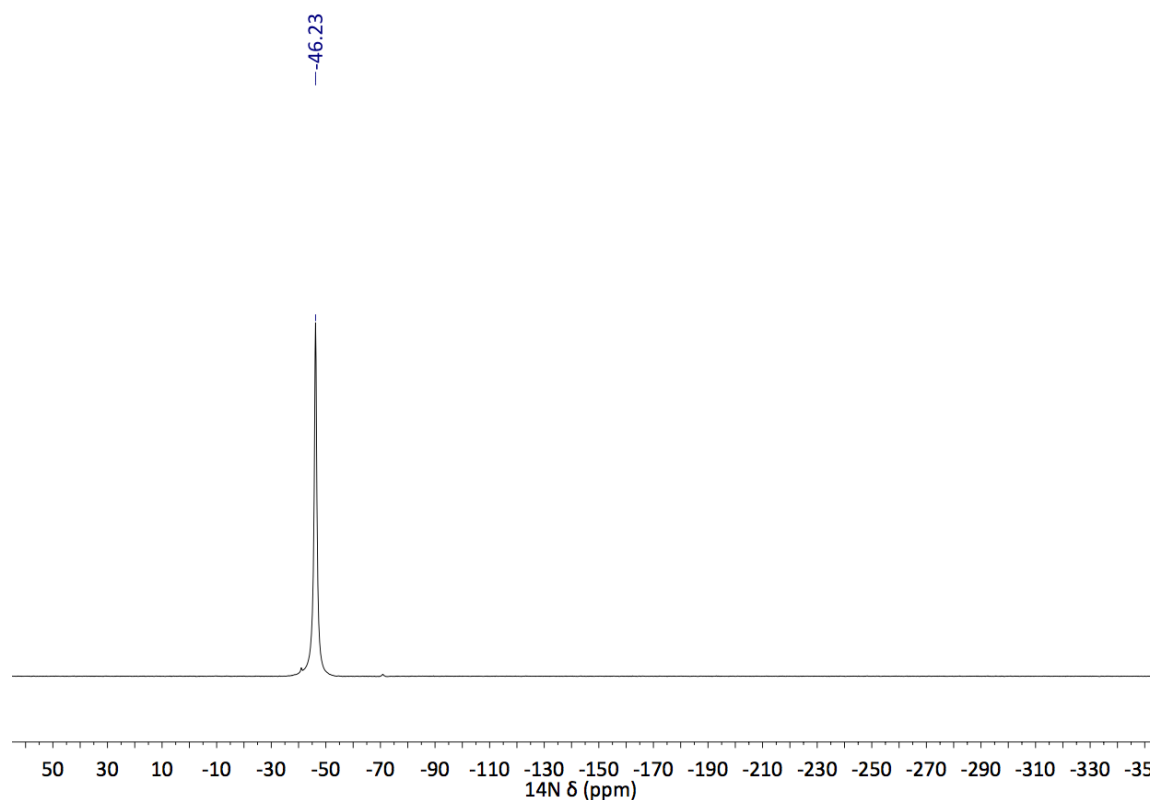


Figure 11. Nitrogen spectrum (^{14}N) of 3-nitrato-3-methyloxetane.

1.5.3 X-Ray Diffraction and Hirshfeld Analysis

The crystals unfortunately had a twinning problem. Data collection was performed with an Oxford Xcalibur3 diffractometer with a CCD area detector, equipped with a multilayer monochromator; a Photon 2 detector and a rotating-anode generator were employed for data collection using Mo $K\alpha$ radiation ($\lambda = 0.7107 \text{ \AA}$). Data collection and reduction were carried out using the CRYSTALISPRO software.^[28] The structures were solved by direct methods (SIR-2014)^[29] and refined (SHELXLE)^[30] by full-matrix least-squares on F2 (SHELXL)^[31,32] and finally checked using the PLATON software^[33] integrated in the WINGX software suite.^[34] The non-hydrogen atoms were refined anisotropically, and the hydrogen atoms were located and freely refined. All Diamond 3 plots are shown with thermal ellipsoids at the 50% probability level, and hydrogen atoms are shown as small spheres of arbitrary radius. The twin reflexes were cut out.

1 Oxygen-Rich Oxetanes

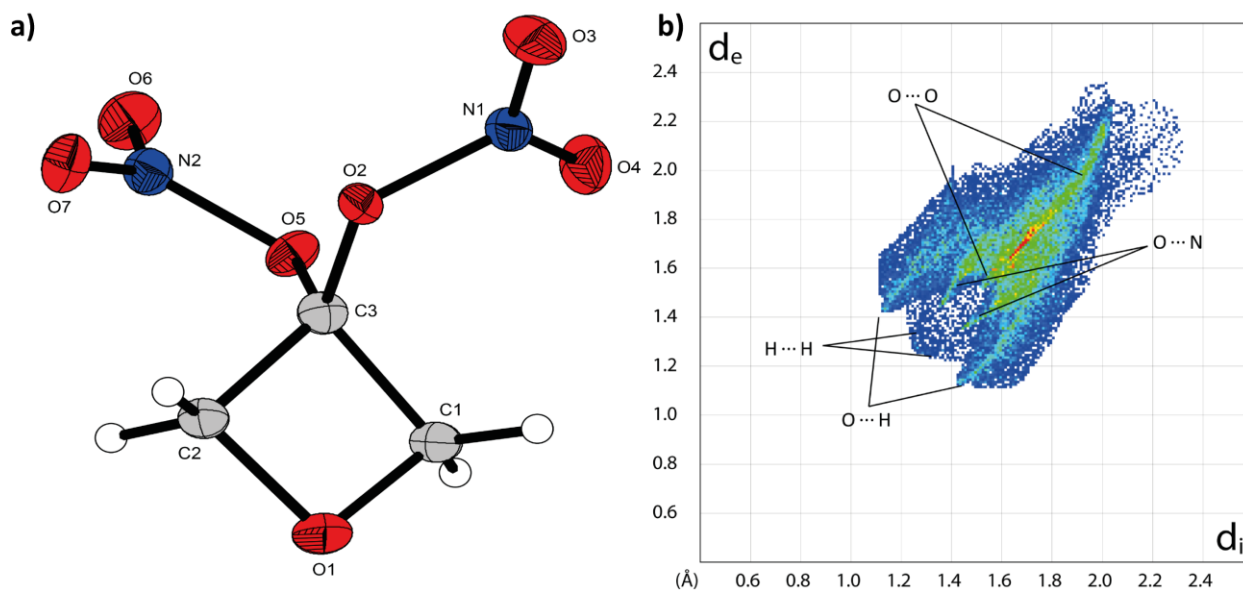


Figure 12. a) Molecular structure of 3,3-dinitratoxetane. Thermal ellipsoids are drawn at 50% probability level. b) Two-dimensional fingerprint plot in crystal stacking of 3,3-dinitratoxetane.

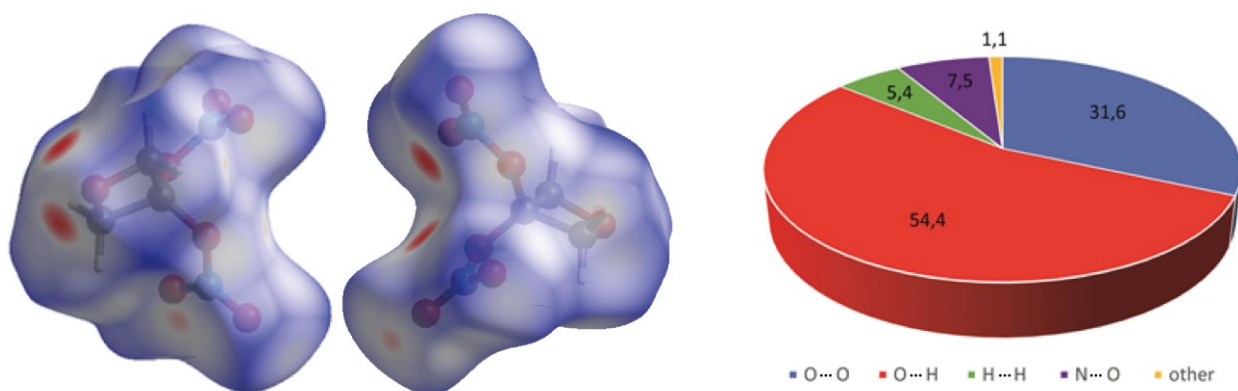


Figure 13. Left: Calculated Hirshfeld surfaces of compound 1. Right: Population of close contacts in compound 1.

Table 2. Detailed crystallographic information of 3,3-dinitratooxetane (**1**).

	1
Formula	C ₃ H ₄ N ₂ O ₇
FW [g mol ⁻¹]	180.08
Crystal System	monoclinic
Space Group	P2 ₁ /c
Color / Habit	colorless block
Size [mm]	0.20 x 0.12 x 0.05
a [Å]	9.259(2)
b [Å]	12.501(3)
c [Å]	5.7467(11)
α [°]	90
β [°]	92.46(2)
γ [°]	90
V [Å ³]	664.6(3)
Z	4
ρ _{calc.} [g cm ⁻³]	1.800
μ [mm ⁻¹]	0.183
F (000)	368
λ _{MoKα} [Å]	0.71073
T [K]	107
ϑ min-max [°]	2.739, 26.370
Dataset h; k; l	-11:11; -8:15; -7:7
Reflect. coll.	1313
Independ. Refl.	1313
R _{int.}	0.057
Reflection obs.	822
No. parameters	109
R1 (obs.)	0.0749
wR2 (all data)	0.1672
S	1.049
Resd. Dens. [e Å ⁻³]	-0.395, 0.365
Device Type	Oxford XCalibur3 CCD
Solution	Sir2014
Refinement	SHELXLE
Absorpt. corr.	Multi-scan
CCDC	2013564

1.5.4 Heat of formation calculation

The atomization was used to determine the heat of formation of **1–3** using the atom energies in **Table 3**.

$$\Delta_f H^\circ_{(g, M, 298)} = H_{(\text{molecule}, 298)} - \sum H^\circ_{(\text{atoms}, 298)} + \sum \Delta_f H^\circ_{(\text{atoms}, 298)}$$

Table 3. CBS-4M electronic enthalpies for atoms C, H, N and O and their literature values.

	$-H^{298} / \text{a.u.}$	$\Delta_f H^\circ_{\text{gas}} [35]$
H	0.500991	217.998
C	37.786156	716.68
N	54.522462	472.68
O	74.991202	249.18

The Gaussian16 program package was used to calculate room temperature enthalpies on the CBS-4M level of theory.^[36] In order to obtain the energy of formation for the solid phase of **1**, the Trouton's Rule has to be applied ($\Delta H_{\text{sub}} = 188 \cdot T_m$). As compounds **2** and **3** are liquid, a different factor is applied ($\Delta H_{\text{sub}} = 90 \cdot T_m$).

Table 4. Heat of formation calculation results for compounds **1–3**.

M	$-H^{298} [a] [\text{a.u.}]$	$\Delta_f H^\circ(g, M) [b] [\text{kJ mol}^{-1}]$	$\Delta_{\text{sub}} H^\circ (M) [c] [\text{kJ mol}^{-1}]$	$\Delta_f H^\circ(s) [d] [\text{kJ mol}^{-1}]$	Δn	$\Delta_f U(s) [e] [\text{kJ kg}^{-1}]$
1	751.610116	-233.4	69.2122	-302.6	-6.5	-1590.9
2	472.193794	-129.6	38.3355	-168.0	-5.0	-1306.5
3	511.451024	-208.6	37.2735	-245.8	-6.0	-1735.1

[a] CBS-4M electronic enthalpy; [b] gas phase enthalpy of formation; [c] sublimation enthalpy; [d] standard solid state enthalpy of formation; [e] solid state energy of formation.

1.5.5 Thermal Analysis

The thermal behavior of compounds **1–3** was analyzed by DSC at a heating rate of 5°C min^{-1} . The obtained thermogram and its evaluation is depicted in **Figure 14**.

1 Oxygen-Rich Oxetanes

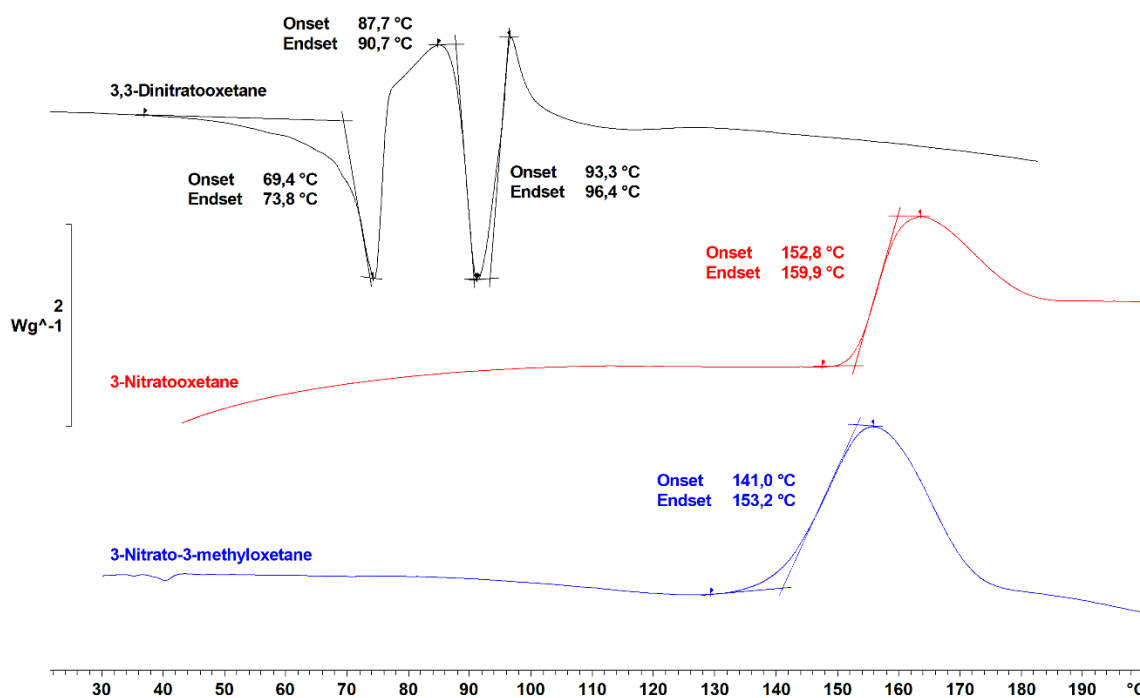


Figure 14. DSC evaluation result for compounds 1–3 (exo-up).

1.6 References

- [1] J. A. Burkhard, G. Wuitschik, M. Rogers-Evans, K. Müller and E. M. Carreira, *Angew. Chem. Int. Ed.* **2010**, *49*, 9052-9067.
- [2] J. A. Burkhard, G. Wuitschik, M. R. Evans, K. Müller and E. M. Carreira, *MEDCHEM NEWS* **2012**, *22*, 8-15.
- [3] <https://spirochem.com/catalog/oxetanes.html> (accessed January **2021**)
- [4] S. A. Ruider, S. Müller and E. M. Carreira, *Angew. Chem. Int. Ed.* **2013**, *52*, 11908-11911.
- [5] M. P. Dreyfuss and P. Dreyfuss, in *Encyclopedia of Polymer Science and Technology* **2011**, DOI: 10.1002/0471440264.pst520.
- [6] H. G. Ang and S. Pisharath, *Energetic Polymers: Binders and Plasticizers for Enhancing Performance*, Wiley, **2012**.
- [7] K. Baum, P. T. Berkowitz, V. Grakauskas and T. G. Archibald, *J. Org. Chem.* **1983**, *48*, 2953–2956.
- [8] *US Pat.*, US8030440B1, **2011**.
- [9] T. Urbanski, *Chemie und Technologie der Explosivstoffe*, VEB Dt. Verl. f. Grundstoffindustrie, Leipzig, **1963**.
- [10] G. Travagli, *Gazzetta Chimica Italiana* **1938**, *68*, 718.
- [11] M. Reichel, B. Krumm, Y. V. Vishnevskiy, S. Blomeyer, J. Schwabedissen, H.-G. Stammer, K. Karaghiosoff and N. W. Mitzel, *Angew. Chem. Int. Ed.* **2019**, *58*, 18557–18561.
- [12] J. Kacmarek, F. H. Jarke, J. Shamir, I. J. Solomon and M. Lustig, *J. Org. Chem.* **1975**, *40*, 1851–1854.

1 Oxygen-Rich Oxetanes

- [13] D. Fischer, T. M. Klapötke and J. Stierstorfer, *Chem. Comm.* **2016**, 52, 916–918.
- [14] D. E. Dosch, M. Reichel, M. Born, T. M. Klapötke and K. Karaghiosoff, *Cryst. Growth Des.* **2021**, 21, 243–248.
- [15] Y. Ma, A. Zhang, X. Xue, D. Jiang, Y. Zhu and C. Zhang, *Cryst. Growth Des.* **2014**, 14, 6101–6114.
- [16] M. A. Spackman and D. Jayatilaka, *CrystEngComm* **2009**, 11, 19–32.
- [17] M. Reichel, D. Dosch, T. Klapötke and K. Karaghiosoff, *J. Am. Chem. Soc.* **2019**, 141, 19911–19916.
- [18] T. M. Klapötke, *Chemistry of High-Energy Materials*, De Gruyter, Berlin, Boston, 5th ed., **2019**.
- [19] T. M. Klapötke, *Energetic Materials Encyclopedia*, De Gruyter, Berlin, 2nd ed., **2021**.
- [20] J. Liu, *Nitrate Esters Chemistry and Technology*, Springer Singapore, 1 edn., **2019**.
- [21] <http://www.bam.de>
- [22] NATO Standardization Agreement (STANAG) on Explosives, *Impact Sensitivity Tests*, no. 4489, 1st ed., September 17, **1999**.
- [23] WIWEB-Standardarbeitsanweisung 4-5.1.02, Ermittlung der Explosionsgefährlichkeit, hier der Schlagempfindlichkeit mit dem Fallhammer, November 8, **2002**.
- [24] NATO Standardization Agreement (STANAG) on Explosives, *Friction Sensitivity Tests*, no. 4487, 1st ed., August 22, **2002**.
- [25] WIWEB-Standardarbeitsanweisung 4-5.1.03, Ermittlung der Explosionsgefährlichkeit oder der Reibeempfindlichkeit mit dem Reibeapparat, November 8, **2002**.
- [26] Impact: Insensitive >40 J, less sensitive ≤35 J, sensitive ≤4 J, very sensitive ≤3 J; friction: Insensitive >360 N, less sensitive=360 N, sensitive 80 N, very sensitive ≤80 N, extreme sensitive ≤10 N; According to the UN Recommendations on the Transport of Dangerous Goods (+) indicates: not safe for transport.
- [27] R. L. Willer, K. Baum, W.-H. Lin, *US 8030440 B1*, 2011.
- [28] CrysAlisPRO (Version 171.33.41); Oxford Diffraction Ltd., **2009**.
- [29] Burla, M. C.; Caliandro, R.; Carrozzini, B.; Cascarano, G. L.; Cuocci, C.; Giacovazzo, C.; Mallamo, M.; Mazzone, A.; Polidori, G. Crystal structure determination and refinement via SIR2014. *J. Appl. Crystallogr.* **2015**, 48, 306.
- [30] Hübschle, C. B.; Sheldrick, G. M.; Dittrich, B. ShelXle: a Qt graphical user interface for SHELXL. *J. Appl. Crystallogr.* **2011**, 44, 1281.
- [31] Sheldrick, G. M. SHELXL-97, Program for the Refinement of Crystal Structures; University of Göttingen: Germany, **1997**.
- [32] Sheldrick, M. A short history of SHELX. *Acta Crystallogr., Sect. A: Found. Crystallogr.* **2008**, 64, 112.

1 Oxygen-Rich Oxetanes

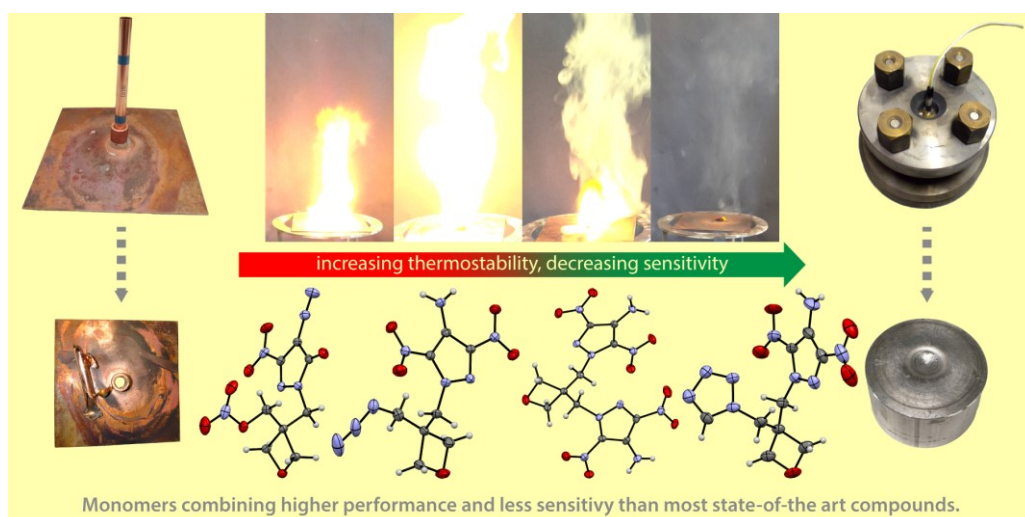
- [33] Spek, A. L. PLATON, A Multipurpose Crystallographic Tool; Utrecht University: The Netherlands, **1991**.
- [34] Farrugia, L. J., WinGX and ORTEP for Windows: an update. *J. Appl. Crystallogr.* **2012**, *45*, 849.
- [35] M. W. Chase Jr., NIST-JANAF Thermochemical Tables, Fourth Edition, *J. Phys. Chem. Ref. Data*, *Monograph 9*, **1998**, 1 – 1951.
- [36] M. J. Frisch, G. W. Trucks, H. B. Schlegel, G. E. Scuseria, M. A. Robb, J. R. Cheeseman, G. Scalmani, V. Barone, G. A. Petersson, H. Nakatsuji, X. Li, M. Caricato, A. V. Marenich, J. Bloino, B. G. Janesko, R. Gomperts, B. Mennucci, H. P. Hratchian, J. V. Ortiz, A. F. Izmaylov, J. L. Sonnenberg, D. Williams-Young, F. Ding, F. Lipparini, F. Egidi, J. Goings, B. Peng, A. Petrone, T. Henderson, D. Ranasinghe, V. G. Zakrzewski, J. Gao, N. Rega, G. Zheng, W. Liang, M. Hada, M. Ehara, K. Toyota, R. Fukuda, J. Hasegawa, M. Ishida, T. Nakajima, Y. Honda, O. Kitao, H. Nakai, T. Vreven, K. Throssell, J. A. Montgomery, Jr., J. E. Peralta, F. Ogliaro, M. J. Bearpark, J. J. Heyd, E. N. Brothers, K. N. Kudin, V. N. Staroverov, T. A. Keith, R. Kobayashi, J. Normand, K. Raghavachari, A. P. Rendell, J. C. Burant, S. S. Iyengar, J. Tomasi, M. Cossi, J. M. Millam, M. Klene, C. Adamo, R. Cammi, J. W. Ochterski, R. L. Martin, K. Morokuma, O. Farkas, J. B. Foresman, and D. J. Fox, Gaussian16 ,Gaussian, Inc., Wallingford, CT, USA, **2016**.

2 Oxetanes based on LLM-116

Highly energetic, insensitive and thermostable oxetane monomers based on the powerful explosive LLM-116

Max Born, Konstantin Karaghiosoff, Thomas M. Klapötke and Michael Voggenreiter

As published in *ChemPlusChem* **2022**, 87, e202200049; DOI: 10.1002/cplu.202200049



2.1 Abstract

3-Bromomethyl-3-hydroxymethyloxetane (BMHMO) represents an inexpensive and versatile precursor for the synthesis of both asymmetrically and symmetrically 3,3-disubstituted oxetane derivatives. In the present work, its synthesis was significantly improved and various energetic oxetanes based on the powerful explosive LLM-116 (4-amino-3,5-dinitro-1*H*-pyrazole) were prepared. Compared to other energetic oxetane monomers, these are superior in terms of performance, thermostability and sensitivity to mechanical stimuli. Next to a symmetric LLM-116 derivative, three asymmetric compounds were prepared using azido-, nitrate- and tetrazolyl-moieties. All compounds were intensively characterized by vibrational-, mass- and multinuclear (^1H , ^{13}C , ^{14}N) NMR spectroscopy, differential scanning calorimetry and elemental analysis. The molecular structures were elucidated by single crystal X-ray diffraction. Hirshfeld analysis was used to estimate their sensitivity, which was determined experimentally using BAM standard procedures. Their performance was calculated using the EXPLO5 V6.04 thermochemical code and both a small-scale-reactivity test (SSRT) and initiation test were performed to evaluate and demonstrate their insensitivity and performance.

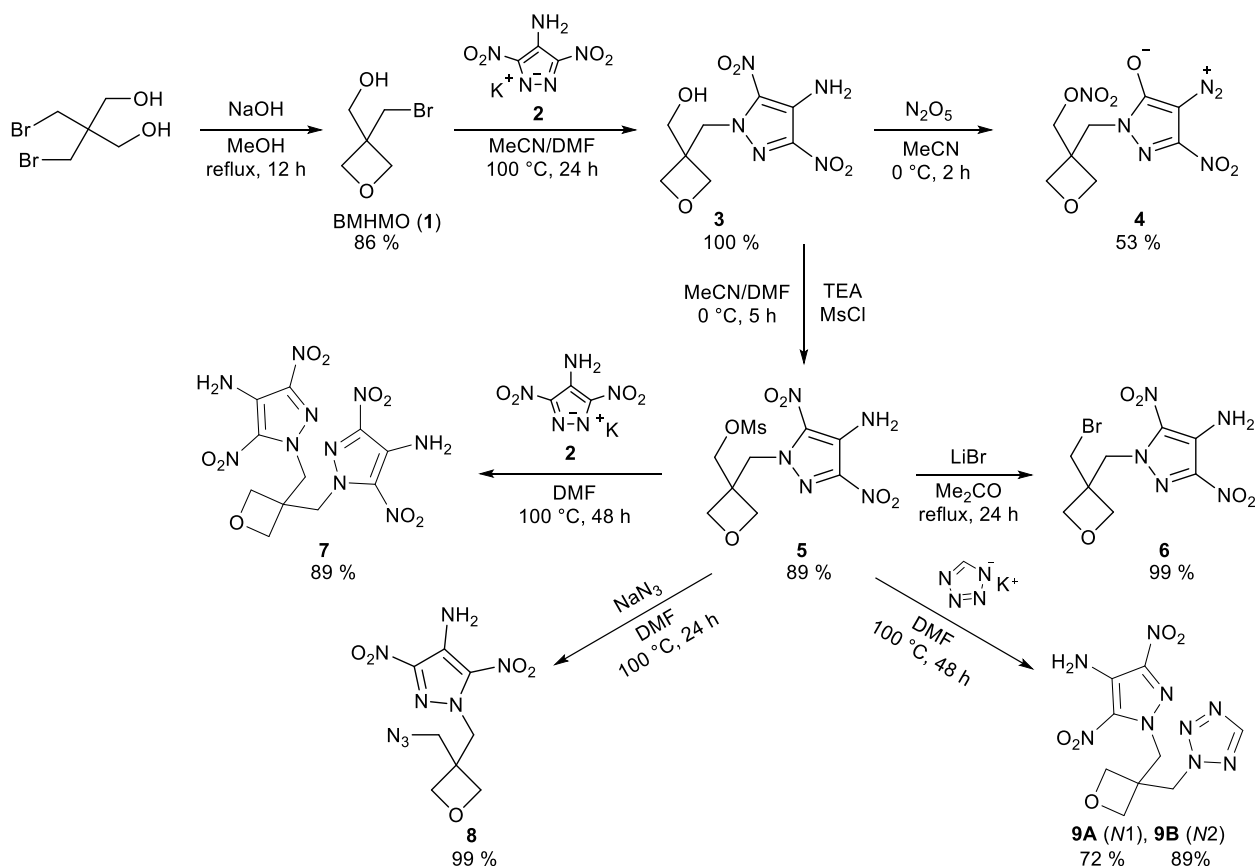
2.2 Introduction

the art in the field of energetic polymers is mainly represented by well-known polyethers such as GAP, polyBAMO, polyAMMO, polyNIMMO and polyGLYN.^[1] Unfortunately, the respective monomers show performances way inferior to TNT or more recent developments in the field of secondary explosives. They can be subdivided into two groups – azides, which feature relatively high thermostability at the price of poor oxygen balance and organic nitrates with improved oxygen balance at the cost of thermostability below modern requirements.^[2] Their polymers are preferred over non-energetic binders, but their energetic contribution in formulations is low. Therefore, new monomers combining higher performance and thermostability with less sensitivity are highly desirable. For example, binders prepared thereof could find application in especially safe low-vulnerability ammunitions (LOVA) and propellants.^[3] In this context, a patent describes 3-bromomethyl-3-hydroxymethyl-oxetane (BMHMO) as very suitable starting material for the preparation of asymmetric oxetane monomers. For instance, the preparation of the powerful compound 3-azidomethyl-3-nitratomethyloxetane is disclosed.^[4] Indeed, BMHMO shows advantageous properties. It can be prepared inexpensively by *Williamson* ether synthesis and is chemically very versatile. For example, the excellent leaving group enables

2 Oxetanes based on LLM-116

functionalization with nucleophiles and follow-up reactions with electrophiles making use of the hydroxy group to afford asymmetric species. Conversion of this group into a leaving group enables access to either symmetric or asymmetric derivatives by further substitution reactions. Beyond, the present methylene spacers diminish the adverse effect of mostly electron-withdrawing explosophoric groups on the oxetane oxygen atom. This is of advantage as the success of cationic ring-opening polymerization strongly depends on the basicity of the oxygen atom.^[5] However, the scaffold of BMHMO imposes a detrimental carbon-hydrogen ballast rendering it beneficial to use larger energetic motifs as substituents to mitigate or compensate this influence. For this purpose, powerful secondary explosives with functional groups like 4-amino-3,5-dinitro-1*H*-pyrazole (LLM-116 or ADNP) are very promising. ADNP was first described as protected compound in 1993 by *Vinogradov* and later as unprotected compound by *Shevelev* in 1998.^[6] Since then, it has been made accessible by several synthetic routes, whereas 4-chloro-1*H*-pyrazole provides the highest yield when used as starting material.^[7] ADNP impresses with a high density (1.90 g cm^{-3}) and correspondingly high performance ($\text{VoD} = 8680 \text{ m s}^{-1}$, $p_{\text{C-J}} = 32.8 \text{ kbar}$).^[8] Already in 2014, it was employed in a pilot scale study by *Ek* and *Latypov* and prepared in 200 g batches.^[7] Due to its favorable properties, ADNP has been increasingly used for the synthesis of new energetic materials since 2011.^[9-11] Herein, we report an significantly improved synthesis of BMHMO, rendering it an even more attractive starting material for the synthesis of inexpensive, energetic oxetane monomers. Ultimately, it was used to prepare symmetric and asymmetric derivatives based on LLM-116. Here, high yields and the preferential use of commercially available materials contribute to low costs. The molecular structures of all products were elucidated by X-Ray diffraction also allowing Hirshfeld analysis which made the high insensitivity of some target compounds and the results of the SSRT and initiation test comprehensible. In terms of performance and thermostability, the target compounds are largely superior to prior art energetic oxetane monomers. Based on the fine balance of these new monomers between performance, thermostability and insensitivity, they are promising candidates for the preparation of energetic polymers with improved properties in these key-aspects.

2 Oxetanes based on LLM-116



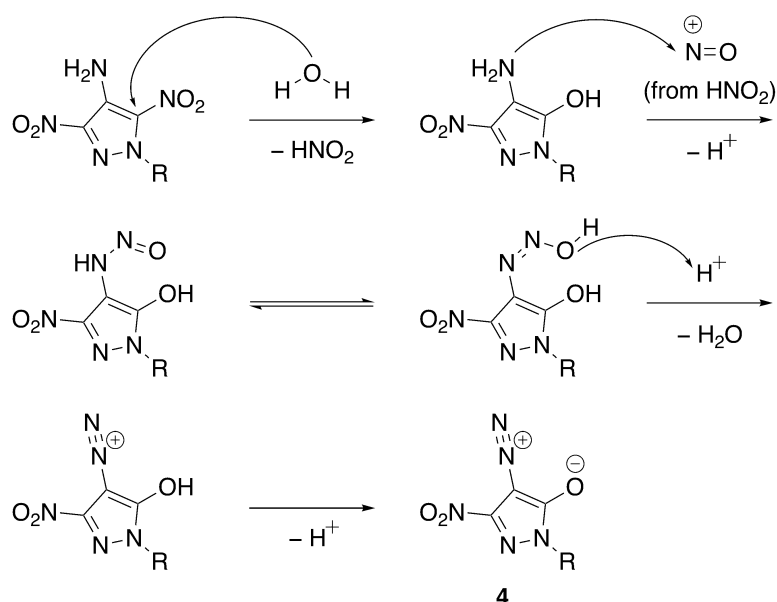
Scheme 1. Synthetic pathway starting with the ring-closure of 2,2-bis(bromomethyl)propane-1,3-diol toward BMHMO (1). Subsequent substitution using the potassium salt of LLM-116 affords compound 3. Nitration results in target compound (4) while mesylation gives compound 5 providing access to target compounds 6–9 in high overall yield.

2.3 Results and Discussion

2.3.1 Synthetic Procedures

The *Williamson* reaction to give 3-bromomethyl-3-hydroxymethyloxetane (BMHMO, 1) was significantly improved by changing base and solvent from NaOEt/EtOH to NaOH/MeOH to give a crude yield of 93%. Subsequent vacuum distillation removed by-products (spiro-compound) and unreacted starting material to afford pure BMHMO as colorless oil in 85% (+33%) yield while the literature reports only 52% after purification.^[4] Reaction of 1 with the potassium salt of 4-amino-3,5-dinitro-1H-pyrazole (K-ADNP, 2) in DMF led to alcohol 3 which was isolated by the precipitation of inorganic salts using ethyl acetate, filtration through a Celite plug and rotary evaporation to remove all volatiles. Residual traces of DMF were co-evaporated (cold ether) to afford 3 as bright-yellow solid in quantitative yield (**Scheme 1**). It was tried to obtain the corresponding nitrate 4 using acetyl nitrate as mild and cost-efficient nitrating agent but several attempts failed (recovery of starting material). However, aprotic nitration using dinitrogen

pentoxide was successful while minimizing the risk of undesired ring-opening of the oxetane ring by hydrolysis. Unfortunately, the pyrazole motif suffered from severe chemical changes and the zwitterionic diazonium olate **4** was obtained. Similar zwitterionic pyrazole compounds are known to literature but usually obtained by targeted diazotation reactions.^[12] Fischer reported a very similar diazonium olate by nitrating the structurally related bis(4-amino-3,5-dinitropyrazolyl)methane with mixed acid followed by quenching on water.^[10] However, no mechanism for the formation of this particular structure was proposed. As nitro groups are prone to act as leaving groups in aromatic nucleophilic substitution reactions, we assume a nucleophilic attack of water upon quenching. This leads to the formation of nitrous acid as source of nitrosyl cations. These cause a quick, subsequent diazotation reaction toward compound **4** (Scheme 2).



Scheme 2. Proposed mechanism for the formation of diazonium olate **4**

Despite various solvent/anti-solvent precipitation attempts, the crude compound remained an extremely viscous oil. Ultimately, column chromatography (SiO₂, EtOAc) afforded **4** in 53% yield as orange solid. To enable further substitution reactions, compound **3** was mesylated to provide a good leaving group. Due to the tailored solvent system, methanesulfonic ester **5** precipitated as lemon-yellow solid after a short reaction time and was obtained by suction filtration in high purity and yield (85%). Since particularly weak or sterically demanding nucleophiles are not always able to readily substitute the mesyl group, compound **5** was converted to the bromo-species **6** in a Finkelstein-type reaction using lithium bromide in acetone to provide an alternative leaving group. Filtration through silica (EtOAc) to separate inorganic salts gave compound **6** in high purity and quantitative yield (Scheme 1). However, all follow-up substitution reactions were

successfully performed using mesylate **5** thus avoiding this additional step. DMF was employed as solvent as it allows high reaction temperatures and removal by rotary evaporation while it dissolves sodium azide, K-ADNP and potassium tetrazol-1-ide rather well. The reaction of **5** with K-ANDP (**2**) was complete after 48 h according to TLC. The high reaction time can be explained by the steric demand of the nucleophile. All inorganic salts were separated as previously described and DMF was evaporated. The crude material was suspended in diethyl ether and collected by suction filtration to give **7** in high yield and purity (89%) as yellow solid. Compound **8** was prepared analogously from **5** using sodium azide. The same work-up routine was applied and traces of DMF removed by co-evaporation to give **8** in 99% yield. Dissolution of **8** in a small amount of acetone followed by precipitation (*n*-hexane) gave pure **8** as bright yellow solid without yield loss. As in case of compound **7**, the reaction of **5** with potassium tetrazol-1-ide required a prolonged reaction time of 48 h according to TLC. The work-up was performed as described before and the crude isomeric mixture (**9A**, **9B**) was suspended in a small amount of acetone prior to the addition of an excess of diethyl ether. After suction filtration, a yield of 98% was obtained and ¹H NMR spectroscopy revealed a *N*1/*N*2 ratio of 1:2. The regioisomers were separated by refluxing the mixture in toluene and filtration of the hot suspension. The filtrate was evaporated to give pure *N*2-isomer (**9B**) with a yield of 89%. The filter residue contained 10% *N*2-isomer (¹H NMR) and was recrystallized from acetone to give 72% of *N*1-isomer (**9A**) also as yellow solid. Thereby, an overall yield of 84% (*N*1, *N*2) was achieved without column chromatography.

2.3.2 Crystallography

Single crystals of the following compounds were obtained by slow evaporation of their solutions using ethyl acetate (**4**, **8**), DMF (**7**), toluene (**9B**) and acetone (**9A**). Detailed crystallographic data can be found in the Supporting Information. Compound **4** crystallizes in the monoclinic space group $P2_1/n$ with four molecules in the unit cell and a calculated density of 1.667 g cm⁻³ at 123 K (**Figure 1a**). The bond lengths of C6–O5 (1.218(2) Å) corresponds to a C=O double bond.^[13] Further, C7–N5 has a length of 1.327(2) Å which is approximately the length of a C=N double bond.^[14] The diazo group is nearly linear with an angle of 176.2° (C7–N5–N6) and shows a very short interatomic distance of 1.110(2) Å (N5–N6) which can be attributed to a N≡N triple bond.

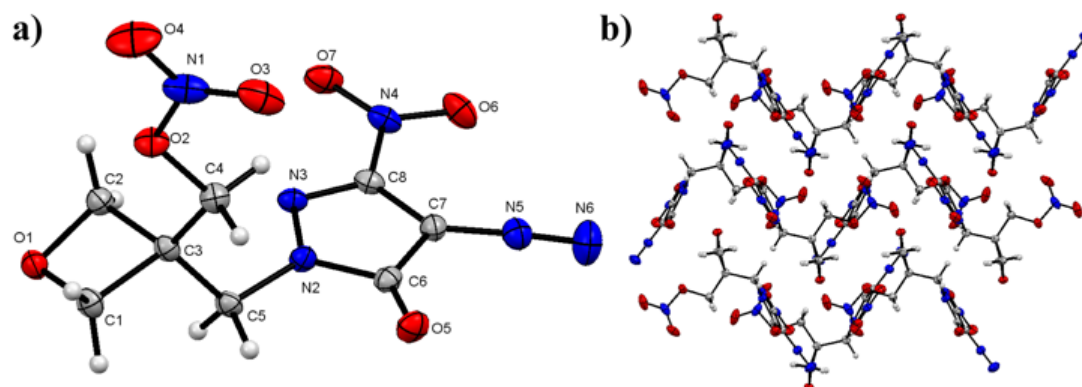


Figure 1. a) Molecular structure of **4** in the crystal. Thermal ellipsoids are drawn at the 50% probability level. b) View along the a axis – the molecules form a wave-like pattern.

The angles within the oxetane ring range between $91.14(9)^\circ$ at O1–C2–C3 and $91.52(9)^\circ$ at O1–C1–C3. The smallest angle is observed at C1–C3–C2 ($84.72(9)^\circ$). The oxetane ring shows a puckering angle of 12.5° which is slightly larger than the puckering angle found in unsubstituted oxetane (8.7° , 140 K).^[15] The nitro group of the pyrazole motif essentially matches the pyrazole plane. In the crystal, the molecules are arranged to form a wave-like pattern along the a axis (**Figure 1b**).

Compound **7** crystallizes in the monoclinic space group $P2_1/n$ with four formula units in the unit cell. The crystal contains one dimethylformamide molecule per formula unit and displays a density of 1.639 g cm^{-3} at 123 K (**Figure 2**).

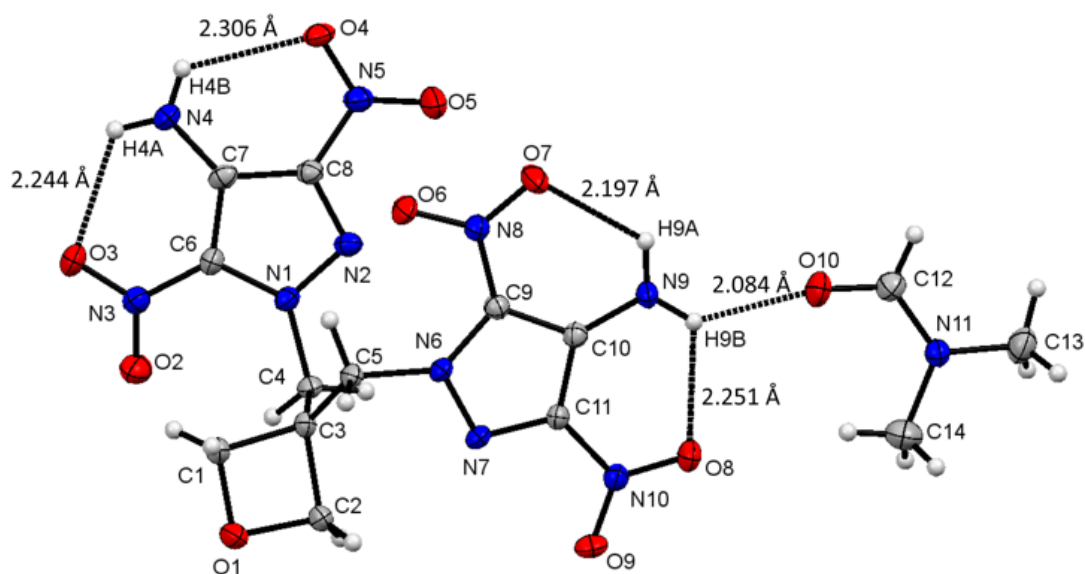


Figure 2. Molecular structure of **7** in the crystal and interactions with the crystallized dimethylformamide molecule. Thermal ellipsoids are drawn at the 50% probability level.

The angles within the oxetane ring vary from $83.82(2)^\circ$ at C1–C3–C2 to $91.72(2)^\circ$ at O1–C2–C3. The oxetane ring is strongly folded with a puckering angle of 15.9° which is considerably larger than the corresponding angle in unsubstituted oxetane (8.7° at 140 K).^[15] One of the pyrazole rings has both nitro groups in the ring plane, the other pyrazole ring has the nitro group at C6 twisted by 16.81° and the nitro group at C8 twisted by 3.28° . The amino group at C7 features intramolecular interactions with the neighbored nitro groups with distances of $2.306(2) \text{ \AA}$ and $2.244(2) \text{ \AA}$. The other amino group at C10 shows the same interaction with distances of $2.197(2) \text{ \AA}$ and $2.251(2) \text{ \AA}$. In addition, an intermolecular hydrogen bridge is found between this amino group and the oxygen atom of the dimethyl formamide molecule with a distance of $2.084(2) \text{ \AA}$. Compound **8** crystallizes in the monoclinic space group $P2_1/c$ with four formula units in the unit cell and a density of 1.608 g cm^{-3} at 123 K (**Figure 3a**). The angles within the oxetane motif vary from $84.72(2)^\circ$ at C1–C3–C2 to $92.72(2)^\circ$ at C1–O1–C3. The oxetane ring is found to be essentially planar and the azido group is almost linear (N1–N2–N3, $174.0(3)^\circ$). The nitro groups at C8 and C6 are twisted out of the pyrazole plane by 19.58° and 5.62° , respectively. The molecule displays an intramolecular hydrogen bond from H7B to O4 with a distance of $2.204(2) \text{ \AA}$ (**Figure 3b**). Further, there are intermolecular hydrogen bonds of the amino group to two adjacent molecules. One between H7B to O5 (nitro group) with a distance of $2.254(2) \text{ \AA}$ and another between H7A and O1 (oxetane ring) with a length of $1.986(2) \text{ \AA}$. These hydrogen bonds contribute to a stabilization the molecule in the solid state.

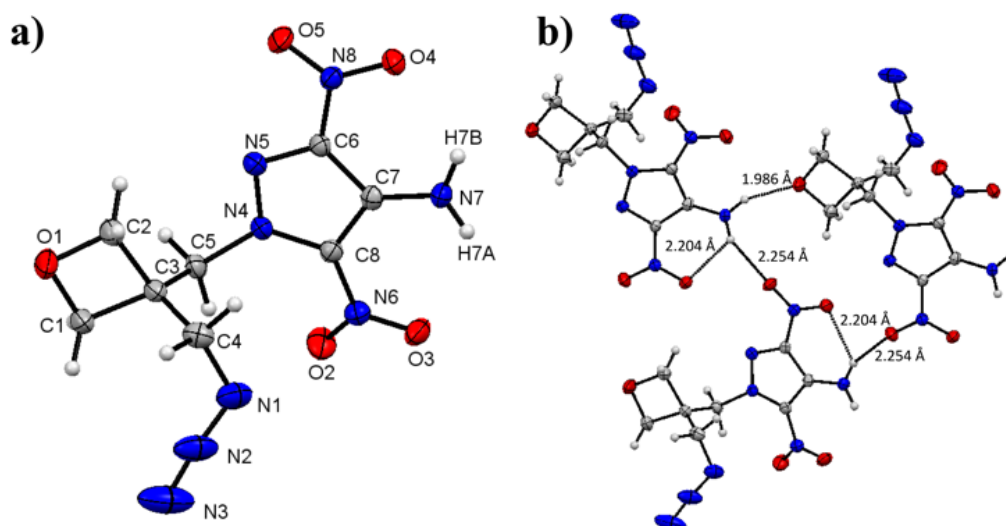


Figure 3. a) Molecular structure of **8** in the crystal. Thermal ellipsoids are drawn at the 50% probability level. **b)** Intra- and intermolecular hydrogen bonding in the crystal structure of **8**.

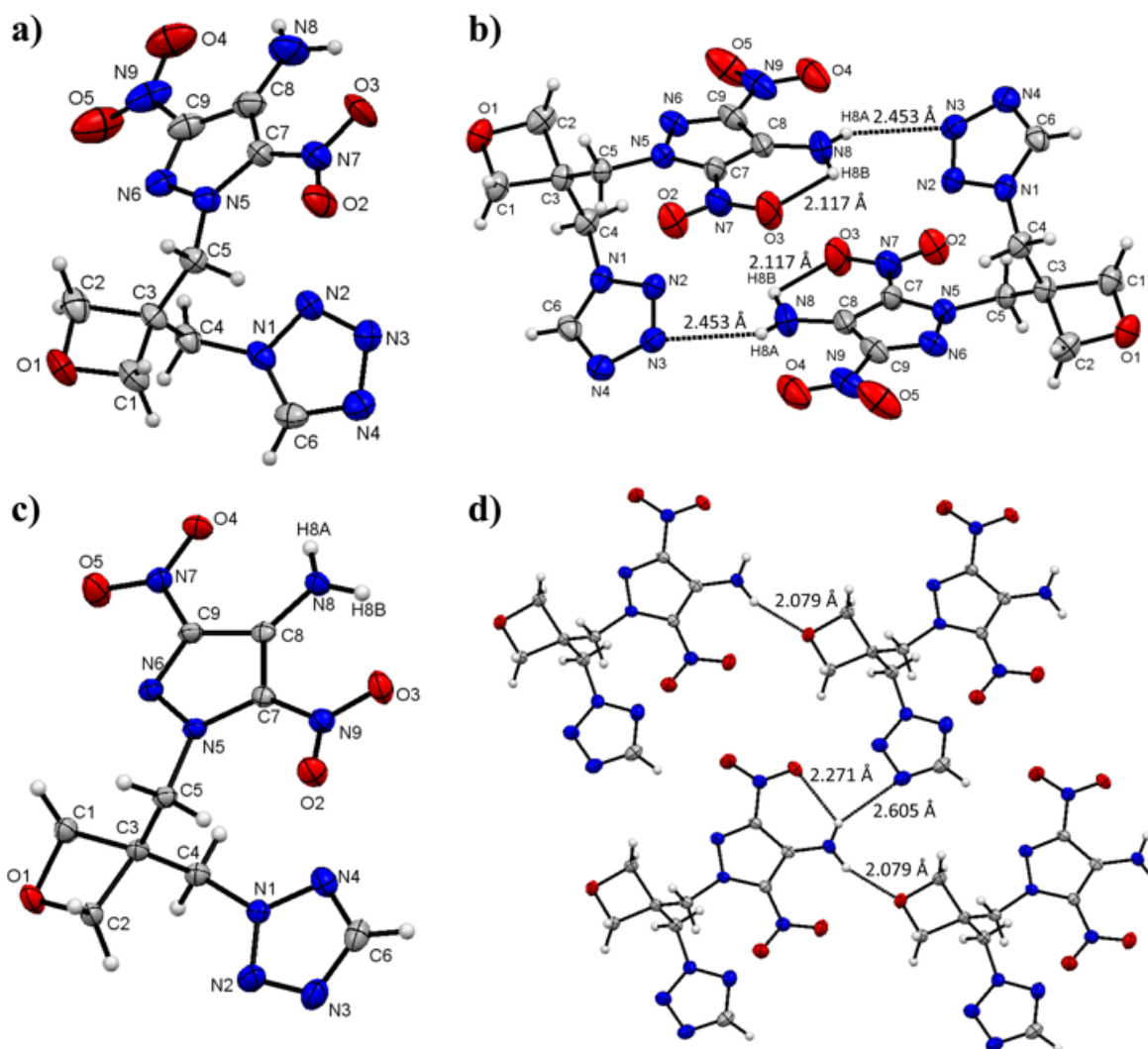


Figure 4. Molecular structure of **9A** (a) and the corresponding pairs formed in the solid state (b). Crystal structure of **9B** (c) and the network which is formed in the crystal (d). Thermal ellipsoids are drawn at the 50% probability level.

Compound **9A** crystallizes in the monoclinic space group $P2_1/c$ with four formula units in the unit cell and **9B** crystallizes in the triclinic space group $P\bar{1}$ with two formula units in the unit cell (**Figure 4**). Compound **9B** has a density of 1.691 g cm^{-3} at 123 K which is marginally higher than the density of **9A** (1.630 g cm^{-3}) at 123 K. The puckering angle in the oxetane ring of **9B** is 14.5° while **9A** exhibits a way smaller puckering angle of 10.2° . For compound **9A**, two molecules arrange in pairs due to strong hydrogen bonding between the amino group and the tetrazole ring (N3) of a neighboring molecule with a distance of $2.453(5) \text{ \AA}$. Intramolecular hydrogen bonding is found between the amino group (H8B) and an adjacent nitro group (O3) with a distance of $2.117(4) \text{ \AA}$. An analogous intramolecular hydrogen bond is observed in case of compound **9B** involving H8A of the amino group and the neighboring oxygen atom O4 of the nitro group with a distance of $2.271(3) \text{ \AA}$. In addition, H8A shows an intermolecular short contact bond to the

tetrazole moiety (N3) of an adjacent molecule with a distance of 2.605(3) Å, which is quite long for a hydrogen bond. Moreover, an intermolecular short contact bond with a distance of 2.079(3) Å is found between H8B of the amino group and the oxetane oxygen atom O1 of a neighboring molecule.

2.3.3 Hirshfeld Analysis

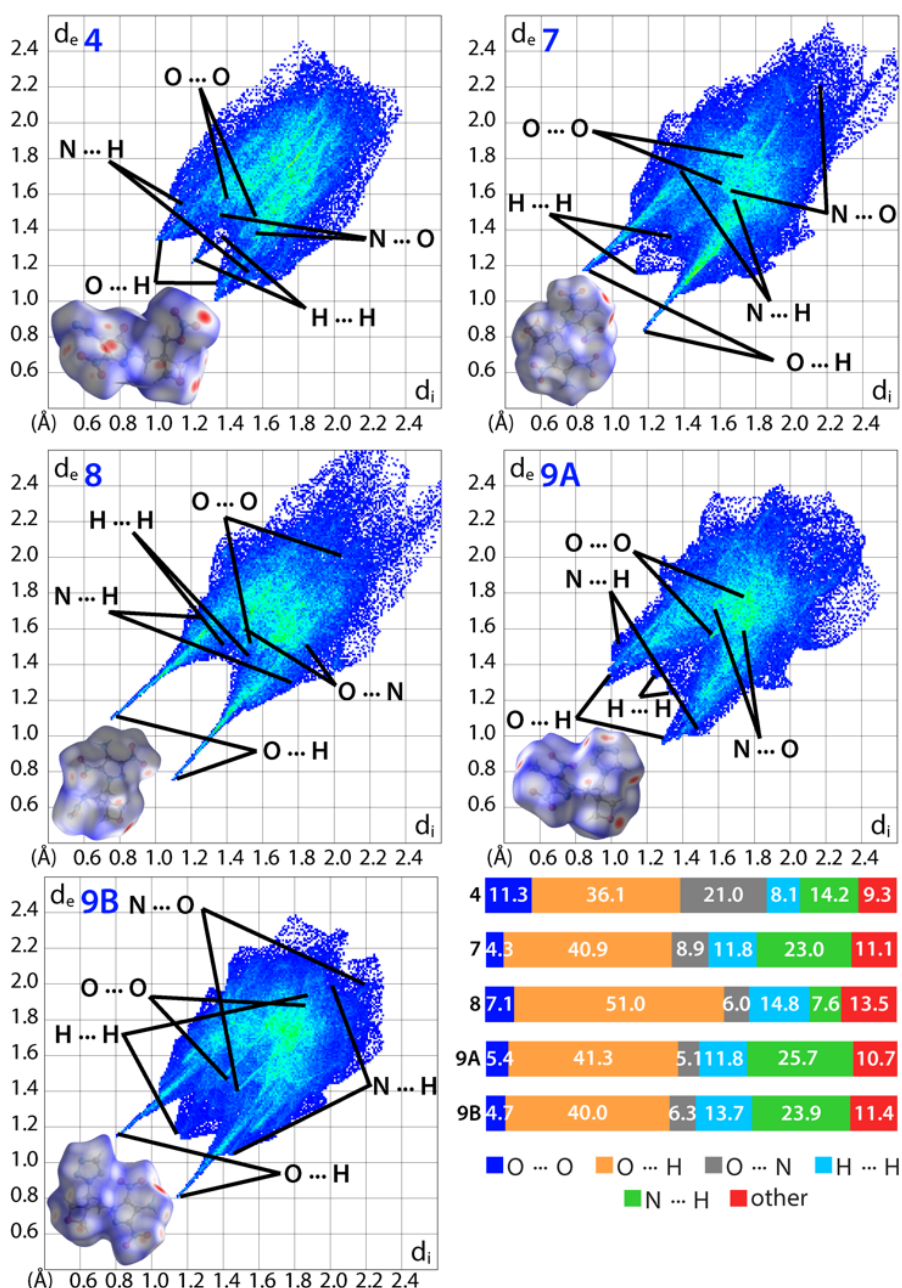


Figure 5. Calculated Hirshfeld surfaces and 2D fingerprint plots for compounds **4** and **7–9**. The bar chart summarizes the respective populations of close contacts in the crystal.

When a mechanical force acts upon a solid energetic material, it causes vertical compression and horizontal sliding of layers in the crystal leading to internal strains.^[16] If the related strain energy is higher than the lowest bond dissociation energy in the molecule, decomposition will occur.^[17] In this context, intermolecular interactions can have a stabilizing or destabilizing effect establishing a direct correlation with an energetic materials' sensitivity.^[17,18] A valuable tool to explore these interactions is Hirshfeld analysis.^[19,20] Hence, we calculated the Hirshfeld surface (HFS) of all target compounds using CrystalExplorer V17.5 to find correlations.^[21] On the HFS, close contact interactions are shown as red dots. In addition, we visualized all interactions and their distances $d_i + d_e$ (d_i = distance from HFS to the closest atom interior, d_e = distance from HFS to closest atom exterior) in a 2D fingerprint plot (**Figure 5**).^[22] Interactions with distances below 2.4 Å are considered strong, while interactions with distances larger than roughly 3 Å are considered weak. Especially characteristic for sensitive compounds are high populations of repulsive O...O interactions next to destabilizing, repulsive O...N or H...H contacts. High sensitivity is particularly encountered when these are poorly balanced by stabilizing interactions like N...H or O...H close contacts.^[17,18] Further, a comparison of the respective percentages (bar diagram, Fig. 5) and the interaction distances ($d_i + d_e$) enables a weighting. This allows a reasonable estimation of the sensitivity and a ranking of the compounds relative to each other. For example, compound **4** shows stabilizing strong ($d_i + d_e < 2.4$ Å) O...H interactions (36.1%) and moderately strong N...H (14.2%) interactions. These are counterbalanced by strong, repulsive H...H interactions and weak ($d_i + d_e > 3$ Å) destabilizing O...N (21.0%) and O...O interactions (11.3%). Even if these are weak, their high proportion significantly counteracts the stabilizing interactions. Therefore, a significant sensitivity toward mechanical stimuli can be anticipated. In comparison, compound **7** shows a significantly higher proportion of strong O...H interactions (40.9%). The stabilizing N...H interactions are weak, but their high proportion (23.0%) significantly contributes to the overall stabilization. With a total of 63.9%, they easily compensate found destabilizing interactions – these are made up by a low population of strong, repulsive H...H interactions (11.8%) next to weak O...N (8.9%) and O...O (4.2%) interactions with almost negligible proportions. As a consequence, low sensitivity can be expected. The highest population of strong O...H interactions (51.0%) is found in case of compound **8**. Additional stabilization arises from of weak N...H interactions (7.6%). These are only attenuated by few and weak destabilizing interactions. Hereby, repulsive H...H interactions (14.8%) represent the largest fraction, along with O...O and O...N interactions, with a cumulative share of only 13.1%. As stabilizing

interactions (58.6%) clearly dominate, a low sensitivity is indicated. Since compounds **9A** and **9B** are regioisomers, very similar sensitivity might be expected. This is indeed reflected by very similar interaction proportions. Both compounds are equally dominated by strong O⋯H interactions with populations of 41.3% and 40%, respectively, and N⋯H interactions with high percentages of 25.7% and 23.9%. In compound **9A**, this interaction has a higher significance, as the proportion is higher and the relative share of strong interactions ($d_i + d_e < 2.4 \text{ \AA}$) is more pronounced. The total population of stabilizing interactions is the highest of all investigated compounds with 67.0% (**9A**) and 63.9% (**9B**). Rather weak, repulsive H⋯H interactions impose a destabilizing effect on both **9A** (11.8%) and **9B** (13.7%). The same applies to O⋯N interactions with populations of 5.1% (**9A**) and 6.3% (**9B**) next to O⋯O interactions with proportions of 5.4% and 4.7%, respectively. Due to their low population and weak nature, they cause negligible destabilization. Based on found interactions, their population and respective strength, **9A** and **9B** should not only be very insensitive, but the least sensitive of all investigated compounds – closely followed by compounds **7** and **8** with compound **4** showing the highest sensitivity. This agrees well with the experimental values for impact and friction sensitivity (Table 2). However, an absolute difference in case of **7–9** cannot be quantified due their generally high insensitivity.

2.3.4 Thermal Analysis

Thermal analysis of all compounds was performed by differential scanning calorimetry (DSC) at a heating rate of 5° min^{-1} . Here, compound **4** shows the lowest melting point (95° C) and due the presence of the diazonium and the nitrate ester functionality, which impose thermal instability, also the lowest decomposition temperature (184° C) of all investigated compounds. Considerably higher decomposition temperatures were found for compounds **7–9**. Compound **8** shows a melting point at 101° C and a decomposition temperature of 238° C , which is very high as most organic azides already decompose at roughly 180° C according to literature.^[23] This can be attributed to stabilizing effects in the crystal (see Hirshfeld discussion). While isomer **9B** features a high melting point of 161° C and decomposes at 241° C , compounds **7** and **9A** do not show a melting point and directly decompose exothermically at 246° C and 241° C . The different and thus interesting thermal behavior of regioisomers **9A** (*N1*) and **9B** (*N2*) can be attributed to interactions in the crystal. In direct comparison, the *N1*-isomer shows a higher proportion of stabilizing interactions (O⋯H, N⋯H) and a lower proportion of repulsive H⋯H interactions (**Figure 5**). Specifically, the intermolecular hydrogen bond (H8A–N3, $d = 2.453 \text{ \AA}$) is shorter and

thus stronger than the analogous interaction in the *N2* isomer with a distance of 2.605 Å. Further and contrary to the *N2*-isomer, parallel-displaced π -stacking interactions occur between spatially opposing pyrazole rings as well as tetrazole rings. In sum, the higher interactions prevent melting of **9A** prior to decomposition. Overall, **7** is the most thermostable compound of all, followed by **9B**, **9A**, **8** and organic nitrate **4**. As a result, the decomposition temperatures essentially correlate with the ratio of stabilizing and destabilizing effects in the crystal as indicated by Hirshfeld analysis. The effect of substitution is particularly interesting in case of compounds **7–9**, since the parent compound (ADNP) decomposes already at 183.6 °C when a heating rate of 10 °C min⁻¹ is applied.^[24]

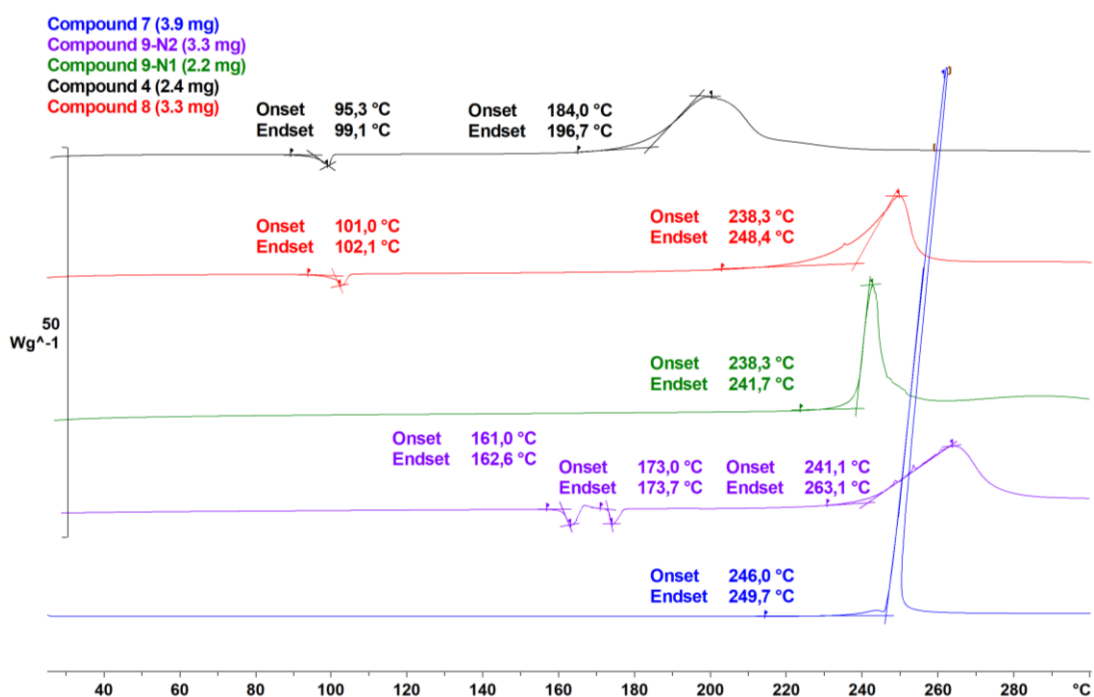


Figure 6. DSC thermogram of compounds **4** and **7–9**.

2.3.5 Small-scale Shock Reactivity and Initiation Test

In order to evaluate the explosive performance of compounds **4** and **7–9**, a small-scale shock reactivity test (SSRT) was performed (Figure 7). This test is suitable to assess the shock reactivity (explosiveness) of an energetic material – often below its critical diameter and without requiring transition to detonation.^[25] It combines the advantages of both lead block test and gap test while it requires small quantities of roughly 500 mg.^[26] In each test, the same sample volume V_S is used (284 mm³) and the required amount of explosive (m_E) is calculated by the formula $m_E = V_S \cdot \rho_{XR} \cdot 0.95$ where ρ is the density determined via X-ray or helium pycnometry. Regarding the setup, each sample was pressed into a perforated steel block on top of an aluminum witness

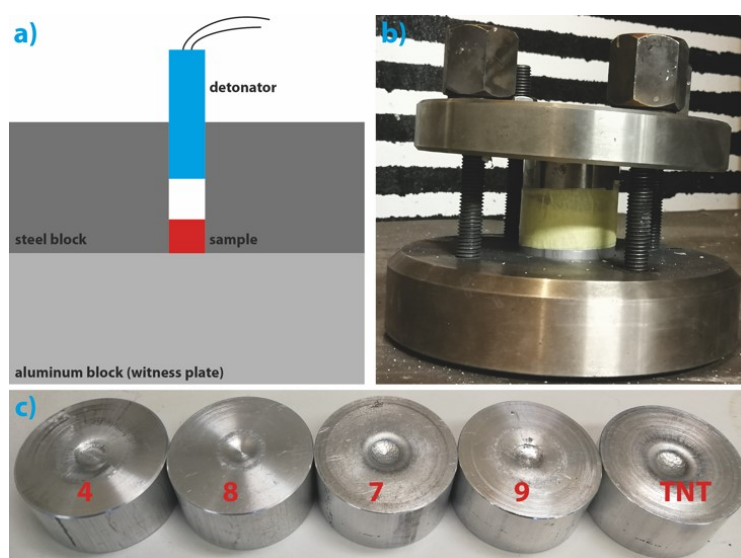


Figure 7. a) Schematic setup of a SSRT. b) Steel block and witness plate confined between heavy steel plates prior to the test. c) Aluminum witness plates with dents caused by the respective sample.

block with a pressure of three tons and five seconds duration. Subsequently, the arrangement is confined between two steel plates (**Figure 7b**). The pressed charge is then initiated by a commercial detonator (Orica Dynadet C2) using an air gap of 1.5 cm. The obtained dent sizes of the witness blocks can be compared to each other by filling them with finely powdered SiO_2 and measuring the respective weight. Alternatively, the actual dent volumes can be measured using a 3D profilometer. Hereby, the performance of the energetic materials can be compared relative to each other. As all investigated compounds show calculated performances comparable to 2,4,6-trinitrotoluene (TNT), it was used as reference. Interestingly, almost no indentation was obtained in case of compound **8** and plenty of unaffected material was found (see ESI). In case of compounds **4**, **7** and **9**, significant dents were obtained, but much smaller than in case of TNT (**Table 1**) and thus far behind expectation. Since the critical diameter has little relevance in this test and its determination would require the detonation of numerous charges on a multigram scale at different charge diameters, the insensitivity of the investigated compounds was considered to be the main cause. In this case, the applied shock impulse would be insufficient

Table 1. Mass of explosive versus dent size in the SSRT

Compound	4	7	8	9	TNT
m_e (mg)	426	459	424	428	445
V_{dent} (mm ³)	160	298	34	162	343

for complete initiation making the results plausible. To prove this assumption, all compounds were subjected to a systematic initiation test in closed copper tubes with an inner diameter of 7 mm which is comparable to the SSRT diameter of 7.5 mm (**Figure 8**). Each tube was filled with 200 mg of the respective compound prior to pressing the charge (3 tons, 5 seconds). Afterward, each tube was charged with 50 mg of loosely packed military-grade lead azide (LA) and placed on top of a copper witness plate. Then, the primary explosive was initiated by the spark of an electrical igniter. In case of compound **4**, the main charge (200 mg) was initiated by LA causing the destruction of the copper tube and an indentation of the witness plate. In case of compounds **7–9**, the copper tubes were left completely intact as only the LA top charge detonated proving the extreme insensitivity of these compounds (**Figure 8c**). Therefore, the test was repeated for compounds **7–9** using an additional booster charge of 50 mg PETN which was pressed onto the sample charge and 50 mg of unpressed lead azide was again added prior to firing the charges with an electrical igniter. In all cases, the copper tube was destroyed and the witness plate perforated (**8, 9**) or heavily dented (**7**) (**Figure 8d**). It can be concluded that all compounds except **4** are too insensitive to be initiated by the detonation of a lead azide primary charge. Instead, a booster explosive such as PETN is required for initiation. Therefore, compounds **7–9** have proofed to combine notable performance and thermostability with low sensitivity.

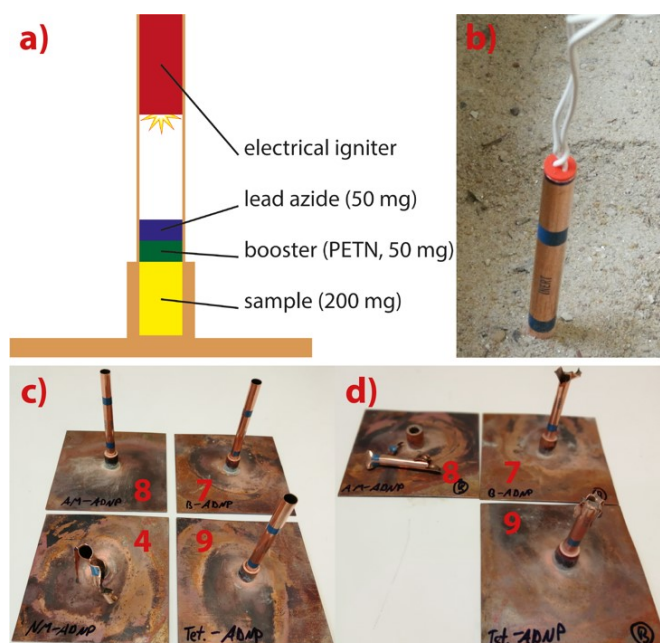


Figure 8. a) Schematic test setup. b) Prepared charge in a sandbox. c) Negative (**7, 8, 9**) and positive result (**4**) using lead azide. d) Positive result using PETN as booster (**7, 8, 9**).

2.3.6 Energetic Properties

All compounds were determined to be very insensitive towards impact and friction except **4** which is sensitive towards impact (3 J) but rather insensitive towards friction (288 N). All target compounds possess a combined nitrogen and oxygen content (N+O) between 63.4 % (**9**) and 66.3 % (**4**). The Gaussian16 program package was used to calculate room temperature enthalpy of formation for all energetic target compounds at the CBS-4M level of theory using the atomization method.^[27,28] All compounds exhibit a positive heat of formation in a range of 105.2 to 263.0 kJ mol⁻¹. The EXPLO5 V6.04 code was used to calculate the energetic performance of compounds **4** and **7–9**. Isomers **9B** and **9A** show a calculated detonation velocity of 6820 m s⁻¹ and 7088 m s⁻¹ linked to detonation pressures of 16.7 and 18.3 GPa, respectively, which are therefore in the range of TNT (6809 m s⁻¹, 18.7 GPa). The same applies to azide **8** which features comparable performance. In contrast, compounds **4** and **7** outperform TNT with detonation velocities of 7124 and 7335 m s⁻¹ and detonation pressures of 20.1 GPa and 20.9 GPa, respectively (**Table 2**). As compound **7** combines the highest performance and thermal stability of all presented compounds with great insensitivity, it is likely the most promising compound for the preparation of future energetic binders with superior characteristics in these aspects. With respect to performance, all compounds are superior to state-of-the-art energetic oxetane monomers (Table S5 (ESI) and Table 2). With exception of compound **4**, this also applies to the thermal stability.

2.4 Conclusion

The synthesis of BMHMO (**1**) was significantly improved compared to literature methods to provide a yield of 85% (+33%) rendering it an inexpensive and versatile precursor for the synthesis of both energetic and non-energetic oxetanes. Substitution using K-ADNP (**2**) afforded alcohol **3** in quantitative yield which can directly provide various energetic monomers using suitable electrophiles (**4**). Beyond, mesylation gave sulfonic ester **5** which was used to obtain symmetric compound **7** and asymmetric derivatives **8** and **9** in high yield. With exception of compound **4**, all compounds show an interplay of performance, thermostability, and insensitivity unparalleled in the field of energetic oxetanes and exhibit an advantageous, positive heat of formation. Their calculated performance is in range of the standard military explosive TNT (**8, 9**) or even higher (**4, 7**). Thus, they are clearly superior to typical energetic oxetane monomers which constitute the current state of the art (e.g., NIMMO, AMMO, BAMO). The molecular structures

2 Oxetanes based on LLM-116

Table 2. Physiochemical properties of compounds **4**, **7**, **8**, **9A** and **9B** in comparison to **NIMMO** and **TNT**.

	4	7	8	9A (N1)	9B (N2)	NIMMO	TNT
Formula	C ₈ H ₈ N ₆ O ₇	C ₁₁ H ₁₂ N ₁₀ O ₉	C ₈ H ₁₀ N ₈ O ₅	C ₉ H ₁₁ N ₉ O ₅	C ₉ H ₁₁ N ₉ O ₅	C ₅ H ₉ NO ₄	C ₇ H ₅ N ₃ O ₆
FW [g·mol ⁻¹]	300.19	428.28	298.22	325.27	325.27	147.13	227.12
IS ^[a] [J]	3	>40	>40	>40	>40	> 40	15
FS ^[b] [N]	288	>360	>360	>360	>360	360	> 353
N / N+O ^[c] [%]	28.0/65.3	32.7/66.3	37.6/64.4	38.8/63.4	38.8/63.4	9.5/52.2	18.5/60.5
Ω _{CO} , Ω _{CO₂} ^[d] [%]	-26.6, -69.3	-29.9, -71.0	-42.9, -85.8	-46.7, -91.0	-46.7, -91.0	-59.8, -114	-24.7, -74.0
T _m ^[e] / T _{dec.} ^[f] [°C]	95/184	-/246	101/238	-/238	161/241	-14/170	81/290
ρ ^[g] [g·cm ⁻³]	1.62	1.70	1.56	1.64	1.59	1.19	1.64
ΔH _f ^[h] [kJ·mol ⁻¹]	115.2	105.2	315.3	238.0	263.0	-268.9	-219.0
EXPLO5 V6.04							
-ΔE _U ^[i] [kJ·kg ⁻¹]	4634	4206	4244	3769	3682	3949	4380
T _{C-J} ^[j] [K]	3276	2981	2948	2669	2649	2507	3190
D _{C-J} ^[k] [m·s ⁻¹]	7124	7335	6962	7088	6820	5906	6809
p _{C-J} ^[l] [GPa]	20.1	20.9	17.8	18.3	16.7	10.6	18.7
V ₀ ^[m] [dm ³ ·kg ⁻¹]	707	710	746	730	734	827	640

[a] Impact sensitivity (BAM drop hammer, method 1 of 6); [b] friction sensitivity (BAM drop hammer, method 1 of 6); [c] Nitrogen and oxygen content; [d] Oxygen balance toward carbon monoxide ($\Omega_{CO} = (nO - xC - yH/2)(1600/FW)$) and carbon dioxide ($\Omega_{CO_2} = (nO - 2xC - yH/2)(1600/FW)$); [e] melting point (DTA, $\beta = 5 \text{ }^\circ\text{C}\cdot\text{min}^{-1}$); [f] temperature of decomposition (DTA, $\beta = 5 \text{ }^\circ\text{C}\cdot\text{min}^{-1}$); [g] density at 298 K ($\rho_{X\text{-ray}}/1.028$) or helium pycnometry (7) ; [h] standard molar enthalpy of formation; [i] detonation energy; [j] detonation temperature; [k] detonation velocity; [l] detonation pressure [m] Volume of detonation products (assuming only gaseous products).

of all compounds were elucidated by single crystal X-ray crystallography allowing a sensitivity estimation via Hirshfeld analysis next to the practical evaluation. Compound **4** was found to be rather sensitive, while compounds **7–9** are highly insensitive which was also reflected by the SSRT and initiation test. Like other energetic oxetanes we are studying, **4** and **8** show melting points around 100 °C. Hence, higher performances may even allow oxetanes to enter the field of melt-cast explosives. For now, compounds **7–9** compounds are most well-suited to prepare low-sensitivity energetic binders with enhanced performance to be applied in low-vulnerability ammunitions (LOVA). Unfortunately, the steric demand of compound **7** is very likely to complicate its homopolymerization. However, copolymerization with sterically less demanding compounds (e.g., THF) may even benefit from the bulky substituents as back-biting reactions become effectively suppressed. Based on the current results, we conclude that BMHMO and ADNP are promising structural motifs for the synthesis of energetic monomers surpassing the prior art in key-aspects like performance, sensitivity and thermostability. We anticipate, that these motifs and the investigated compounds are helpful to develop the next generation of energetic binders and to lessen the lack of available monomers for their preparation.

Financial support of this work by the Ludwig-Maximilians University of Munich (LMU), the Office of Naval Research (ONR) under grant no. ONR N00014-19-1-2078 and the Strategic Environmental Research and Development Program (SERDP) grant WP19-1287 under contract no. W912HQ19C0033 is gratefully acknowledged. The authors also thank Stefan Huber for his help regarding sensitivity evaluations and Jakob Plank for his extensive help with all preparative tasks as well as Maximilian Benz for the dent volume measurements (SSRT). The authors declare no conflict of interest.

2.5 Supporting Information

2.5.1 Experimental part and general methods

Caution! All disclosed compounds are powerful energetic materials with sensitivities towards stimuli like shock, friction and electrostatic discharge. Therefore, proper security precautions (safety glasses, face shield, earthed equipment and shoes, Kevlar gloves and ear protection) have to be applied while preparing and handling the described compounds.

All reagents and solvents were used as received (Sigma-Aldrich, Acros Organics, ABCR, TCI). Potassium tetrazol-1-ide was used from a workgroup internal stockpile. FTIR spectra were recorded on a Perkin Elmer Spectrum One FT-IR instrument using neat compounds. Raman

2 Oxetanes based on LLM-116

spectra were obtained on a Bruker MultiRam FT Raman spectrometer and a neodymium-doped yttrium aluminum garnet (Nd:YAG) laser ($\lambda = 1064$ nm, 1074 mW). ^1H , ^{13}C and ^{14}N spectra were recorded using a Bruker AV400 or JEOL ECX400 using TMS (^1H and ^{13}C) or nitromethane (^{14}N) as internal reference. Thermal characteristics were determined using an OZM 552-Ex Differential Thermal Analyzer with Meavy 2.1.2 software or a Mettler Toledo DSC822e and a heating rate of $5\text{ }^\circ\text{C min}^{-1}$ and Mettler Toledo STAR^e Version 16.20 evaluation software. Mass spectra were obtained using a ThermoFinnigan MAT 90 or MAT 95. Elemental analyses were conducted on an Elementar Vario EL or Elementar Vario Micro using pyrolysis and subsequent gas analysis. Crystallographic measurements were performed on an Xcalibur Sapphire3. Helium pycnometry was performed using a Quantachrome Ultrapyc 1200e device. The sensitivity data was collected using a BAM (Bundesanstalt für Materialforschung) drophammer according to STANAG 4489 modified instruction and a BAM friction tester according to STANAG 4487 modified instruction.²⁹
³⁰ The classification of the tested compounds results from the 'UN Recommendations on the Transport of Dangerous Goods'.³¹ The dents of the SSRT were measured using a Keyence VR 5100 3D profilometer.

3-Bromomethyl-3-hydroxymethyloxane (BMHMO, **1**)

2,2-bis(bromomethyl)propane-1,3-diol (20.0 g, 76.4 mmol) was dissolved in methanol (200 mL) and sodium hydroxide (3.67 g, 91.8 mmol, 1.2 eq.) was added under vigorous stirring. The solution was refluxed for 12 hours prior to rotary evaporation. Dichloromethane (300 mL) was added to the suspension and all inorganics were removed by filtering through Celite. The solvent was removed to give a yellowish oil which was subject to vacuum distillation (10^{-3} mbar). By-products (e.g. spiro-compound) distilled over at $100\text{ }^\circ\text{C}$, followed by the target compound which distilled over at $120\text{--}130\text{ }^\circ\text{C}$ to give 11.9 g (86%) of BMHMO (**1**) as colorless oil.

^1H NMR: (400 MHz, CDCl_3): 2.86 (t, 1H, $J = 5.1$ Hz, OH), 3.74 (s, 2H, CH_2), 3.90 (d, 2H, $J = 5.1$ Hz, CH_2), 4.44 (m, 4H, CH_2) ppm. **IR** (ATR, cm^{-1}): $\tilde{\nu} = 3376$ (m), 2952 (m), 2877 (m), 1434 (m), 1269 (m), 1228 (m), 1108 (m), 1036 (vs), 968 (vs), 913 (s), 851 (m), 832 (s), 700 (s), 642 (s), 502 (s), 459 (s), 430 (s), 405 (s). **Raman** (1075 nm, 1000 mW, $25\text{ }^\circ\text{C}$, cm^{-1}): $\tilde{\nu} = 3015$ (14), 2963 (58), 2884 (68), 1490 (38), 1347 (12), 1272 (24), 1229 (14), 1143 (18), 1112 (18), 1069 (14), 971 (34), 923 (16), 832 (20), 703 (14), 647 (100), 504 (14). **HRMS (EI):** $m/z = 180.9856$ [$\text{C}_5\text{H}_{10}\text{O}_2\text{Br}^+$], 162.9750 [$\text{C}_5\text{H}_8\text{OBr}^+$], 148.9594 [$\text{C}_4\text{H}_6\text{OBr}^+$], 132.9646 [$\text{C}_4\text{H}_6\text{Br}^+$], 92.9334 [CH_2Br^+], 71.0491 [$\text{C}_4\text{H}_7\text{O}^+$]. **EA** ($\text{C}_5\text{H}_9\text{BrO}_2$) calcd.: H 5.01, C 33.17; found: H 5.56, C 33.98%.

Potassium 4-amino-3,5-dinitropyrazol-1-ide (2)

4-Amino-3,5-dinitro-1*H*-pyrazole (5.00 g, 28.9 mmol) was dissolved in boiling water (100 mL) and the pH-value was set to 9 by the dropwise addition of a saturated aqueous potassium hydroxide solution. The solution was then cooled to 5 °C by means of an ice bath and ethanol (200 mL) was added. The precipitated yellow solid was collected by suction filtration and washed with ethanol (50 mL) and diethyl ether (50 mL) to give 5.77 g (27.3 mmol, 94%) of potassium 4-amino-3,5-dinitropyrazol-1-ide (**2**) as yellow solid.

IR (ATR, cm^{-1}): $\tilde{\nu}$ = 3507 (w), 3391 (m), 3272 (w), 3226 (w), 3167 (w), 1628 (s), 1455 (s), 1425 (s), 1393 (s), 1288 (vs), 1201 (s), 1133 (s), 914 (s), 835 (s), 758 (s), 671 (m), 503 (s), 430 (s). **Raman** (1075 nm, 1000 mW, 25 °C, cm^{-1}): $\tilde{\nu}$ = 1627 (14), 1569 (8), 1443 (24), 1422 (24), 1389 (70), 1308 (17), 1303 (17), 1272 (30), 1251 (51), 830 (100), 722 (49), 647 (9). **EA** ($\text{C}_3\text{H}_2\text{KN}_5\text{O}_4$) calcd.: N 33.16, H 0.95, C 17.06; found: N 33.33, H 0.96, C 17.01 %. **DSC** (5 °C min^{-1}): 74.8 °C (m.p.), 312.3 °C (dec.). **IS**: > 40 J. FS > 360 N.

(3-((4-amino-3,5-dinitro-1*H*-pyrazol-1-yl)methyl)oxetan-3-yl)methanol (3)

Compound **2** (2.00 g, 9.47 mmol) and BMHMO (2.23 g, 12.3 mmol, 1.3 eq.) were added to a mixture of MeCN (20 mL) and DMF (8 mL). The suspension was heated to 100 °C resulting in a solution. The temperature was maintained for 24 h and the reaction mixture was subsequently allowed to cool to ambient temperature and poured into ethyl acetate (250 mL). The suspension was filtered through Celite and the solvents removed using a rotary evaporator (100 °C, 20 mbar) to give a yellow, oily residue. Cold diethyl ether (30 mL) was added two times and evaporated to remove any traces of DMF and 2.59 g (9.49 mmol, 100 %) of compound **3** were obtained as yellow solid.

¹H NMR (400 MHz, DMSO- d_6) δ = 3.65 (d, 2H, J = 5.2 Hz, CH_2), 4.30 (d, 2H, J = 6.4 Hz, CH_2 (Ox.)), 4.46 (d, 2H, J = 6.5 Hz, CH_2 (Ox.)), 4.90 (s, 2H, CH_2), 5.04 (bs or t, 1H, J = 5.3 Hz, OH), 7.28 (s, 2H, NH_2) ppm. **¹³C NMR** (101 MHz, DMSO- d_6) δ = 44.8, 55.0, 63.5, 75.0, 130.5, 132.5, 140.3 ppm. **¹⁴N NMR** (27 MHz, DMSO- d_6) δ = -26.7 ppm. **IR** (ATR, cm^{-1}): $\tilde{\nu}$ = 3448 (m), 3317 (m), 1633 (s), 1516 (m), 1471 (vs), 1443 (s), 1372 (m), 1349 (m), 1302 (vs), 1259 (s), 1225 (m), 1207 (m), 1055 (s), 988 (m), 948 (s), 910 (s), 891 (m), 827 (s), 788 (s), 761 (m), 747 (m), 736 (m), 661 (m), 487 (s), 467 (s). **Raman** (1075 nm, 1000 mW, 25 °C, cm^{-1}): $\tilde{\nu}$ = 2980 (4), 1632 (15), 1584 (7), 1470 (8), 1401 (21), 1372 (100), 1353 (17), 1310 (20), 1229 (4), 990 (4), 913 (3), 832 (20), 792 (11), 664 (4). **EA** ($\text{C}_8\text{H}_{10}\text{N}_8\text{O}_5$) calcd.: C 35.17, H 4.06, N, 25.63 %; found: C 34.81, H 4.02, N 25.67%. **HRMS (EI⁺)**:

2 Oxetanes based on LLM-116

$m/z = 273.0705 [C_8H_{11}N_5O_6]^+$, $179.0548 [C_6H_{11}O_6]^+$, $112.0132 [C_3H_2O_2N_3]^+$. **DSC** ($5\text{ }^\circ\text{C min}^{-1}$): $180.2\text{ }^\circ\text{C}$ (m.p.), $210.5\text{ }^\circ\text{C}$ (dec.). IS: $> 40\text{ J}$. FS $> 360\text{ N}$. $R_f = 0.65$ (SiO_2 , EtOAc).

(3-((4-diazo-3-nitro-5-oxo-4,5-dihydro-1H-pyrazol-1-yl)methyl)oxetan-3-yl)methyl nitrate (4)

Compound **3** (1.50 g, 5.49 mmol) was added to a solution dinitrogen pentoxide (2.36 g, 12.9 mmol, 2.36 eq.) in acetonitrile (20 mL) at $0\text{ }^\circ\text{C}$ using an ice bath. The yellow solution was stirred for two hours at the initial temperature and was then poured into ice water (200 mL). The aqueous phase was extracted with ethyl acetate (3x 30 mL) and the organic phase was washed with water (2 x 50 mL) and saturated sodium bicarbonate solution (2 x 30 mL). The organic phase was dried over sodium sulfate and the solvent removed by rotary evaporation to give a yellow semi-solid. The crude material was purified by column chromatography (SiO_2 , EtOAc) to give 0.87 g (2.90 mmol, 53%) of compound **4** as bright yellow solid.

$^1\text{H NMR}$ (400 MHz, DMSO-d_6) $\delta = 4.26$ (s, 2H, CH_2), 4.45 (d, 2H, $J = 6.6\text{ Hz}$, CH_2 (Ox.)), 4.53 (d, 2H, $J = 6.5\text{ Hz}$, CH_2 (Ox.)), 4.76 (s, 2H, CH_2) ppm. $^{13}\text{C NMR}$ (101 MHz, DMSO-d_6) $\delta = 42.3, 46.8, 73.3, 74.5, 143.7, 162.0$ ppm. $^{14}\text{N NMR}$ (27 MHz, DMSO-d_6) $\delta = -28.8, -41.9, -141.3$ ppm. **IR** (ATR, cm^{-1}): $\tilde{\nu} = \text{Raman}$ (1075 nm, 1000 mW, $25\text{ }^\circ\text{C}$, cm^{-1}): $\tilde{\nu} = \text{EA}$ ($\text{C}_8\text{H}_8\text{N}_6\text{O}_7$) calcd.: N 27.90, H 3.01, C 31.90; found: N 27.86, H 2.93, C 31.99 %. **HRMS (ESI $^+$)**: $m/z = 300.0460 [C_8H_8N_6O_7]^+$, $254.0555 [C_8H_8N_5O_5]^+$, $156.0004 [C_1H_4O_7N_2]^+$. **DSC** ($5\text{ }^\circ\text{C min}^{-1}$): $95.3\text{ }^\circ\text{C}$ (m.p.), $184.0\text{ }^\circ\text{C}$ (dec.). $R_f = 0.65$ (SiO_2 , EtOAc).

(3-((4-amino-3,5-dinitro-1H-pyrazol-1-yl)methyl)oxetan-3-yl)methyl methanesulfonate (5)

Compound **3** (0.50 g, 1.83 mmol) was dissolved in a mixture of acetonitrile (20 mL) and DMF (2 mL) and triethylamine (370 mg, 3.66 mmol, 2 eq.) was added. The orange solution was cooled to $0\text{ }^\circ\text{C}$ using an ice bath and a solution of methane sulfonyl chloride (252 mg, 2.19 mmol, 1.2 eq.) in acetonitrile (2 mL) was added dropwise. The instantaneous precipitation of a bright yellow solid was observed and the reaction mixture was stirred for 5 hours at the initial temperature and subsequently poured onto ice (50 g). The ice was allowed to melt and the solid was collected by suction filtration and washed with cold ethanol (20 mL) and diethyl ether (20 mL) to give 575 mg (89%) of compound **5** as yellow powder.

$^1\text{H NMR}$ (400 MHz, DMSO-d_6) $\delta = 3.21$ (s, 3H, CH_3), 4.40 (d, 2H, $J = 6.8\text{ Hz}$, CH_2), 4.57 (d, 2H, $J = 6.8\text{ Hz}$, CH_2 (Ox.)), 5.02 (s, 2H, CH_2), 7.34 (s, 2H, NH_2) ppm. $^{13}\text{C NMR}$ (101 MHz, DMSO-d_6) $\delta = 36.5, 42.9, 54.4, 70.7, 74.3, 130.6, 132.4, 140.5$ ppm. **IR** (ATR, cm^{-1}): $\tilde{\nu} = 3460$ (m), 3307 (w), 1633 (s),

2 Oxetanes based on LLM-116

1519 (m), 1473 (s), 1456 (m), 1448 (m), 1344 (s), 1307 (vs), 1291 (s), 1178 (s), 1142 (w), 1058 (m), 1007 (m), 989 (s), 973 (s), 955 (m), 929 (m), 884 (w), 859 (s), 840 (s), 830 (s), 788 (s), 760 (m), 746 (w), 718 (w), 666 (m), 535 (s), 503 (s), 488 (s), 461 (s). **Raman** (1075 nm, 1000 mW, 25 °C, cm^{-1}): $\tilde{\nu}$ = 2977 (6), 2946 (6), 1636 (19), 1586 (9), 1470 (11), 1403 (24), 1376 (100), 1351 (19), 1326 (30), 1310 (24), 1293 (9), 1279 (6), 1170 (7), 954 (6), 832 (22), 790 (13), 763 (6), 535 (6). **EA** ($\text{C}_9\text{H}_{13}\text{N}_5\text{O}_8\text{S}$) calcd.: N 19.94, H 3.73, C 30.77; found: N 19.92, H 3.69, C 30.85 %. **HRMS (EI⁺)**: m/z = 351.0473 [$\text{C}_9\text{H}_{13}\text{N}_5\text{O}_8^{32}\text{S}_1$]⁺, 334.0433 [$\text{C}_9\text{H}_{12}\text{N}_5\text{O}_7^{32}\text{S}_1$]⁺, 179.0549 [$\text{C}_6\text{H}_{11}\text{O}_6$]⁺. **DSC** (5 °C min^{-1}): 188.4 °C (dec.). R_f = 0.59 (SiO_2 , EtOAc/petrol ether/toluene 3:1:1).

1-((3-(bromomethyl)oxetan-3-yl)methyl)-3,5-dinitro-1H-pyrazol-4-amine (6)

Compound **5** (0.50 g, 1.42 mmol) was suspended in acetone (10 mL) and lithium bromide (247 mg, 2.85 mmol, 2 eq.) was added. The reaction mixture was set to reflux for 24 h and the solvent was removed by rotary evaporation. Ethyl acetate was added to dissolve the crude compound and all inorganic were removed filtration through a silica-plug which was thoroughly rinsed with ethyl acetate. The solvent was again removed by rotary evaporation to give 476 mg (99 %, 1.42 mmol) of compound **6** as intense yellow solid.

¹H NMR (400 MHz, acetone- d_6) δ = 4.01 (s, 2H, CH_2), 4.46 (d, 2H, J = 6.8 Hz, CH_2), 4.65 (d, 2H, J = 6.8 Hz, CH_2 (Ox.)), 5.19 (s, 2H, CH_2), 7.01 (s, 2H, NH_2) ppm. **¹³C NMR** (101 MHz, acetone- d_6) δ = 38.1, 45.6, 56.3, 77.2, 131.4 ppm. **¹⁴N NMR** (27 MHz, acetone- d_6) δ = -23.6, -28.4 ppm. **IR** (ATR, cm^{-1}): $\tilde{\nu}$ = 3443 (w), 3315 (w), 1644 (s), 1515 (m), 1473 (s), 1431 (s), 1409 (m), 1377 (w), 1309 (vs), 1269 (s), 1256 (m), 1244 (s), 1197 (m), 1155 (m), 1084 (m), 1044 (m), 954 (s), 906 (s), 864 (m), 850 (m), 825 (s), 788 (s), 760 (m), 747 (m), 663 (m), 642 (s), 611 (m), 521 (vs), 449 (s). **Raman** (1075 nm, 1000 mW, 25 °C, cm^{-1}): $\tilde{\nu}$ = 2965 (6), 1636 (19), 1575 (7), 1472 (13), 1436 (11), 1411 (13), 1386 (45), 1372 (100), 1339 (25), 1326 (22), 1310 (18), 1258 (13), 1227 (10), 830 (23), 792 (10), 699 (6), 670 (7), 643 (7). **EA** ($\text{C}_9\text{H}_{13}\text{N}_5\text{O}_8\text{S}$) calcd.: N 20.84, H 3.00, C 28.59; found: N 21.02, H 3.00, C 28.79 %. **HRMS (EI⁺)**: m/z = 335.9924 [$\text{C}_8\text{H}_{11}\text{N}_5\text{O}_5^{79}\text{Br}$]⁺, 334.9863 [$\text{C}_8\text{H}_{10}\text{N}_5\text{O}_5^{79}\text{Br}$]⁺, 226.0706 [$\text{C}_8\text{H}_{10}\text{O}_4\text{N}_4$]⁺, 179.0570 [$\text{C}_7\text{H}_7\text{O}_2\text{N}_4$]⁺. **DSC** (5 °C min^{-1}): 157.3 °C (m.p.), 197.5 °C (dec.). R_f = 0.83 (SiO_2 , EtOAc/petrol ether/toluene 3:1:1).

1,1'-(oxetane-3,3-diylbis(methylene))bis(3,5-dinitro-1H-pyrazol-4-amine) (7)

Compound **5** (500 mg, 1.42 mmol) and potassium 4-amino-3,5-dinitropyrazol-1-ide (300 mg, 1.42 mmol) were dissolved in DMF (10.0 mL) and the reaction mixture heated to 100 °C for 48 h which

was accompanied by the formation of a colorless precipitate. The mixture was then poured into ethyl acetate (100 mL) to precipitate all inorganics and filtered through Celite to give a bright yellow solution. The solvent was evaporated and the obtained solid recrystallized from ethyl acetate to give 541 mg (89%) of compound **7** as yellow solid.

¹H-NMR (400 MHz, dms_o-d₆): δ = 4.57 (s, 4H, CH₂), 5.09 (s, 4H, CH₂), 7.31 (s, 4H, NH₂) ppm. **¹³C NMR** (101 MHz, dms_o-d₆) δ = 43.6, 55.4, 75.7, 130.5, 132.2, 140.1 ppm. **¹⁴N NMR** (27 MHz, dms_o-d₆) δ = -19.8 ppm. **IR** (ATR, cm⁻¹): $\tilde{\nu}$ = 3487 (w), 3422 (w), 3370 (m), 3282 (w), 3199 (w), 1634 (s), 1523 (m), 1505 (m), 1490 (m), 1466 (s), 1452 (s), 1430 (s), 1396 (m), 1371 (m), 1353 (m), 1297 (vs), 1276 (vs), 1217 (m), 1142 (m), 1050 (m), 978 (m), 964 (s), 946 (s), 889 (m), 829 (s), 796 (s), 787 (s), 758 (m), 747 (m), 667 (s), 643 (m), 482 (vs), 457 (s). **Raman** (1075 nm, 1000 mW, 25 °C, cm⁻¹): $\tilde{\nu}$ = 2969 (4), 1640 (15), 1584 (8), 1565 (8), 1528 (5), 1474 (14), 1432 (10), 1372 (100), 1355 (66), 1320 (32), 1301 (22), 1241 (11), 1187 (5), 979 (5), 946 (5), 832 (29), 797 (13), 792 (14), 739 (6), 670 (5), 645 (4), 622 (6), 518 (5). **EA** (C₁₁H₁₂N₁₀O₉) calcd.: N 32.71, H 2.28, C 30.85; found: N 32.00, H 2.88, C 30.84 %. **HRMS (EI⁺)**: m/z = 428.0800 [C₁₁H₁₂N₁₀O₉]⁺, 411.0831 [C₁₁H₁₁N₁₀O₈]⁺, 179.0569 [C₇H₇N₄O₂]⁺; **DSC** (5 °C min⁻¹): 246.0 °C (dec.). **R_f** = 0.25 (SiO₂, EtOAc).

1-((3-(azidomethyl)oxetan-3-yl)methyl)-3,5-dinitro-1H-pyrazol-4-amine (**8**)

Compound **5** (500 mg, 1.42 mmol) was dissolved in dimethylformamide (20 mL) together with sodium azide (185 mg, 2.85 mmol, 2 eq.) and the reaction mixture was heated to 100 °C for 24 h to give a deep orange solution. The reaction mixture was poured into ethyl acetate (150 mL) and the resulting suspension was filtered through Celite to remove all salts. The solvent was removed by rotary evaporation (40 °C, 240 mbar; 100 °C, 20 mbar) to give a slightly orange solid. Residues of dimethylformamide were removed by co-evaporation with cold diethyl ether (20 mL) and cold ethyl acetate (20 mL) to give 421.3 mg (1.41 mmol, 99%) of compound **8** as yellow to orange solid. If necessary, the compound can be dissolved in the minimum amount of acetone and precipitated with *n*-Hexane to give a bright yellow solid with no yield loss.

¹H NMR (400 MHz, acetone-d₆) δ = 3.94 (s, 2H, CH₂), 4.44 (d, 2H, *J* = 6.8 Hz, CH₂), 4.63 (d, 2H, *J* = 6.8 Hz, CH₂ (Ox.)), 5.09 (s, 2H, CH₂), 7.00 (bs, 2H, NH₂) ppm. **¹³C NMR** (101 MHz, acetone-d₆) δ = 44.9, 55.3, 56.2, 76.5, 131.4, 133.6, 141.7 ppm. **¹⁴N NMR** (27 MHz, acetone-d₆) δ = -23.0, -27.8, -133.8, -172.5 ppm. **IR** (ATR, cm⁻¹): $\tilde{\nu}$ = 3447 (m), 3294 (m), 3207 (w), 2886 (w), 2096 (s), 1636 (s), 1582 (w), 1516 (m), 1470 (vs), 1442 (s), 1373 (m), 1302 (vs), 1274 (vs), 1240 (s), 1206 (s), 1141 (m), 1102 (m), 1052 (m), 979 (s), 958 (m), 915 (s), 889 (m), 865 (m), 828 (s), 789 (s), 761 (m).

Raman (1075 nm, 1000 mW, 25 °C, cm^{-1}): $\tilde{\nu}$ = 2977 (4), 2892 (2), 2105 (1), 1638 (13), 1590 (7), 1488 (2), 1470 (7), 1445 (3), 1403 (15), 1374 (100), 1353 (15), 1306 (19), 1245 (3), 1150 (2), 994 (3), 925 (2), 830 (24), 792 (11), 674 (3), 618 (2). **EA** ($\text{C}_8\text{H}_{10}\text{N}_8\text{O}_5$) calcd.: N 37.58, H 3.38, C 32.22; found: N 37.45, H 3.32, C 32.41 %. **HRMS (EI⁺)**: m/z = 298.0769 [$\text{C}_8\text{H}_{10}\text{N}_8\text{O}_5$]⁺, 194.0675 [$\text{C}_7\text{H}_8\text{N}_5\text{O}_2$]⁺. **DSC** (5 °C min^{-1}): 101.0 °C (m.p.), 238.3 °C (dec.).

1-((3-((1H-tetrazol-1-yl)methyl)oxetan-3-yl)methyl)-3,5-dinitro-1H-pyrazol-4-amine (9A) and 1-((3-((2H-tetrazol-2-yl)methyl)oxetan-3-yl)methyl)-3,5-dinitro-1H-pyrazol-4-amine (9B)

Compound **5** (2.00 g, 5.69 mmol) and potassium tetrazol-1-ide (924 mg, 8.54 mmol, 1.5 eq.) were dissolved in DMF (50.0 mL) and the reaction mixture heated to 100 °C for 48 h which was accompanied by the formation of a gelatinous precipitate. The mixture was then poured into ethyl acetate (200 mL) to precipitate all inorganics and filtered through Celite to give an orange solution. All volatiles were evaporated and a small quantity of acetone (10 mL) added to the obtained slurry. Diethyl ether was added (100 mL) to precipitate the target compound as bright orange solid which was collected by suction filtration to give 1.81 g (98%) of the isomeric mixture (**9A**, **9B**) which was afterward refluxed in toluene. The suspension was filtered hot to give 1.07 g (89%) of compound **9A** as yellow solid. The filter residue was recrystallized from hot acetone to give 439 mg (72%) of compound **9B** as yellow solid corresponding to an overall yield of 84%.

Compound 9A (N2):

¹H-NMR (400 MHz, acetone- d_6): δ = 4.71 (d, J = 7.1 Hz, 2H, CH_2), 4.75 (d, J = 7.1 Hz, 2H, CH_2), 5.08 (s, 2H, CH_2), 5.29 (s, 2H, CH_2), 6.99 (s, 2H, NH_2), 8.75 (s, 1H, CH) ppm. **¹³C NMR** (101 MHz, acetone- d_6) δ = 44.9, 55.7, 56.1, 76.5, 131.3, 141.6, 154.0 ppm. **¹⁴N NMR** (27 MHz, acetone- d_6) δ = -23.6, -28.4, -101.8 ppm. **IR** (ATR, cm^{-1}): $\tilde{\nu}$ = 3444 (w), 3322 (m), 3138 (w), 2966 (w), 2890 (w), 1635 (s), 1582 (w), 1515 (m), 1466 (s), 1434 (s), 1412 (m), 1393 (w), 1380 (w), 1370 (w), 1356 (m), 1306 (vs), 1278 (vs), 1246 (m), 1186 (m), 1148 (m), 1132 (m), 1066 (m), 1024 (s), 1006 (m), 985 (m), 970 (s), 925 (m), 906 (m), 827 (s), 798 (s), 763 (s), 749 (m), 709 (m), 689 (m), 671 (m), 663 (m), 615 (m), 526 (s), 470 (s). **Raman** (1075 nm, 1000 mW, 25 °C, cm^{-1}): $\tilde{\nu}$ = 2969 (7), 2955 (6), 1640 (23), 1582 (9), 1567 (6), 1522 (6), 1476 (12), 1438 (16), 1413 (30), 1393 (69), 1380 (100), 1339 (66), 1279 (11), 1254 (19), 1247 (16), 1189 (6), 1025 (7), 1008 (5), 973 (6), 828 (36), 797 (13), 765 (7), 695 (9), 672 (9), 502 (5), 471 (5). **EA** ($\text{C}_9\text{H}_{11}\text{N}_9\text{O}_5$) calcd.: N 38.76, H 3.41, C 33.24; found: N 39.03, H 3.50, C 33.48 %. **HRMS (EI⁺)**: m/z = 325.0889 [$\text{C}_9\text{H}_{11}\text{N}_9\text{O}_5$]⁺, 324.0812 [$\text{C}_9\text{H}_{10}\text{N}_9\text{O}_5$]⁺, 298.0895 [$\text{C}_9\text{H}_{12}\text{N}_7\text{O}_5$]⁺; 172.0112 [$\text{C}_3\text{H}_2\text{N}_5\text{O}_4$]⁺. **DSC** (5 °C min^{-1}): 161.0 °C (m.p.), 241.1 °C (dec.).

Compound 9B (N1):

¹H-NMR (400 MHz, acetone-d₆): δ = 4.69 (d, *J* = 7.1 Hz, 2H, CH₂), 4.73 (d, *J* = 7.2 Hz, 2H, CH₂), 5.08 (s, 2H, CH₂), 5.12 (s, 2H, CH₂), 7.01 (s, 2H, NH₂), 9.26 (s, 1H, CH) ppm. **¹³C NMR** (101 MHz, acetone-d₆) δ = 45.0, 51.3, 55.7, 77.6, 124.7, 145.4 ppm. **¹⁴N NMR** (27 MHz, dms_o-d₆) δ = -29.0 ppm. **IR** (ATR, cm⁻¹): $\tilde{\nu}$ = 3484 (w), 3366 (m), 3130 (w), 3044 (w), 2963 (w), 2896 (w), 1634 (s), 1509 (m), 1487 (m), 1469 (vs), 1437 (m), 1389 (m), 1360 (m), 1344 (m), 1319 (vs), 1299 (vs), 1258 (m), 1245 (m), 1215 (m), 1162 (m), 1135 (m), 1107 (s), 1060 (m), 973 (s), 952 (s), 911 (s), 890 (m), 839 (m), 830 (s), 791 (s), 759 (m), 749 (m), 721 (m), 680 (m), 667 (m), 619 (w), 450 (s). **Raman** (1075 nm, 1000 mW, 25 °C, cm⁻¹): $\tilde{\nu}$ = 2975 (14), 2897 (5), 1627 (22), 1563 (14), 1524 (5), 1478 (17), 1468 (18), 1440 (6), 1428 (5), 1399 (53), 1368 (100), 1357 (99), 1314 (19), 1297 (11), 1283 (12), 1249 (5), 1218 (6), 1033 (6), 988 (6), 832 (31), 792 (14), 736 (6). **EA** (C₉H₁₁N₉O₅) calcd.: N 38.76, H 3.41, C 33.24; found: N 37.76, H 3.34, C 32.97 %. **HRMS (EI⁺)**: *m/z* = 325.0890 [C₉H₁₁N₉O₅]⁺, 324.0812 [C₉H₁₀N₉O₅]⁺, 295.0910 [C₉H₁₁N₈O₄]⁺; 172.0111 [C₃H₂N₅O₄]⁺. **DSC** (5 °C min⁻¹): 238.3 °C (dec.).

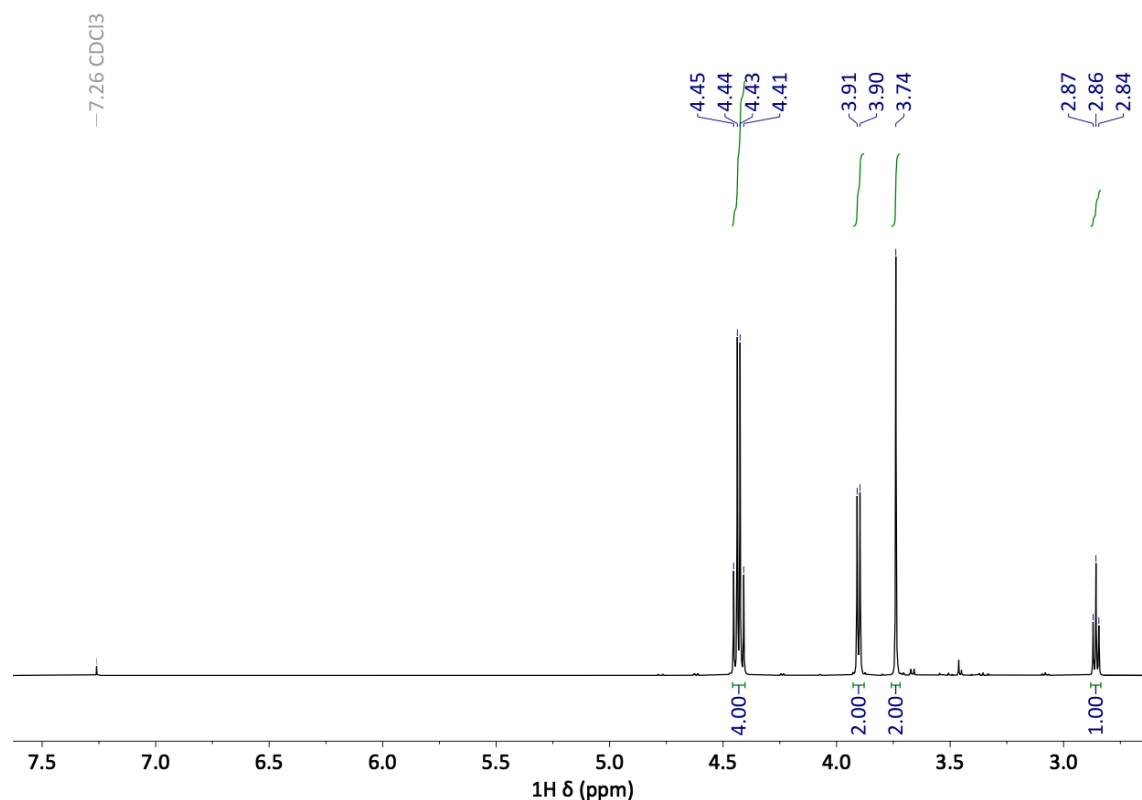
2.5.2 NMR Spectra

Figure 9. Proton spectrum (¹H) of 3-bromomethyl-3-hydroxymethyloxetane (BMHMO, 1).

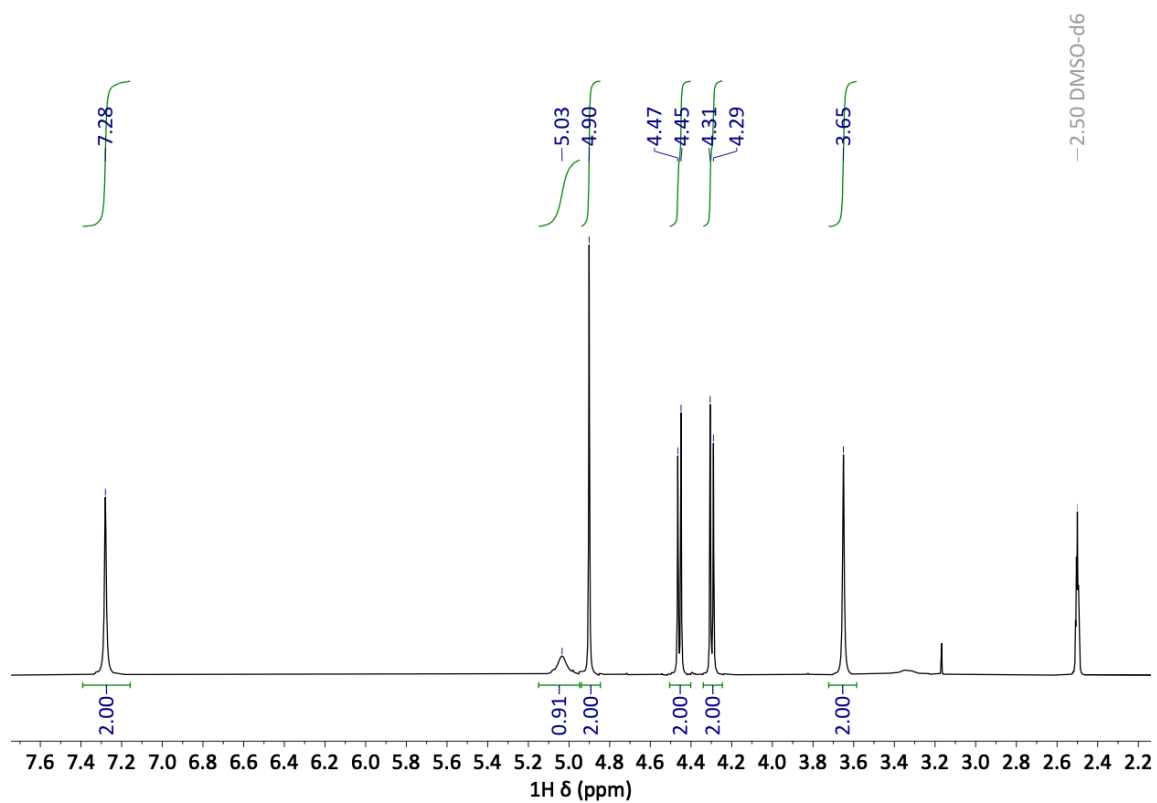


Figure 10. Proton spectrum (^1H) of compound **3**.

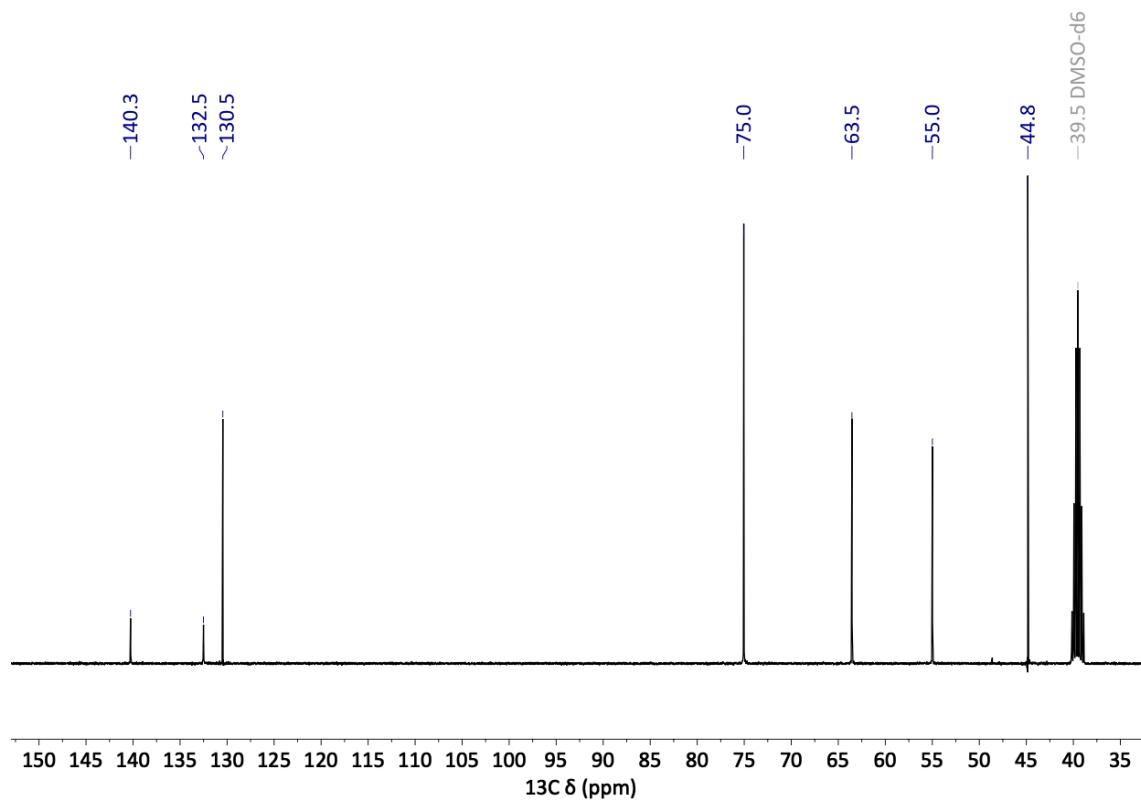


Figure 11. Carbon spectrum (^{13}C) of compound **3**.

2 Oxetanes based on LLM-116

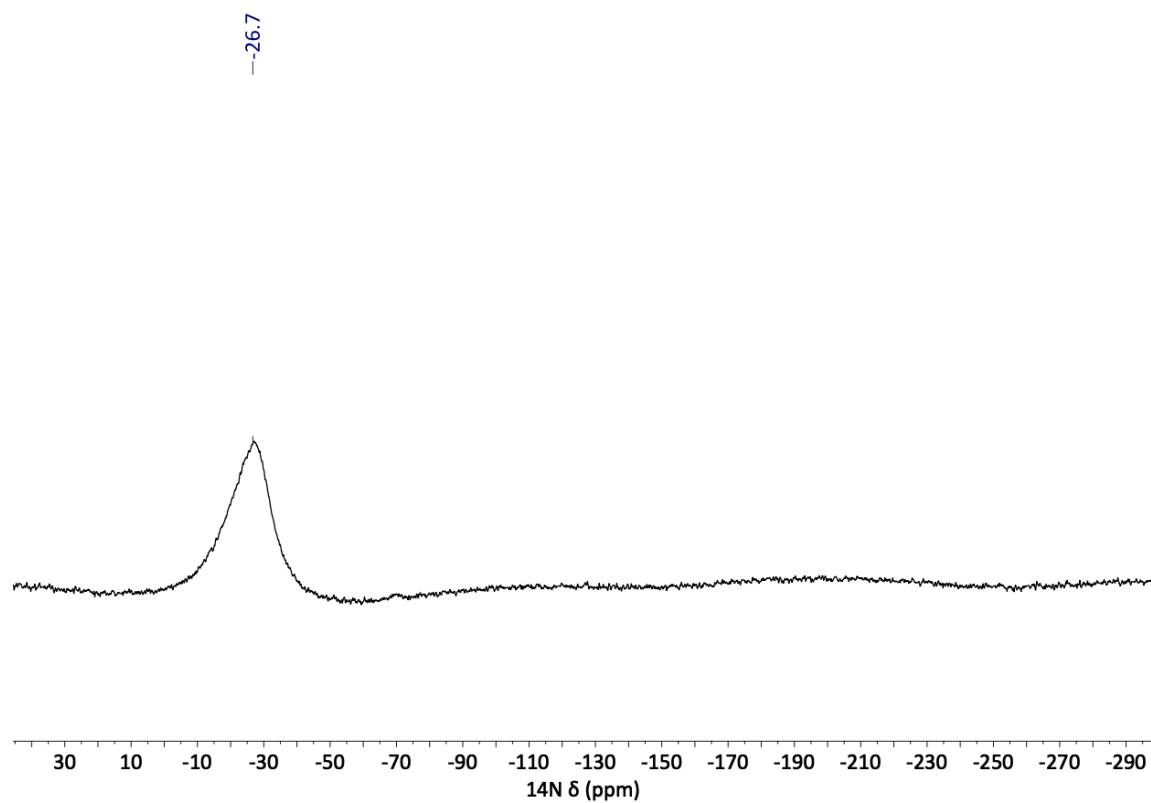


Figure 12. Nitrogen spectrum (^{14}N) of compound 3.

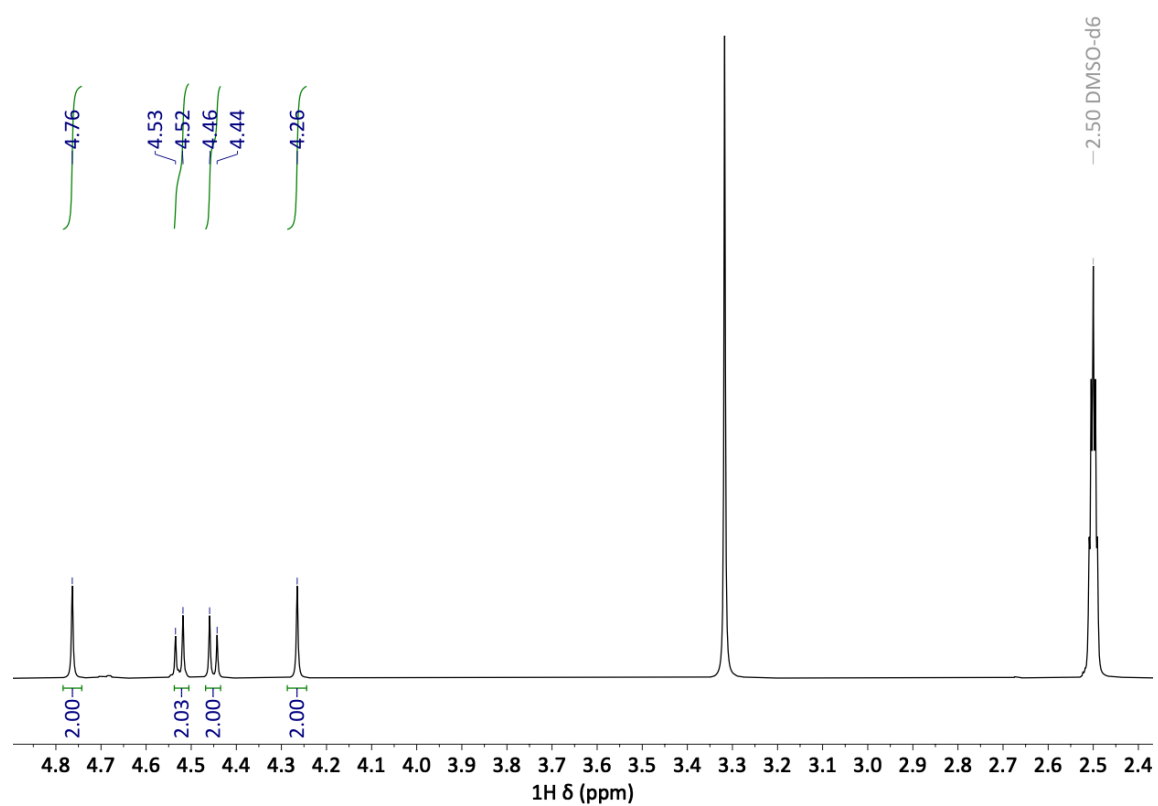


Figure 13. Proton spectrum (^1H) of compound 4.

2 Oxetanes based on LLM-116

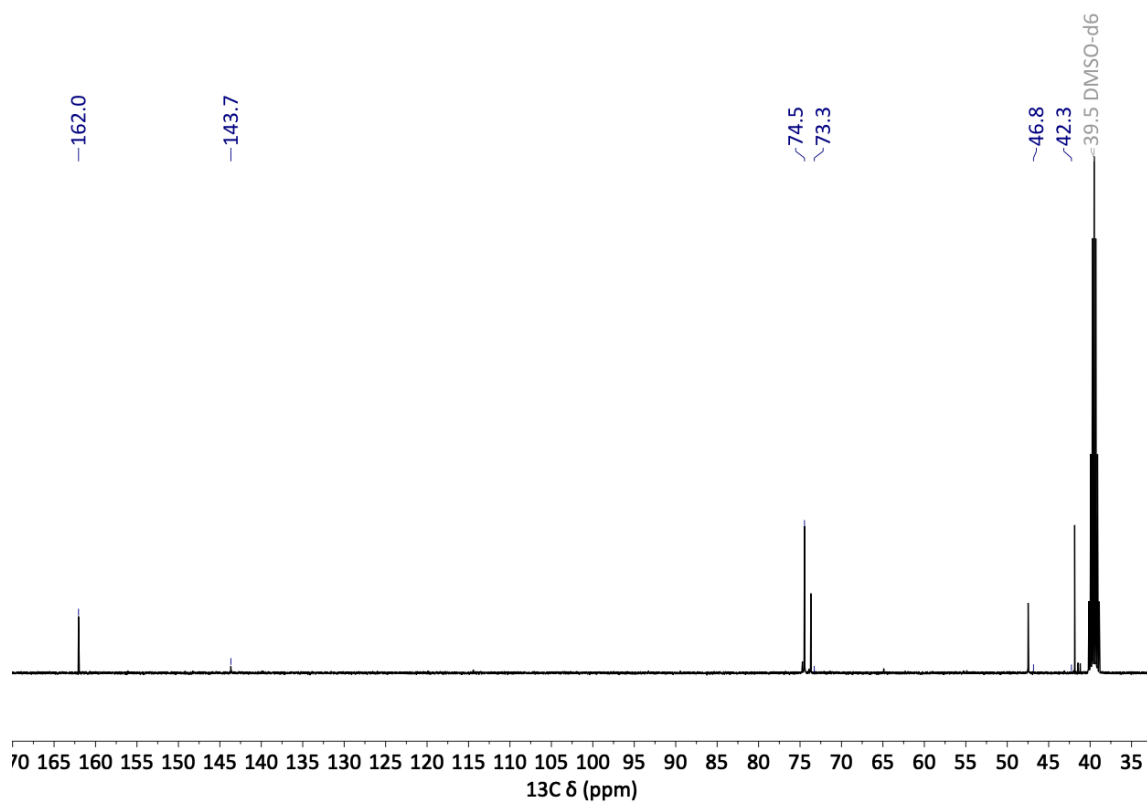


Figure 14. Carbon spectrum (^{13}C) of compound 4.

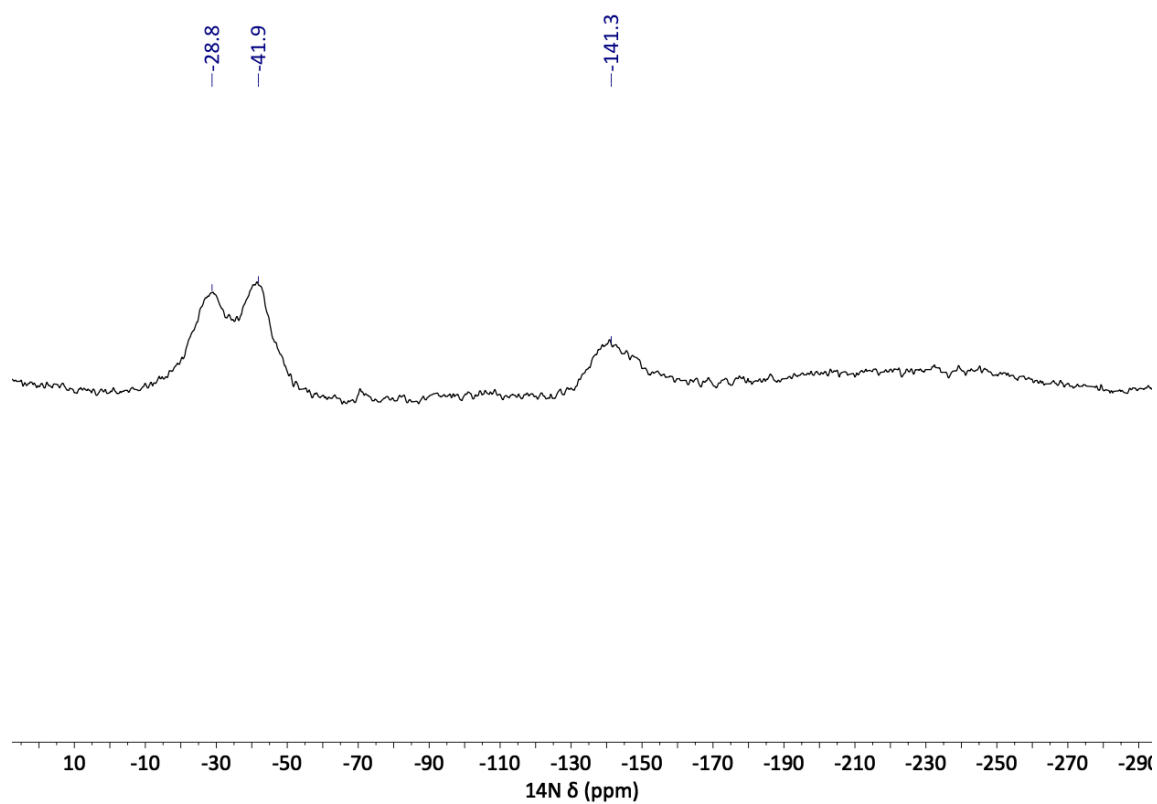


Figure 15. Nitrogen spectrum (^{14}N) of compound 4.

2 Oxetanes based on LLM-116

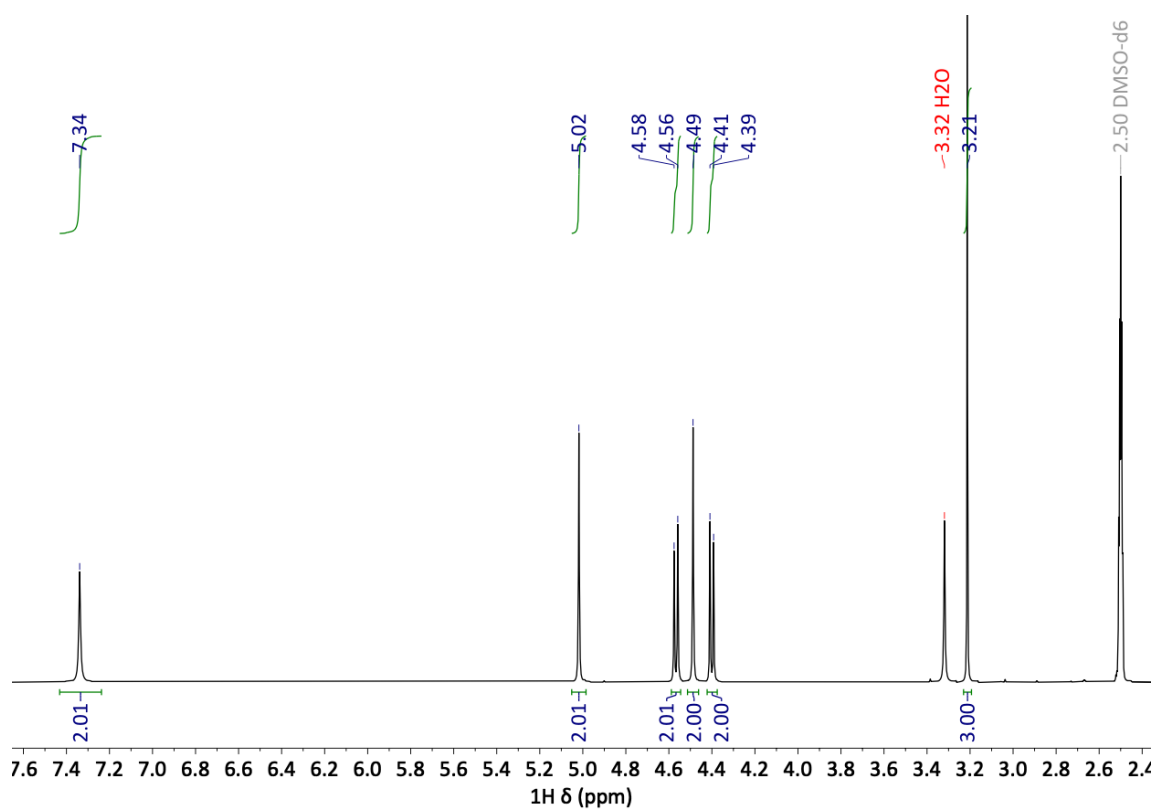


Figure 16. Proton spectrum (^1H) of compound 5.

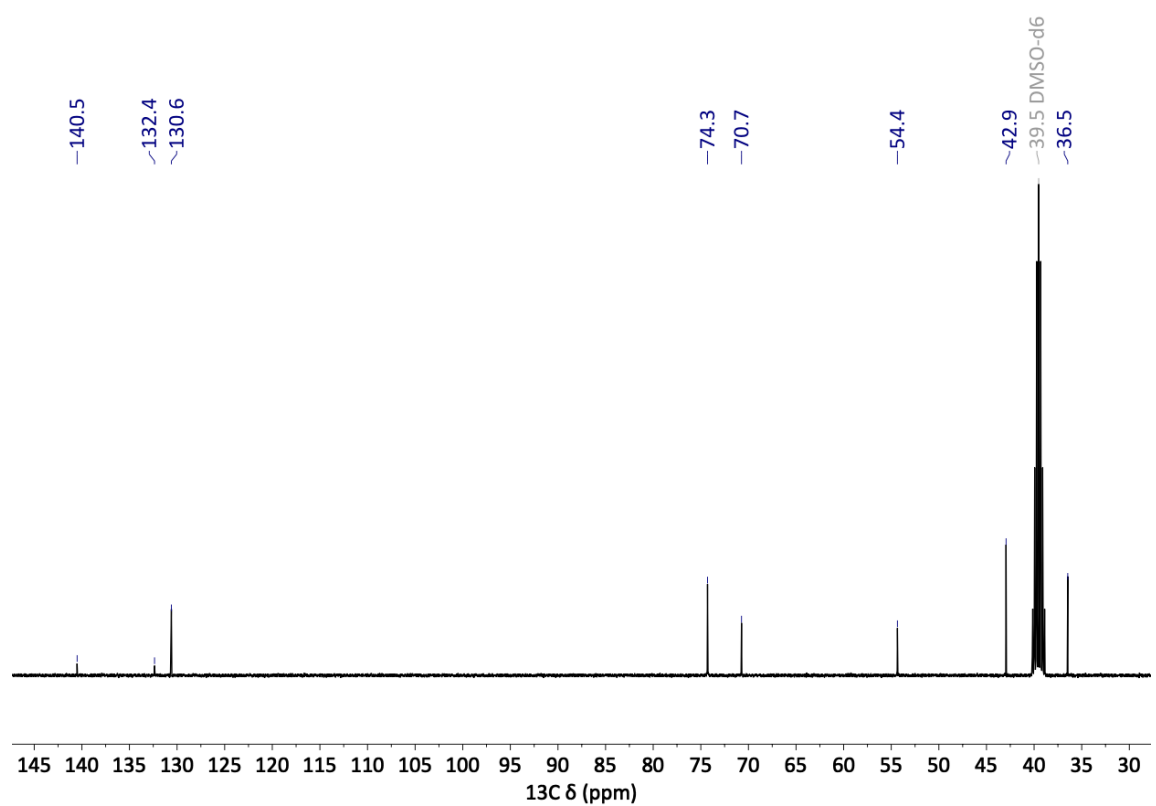


Figure 17. Carbon spectrum (^{13}C) of compound 5.

2 Oxetanes based on LLM-116

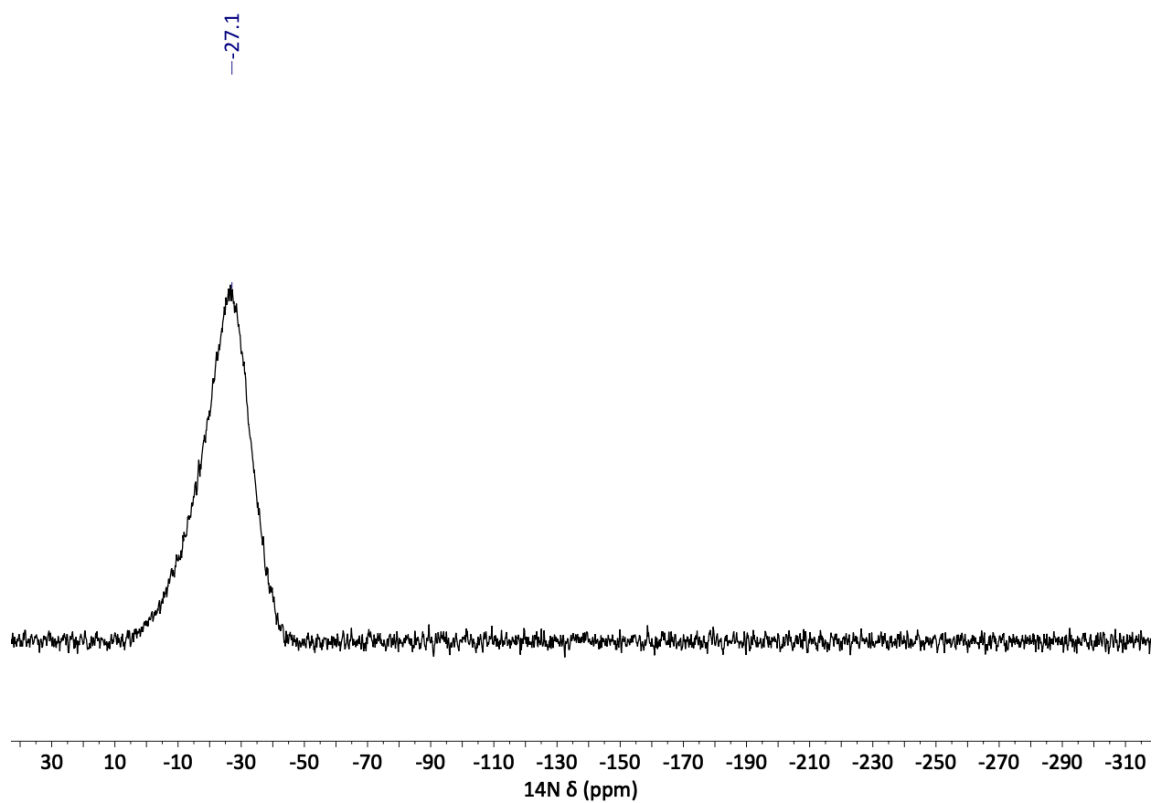


Figure 18. Nitrogen spectrum (^{14}N) of compound 5.

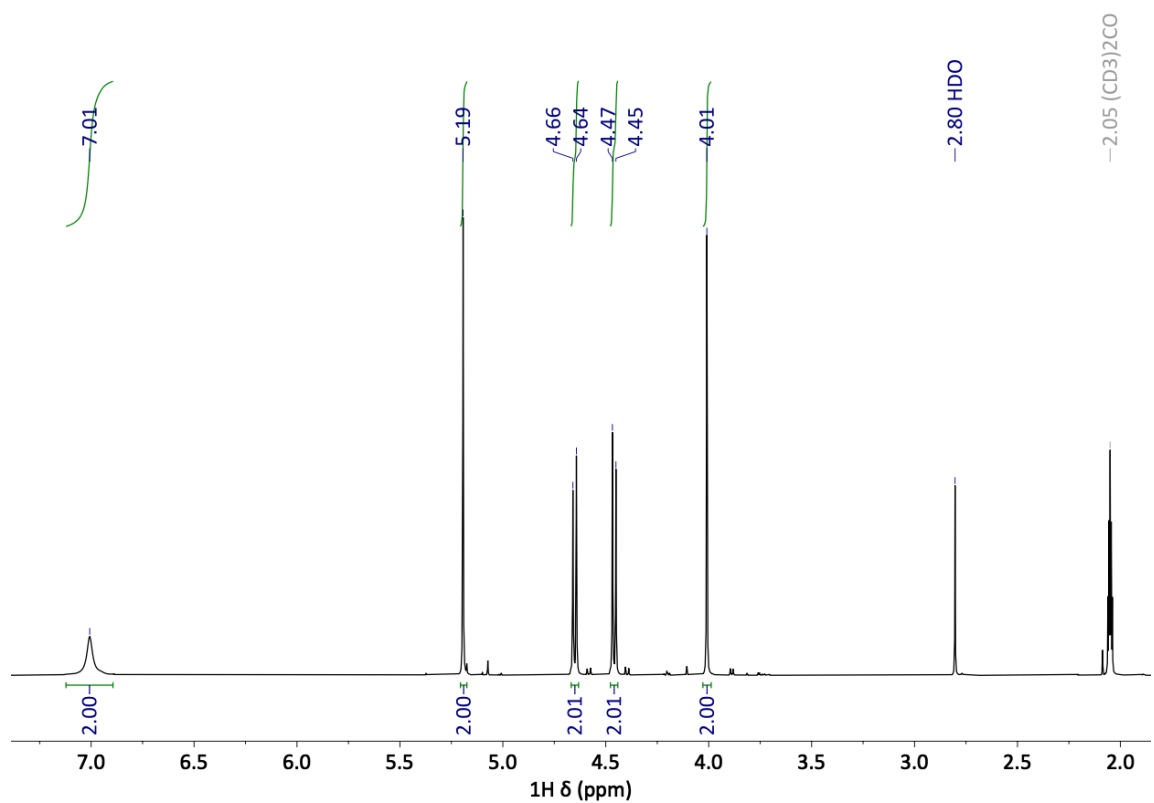


Figure 19. Proton spectrum (^1H) of compound 6.

2 Oxetanes based on LLM-116

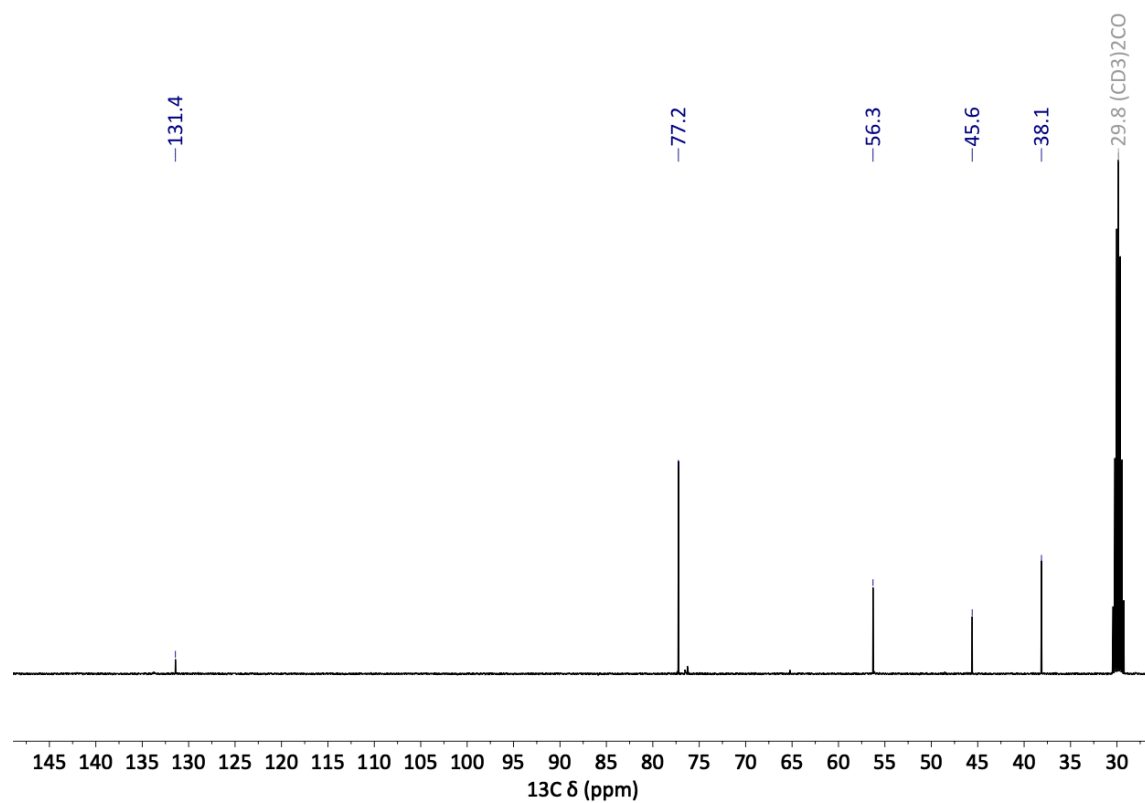


Figure 20. Carbon spectrum (^{13}C) of compound 6.

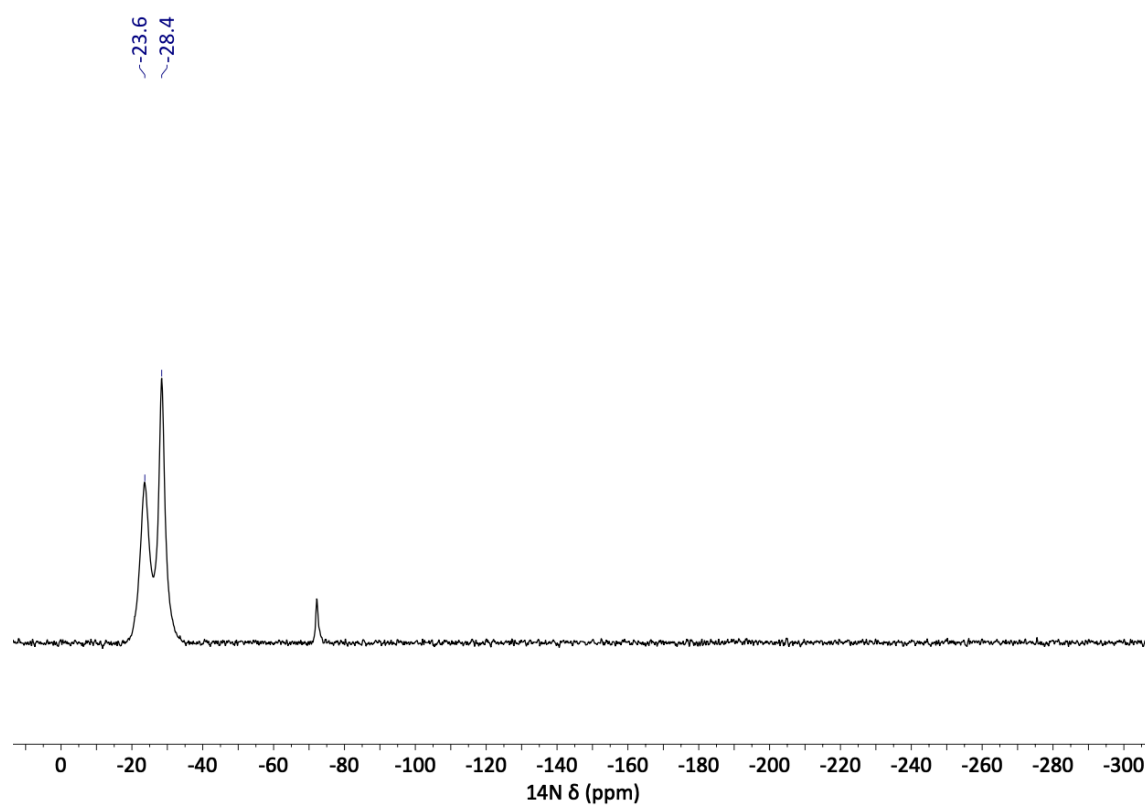


Figure 21. Nitrogen spectrum (^{14}N) of compound 6.

2 Oxetanes based on LLM-116

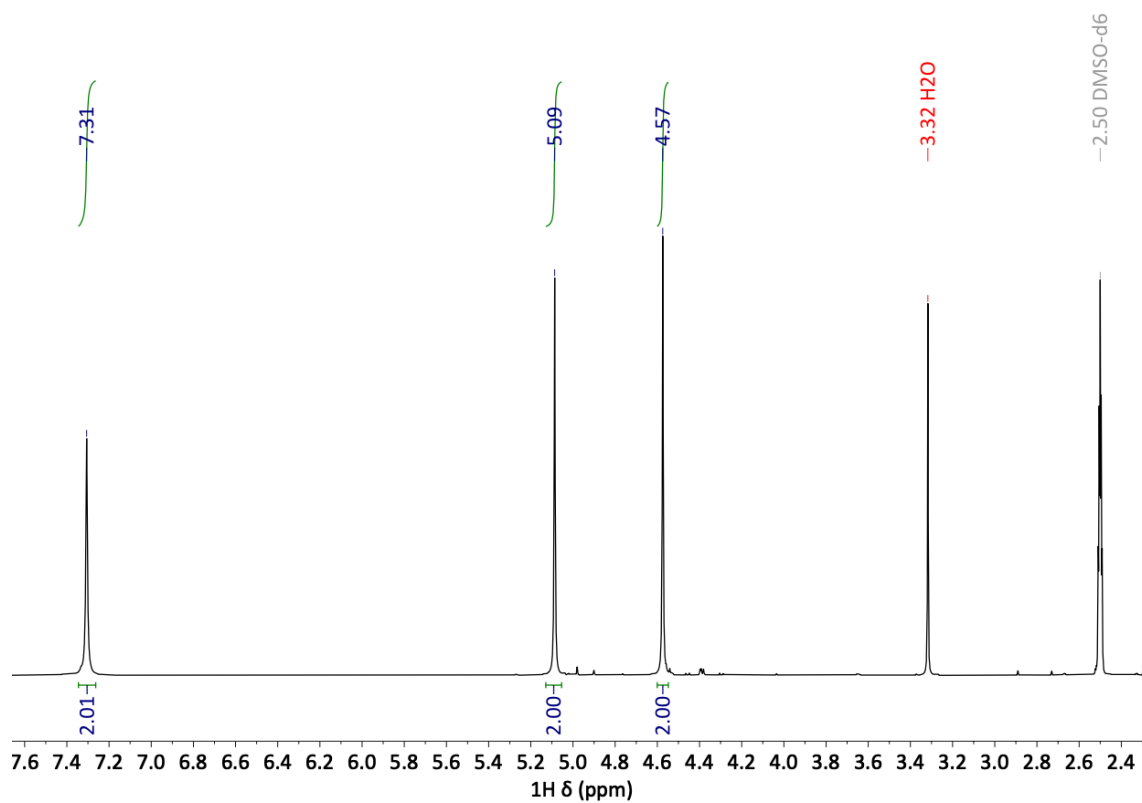


Figure 22. Proton spectrum (^1H) of compound 7.

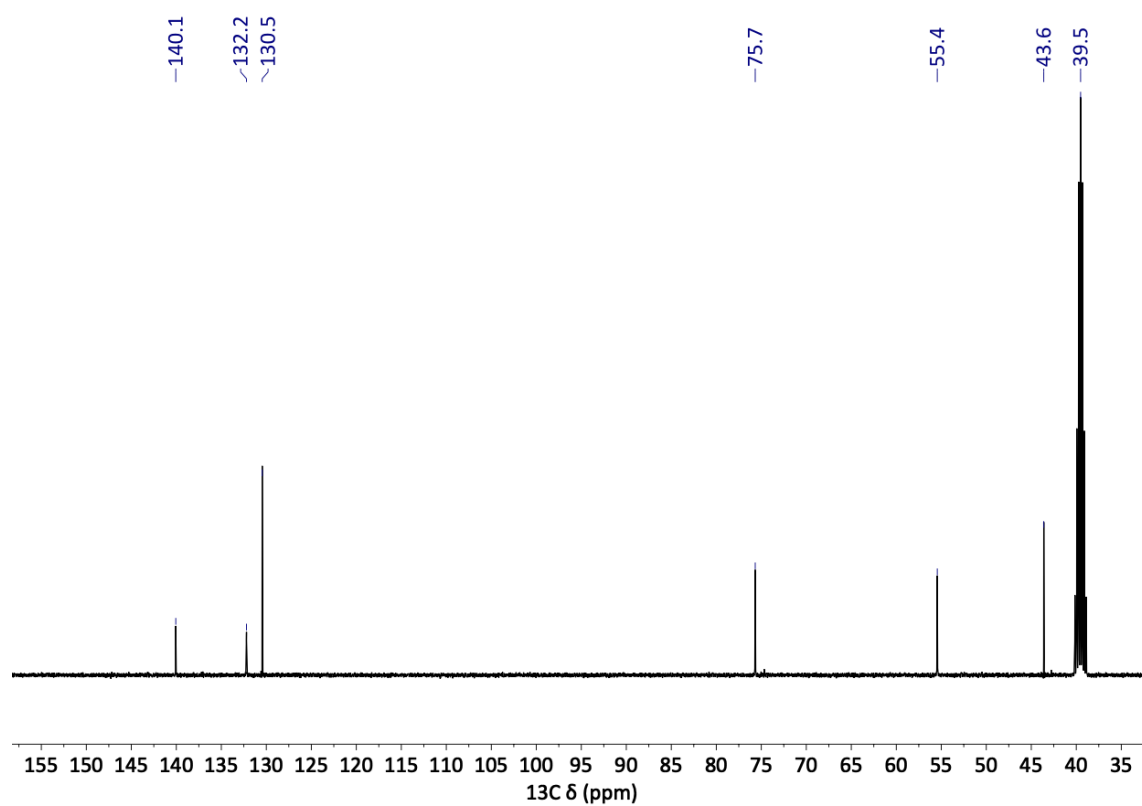


Figure 23. Carbon spectrum (^{13}C) of compound 7.

2 Oxetanes based on LLM-116

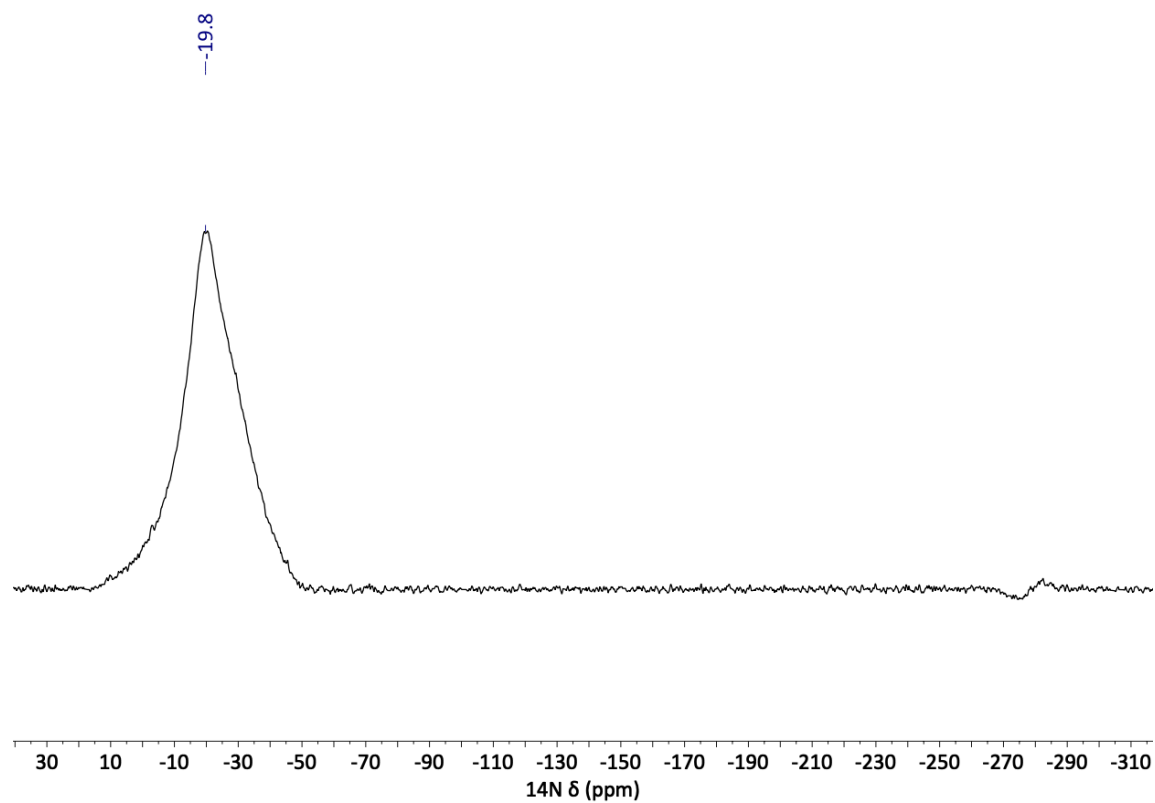


Figure 24. Nitrogen spectrum (^{14}N) of compound 7.

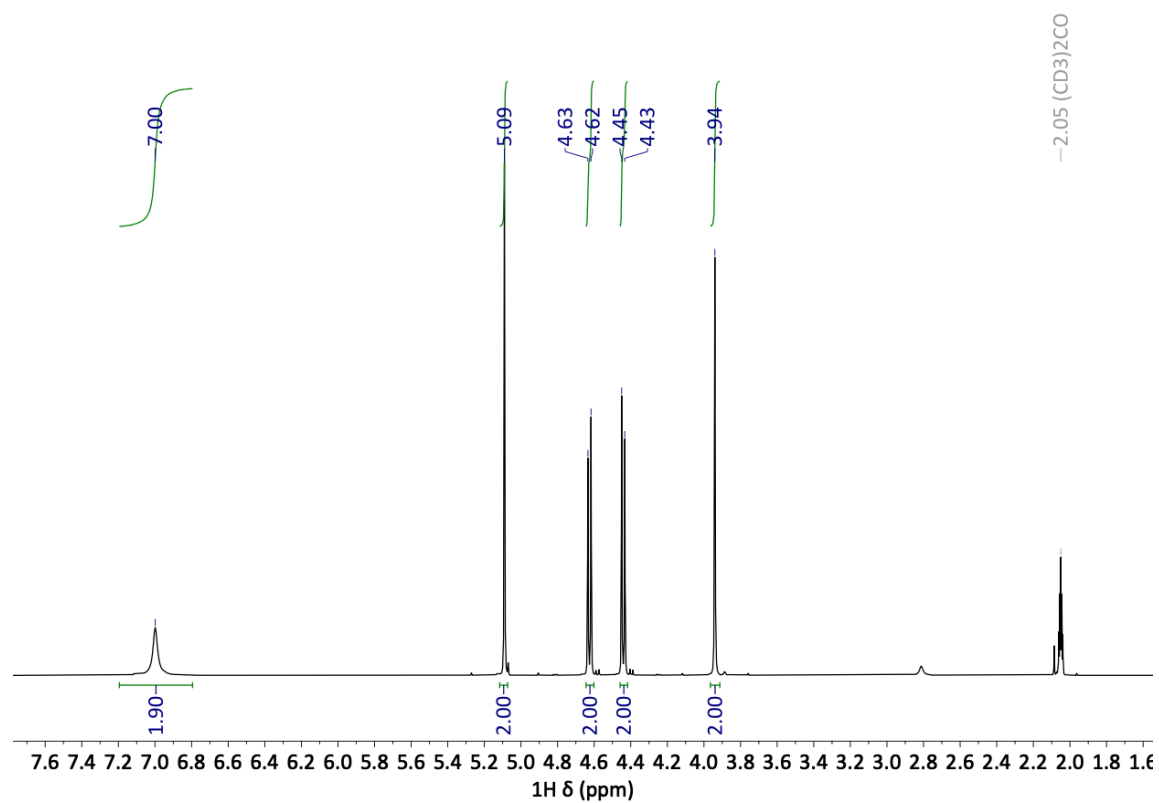


Figure 25. Proton spectrum (^1H) of compound 8.

2 Oxetanes based on LLM-116

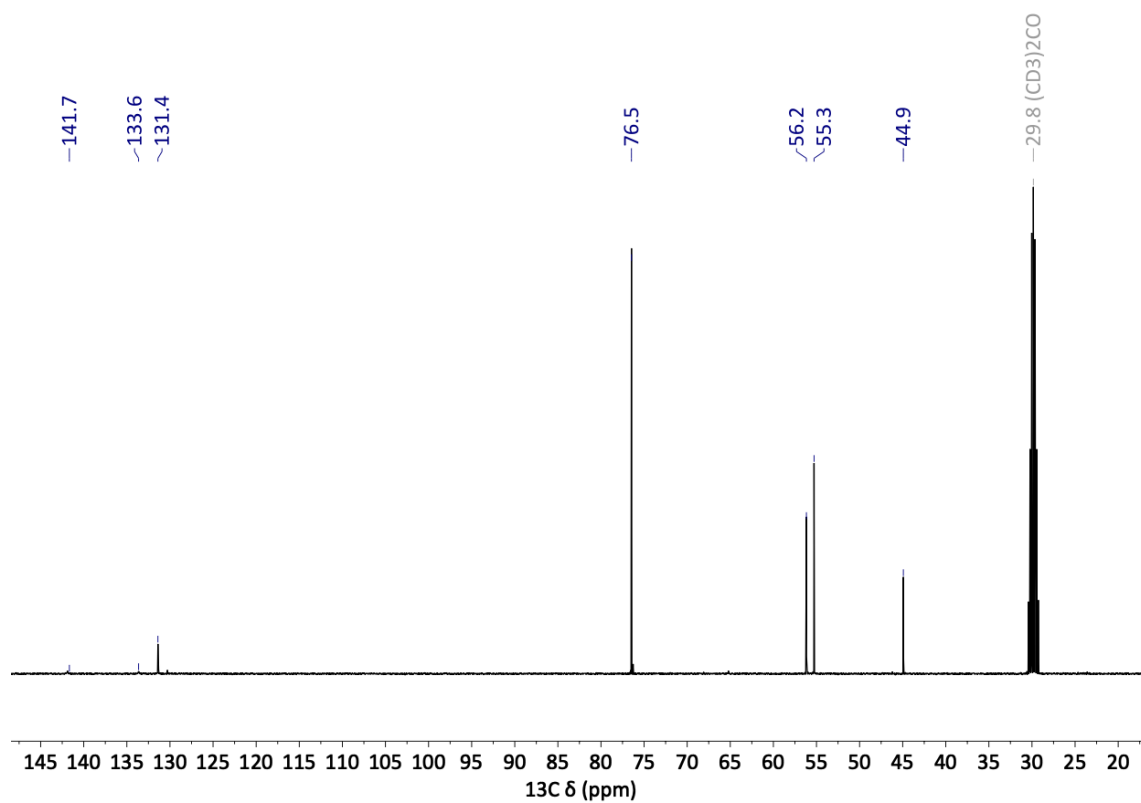


Figure 26. Carbon spectrum (¹³C) of compound 8.

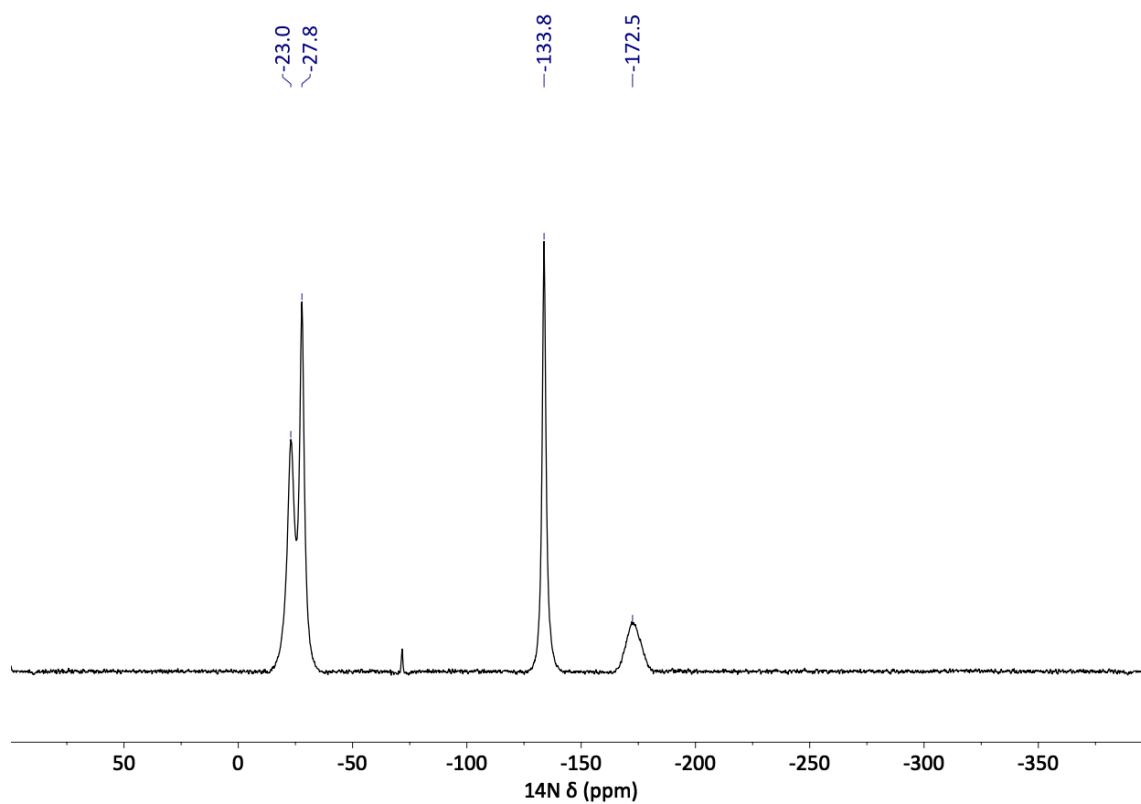


Figure 27. Nitrogen spectrum (¹⁴N) of compound 8.

2 Oxetanes based on LLM-116

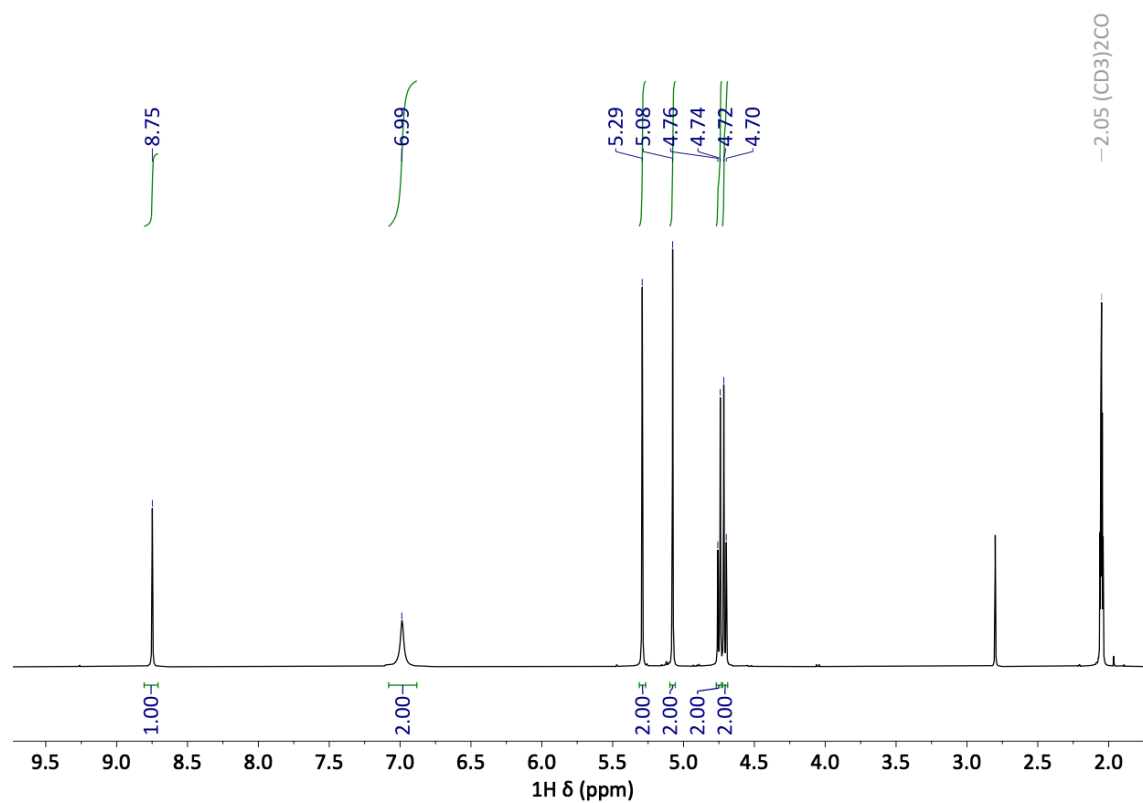


Figure 28. Proton spectrum (^1H) of compound 9A.

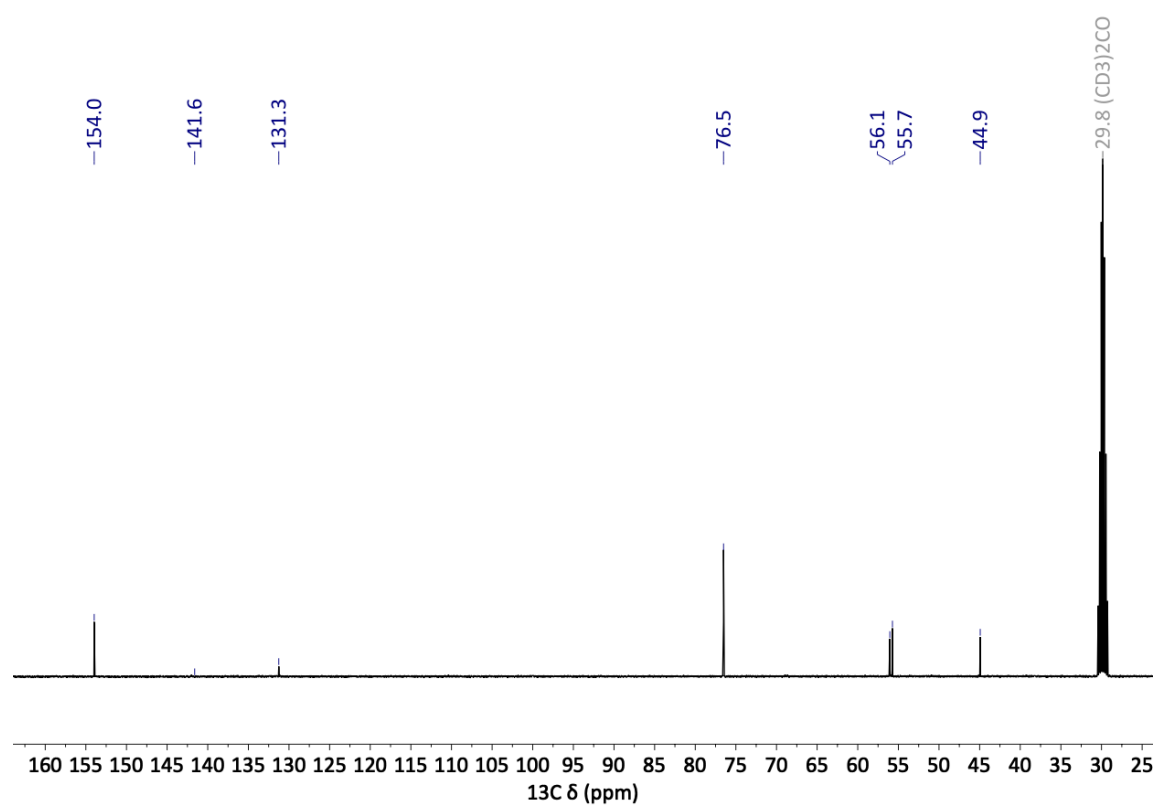


Figure 29. Carbon spectrum (^{13}C) of compound 9A.

2 Oxetanes based on LLM-116

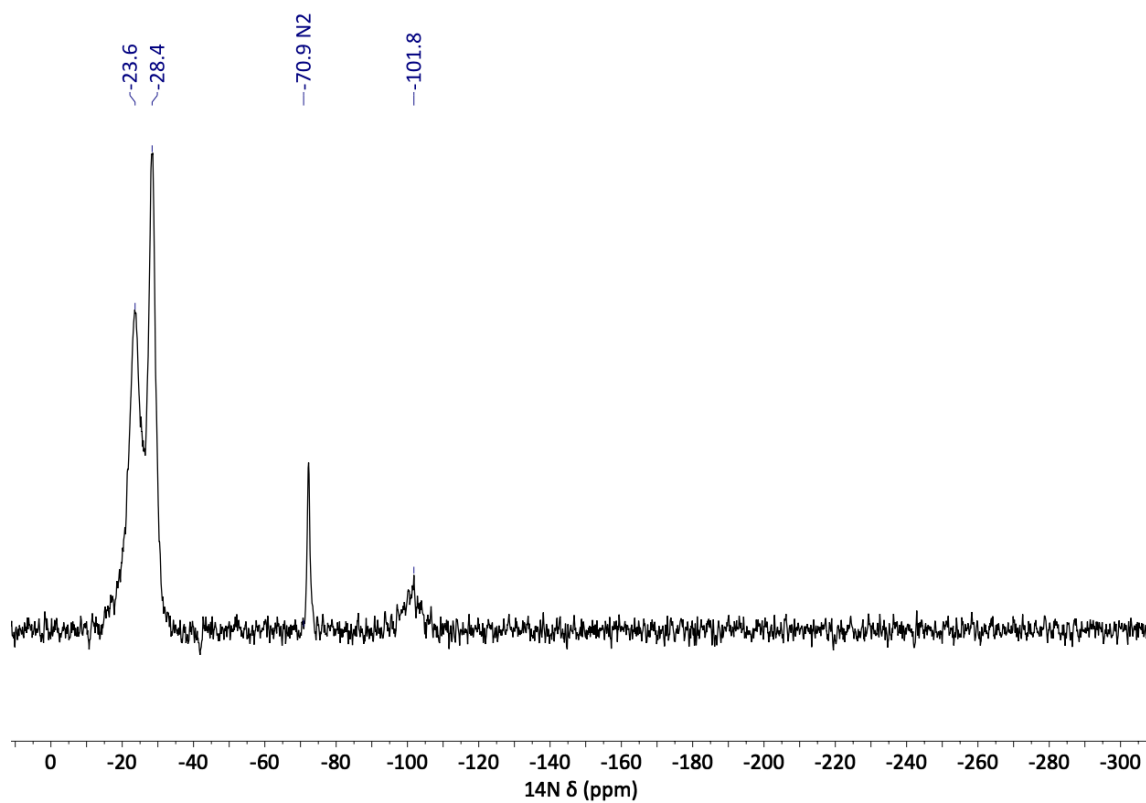


Figure 30. Nitrogen spectrum (^{14}N) of compound 9A.

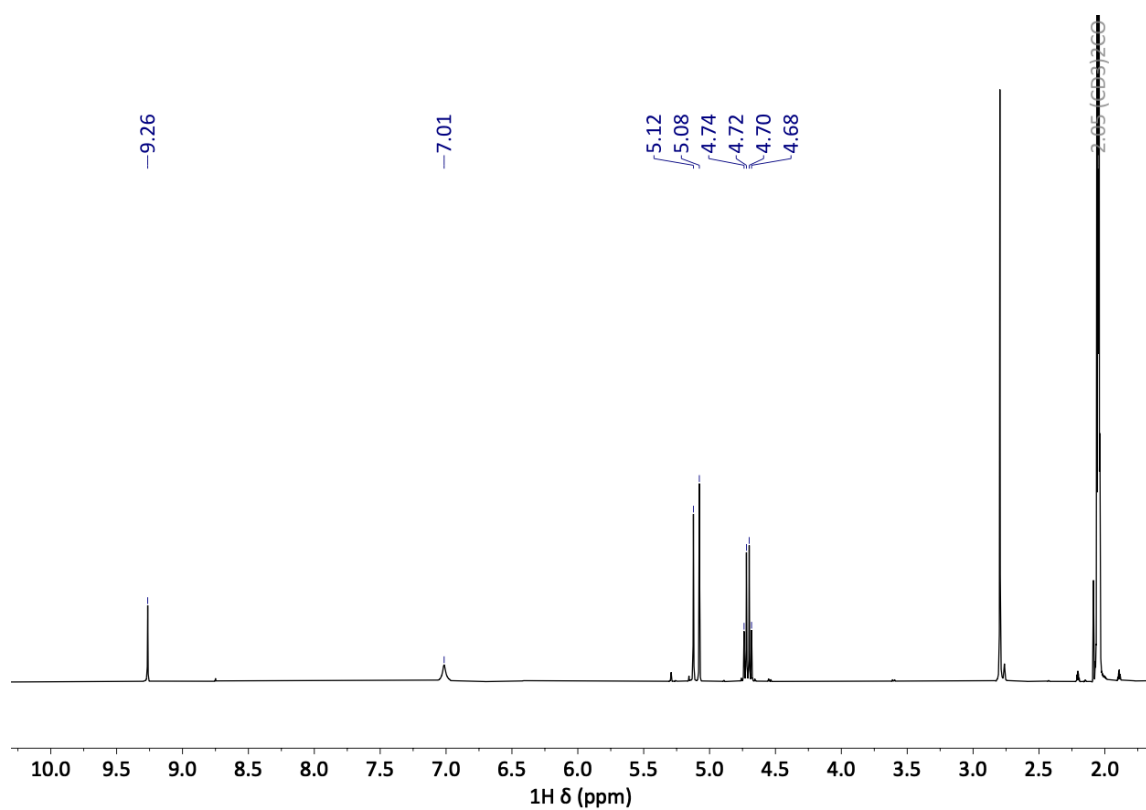


Figure 31. Proton spectrum (^1H) of compound 9B.

2 Oxetanes based on LLM-116

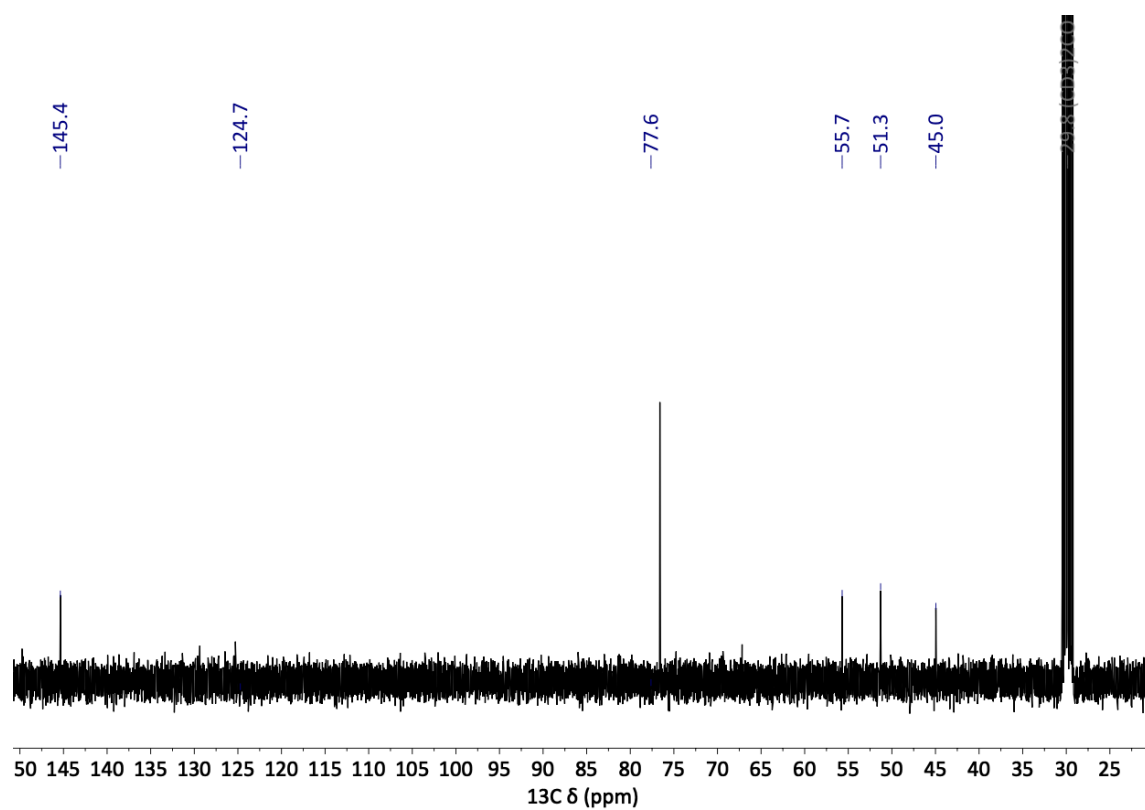


Figure 32. Carbon spectrum (^{13}C) of compound 9B.

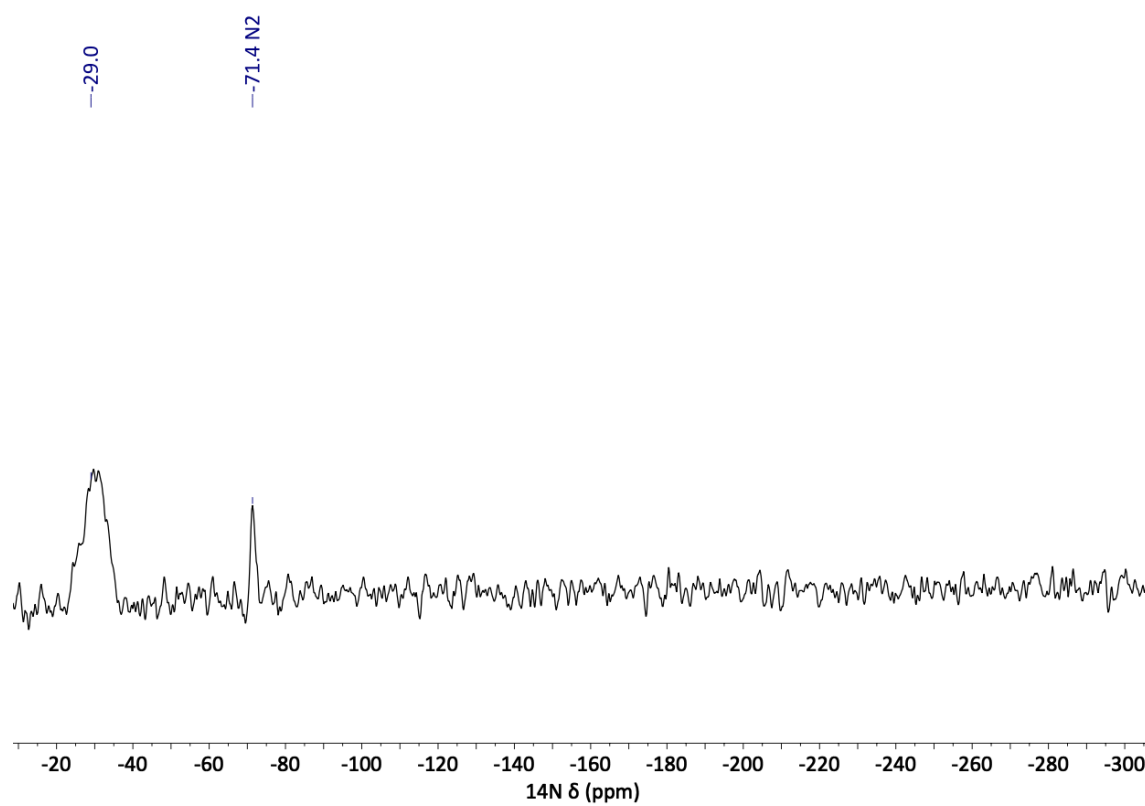


Figure 33. Nitrogen spectrum (^{14}N) of compound 9B.

2.5.3 Crystallography and Hirshfeld Analysis

Crystal structure data was obtained from an Oxford Xcalibur3 diffractometer with a Spellman generator (voltage 50kV, current 40mA) and a Kappa CCD area for data collection using Mo-K α radiation ($\lambda=0.71073\text{\AA}$) or a Bruker D8 Venture TXS diffractometer equipped with a multilayer monochromator, a Photon 2 detector and a rotation-anode generator (Mo-K α radiation). The data collection was performed using the CRYSTALIS RED software.^[32] The solution of the structure was performed by direct methods and refined by full-matrix least-squares on F² (SHELXT)^[33] implemented in the OLEX2^[34] software suite. The non-hydrogen atoms were refined anisotropically and the hydrogen atoms were located and freely refined. The absorption correction was carried out by a SCALE3 ABSPACK multiscan method.^[35] The MERCURY 2020.3.0 plots show thermal ellipsoids at the 50% probability level and hydrogen atoms are shown as small spheres of arbitrary radius. The SADABS program embedded in the Bruker APEX3 software was used for multi-scan absorption corrections in all structures.^[36] Hirshfeld analysis was performed using the CrystalExplorer17 software.^[37]

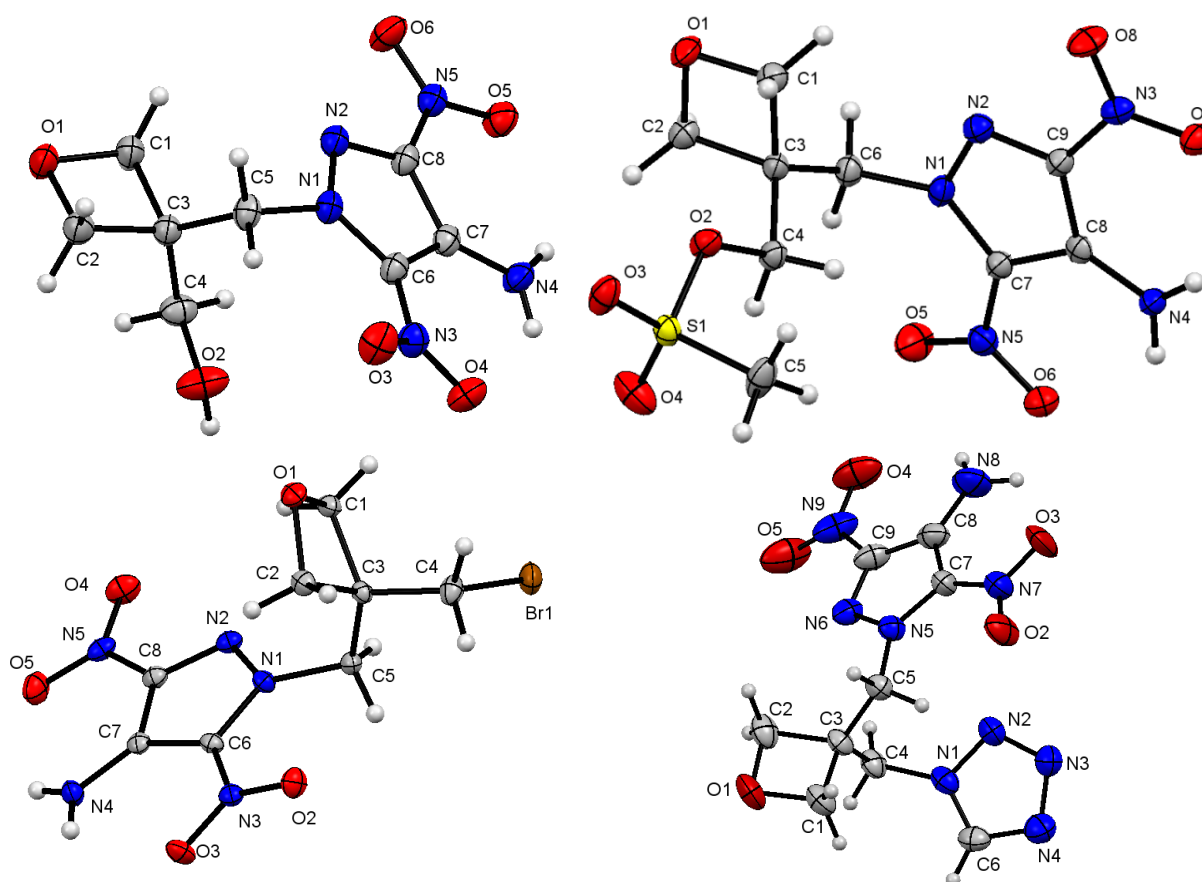


Figure 34. Molecular structures of compounds **3** (top left), **5** (top right), **6** (bottom left) and isomer **9B** (bottom right) in the crystal. Ellipsoids drawn at the 50% probability level.

(3-((4-amino-3,5-dinitro-1H-pyrazol-1-yl)methyl)oxetan-3-yl)methanol (3)

Compound **3** crystallizes in the monoclinic space group $P2_1/c$ with 4 formula units in the unit cell and a density of 1.614 g cm^{-3} at 123 K. All bond lengths are in the range of the standard bond lengths. The angles in the oxetane motif range from $91.3(1)^\circ$ (C3–C1–O1) over $91.2(1)^\circ$ (O1–C2–C3) down to $91.0(1)^\circ$ (C1–O1–C2) while the smallest angle is found at C1–C3–C2 ($85.4(1)^\circ$). The angles between the sp^3 -hybridized C3 atom and the substituents are slightly larger than ideal tetrahedral angles with $116.6(2)^\circ$ at C1–C3–C5 and $114.1(1)^\circ$ at C2–C3–C4. The oxetane ring has a puckering angle of 10.6° which is significantly higher than in the parent compound oxetane ($8.7(2)^\circ$, 140 K).^[15] The increased puckering angle is caused by the substituents in 3-position. The pyrazole motif is found to be almost planar with a torsion of only 1.8° . The nitro-groups are twisted out of the pyrazole plane with a torsion of 2.9° for the nitro group connected to C8. The other nitro group reveals a much higher torsion of 18.9° against the pyrazole plane.

(3-((4-amino-3,5-dinitro-1H-pyrazol-1-yl)methyl)oxetan-3-yl)methyl methanesulfonate (5)

Compound **5** crystallizes in the monoclinic space group $P2_1/c$ with 4 formula units in the unit cell and a density of 1.716 g cm^{-3} at 123 K. All bond lengths are in the range of the standard bond lengths. The angles in the oxetane ring range from $91.8(2)^\circ$ () over $91.5(2)^\circ$ to $91.4(2)^\circ$. The smallest angle is found at C1–C3–C2 ($85.3(2)^\circ$). As expected, deviance from the ideal tetrahedral angle are found at the sp^3 -hybridized C3 atom with $115.8(2)^\circ$ at C1–C3–C6 and $116.1(2)^\circ$ at C2–C3–C4. The oxetane ring as well as the pyrazole ring are both planar. The nitro groups are only slightly twisted out of the pyrazole plane with 8.8° at C9 and 6.3° at C7 respectively. The planarity of the oxetane motif is caused by the introduction of the mesyl leaving group as the direct precursor (**3**) shows a higher puckering angle than the unsubstituted parent compound oxetane.

1-((3-(bromomethyl)oxetan-3-yl)methyl)-3,5-dinitro-1H-pyrazol-4-amine (6)

Compound **6** crystallizes in the monoclinic space group $P2_1/c$ with 4 molecules in the unit cell and a density of 1.890 g cm^{-3} at 123 K. All bond lengths are in the range of the standard bond lengths. Within the oxetane motif, a bond angle of $91.0(2)^\circ$ is found at both O1–C2–C3 and C3–C1–O1 while a slightly smaller angle is found at C1–O1–C2 ($90.2(2)^\circ$). The smallest angle is again found at C2–C3–C1 ($84.3(2)^\circ$). Surprisingly, an almost ideal tetrahedral angle of $109.0(2)^\circ$ is found at C2–C3–C4 causing the angle at C1–C3–C5 to be even larger ($121.0(2)^\circ$) than in aforementioned compounds. The oxetane motif shows an extremely strong puckering with an angle of 19.9° caused by the exchange of the mesyl group for a bromine atom. The pyrazole moiety is almost

planar. Both nitro groups are rotated out of the pyrazole plane with torsion angles of 3.5° at C8 and 7.1° at C6 respectively.

1-((3-((1*H*-tetrazol-1-yl)methyl)oxetan-3-yl)methyl)-3,5-dinitro-1*H*-pyrazol-4-amine (9B)

Compound **9B** crystallizes the monoclinic space group $P2_1/c$ with 4 formula units per unit cell and a density of 1.630 g cm⁻³ at 123 K. The angles in the oxetane ring range from 85.0(2)° at C1–C3–C2 to 91.6(2)° at C1–O1–C2. The pyrazole as well as the tetrazole motif are planar. The puckering angle of 10.2° corresponds well to the puckering angle reported by *Luger* for the unsubstituted parent compound.^[15] In the crystal structure, two molecules arrange in pairs due to strong hydrogen bonding between the amino group and the tetrazole-moiety (N3) with a distance of 2.45(5) Å. Intramolecular hydrogen bonding is found between the amino-group and a neighboring nitro group with a distance of 2.12(4) Å. These bonds are assumed the cause a stabilization of the overall compound.

Table 3. Detailed crystallographic information of compounds **3–6**.

	3	4	5	6
Formula	C ₈ H ₁₁ N ₅ O ₆	C ₈ H ₈ N ₆ O ₇	C ₉ H ₁₃ N ₅ O ₈ S	C ₈ H ₁₀ BrN ₅ O ₅
FW [g mol ⁻¹]	273.22	300.19	351.30	336.12
Crystal System	monoclinic	monoclinic	monoclinic	monoclinic
Space Group	$P2_1/c$	$P2_1/n$	$P2_1/c$	$P2_1/c$
Color / Habit	yellow block	brown block	yellow block	yellow block
Size [mm]	0.40 x 0.40 x 0.10	0.25 x 0.25 x 0.25	0.50 x 0.25 x 0.20	0.35 x 0.30 x 0.20
a [Å]	10.8018(6)	11.3896(4)	12.6134(6)	5.6775(3)
b [Å]	9.7487(4)	9.4491(3)	10.1342(4)	17.9225(8)
c [Å]	11.8318(7)	11.5447(4)	10.9720(5)	11.8409(6)
α [°]	90	90	90	90
β [°]	115.498(7)	105.683(3)	104.236(5)	101.295(5)
γ [°]	90	90	90	90
V [Å ³]	1124.58(12)	1196.20(7)	1359.44(11)	1181.53(10)
Z	4	4	4	4
ρ _{calc.} [g cm ⁻³]	1.614	1.667	1.716	1.890
μ [mm ⁻¹]	0.139	0.148	0.295	3.507
F (000)	568	616	728	672
λ _{MoKα} [Å]	0.71073	0.71073	0.71073	0.71073
T [K]	123	123	123	123
θ min-max [°]	3.473, 26.368	2.229, 30.502	2.776, 26.371	2.273, 30.505

2 Oxetanes based on LLM-116

Dataset h; k; l	-13:13; -12:11; -14:14	-16:16; -12:13; -16:13	-15:15; -12:12; -13:13	-8:8; -25:25; -16:16
Reflect. coll.	8061	12680	19746	23528
Independ. Refl.	2305	3646	2769	3586
R _{int} .	0.033	0.023	0.049	0.029
Reflection obs.	1834	3030	2301	2848
No. parameters	184	190	260	184
R1 (obs.)	0.0380	0.0296	0.0399	0.0380
wR2 (all data)	0.0975	0.0942	0.0976	0.0918
S	1.041	1.017	1.020	1.045
Resd. Dens. [e Å ⁻³]	-0.189, 0.289	-0.195, 0.419	-0.290, 0.481	-0.489, 0.933
Device Type	Oxford XCalibur3 CCD	Oxford XCalibur3 CCD	Oxford XCalibur3 CCD	Oxford XCalibur3 CCD
Solution	SHELXS-97	SHELXS-97	SHELXS-97	SHELXS-97
Refinement	SHELXL 2014-3	SHELXL 2014-3	SHELXL 2014-3	SHELXL 2014-3
Absorpt. corr. CCDC	Multi-scan 2097524	Multi-scan 2097531	Multi-scan 2097526	Multi-scan 2097528

	7	8	9A	9B
Formula	C ₁₄ H ₁₉ N ₁₁ O ₁₀	C ₈ H ₁₀ N ₈ O ₅	C ₉ H ₁₁ N ₉ O ₅	C ₉ H ₁₁ N ₉ O ₅
FW [g mol ⁻¹]	501.37	298.24	325.27	325.27
Crystal System	monoclinic	monoclinic	triclinic	monoclinic
Space Group	P2 ₁ /n	P2 ₁ /c	P-1	P2 ₁ /c
Color / Habit	yellow block	yellow plate	yellow plate	yellow block
Size [mm]	0.25 x 0.10 x 0.05	0.20 x 0.10 x 0.02	0.30 x 0.30 x 0.02	0.20 x 0.10 x 0.02
a [Å]	13.7945(8)	12.2346(9)	8.5694(8)	11.4135(10)
b [Å]	10.0128(4)	9.7192(4)	9.0576(9)	7.3682(7)
c [Å]	15.9803(11)	11.4141(8)	9.8868(10)	15.9533(13)
α [°]	90	90	111.396(9)	90
β [°]	113.001(7)	114.824(9)	106.502(9)	98.914(2)
γ [°]	90	90	102.627(8)	90
V [Å ³]	2031.7(2)	1231.85(16)	638.89(12)	1325.4(2)
Z	4	4	2	4
ρ _{calc.} [g cm ⁻³]	1.639	1.608	1.691	1.630
μ [mm ⁻¹]	0.140	0.136	0.141	0.136
F (000)	1040	616	336	672
λ _{MoKα} [Å]	0.71073	0.71073	0.71073	0.71073
T [K]	123	123	123	123

2 Oxetanes based on LLM-116

ϑ min-max [°]	2.461, 26.371	3.575, 26.368	2.415, 26.355	3.052, 26.022
Dataset h; k; l	-17:17; -12:12; -19:19	-15:15; -12:12; -7:14	-10:10; -10:11; -12:12	-14:14; -9:9; -19:19
Reflect. coll.	25112	9467	4961	18850
Independ. Refl.	4131	2509	2600	2592
R_{int}	0.078	0.058	0.025	0.090
Reflection obs.	2873	1780	1941	1649
No. parameters	341	198	221	220
R1 (obs.)	0.0534	0.0475	0.0418	0.0682
wR2 (all data)	0.1269	0.1105	0.0956	0.1301
S	1.053	1.012	1.013	1.061
Resd. Dens. [$\text{e} \text{ \AA}^{-3}$]	-0.280, 0.515	-0.266, 0.263	-0.206, 0.284	-0.257, 0.275
Device Type	Oxford XCalibur3 CCD	Oxford XCalibur3 CCD	Oxford XCalibur3 CCD	Oxford XCalibur3 CCD
Solution	SHELXS-97	SHELXS-97	SHELXS-97	SHELXS-97
Refinement	SHELXL 2014-3	SHELXL 2014-3	SHELXL 2014-3	SHELXL 2014-3
Absorpt. corr.	Multi-scan	Multi-scan	Multi-scan	Multi-scan
CCDC	2097525	2097527	2097529	2097530

Hirshfeld analysis showed stabilizing and quite strong O \cdots H interactions for compounds **4**, **7**, **8** and **9A/B** ranging from 36.1 % for compound **4** to 51.0 % for compound **8** all with a distance of 2.1 Å to 2.4 Å. Further, all investigated compounds feature stabilizing N \cdots H close contacts with a distance around 2.4 Å and population of 7.6 % for compound **8** up to 25.7 % for **9B**. Compound **4** has a high percentage of destabilizing close contacts (O \cdots O (11.3 %), O \cdots N (21.0 %) and H \cdots H (8.1 %)) compared to compounds **7**, **8** and **9A/B**, which feature fewer destabilizing interactions. Accordingly, compound **4** was found to be the most sensitive while all other compounds were found to be highly insensitive.

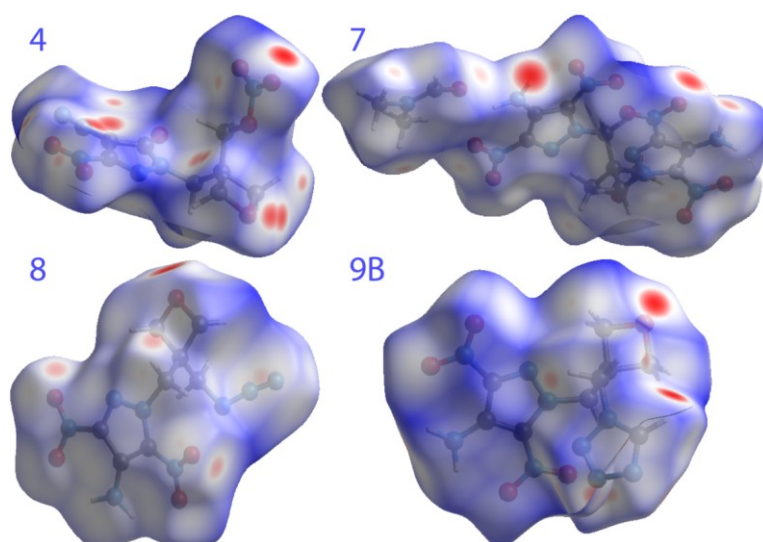


Figure 35. Enlarged depiction of the calculated Hirshfeld surfaces for compounds **4** and **7–9B**.

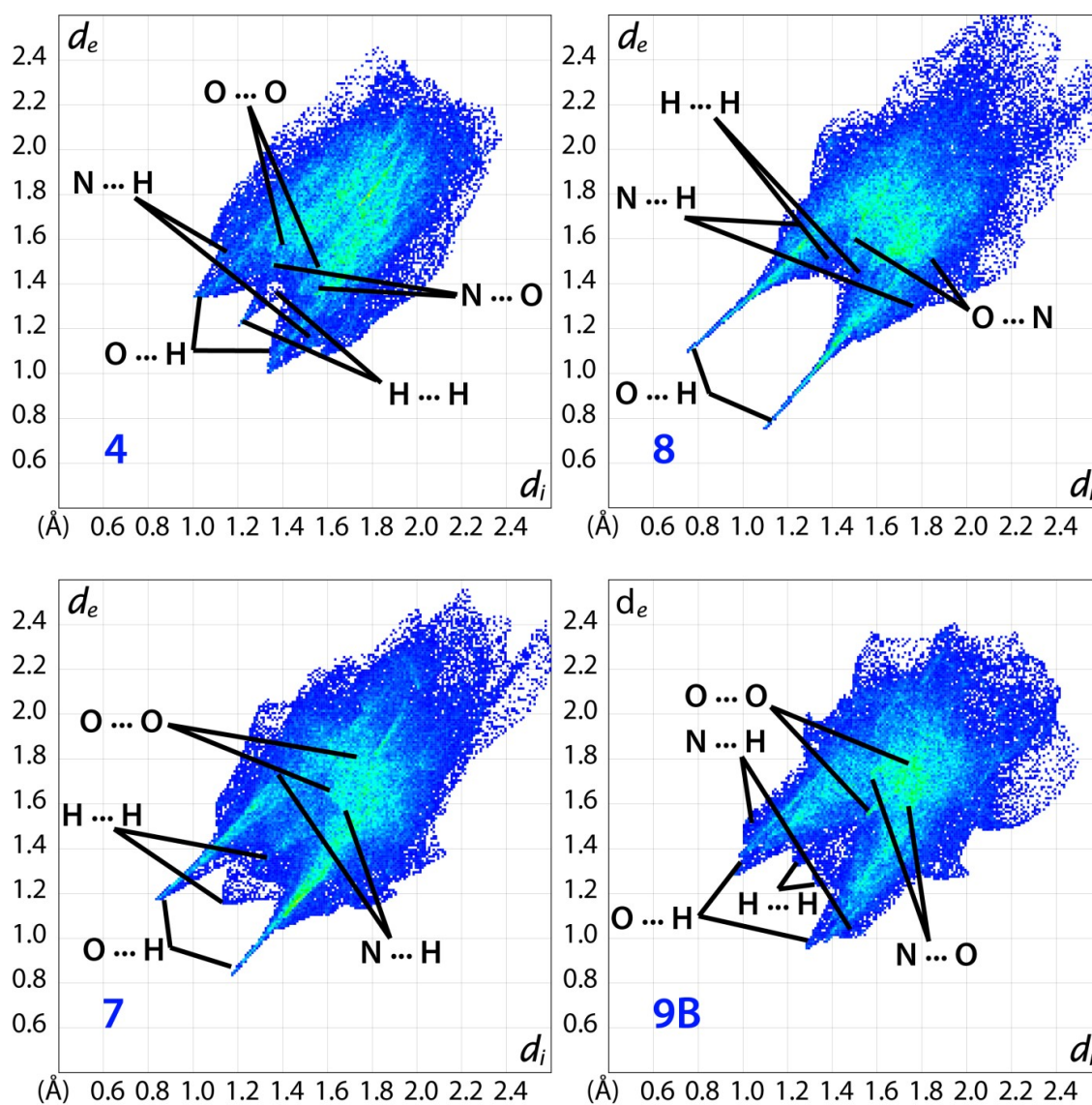


Figure 36. Enlarged depiction of obtained 2D fingerprint plots revealing close interactions.

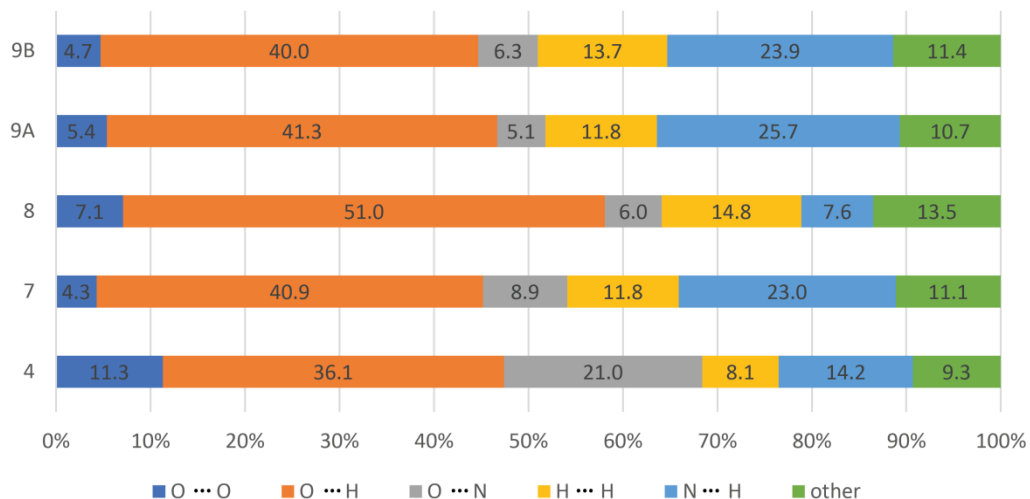


Figure 37. Interaction percentages as determined by Hirshfeld analysis.

2.5.4. Heat of Formation Calculation

The atomization method was used to determine the heat of formation of energetic target compounds (**4**, **7–9**) using the atom energies in **Table 4**.

$$\Delta_f H^\circ_{(g, M, 298)} = H_{(molecule, 298)} - \sum H^\circ_{(atoms, 298)} + \sum \Delta_f H^\circ_{(atoms, 298)}$$

Table 4. CBS-4M electronic enthalpies for atoms C, H, N and O and their literature values.

	$-H^{298} / \text{a.u.}$	$\Delta_f H^\circ_{\text{gas}} [38]$
H	0.500991	217.998
C	37.786156	716.68
N	54.522462	472.68
O	74.991202	249.18

The Gaussian16 program package was used to calculate room temperature enthalpies on the CBS-4M level of theory.^[27] In order to obtain the heat of formation for compounds **4** and **7–9**, Trouton's Rule has to be applied ($\Delta H_{\text{sub}} = 188 \cdot T_m$).

Table 5. Heat of formation calculation results for all target compounds (**4**, **7**, **8**, **9A/B**).

M	$-H^{298} [a]$ [a.u.]	$\Delta_f H^\circ(g, M) [b]$ [kJ mol ⁻¹]	$\Delta_{\text{sub}} H^\circ (M) [c]$ [kJ mol ⁻¹]	$\Delta_f H^\circ(s) [d]$ [kJ mol ⁻¹]	Δn	$\Delta_f U(s) [e]$ [kJ kg ⁻¹]
4	1162.892687	184.4	69.2498	115.2	-10.5	470.3
7	1648.381352	202.8	97.6002	105.2	-15.5	335.4
8	1123.216883	385.6	70.3402	315.3	-11.5	1152.7

9A (N1)	1216.578143	344.6	81.6202	263.0	-12.5	903.8
9B (N2)	1216.564679	379.9	96.1526	283.8	-12.5	967.8

[a] CBS-4M electronic enthalpy; [b] gas phase enthalpy of formation; [c] sublimation enthalpy; [d] standard solid-state enthalpy of formation; [e] solid state energy of formation.

2.5.5 Thermal Analysis

The thermal behavior of target compounds (**4**, **7**, **8**, **9A/B**) and all precursors was analyzed by differential scanning calorimetry (DSC) at a heating rate of $5^{\circ}\text{C min}^{-1}$. The obtained thermograms and respective evaluations are depicted.

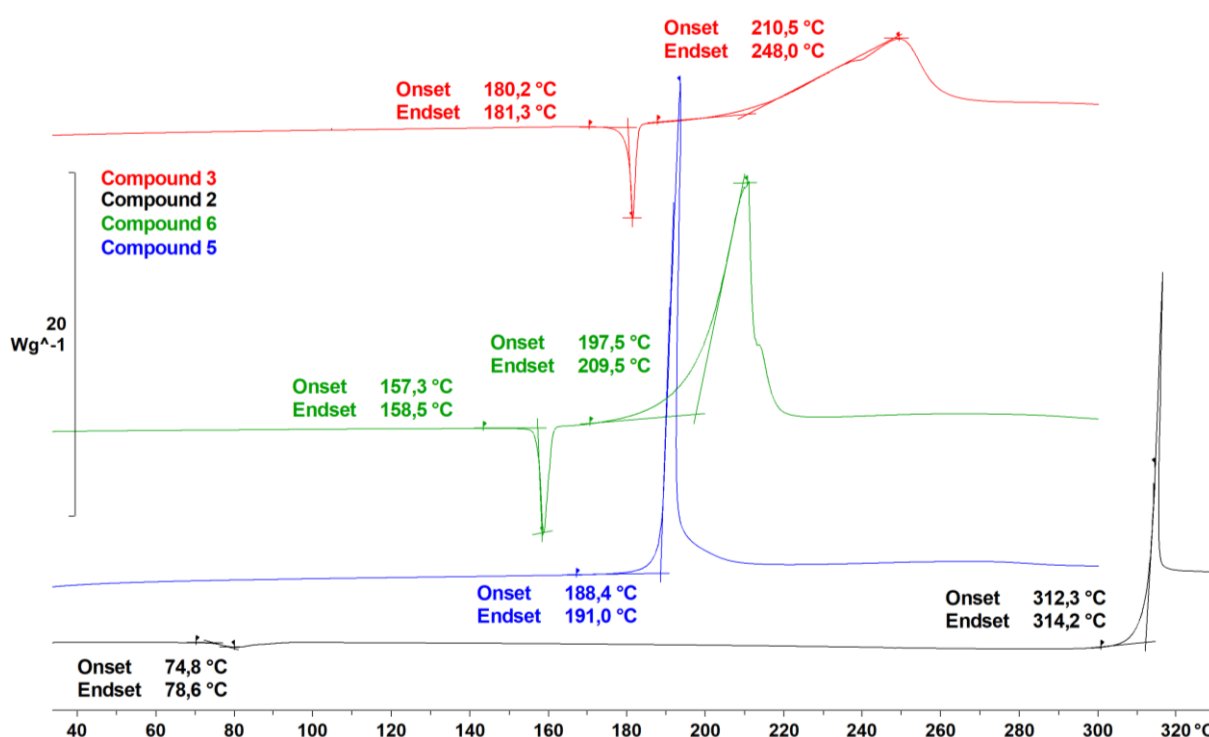


Figure 38. DSC evaluation of energetic precursor compounds (**2**, **3**, **5**, **6**).

2.5.6 Performance Calculation for State-of-the-art Monomers (Comparison)

To facilitate a performance comparison of obtained compounds with the prior art in the field of energetic oxetanes, the performance of the most prevalent oxetane monomers was calculated using the EXPLO5 V6.04 thermochemical code. For this purpose, the heats of formation were calculated as described in the previous section. Aforementioned prior art is mainly made up by the organic azides 3-azidomethyl-3-methyloxetane (AMMO), 3,3-bis(azidomethyl)oxetane (BAMO) and the less known 3-azidooxetane (3AO). The most well-known organic nitrate is 3-nitratomethyl-3-methyloxetane (NIMMO) among the less prevalent direct comparison nitrates

2 Oxetanes based on LLM-116

3-nitratooxetane (3NO) and 3-azidomethyl-3-nitratomethyloxetane (AMNMO). In direct comparison to compound **7**, it becomes evident that the latter is superior in all relevant parameters such as detonation velocity, detonation pressure, thermostability and sensitivity (**Table 6**).

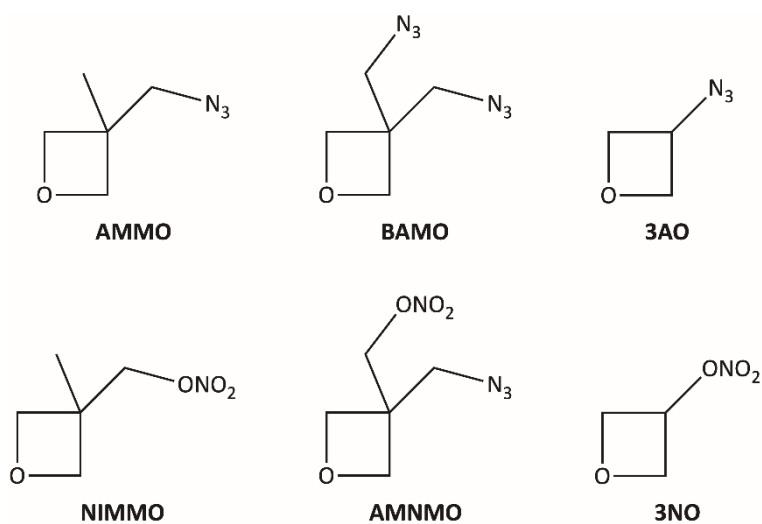


Figure 39. Molecular structures of the most prevalent energetic oxetane monomers (state of the art).

Table 6. Physicochemical and energetic properties of AMMO, BAMO, 3AO NIMMO and AMNMO as state-of-the-art monomers in comparison to compound 7.

	AMMO	BAMO	3AO	NIMMO	3NO^[39]	AMNMO	7
Formula	C ₅ H ₉ N ₃ O	C ₅ H ₈ N ₆ O	C ₃ H ₅ N ₃ O	C ₅ H ₉ NO ₄	C ₃ H ₅ NO ₄	C ₅ H ₈ N ₄ O ₄	C ₁₁ H ₁₂ N ₁₀ O ₉
FW [g·mol ⁻¹]	127.15	168.16	99.09	147.13	119.08	188.14	428.28
IS ^[a] [J]	> 40	40	3	> 40	40	7	>40
FS ^[b] [N]	360	360	>192	360	>360	288	>360
Ω ^[c] [%]	-106.96	-76.12	-72.7	-59.81	-20.15	-42.52	-29.9
T _m ^[d] / T _b ^[e] / T _{dec} ^[f] [°C]	-/178/210	-/-/207.3	-/140/190	-13.8/-/170.3	-/-/153	-12.4/-/178.2	-/-/246
ρ ^[g] [g·cm ⁻³]	1.05	1.23	1.18	1.19	1.34	1.33	1.70
ΔH _f ^[h] [kJ·mol ⁻¹]	148.3	510.5	225.6	-268.9	-168.0	93.8	105.2
EXPLO5 V6.04							
-Δ _E U ^[i] [kJ·kg ⁻¹]	3411	4479	4520	3949	5089	4768	4206
T _{C-J} ^[j] [K]	2086	2786	2813	2507	3394	3129	2981
p _{C-J} ^[k] [GPa]	7.69	12.4	11.5	10.6	16.6	15.2	20.9
D _{C-J} ^[l] [m·s ⁻¹]	5544	6548	6307	5906	6771	6729	7335
V ₀ ^[m] [dm ³ ·kg ⁻¹]	803	797	820	827	829	817	710

[a] Impact sensitivity (BAM drophammer, method 1 of 6); [b] friction sensitivity (BAM drophammer, method 1 of 6); [c] Oxygen balance regarding carbon monoxide ($\Omega_{CO} = (nO - xC - yH/2)(1600/FW)$); [d] melting point (DSC, $\beta = 5 \text{ }^\circ\text{C}\cdot\text{min}^{-1}$); [e] boiling point (DSC, $\beta = 5 \text{ }^\circ\text{C}\cdot\text{min}^{-1}$); [f] decomposition temperature (DSC, $\beta = 5 \text{ }^\circ\text{C}\cdot\text{min}^{-1}$); [g] density at 298 K; [h] standard molar enthalpy of formation; [i] detonation energy; [j] detonation temperature; [k] detonation pressure; [l] detonation velocity; [m] volume of detonation gases at standard temperature and pressure conditions.

2.5.7 Practical Tests

Hot-plate test

A hot-plate test was performed by placing 50 mg of each target compound on a copper plate prior to heating with a bunsen burner. Compounds **4** and **8** show a violent deflagration while compound **7** partially sublimates before it ignites. Compound **9** thermally decomposes without visible flame.



Figure 40. Deflagration of compound **4**.



Figure 41. Violent deflagration of compound **8**.



Figure 42. Partial sublimation of compound **7** prior to ignition.

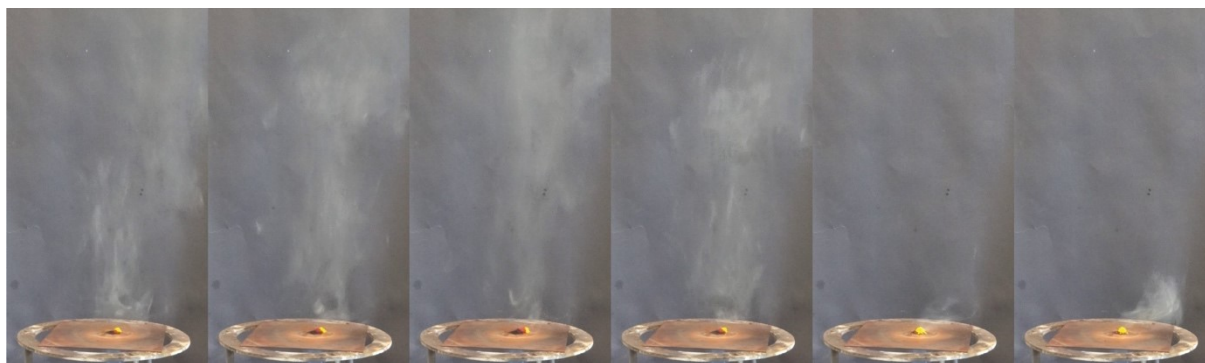


Figure 43. Decomposition of compound 9 (isomeric mixture) without visible flame.

SSRT (small-scale reactivity test)

The small-scale reactivity tests were performed as described and the dents volume of each aluminum witness plate was measured using a 3D profilometer.



Figure 44. Aluminum witness blocks and indentation caused by the respective compound (4, 7, 8, 9).

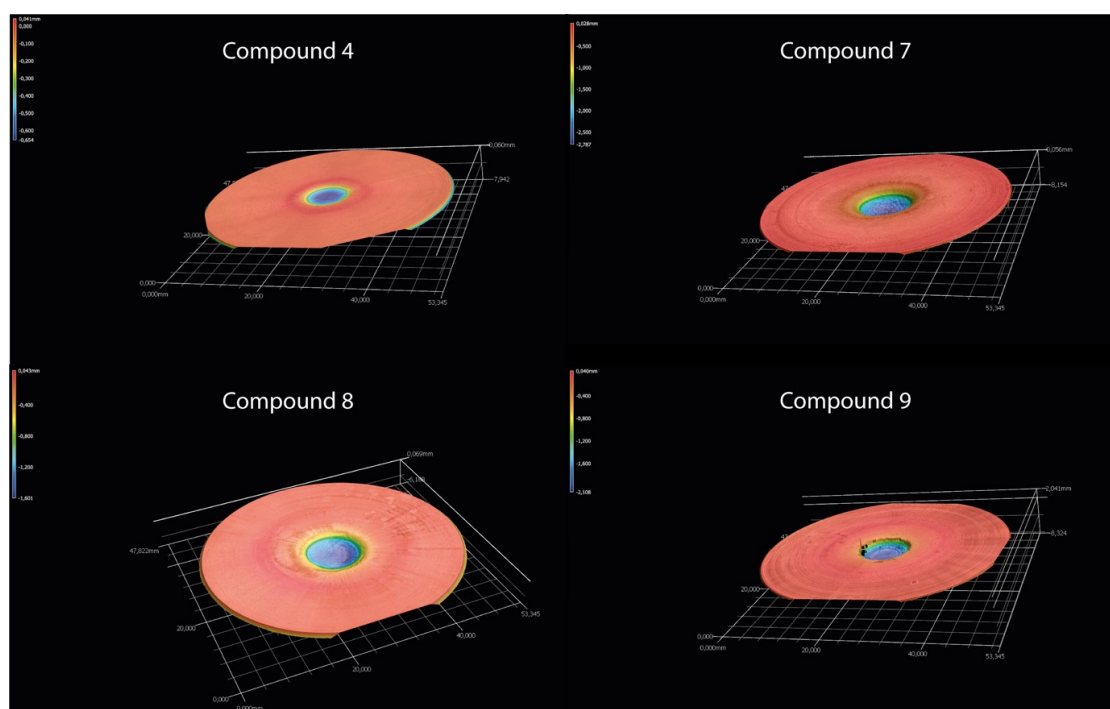


Figure 45. Dent volume determination using a 3D profilometer.

Initiation test

The initiation tests were performed as described in the main document.



Figure 46. Negative test results using neat lead azide (left) and bottom of the respective witness plates (right).

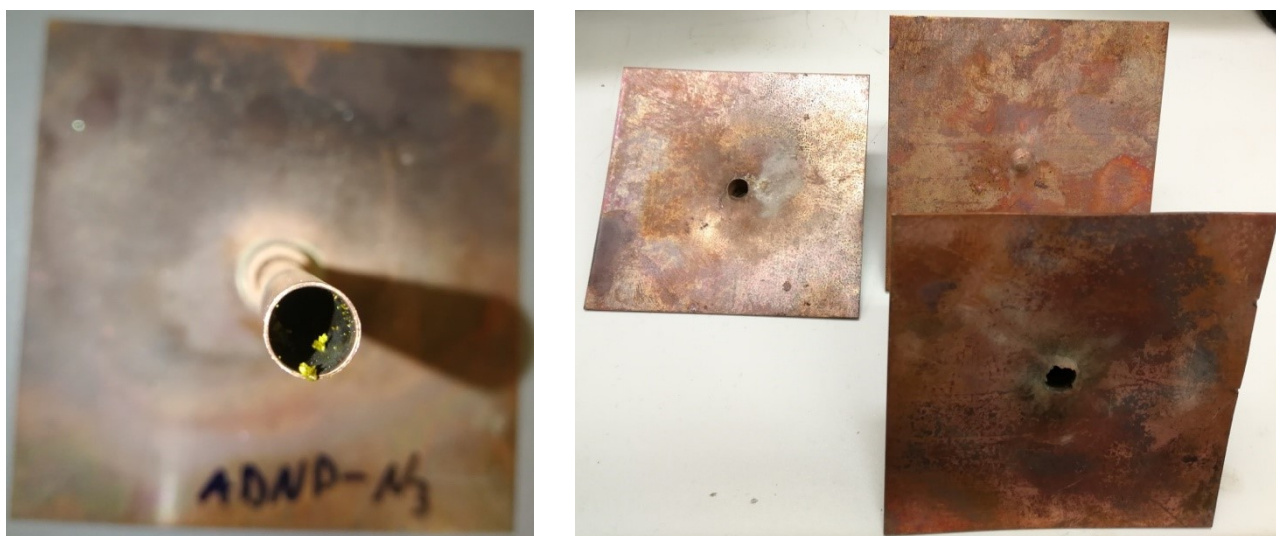


Figure 47 Unaffected material (compound **8**) after detonation of 50 mg lead azide (left) and witness plates after successful initiation using PETN as booster charge.

2.6 References

- [1] H. G. Ang, S. Pisharath, *Energetic Polymers: Binders and Plasticizers for Enhancing Performance*; Wiley-VCH, Germany, **2012**.
- [2] T. M. Klapötke, *Chemistry of High-Energy Materials*, 5th ed., deGruyter, Berlin/Boston, **2019**.
- [3] M. S. Kirshenbaum, L. Avrami, B. Strauss, *Sensitivity Characterization of low vulnerability (LOVA) propellants*, US Army Armament Research and Development Command, **1983**.
- [4] G. E. Manser, A. A. Malik, T. G. Archibald, *3-Azidomethyl-3-Nitratomethyloxetane*. US 5489700, **1996**.
- [5] M. P. Dreyfuss, P. Dreyfuss, *Oxetane Polymers*. In *Encyclopedia of Polymer Science and Technology*, (Ed.), John Wiley & Sons: Hoboken, New Jersey, **2011**.
- [6] V. M. Vinogradov, T. I. Cherkasova, I. L. Dalinger, S. A. Shevelev, *Russ. Chem. Bull.* **1993**, *42*, 1552.
- [7] S. Ek, N. V. Latypov, *J. Heterocycl. Chem.* **2014**, *51*, 1621.
- [8] T. M. Klapötke, *Energetic Materials Encyclopedia*; DeGruyter: Berlin/Boston, **2021**.
- [9] Y. Zhang, Y. Huang, D. A. Parrish, J. M. Shreeve, *J. Mater. Chem.* **2011**, *21*, 6891.
- [10] D. Fischer, J. L. Gottfried, T. M. Klapötke, K. Karaghiosoff, J. Stierstorfer, T. G. Witkowski, *Angew. Chem. Int. Ed.* **2016**, *55*, 16132.
- [11] M.-X. Zhang, P. F. Pagoria, G. H. Imler, D. J. Parrish, *Heterocycl. Chem.* **2019**, *56*, 781.
- [12] L. Dalinger, I. T. Cherkasova, A. Shevelev, *Mendeleev Commun.* **1997**, *7* (2), 58-59.
- [13] A. G. Orpen, L. Brammer, F. H. Allen, O. Kennard, D. G. Watson, R. Taylor, *Struct. Correl.* **1994**, p 752.
- [14] P. F. de Athayde-Filho, J. Miller, A. M. Simas, B. F. Lira, J. A. de Souza Luis, J. Zuckerman-Schpector, *Synthesis* **2003**, *5*, 685.
- [15] P. Luger, J. Buschmann, *J. Am. Chem. Soc.* **1984**, *106*, 7118.
- [16] J. Zhang, Q. Zhang, T. T. Vo, D. A. Parrish, J. M. Shreeve, *J. Am. Chem. Soc.* **2015**, *137*, 1697.
- [17] M. Reichel, D. E. Dosch, T. M. Klapötke, K. Karaghiosoff, *J. Am. Chem. Soc.* **2019**, *141*, 19911.
- [18] M. Reichel, M. Born, D. E. Dosch, T. M. Klapötke, K. Karaghiosoff *Cryst. Growth Des.* **2021**, *21*, 243.
- [19] M. A. Spackman, D. Jayatilaka, *CrystEngComm* **2009**, *11*, 19.
- [20] J. J. McKinnon, M. A. Spackman, A. S. Mitchell, *Acta Crystallographica Section B* **2004**, *60*, 627.
- [21] M. J. Turner, J. J. McKinnon, S. K. Wolff, D. J. Grimwood, P. R. Spackman, D. Jayatilaka, M. A. Spackman, *CrystalExplorer17* (**2017**). University of Western Australia. <https://hirshfeldsurface.net>.
- [22] M. A. Spackman, J. J. McKinnon, *CrystEngComm* **2002**, *4*, 378.
- [23] T. Keicher, S. Löbbecke, *Organic Azides*; John Wiley & Sons: Hoboken, New Jersey, **2010**.
- [24] R. D. Schmidt, G. S. Lee, P. F. Pagoria, A. R. Mitchell, R. Gilardi, *J. Heterocycl. Chem.* **2001**, *38*, 1227.
- [25] J. E. Felts, H. W. Sandusky, R. H. Granholm, In *AIP Conference Proceedings 2009*, American Institute of Physics, Vol. 1195, pp 233–236.
- [26] R. Meyer, J. Köhler, A. Homburg *Explosives*, 6th ed.; Wiley-VCH: Weinheim, **2007**.

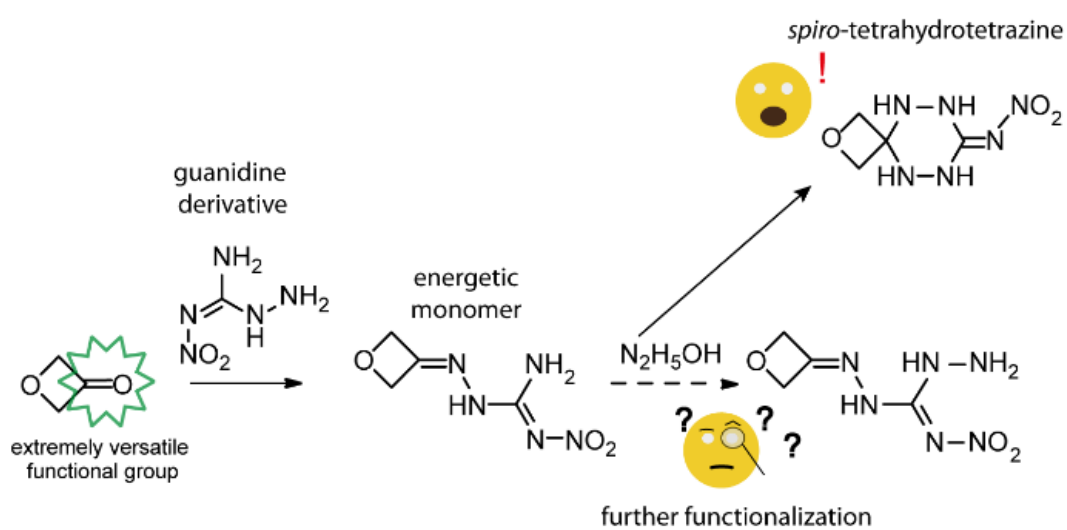
- [27] M. J. Frisch, G. W. Trucks, H. B. Schlegel, G. E. Scuseria, M. A. Robb, J. R. Cheeseman, G. Scalmani, V. Barone, G. A. Petersson, H. Nakatsuji, X. Li, M. Caricato, A. V. Marenich, J. Bloino, B. G. Janesko, R. Gomperts, B. Mennucci, H. P. Hratchian, J. V. Ortiz, A. F. Izmaylov, J. L. Sonnenberg, D. Williams-Young, F. Ding, F. Lipparini, F. Egidi, J. Goings, B. Peng, A. Petrone, T. Henderson, D. Ranasinghe, V. G. Zakrzewski, J. Gao, N. Rega, G. Zheng, W. Liang, M. Hada, M. Ehara, K. Toyota, R. Fukuda, J. Hasegawa, M. Ishida, T. Nakajima, Y. Honda, O. Kitao, H. Nakai, T. Vreven, K. Throssell, J. A. Montgomery, Jr., J. E. Peralta, F. Ogliaro, M. J. Bearpark, J. J. Heyd, E. N. Brothers, K. N. Kudin, V. N. Staroverov, T. A. Keith, R. Kobayashi, J. Normand, K. Raghavachari, A. P. Rendell, J. C. Burant, S. S. Iyengar, J. Tomasi, M. Cossi, J. M. Millam, M. Klene, C. Adamo, R. Cammi, J. W. Ochterski, R. L. Martin, K. Morokuma, O. Farkas, J. B. Foresman, D. J. Fox, Gaussian16, Gaussian, Inc., Wallingford, CT, USA, **2016**.
- [28] T. Altenburg, T. M. Klapötke, A. Penger, J. Stierstorfer, *Z. Anorg. Allg. Chem.* **2010**, 636, 463.
- [29] NATO Standardization Office, NATO STANAG 4489: Explosives. Impact Sensitivity Tests, **1999**.
- [30] NATO Standardization Office, NATO STANAG 4487: Explosives. Friction Sensitivity Tests, **2002**.
- [31] United Nations (UN), UN Recommendations on the Transport of Dangerous Goods, Manual of Tests and Criteria, **2009**.
- [32] CrysAlisPro, Oxford Diffraction Ltd., *version 171.33.41*, **2009**.
- [33] G. M. Sheldrick, *Acta Cryst.*, **2015**, A71, 3 – 8.
- [34] O. V. Dolomanov, L. J. Bourhis, R. J. Gildea, J. A. K. Howard, H. Puschmann, *J. Appl. Cryst.*, **2009**, 42, 339–341.
- [35] *SCALE3 ABSPACK – An Oxford Diffraction program* (1.0.4, gui: 1.0.3), Oxford Diffraction Ltd., **2005**.
- [36] *APEX3*. Bruker AXS Inc., Madison, Wisconsin, USA.
- [37] M. J. Turner, J. J. McKinnon, S. K. Wolff, D. J. Grimwood, P. R. Spackman, D. Jayatilaka and M. A. Spackman, *CrystalExplorer17* (2017). University of Western Australia. <https://hirshfeldsurface.net>.
- [38] M. W. Chase, NIST-JANAF Thermochemical Tables, Fourth Edition, *J. Phys. Chem. Red. Data, Monograph 9*, **1998**, 1.
- [39] M. Born, T. C. Fessard, L. Göttemann, T. M. Klapötke, J. Stierstorfer and M. Voggenreiter, *Chem. Comm.* **2021**, 57, 2804–2807.

3 Spiro Oxetanes

Energetic but insensitive spiro-tetrahydrotetrazines based on oxetane-3-one

Thomas C. Fessard, Ivan Gospodinov, Thomas M. Klapötke, Jörg Stierstorfer and Michael Voggenreiter

Accepted author manuscript, *Journal of Heterocyclic Chemistry* 2022.



3.1 Abstract

Energetic oxetanes were first described in the 1970s such as 3,3-bis(azidomethyl)oxetanes (BAMO) and 3-(nitratomethyl)-3-(methyl)oxetanes (NIMMO). Over the past few years, oxetanes were hardly available only as special purpose chemicals for the pharmaceutical industry. Oxetan-3-one is condensed with energetic compound with a hydrazino function such as amino-nitroguanidine and picryl hydrazine to form energetic Schiff bases. Hydrazinolysis of the guanidine derivatives lead to energetic spiro-tetrahydrotetrazines which are quite rare in literature. All products were characterized by their crystal structure using single crystal X-ray diffraction. Further, the new compounds were analyzed using IR, EA, DTA and multinuclear NMR spectroscopy (^1H and ^{13}C). The sensitivities towards external stimuli such as friction and impact were determined according to BAM standards and the energetic performances were calculated using the EXPLO5 code.

3.2 Introduction

In 1878, *Reboul* discovered and described oxetanes as small strained four membered heterocycles.^[1] Since then, the availability of different oxetanes greatly increased, especially due to better and new synthetic approaches.^[2-4] The pharmaceutical industry has an enormous interest in oxetanes because of the chemical similarity and stability of gem-dimethyl and carbonyl groups, resulting in better commercial availability.^[4] Oxetanes are often used as substitutes for these gem-dimethyl and also carbonyl groups in pharmaceuticals, due to their non-toxic degradation in the human body and better solubility.^[4] Some work has focused mainly on substitution in the 3-position of oxetanes, as these units are achiral and incorporation into a drug for medical use does not add a stereocenter.^[5] In 1984, *Luger* successfully characterized the unsubstituted parent compound oxetane and showed that the planar structure minimizes the ring strain.^[6] Nearly at the same time several energetic oxetanes were synthesized such as 3,3-bis(azidomethyl)oxetane (BAMO) or 3-(nitratomethyl)-3-(methyl)oxetane (NIMMO).^[7-10] These energetic oxetanes can be polymerized via cationic ring-opening polymerization (CROP) which offered the development of further energetic polymers.^[11] A good starting point for new energetic monomers is the commonly available oxetan-3-one which offers the carbonyl function as reactive site.^[5] Carbonyl functions in general are very versatile chemical functional groups (**Figure 1**) and are able to react for example with hydrogen peroxide under acidic conditions to form peroxy-compounds.^[12,13] Various addition reactions such as the addition of dinitrogen

3 Spiro Oxetanes

pentoxide to the carbonyl function to obtain unstable dinitrates ^[14,15] and the addition of trimethylsilyl cyanide or a cyanide salt to synthesize hydroxy-carbonitriles are also well reported in the literature. ^[16–18] However, oxetan-3-one is an extremely versatile building block for 3-monosubstituted and 3,3-disubstituted oxetanes as shown for the 3,3-dinitratoxetane by our group. ^[14] Another type of reaction is the addition of metal alkoxides to obtain hemiacetals. ^[19,20] The C=O double bond can also be reduced with elemental hydrogen to synthesize simple hydroxy compounds. ^[21,22] Further, carbonyl compounds can condense easily and fast to form Schiff bases under acid catalysis. ^[23–25] Herein, we report several condensation reactions of oxetan-3-one with different energetic compounds having a hydrazino function such as aminoguanidine (AQ), amino-nitroguanidine (ANQ) and picryl hydrazine (PicHy). The guanidine derivatives can be further functionalized with hydrazine.

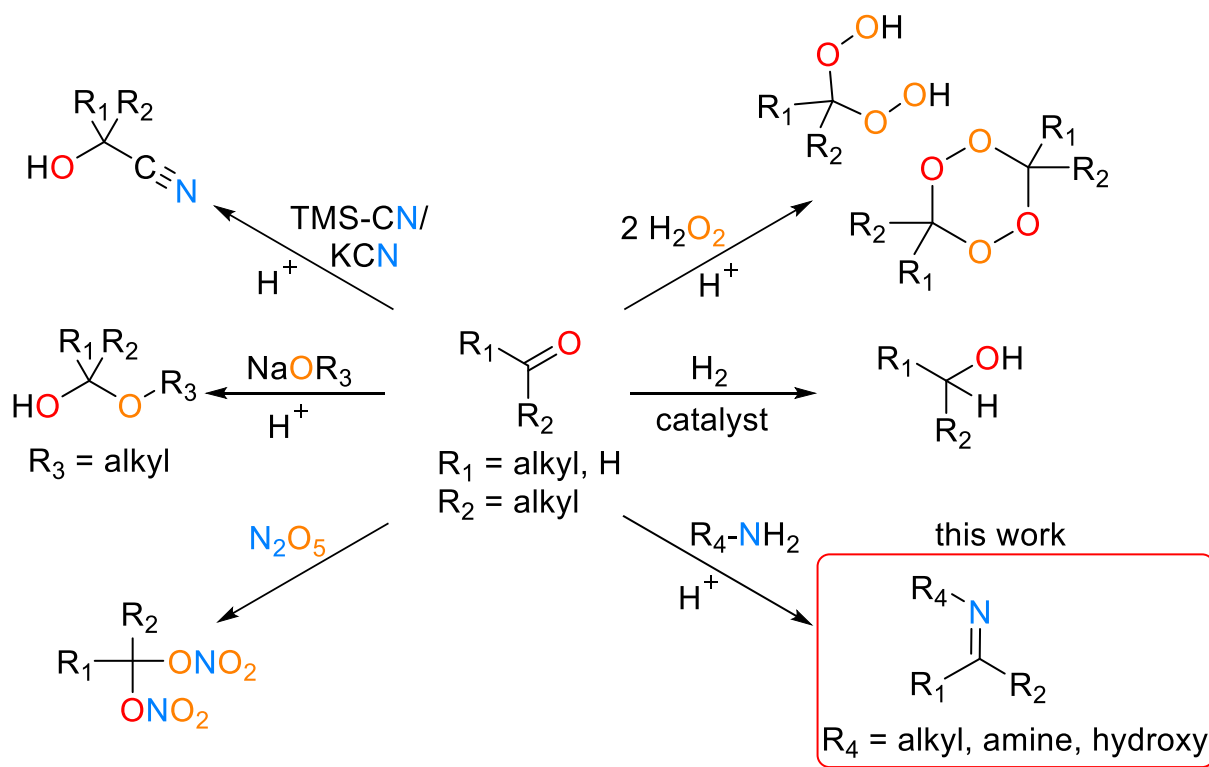
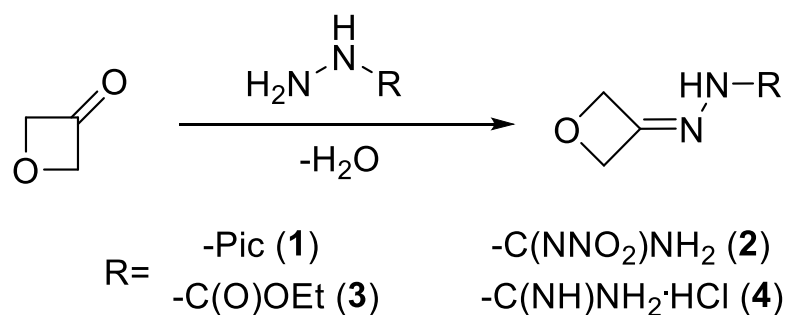


Figure 1. General reactions of carbonyl compounds with the focus on the condensation reaction to form a Schiff base in this work.

3.3 Results and Discussion

3.3.1 Synthetic Procedures

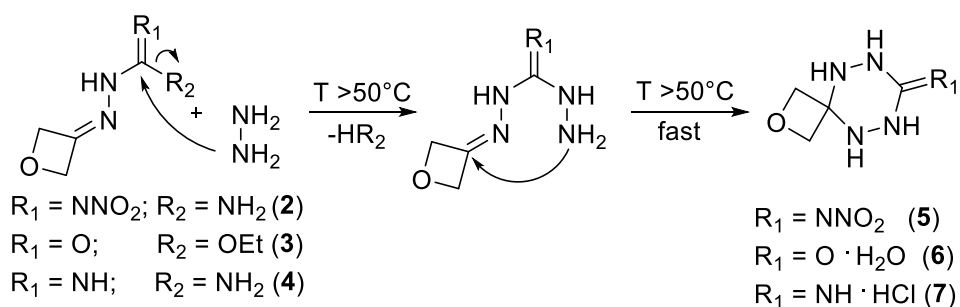
Commercially available oxetan-3-one (SpiroChemAG), aminoguanidine hydrochloride (Sigma-Aldrich) and 1,3-diaminoguanidine hydrochloride (Sigma-Aldrich) were used as received. Amino-nitroguanidine ^[26], picryl hydrazine ^[27], ethyl hydrazine carboxylate ^[28] were synthesized according to literature procedures. Oxetan-3-one was heated with picryl hydrazine in ethanol and a catalytical amount of concentrated hydrochloric acid to nearly boiling. After a short period of 5 to 10 minutes at 90°C, the mixture was cooled to room temperature and the pure orange precipitate **1** was collected in 92% yield. The same protocol can be applied for the reaction with amino-nitroguanidine, ethyl hydrazine carboxylate and aminoguanidine to obtain the corresponding colorless compounds **2–4**. (**Scheme 1**). The hydrazinolysis of compounds **2–4** did



Scheme 1. Reaction of oxetan-3-one with different compounds with a hydrazine function to obtain Schiff bases (**1–4**).

not lead to the open form compound but instead gave interesting *spiro*-1,2,4,5-tetrahydro-1,2,4,5-tetrazine derivatives (**5–7**). It is assumed, that first hydrazine cleaves the respective residue R₂ (**Scheme 2**) and the open form product is formed. In a second reaction step, the reactive hydrazine function attacks rapidly at the C=N double bond to form the thermodynamically favorable tetrazine derivative. Probably the *spiro*-tetrahydro-tetrazine formation proceeds in a concerted manner. Such derivatives are neither well present in the literature nor structurally well characterized.^[29,30] However, the reaction of oxetan-3-one with 1,3-diaminoguanidine also lead to compound **7**, probably in the same manner as the hydrazinolysis reaction of **4**.

3 Spiro Oxetanes



Scheme 2. Hydrasinolysis reaction of compounds **2–4**. Hydrazine cleaves R_2 to form the open intermediate, which then cyclizes rapidly intramolecularly to form the *spiro*-tetrahydrotetrazine derivatives (**5–7**).

3.3.2 Crystallography

A detailed crystallographic discussion can be found in the Supporting Information. Thermal ellipsoids are drawn at the 50% probability level and hydrogen atoms are shown as small spheres of arbitrary radius. The single crystals suitable for X-ray diffraction were obtained by recrystallization from ethyl acetate (**1, 2**), water (**4, 6, 7**) or methanol (**5**). Structures were deposited with the CCDC database under the following numbers: 2157490 (**1**), 2157477 (**2**), 2157480 (**4**), 2157481 (**5**), 2157478 (**6**), 2157482 (**7**).

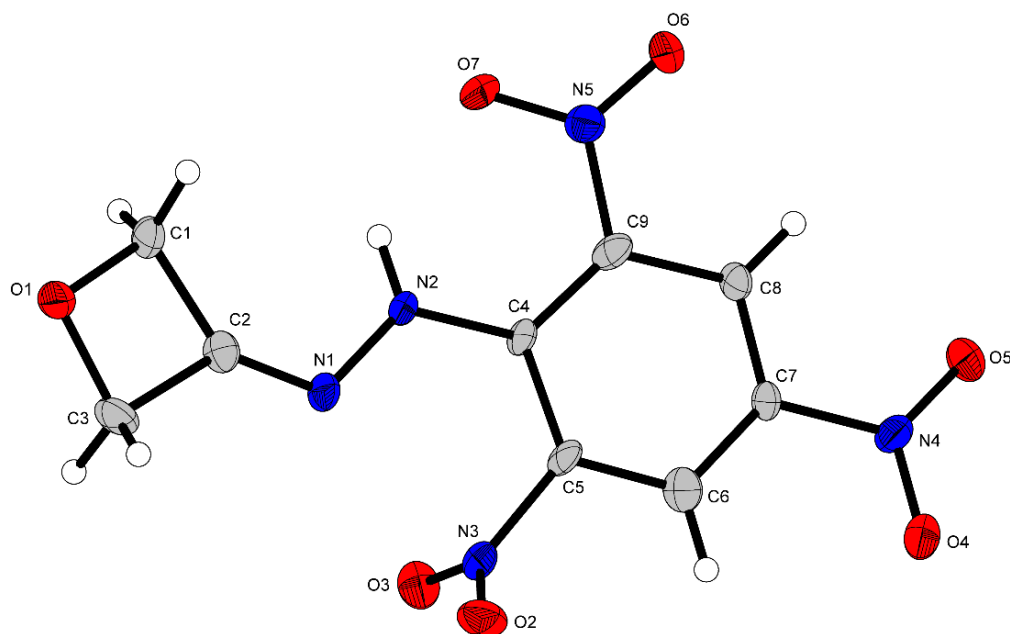


Figure 2. Crystal structure of 1-(oxetan-3-ylidene)-2-(2,4,6-trinitrophenyl)-hydrazine (**1**).

3 Spiro Oxetanes

1-(Oxetan-3-ylidene)-2-(2,4,6-trinitrophenyl)-hydrazine (**1**) crystallizes in the triclinic space group $P\bar{1}$ with 4 molecules in the unit cell and a density of 1.703 g cm^{-3} at 101 K (**Figure 2**). The bond length of C2–N1 ($1.276(6) \text{ \AA}$) is slightly shorter than typical C=N double bond ($\sim 1.30 \text{ \AA}$).^[31] N1–N2 ($1.380(5) \text{ \AA}$) is only slightly shorter than a N–N single bond ($\sim 1.41 \text{ \AA}$) and but much larger than a N=N double bond ($\sim 1.24 \text{ \AA}$).^[31] One nitro group at the *ortho*-position (O2–N3–O3) stands perpendicular ($91.0(5)^\circ$) to the aromatic ring. The other nitro group is twisted only $22.9(5)^\circ$ due to an intramolecular hydrogen bond of the hydrogen of N2 to O7 with a distance of 2.019 \AA .

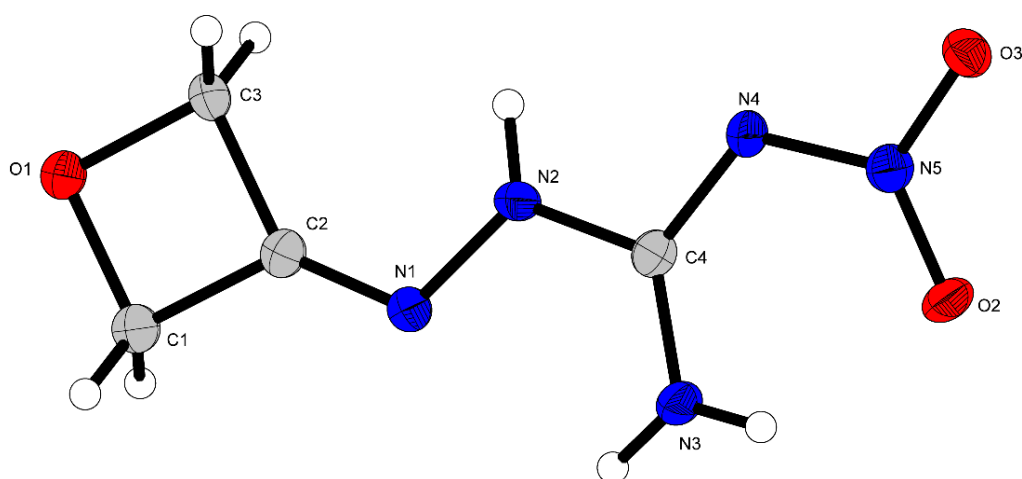


Figure 3. Molecular moiety of *N*-nitro-2-(oxetan-3-ylidene)hydrazine-1-carboximidamide (**2**).

N-nitro-2-(oxetan-3-ylidene)hydrazine-1-carboximidamide (**2**) crystallizes in the orthorhombic space group $Pna2_1$ with 4 molecules in the unit cell and a density of 1.567 g cm^{-3} at 119 K (**Figure 3**). The electrons in the nitroguanidine moiety indicate a delocalization with bond lengths of $1.307(4) \text{ \AA}$ (C4–N3), $1.366(4) \text{ \AA}$ (C4–N4), and 1.351 \AA (C4–N2). The oxetane ring has a puckering angle of 7.07° which is in the range of the reported puckering angle of Luger (8.7° at 140 K).^[6]

Compound **4** crystallizes monoclinic ($P2_1/n$) with 8 formula units in the unit cell and a density 1.465 g cm^{-3} at 119 K (**Figure 4**). The bond lengths are in the same range, as discussed for compound **2**, suggesting delocalization of electrons in the guanidine moiety. The molecule is essentially planar except the oxetane ring which is 15.66° off the planarity of the guanidine fragment. The molecules arrange themselves in the crystal as a light zig-zag pattern with an interlayer distance of 3.422 \AA .

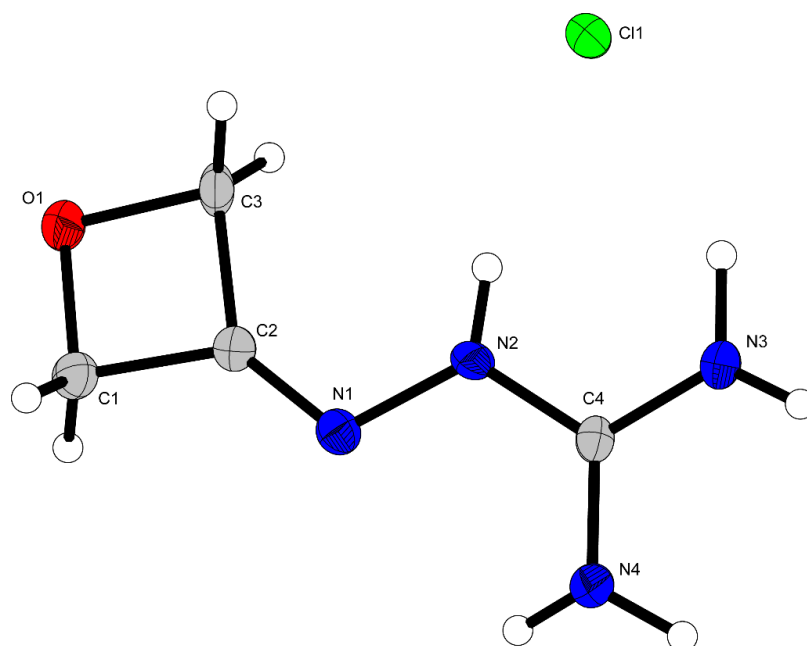


Figure 4. Crystal structure of amino(2-(oxetan-3-ylidene)hydrazineyl)-methaniminium chloride (**4**).

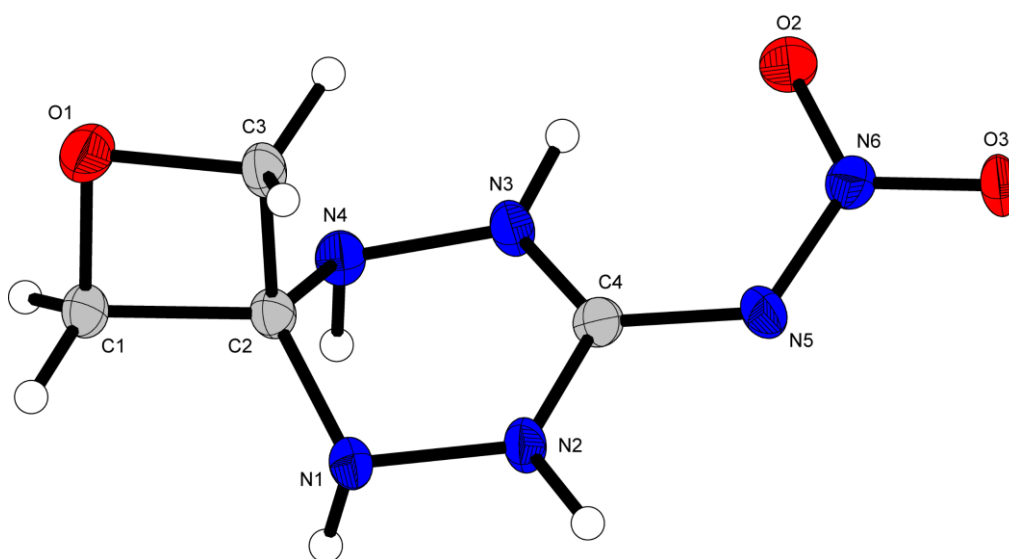


Figure 5. Crystal structure of *N*-(2-oxa-5,6,8,9-tetraazaspiro[3.5]nonan-7-ylidene)nitramide (**5**).

N-(2-oxa-5,6,8,9-tetraazaspiro[3.5]nonan-7-ylidene)nitramide (**5**) crystallizes in the monoclinic space group $I2/a$ with a density of 1.685 g cm^{-3} at 102 K which is significantly higher than the parent compound **2** with 1.567 g cm^{-3} (**Figure 5**). Further, the bond lengths at C4 is very similar to the carbon atom of the guanidine derivatives. The tetrahydropyridazine ring has a half-chair or envelope-like conformation being planar in N2–C4–N3–N4. The oxetane has a puckering of 16.38° which is larger than the reported puckering angle of 8.7° (140 K) for unsubstituted oxetane.^[6] Further, the oxetane ring stands nearly perpendicular to the tetrahydropyridazine ring (81.24°).

3 Spiro Oxetanes

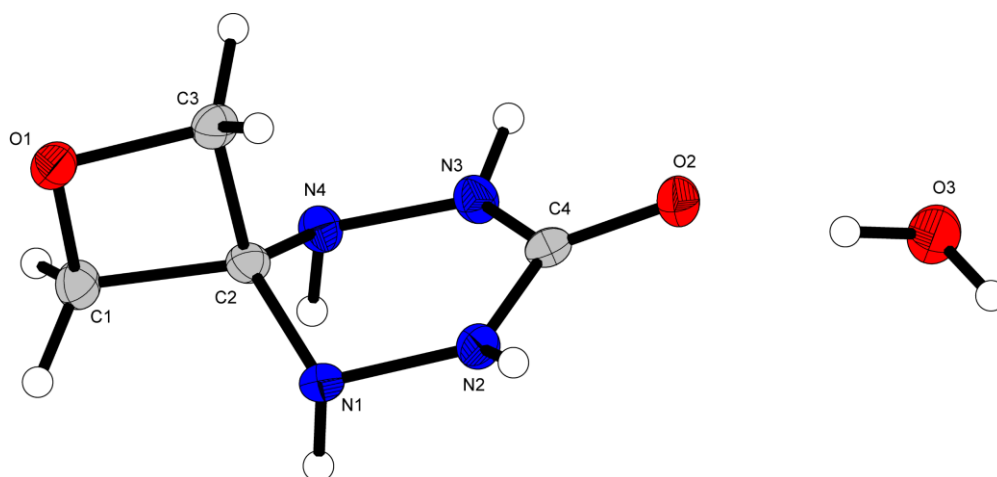


Figure 6. Crystal structure of 2-oxa-5,6,8,9-tetraazaspiro[3.5]nonan-7-one monohydrate (**6**).

2-Oxa-5,6,8,9-tetraazaspiro[3.5]nonan-7-one (**6**) crystallizes as monohydrate in the monoclinic space group $P21/n$ with 4 molecules in the unit cell and a density of 1.547 g cm^{-3} at 103 K (**Figure 6**). The bond lengths are in the same range of the lengths for **5**, except the C4–O2 which has a length of a standard C–O double bond.^[31] The tetrahydropyridazine ring features an envelope-like conformation as compound **5**. Only C2 is out of the tetrazine plane. As discussed beforehand, the oxetane ring stands approximately perpendicular to the tetrahydropyridazine ring with an angle of 84.65° . The water molecule bridges three molecules via hydrogen bond, forming a three-dimensional network.

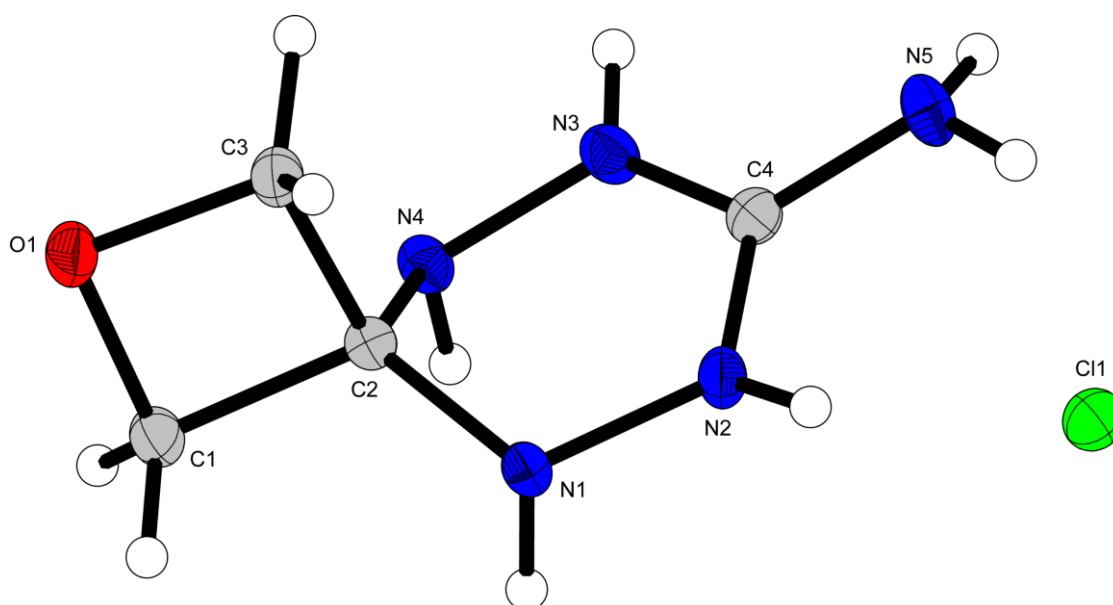


Figure 7. Crystal structure of 2-oxa-5,6,8,9-tetraazaspiro[3.5]nonan-7-imine hydrochloride (**7**).

3 Spiro Oxetanes

2-Oxa-5,6,8,9-tetraazaspiro[3.5]nonan-7-iminium chloride (**7**) crystallizes also monoclinic ($P2_1/c$) with 4 molecules in the unit cell and a density of 1.617 g cm^{-3} at 102 K (**Figure 7**). The conformation of the tetrazine moiety is also a half chair conformation with C2–N1–N2–C4 in a plane. The oxetane ring has an angle of 65.64° towards the tetrazine ring. Further, the oxetane itself has a puckering angle of 14.77° which is near the puckering angle of compound **5**.

3.3.3 Spectroscopic Analysis

For better comparison all NMR spectra were recorded using DMSO- d_6 as solvent. A detailed NMR discussion can be found in the Supporting Information. The chemical shifts of the relevant positions (^1H and ^{13}C) are summarized in **Table 1** and quoted in ppm. The methylene groups of the oxetane ring can be found around 5.20 ppm as multiplets for compounds **1–4**. The tetrahydrotetrazines **5–7** have only singlets for the oxetane CH_2 groups at around 4.30 ppm. In ^{13}C NMR, the methylene signals of the oxetane ring are found at about 80 ppm, but two signals are found for **1–4** due to the E/Z isomerism of the C=N bond, compared to only one signal for **5–7**. Furthermore, the C2 signal is found at 150 ppm except for the *spiro*-tetrahydrotetrazines which have a significant shift upfield to 67 ppm. The C4 signal is essentially unchanged for all compounds at about 153 ppm. Compounds **1–4** exhibit NH signals at around 10–11 ppm. Compounds **5–7** also have additional NH signals but now shifted upfield compared to the parent compounds.

Table 1. Comparison of the relevant NMR shifts all quoted in ppm.

	CH ₂ (oxetane)		NH	NH ₂	C2	C4
	δ ^1H	δ ^{13}C	δ ^1H	δ ^1H	δ ^{13}C	δ ^{13}C
1	5.44 (m) 5.28 (m)	80.0 79.8	10.87	-	157.1	-
2	5.27 (m)	80.4 80.0	11.34	8.78 (s) 8.41 (s)	158.3	153.4
3	5.17 (m)	80.4 80.1	10.49	-	148.2	153.7
4	5.29 (s)	80.1 79.7	11.75	7.64	155.6	153.1
5	4.33 (s)	77.2	9.73 7.08	-	67.8	152.4
6	4.29 (s)	76.9	7.78 5.03	-	67.7	154.6
7	4.33 (s)	77.1	9.76 7.09	5.86	67.8	152.4

3.3.4 Physicochemical Properties

All compounds were investigated for their physicochemical properties. The sensitivities towards impact and friction as well as their thermal decomposition temperature were determined experimentally. The enthalpies of formation for **1**, **2**, **4–7** were calculated using the atomization method on the CBS-4M level of theory in the Gaussian software suite.^[35] The detonation parameters were calculated with the program EXPLO5 V6.05 using the calculated enthalpies of formation accompanied by the densities according to the crystal structures, or in case of compound **6**, determined pycnometrically for the anhydrous compound.^[33] The calculated as well as the experimentally determined values are summarized in **Table 2** and compared to the values of BAMO.^[32] All investigated compounds are insensitive towards mechanical stimuli such as friction or impact which is also BAMO. Further, all compounds exhibit a negative oxygen balance between -29.6% for **4** to -73.0% for **7** with respect to the formation of CO. Also, compound **4** has the lowest density with 1.423 g cm^{-3} and the picryl derivative **1** as well as the nitriminotetrahydro-tetrazine **5** have the highest densities with 1.654 g cm^{-3} and 1.637 g cm^{-3} respectively. All compounds exceed the energetic performance of BAMO especially compound **5**, which has a detonation velocity of nearly 8000 m s^{-1} . The other compounds have detonation velocities in the range of 6798 m s^{-1} (**4**) to 7279 m s^{-1} (**6**). Further, the detonation pressures are in between 15.2 GPa for compound **7** and 23.2 GPa for compound **5** which is an increase of at least 23% to 87 % compared to BAMO. The synthesized molecules decompose between 151°C (**5**) to 200°C (**4**). Along the tetrahydrotetrazines, compound **6** is the most thermally stable one with a decomposition temperature of 192°C . Only compounds **1** and **3** have melting points of 170°C shortly before decomposition at 177°C and 113°C with a decomposition point of 198°C . With respect to BAMO, all compounds are almost similar in thermal stability, but do not succeed in surpassing it.

3.4 Conclusion

In this work, oxetan-3-one is utilized by the versatility of the keto function to obtain various energetic monomers suitable for ring opening polymerization. The condensation reactions to form the Schiff base compounds **1–4** are fast and work in high yields and purity. Further reaction with hydrazine of compounds **2–4** lead to unexpected but energetic *spiro*-tetrahydrotetrazines which were intensively characterized. The crystal structures of the *spiro*-tetrahydrotetrazines give more insight into the reactivity and stability among these poorly described compounds.

3 Spiro Oxetanes

Table 2. Physiochemical properties of compounds **1**, **2** and **4–7** compared to **BAMO**.^[32]

	1	2	4	5	6	7	BAMO ^[32]
Formula	C ₉ H ₇ N ₅ O ₇	C ₄ H ₇ N ₅ O ₃	C ₄ H ₉ N ₄ OCl	C ₄ H ₈ N ₆ O ₃	C ₄ H ₈ N ₄ O ₂	C ₄ H ₁₀ N ₅ OCl	C ₅ H ₈ N ₆ O
<i>FW</i> [g·mol ⁻¹]	297.2	173.1	164.4	188.2	162.1	179.6	168.2
<i>IS</i> ^{a)} [J]	>40	>40	>40	>40	>40	>40	40
<i>FS</i> ^{b)} [N]	>360	>360	>360	>360	>360	>360	360
<i>N+O</i> ^{c)} [%]	61.3	68.2	43.8	70.2	64.2	47.9	59.5
Ω_{CO} ^{d)} [%]	-29.6	-41.6	-73.0	-42.5	-59.2	-71.3	-76.1
<i>T_m</i> ^{e)} / <i>T_{dec}</i> ^{f)} [°C]	170/177	-/191	-/200	-/151	-/192	-/168	-/207
ρ ^{g)} [g·cm ⁻³]	1.654	1.526	1.423	1.637	1.57*	1.571	1.23
$\Delta_f H^\circ$ ^{h)} [kJ·mol ⁻¹]	238.1	107.8	323.8	223.1	-71.3	-17.4	510.5
EXPLO5 V6.05 ^[33]							
$-\Delta_E U^\circ$ ⁱ⁾ [kJ kg ⁻¹]	4919	4234	4100	4650	2745	2084	4479
<i>T_{C-J}</i> ^{j)} [K]	3424	2848	2773	2952	1930	1712	2786
ρ_{C-J} ^{k)} [GPa]	20.2	18.1	17.3	23.2	17.3	15.2	12.4
<i>D_{C-J}</i> ^{l)} [m·s ⁻¹]	7062	7146	6798	7989	7279	6821	6548
<i>V₀</i> ^{m)} [dm ³ ·kg ⁻¹]	658	814	795	834	817	810	797

^{a)} Impact sensitivity (BAM drophammer, method 1 of 6). ^{b)} friction sensitivity (BAM friction tester, method 1 of 6). ^{c)} combined nitrogen and oxygen content. ^{d)} oxygen balance toward carbon monoxide ($\Omega_{CO} = (nO - xC - yH/2)(1600/FW)$). ^{e)} Melting point (DTA, $\beta = 5 \text{ }^\circ\text{C}\cdot\text{min}^{-1}$). ^{f)} temperature of decomposition (DTA, $\beta = 5 \text{ }^\circ\text{C}\cdot\text{min}^{-1}$). ^{g)} density recalculated to 298 K with the formula: $\rho_{298K} = \rho_T / [1 + \alpha_V(298 \text{ K} - T)]$ where $\alpha_V = 1.6 \times 10^{-4} \text{ K}^{-1}$.^[34] ^{h)} standard molar enthalpy of formation. ⁱ⁾ detonation energy. ^{j)} detonation temperature. ^{k)} detonation velocity. ^{l)} detonation pressure. ^{m)} volume of detonation gases at standard temperature and pressure conditions. *pycnometrically determined

3 Spiro Oxetanes

The energetic properties of the synthesized and insensitive compounds were calculated and it was shown that the nitrimino-derivatives **2** and **5** have good detonation performances, especially **5** which has a detonation velocity of nearly 8000 m s⁻¹. The major drawback is the poor thermal stability of all compounds with decomposition points below 200°C. Probably polymerization is not possible due to the reactive NH sites of the *spiro*-compounds. But in summary, all compounds are promising in the search for new energetic monomers which can be suitable for ring-opening polymerization.

For financial support of this work by Ludwig-Maximilians University (LMU), the Office of Naval Research (ONR) under grant no. ONR N00014-19-1-2078 and the Strategic Environmental Research and Development Program (SERDP) under contract no. W912HQ19C0033 are gratefully acknowledged.

3.5 Supporting Information

3.5.1 Experimental Part and General Methods

Chemicals and solvents were employed as received (SpiroChemAG, Sigma-Aldrich, TCI). ¹H and ¹³C and spectra were recorded using a Bruker AMX 400 instrument. The chemical shifts quoted in ppm refer to tetramethylsilane (¹H, ¹³C). Decomposition temperatures were determined on an OZM Research DTA 552–Ex instrument with a heating rate of 5°C min⁻¹. Infrared (IR) spectra were recorded using a Perkin-Elmer Spektrum One FT–IR instrument. Elemental analyses were performed with an Elementar Vario el by pyrolysis of the sample and subsequent analysis of formed gases. The sensitivity data were collected using a BAM (Bundesanstalt für Materialforschung) drophammer^[36] according to STANAG 4489^[37] modified instruction^[38] and a BAM friction tester^[36] according to STANAG 4487^[39] modified instruction.^[40] The classification of the tested compounds results from the 'UN Recommendations on the Transport of Dangerous Goods'.^[41]

1-(Oxetan-3-ylidene)-2-(2,4,6-trinitrophenyl)-hydrazine (**1**)

Picrylhydrazine (0.675 g 2.78 mmol, 1.0 eq.) was dissolved in ethanol (10 mL) at 40°C and 4 drops of concentrated HCl were added. Oxetan-3-one (0.200 g, 2.78 mmol, 1.0 eq.) was added dropwise and the solution was heated to 90°C and subsequently cooled to room temperature. The precipitated bright orange solid was filtered and dried to give **1** (0.761 g, 2.57 mmol, 92%).

3 Spiro Oxetanes

DTA (T_{onset} , $5^{\circ}\text{C min}^{-1}$): 170°C (mp.), 177°C (dec.); **FT-IR** (ATR): $\tilde{\nu}$ = 3281 (w), 3039 (m), 1614 (s), 1590 (m), 1539 (m), 1429 (w), 1307 (w), 1177 (w), 1103 (m), 942 (s), 844 (w), 739 (m), 715 (m), 686 (m), 514 (s), 436 (m) cm^{-1} ; **$^1\text{H NMR}$** (400 MHz, DMSO- d_6 , 25°C): δ = 10.87 (br s, 1H, NH), 8.90 (s, 2H, 2 x $\text{C}_{\text{Harom.}}$), 5.45 – 5.43 (m, 2H, $\text{CH}_2_{\text{oxetane}}$), 5.29 – 5.27 (m, 2H, $\text{CH}_2_{\text{oxetane}}$) ppm; **$^{13}\text{C NMR}\{^1\text{H}\}$** (101 MHz, DMSO- d_6 , 25°C): δ = 157.1, 137.0, 136.4, 135.8, 125.6, 80.0, 79.8 ppm; **EA** ($\text{C}_9\text{H}_7\text{N}_5\text{O}_7$) calcd.: C 36.37, H 2.37, N 23.57; found: C 36.51 H 2.40 N 23.33; **BAM drophammer** $>40\text{ J}$ ($>500\ \mu\text{m}$); **Friction test** $>360\text{ N}$ ($>500\ \mu\text{m}$).

N-nitro-2-(oxetan-3-ylidene)hydrazine-1-carboximidamide (2)

Amino-nitroguanidine (0.496 g, 4.16 mmol, 1.0 eq.) was suspended in ethanol (10 mL) and 5 drops of concentrated HCl were added. Oxetan-3-one (0.300 g, 4.16 mmol, 1.0 eq.) dissolved in ethanol (5 mL) was added and the mixture was refluxed for 3 hours. After cooling to room temperature, the colorless precipitate was collected, washed with a small amount of ethanol and dried to give **2** (0.560 g, 3.24 mmol, 78 %).

DTA (T_{onset} , $5^{\circ}\text{C min}^{-1}$): 191°C (dec.); **IR** (ATR): $\tilde{\nu}$ = 3253 (w), 3090 (m), 1622 (m), 1573 (s), 1388 (m), 1218 (m), 1138 (m), 1048 (s), 944 (s), 856 (m), 792 (m), 714 (w), 579 (m), 540 (s), 462 (s) 416 (m) cm^{-1} ; **$^1\text{H NMR}$** (400 MHz, DMSO- d_6 , 25°C): δ = 11.34 (s, 1H, NH), 8.78 (br s, 1H, NH), 8.41 (br s, 1H, NH), 5.29 – 5.24 (m, 4H, 2 x $\text{CH}_2_{\text{oxetane}}$) ppm; **$^{13}\text{C NMR}\{^1\text{H}\}$** (101 MHz, DMSO- d_6 , 25°C): δ = 158.3, 153.4, 80.4, 80.0 ppm; **EA** ($\text{C}_4\text{H}_7\text{N}_5\text{O}_3$) calcd.: C 27.75, H 4.08, N 40.19; found: C 27.90 H 4.01 N 40.22; **BAM drophammer** $>40\text{ J}$ ($>500\ \mu\text{m}$); **Friction test** $>360\text{ N}$ ($>500\ \mu\text{m}$).

Ethyl 2-(oxetan-3-ylidene)hydrazine-1-carboxylate (3)

Ethyl hydrazinecarboxylate (0.722 g, 6.94 mmol, 1.0 eq.) and oxetan-3-one (0.500 g, 6.94 mmol, 1.0 eq.) were mixed in ethanol (20 mL) and refluxed for 3 hours. After cooling to room temperature, the colorless precipitate was collected and dried to give **3** (0.703 g, 4.43 mmol, 67%).

DTA (T_{onset} , $5^{\circ}\text{C min}^{-1}$): 113°C (mp.), 198°C (dec.); **IR** (ATR): $\tilde{\nu}$ = 3121 (w), 1693 (s), 1500 (w), 1431 (m), 1384 (m), 1338 (m), 1310 (w), 1270 (w), 1182 (m), 1047 (m), 972 (m), 947 (s), 853 (m), 766 (m), 673 (w), 574 (m) cm^{-1} ; **$^1\text{H NMR}$** (400 MHz, DMSO- d_6 , 25°C): δ = 10.49 (br s, 1H, NH), 5.19 – 5.15 (m, 4H, 2 x $\text{CH}_2_{\text{oxetane}}$), 4.12 – 4.07 (q, 2H, CH_2), 1.22 – 1.18 (t, 3H, CH_3) ppm; **$^{13}\text{C NMR}\{^1\text{H}\}$** (101 MHz, DMSO- d_6 , 25°C): δ = 153.7, 148.2, 80.4, 80.1, 60.5, 14.5 ppm; **EA** ($\text{C}_6\text{H}_{10}\text{N}_2\text{O}_3$) calcd.:

3 Spiro Oxetanes

C 45.57, H 6.37, N 17.71; found: C 45.95 H 6.02 N 17.91; **BAM drophammer** >40 J (>500 μm); **Friction test** >360 N (>500 μm).

Amino(2-(oxetan-3-ylidene)hydrazineyl) methaniminium chloride (4)

Aminoguanidine hydrochloride (0.460 g, 4.16 mmol, 1.0 eq.) was suspended in ethanol (15 mL) and heated to 55°C, then oxetan-3-one (0.300 g, 4.16 mmol, 1.0 eq.) was added and the mixture heated to 85°C for 1.5 hours. The solution was cooled and the colorless precipitate was collected and washed with a small amount of ethanol and dried to give **4** (0.589 g, 3.58 mmol, 86%).

DTA (T_{onset} , 5 °C min⁻¹): 200°C (dec.); **IR** (ATR): $\tilde{\nu}$ = 3254 (m), 2939 (w), 1669 (s), 1625 (s), 1429 (w), 1265 (w), 1124 (m), 985 (m), 965 (m), 944 (s), 858 (m), 755 (w), 698 (w), 537 (s) cm⁻¹; **¹H NMR** (400 MHz, DMSO-d₆, 25 °C): δ = 11.75 (s, 1H, NH), 7.64 (br s, 4H, 2 x NH₂), 5.29 (s, 4H, 2 x CH₂ oxetane) ppm; **¹³C NMR{¹H}** (101 MHz, DMSO-d₆, 25 °C): δ = 155.6, 153.1, 80.1, 79.7 ppm; **EA** (C₄H₉N₄OCl) calcd.: C 29.19, H 5.51, N 34.03; found: C 28.91 H 5.23 N 33.88; **BAM drophammer** >40 J (>500 μm); **Friction test** >360 N (>500 μm).

N-(2-oxa-5,6,8,9-tetraazaspiro[3.5]nonan-7-ylidene)nitramide (5)

Compound **2** (0.210 g, 1.21 mmol, 1.0 eq.) was dissolved in water (10 mL) and heated to 55°C. Hydrazine hydrate (0.073 g, 1.46 mmol, 1.2 eq.) was added and the mixture stirred until a yellow solution was formed. The solvent was removed, yielding 0.174 g (0.93 mmol, 77%) of **5** as yellow solid.

DTA (T_{onset} , 5°C min⁻¹): 151°C (dec.); **IR** (ATR): $\tilde{\nu}$ = 3203 (m), 3125 (m), 1645 (s), 1615 (s), 1408 (m), 1223 (m), 963 (s), 941 (s), 851 (s), 813 (s), 793 (m), 712 (m), 559 (s), 508 (s), 451 (s) cm⁻¹; **¹H NMR** (400 MHz, DMSO-d₆, 25 °C): δ = 9.73 (s, 2H, 2 x NH), 7.08 (s, 2H, 2 x NH), 4.33 (s, 4H, 2 x CH₂ oxetane) ppm; **¹³C NMR{¹H}** (101 MHz, DMSO-d₆, 25 °C): δ = 152.4, 77.2, 67.8 ppm; **EA** (C₄H₈N₆O₃) calcd.: C 25.54, H 4.29, N 44.67; found: C 25.77 H 4.53 N 44.28; **BAM drophammer** >40 J (>500 μm); **Friction test** >360 N (>500 μm).

2-Oxa-5,6,8,9-tetraazaspiro[3.5]nonan-7-one (6)

Compound **4** (0.300 g, 1.90 mmol, 1.0 eq.) was mixed with hydrazine hydrate (6 mL) in ethanol/water (5 mL/5 mL) and heated to 80°C for 1.5 hours. The solvent was removed to give the colorless product **6** which was purified by washing with methanol and diethyl ether (0.170 g, 1.18 mmol, 62%).

3 Spiro Oxetanes

DTA (T_{onset} , 5 °C min⁻¹): 192°C (dec.); **IR** (ATR): $\tilde{\nu}$ = 3254 (m), 3205 (m), 1646 (s), 1614 (m), 1466 (m), 1394 (s), 1288 (w), 1247 (m), 1213 (m), 1148 (m), 1123 (w), 1034 (w), 1013 (w), 947 (s), 912 (m), 840 (s), 708 (s), 665 (s), 642 (s), 523 (s). 477 (s) cm⁻¹; **¹H NMR** (400 MHz, DMSO-d₆, 25 °C): δ = 7.78 (s, 2H, 2 x NH), 5.06 (s, 2H, 2 x NH), 4.29 (s, 4H, 2 x CH₂_{oxetane}) ppm; **¹³C NMR{¹H}** (101 MHz, DMSO-d₆, 25 °C): δ = 154.6, 76.9, 67.7 ppm; **EA** (C₄H₈N₄O₂) calcd.: C 33.33, H 5.59, N 38.87; found: C 33.60 H 5.81 N 38.75; **BAM drophammer** >40 J (>500 μ m); **Friction test** >360 N (>500 μ m).

2-Oxa-5,6,8,9-tetraazaspiro[3.5]nonan-7-imine hydrochloride (**7**)

Procedure I: Diamino guanidine hydrochloride (1.57 g, 12.48 mmol, 3.0 eq.) was suspended in water/ethanol (10 mL/10 mL) and heated to 70°C. Oxetan-3-one (0.300 g, 4.16 mmol, 1.0 eq.) dissolved in ethanol (2 mL) was added and the mixture heated at 70°C for 2 hours. The solvent was removed and the residue dissolved in hot ethanol and filtrated hot. The solvent is removed to give 0.486 g (2.71 mmol, 65%) of **7** as colorless solid.

Procedure II: Compound **4** (0.200 g, 1.22 mmol, 1.0 eq.) was mixed with hydrazine hydrate (4 mL) in ethanol/water (5 mL/5 mL) and heated to 80°C for 1.5 hours. The solvent was removed, the mixture was mixed with methanol and filtered. The residue was collected and dried to give 0.143 g (0.796 mmol, 65%) of **7** as colorless solid.

DTA (T_{onset} , 5 °C min⁻¹): 168°C (dec.); **IR** (ATR): $\tilde{\nu}$ = 3200 (m), 3123 (m), 1645 (s), 1613 (s), 1419 (m), 1356 (w), 1223 (w), 1048 (m), 963 (s), 941 (s), 852 (s), 812 (s), 793 (s), 711 (m), 670 (m), 555 (s). 507 (s), 444 (s) cm⁻¹; **¹H NMR** (400 MHz, DMSO-d₆, 25 °C): δ = 9.76 (s, 2H, 2 x NH), 7.09 (s, 2H, 2 x NH), 5.86 (s, 2H, NH₂), 4.33 (s, 4H, 2 x CH₂_{oxetane}) ppm; **¹³C NMR{¹H}** (101 MHz, DMSO-d₆, 25 °C): δ = 152.4, 77.1, 67.8 ppm; **EA** (C₄H₁₀N₅OCl) calcd.: C 26.75, H 5.61, N 38.99; found: C 26.54 H 5.72 N 38.42; **BAM drophammer** >40 J (>500 μ m); **Friction test** >360 N (>500 μ m).

3.5.2 NMR Discussion and Spectra

Compound **1** has a broad singlet for the NH proton at 10.87 ppm in the ¹H NMR spectrum. The oxetane ring should be symmetric and actually give only one signal, but due to the C=N double bond an E/Z isomerism is present. For this reason, the 4 protons of the oxetane are not chemically equivalent and two multiplets of each of the chemically equivalent two protons are found. The ¹³C NMR spectrum also has two signals at 80.0 ppm and 79.8 ppm for the CH₂ groups of the oxetane ring, which are attributed to E/Z isomerism. The third signal of the oxetane ring is located in the downfield region at 157.1 ppm. In the proton NMR, compound **2** has one sharp singlet at

3 Spiro Oxetanes

11.34 ppm for the NH signal and two broad singlets at 8.78 ppm and 8.41 ppm for the NH₂ group. This splitting is known due to the hindered rotation. The oxetane ring protons are found as one multiplet at 5.27 ppm. In the ¹³C NMR spectrum, two downfield shifted carbon atoms are found at 158.3 ppm and at 153.4 ppm, which can be assigned to the oxetane ring C2 and the guanidine carbon, respectively. As discussed for the previous compound **1**, the oxetane ring CH₂ groups are found as two signals at 80.4 ppm and 80.0 ppm. For compound **3**, four signals are found in the ¹H NMR spectrum. A broad signal at 10.49 ppm is found for the NH proton and a multiplet for the oxetane ring protons is located at 5.17 ppm. The ethyl group exhibits the expected signals at 4.09 ppm as quartet and at 1.20 ppm as singlet. The carbon NMR spectrum of **3** shows two downfield shifted carbons at 153.7 ppm and 148.2 ppm for the C=N of the oxetane and the carbonyl group, respectively. As before, the oxetane methylene groups are found in the same region of about 80 ppm and the ethyl residue is located at 60.5 ppm and 14.5 ppm. Compound **4** exhibits a singlet for the NH group at 11.75 ppm and another broad singlet for both NH₂ groups at 7.64 ppm, which is due to chemical equivalence by protonation and the delocalization of the electrons in the whole fragment. The oxetane ring appears as singlet at 5.29 ppm due to the delocalization of electrons in the complete aminoguanidine motif. Contrary to the proton NMR, the ¹³C NMR spectrum of compound **4** has two signals for the oxetane CH₂ groups at 80.1 ppm and 79.7 ppm. The two other carbon atoms are found at 155.6 ppm and 153.1 ppm which is in accordance with the shifts of compound **2**. Compound **5** has 3 singlet signals in the ¹H NMR spectrum. A singlet at 9.73 ppm which can be assigned to the two NH protons neighbored to the nitrimine group due to the electron withdrawing effect. For the other two NH protons, a singlet at 7.08 ppm is found. The CH₂ groups of the oxetanes are now symmetrical compared to the parent compound **2** and shifted upfield to 4.33 ppm. In the ¹³C NMR spectrum, the oxetane substituted carbon atom is drastically shifted upfield to 67.8 ppm. The methylene group signals are found at 77.2 ppm. The C4 signal of the nitrimine group is essentially unchanged at 152.4 ppm. The NH protons of **6** are found as a singlet at 7.78 ppm and 5.03 ppm, similar to compound **5**, but not as downfield shifted due to the keto-group. The ¹³C spectrum is also somewhat analogous to that of the beforementioned compound, with signals at 154.5 ppm, 76.9 ppm and 67.7 ppm. The ¹H NMR of compound **7** has a two singlet signals for the NH groups at 9.76 ppm and 7.09 ppm and further a slightly broadened singlet for the NH₂ function at 5.86 ppm. The protons of the oxetane ring are found as a singlet at 4.33 ppm, which is in the same region as for the other tetrazine compounds. Also, ¹³C NMR revealed almost the same shifts

3 Spiro Oxetanes

as for the other tetrahydrotetrazines, at 152.4 ppm for C4, 77.1 ppm for the oxetane methylene groups, and 67.8 ppm for C2.

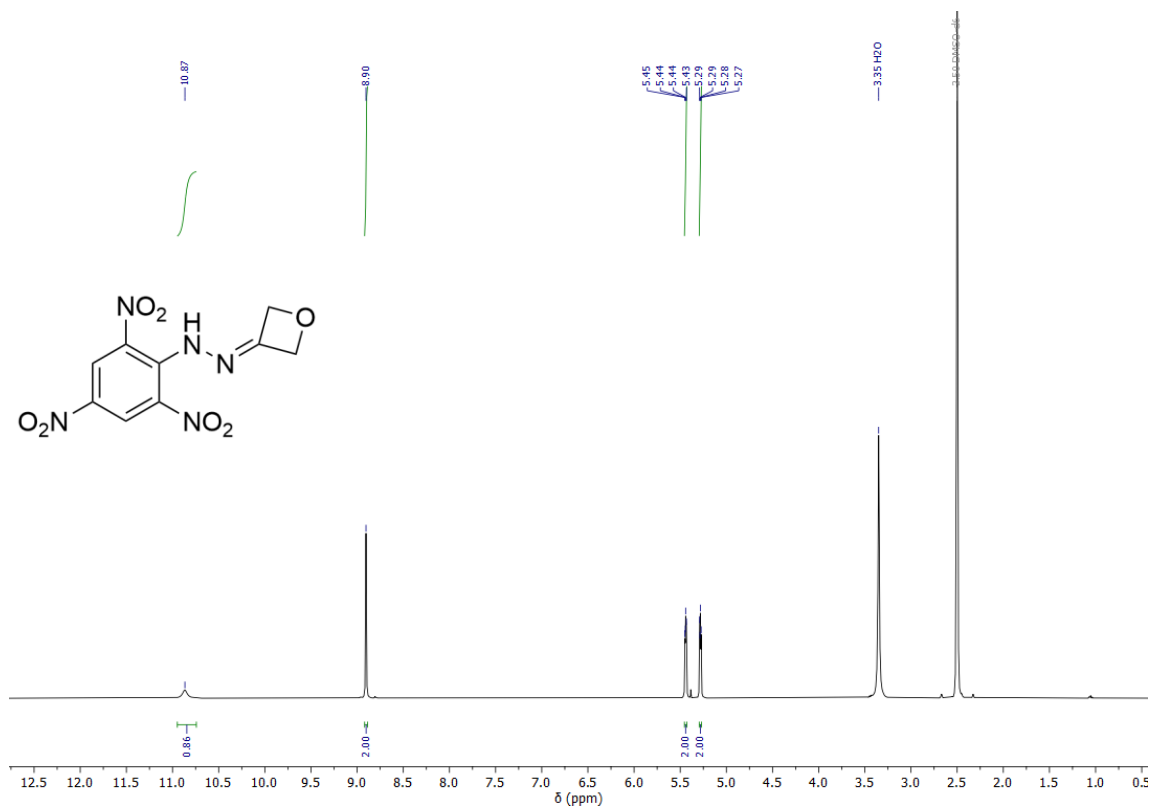


Figure 8. ¹H NMR spectrum of compound 1.

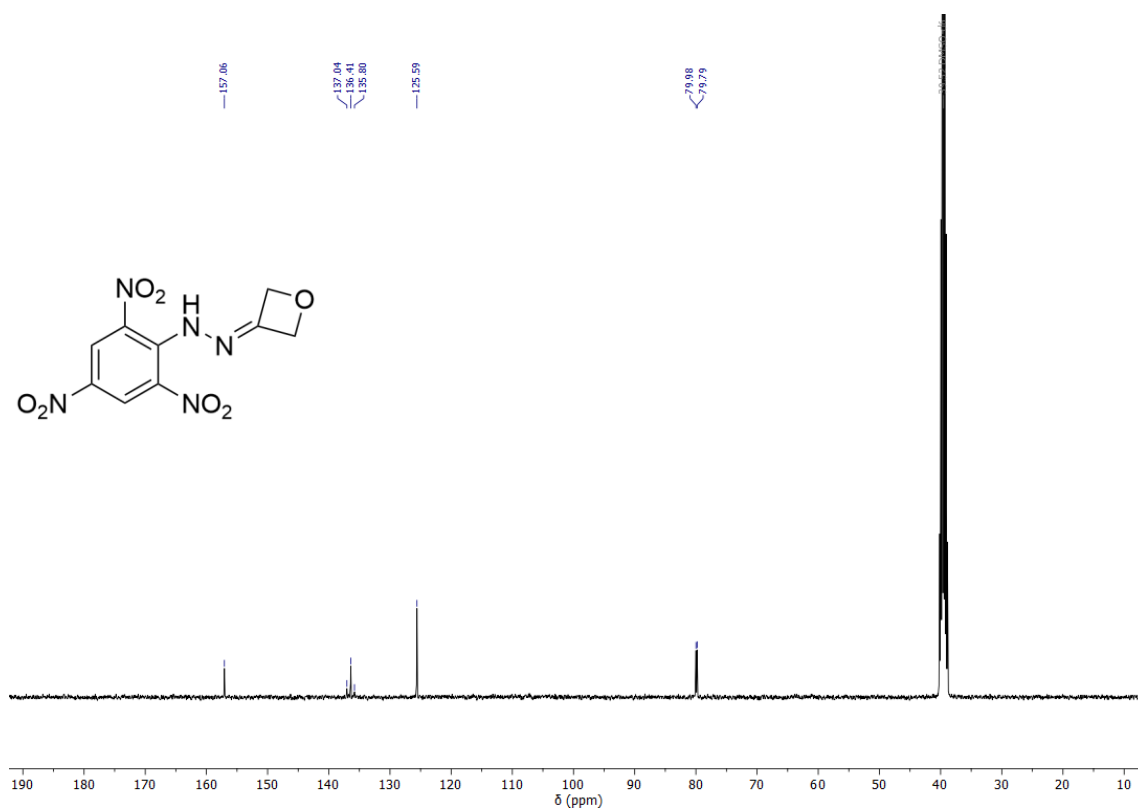


Figure 9. ¹³C NMR spectrum of compound 1.

3 Spiro Oxetanes

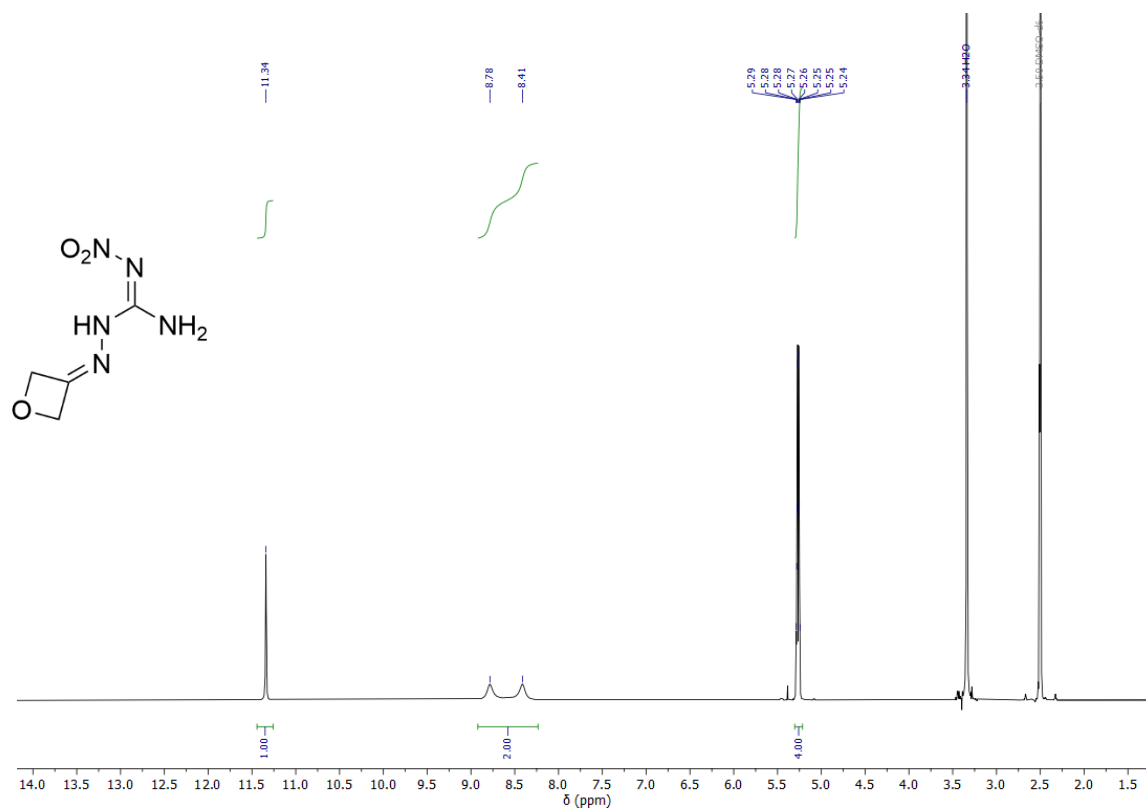


Figure 10. ¹H NMR spectrum of compound 2.

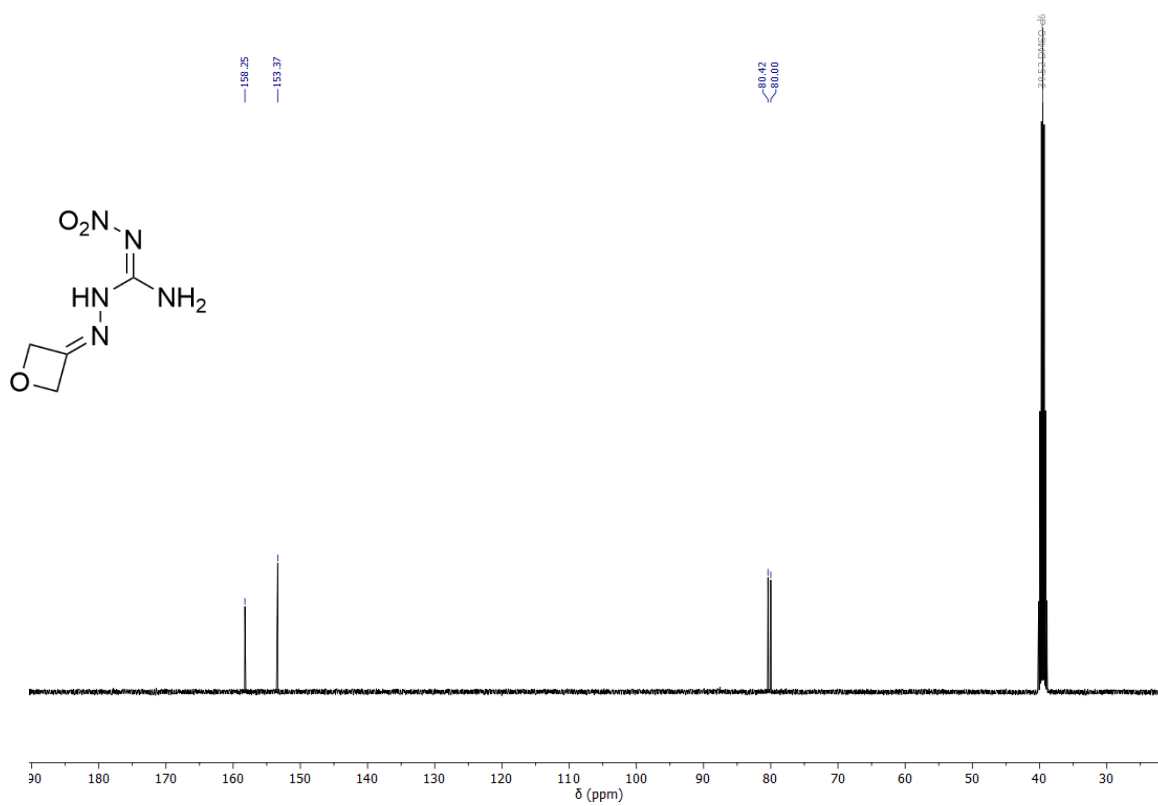


Figure 11. ¹³C NMR spectrum of compound 2.

3 Spiro Oxetanes

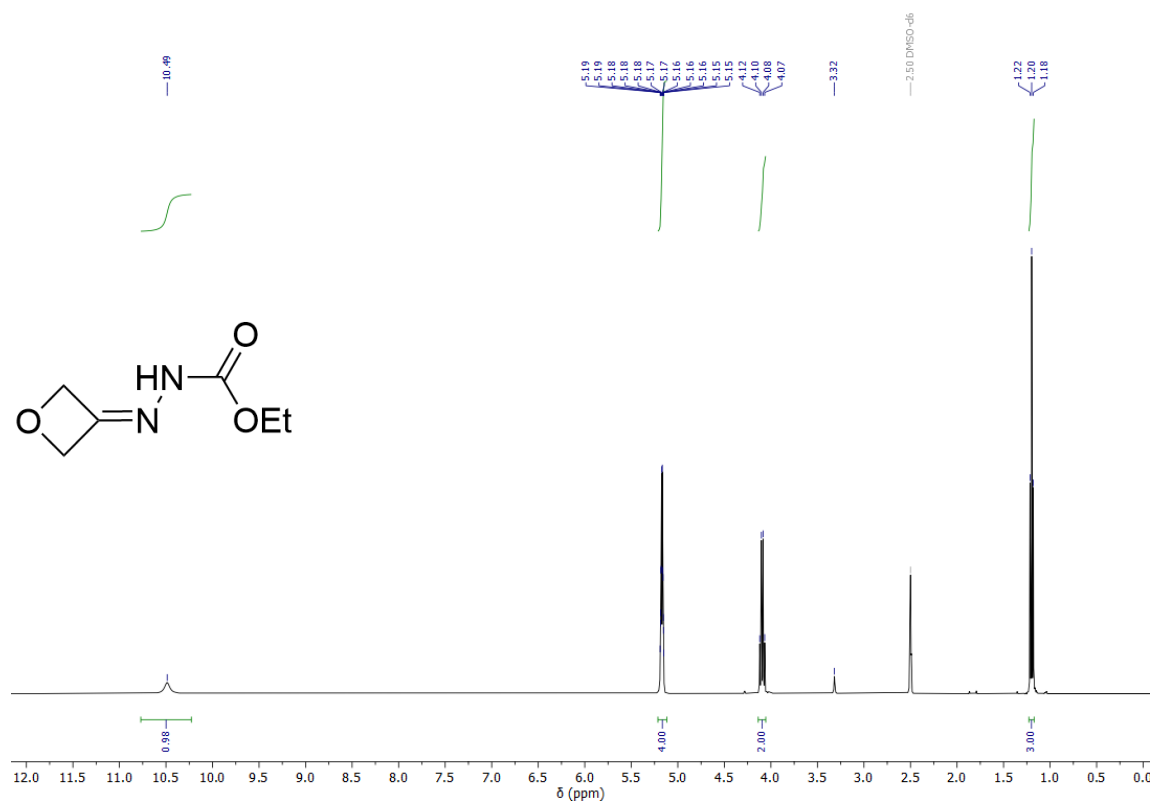


Figure 12. ¹H NMR spectrum of compound 3.

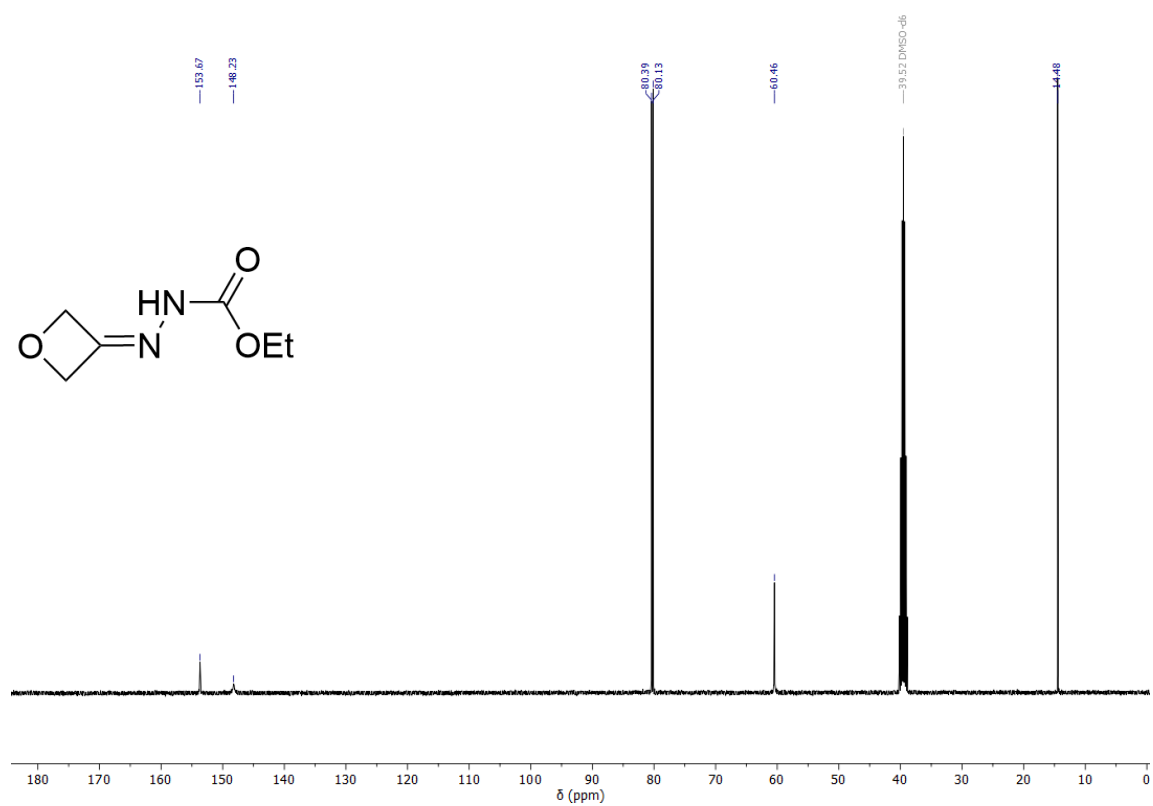


Figure 13. ¹³C NMR spectrum of compound 3.

3 Spiro Oxetanes

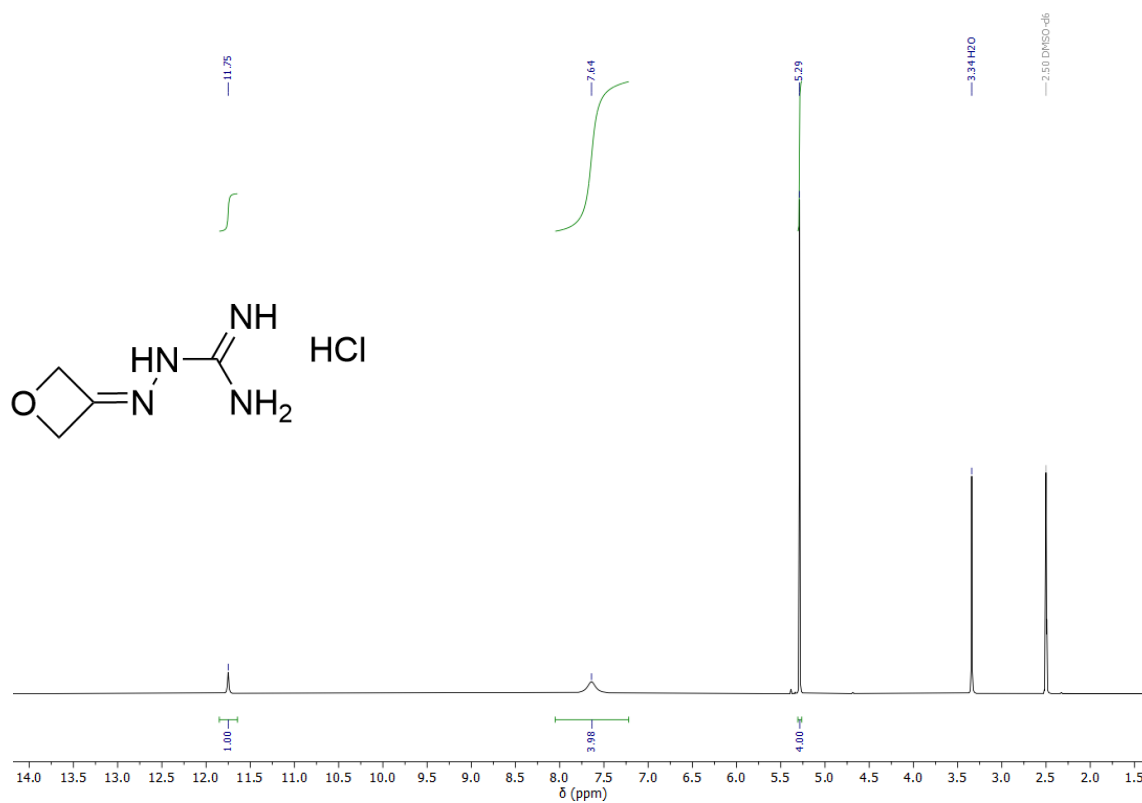


Figure 14. $^1\text{H NMR}$ spectrum of compound 4.

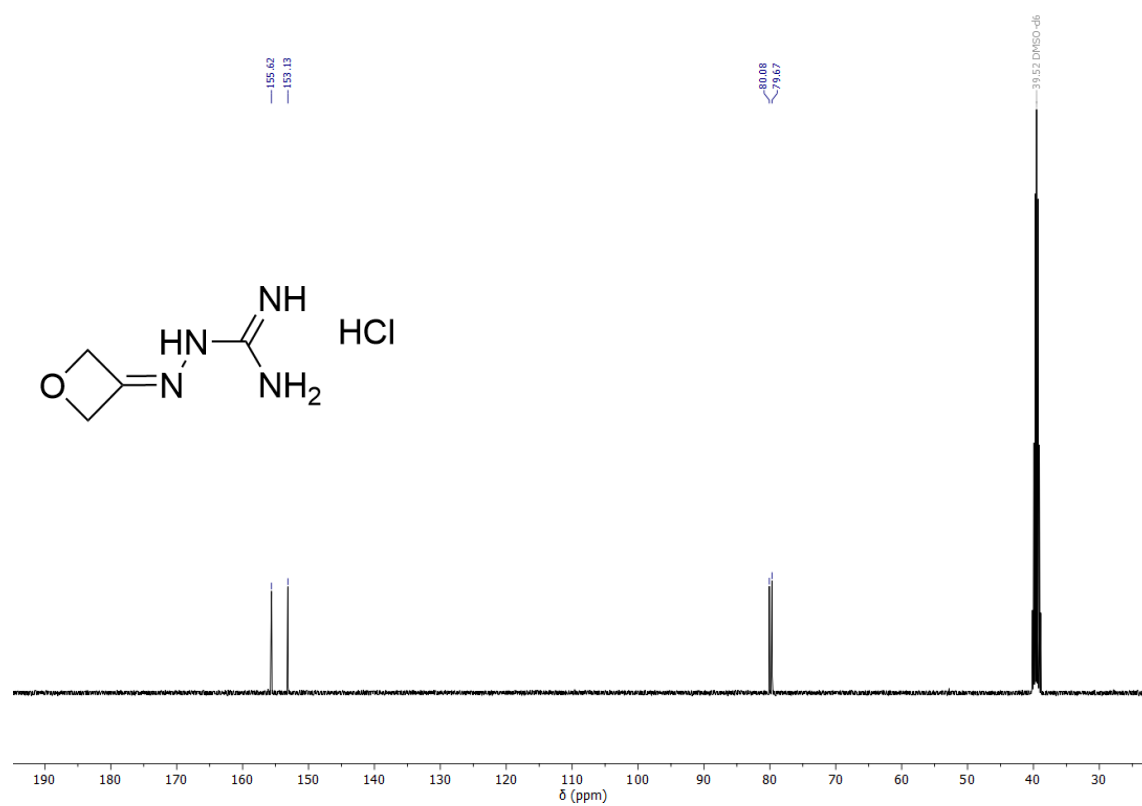


Figure 15. $^{13}\text{C NMR}$ spectrum of compound 4.

3 Spiro Oxetanes

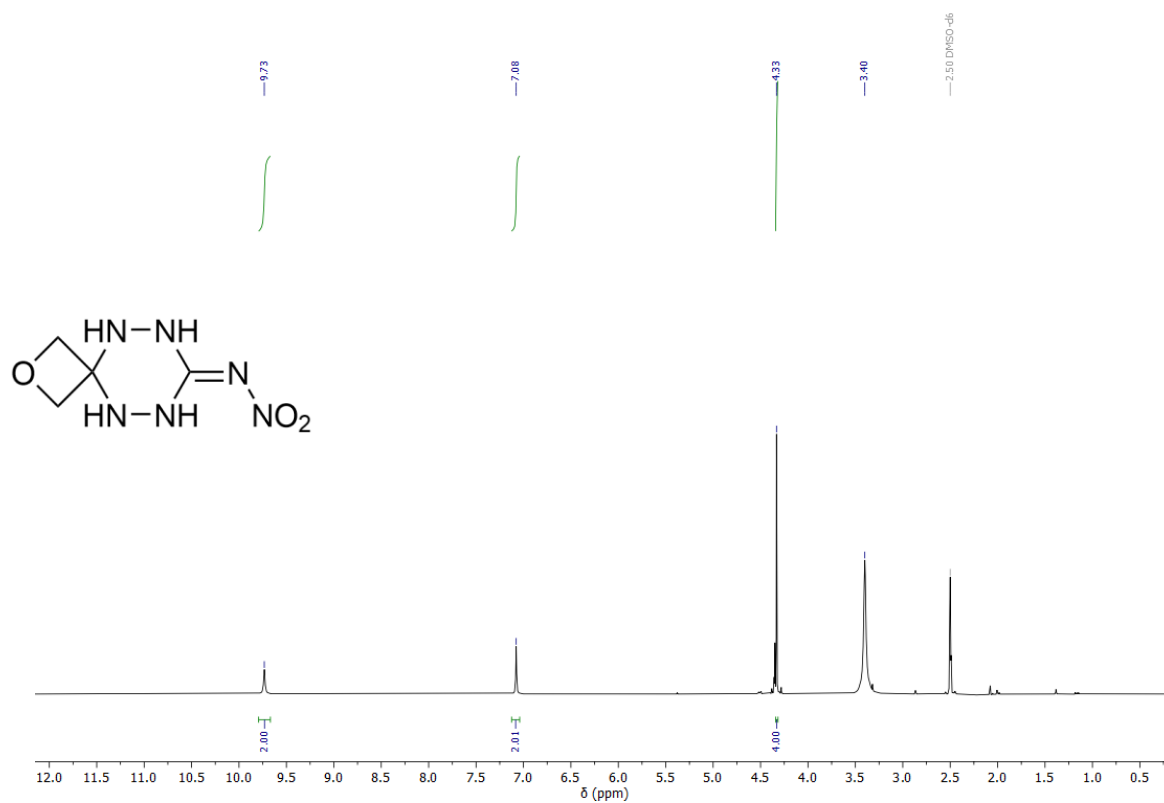


Figure 16. ^1H NMR spectrum of compound 5.

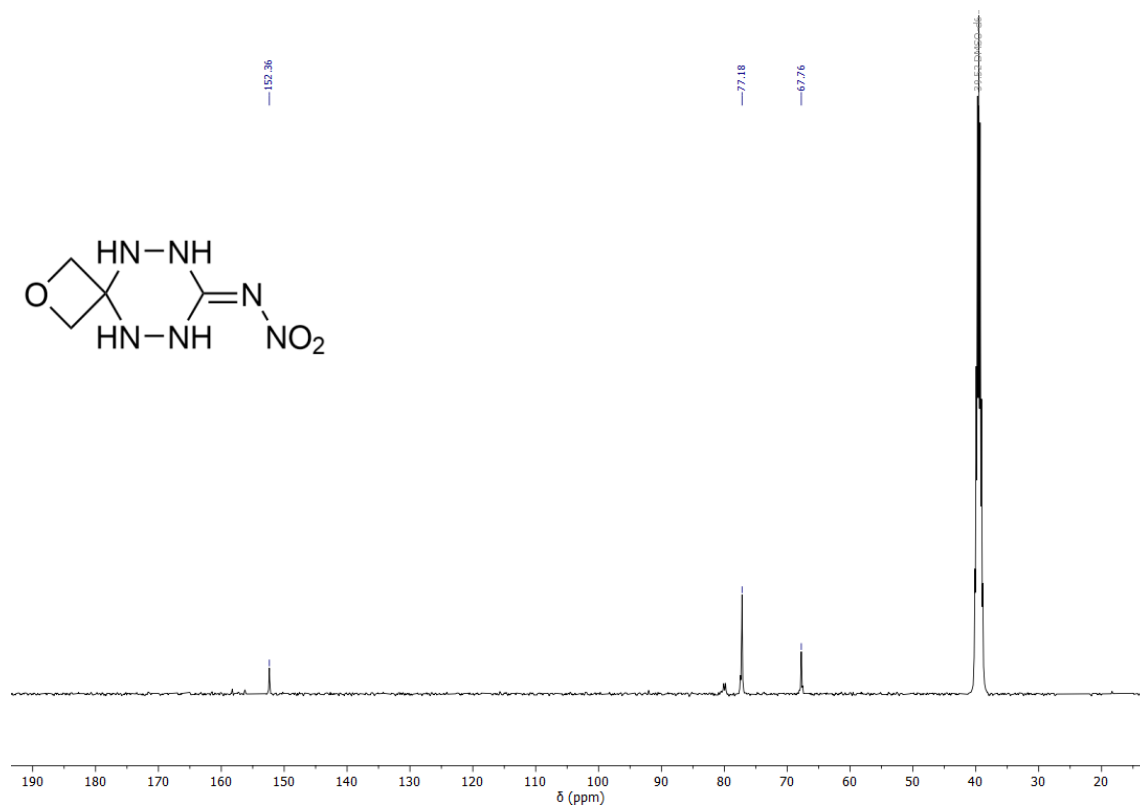


Figure 17. ^{13}C NMR spectrum of compound 5.

3 Spiro Oxetanes

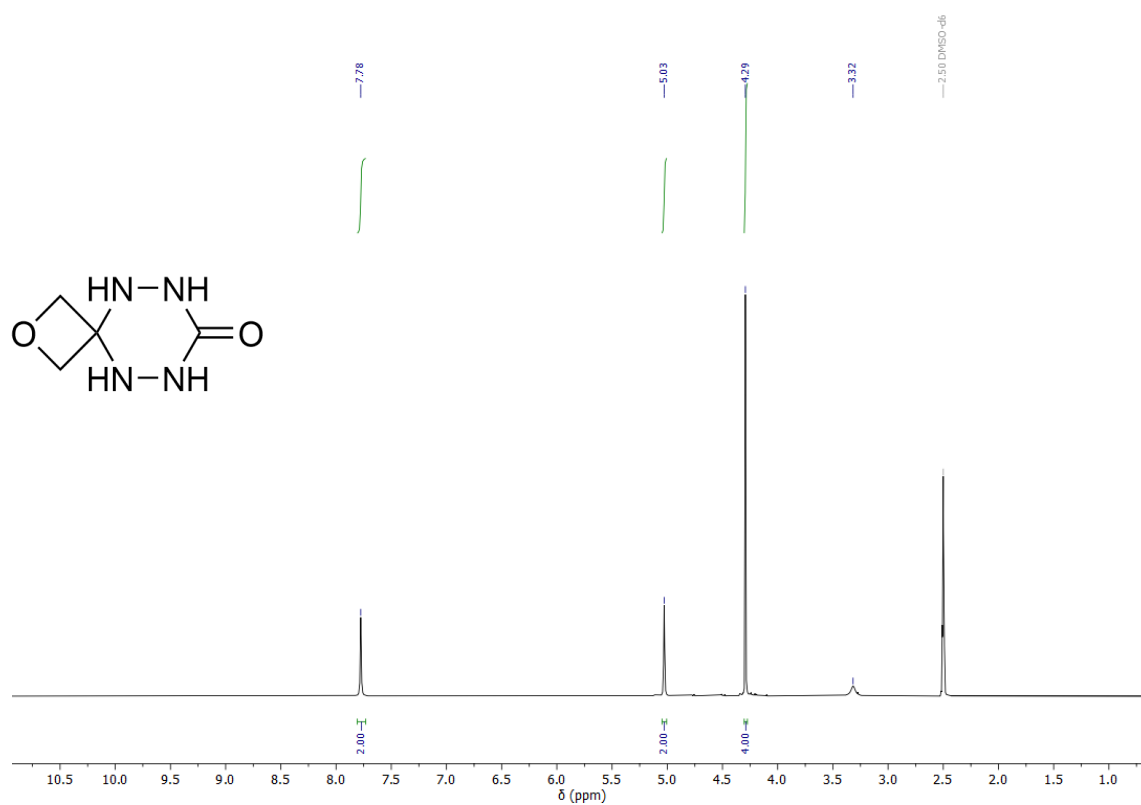


Figure 18. ¹H NMR spectrum of compound 6.

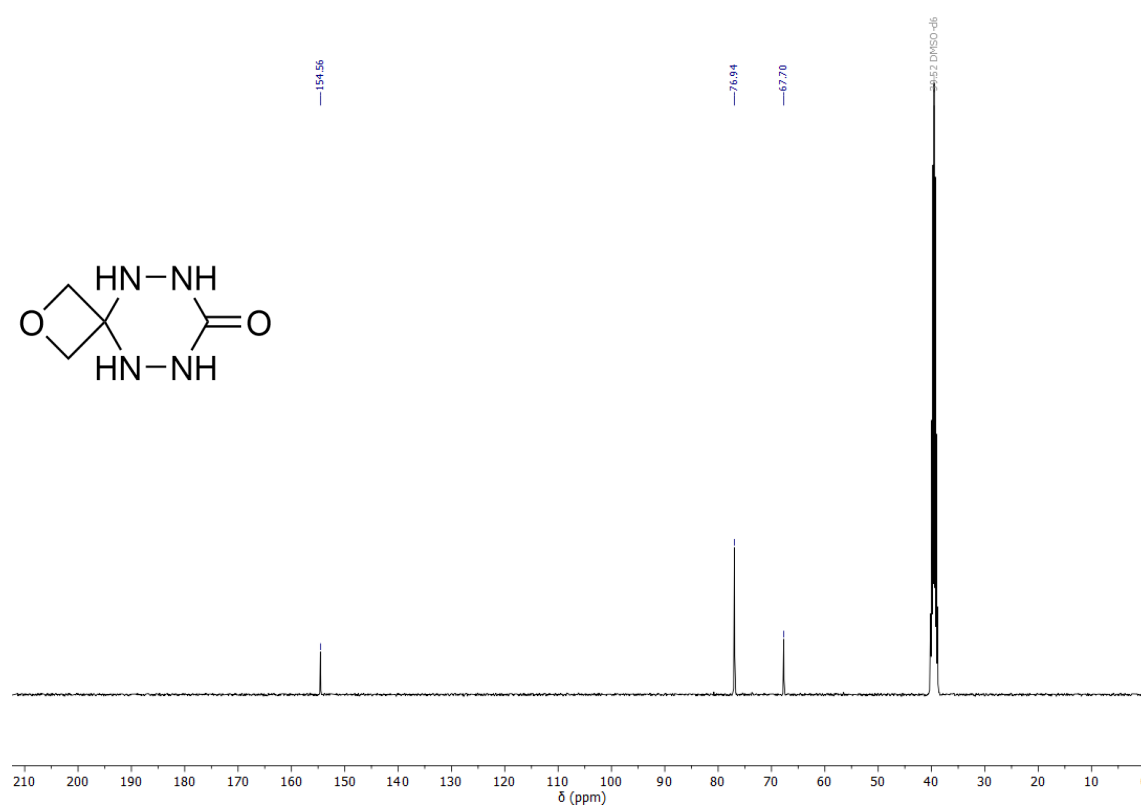


Figure 19. ¹³C NMR spectrum of compound 6

3 Spiro Oxetanes

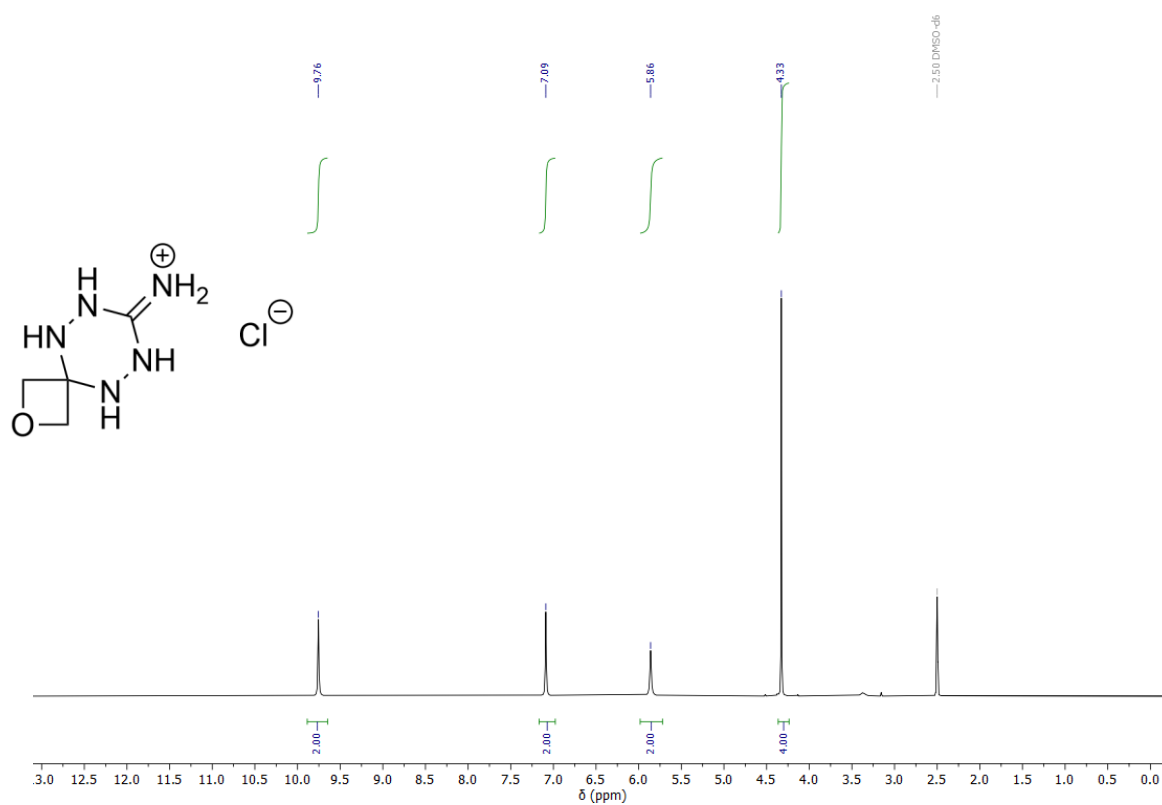


Figure 20. ¹H NMR spectrum of compound 7.

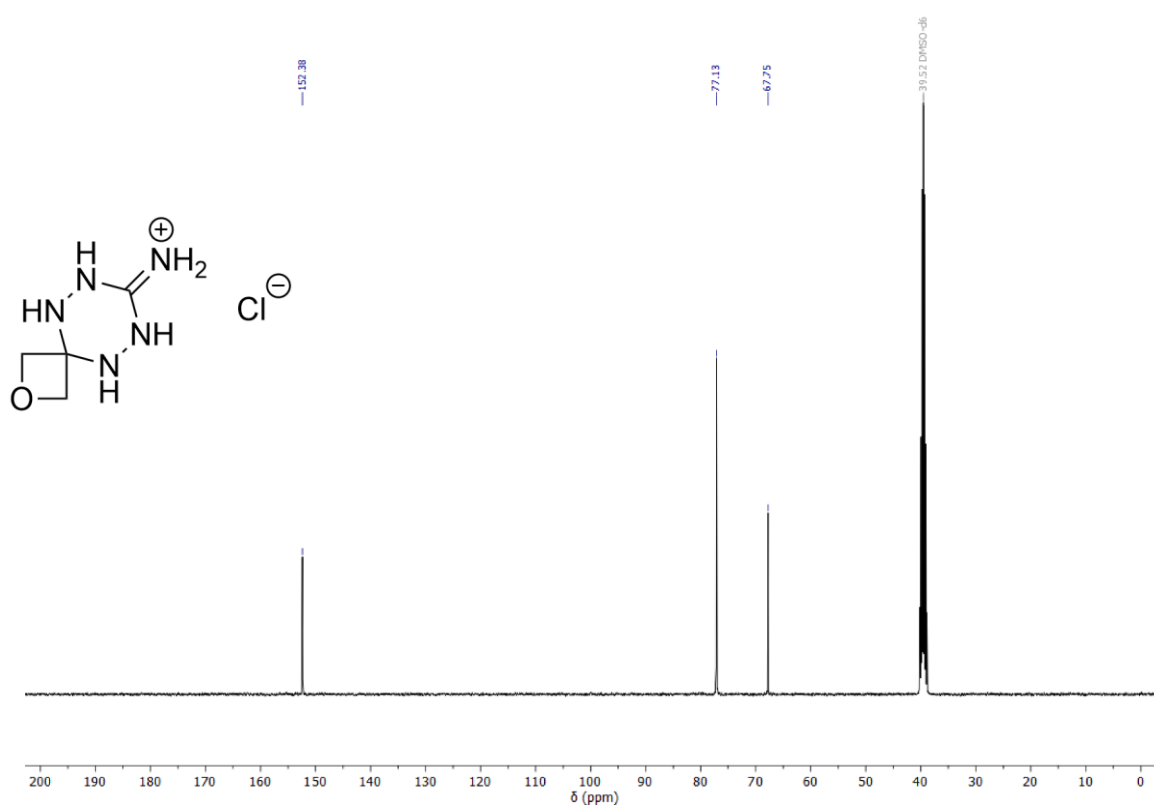


Figure 21. ¹³C NMR spectrum of compound 7

3.5.3 X-ray Diffraction

Crystal structure data were obtained from an Oxford Xcalibur3 diffractometer with a Spellman generator (voltage 50kV, current 40mA) and a Kappa CCD area for data collection using Mo-K α radiation ($\lambda=0.71073\text{\AA}$) or a Bruker D8 Venture TXS diffractometer equipped with a multilayer monochromator, a Photon 2 detector and a rotation-anode generator (Mo-K α radiation). The data collection was performed using the CRYSTALIS RED software.^[42] The solution of the structure was performed by direct methods and refined by full-matrix least-squares on F² (SHELXT)^[43] implemented in the OLEX2^[44] software suite. The non-hydrogen atoms were refined anisotropically and the hydrogen atoms were located and freely refined. The absorption correction was carried out by a SCALE3 ABSPACK multiscan method.^[45] The DIAMOND2 plots shown with thermal ellipsoids at the 50% probability level and hydrogen atoms are shown as small spheres of arbitrary radius. The SADABS program embedded in the Bruker APEX3 software was used for multi-scan absorption corrections in all structures.^[46]

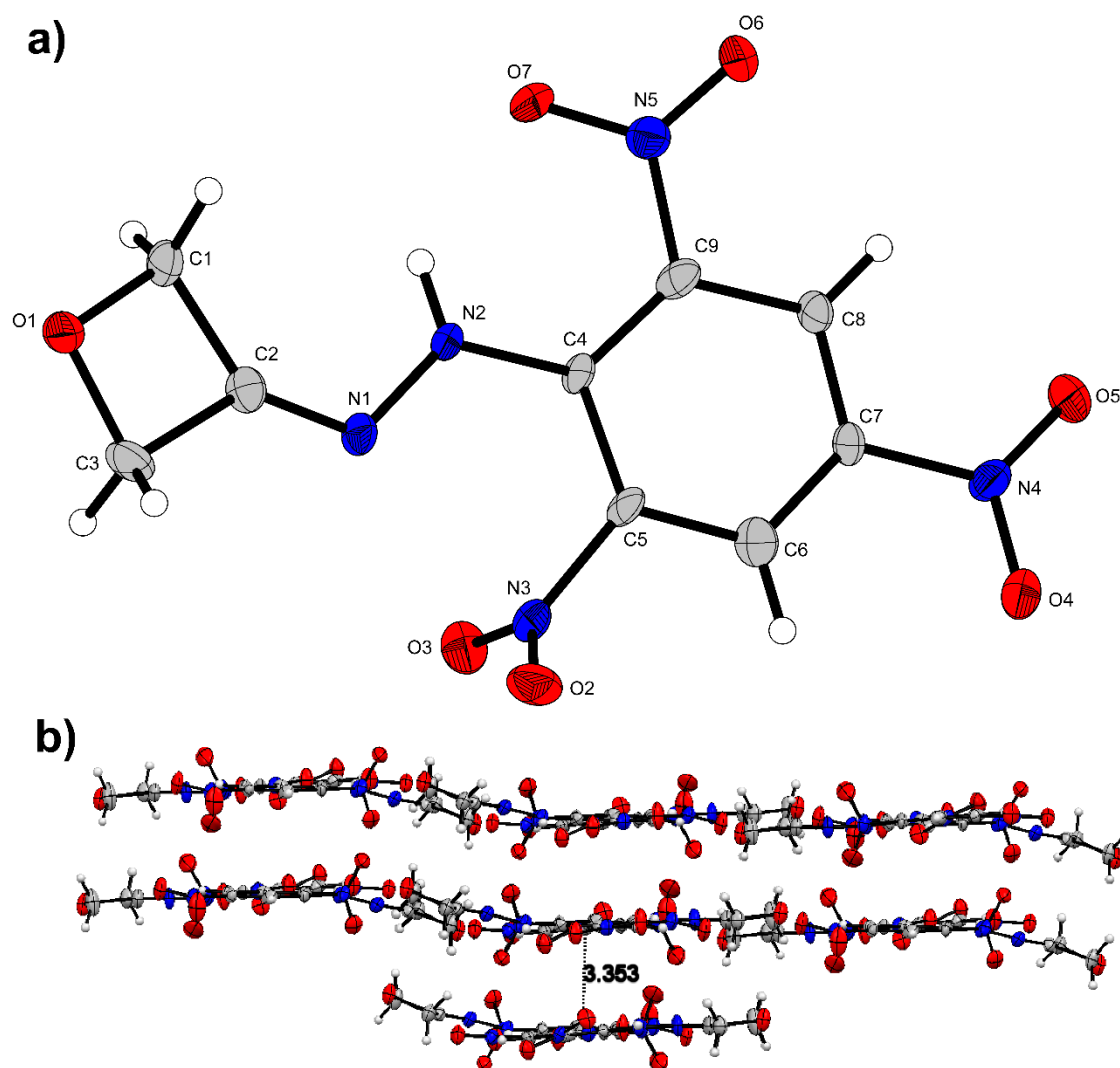


Figure 22. **a)** Crystal structure of **1**. **b)** Layers of **1** with an interlayer distance of 3.353 Å.

1-(Oxetan-3-ylidene)-2-(2,4,6-trinitrophenyl)hydrazine (**1**) crystallizes in the triclinic space group $P\bar{1}$ with 4 molecules in the unit cell and a density of 1.703 g cm^{-3} at 101 K. The bond length of C2–N1 (1.276(6) Å) is slightly shorter than typical C=N double bond (~ 1.30 Å). N1–N2 (1.380(5) Å) is only slightly shorter than a N–N single bond (~ 1.41 Å) and but much larger than a N–N double bond (~ 1.24 Å). One nitro group at the *ortho*-position (O2–N3–O3) stands perpendicular ($91.0(5)^\circ$) to the aromatic ring. The other nitro group is twisted only $22.9(5)^\circ$ due to an intramolecular hydrogen bond of the hydrogen of N2 to O7 with a distance of 2.019 Å. The oxetane ring has a puckering angle of 9.26° . The aromatic ring and N2 form a plane on which the oxetane ring together with N1 is located with an angle of 14.57° . The molecules form layers with π -stacking of the benzol rings and an interlayer distance of 3.353 Å.

3 Spiro Oxetanes

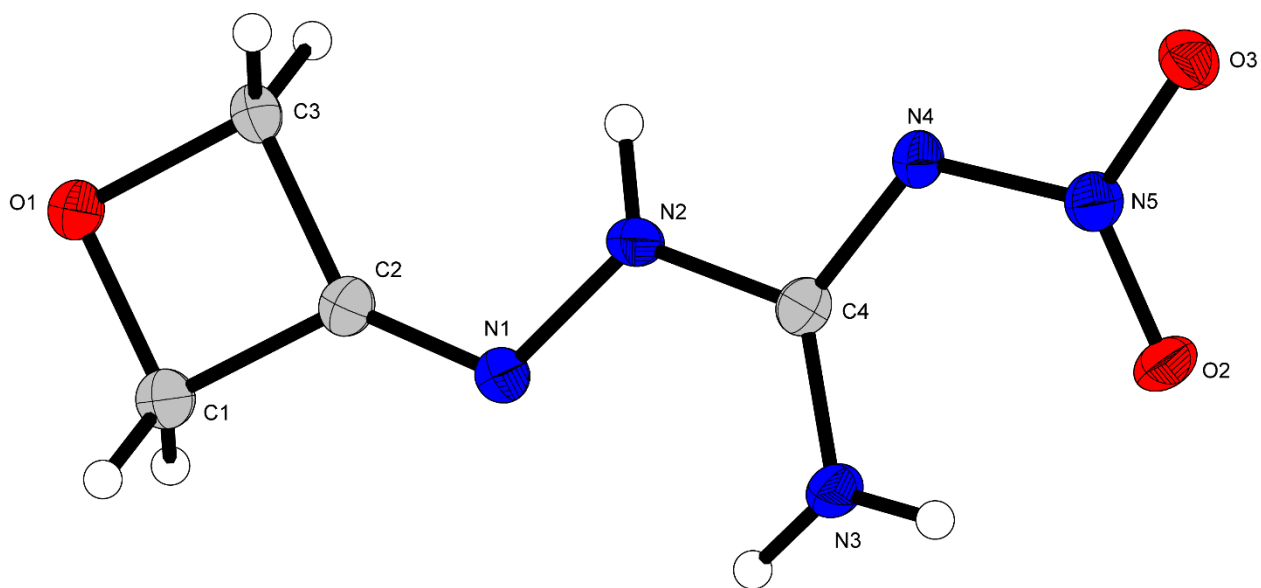


Figure 23. Crystal structure of **2**.

N-nitro-2-(oxetan-3-ylidene)hydrazine-1-carboximidamide (**2**) crystallizes in the orthorhombic space group $Pna2_1$ with 4 molecules in the unit cell and a density of 1.567 g cm^{-3} at 119 K. The electrons in the nitroguanidine moiety indicate a delocalization with bond lengths of $1.307(4) \text{ \AA}$ (C4–N3), $1.366(4) \text{ \AA}$ (C4–N4), and 1.351 \AA (C4–N2). The oxetane ring has a puckering angle of 7.07° . An intramolecular hydrogen bond is formed from O2 to H32 with a distance of $1.991(5) \text{ \AA}$. Further, several intermolecular hydrogen bonds are observed from H32 to O1, H31 to O3, H2 to O3 with distances of $2.16(4) \text{ \AA}$, $2.30(4) \text{ \AA}$ and 2.08 \AA , respectively.

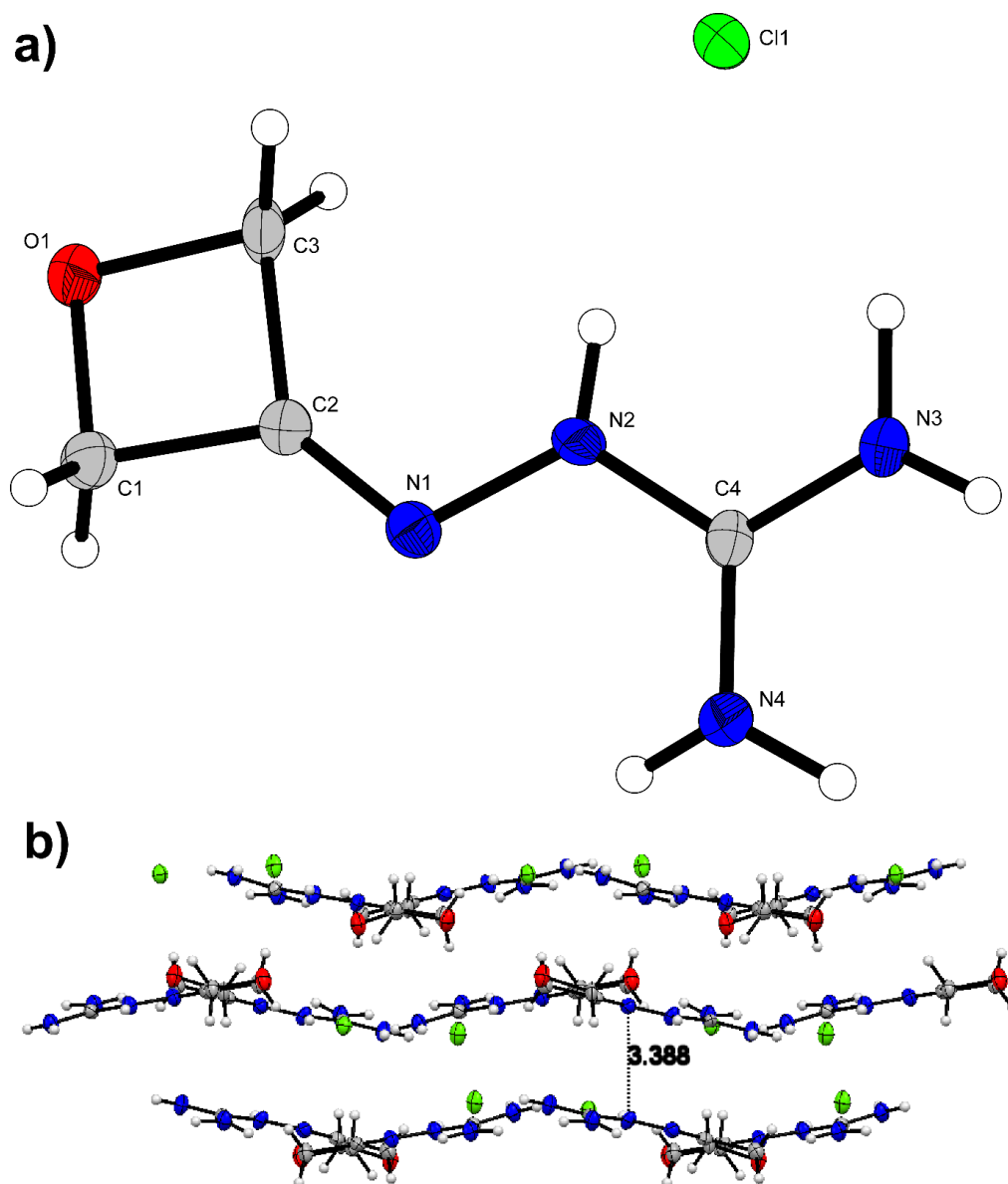


Figure 24. a) Crystal structure of **4**.

b) Wave-like layers of **4** with an interlayer distance of 3.388 Å.

Compound **4** crystallizes monoclinic ($P2_1/n$) with 8 formula units in the unit cell and a density 1.465 g cm^{-3} at 119 K. The bond lengths are in the same range, as discussed for compound **2**, suggesting delocalization of electrons in the guanidine moiety. The molecule is essentially planar except the oxetane ring which is 15.66° off the planarity of the guanidine fragment. The oxygen atom of the oxetane ring functions as hydrogen bond acceptor of H8 having a distance of 2.192 \AA . H5 and H6 have intramolecular hydrogen bonds to the chloride anion with distances of 2.295 \AA and 2.406 \AA . The molecules arrange themselves in the crystal as a light zig-zag pattern with an interlayer distance of 3.422 \AA .

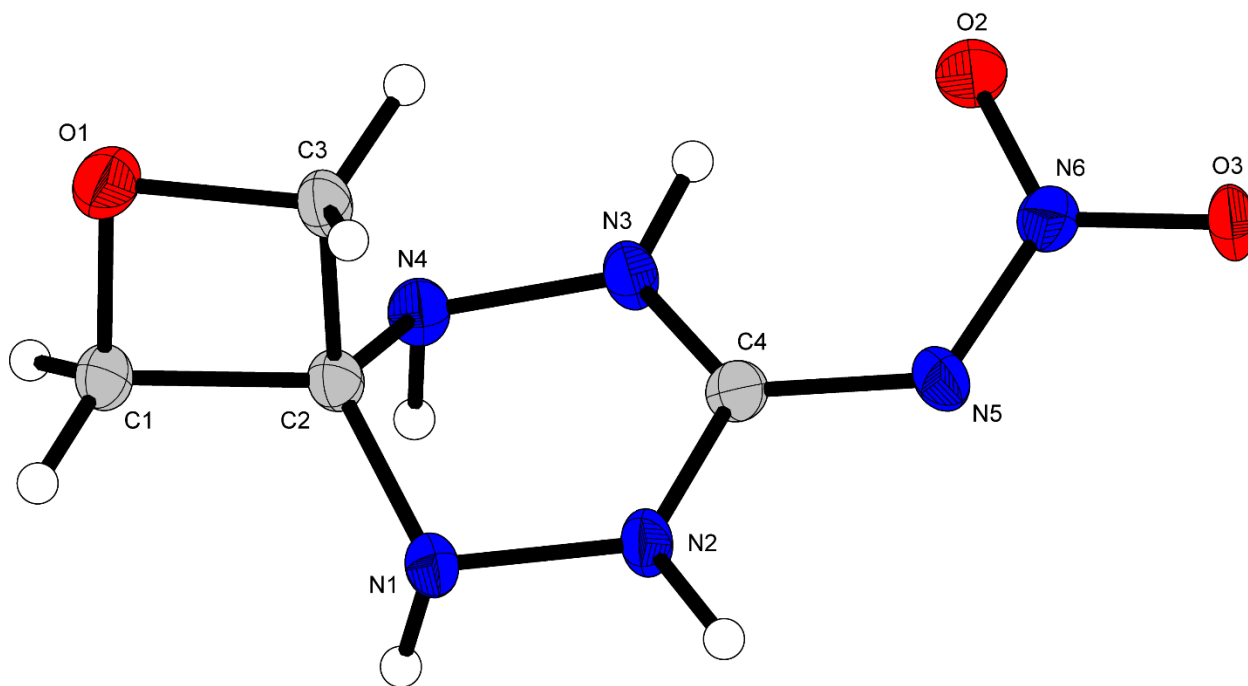


Figure 25. Crystal structure of **5**.

N-(2-oxa-5,6,8,9-tetraazaspiro[3.5]nonan-7-ylidene)nitramide (**5**) crystallizes in the monoclinic space group *I2/a* with a density of 1.685 g cm^{-3} at 102 K which is significantly higher than the parent compound **2** with 1.567 g cm^{-3} . Further, the bond lengths at C4 is very similar to the carbon atom of the guanidine derivatives. The tetrahydropyridazine ring has a half-chair or envelope-like conformation being planar in N2–C4–N3–N4. The oxetane has a puckering of 16.38° . Further, the oxetane ring stands nearly perpendicular to the tetrahydropyridazine ring with an angle of 81.24° . The molecule has one intramolecular hydrogen bond from H8 to O2 with a distance of 1.936 \AA . Several intermolecular hydrogen bonds can be observed in the crystal structure with oxygen being the acceptor atom. First, the oxetane oxygen O1 to H5 and H8 with distances of 2.646 \AA and 2.408 \AA . Next, hydrogen bonds to oxygen atoms of the nitro group can be found, O2–H7 (2.471 \AA), O3–H5 (2.342 \AA) and O3–H6 (2.429 \AA). Last, N5 functions also as acceptor atom to H6 with a distance of 1.933 \AA .

3 Spiro Oxetanes

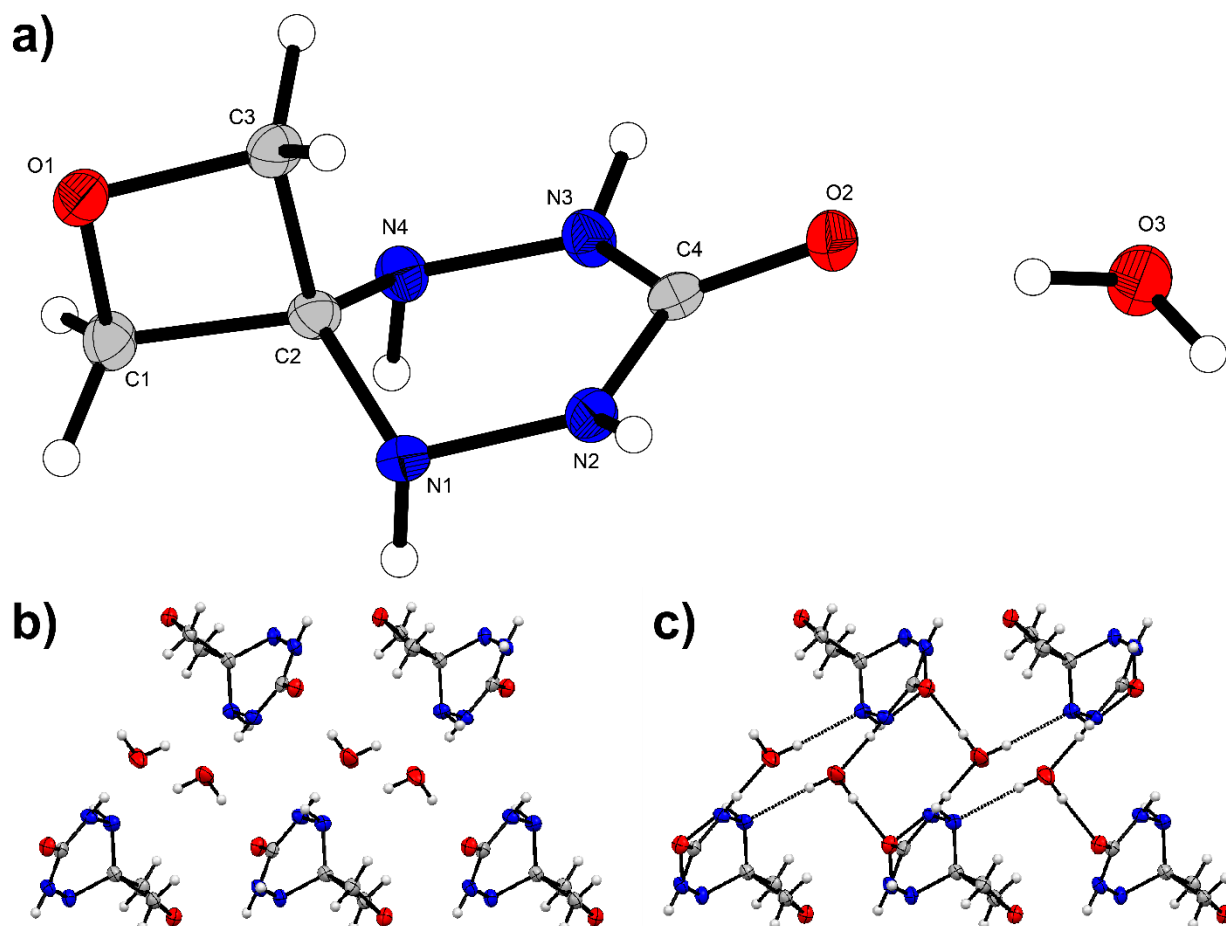


Figure 26. a) Crystal structure of **6** · H₂O. b) View along the b-axis with water molecules laying in between sheets of the tetrazine compound. c) View along the b-axis with visualized hydrogen bonds of the water molecules between the tetrahydrotetrazines.

2-Oxa-5,6,8,9-tetraazaspiro[3.5]nonan-7-one (**6**) crystallizes as monohydrate in the monoclinic space group *P21/n* with 4 molecules in the unit cell and a density of 1.547 g cm⁻³ at 103 K. The bond lengths are in the same range of the lengths for **5**, except the C4–O2 which has a length of a standard C–O double bond. The tetrahydrotetrazine ring features an envelope-like conformation as compound **5**. Only C2 is out of the tetrazine plane. As discussed beforehand, the oxetane ring stands approximately perpendicular to the tetrahydrotetrazine ring with an angle of 84.65°. Further the oxetane moiety has a puckering angle of 10.19°. The oxygen atom of the oxetane functions as hydrogen bond acceptor to H6 with a distance of 2.066 Å. Also, the keto-group is an acceptor to H5 (2.269 Å) and H8 (2.681 Å). The water molecule bridges three molecules via quite short hydrogen bonds, namely O2–H9 (1.810 Å), H10–N4 (2.105 Å) and O3–H7 (1.919 Å), forming a three-dimensional network.

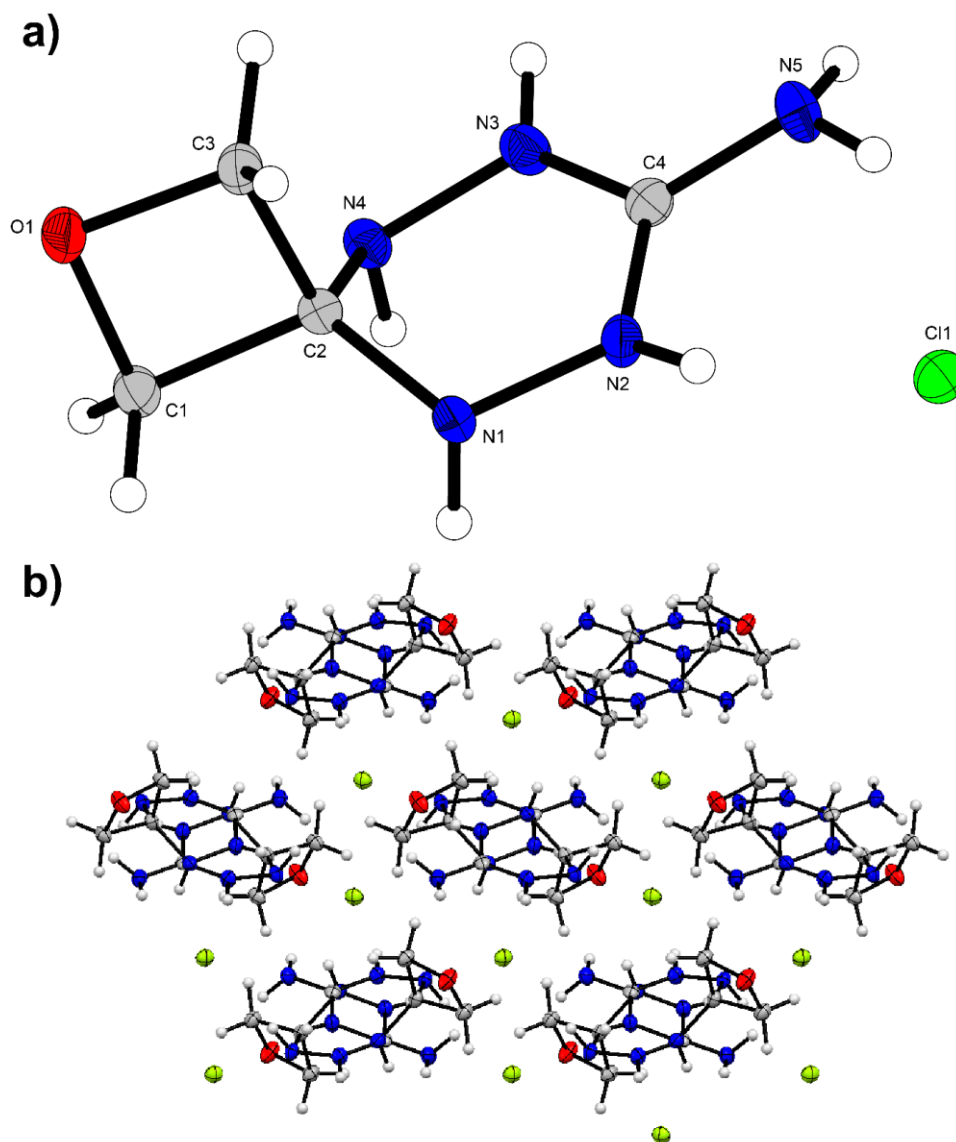


Figure S19. a) Crystal structure of **7**. b) View along the a-axis with the chloride anion forming the network.

2-Oxa-5,6,8,9-tetraazaspiro[3.5]nonan-7-iminium chloride (**7**) crystallizes also monoclinic ($P2_1/c$) with 4 molecules in the unit cell and a density of 1.617 g cm^{-3} at 102 K (**Figure 7**). The bond lengths are similar to the ones of **5**. The conformation of the tetrazine moiety is also a half chair conformation with C2–N1–N2–C4 in a plane. The oxetane ring has an angle of 65.64° towards the tetrazine ring. Further, the oxetane itself has a puckering angle of 14.77° which is near the puckering angle of compound **5**. H7 forms an intermolecular hydrogen bond to O1 with a distance of 2.354 \AA . The chloride anion forms a three-dimensional network, bridging 4 molecules. The Cl anion forms intramolecular hydrogen bonds with H6 (2.302 \AA) and H10 (2.751 \AA) and further intermolecular hydrogen bonds with H5 (2.552 \AA), H8 (2.628 \AA) and H9 (2.381 \AA).

Table 3. Crystallographic data and structure refinement details for the prepared compounds.

	1	2	4
Formula	C ₉ H ₇ N ₅ O ₇	C ₄ H ₇ N ₅ O ₃	C ₄ H ₉ N ₄ O Cl
FW [g mol ⁻¹]	297.20	173.15	164.60
Crystal system	triclinic	orthorhombic	monoclinic
Space group	P-1 (No. 2)	Pna21 (No. 33)	P21/n (No. 14)
Color / Habit	yellow plateletk	colorless block	colorless platelet
Size [mm]	0.50 x 0.50 x 0.10	0.10 x 0.10 x 0.50	0.05 x 0.50 x 0.50
a [Å]	6.0897(8)	12.887(3)	10.3577(8)
b [Å]	9.3761(9)	11.380(4)	13.3053(9)
c [Å]	20.622(4)	5.0056(12)	10.8302(7)
α [°]	94.216(11)		90
β [°]	93.917(13)		90.206(6)
γ [°]	98.100(10)		90
V [Å ³]	1158.9(3)	734.1(4)	1492.53(18)
Z	4	4	8
ρ _{calc.} [g cm ⁻³]	1.703	1.567	1.465
μ [mm ⁻¹]	0.150	0.134	0.451
F(000)	608	360	688
λ _{MoKα} [Å]	0.71073	0.71073	0.71073
T [K]	101	119	101
θ Min-Max [°]	2.2, 25.2	2.4, 26.4	2.4, 26.4
Dataset	-7: 7 ; -11: 11 ; -25: 25	-16: 14 ; -14: 13 ; - 6: 6	-8: 12 ; -16: 16 ; -13: 13
Reflections collected	5471	5734	7171
Independent refl.	3671	1485	3031
R _{int}	0.066c	0.049	0.044
Observed reflections	3671	1212	2224
Parameters	380	138	253
R ₁ (obs) ^[a]	0.0586	0.0424	0.0649
wR ₂ (all data) ^[b]	0.1371	0.0916	0.1505
S ^[c]	0.972	1.04	1.07
Resd. dens [e Å ⁻³]	-0.361, 0.358	-0.18, 0.22	-0.33, 0.40
Device type	Oxford Xcalibur3	Oxford Xcalibur3	Oxford Xcalibur3
Solution	SHELXT	SHELXT	SHELXT
Refinement	SHELXL-2018	SHELXL-2018	SHELXL-2018
Absorption correction	multi-scan	multi-scan	multi-scan
CCDC	2157490	2157477	2157480

^[a] $R_1 = \sum ||F_o| - |F_c|| / \sum |F_o|$; ^[b] $wR_2 = [\sum [w(F_o^2 - F_c^2)^2] / \sum [w(F_o^2)]]^{1/2}$; $w = [\sigma^2(F_o^2) + (xP)^2 + yP]^{-1}$ and $P = (F_o^2 + 2F_c^2) / 3$;

^[c] $S = \{\sum [w(F_o^2 - F_c^2)^2] / (n-p)\}^{1/2}$ (n = number of reflections; p = total number of parameters).

Table 4. Crystallographic data and structure refinement details for the prepared compounds.

	5	6	7
Formula	C ₄ H ₈ N ₆ O ₃	C ₄ H ₁₀ N ₄ O ₂	C ₄ H ₁₀ N ₅ O Cl
FW [g mol ⁻¹]	188.16	162.16	179.62
Crystal system	monoclinic	monoclinic	monoclinic
Space group	I2/a (No. 15)	P21/c (No. 14)	P21/c (No. 14)
Color / Habit	colorless block	colorless block	colorless block
Size [mm]	0.10 x 0.20 x 0.40	0.10 x 0.25 x 0.50	0.10 x 0.20 x 0.20
a [Å]	8.4618(14)	11.135(3)	10.3623(11)
b [Å]	10.3310(16)	5.7344(7)	7.7338(6)
c [Å]	16.985(3)	11.913(3)	10.3200(12)
α [°]	90	90	90
β [°]	92.144(16)	113.71(3)	116.844(14)
γ [°]	90	90	90
V [Å ³]	1483.8(4)	696.5(3)	737.92(16)
Z	8	4	4
ρ _{calc.} [g cm ⁻³]	1.685	1.546	1.617
μ [mm ⁻¹]	0.143	0.131	0.467
F(000)	784	344	376
λ _{MoKα} [Å]	0.71073	0.71073	0.71073
T [K]	102	103	102
θ Min-Max [°]	2.3, 26.4	2.0, 26.4	2.2, 26.4
Dataset	-10: 10 ; -12: 8 ; -21: 14	-10: 13 ; -7: 6 ; -14: 14	-12: 12 ; -9: 9 ; -12: 12
Reflections collected	3290	2874	5895
Independent refl.	1520	1425	1503
R _{int}	0.059	0.027	0.042
Observed reflections	872	1096	1202
Parameters	150	140	140
R ₁ (obs) ^[a]	0.0772	0.0431	0.0389
wR ₂ (all data) ^[b]	0.1946	0.1077	0.0856
S ^[c]	1.04	1.05	1.04
Resd. dens [e Å ⁻³]	-0.32, 0.36	-0.19, 0.32	-0.22, 0.32
Device type	Oxford Xcalibur3	Oxford Xcalibur3	Oxford Xcalibur3
Solution	SHELXT	SHELXT	SHELXT
Refinement	SHELXL-2018	SHELXL-2018	SHELXL-2018
Absorption correction	multi-scan	multi-scan	multi-scan
CCDC	2157481	2157478	2157482

^[a]R₁ = Σ||F_o| - |F_c|| / Σ|F_o|; ^[b]wR₂ = [Σ[w(F_o² - F_c²)²] / Σ[w(F_o²)]^{1/2}; w = [σ²(F_o²) + (xP)² + yP]⁻¹ and P = (F_o² + 2F_c²) / 3; ^[c]S = {Σ[w(F_o² - F_c²)²] / (n - p)}^{1/2} (n = number of reflections; p = total number of parameters).

3.5.4 Thermal analysis

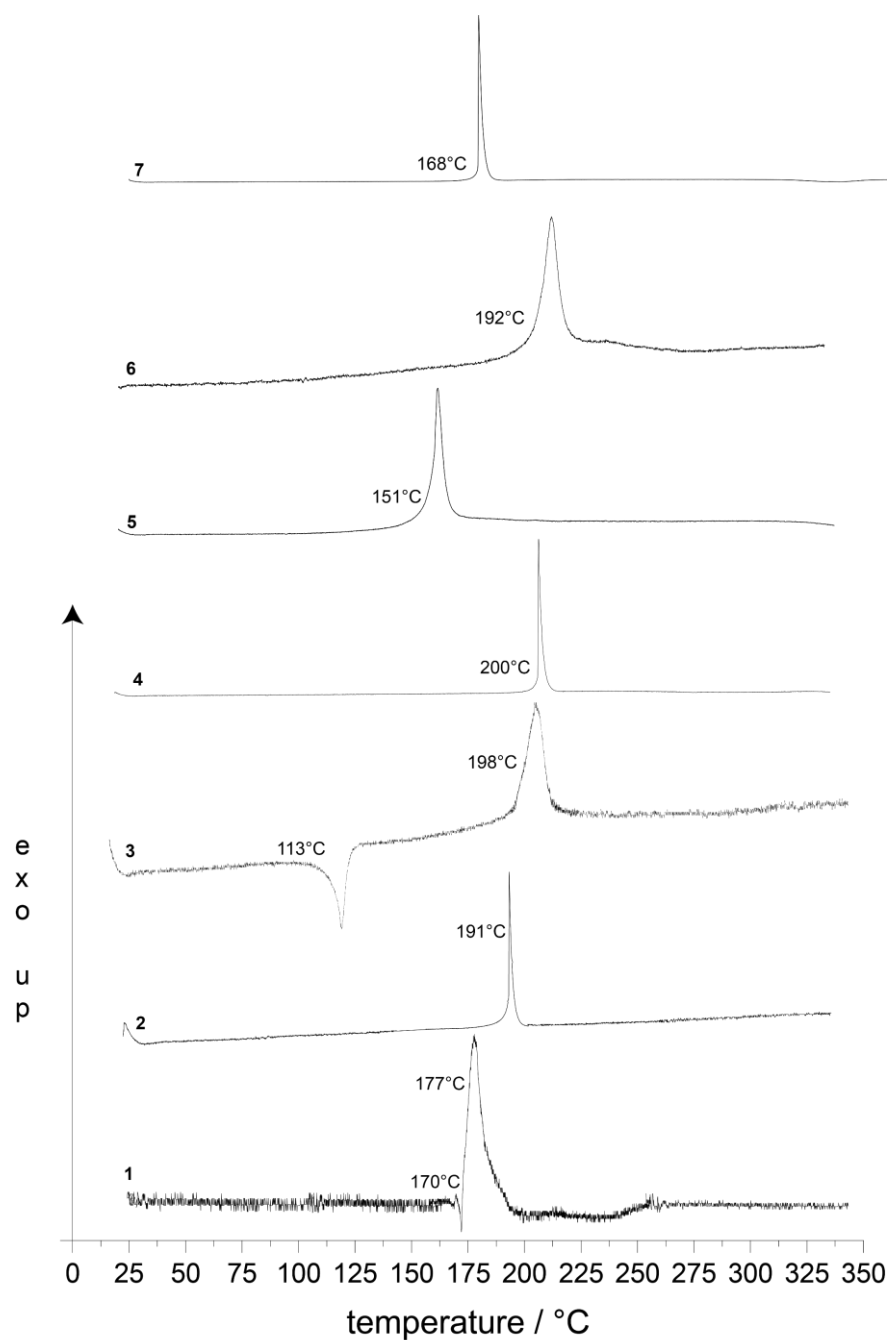


Figure S20. Differential thermal analysis plots of compounds 1–7.

3.5.5 Heat of Formation Calculation

The atomization method was used to determine the heat of formation of **1**, **2**, **4–7** using the atom energies in **Table 5**.

$$\Delta_f H^\circ_{(g, M, 298)} = H_{(molecule, 298)} - \sum H^\circ_{(atoms, 298)} + \sum \Delta_f H^\circ_{(atoms, 298)}$$

3 Spiro Oxetanes

Table 5. CBS-4M electronic enthalpies for atoms C, H, N and O and their literature values.

	$-H^{298} / \text{a.u.}$	$\Delta_f H^\circ_{\text{gas}} [47]$
H	0.500991	217.998
C	37.786156	716.68
N	54.522462	472.68
O	74.991202	249.18

The Gaussian16 program package was used to calculate room temperature enthalpies on the CBS-4M level of theory.^[35] In order to obtain the energy of formation for the solid phase, the Trouton's Rule has to be applied ($\Delta H_{\text{sub}} = 188 \cdot T_m$).

Table 6. Heat of formation calculation results for compounds **1**, **2**, **4–7**.

M	$-H^{298} [a] [\text{a.u.}]$	$\Delta_f H^\circ(\text{g}, \text{M}) [b] [\text{kJ mol}^{-1}]$	$\Delta_{\text{sub}} H^\circ (\text{M}) [c] [\text{kJ mol}^{-1}]$	$\Delta_f H^\circ(\text{s}) [d] [\text{kJ mol}^{-1}]$	Δn	$\Delta_f U(\text{s}) [e] [\text{kJ kg}^{-1}]$
1	1145.613114	321.4	83.3122	238.1	-9.5	880.4
2	655.021183	195.0	87.2602	107.8	-7.5	729.9
4	910.789869	839.4	---	323.8	-7.5	2080.1
5	710.266628	302.9	79.7402	223.1	-8.5	1297.9
6	525.884738	16.1	87.4482	-71.3	-7.0	-375.4
7	966.205753	499.7	---	-17.4	-8.5	20.4

[a] CBS-4M electronic enthalpy; [b] gas phase enthalpy of formation; [c] sublimation enthalpy; [d] standard solid state enthalpy of formation; [e] solid state energy of formation.

3.6 References

- [1] M. Reboul, *Ann. Chim.* **1878**, *14*, 495–497.
- [2] C. R. Noller, *Organic Syntheses, Coll.* **1955**, *Vol. 3*, 835.
- [3] Re. Leikkala, Ra. Leikkala, B. Moku, K. P. Rakesh, H.-L. Qin, *Beilstein J. Org. Chem.* **2019**, *15*, 976–980.
- [4] J. A. Bull, R. A. Croft, O. A. Davis, R. Doran, K. F. Morgan, *Chem. Rev.* **2016**, *116*, 12150–12233.
- [5] J. A. Burkhard, G. Wuitschik, M. Rogers-Evans, K. Müller, E. M. Carreira, *Angew. Chem. Int. Ed.* **2010**, *49*, 9052–9067.
- [6] P. Luger, J. Buschmann, *J. Am. Chem. Soc.* **1984**, *106*(23), 7118–7121.
- [7] W. R. Carpenter, *J. Org. Chem.* **1962**, *27*(6), 2085–2088.
- [8] M. B. Frankel, E. R. Wilson, *J. Chem. Eng. Data* **1981**, *26*, 219.
- [9] J. C. Hoffsommer, D. J. Glover, N. E. Burlinson, *J. Org. Chem.* **1983**, *48*(3), 315–321.
- [10] P. Golding, R. W. Millar, N. C. Paul, D. H. Richards, *Tetrahedron* **1993**, *49*(32), 7051–7062.
- [11] T. G. Archibald, R. P. Carlson, A. A. Malik, G. E. Manser, *US patent No. 5663289*, **1997**.
- [12] G. R. Peterson, W. P. Bassett, B. L. Weeks, L. J. Hope-Weeks, *Cryst. Growth Des.* **2013**, *13*, 2307–2311.
- [13] N.-D. H. Gamage, B. Stiasny, J. Stierstorfer, P. D. Martin, T. M. Klapötke, C. H. Winter, *Chem. Commun.* **2015**, *51*, 13298–13300.
- [14] M. Born, T. C. Fessard, L. Göttemann, T. M. Klapötke, J. Stierstorfer, M. Voggenreiter, *Chem. Commun.* **2021**, *57*, 2804–2807.
- [15] D. Fischer, T. M. Klapötke, J. Stierstorfer, *Chem. Commun.* **2016**, *52*, 916–918.
- [16] T. Kanai, K. Iwamoto, *US patent No. 2020/0017450A1*, **2020**.
- [17] E. Brunet, M. S. Batra, F. J. Aguilar, J. L. G. Ruano, *Tetrahedron* **1991**, *32*(39), 5423–5424.
- [18] I. Choudhury-Mukherjee, H. A. Schenck, S. Cechova, T. N. Pajewski, J. Kapur, J. Ellena, D. S. Cafiso, M. L. Brown, *J. Med. Chem.* **2003**, *46*, 2494–2501.
- [19] S. Huang, A. K. Miller, W. Wu, *Tetrahedron Letters* **2009**, *50*, 6584–6585.
- [20] J. M. Bell, D. G. Kubler, P. Sartwell, R. G. Zepp, *J. Org. Chem.* **1965**, *30*(12), 4284–4292.
- [21] H. Yang, N. Huo, P. Yang, H. Pei, H. Lv, X. Zhang, *Org. Lett.* **2015**, *17*, 4144–4147.
- [22] L. Zhang, Y. Tang, Z. Han, K. Ding, *Angew. Chem. Int. Ed.* **2019**, *58*, 4973–4977.
- [23] A. R. Katritzky, A. Denisenko, S. N. Denisenko, *J. Heterocyclic Chem.* **2000**, *37*, 1309–1314.
- [24] C. DeMonte, S. Carradori, D. Secci, M. D’Ascenzio, P. Guglielmi, A. Mollica, S. Morronem S. Scarpa, A. M. Agliano, S. Giantulli, I. Silverstri, *Eur. J. Med. Chem.* **2015**, *105*, 245–262.
- [25] X. Mo, T. D. R. Morgan, H. T. Ang, D. G. Hall, *J. Am. Chem. Soc.* **2018**, *140*, 5264–5271.
- [26] N. Fischer, T. M. Klapötke, J. Stierstorfer, *Z. Naturforsch.* **2012**, *67b*, 573–588.
- [27] M. Atakol, A. Atakol, A. Ö. Yigiter, I. Svoboda, O. Atakol, *J. Therm. Anal. Calorim* **2017**, *127*, 1931–1940.

3 Spiro Oxetanes

- [28] C.-X. Tan, Y.-X. Shi, J.-Q. Weng, X.-H. Liu, W.-G. Zhao, B.-J. Li, *Lett. Drug. Des. Discov.* **2014**, *11*(7), 940–943.
- [29] R. W. Lamon, *J. Org. Chem.* **1969**, *34*(3), 756–758.
- [30] K. Karger, K. Bechthold, G. Maas, *Zeitschrift für Naturforschung B*, **2020** *75*(6–7), 517–528.
- [31] A. G. Orpen, L. Brammer, F. H. Allen, O. Kennard, D. G. Watson, R. Taylor, *Struct. Correl.* **1994**, 752–858.
- [32] M. Born, K. Karaghiosoff, T. M. Klapötke M. Voggenreiter, *ChemPlusChem* **2022**, *87*, e202200049.
<https://doi.org/10.1002/cplu.202200049>.
- [33] M. Suceska, EXPLO5 program, Zagreb, Croatia, **2018**.
- [34] T. M. Klapötke, *Chemistry of High-Energy Materials 2019*, Berlin, Boston: de Gruyter.
- [35] M. J. Frisch, G. W. Trucks, H. B. Schlegel, G. E. Scuseria, M. A. Robb, J. R. Cheeseman, G. Scalmani, V. Barone, B. Mennucci, G. A. Petersson, H. Nakatsuji, M. Caricato, X. Li, H. P. Hratchian, A. F. Izmaylov, J. Bloino, G. Zheng, J. L. Sonnenberg, M. Hada, M. Ehara, K. Toyota, R. Fukuda, J. Hasegawa, M. Ishida, T. Nakajima, Y. Honda, O. Kitao, H. Nakai, T. Vreven, J. A. Montgomery, Jr., J. E. Peralta, F. Ogliaro, M. Bearpark, J. J. Heyd, E. Brothers, K. N. Kudin, V. N. Staroverov, R. Kobayashi, J. Normand, K. Raghavachari, A. Rendell, J. C. Burant, S. S. Iyengar, J. Tomasi, M. Cossi, N. Rega, J. M. Millam, M. Klene, J. E. Knox, J. B. Cross, V. Bakken, C. Adamo, J. Jaramillo, R. Gomperts, R. E. Stratmann, O. Yazyev, A. J. Austin, R. Cammi, C. Pomelli, J. W. Ochterski, R. L. Martin, K. Morokuma, V. G. Zakrzewski, G. A. Voth, P. Salvador, J. J. Dannenberg, S. Dapprich, A. D. Daniels, Ö. Farkas, J. B. Foresman, J. V. Ortiz, J. Cioslowski, D. J. Fox, *Gaussian 09, Revision A.1*, Gaussian, Inc., Wallingford CT, **2009**.
- [36] <http://www.bam.de>
- [37] NATO Standardization Agreement (STANAG) on Explosives, Impact Sensitivity Tests, no. 4489, 1st ed., September 17, **1999**.
- [38] WIWEB-Standardarbeitsanweisung 4-5.1.02, Ermittlung der Explosionsgefährlichkeit, hier der Schlagempfindlichkeit mit dem Fallhammer, November 8, **2002**.
- [39] NATO Standardization Agreement (STANAG) on Explosives, Friction Sensitivity Tests, no. 4487, 1st ed., August 22, **2002**.
- [40] WIWEB-Standardarbeitsanweisung 4-5.1.03, Ermittlung der Explosionsgefährlichkeit oder der Reibeempfindlichkeit mit dem Reibeapparat, November 8, **2002**.
- [41] Impact: Insensitive >40 J, less sensitive ≤35 J, sensitive ≤4 J, very sensitive ≤3 J; friction: Insensitive >360 N, less sensitive=360 N, sensitive 80 N, very sensitive ≤80 N, extreme sensitive ≤10 N; According to the UN Recommendations on the Transport of Dangerous Goods (+) indicates: not safe for transport.
- [42] CrysAlisPro, Oxford Diffraction Ltd., *version 171.33.41*, **2009**.
- [43] G. M. Sheldrick, *Acta Cryst.* **2015**, *A71*, 3 – 8.

3 Spiro Oxetanes

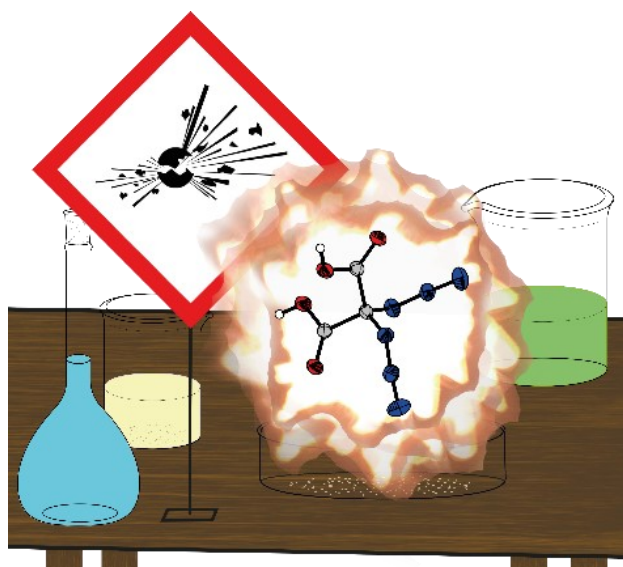
- [44] O. V. Dolomanov, L. J. Bourhis, R. J. Gildea, J. A. K. Howard, H. Puschmann, *J. Appl. Cryst.* **2009**, *42*, 339 – 341.
- [45] SCALE3 ABSPACK –An Oxford Diffraction program (1.0.4, gui: 1.0.3), Oxford Diffraction Ltd., **2005**.
- [46] APEX3. Bruker AXS Inc., Madison, Wisconsin, USA.
- [47] M. W. Chase Jr., NIST-JANAF Thermochemical Tables, Fourth Edition, *J. Phys. Chem. Red. Data, Monograph 9* **1998**, 1 – 1951.

4 Geminal Diazides

Synthesis and Characterization of Geminal Diazido Derivatives based on Diethyl Malonate

Alexander G. Harter, Thomas M. Klapötke, Christian Riedelsheimer, Jörg Stierstorfer, Michael Voggenreiter

As published in *European Journal of Inorganic Chemistry*, **2021**, 23, 2241–2247.
DOI: 10.1002/ejic.202100212



4.1 Abstract

New geminal diazide derivatives based on diethyl 2,2-diazidomalonate (**1**) are presented. 2,2-Diazidomalononic acid (**2**) as well as four alkaline and nitrogen rich salts of 2,2-diazidomalonate (**3–6**) were synthesized and extensively characterized e.g. by low temperature X-ray diffraction. All compounds, which represent promising starting materials for further nitrogen-rich materials, were analyzed by ^1H and ^{13}C NMR spectroscopy, elemental analysis, differential thermal analysis (DTA) and regarding their sensitivity towards impact, friction and electrostatic discharge according to BAM standard techniques. In addition, all synthesized compounds were evaluated regarding their energetic behavior using the EXPLO5 code and compared to TNT in order to provide a comparison to a well-known energetic material. In addition, two selected compounds were investigated towards their aquatic toxicity, using the bioluminescent bacteria *vibrio fischeri*.

4.2 Introduction

Organic azides have been well investigated during the past decades, as they are widely used in various different fields of application ranging from pharmaceutical and medical science^[1,2] over precursors for click chemistry^[3] to chemical biology^[4] and the agricultural sector^[5]. The azido moiety is also commonly found in the area of energetic materials^[6], with many materials like plasticizers, hypergolic ionic liquids and binders containing at least one functional azido group.^[7,8]

Figure 1 shows a selection of commonly used organic azides in exemplary fields of application, as well as an example for the importance of geminal diazides in cyclisation reactions towards tetrazoles.^[9]

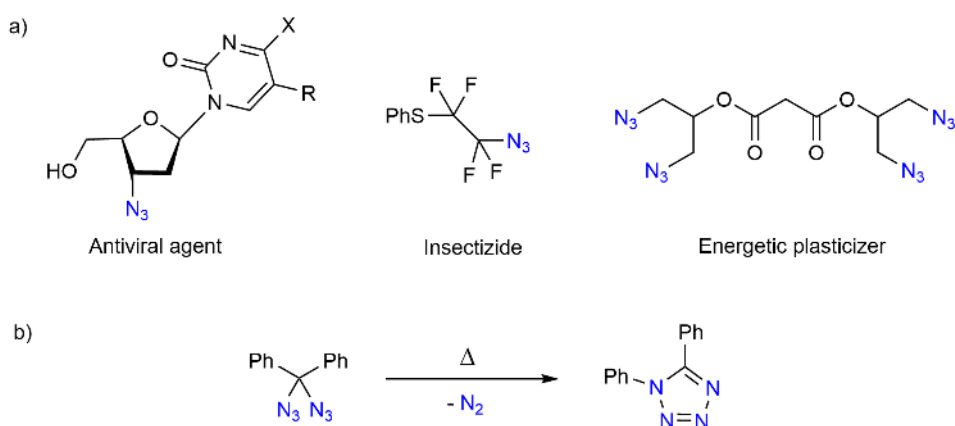


Figure 1. a) Selected applications of organic azides. b) Synthesis of a 1,5-tetrazole starting from a geminal diazide.

4 Geminal Diazides

Some of the reasons for the attractiveness of the azido group in energetic materials are its thermodynamic properties, as it has a high positive heat of formation and adds about 260 kJ mol^{-1} of endothermic energy to a carbon-based molecule.^[10] In terms of developing more environmentally friendly and less toxic energetic materials, which has been of growing interest during the last decades, the azido group plays an important role, as it exclusively releases nitrogen gas during decomposition. However, the functionalization with azido groups is not without risks, as it is well reported, that it possibly increases the sensitivity of molecules towards external stimuli like impact and friction.^[11] Therefore, azido compounds are known for their explosive behavior, when handled without the necessary care.^[12] The subclass of geminal diazides has been discovered by *Forster et al.* in 1908, but is insufficiently investigated until today.^[13] In 2015 *Kirsch et al.* summarized the few reports on reactions involving geminal diazides, and named their potentially explosive character as a possible reason for the lack of research done regarding this topic.^[14] In the following years the spectrum of reactions evolving around the geminal diazido group was further expanded, including click chemistry^[15,16,17], fullerene addition^[18], polymerization^[19] and other new synthetic approaches^[20], summarized in **Figure 2**, but the questions about hazards regarding its explosive behavior still remained unanswered. Therefore, this work focuses on the synthesis of new geminal diazido derivatives based on diethyl malonate and intensively characterizing both new and literature known geminal diazides regarding their energetic and structural properties.

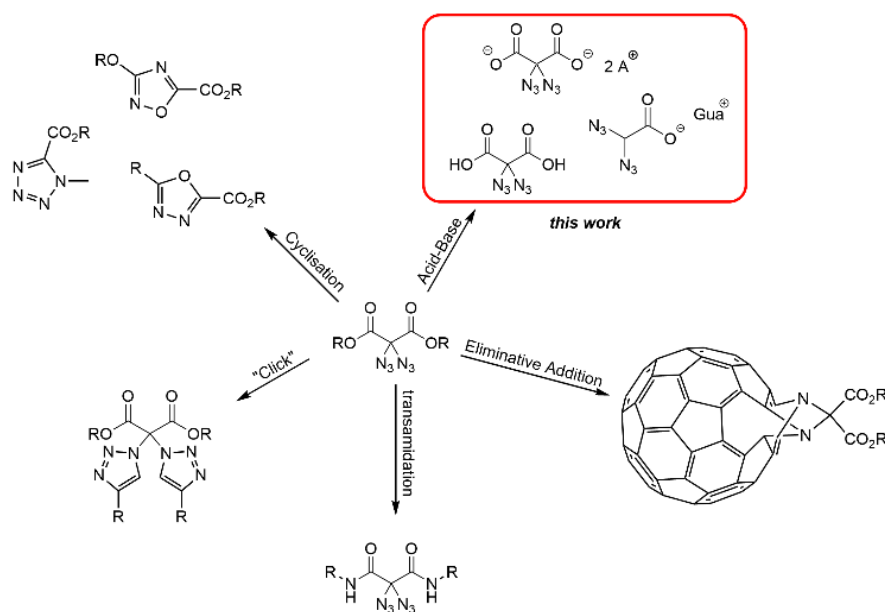
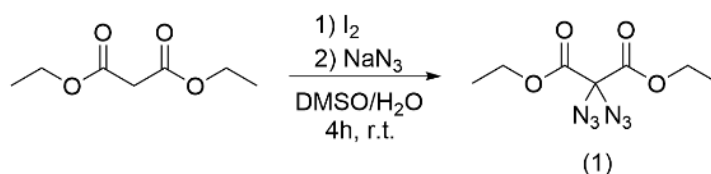


Figure 2. Extension of known reaction types starting from geminal diazide esters with acid base chemistry.

4.3 Results and Discussion

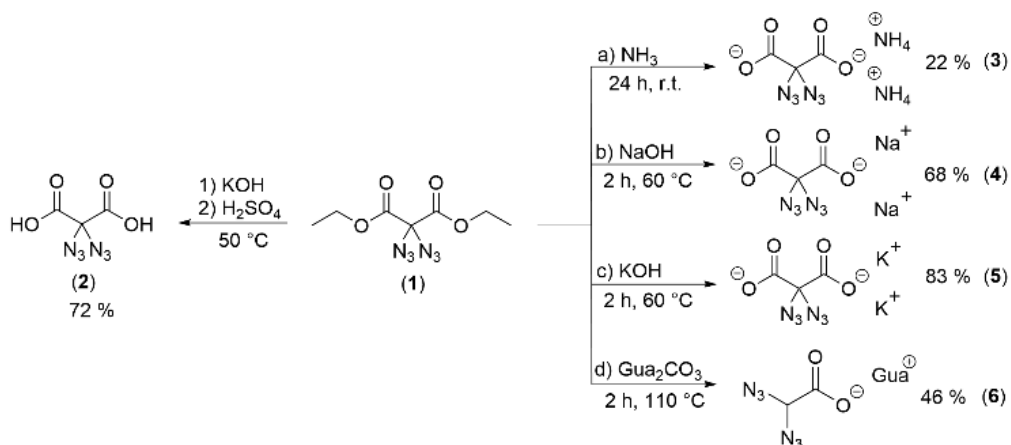
4.3.1 Synthesis

Diethyl 2,2-diazidomalonate (**1**) was synthesized according to a literature procedure, which is shown in Scheme 1.^[21] Diethyl malonate is iodized on the carbon atom between the ester groups in a slightly basic aqueous solution, followed by an iodine azide exchange, which leads to the desired geminal diazide.



Scheme 1. Synthesis of diethyl 2,2-diazidomalonate (**1**).

The synthetic route to the ionic compounds **3–6**, as well as the neutral compound **2** is depicted in scheme 2. All compounds can be formed by Brønsted acid-base chemistry. Hereby, the ethyl residue is cleaved by the basic reactants and the carboxylate-salt formation takes place. Diethyl 2,2-diazidomalonate (**1**) is mixed with water and is reacted with an equimolar amount of the respective base at slightly elevated temperatures. An exception is the guanidinium salt, which only reacts at higher temperatures. Under these conditions, CO₂ is released from **1** and compound **6** is formed. Compound **2** is formed in a similar manner, but acidified with sulfuric acid after formation of the potassium salt in order to form the dicarboxylic acid. The synthesis of 2,2-diazidomalonic acid (**2**) was described in literature, but the compound insufficiently characterized.^[22]



Scheme 2. Synthesis of compounds **2–6** via acid base chemistry.

4.3.2 Crystal Structures

Measurable crystals could be obtained for the compounds **2–6**, either directly from the reaction mixture or by recrystallization from the following solvents (**2**: diethyl ether, **3, 6**: water, **4, 5**: acetone). General information on the X-ray measurements and refinements are given in the SI. Structures were deposited with the CCDC database under the following numbers (**2**: 2068210, **3**: 2068206, **4**: 2068209, **5**: 2068208, **6**: 2068207).

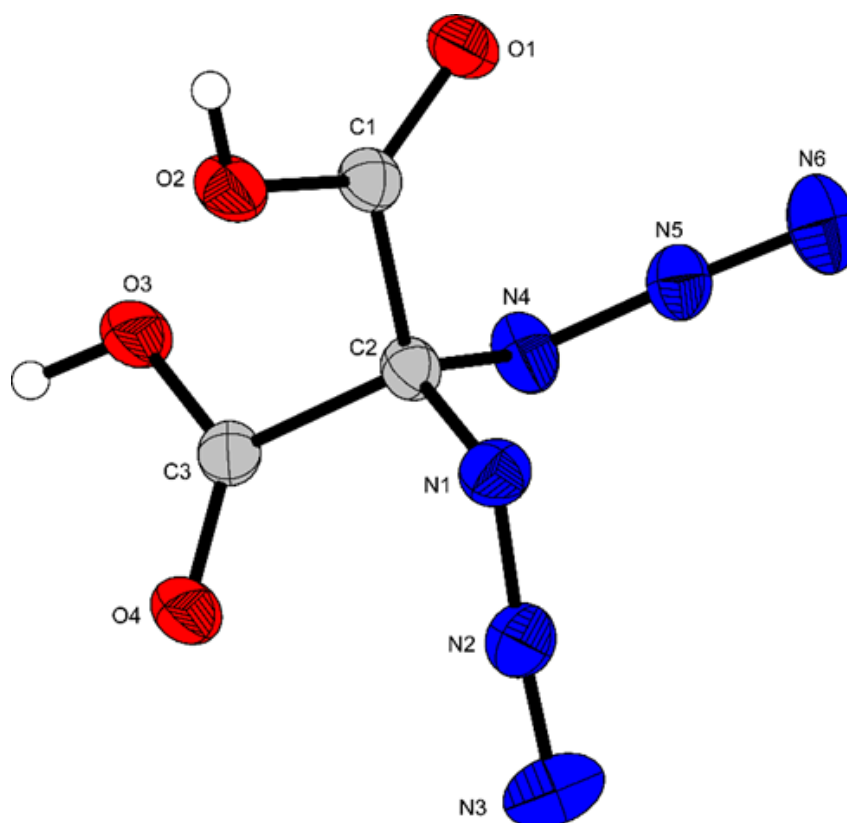


Figure 3. Molecular unit of 2,2-diazidomalonic acid (**2**). Thermal ellipsoids of non-hydrogen atoms are drawn at the 50 % probability level and hydrogen atoms are shown as small spheres of arbitrary radius.

2,2-Diazidomalonic acid (**2**) crystallizes in the orthorhombic space group $Pna2_1$ with a density of 1.705 g cm^{-3} at 173 K and four formula units per unit cell (**Figure 3**). Due to the mutual repulsion of the functional groups, a symmetrical tetrahedral structure is expected. This is confirmed when looking at the angles around the C2 atom. In each case, the angles of the azide groups but also the carboxyl groups are nearly identical, and correspond almost to the 109.5° of a tetrahedral conformation (C1–C2–C3 109.5° , N1–C2–C3 113.9° , N4–C2–C1 112.6° , N1–C2–N4 114.4°). Strong intermolecular hydrogen bonds can be observed between the carboxylic acid groups (O2–H2...O4, O3–H3...O1). All bond lengths comply with the expected values for C–C, C–N, C–O and N–N single and double bonds.^[23,24]

4 Geminal Diazides

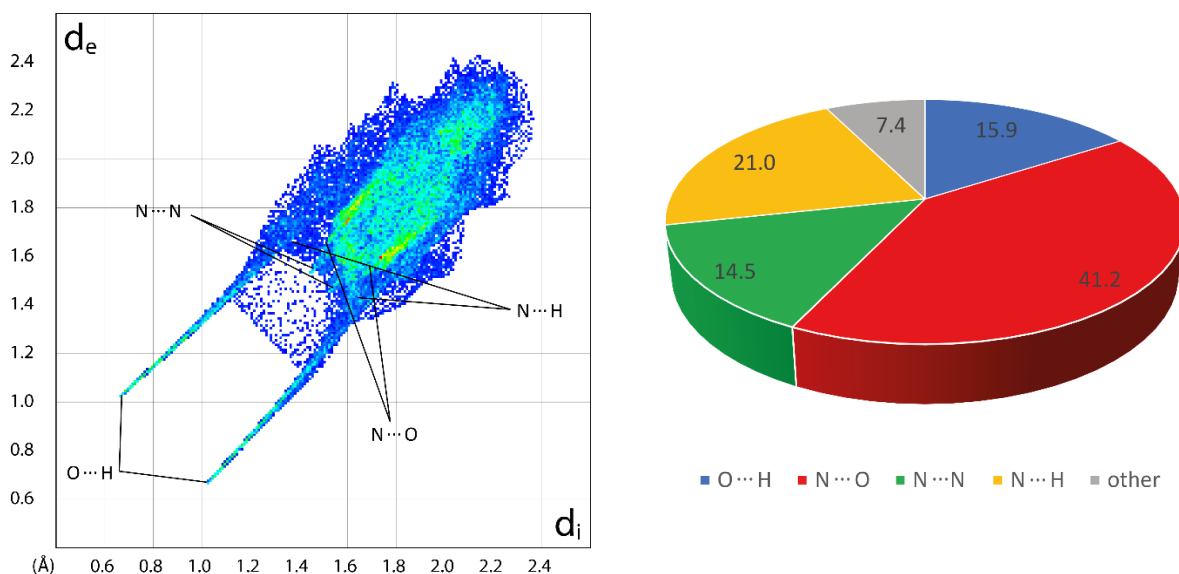


Figure 4. Two-dimensional Hirshfeld fingerprint plot of 2,2-diazidomalonic acid (**2**). Population of close contacts of **2**.

Hirshfeld analysis showed a high percentage of $N \cdots O$ contacts (41.2 %) which have a destabilizing effect (**Figure 4**).^[25,26,27] A stabilizing effect is the $N \cdots H$ interaction (21.0 %) but the distance is large ($>3 \text{ \AA}$) and can be neglected. Further, repulsive $N \cdots N$ interactions (14.5 %) are found which cause strong repulsive interactions in the case of grid deformation caused by mechanical stimuli and therefore indicate a high sensitivity. Strong and stabilizing $O \cdots H$ interactions are found (15.9 %) having a distance of below 2 \AA .^[25,26,27] In total, the destabilizing $N \cdots N$ interactions are quite counterbalanced by the strong $O \cdots H$ interactions and the molecule should be sensitive and a low thermal stability must be assumed.

Diammonium 2,2-diazidomalonate (**3**) crystallizes in the triclinic space group $P-1$ with a density of 1.546 g cm^{-3} at 110 K (**Figure 5**). The cell volume is $472.9(2) \text{ \AA}^3$ with two formula units per cell. The cell constants are $a = 7.0256(17) \text{ \AA}$, $b = 7.3752(13) \text{ \AA}$ and $c = 10.523(3) \text{ \AA}$. Due to the mutual repulsion of the functional groups, a symmetrical tetrahedral structure is expected. This is confirmed when looking at the angles around the C1 atom. In each case, the angles of an azide and a carboxyl group are identical, and correspond almost to the 109.5° of a tetrahedral conformation ($N1-C1-N4$ 113.1° , $N1-C1-C2$ 113.1° , $N1-C1-C3$ 105.4° , $N4-C1-C2$ 105.2°). All bond lengths comply with the expected values for C–C, C–N, C–O and N–N single and double bonds.

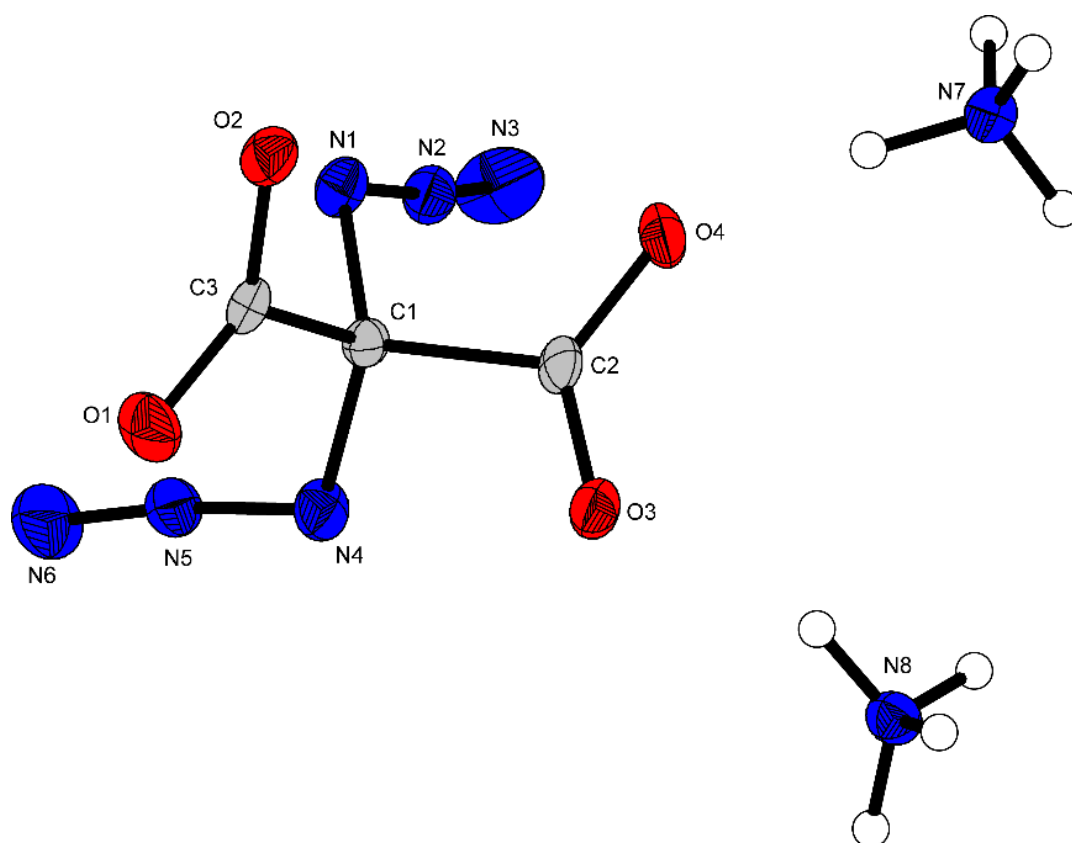


Figure 5. Molecular unit of diammonium 2,2-diazidomalonate (**3**). Thermal ellipsoids of non-hydrogen atoms are drawn at the 50 % probability level and hydrogen atoms are shown as small spheres of arbitrary radius.

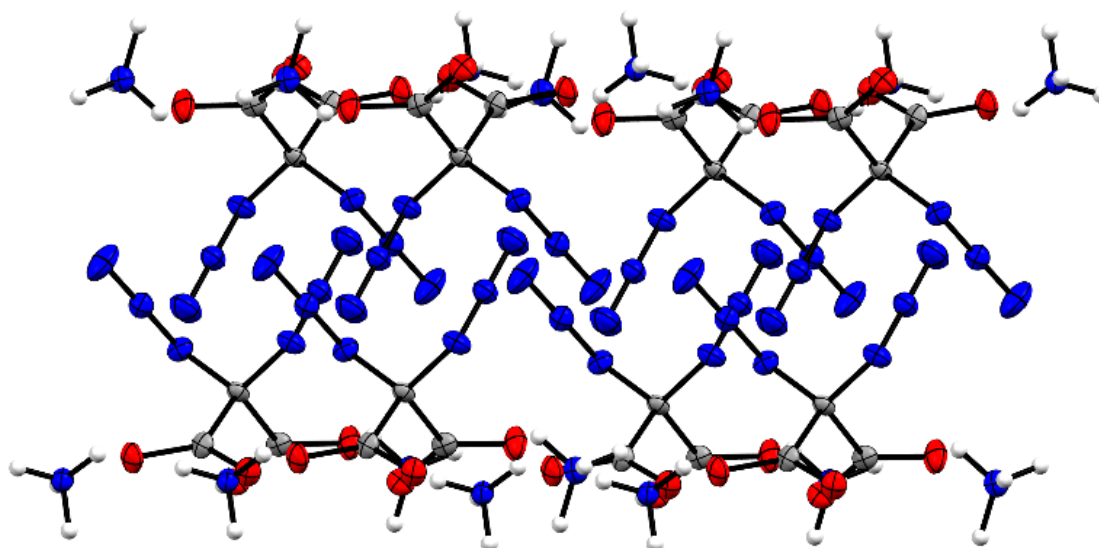


Figure 6. Layered arrangement of eight diammonium 2,2-diazidomalonate (**3**) molecules. Thermal ellipsoids of non-hydrogen atoms are drawn at the 50 % probability level and hydrogen atoms are shown as small spheres of arbitrary radius.

4 Geminal Diazides

Compound **3** forms a layered structure consisting of one layer of the azido moieties surrounded by two layers of the ionic carboxyl and ammonium moieties, shown in **Figure 6**. The repulsing azido groups interact with each other at a distance of 3.07 Å.

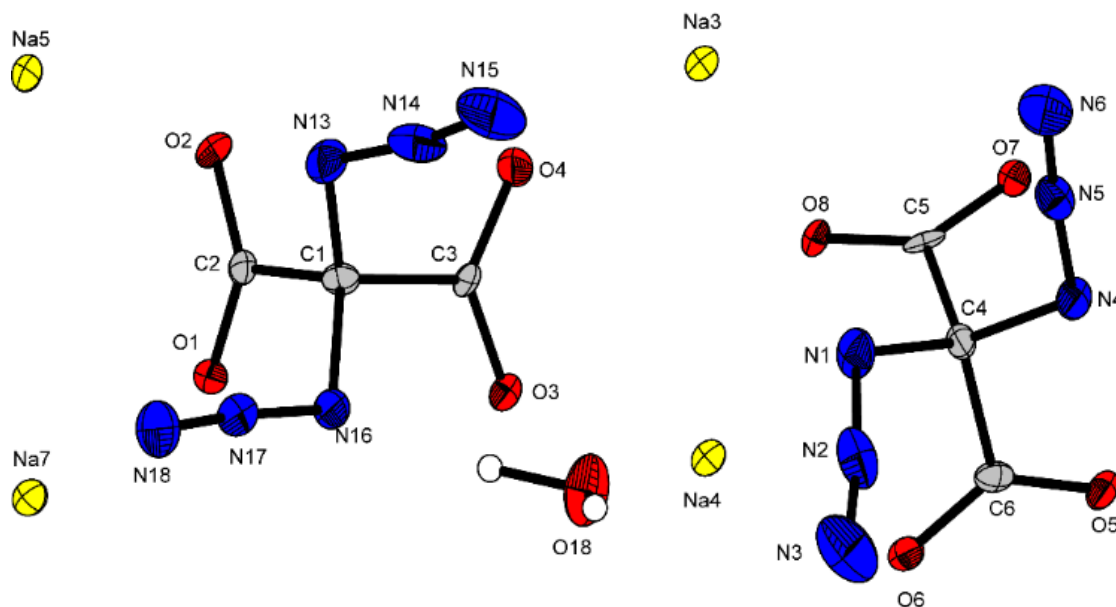


Figure 7. Molecular unit of disodium 2,2-diazidomalonate (**4**). Thermal ellipsoids of non-hydrogen atoms are drawn at the 50 % probability level and hydrogen atoms are shown as small spheres of arbitrary radius.

Disodium 2,2-diazidomalonate semihydrate (**4**) crystallizes in the monoclinic space group $P2_1/c$ with a density of 1.904 g cm^{-3} at 123 K and one water molecule per two malonate molecules (**Figure 7**). In regard to the molecular structure, compound **4** shows a high similarity to compound **3**. It has symmetrical bond angles around the C1 atom and forms an almost tetrahedral structure (N13–C1–C2 108.3° , N13–C1–N16 112.4° , N16–C1–C2 112.0° , N16–C1–C3 106.6°). Compound **2** crystallizes with two water molecules per unit cell. All bond lengths comply with the expected values for C–C, C–N, C–O and N–N single and double bonds.

Dipotassium 2,2-diazidomalonate (**5**) crystallizes in the triclinic space group $P-1$ with a density of 1.981 g cm^{-3} at 173 K (**Figure 8**). The cell volume is $439.70(2) \text{ \AA}^3$ with two formula units per cell. The cell constants are $a = 6.8277(1) \text{ \AA}$, $b = 7.1525(2) \text{ \AA}$ and $c = 10.3164(2) \text{ \AA}$. Compound **5** shows comparable bond angles and lengths as compound **1** and **2**, forming a tetrahedral structure (N1–C2–C1 112.4° , N1–C2–C3 105.6° , N4–C2–C1 106.1° , N4–C2–C3 112.7°).

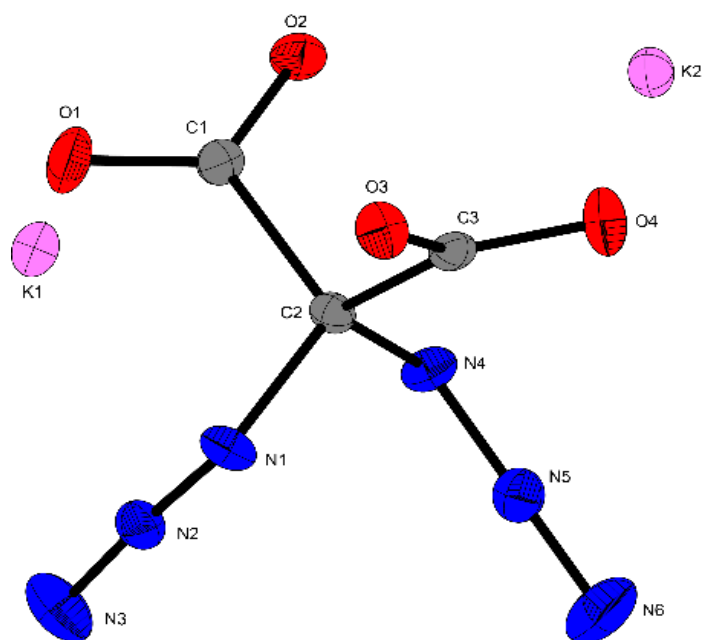


Figure 8. Molecular unit of dipotassium 2,2-diazidomalonate (**5**). Thermal ellipsoids of non-hydrogen atoms are drawn at the 50 % probability level.

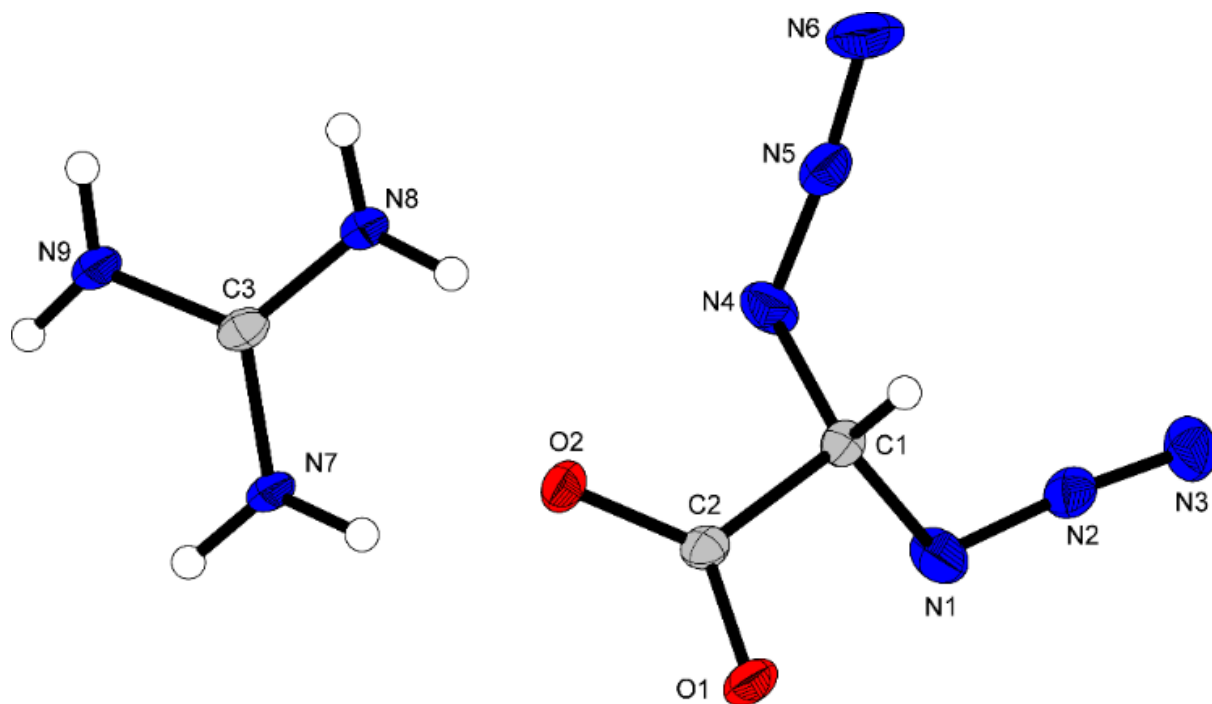


Figure 9. Molecular unit of guanidinium 2,2-diazoacetate (**6**). Thermal ellipsoids of non-hydrogen atoms are drawn at the 50 % probability level and hydrogen atoms are shown as small spheres of arbitrary radius.

4 Geminal Diazides

Guanidinium 2,2-diazoacetate (**6**) crystallizes in the orthorhombic space group $Pna2_1$ with a density of 1.534 g cm^{-3} at 102 K (**Figure 9**). The cell volume is $871.31(19) \text{ \AA}^3$ with four formula units per cell. The cell constants are $a = 15.725(2) \text{ \AA}$, $b = 7.6451(9) \text{ \AA}$ and $c = 7.2477(10) \text{ \AA}$. Regarding its molecular structure compound **6** corresponds surprisingly well with compound **3–5**, even though the missing carboxyl group is replaced by the much smaller hydrogen atom. This is confirmed when looking at the bond angles, which lie in the same range as the ones of previously discussed structure ($\text{N1–C1–N4 } 110.0^\circ$, $\text{N1–C1–C2 } 107.4^\circ$, $\text{N4–C1–C2 } 110.0^\circ$, $\text{C2–C1–H1 } 106.2^\circ$).

4.3.3 Physicochemical Properties

Since the focus of this work was the determination of the energetic properties of the synthesized geminal diazides, all compounds were characterized regarding their physicochemical properties. Therefore, their thermal behavior, detonation parameters and sensitivities towards impact, friction and electrostatic discharge were determined experimentally or computationally and compared to TNT, shown in **Table 1**. TNT was chosen as a comparable because it is a well-known energetic material, regarding the characterization and handling in an industrial scale.^[28]

The thermal behavior of all compounds was measured by differential thermal analysis. All measured compounds show rather low decomposition temperatures ranging from $105 \text{ }^\circ\text{C}$ to $147 \text{ }^\circ\text{C}$, with compound **1** having the highest and compound **5** the lowest value. In regard to the endothermic peaks, no melting points could be observed, with compound **6** showing a water loss at $89 \text{ }^\circ\text{C}$ due to its hygroscopicity. In comparison to TNT all measured compounds are significantly less stable towards thermal influences. It has to be mentioned that compound **2** detonated violently upon direct heating on a metal spatula. All synthesized compounds show an exceptionally high combined nitrogen and oxygen content up to almost 80 % for compounds **2**, **3** and **6**. The sensitivity values towards impact, friction and electrostatic discharge were determined according to the BAM standards.^[30] Compound **2** ($\text{IS} = 1 \text{ J}$, $\text{FS} = 1 \text{ N}$) shows the highest sensitivity towards external stimuli, followed by the potassium salt (**5**, $\text{IS} = 5 \text{ J}$, $\text{FS} = 288 \text{ N}$, $\text{ESD} = 0.16 \text{ mJ}$). Both are significantly more sensitive than TNT and should therefore be handled with the appropriate care. Compound **2** exceeds the values, estimated by the Hirshfeld analysis, significantly, which is unexpected. Compound **1**, **3**, **4** and **6** are insensitive towards all external stimuli. The insensitivity for the sodium salt (**4**, $\text{IS} = >40 \text{ J}$, $\text{FS} = >360 \text{ N}$, $\text{ESD} = 1.00 \text{ mJ}$) can be

4 Geminal Diazides

Table 1. Physiochemical properties of compounds **1–6** and TNT.^[29]

	1	2	3	4 · 0.5 H₂O	5	6	TNT
Formula	C ₇ H ₁₀ N ₆ O ₄	C ₃ H ₂ N ₆ O ₄	C ₃ H ₈ N ₈ O ₄	C ₃ N ₆ O ₄ Na ₂	C ₃ N ₆ O ₄ K ₂	C ₃ H ₇ N ₉ O ₂	C ₇ H ₅ N ₃ O ₆
FW [g·mol ⁻¹]	242.20	186.09	220.15	230.05	262.27	201.15	227.13
IS ^[a] [J]	>40	1	>40	>40	5	>40	15
FS ^[b] [N]	>360	1	>360	> 360	288	>360	>360
ESD ^[c] [J]	–	–	0.60	1.00	0.16	0.54	0.70
N+O ^[d] [%]	61.12	79.55	79.97	65.18	56.44	78.58	55.52
Ω _{CO₂} ^[e] [%]	–99	–26	–43	–19	–25	–23	–74
T _{endo} ^[f] / T _{exo} ^[g] [°C]	–/147	–/116	–/115	–/126	–/105	89/140	79/306
ρ ^[h] [g·cm ⁻³]	1.20	1.67	1.50	1.86	1.95	1.45	1.63
Δ _f H ^o ^[i] [kJ·mol ⁻¹]	–523	–563	–270	–786	–455	–555	–261
EXPLO5 V6.05							
–Δ _E U ^o ^[j] [kJ·kg ⁻¹]	2927	3453	1226	3167	2471	1025	4399
T _{C-J} ^[k] [K]	2245	2966	2299	2342	1857	2494	3192
ρ _{C-J} ^[l] [GPa]	8.8	20.5	16.3	14.8	19.0	16.2	18.8
D _{C-J} ^[m] [m·s ⁻¹]	5509	7348	6912	6589	7275	6998	6878
V ^o ^[n] [dm ³ ·kg ⁻¹]	782	741	883	449	419	874	642

[a] Impact sensitivity (BAM drophammer, method 1 of 6); [b] friction sensitivity (BAM drophammer, method 1 of 6); [c] electrostatic discharge device (OZM research); [d] combined nitrogen and oxygen content; [e] oxygen balance toward carbon dioxide ($\Omega_{CO_2} = (nO - 2xC - yH/2)(1600/FW)$); [f] endothermic event (DTA, $\beta = 5 \text{ }^\circ\text{C}\cdot\text{min}^{-1}$); [g] temperature of decomposition (DTA, $\beta = 5 \text{ }^\circ\text{C}\cdot\text{min}^{-1}$); [h] density at 298 K (for **1** determined volumetrically with a Hamilton syringe 100 μL); [i] standard molar enthalpy of formation; [j] detonation energy; [k] detonation temperature; [l] detonation velocity; [m] detonation pressure; [n] volume of detonation gases at standard temperature and pressure conditions.

4 Geminal Diazides

explained by the crystal water, which generally reduces those values. For compound **1** and **2** no values regarding electrostatic discharge sensitivities could be obtained, since those are liquids. The detonation parameters were determined with EXPLO5 (V6.05) based on densities, obtained from the crystal structures and the heats of formation calculated with the CBS-4M method. The density of compound **1** was determined volumetrically with a Hamilton syringe. The densities of compound **2–6** show a broad range from 1.45 g cm⁻³ to 1.95 g cm⁻³. The distribution of the densities fits the expectations, with the alkaline metal salts (compound **4** and **5**) showing the highest values, followed by the malonic acid (**2**) and the nitrogen rich salts (compound **3** and **6**) at the lower end. With respect to their detonation velocities and pressures compounds **2–6** are all in the range of TNT, with detonation velocities around 7000 m s⁻¹ and detonation pressures between 14.8 GPa and 20.5 GPa. Compound **1** shows significantly lower detonation parameters with $V_D = 5509 \text{ m s}^{-1}$ and $p_{Cl} = 8.8 \text{ GPa}$, which can be explained by its relatively high carbon content. Compounds **2**, **3**, **5** and **6** exceed TNT in terms of their detonation velocity, with 2,2-diazidomalonic acid (**2**) showing the highest value of $V_D = 7348 \text{ m s}^{-1}$ and $p_{Cl} = 20.5 \text{ GPa}$.

4.3.4 Toxicity Assessment

The ecotoxicological impact of this class of geminal diazides was determined by EC₅₀ measurements based on the bioluminescent *Vibrio fischeri* NRRL-B-11177 marine bacteria strain. Therefore, compound **2** and **3** were used as representative examples, and their EC₅₀ values measured after 15 and 30 minutes and compared to the literature known values of TNT^[31]. The EC₅₀ value refers to the concentration of a toxicant which induces a response of 50 % after a specific exposure time. In this case the EC₅₀ value is determined by inhibition of the luminescence by 50 %, when exposed to the toxicant.^[32] Based on the resulting effective concentration the measured substances were classified as nontoxic (>1.00 g L⁻¹), toxic (0.10–1.00 g L⁻¹), and very toxic (<0.10 g L⁻¹). The measured values are shown in Table 2. Compound **2** can be described as nontoxic, since its EC₅₀ value is above 1 g L⁻¹. Compound **3** is classified as toxic with values of 0.45 g L⁻¹ and 0.41 g L⁻¹ after 15 min and 30 min, respectively.

Table 2. EC₅₀ values of **2**, **3** and TNT.

EC ₅₀ (g L ⁻¹)			
Incubation	2	3	TNT
15 min	3.76	0.45	–
30 min	2.16	0.41	0.0036

4.4 Conclusion

In this work, we describe the geminal 2,2-diazidomalononic acid (**2**) as well as their twice deprotonated sodium (**3**), potassium (**4**) and ammonium (**5**) salts. The reaction of 2,2-diazidomalononic acid with guanidinium carbonate yielded guanidinium diazidoacetate. Crystal structures of all synthesized compounds were determined. The densities range from 1.45 g cm^{-3} for the guanidinium salt (**6**) to 1.95 g cm^{-3} for the potassium salt (**5**). All compounds were characterized via NMR, as well as regarding their physiochemical properties, including thermal behavior and sensitivity towards impact, friction and electrostatic discharge. Compound **2** is a highly sensitive substance with values of 1 J impact and 1 N friction and should be handled with extreme care. All other compounds are rather low or not sensitive except the potassium salt (**5**) which has an impact sensitivity of 5 J and a friction sensitivity of 288 N. In addition, all compounds were analyzed towards their detonation parameters, calculated with the EXPLO5 code. Compounds **2**, **3**, **5** and **6** exceed TNT in terms of their detonation velocity with values up to 7348 m s^{-1} for compound **2**. Finally, selected compounds were evaluated by the luminous bacteria inhibition test in regard to their ecotoxicological impact, while it can be assumed, that the salts are lower in toxicity than the neutral form. Potassium salt **3** is categorized as nontoxic, however the malonic acid shows toxicity towards aqueous organisms. In order to give an assessment of possible hazards, when working with geminal diazides all compounds were compared to TNT. Geminal diazides are a versatile class of compounds, which have hereby been proven to show energetic behavior.

For financial support of this work by the Ludwig-Maximilians University (LMU), the Office of Naval Research (ONR) under grant no. ONR N00014-19-1-2078 and the Strategic Environmental Research and Development Program (SERDP) under contract no. W912HQ19C0033 are gratefully acknowledged. The authors thank *Stefan Huber* for his help with the sensitivity measurement and *Jasmin Lechner* for graphical support.

4.5 Supporting Information

4.5.1 Experimental Section

Caution! Geminal Diazides are energetic materials with high sensitivities towards shock and friction. Therefore, proper security precautions (safety glass, face shield, earthened equipment

4 Geminal Diazides

and shoes, Kevlar gloves and ear plugs) have to be applied while synthesizing and handling the described compounds.

Chemicals and solvents were employed as received (Sigma-Aldrich, Acros, TCI, Spirochem AG). ^1H , ^{13}C and ^{14}N spectra were recorded using a Bruker AMX 400 instrument. The chemical shifts quoted in ppm refer to tetramethylsilane (^1H , ^{13}C) and nitromethane (^{14}N). Decompositions temperatures were determined on a Mettler Toledo DSC822e at a heating rate of $5\text{ }^\circ\text{C min}^{-1}$ using $40\ \mu\text{L}$ aluminum crucibles and nitrogen purge gas at a flow rate of $30\ \text{mL min}^{-1}$. Evaluations of thermal behavior were performed using the STAR^e Software Version 16.20. Infrared (IR) spectra were recorded using a Perkin-Elmer Spektrum One FT-IR instrument. Raman spectra were obtained using a Bruker MultiRam FT Raman spectrometer and a neodymium-doped yttrium aluminum garnet (Nd:YAG) laser ($\lambda = 1064\ \text{nm}$, $1074\ \text{mW}$). Elemental analyses were performed with an Elementar Vario el by pyrolysis of the sample and subsequent analysis of formed gases (standard deviation liquids: $\pm 0.5\%$). The sensitivity data were collected using a BAM (Bundesanstalt für Materialforschung) drophammer^[33] according to STANAG 4489^[34] modified instruction^[35] and a BAM friction tester^[36] according to STANAG 4487^[37] modified instruction. The classification of the tested compounds results from the 'UN Recommendations on the Transport of Dangerous Goods'.^[38]

Diethyl 2,2-diazidomalonate (1)

Diethyl 2,2-diazidomalonate (**1**) was synthesized according to literature. The pure product was obtained as a colorless oil in yields of 80 %.

$^1\text{H NMR}$ (400 MHz, DMSO-d_6): δ (ppm) = 4.36 (q, 4H, OCH_2CH_3), 1.32 (t, 6H, CH_3); $^{13}\text{C NMR}$ (101 MHz, DMSO-d_6): δ (ppm) = 163.5 (CO_2Et), 79.8 ($\text{C}(\text{N}_3)_2$), 64.9 (OCH_2CH_3), 13.9 (OCH_2CH_3); **IR** (ATR, rel. int.): $\tilde{\nu}$ (cm^{-1}) = 2987 (w), 2359 (w), 2340 (w), 2119 (s), 1754 (s), 1467 (w), 1447 (w), 1393 (w), 1369 (w), 1298 (m), 1226 (s), 1095 (m), 1066 (s), 1043 (s), 1016 (s), 854 (m), 822 (w), 770 (m), 739 (m), 667 (w); **Elemental analysis**: calcd. (%) for $\text{C}_7\text{H}_{10}\text{N}_6\text{O}_4$ ($242.20\ \text{g mol}^{-1}$): C 34.71, H 4.16, N 34.70; found: C 35.28, H 3.91, N 33.87; **Sensitivities**: BAM impact: $>40\ \text{J}$, BAM friction: $>360\ \text{N}$; **DTA** ($5\text{ }^\circ\text{C min}^{-1}$): $T_{\text{exo}} = 147\text{ }^\circ\text{C}$.

2,2-Diazidomalononic acid (2)

Diethyl 2,2-diazidomalonate (**1**) (500 mg, 2.06 mmol, 1.0 eq.) was mixed with 1 ml water and potassium hydroxide (500 mg, 8.26 mmol, 4 eq.) was added to the mixture. The mixture was

4 Geminal Diazides

stirred at 50 °C until there was no trace of the undissolved diethyl 2,2-diazidomalonate (**1**) visible. Afterwards an aqueous solution of 30 % sulfuric acid (2,70 g, 8.26 mmol, 4 eq.) was added to the solution. After extraction with diethyl ether (20 ml) the organic phase was dried over magnesium sulfate and left for crystallization. 2,2-Diazidomalononic acid (**2**) (275 mg, 1.48 mmol, 72 %) was obtained as colorless crystals, which are highly hydroscopic.

¹H NMR (400 MHz, CDCl₃): δ (ppm) = 8.79; **¹³C NMR** (101 MHz, CDCl₃): δ (ppm) = 166.0, 79.9; **IR** (ATR, rel. int.): $\tilde{\nu}$ (cm⁻¹) = 2926 (w), 2102 (s), 1734 (m), 1407 (w), 1196 (s), 975 (m), 899 (m), 687 (m), 550 (m), 467 (m), 433 (m); **Elemental analysis**: calcd. (%) for C₇H₁₀N₆O₄ (242.20 g mol⁻¹): C 34.71, H 4.16, N 34.70; found: C 35.28, H 3.91, N 33.87; **Sensitivities**: BAM impact: 1 J, BAM friction: 1 N; **DTA** (5 °C min⁻¹): T_{exo} = 115 °C.

Diammonium 2,2-diazidomalonate (3)

Diethyl 2,2-diazidomalonate (**1**) (1.0 g, 4.12 mmol, 1.0 eq.) was mixed with 10 ml water and ammonia (2.4 ml, 16.48 mmol, 4.0 eq.) was added to the solution. The solution was left to stir for 24 hours at room temperature after which the remaining solvent was removed in vacuo. The oil-like product was allowed to stand for crystallization and was then washed with diethyl ether, yielding a white microcrystalline solid (200 mg, 0,91 mmol, 22 %).

¹H NMR (400 MHz, DMSO-d₆): δ (ppm) = 6.90 (s, 8H); **¹³C NMR** (101 MHz, DMSO-d₆): δ = 169.0, 114.4; **IR** (ATR, rel. int.): $\tilde{\nu}$ (cm⁻¹) = 3171 (m), 3007 (m), 2850 (m) 2263 (w), 2131 (m), 2106 (s), 1611 (s), 1425 (s), 1382 (s), 1309 (s), 1238 (w), 1209 (s), 1156 (w), 1107 (w), 1046 (w), 1026 (w), 1007 (m), 832 (w), 783 (m), 715 (s), 599 (m), 555 (m), 472 (m), 437 (w), 424 (w); **Elemental analysis**: calcd. (%) for C₃H₈N₈O₄ (220.07 g mol⁻¹): C 16.37, H 3.66, N 50.90; found: C 16.33, H 3.68, N 51.49; **Sensitivities** (grain size: 100 - 300 μm): BAM impact: >40 J, BAM friction: >360 N, ESD: 0.608 J.; **DTA** (5 °C min⁻¹): T_{exo} = 115 °C.

Disodium 2,2-diazidomalonate semihydrate (4)

Diethyl 2,2-diazidomalonate (**1**) (250 mg, 1.03 mmol, 1.0 eq.) was mixed with 5 ml water and sodium hydroxide (82.6 mg, 2.06 mmol, 2.0 eq.) was added to the solution. The solution was left to stir for 1 h at room temperature, followed by 2 h at 60 °C. The remaining solvent was concentrated in vacuo. Disodium 2,2-diazidomalonate monohydrate was obtained as a yellow powder (175 mg, 0,71 mmol, 68 %), which was recrystallized from acetone for x-ray measurements.

4 Geminal Diazides

¹³C NMR (101 MHz, DMSO-d₆): δ (ppm) = 170.6, 108.9; **IR** (ATR, rel. int.): $\tilde{\nu}$ (cm⁻¹) = 3757 (w), 3662 (w), 3537 (w) 2432 (w), 2104 (s), 1667 (s), 1634 (s), 1606 (m), 1403 (m), 1315 (s), 1206 (s), 1128 (w), 1059 (w), 1041 (w), 1007 (m), 843 (w), 817 (w), 789 (s), 722 (m), 708 (m), 693 (m), 601 (w), 568 (w), 559 (w), 470 (m), 435 (w), 411 (w); **Elemental analysis**: calcd. (%) for C₃H₂N₆O₅Na₂ (248.07 g mol⁻¹): C 14.53, H 0.81, N 33.88; found: C 14.29, H 0.58, N 30.22; **Sensitivities** (grain size: 100 – 500 μ m): BAM impact: >40 J, BAM friction: >360 N, ESD: 1.0 J.; **DTA** (5 °C min⁻¹): T_{exo} = 126 °C.

Dipotassium 2,2-diazidomalonate (5)

Diethyl 2,2-diazidomalonate (**1**) (250 mg, 1.03 mmol, 1.0 eq.) was mixed with 5 ml water and potassium hydroxide (115,8 mg, 16.48 mmol, 2.0 eq.) was added to the solution. The solution was left to stir for 1 h at room temperature, followed by 2 h at 60 °C. The remaining solvent was concentrated in vacuo. After recrystallization from acetone dipotassium 2,2-diazidomalonate was obtained as a white crystalline solid (210 mg, 0,80 mmol, 83 %).

¹³C NMR (101 MHz, CDCl₃): δ = 170.6, 107.9; **IR** (ATR, rel. int.): $\tilde{\nu}$ (cm⁻¹) = 3322 (w), 2432 (w), 2265 (w) 2133 (m), 2103 (s), 2047 (w), 1645 (s), 1628 (s), 1397 (m), 1379 (m), 1344 (m), 1312 (s), 1243 (s), 1214 (s), 1124 (w), 1036 (w), 1024 (w), 1003 (s), 831 (m), 809 (w), 784 (s), 737 (s), 707 (s), 597 (m), 557 (m), 472 (s), 423 (w); **Elemental analysis**: calcd. (%) for C₃N₆O₄K₂ (261.93 g mol⁻¹): C 13.74, N 32.04; found: C 13.20, N 30.53; **Sensitivities** (grain size: 500 - 1000 μ m): BAM impact: 5 J, BAM friction: 288 N, ESD: 0.16 J.; **DTA** (5 °C min⁻¹): T_{exo} = 105 °C.

Guanidinium 2,2-diazoacetate (6)

Diethyl 2,2-diazidomalonate (**1**) (250 mg, 1.03 mmol, 1.0 eq.) was mixed with 10 ml water and guanidinium carbonate (93 mg, 0.52 mmol, 0.5 eq.) was added to the solution. The solution was left to stir for 2 h at 110 °C. The remaining solvent was concentrated in vacuo. A yellow hygroscopic powder (105 mg, 0,47 mmol, 46 %) was obtained, which was recrystallized from water for x-ray measurements.

¹H NMR (400 MHz, DMSO-d₆): δ (ppm) = 7.31 (s, 6H), 4.65 (s, 1H); **¹³C NMR** (101 MHz, DMSO-d₆): δ (ppm) = 169.7, 158.4, 75.5; **IR** (ATR, rel. int.): $\tilde{\nu}$ (cm⁻¹) = 3343 (m), 3134 (m), 2116 (m), 2042 (m), 1651 (s), 1612 (s), 1396 (m), 1321 (m), 1302 (m), 1267 (m), 1238 (m), 1062 (w), 1033 (w), 1009 (w), 986 (m), 881 (w), 788 (m), 744 (m), 526 (s), 459 (s), 407 (s); **Elemental analysis**: calcd. (%) for C₇H₁₄N₆O₆ (237.18 g mol⁻¹): C 15.19, H 4.67, N 53.15; found: C 14.90, H 5.01, N 66.92;

Sensitivities (grain size: > 1000 μm): BAM impact: >40 J, BAM friction: >360 N, ESD: 0.54 J; **DTA** ($5\text{ }^\circ\text{C min}^{-1}$): $T_{\text{endo}} = 89\text{ }^\circ\text{C}$, $T_{\text{exo}} = 140\text{ }^\circ\text{C}$.

4.5.2 X-ray Diffraction

Crystal structure data were obtained by measurements on an Oxford Xcalibur3 diffractometer with a Spellman generator (voltage 50 kV, current 40 mA) and a Kappa CCD area for data collection using Mo-K α radiation ($\lambda = 0.71073\text{ \AA}$) or a Bruker D8 Venture TXS diffractometer equipped with a multilayer monochromator, a Photon 2 detector and a rotation-anode generator (Mo-K α radiation). The data collection was performed using the CRYSTALIS RED software.^[39] The solution of the structure was performed by direct methods and refined by full-matrix least-squares on F2 (SHELXT)^[40] implemented in the OLEX2^[41] software suite. The non-hydrogen atoms were refined anisotropically and the hydrogen atoms were located and freely refined. The absorption correction was carried out by a SCALE3ABSPACK multiscan method.^[42] The DIAMOND2 plots shown with thermal ellipsoids at the 50% probability level and hydrogen atoms are shown as small spheres of arbitrary radius. The SADABS program embedded in the Bruker APEX3 software was used for multi-scan absorption corrections in all structures.^[43]

Table 3. Crystallographic data and structure refinement details for the prepared compounds **2-4**.

	2,2 Diazidomalic acid (2)	Diammonium 2,2-diazidomalonate (3)	Disodium 2,2-diazidomalonate semihydrate (4)
Formula	C ₃ H ₂ N ₆ O ₄	C ₃ H ₈ N ₈ O ₄	C ₁₂ H ₄ N ₂₄ Na ₈ O ₁₈
FW [g mol ⁻¹]	186.11	220.17	956.31
Crystal system	orthorhombic	triclinic	monoclinic
Space group	<i>Pna</i> 2 ₁ (No. 33)	<i>P</i> -1 (No. 2)	<i>P</i> 2 ₁ / <i>c</i> (No. 14)
Color / Habit	colourless rod	colourless block	colourless platelet
Size [mm]	0.02 x 0.03 x 0.14	0.08 x 0.10 x 0.30	0.10 x 0.18 x 0.25
a [Å]	11.1440(4)	7.0256(17)	11.6751(6)
b [Å]	5.9329(2)	7.3752(13)	12.5066(7)
c [Å]	10.9654(4)	10.523(3)	23.215(2)
α [°]		105.015(18)	90
β [°]		100.15(2)	100.154(7)
γ [°]		110.12(2)	90
V [Å ³]	724.99(4)	472.9(2)	3336.7(4)
Z	4	2	4
ρ _{calc.} [g cm ⁻³]	1.705	1.546	1.904
μ [mm ⁻¹]	0.156	0.138	0.255
F(000)	376	228	1904
λ _{MoKα} [Å]	0.71073	0.71073	0.71073
T [K]	173	110	123
θ Min-Max [°]	3.7, 26.4	2.1, 26.4	1.8, 26.4
Dataset	-13: 13 ; -7: 7 ; -13: 13	-8: 7 ; -9: 9 ; -13: 12	-14: 14 ; -15: 15 ; -29: 29
Reflections collected	13833	2952	26923
Independent refl.	1468	1885	6832
R _{int}	0.032	0.047	0.069
Observed reflections	1432	1215	3259
Parameters	126	169	566
R ₁ (obs) ^[a]	0.0220	0.0661	0.0532
wR ₂ (all data) ^[b]	0.0605	0.1360	0.1313
S ^[c]	1.07	1.05	0.99
Resd. dens [e Å ⁻³]	-0.14, 0.23	-0.32, 0.31	-0.38, 0.41
Device type	Bruker D8 Venture TXS	Xcalibur Sapphire3	Xcalibur Sapphire3
Solution	SIR-92	SIR-92	SIR-92
Refinement	SHELXL-2018	SHELXL-2018	SHELXL-2018
Absorption correction	Multi-Scan	Multi-Scan	Multi-Scan
CCDC	2068210	2068206	2068209

^[a]R₁ = $\sum ||F_o| - |F_c|| / \sum |F_o|$; ^[b]wR₂ = $[\sum [w(F_o^2 - F_c^2)^2] / \sum [w(F_o^2)]]^{1/2}$; $w = [\sigma^2(F_o^2) + (xP)^2 + yP]^{-1}$ and $P = (F_o^2 + 2F_c^2) / 3$; ^[c]S = $\{\sum [w(F_o^2 - F_c^2)^2] / (n-p)\}^{1/2}$ (n = number of reflections; p = total number of parameters).

Table 4. Crystallographic data and structure refinement details for the prepared compounds **5** and **6**.

	Dipotassium 2,2-diazidomalonate (5)	Guanidinium 2,2-diazoacetate (6)
Formula	C ₃ N ₆ O ₄ K ₂	C ₃ H ₆ N ₉ O ₂
FW [g mol ⁻¹]	262.29	201.18
Crystal system	Triclinic	orthorhombic
Space group	<i>P</i> -1 (No. 2)	<i>Pna</i> 2 ₁ (No. 33)
Color / Habit	colourless block	colorless platelet
Size [mm]	0.11 x 0.33 x 0.49	0.12 x 0.15 x 0.20
a [Å]	6.8277(1)	15.725(2)
b [Å]	7.1525(2)	7.6451(9)
c [Å]	10.3164(2)	7.2477(10)
α [°]	103.163(2)	
β [°]	101.170(2)	
γ [°]	110.137(2)	
V [Å ³]	439.70(2)	871.31(19)
Z	2	4
ρ _{calc.} [g cm ⁻³]	1.981	1.534
μ [mm ⁻¹]	1.084	0.129
F(000)	260	416
λ _{MoKα} [Å]	0.71073	0.71073
T [K]	173	102
θ Min-Max [°]	4.2, 26.0	3.0, 25.0
Dataset	-8: 8 ; -8: 8 ; -12: 12	-18: 18 ; -8: 9 ; -8: 8
Reflections collected	6268	8310
Independent refl.	1719	1504
R _{int}	0.022	0.047
Observed reflections	1599	1365
Parameters	137	155
R ₁ (obs) ^[a]	0.0196	0.0400
wR ₂ (all data) ^[b]	0.0512	0.0814
S ^[c]	1.06	1.12
Resd. dens [e Å ⁻³]	-0.23, 0.39	-0.19, 0.19
Device type	Xcalibur Sapphire3	Bruker D8 Venture TXS
Solution	SIR-92	SIR-92
Refinement	SHELXL-2018	SHELXL-2018
Absorption correction	Multi-Scan	Multi-Scan
CCDC	2068208	2068207

^[a]R₁ = $\sum ||F_o| - |F_c|| / \sum |F_o|$; ^[b]wR₂ = $[\sum [w(F_o^2 - F_c^2)^2] / \sum [w(F_o^2)]]^{1/2}$; w = $[\sigma^2(F_o^2) + (xP)^2 + yP]^{-1}$ and $P = (F_o^2 + 2F_c^2) / 3$; ^[c]S = $\{\sum [w(F_o^2 - F_c^2)^2] / (n-p)\}^{1/2}$ (n = number of reflections; p = total number of parameters).

4.5.3 Heat of Formation Calculation and Thermal Analysis

The atomization was used to determine the heat of formation of **1–6** using the atom energies in **Table 5**.

$$\Delta_f H^\circ_{(g, M, 298)} = H_{(molecule, 298)} - \sum H^\circ_{(atoms, 298)} + \sum \Delta_f H^\circ_{(atoms, 298)}$$

Table 5. CBS-4M electronic enthalpies for atoms C, H, N and O and their literature values.

	$-H^{298} / \text{a.u.}$	$\Delta_f H^\circ_{\text{gas}}^{[44]}$
H	0.500991	217.998
C	37.786156	716.68
N	54.522462	472.68
O	74.991202	249.18

The Gaussian16 program package was used to calculate room temperature enthalpies on the CBS-4M level of theory.^[45] In order to obtain the heat of formation for compounds **4** and **7–9**, Trouton's Rule has to be applied ($\Delta H_{\text{sub}} = 188 \cdot T_m$).

Table S4: Heat of formation calculation results for compounds **1–6**.

M	$-H^{298} [a.u.]$ [a.u.]	$\Delta_f H^\circ(g, M)$ [b] [kJ mol ⁻¹]	$\Delta_f H^\circ(s)$ [d] [kJ mol ⁻¹]	Δn	$\Delta_f U(s)$ [e] [kJ kg ⁻¹]
1	900.847328	-88.8	-126.6	-10.0	-420.3
2	743.916874	-31.6	-104.7	-6.0	-482.8
3	742.780754	-95.2	-249.7	-10.0	-1021.7
4	742.780754	-115.4	-785.7	-5.0	-3361.6
5	742.780754	-95.2	-584.6	-5.0	-2181.6
6	555.044724	-117.5	-190.0	-9.0	-1055.6

[a] CBS-4M electronic enthalpy; [b] gas phase enthalpy of formation; [c] sublimation enthalpy; [d] standard solid state enthalpy of formation; [e] solid state energy of formation.

4.6 References

- [1] C. Pan, A. Abdukader, J. Han, Y. Cheng, C. Zhu, *Chem. Eur. J.* **2014**, *20*, 3606.
- [2] T. S. Lin, M. S. Chen, C. McLaren, Y. S. Gao, I. Ghazzouli, W. H. Prusoff, *J. Med. Chem.* **1987**, *30*, 440.
- [3] H. A. Michaels, L. Zhu, *Chem. Asian J.* **2011**, *6*, 2825-2834.
- [4] C. I. Schilling, N. Jung, M. Biskup, U. Schepers, S. Bräse, *Chem. Soc. Rev.* **2011**, *40*, 4840-4871.
- [5] S. Voltrová, M. Muselli, J. Filgas, V. Matoušek, B. Klepetářová, P. Beier, *Org. Biomol. Chem.* **2017**, *15*, 4962.

4 Geminal Diazides

- [6] M. Claßen, S. B. Heimsch, T. M. Klapötke, *Prop., Explos., Pyrotech.* **2019**, *44*, 1515.
- [7] D. Kumari, K. D. B. Yamajala, H. Singh, R. R. Sanghavi, N. A. Shri, K. Raju, S. Banerjee, *Propellants Explos. Pyrotech.* **2013**, *38*, 805-809.
- [8] Y. Tang, J. M. Shreeve, *Chem. Eur. J.*, **2015**, *21*, 7285-7291.
- [9] K. Holzschneider, M. L. Tong, F. Mohr, S. F. Kirsch, *Chem. Eur. J.* **2019** *25* (50), 11725-11733.
- [10] M. A. Petrie, J. A. Sheehy, J. A. Boatz, G. Rasul, G. K. Surya Prakash, G. A. Olah, K. O. Christe, *J. Am. Chem. Soc.* **1997**, *119*, 8802-8808.
- [11] O.V. Dorofeeva, O.N. Ryzhova, M.A. Suntsova, *J. Phys. Chem. A* **2013**, *117*, 6835-6845.
- [12] A. Hassner, M. Stern, H. E. Gottlieb, F. Frolow, *J. Org. Chem.* **1990**, *55*, 2304-2306.
- [13] M. O. Forster, H. E. Fierz, W. P. Joshua, *J. Chem. Soc.* **1908**, *93*, 1070-1074.
- [14] A. P. Häring, S. F. Kirsch, *Molecules* **2015**, *20*, 20042-20062.
- [15] F. Borghi, I. E. Çelik, P. Biallas, F. Mittendorf, S. F. Kirsch, *Eur. J. Org. Chem.*, **2020**, 4389-4398.
- [16] H. Erhardt, F. Mohr, S. F. Kirsch, *Chem. Commun.* **2016**, *52*, 545-548.
- [17] K. Holzschneider, F. Mohr, S. F. Kirsch, *Org. Lett.* **2018**, *20* (22), 7066-7070.
- [18] G. X. Dong; J. S. Li, T. H. Chan, *J. Chem. Soc. Chem. Commun.* **1995**, 1725-1726.
- [19] P. Biallas, J. Heider, S. F. Kirsch, *Polym. Chem.* **2019**, *10*, 60-64.
- [20] H. Erhardt, A. P. Häring, A. Kotthaus, M. Roggel, M. L. Tong, P. Biallas, M. Jübermann, F. Mohr, S. F. Kirsch; *J. Org. Chem.* **2015**, *80*, 12460-12469.
- [21] M. O. Forster, R. Müller, *J. Chem. Soc.* **1910**, *97*, 126-142.
- [22] A. F. Holleman, E. Wiberg, N. Wiberg in *Lehrbuch der anorganischen Chemie*, de Gruyter, New York, **2007**.
- [23] F. H. Allen, O. Kennard, D. G. Watson, L. Brammer, A. G. Orpen, R. Taylor, *J. Chem. Soc., Perkin Trans. 2* **1987**, 1-19.
- [24] D. E. Dosch, M. Reichel, M. Born, T. M. Klapötke and K. Karaghiosoff, *Cryst. Growth Des.* **2021**, *21*, 1, 243-248.
- [25] Y. Ma, A. Zhang, X. Xue, D. Jiang, Y. Zhu and C. Zhang, *Cryst. Growth Des.* **2014**, *14*, 6101-6114.
- [26] M. A. Spackman and D. Jayatilaka, *CrystEngComm* **2009**, *11*, 19-32.
- [27] M. Reichel, D. Dosch, T. Klapötke and K. Karaghiosoff, *J. Am. Chem. Soc.* **2019**, *141*, 19911-19916.
- [28] T. M. Klapötke in *Energetic Materials Encyclopedia*, Vol. 2 E - N, DeGruyter, Berlin, **2021**, pp. 773-968.
- [29] M. Härtel, **2017**: Studies towards the gas-phase detection of hazardous materials by vapor pressure measurements with the transpiration method in combination with vacuum outlet GC/MS. Dissertation, LMU München: Fakultät für Chemie und Pharmazie.

4 Geminal Diazides

- [30] Test Methods According to the UN Recommendations on the Transport of Dangerous Goods, Manual of Test and Criteria, Fourth Revised Edition, United Nations Publication, New York and Geneva, **2003**, ISBN 92-1-139087 7, Sales No. E.03.VIII. 2; 13.4.2 Test 3a (ii) BAM Fallhammer.
- [31] O. Drzyzga, T. Gorontzy, A. Schmidt, *Arch. Environ. Contam. Toxicol.* **1995**, *28*, 229-235.
- [32] T. M. Klapötke, B. Krumm, C. C. Unger, *Inorg. Chem.* **2019**, *58*, 4, 2881- 2887.
- [33] <http://www.bam.de>
- [34] NATO Standardization Agreement (STANAG) on Explosives, *Impact Sensitivity Tests*, no. 4489, 1st ed., September 17, **1999**.
- [35] WIWEB-Standardarbeitsanweisung 4-5.1.02, Ermittlung der Explosionsgefährlichkeit, hier der Schlagempfindlichkeit mit dem Fallhammer, November 8, **2002**.
- [36] NATO Standardization Agreement (STANAG) on Explosives, *Friction Sensitivity Tests*, no. 4487, 1st ed., August 22, **2002**.
- [37] WIWEB-Standardarbeitsanweisung 4-5.1.03, Ermittlung der Explosionsgefährlichkeit oder der Reibeempfindlichkeit mit dem Reibeapparat, November 8, **2002**.
- [38] Impact: Insensitive >40 J, less sensitive ≤35 J, sensitive ≤4 J, very sensitive ≤3 J; friction: Insensitive >360 N, less sensitive=360 N, sensitive 80 N, very sensitive ≤80 N, extreme sensitive ≤10 N; According to the UN Recommendations on the Transport of Dangerous Goods (+) indicates: not safe for transport.
- [39] CrysAlisPro, Oxford Diffraction Ltd. version 171.33.41, **2009**.
- [40] G. M. Sheldrick, *Acta Cryst.*, **2015**, *A71*, 3–8.
- [41] Dolomanov, O. V., Bourhis, L. J., Gildea, R. J., Howard, J. A. K. & Puschmann, H. J., *Appl. Cryst.*, **2009**, *42*, 339–341.
- [42] SCALE3 ABSPACK – An Oxford Diffraction program (1.0.4, gui: 1.0.3), Oxford Diffraction Ltd., **2005**.
- [43] APEX3. Bruker AXS Inc., Madison, Wisconsin, USA.
- [44] M. W. Chase Jr., NIST-JANAF Thermochemical Tables, Fourth Edition, *J. Phys. Chem. Ref. Data, Monograph 9*, **1998**, 1 – 1951.
- [45] M. J. Frisch, G. W. Trucks, H. B. Schlegel, G. E. Scuseria, M. A. Robb, J. R. Cheeseman, G. Scalmani, V. Barone, G. A. Petersson, H. Nakatsuji, X. Li, M. Caricato, A. V. Marenich, J. Bloino, B. G. Janesko, R. Gomperts, B. Mennucci, H. P. Hratchian, J. V. Ortiz, A. F. Izmaylov, J. L. Sonnenberg, D. Williams-Young, F. Ding, F. Lipparini, F. Egidi, J. Goings, B. Peng, A. Petrone, T. Henderson, D. Ranasinghe, V. G. Zakrzewski, J. Gao, N. Rega, G. Zheng, W. Liang, M. Hada, M. Ehara, K. Toyota, R. Fukuda, J. Hasegawa, M. Ishida, T. Nakajima, Y. Honda, O. Kitao, H. Nakai, T. Vreven, K. Throssell, J. A. Montgomery, Jr., J. E. Peralta, F. Ogliaro, M. J. Bearpark, J. J. Heyd, E. N. Brothers, K. N. Kudin, V. N. Staroverov, T. A. Keith, R. Kobayashi, J. Normand, K. Raghavachari, A. P. Rendell, J. C. Burant, S.

4 Geminal Diazides

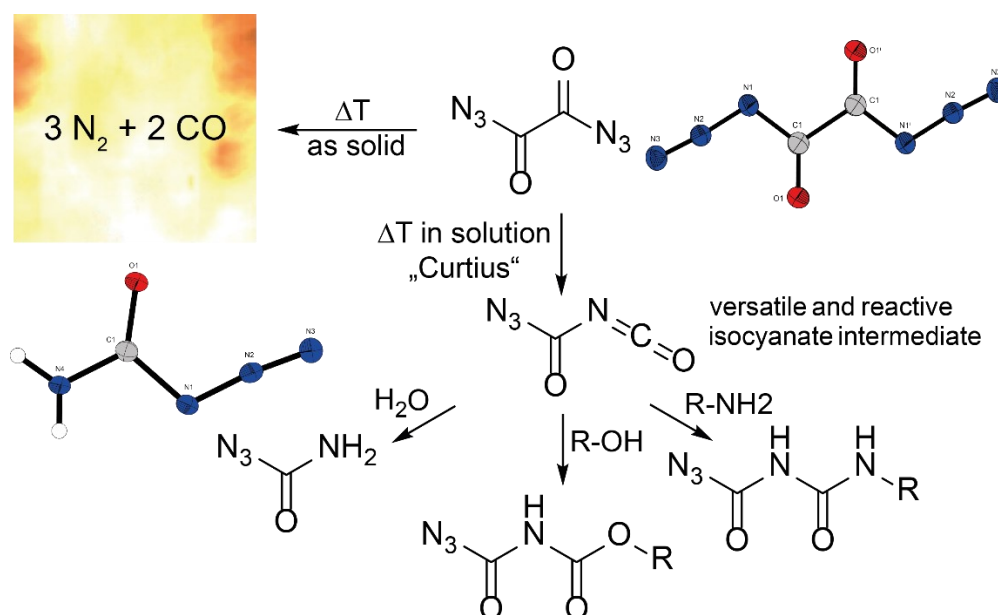
S. Iyengar, J. Tomasi, M. Cossi, J. M. Millam, M. Klene, C. Adamo, R. Cammi, J. W. Ochterski, R. L. Martin, K. Morokuma, O. Farkas, J. B. Foresman, and D. J. Fox, Gaussian16 ,Gaussian, Inc., Wallingford, CT, USA, **2016**.

5 Carbonylazides

Synthesis, Characterization and Energetic Performance of Oxalyl diazide, Carbamoyl azide and *N,N'*-bis(azidocarbonyl)hydrazine

Alexander G. Harter, Thomas M. Klapötke, Jörg Stierstorfer, Michael Voggenreiter and Xiaoqing Zeng

As published in *ChemPlusChem* **2021**, 86(6), 870–874. DOI: 10.1002/cplu.202100214



5.1 Abstract

As pure compounds, small carbonyl azides enjoy a bad reputation, due to the high explosive sensitivity and instability they demonstrate. Consequently, most reported examples have only been poorly characterized. The compounds oxalyl diazide (**1**), carbamoyl azide (**2**), as well as *N,N'*-bis(azidocarbonyl)hydrazine (**3**) were obtained by performing a diazotation reaction on the corresponding hydrazo precursor. Carbamoyl azide (**2**) could also be obtained from oxalyl diazide via *Curtius* rearrangement to the reactive isocyanate, followed by reaction with water. Further, different trapping reactions of the isocyanate with hydroxyl (methanol, oxetan-3-ol) and amino (2-amino-5*H*-tetrazole) functions are described. All products were extensively analyzed using IR, EA, DTA and multinuclear NMR spectroscopy, and the crystal structures elucidated using single crystal X-ray diffraction. In addition, the sensitivities toward friction and impact were determined and the energetic performances of the carbonyl azides were calculated using the EXPLO5 code.

5.2 Introduction

Carbonyl azides were first described more than a century ago by *Curtius* and *Thiele* in 1894.^[1,2] *Curtius* was primarily interested in the explosive nature, as well as the decomposition of carbonyl azides. The low stability of acyl azides limits reports on the synthesis and the characterization of such compounds.^[3] Today, the *Curtius* rearrangement forming isocyanate intermediates and subsequent reaction with water, is a common method to convert carbonyl azides to amines.^[4-6] The number of carbonyl azides, which have been both spectroscopically and structurally characterized has slightly increased in recent years. In 1992, *Willner* and coworkers characterized fluorocarbonyl azide by gas electron diffraction.^[7] *Zeng et al.* published the crystal structure of carbonyl diazide in 2010. This was followed by the work of *Banert et al.* on formyl azide, which was later structurally characterized by *Zeng*.^[8-12] Subsequently, *Zeng et al.* published the structures of *N*-methylcarbamoyl azide, as well as of aryl substituted carbonyl azides such as 1*H*-pyrrole carbonyl azide.^[13,14] Recently, *Benz et al.* successfully synthesized and characterized nitrocarbamoyl azide, which shows remarkable stability.^[15] The publication by *Benz* mentioned the existence of two carbonyl azides, namely, oxalyl diazide and carbamoyl azide, however, neither were characterized (**Fig. 1**).^[2,16-18] It is appropriate to include *N,N'*-bis(azidocarbonyl)hydrazine, which has also been described in the literature, due to the

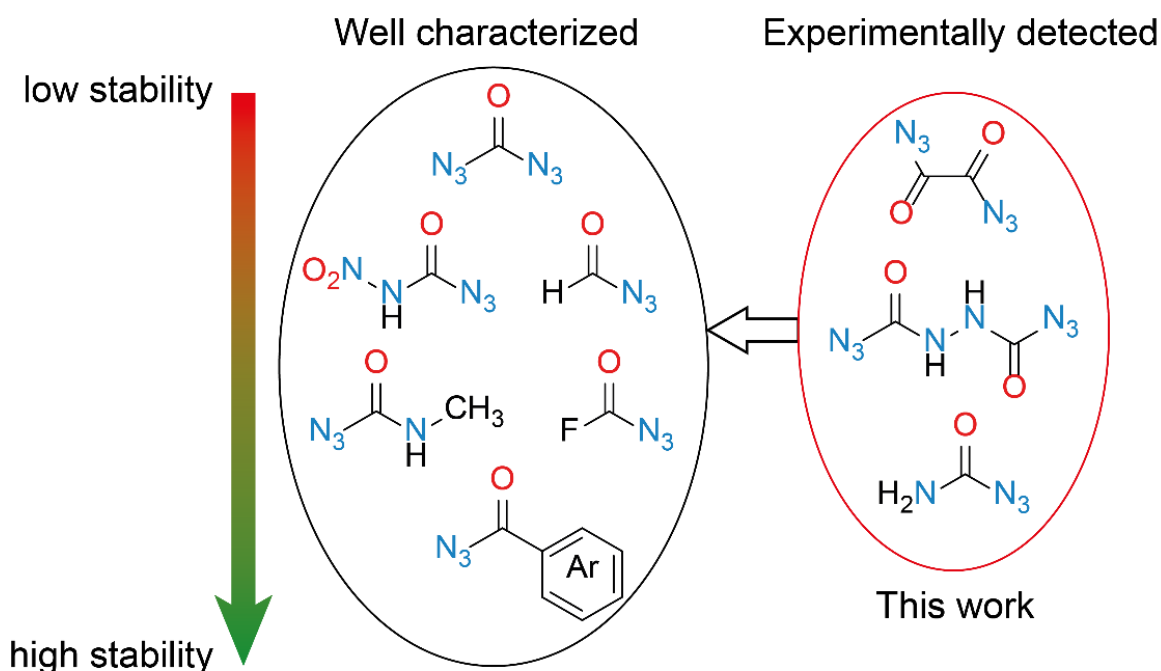


Figure 1. Well-characterized members of the carbonyl azide family arranged with respect to their stability towards heat and external stimuli. This work centers around the structural and physiochemical characterization of the carbonyl azides which have only been mentioned in the literature.

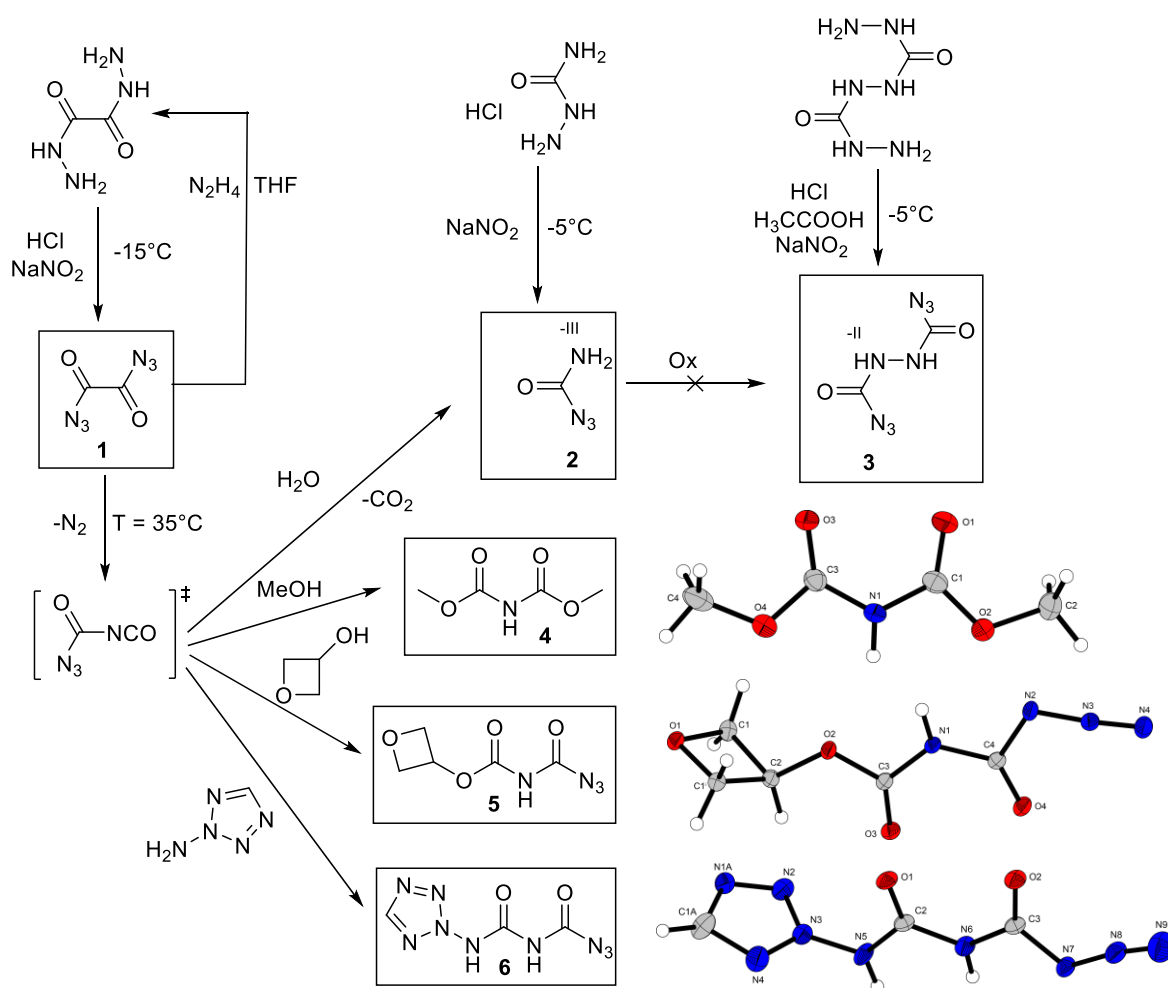
structural relationship it has with both oxalyl diazide and carbamoyl azide.^[19] Not only does this work provide key information on important missing and fundamental members of this class of compounds, namely, on oxalyl diazide (**1**), carbamoyl azide (**2**), and *N,N'*-bis(azidocarbonyl)hydrazine (**3**), it also demonstrates compounds **1–3** to be small, versatile, but very energetic members of the carbonyl azide family. In addition, the decomposition of oxalyl diazide via a Curtius rearrangement to form an isocyanate, as well as subsequent trapping reactions with hydroxyl and amino groups are reported.

5.3 Results and Discussion

The hydrazino precursor compounds were synthesized according to literature procedures.^[16,19] The carbonyl azides (**1–3**) can be synthesized by careful diazotation of the corresponding hydrazo- compounds (**Scheme 1**). The reactions have to be carried out at low temperature in order to achieve high yields: Pure **1** decomposes rapidly in protic solvents at room temperature forming the isocyanate intermediate and reacting with moist air or solvent. Another possible way to obtain **2** is by the Curtius rearrangement of **1**, followed by reaction with water. Furthermore, the reactive isocyanate intermediate can also be trapped with compounds containing a hydroxyl

5 Carbonylazides

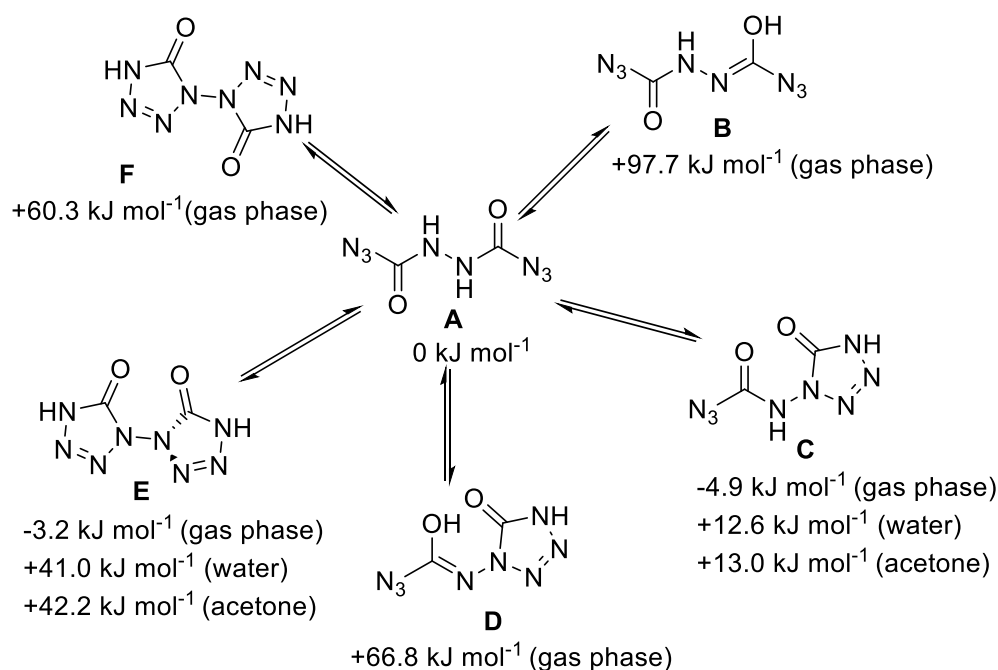
group, resulting in the formation of a carbamate-like carbonyl azide compound.^[17] This strategy also works well if a compound containing an amino functional group is used instead, which produces an acetamide-like carbonyl azide derivative.^[20–22] In this work, methanol was used which reacted with the isocyanate intermediate, and surprisingly, hydrazoic acid was eliminated by methanol and dimethyl iminodicarbonate (**4**) was formed. Furthermore, using oxetan-3-ol and 2-amino-2*H*-tetrazole as reagents, oxetan-3-yl-*N*-azidocarbonyl-carbamate (**5**) and *N*-azidocarbonyl-*N'*-(2*H*-tetrazol-2-yl)-urea (**6**) were obtained. Subsequently, several oxidative coupling reactions were attempted to convert **2** into **3**, using different oxidizing agents.



Scheme 1. Synthetic pathways used in this work to obtain the small carbonyl azide compounds **1–3**, and trapping reaction of the reactive isocyanate intermediate, which is used to obtain compounds **4–6** (CCDC deposition numbers 2077540, 2077535, 2077538). Thermal ellipsoids are drawn at the 50% probability level.

5 Carbonylazides

However, despite these attempts, none of the oxidizing reagents successfully converted **2** into compound **3**, instead only decomposition or the starting material was observed. In this work, the molecular orbitals (MOs) of six different tautomers of *N,N'*-bis(azidocarbonyl)hydrazine (**3**) were calculated using the G09W code (further details in the Supporting Information), and the gas phase energies were calculated at the CBS-4M level. Surprisingly, the mono-tetrazolone tautomer (**C**), as well as the di-tetrazolone tautomer (**E**) are lower in energy than the open amide form (Scheme 2). However, all attempts to synthesize one of these tetrazolone forms (in polar, acidic or basic media) failed. To obtain more insight into which form is present in solution, the three tautomers **A**, **C** and **E** were calculated with the solvents water and acetone at the MP2 level. In agreement with the experimental results in solution, **A** is calculated to be lower in energy in solution than either **C** or **E** (Scheme 2).



Scheme 2. Six different tautomers of *N,N'*-bis(azidocarbonyl)hydrazine (**3**): **A** amide form; **B** iminol form; **C** mono-tetrazolone form; **D** enol-tetrazolone form; **E** di-tetrazolone form (90° twist); **F** di-tetrazolone form (planar, transition state).

Compounds **1** and **2** crystallize in the space group number 14 (*P21/c* for **1** and *P21/n* for **2**) and **3** crystallizes in the monoclinic space group *C2/c* (No. 15). Compound **1** shows the highest density (1.701 g cm⁻³) followed by **3** (1.666 g cm⁻³) and **2** (1.565 g cm⁻³).

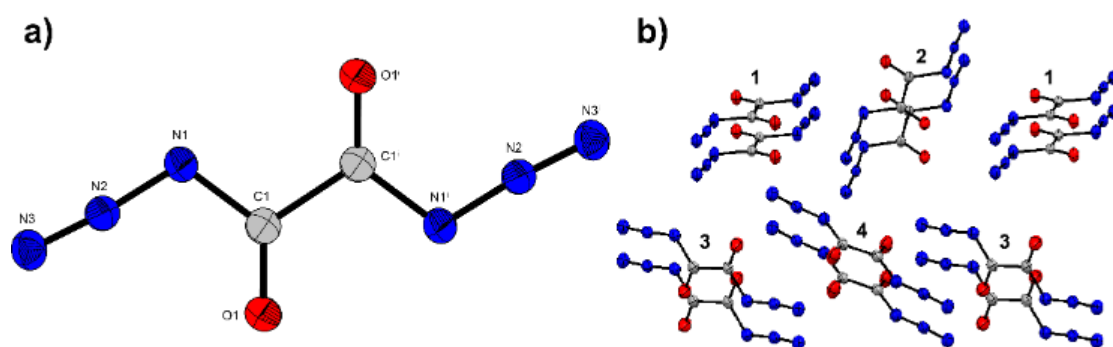


Figure 2. a) Crystal structure of oxalyl diazide (**1**) (Deposition number 2077536). Thermal ellipsoids are drawn at the 50 % probability level. **b)** Crystal packing of oxalyl diazide forming pairs. Ellipsoids are drawn at the 50 % probability level.

The angles of oxalyl diazide (**1**) around C1 are nearly trigonal planar, and the azide moiety has an angle of 174.4° at N1-N2-N3. As is the case in other carbonyl azides, the azido moiety is *syn* to the carbonyl group.^[8,23,24] In the crystal, oxalyl diazide forms pairs as shown above, in which the molecules are arranged alternately (**Fig 2 b**). Oxalyl diazide has no stabilizing, intermolecular hydrogen bonds due to the absence of hydrogen atoms in the molecule, calculated from the Hirshfeld surface (further details in the Supporting Information).

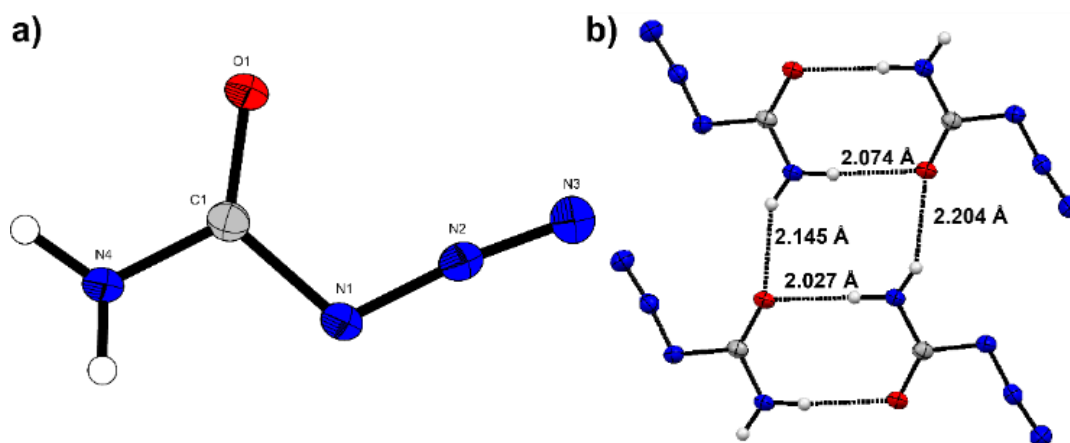


Figure 3. a) Molecular structure of carbamoyl azide (**2**) (Deposition number 2077537). Thermal ellipsoids are drawn at the 50 % probability level. **b)** A network results from hydrogen bonds between the molecules with distance of about 2 Å.

The N2-C1-N1 angle (111.2°) in carbamoyl azide (**2**) deviates from the expected 120° (**Fig. 3 a**). The azide moiety also has an angle of about 174° and is oriented *syn* with respect to the carbonyl group.^[8,23,24] The molecule is planar, and strong hydrogen bonds are present between the molecules (2.027 Å to 2.204 Å) (**Fig. 3 b**).

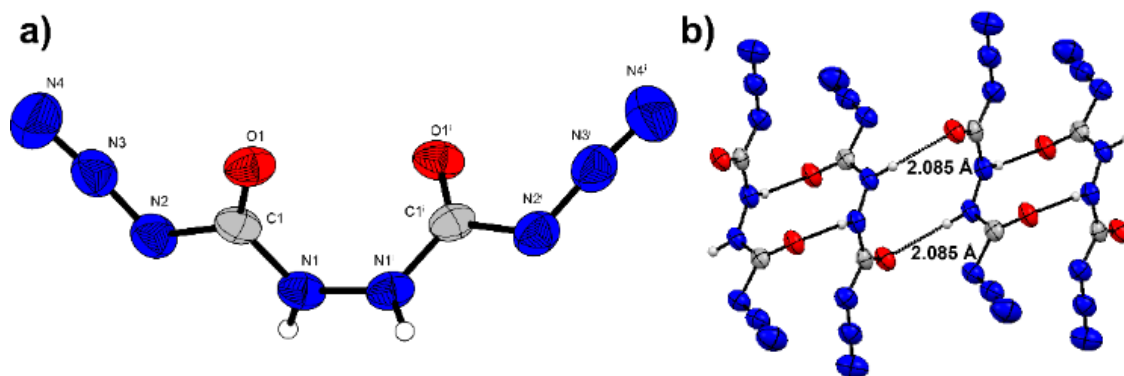


Figure 4. **a)** Crystal structure of *N,N'*-bis(azidocarbonyl)hydrazine (**3**) (Deposition number 2077539). Thermal ellipsoids are drawn at the 50 % probability level. **b)** Hydrogen bond network of *N,N'*-bis(azidocarbonyl)hydrazine with distances of 2.085 Å.

The azide group of *N,N'*-bis(azidocarbonyl)hydrazine (**3**) azide group ($\angle(\text{NNN}) = 173.7^\circ$) is again oriented *syn* with respect to the carbonyl groups,^[8,23,24] and the molecule possesses a center of symmetry between the hydrazino nitrogen atoms (N1, N1'). The molecule is twisted at the hydrazine bridge with a torsion angle of 72.2° . Compound **3** has strong intermolecular hydrogen bonds with a distance of 2.085 Å (**Fig. 4 b**) which results in the formation of a 3-dimensional network.

The azide and carbonyl moieties of **1** are identified by strong bands in the IR spectrum at 2178 cm^{-1} and 1681 cm^{-1} respectively. The FT-IR spectrum of solid **2** shows two medium bands at 3384 and 3247 cm^{-1} corresponding to the amino group, and a strong band at 1674 cm^{-1} for the carbonyl group. In the Ne-matrix and gas phase IR spectra, the bands corresponding to the amino group are observed at 3588 and 3470 cm^{-1} , which corresponds to a dramatic blue-shift from the pure solid (Fig. 5). By contrast, the CO stretching mode which occurs at 1766 cm^{-1} in the matrix IR spectrum and at 1750 cm^{-1} in the gas phase, is significantly red-shifted to 1674 cm^{-1} in the solid. Clearly, these large shifts are due to strong intermolecular hydrogen bonds between the amino and carbonyl groups in the solid state. The asymmetric stretching mode of the azido moiety in the IR (gas, solid, and Ne-matrix) and Raman (solid) spectra remains unchanged at around 2170 cm^{-1} . The IR spectrum of **3** showed weak bands at 3166 cm^{-1} and 3004 cm^{-1} corresponding to the hydrazine bridge, and bands for the azido moieties at 2170 cm^{-1} (medium) and 2150 cm^{-1} (strong).^[19] The carbonyl group in **3** was identified by bands at 1732 cm^{-1} and 1683 cm^{-1} .

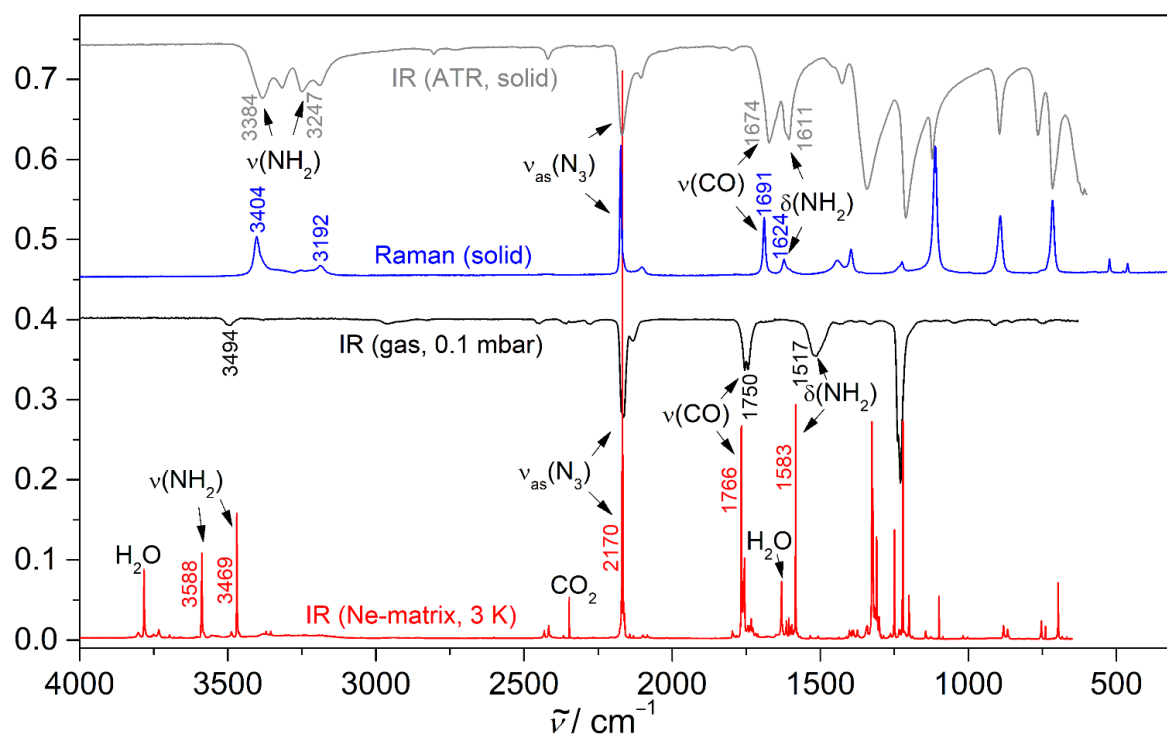


Figure 5. IR and Raman spectra of carbamoyl azide (**2**).

Oxalyl diazide explodes violently at 46 °C after melting. It is extremely sensitive towards external stimuli and was found to be too sensitive to be measured with the capabilities of our test setups (friction <0.1 N, impact <1J). Micro-detonations of **1** occurred repeatedly without any obvious source of stimulus during handling. In contrast to compound **1**, carbamoyl azide (**2**) is insensitive (!) towards friction (>360 N) and shows only low sensitivity towards impact (20 J). Furthermore, **2** is quite thermally stable for a carbonyl azide, showing a melting point of 96 °C and a decomposition point of 133 °C. *N,N'*-bis(azidocarbonyl)hydrazine (**3**) is thermally more stable than **1** or **2**, with a decomposition temperature of 154 °C without melting. The other two carbonyl azide compounds (**5** and **6**) show decomposition temperatures of 135 °C and 145 °C respectively. The detonation parameters were calculated using the EXPLO5 code and compared to the calculated detonation parameters of carbonyl diazide and nitrocarbamoyl azide.^[8,11,15] The calculated detonation velocities range from 6241 m s⁻¹ for the oxetane derivative (**5**) to 8236 m s⁻¹ for oxalyl diazide (**1**).

5 Carbonylazides

Table 1. Physicochemical properties of oxalyl diazide (**1**), carbamoyl azide (**2**), N,N'-bis(azidocarbonyl)hydrazine (**3**), oxetan-3-yl-N-azidocarbonyl-carbamate (**5**), N-azidocarbonyl-N'-(2H-tetrazol-2-yl)-urea (**6**), carbonyl diazide (**CDA**)^[8,11] and nitrocarbamoyl azide (**HNCA**)^[15]

	1	2	3	5	6	CDA ^[8,11]	HNCA ^[15]
Formula	C ₂ N ₆ O ₂	CH ₂ N ₄ O	C ₂ H ₂ N ₈ O ₂	C ₅ H ₆ N ₄ O ₄	C ₃ H ₃ N ₉ O ₂	CN ₆ O	CHN ₅ O ₃
FW [g·mol ⁻¹]	140.06	86.05	170.09	186.13	197.12	112.05	131.05
IS ^[a] [J]	<1	20	1–2	>40	4	<1*	<1
FS ^[b] [N]	<0.1	>360	0.1	>360	360	<0.1*	0.5
N / N+O ^[c] [%]	60.00 / 82.85	65.11 / 83.70	65.88 / 84.69	30.10 / 64.38	63.95 / 80.15	75.00 / 89.28	53.44 / 90.00
Ω _{CO} , Ω _{CO₂} ^[d] [%]	0, -22.8	-18.6, -37.2	-9.4, -28.2	-77.4, -34.4	-44.6, -20.3	0, -14.3	+18.3, +6.1
T _m ^[e] / T _{dec.} ^[f] [°C]	45/46	96/133	-/154	127/135	-/145	-/25–30*	72/83
ρ ^[g] [g·cm ⁻³]	1.701	1.565	1.666	1.604	1.678	1.676	1.708
Δ _f H ^{o[h]} [kJ·mol ⁻¹]	329.7	41.7	309.3	-340.5	353.4	439.5	147.5
EXPLOS V6.05							
-Δ _E U ^{o[i]} [kJ·kg ⁻¹]	4626	2967	4015	2414	3682	5272	5066
T _{C-J} ^[j] [K]	4003	2536	3302	2051	2988	4507	4054
D _{C-J} ^[k] [m·s ⁻¹]	8236	7201	7907	6241	7645	8710	8333
p _{C-J} ^[l] [GPa]	26.5	18.0	23.7	13.8	21.6	29.7	27.0
V ₀ ^[m] [dm ³ ·kg ⁻¹]	768	852	805	715.9	780	825	794
I _{sp} ^[n] [s]	241	189	221	164	209	266	248

[a] Impact sensitivity (BAM drophammer, method 1 of 6); [b] friction sensitivity (BAM drophammer, method 1 of 6); [c] Nitrogen and oxygen content; [d] Oxygen balance toward carbon monoxide ($\Omega_{CO} = (nO - xC - yH/2)(1600/FW)$) and carbon dioxide ($\Omega_{CO_2} = (nO - 2xC - yH/2)(1600/FW)$); [e] melting point (DTA, $\beta = 5 \text{ }^\circ\text{C}\cdot\text{min}^{-1}$); [f] temperature of decomposition (DTA, $\beta = 5 \text{ }^\circ\text{C}\cdot\text{min}^{-1}$); [g] density at 298 K, from X-ray density: $\rho_{X\text{-ray}@100K}/1.0297$; [h] standard molar enthalpy of formation; [i] detonation energy; [j] detonation temperature; [k] detonation velocity; [l] detonation pressure [m] Volume of detonation products (assuming only gaseous products); [n] Specific impulse of neat compound (70.0 bar chamber pressure, isobaric combustion conditions (1 bar), equilibrium expansion); *estimated

5.4 Conclusion

To conclude, oxalyl diazide (**1**), carbamoyl azide (**2**) and *N,N'*-bis(azidocarbonyl)hydrazine (**3**) were synthesized, comprehensively characterized and the solid state structures determined. All three compounds crystallize in the monoclinic space group 14 and have densities ranging from 1.565 g cm⁻³ for **2** to 1.701 g cm⁻³ for **1**. Oxalyl diazide is extremely sensitive towards external stimuli. Both carbamoyl azide and *N,N'*-bis(azidocarbonyl)hydrazine show multiple hydrogen bonds in the crystal structure, which contributes to their thermal stability, with decomposition points of 133 °C and 154 °C, respectively, and also to their lower sensitivities towards external stimuli. The *Curtius* rearrangement of **1** leads to a reactive isocyanate intermediate, which was trapped using water, methanol, oxetan-3-ol and 2-amino-2*H*-tetrazole. The crystal structures were elucidated for all trapping reaction products (**4–6**) and characterized by NMR spectroscopy. Based on the results, numerous new compounds should be accessible in analogous reactions. The ease of synthesis and handling in solution, as well as demonstration of the *Curtius* rearrangement of oxalyl diazide, together with the versatile capture reactions that were performed, will hopefully trigger further research in this field.

Financial support of this work by the Ludwig-Maximilians University of Munich (LMU), the Office of Naval Research (ONR) under grant no. ONR N00014-19-1-2078 and the Strategic Environmental Research and Development Program (SERDP) grant WP19-1287 under contract no. W912HQ19C0033 is gratefully acknowledged. X. Zeng thanks the National Natural Science Foundation of China (22025301) for financial support.

5.5 Supporting Information

5.5.1 Experimental Procedures

CAUTION! *All described compounds are powerful energetic materials with high sensitivities towards shock and friction. Therefore, proper security precautions (safety glass, face shield, earthed equipment and shoes, Kevlar gloves and ear plugs) have to be applied all time while synthesizing and handling the described compounds. Especially oxalyl diazide (**1**) is extremely unstable and lead to several micro-detonations during the work.*

Chemicals and solvents were employed as received (Sigma-Aldrich, Acros, TCI). ¹H, ¹³C and ¹⁴N spectra were recorded using a Bruker AMX 400 instrument. The chemical shifts quoted in ppm

5 Carbonylazides

refer to tetramethylsilane (^1H , ^{13}C) and nitromethane (^{14}N). Decomposition temperatures were determined on an OZM Research DTA 552–Ex instrument with a heating rate of 5°C min^{-1} . Infrared (IR) spectra were recorded using a Perkin-Elmer Spektrum One FT–IR instrument. Elemental analyses were performed with an Elementar Vario el by pyrolysis of the sample and subsequent analysis of formed gases. The sensitivity data were collected using a BAM (Bundesanstalt für Materialforschung) drophammer^[25] according to STANAG 4489^[26] modified instruction^[27] and a BAM friction tester^[25] according to STANAG 4487^[29] modified instruction.^[30] The classification of the tested compounds results from the 'UN Recommendations on the Transport of Dangerous Goods'.^[31]

Oxalyl diazide (1)

Oxalyl dihydrazide was prepared according to the literature procedure.^[16,17] Oxalyl hydrazide (0.45 g, 3.81 mmol, 1.0 eq.) was suspended in concentrated hydrochloric acid (6 mL) and cooled to -15°C . The mixture was layered underneath with chloroform (20 mL). The stirrer speed was set to maximum and an ice-cold solution of sodium nitrite (0.63 g, 9.15 mmol, 2.4 eq.) in water (6 mL) was added dropwise to the mixture. The resulting yellow solution was stirred for 10 minutes and the layers were separated. The aqueous layer was extracted with cold chloroform (20 mL), the organic layers were combined and washed with ice-water (2 x 20 mL) prior to drying. The solvent was removed by slow evaporation leaving transparent crystals of oxalyl diazide (**1**, 0.43 g, 3.07 mmol, 81 %).

DTA (T_{onset} , 5°C min^{-1}): 45°C (mp.) 46°C (dec.); **FT-IR** (ATR): $\tilde{\nu} = 3377$ (w), 2279 (w), 2178 (s), 1681 (s), 1155 (s), 970 (s), 823 (s), 574 (s), 506 (s), 463 (s) cm^{-1} ; **$^{13}\text{C NMR}\{^1\text{H}\}$** (101 MHz, CDCl_3 , 25°C): $\delta = 163.9$ ppm; **$^{14}\text{N NMR}$** (27 MHz, CDCl_3 , 25°C): $\delta = -130.9, -146.6, -252.4$ ppm; **EA** ($\text{C}_2\text{N}_6\text{O}_2$) calcd.: C 17.15, H 0.00, N 60.00; found: C 17.18, H 0.27, N 59.41; **BAM drophammer** < 1 J (> 500 μm); **Friction test** < 0.1 N (> 500 μm).

Carbamoyl azide (2)

Carbamoyl azide was prepared according to Thiele.^[2] Semicarbazide hydrochloride (1.00 g, 8.966 mmol, 1.0 eq.) was dissolved in water (15 mL) and cooled to -5°C . An ice-cold solution of sodium nitrite (0.68 g, 9.862 mmol, 1.1 eq.) in water (7 mL) was added dropwise. After the addition, diethyl ether was added and the mixture stirred for 5 minutes. Ammonium sulfate (~ 9 g) was used to saturate the aqueous phase. The layers were separated and the aqueous phase was

5 Carbonylazides

extracted with diethyl ether (3 x 20 mL) prior to drying. The solvent was removed by rotary evaporation, yielding 0.710 g (8.251 mmol, 92 %) of colorless carbamoyl azide.

DSC (T_{onset} , 5 °C min⁻¹): 96 °C (mp.), 133 (dec.); **FT-IR** (ATR): $\tilde{\nu}$ = 3384 (m), 3247 (m), 2170 (s), 1674 (s), 1611 (s), 1420 (w), 1347 (s), 1212 (s), 888 (m), 760 (w), 713 (s), 509 (s) cm⁻¹; **¹H NMR** (400 MHz, CDCl₃, 25 °C): δ = 5.25 ppm; **¹³C NMR{¹H}** (101 MHz, CDCl₃, 25 °C): δ = 158.1 ppm; **¹⁴N NMR** (27 MHz, CDCl₃, 25 °C): δ = -144.7, -267.3, -302.5 ppm; **EA** (CH₂N₄O) calcd.: C 13.96, H 2.34, N 65.11; found: C 14.18, H 2.16, N 64.90; **BAM drophammer** 20 J (> 500 μ m); **Friction test** >360 N (> 500 μ m).

***N,N'*-bis(azidocarbonyl)hydrazine (3)**

N,N'-Dicarbazoylhydrazine was synthesized according to the literature procedure.^[19] *N,N'*-Dicarbazoylhydrazine (0.207 g, 1.397 mmol, 1.0 eq.) was suspended in a mixture of acetic acid (6 mL), 2 M hydrochloric acid (2 mL) and water (2 mL) and cooled to 0 °C. Sodium nitrite (0.241 g, 3.493 mmol, 2.5 eq.) was dissolved in water (3 mL), cooled to 0 °C and added dropwise to the previously described mixture. After the addition, diethyl ether was added and the mixture stirred for 10 minutes. The layers were separated and the aqueous phase was extracted with diethyl ether (2 x 20 mL). The combined organic layers were washed with ice-water (2 x 25 mL) and brine (20 mL) prior to drying. The solvent was removed by slow evaporation to yield 0.185 g (1.088 mmol, 78 %) of colorless *N,N'*-bis(azidocarbonyl)hydrazine (**3**).

DTA (T_{onset} , 5 °C min⁻¹): 154 °C (dec.); **FT-IR** (ATR): $\tilde{\nu}$ = 3166 (w), 3004 (w), 2170 (m), 2150 (s), 1774 (m), 1732 (m), 1683 (m), 1521 (s), 1163 (s), 1143 (s), 919 (m), 747 (s), 644 (m), 590 (m), 555 (s), 503 (m), 493 (m) cm⁻¹; **¹H NMR** (400 MHz, acetone-d₆, 25 °C): δ = 9.16 ppm; **¹³C NMR{¹H}** (101 MHz, acetone-d₆, 25 °C): δ = 157.7 ppm; **¹⁴N NMR** (27 MHz, acetone-d₆, 25 °C): δ = -144.6 ppm; **EA** (C₂H₂N₈O₂) calcd.: C 14.12, H 1.19, N 65.88; found: C 14.39, H 1.46, N 65.36; **BAM drophammer** 1 – 2 J (> 500 μ m); **Friction test** 0.1 N (> 500 μ m).

Dimethyl Iminodicarbonate (4)

Oxalyl diazide (0.600 g, 4.28 mmol, 1.0 eq.) was dissolved in chloroform (15 mL) and methanol (5 mL) was added. The mixture was stirred at 35 °C for 15 hours. The precipitate was filtered and recrystallized from ethyl acetate to yield 0.518 g (3.89 mmol, 91 %) of dimethyl iminodicarbonate (**4**).

5 Carbonylazides

FT-IR (ATR): $\tilde{\nu}$ = 3205 (m), 3036 (w), 2962 (w), 1805 (m), 1766 (m), 1711 (m), 1532 (s), 1454 (m), 1301 (m), 1209 (m), 1175 (s), 1101 (s), 1040 (s), 910 (w), 783 (m), 729 (m), 703 (m), 558 (w), 443 (m) cm^{-1} ; **$^1\text{H NMR}$** (400 MHz, acetone- d_6 , 25 °C): δ = 9.21 (s, 1H, NH), 3.69 (s, 6H, CH_3) ppm; **$^{13}\text{C NMR}\{^1\text{H}\}$** (101 MHz, acetone- d_6 , 25 °C): δ = 152.4, 52.7 ppm; **EA** ($\text{C}_4\text{H}_7\text{NO}_4$) calcd.: C 36.10, H 5.30, N 10.52; found: C 35.90 H 5.12 N 10.87.

Oxetan-3-yl-*N*-azidocarbonyl-carbamate (5)

Oxalyl diazide (0.625 g, 4.46 mmol, 1.0 eq.) was dissolved in chloroform (15 mL) and oxetan-3-ol (0.330 g, 4.46 mmol, 1.0 eq.) was added and the mixture was stirred for 15 hours at 35 °C. The solvent was removed by rotary evaporation to give 0.781 g (4.20 mmol, 94 %) of colorless oxetan-3-yl-*N*-azidocarbonyl-carbamate.

DTA (T_{onset} , 5 °C min^{-1}): 127 °C (m.p.), 135 °C (dec.); **FT-IR** (ATR): $\tilde{\nu}$ = 3149 (w), 2956 (m), 2160 (m), 1797 (s), 1722 (m), 1538 (s), 1373 (w), 1255 (m), 1164 (s), 1119 (s), 1092 (s), 978 (s), 957 (m), 916 (s), 871 (m), 758 (s), 695 (s), 560 (m), 506 (w), 456 (m) cm^{-1} ; **$^1\text{H NMR}$** (400 MHz, CDCl_3 , 25 °C): δ = 7.44 (br s, 1H, NH), 5.55 – 5.49 (m, 1H, $\text{CH}_{\text{oxetane}}$), 4.93 – 4.89 (m, 2H, $\text{CH}_2_{\text{oxetane}}$), 4.69 – 4.66 ($\text{CH}_2_{\text{oxetane}}$) ppm; **$^{13}\text{C NMR}\{^1\text{H}\}$** (101 MHz, CDCl_3 , 25 °C): δ = 153.3, 149.1, 77.1, 69.9 ppm; **$^{14}\text{N NMR}$** (27 MHz, CDCl_3 , 25 °C): δ = -144.0, -146.8 ppm; **EA** ($\text{C}_5\text{H}_6\text{N}_4\text{O}_4$) calcd.: C 32.27, H 3.25, N 30.10; found: C 32.42 H 3.00 N 29.98; **BAM drophammer** >40 J (> 500 μm); **Friction test** >360 N (> 500 μm).

***N*-Azidocarbonyl-*N'*-(2*H*-tetrazol-2-yl)-urea (6)**

Oxalyl diazide (0.650 g, 4.64 mmol, 1.0 eq.) was dissolved in chloroform (15 mL) and 2*H*-tetrazole-2-amine (0.395 g, 4.64 mmol, 1.0 eq.) was added together with acetonitrile (2 mL). The mixture was heated to 35 °C for 15 hours. The precipitate which formed was filtered and dried to give 0.291 g (1.48 mmol, 32 %) of colorless *N*-azidocarbonyl-*N'*-(2*H*-tetrazol-2-yl)-urea.

DTA (T_{onset} , 5 °C min^{-1}): 145 °C (dec.); **FT-IR** (ATR): $\tilde{\nu}$ = 3289 (m), 3228 (m), 3139 (m), 2191 (m), 2143 (m), 1747 (s), 1689 (w), 1539 (s), 1417 (m), 1280 (m), 1256 (s), 1235 (m), 1163 (s), 1125 (s), 1044 (m), 1015 (s), 994 (s), 903 (m), 876 (m), 732 (m), 709 (s), 667 (s), 654 (s), 592 (s), 546 (s), 504 (s) cm^{-1} ; **$^1\text{H NMR}$** (400 MHz, $\text{DMSO-}d_6$, 25 °C): δ = 10.97 (s, 1H, NH), 8.99 (s, 1H, CH), 6.75 (s, 1H, NH) ppm; **$^{13}\text{C NMR}\{^1\text{H}\}$** (101 MHz, $\text{DMSO-}d_6$, 25 °C): δ = 155.7, 152.3 ppm; **$^{14}\text{N NMR}$** (27 MHz, $\text{DMSO-}d_6$, 25 °C): δ = -134.8, -146.5, -255.4 ppm; **EA** ($\text{C}_3\text{H}_3\text{N}_9\text{O}_2$) calcd.: C 18.28, H 1.53, N 63.95; found: C 18.54 H 1.87 N 63.58; **BAM drophammer** 4 J (> 500 μm); **Friction test** 360 N (> 500 μm).

5.5.2 NMR Discussion and Spectra

The $^{13}\text{C}\{^1\text{H}\}$ NMR spectrum showed one signal at 164 ppm for compound **1** which is in accordance with the shifts reported for carbonyl azide compounds which are in between 150 to 160 ppm.^[15] The ^{13}C NMR of carbamoyl azide (**2**) and *N,N'*-bis(azidocarbonyl)hydrazine (**3**) each show a signal at 158 ppm, which is due to the chemical similarity of both. *N,N'*-bis(azidocarbonyl)hydrazine (**3**) shows a signal at 9.16 ppm in the ^1H NMR spectrum. In addition to this signal, two smaller signals are also found in this region. These two signals indicate a species which is not symmetrical. Either it is a species formed by free rotation around the hydrazine bridge, or it is assumed that they belong to the mono-tetrazolone tautomer formed by free exchange in solution. The ^{14}N NMR spectroscopy for **1** has shows resonance signals at -130.9 ppm for N_γ , -146.6 ppm (N_β) and -252.4 ppm (N_α). The signals for N_α as well as N_γ are shifted to lower field in relation to organic azides in the literature comparable to the carbonyl azides.^[15,31] Only three signals for **2** are found, -144.7 ppm (N_β), -267.3 ppm (N_α), as well as a signal at -302.5 ppm which can be assigned to the amino group. The signal of N_γ is possibly superimposed by the signal of N_β . For compound **3**, only one signal is found at -144.6 ppm which is assigned to N_β which possibly superimposed the N_γ resonance. No N_α signal was observed, however, it is known that for covalent azides, this signal is often very broad in ^{14}N NMR spectra. The very broad resonance typical of the hydrazine bridge of **3** in ^{14}N NMR was not observed.

5 Carbonylazides

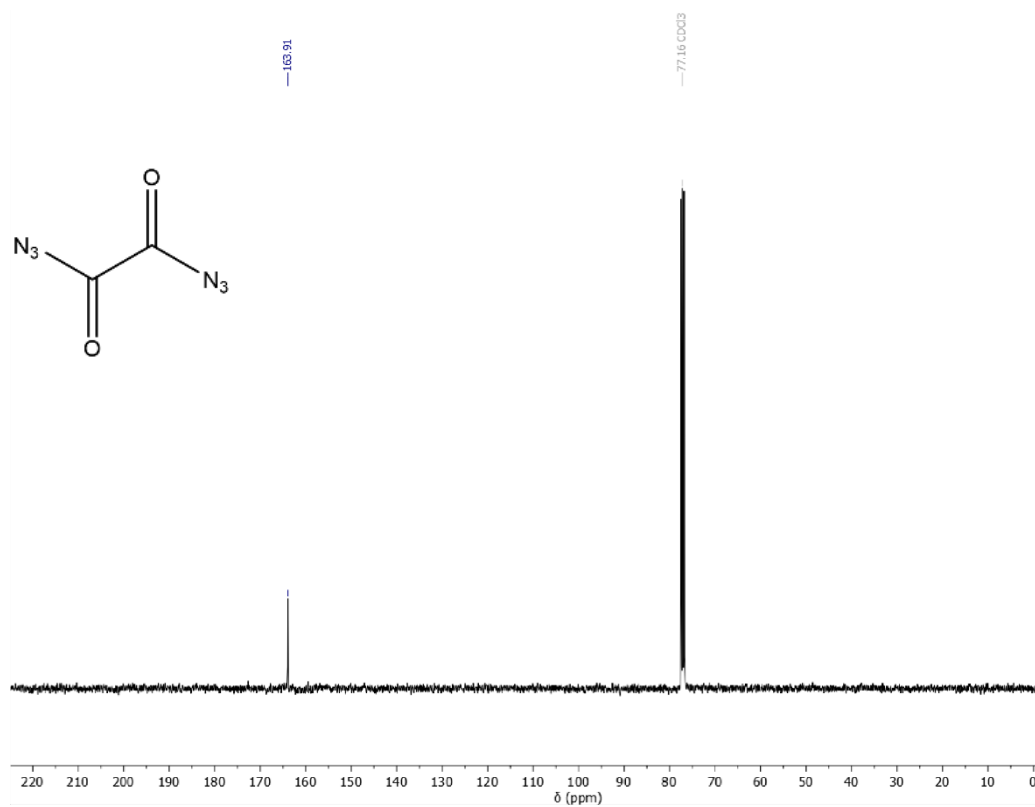


Figure 6. $^{13}\text{C}\{^1\text{H}\}$ NMR spectrum of oxalyl diazide (1).

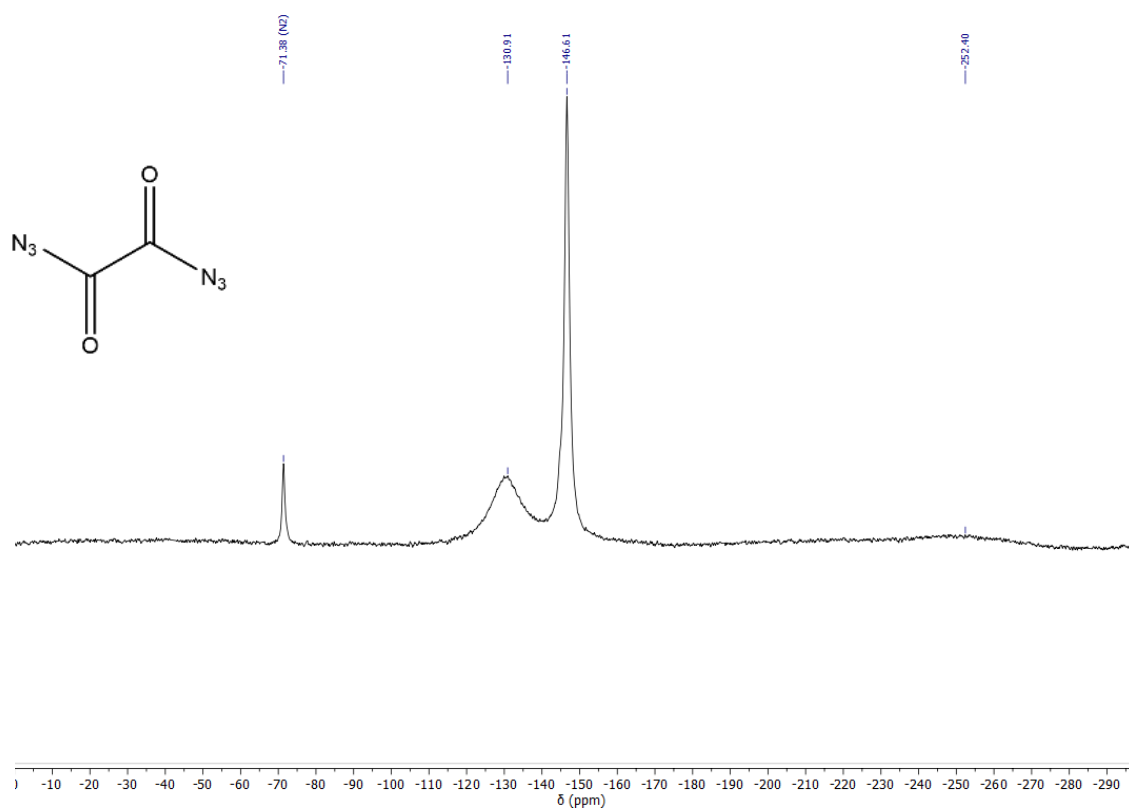


Figure 7. ^{14}N NMR spectrum of oxalyl diazide (1).

5 Carbonylazides

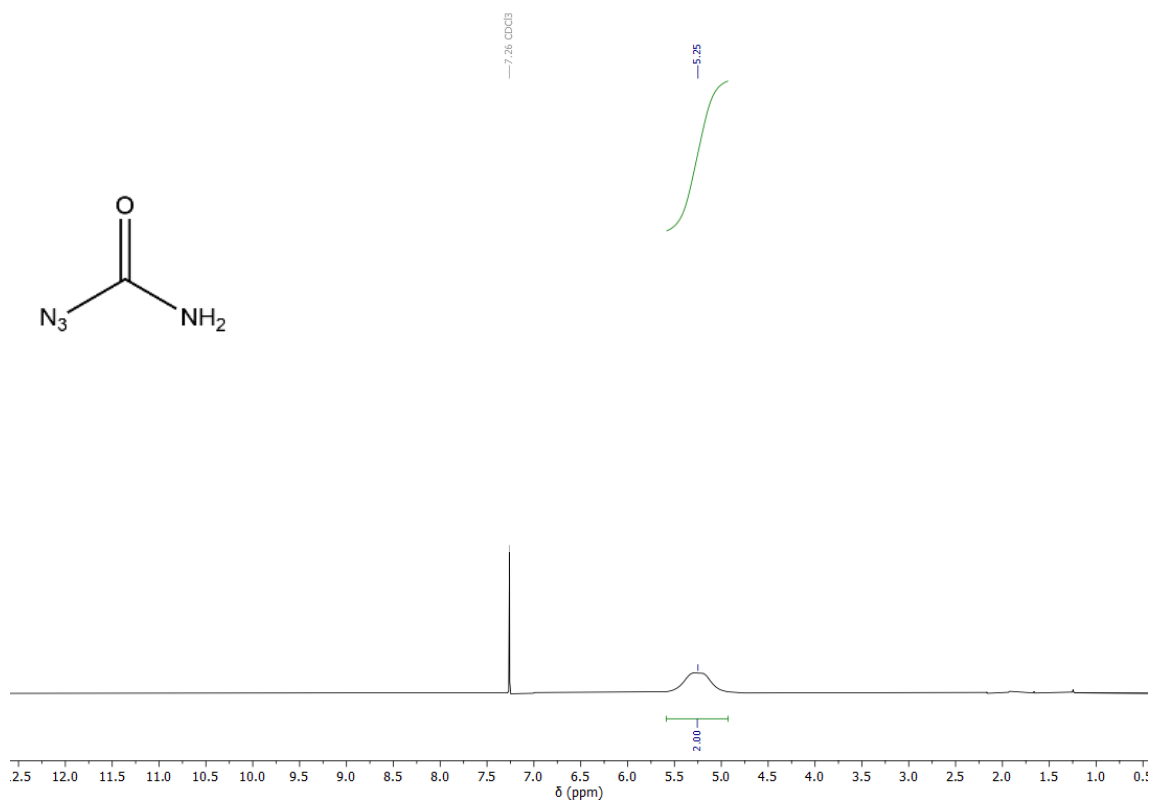


Figure 8. ^1H NMR spectrum of carbamoyl azide (2).

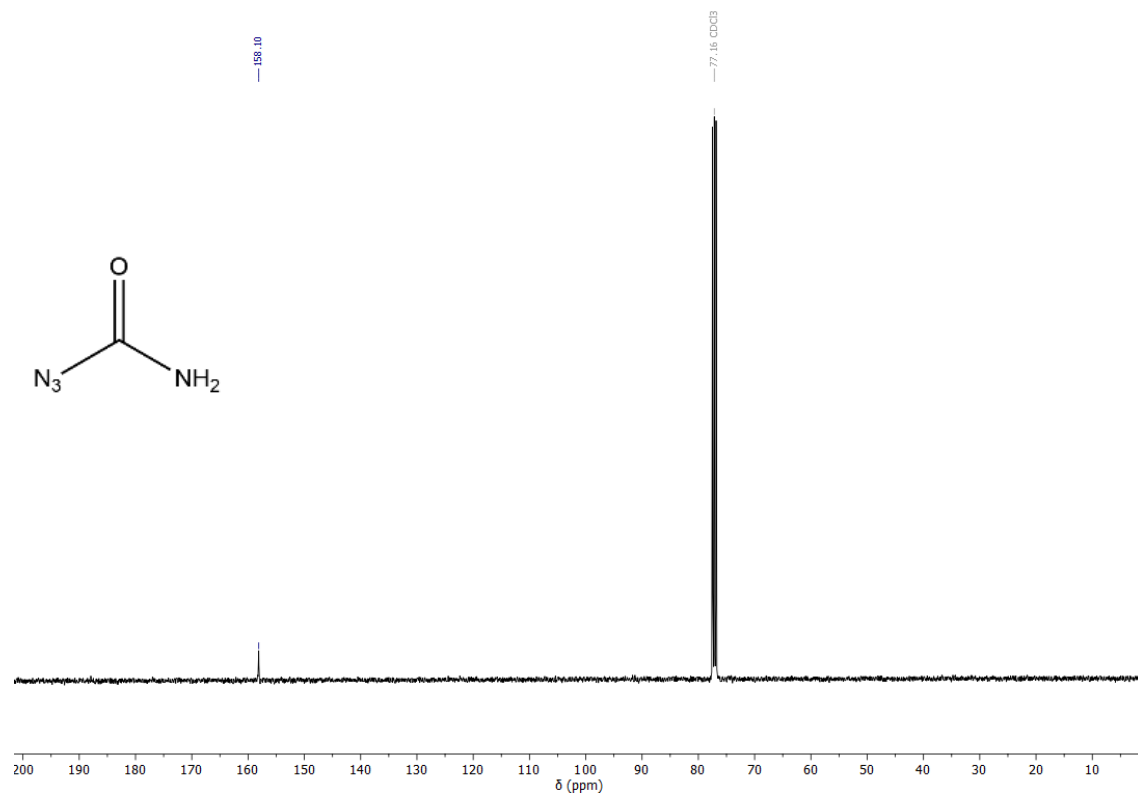


Figure 9. $^{13}\text{C}\{^1\text{H}\}$ NMR spectrum of carbamoyl azide (2).

5 Carbonylazides

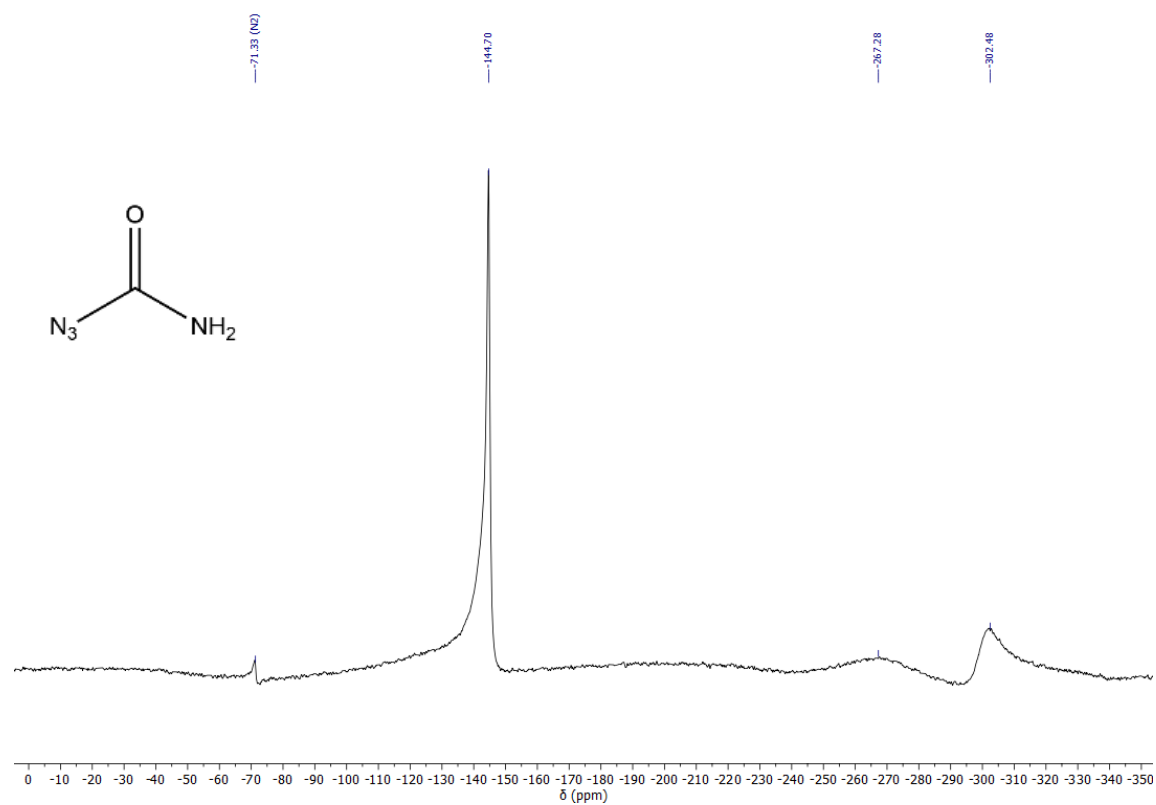


Figure 10. ^{14}N NMR spectrum of carbamoyl azide (2).

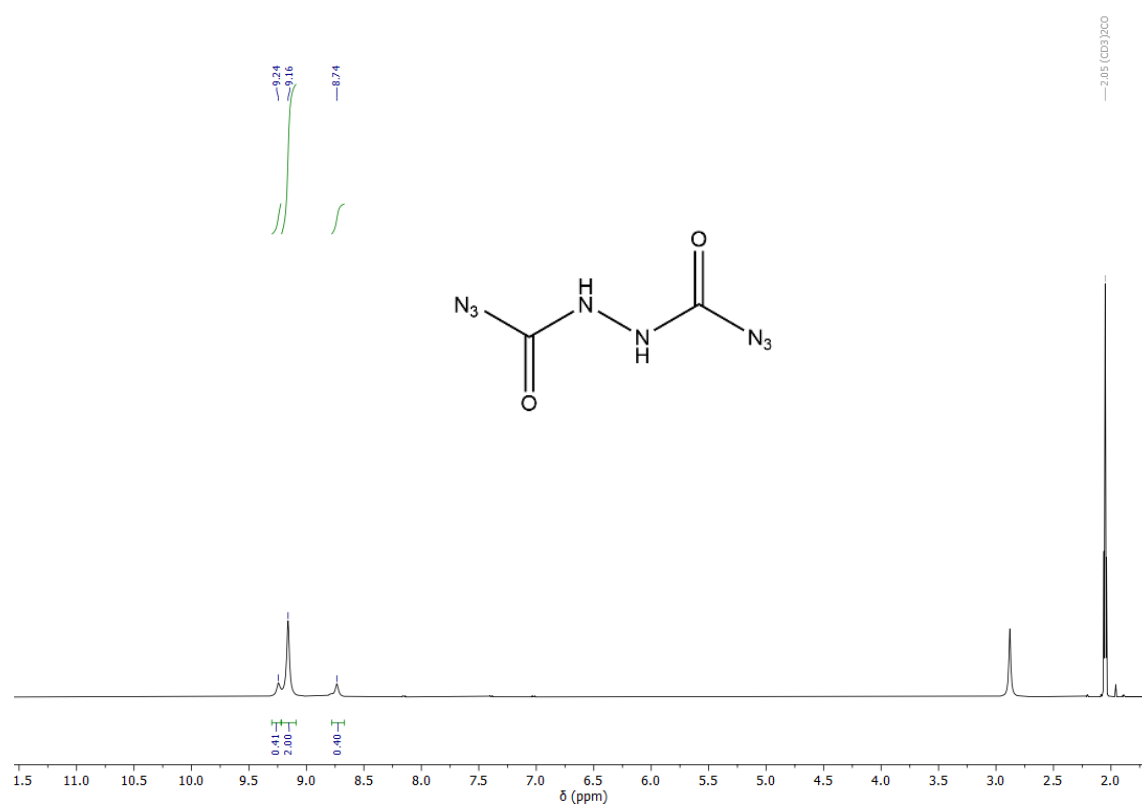


Figure 11. ^1H NMR spectrum of *N,N'*-bis(azidocarbonyl)-hydrazine (3).

5 Carbonylazides

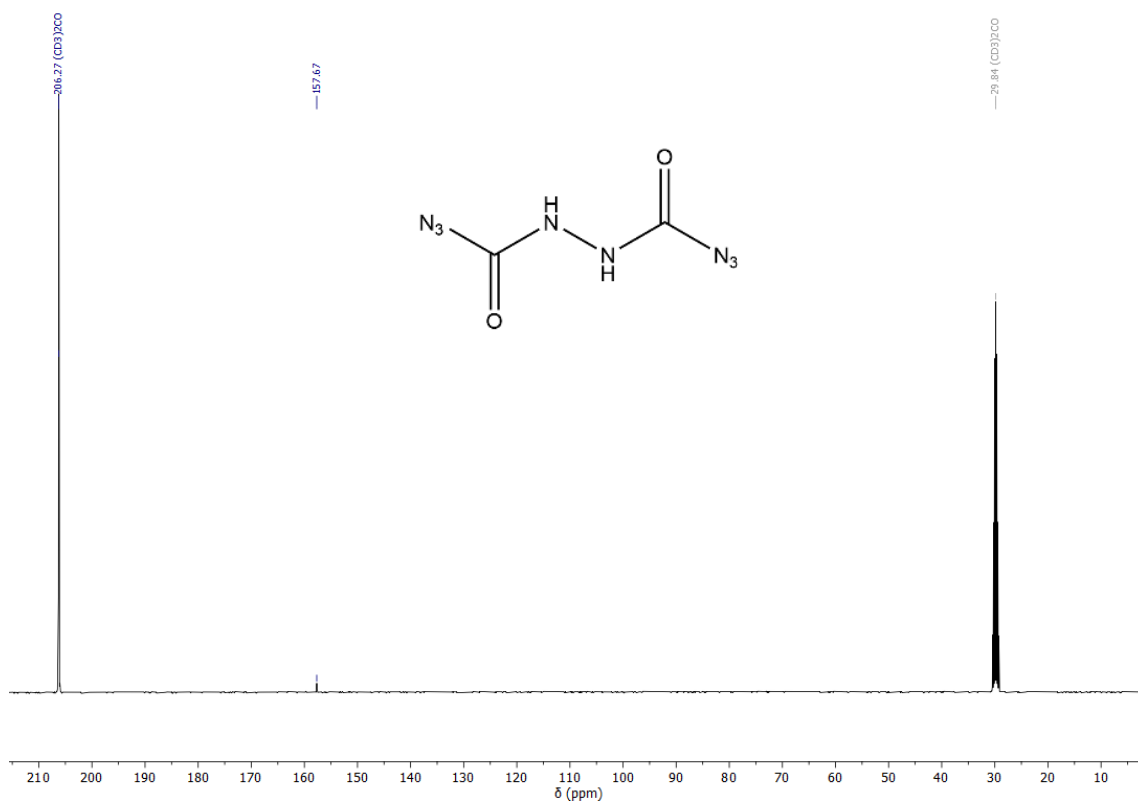


Figure 12. $^{13}\text{C}\{^1\text{H}\}$ NMR spectrum of *N,N'*-bis(azidocarbonyl)-hydrazine (3).

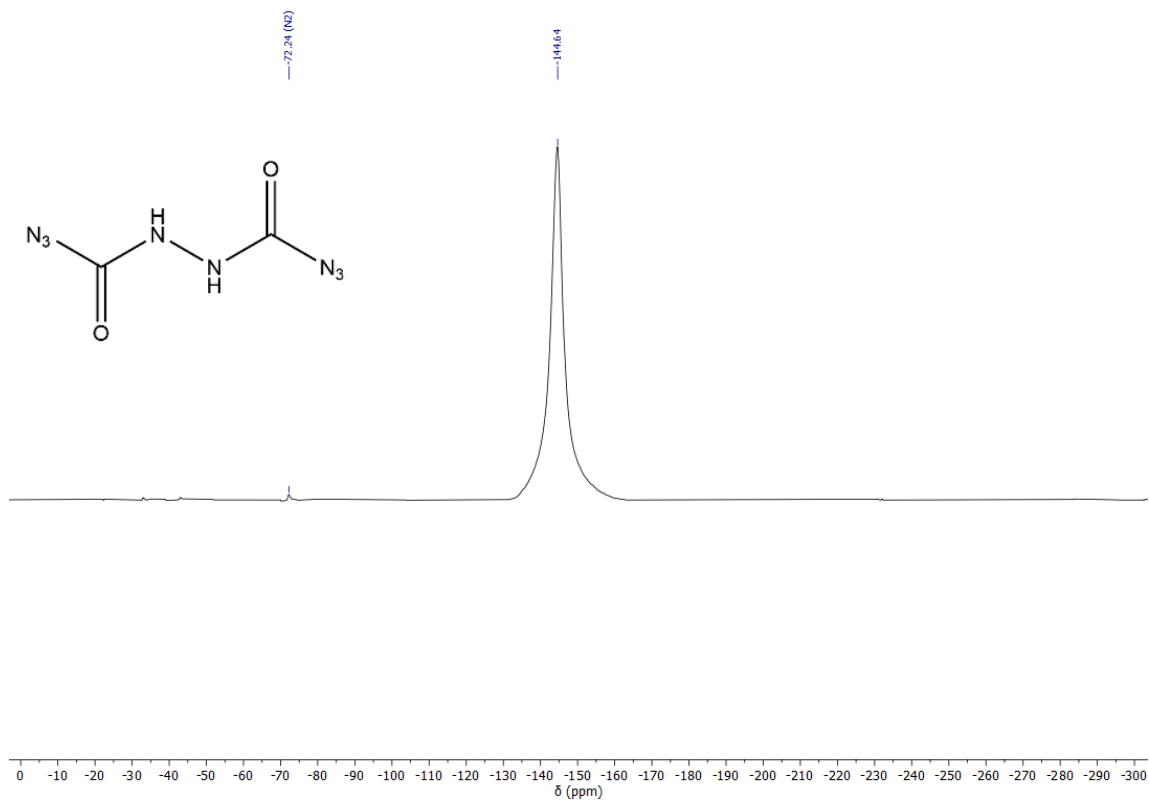


Figure 13. ^{14}N NMR spectrum of *N,N'*-bis(azidocarbonyl)-hydrazine (3).

5 Carbonylazides

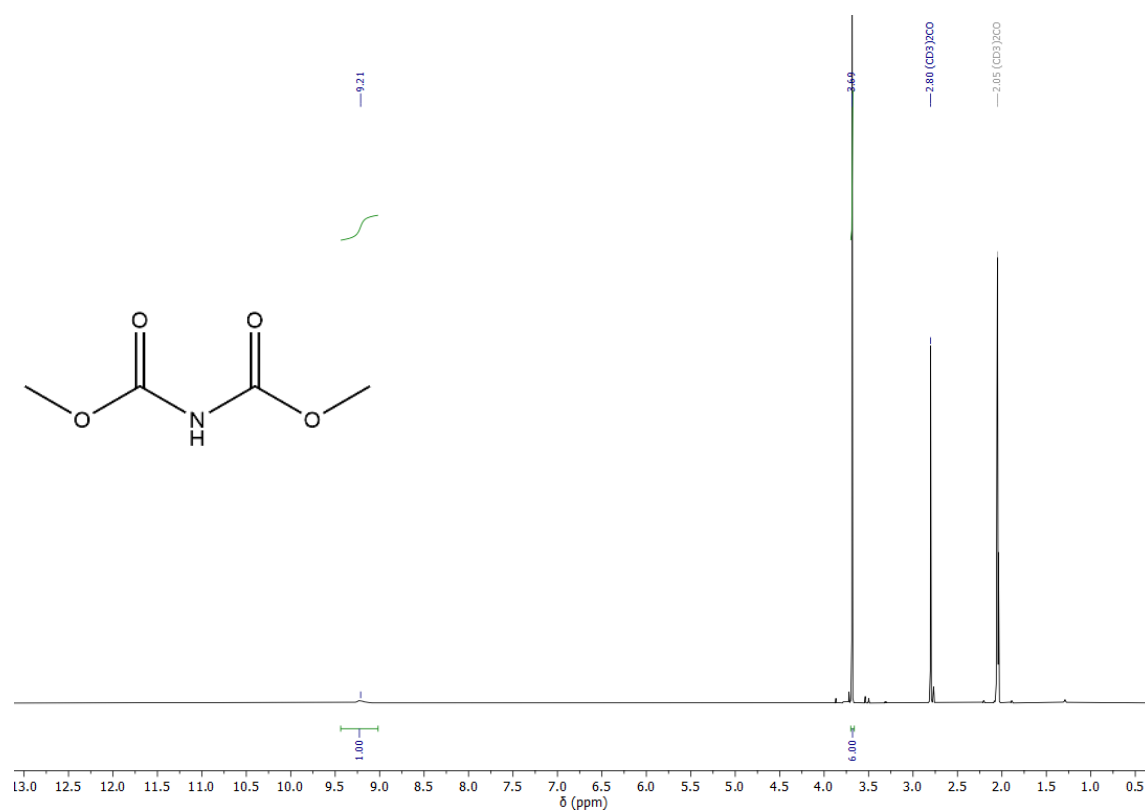


Figure 14. ^1H NMR spectrum of dimethyl iminodicarbonate (4).

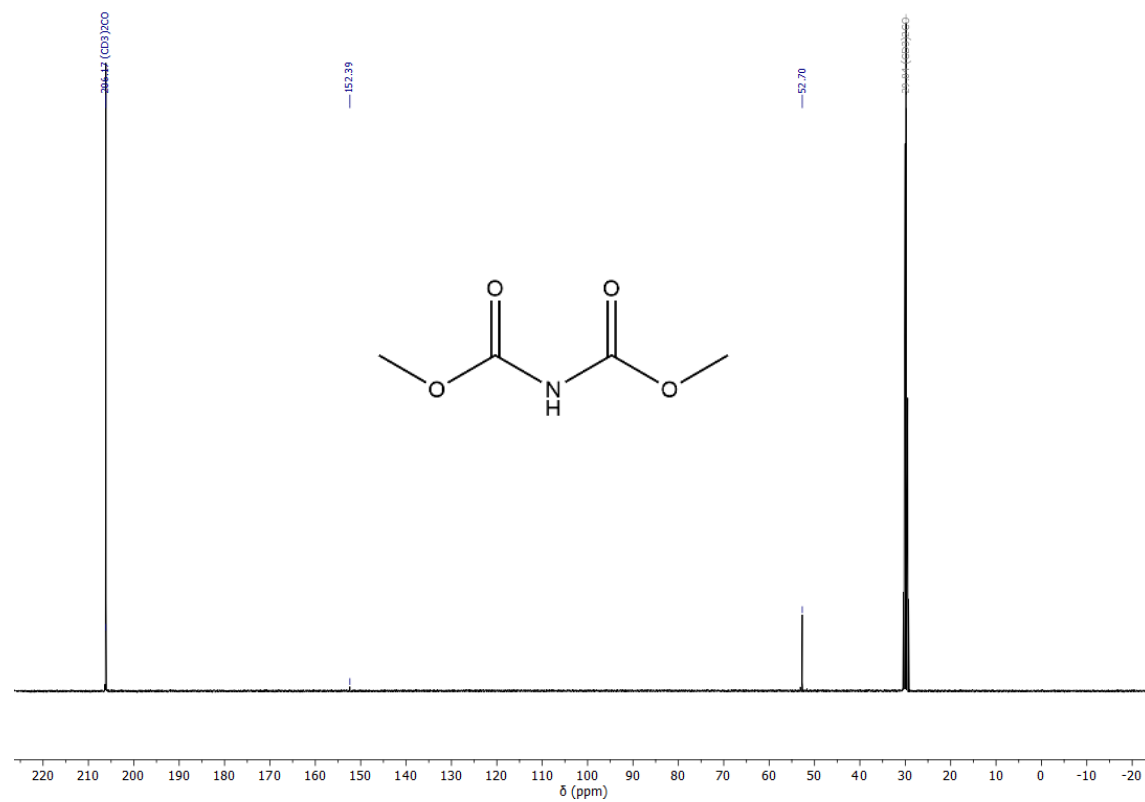


Figure 15. $^{13}\text{C}\{^1\text{H}\}$ NMR spectrum of dimethyl iminodicarbonate (4).

5 Carbonylazides

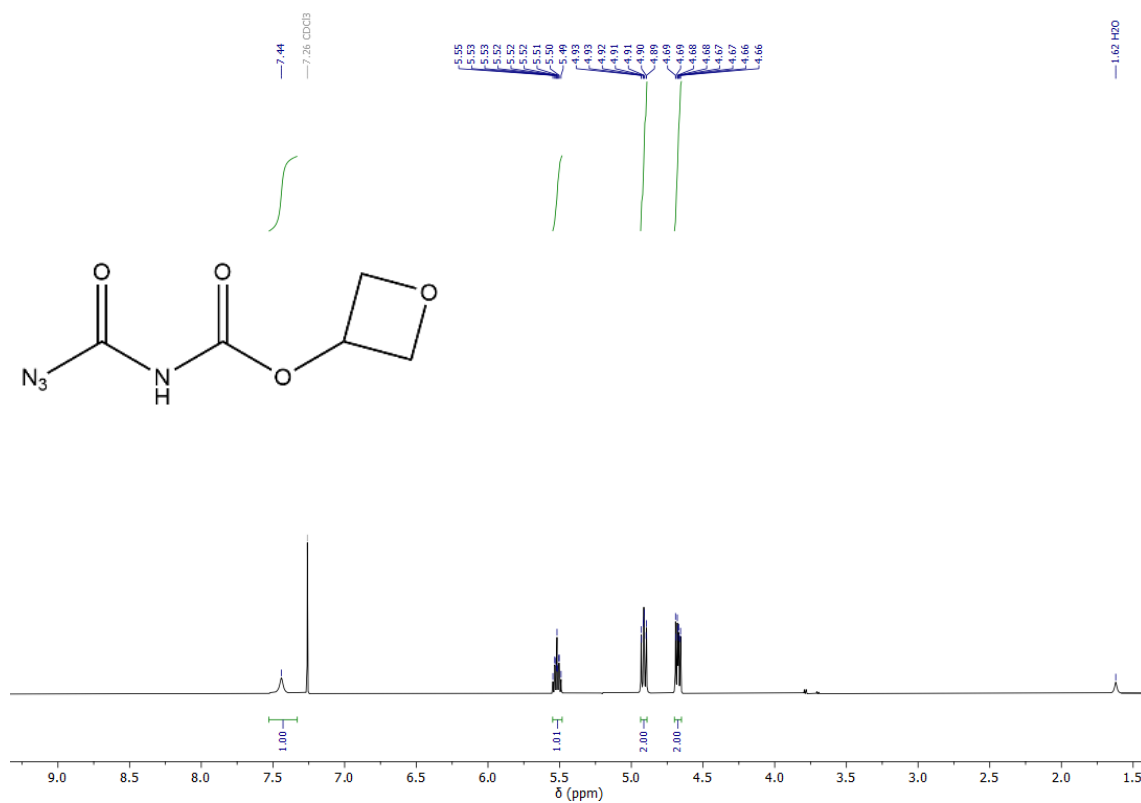


Figure 16. ^1H NMR spectrum of oxetan-3-yl-N-azidocarbonyl-carbamate (5).



Figure 17. $^{13}\text{C}\{^1\text{H}\}$ NMR spectrum of oxetan-3-yl-N-azidocarbonyl-carbamate (5).

5 Carbonylazides

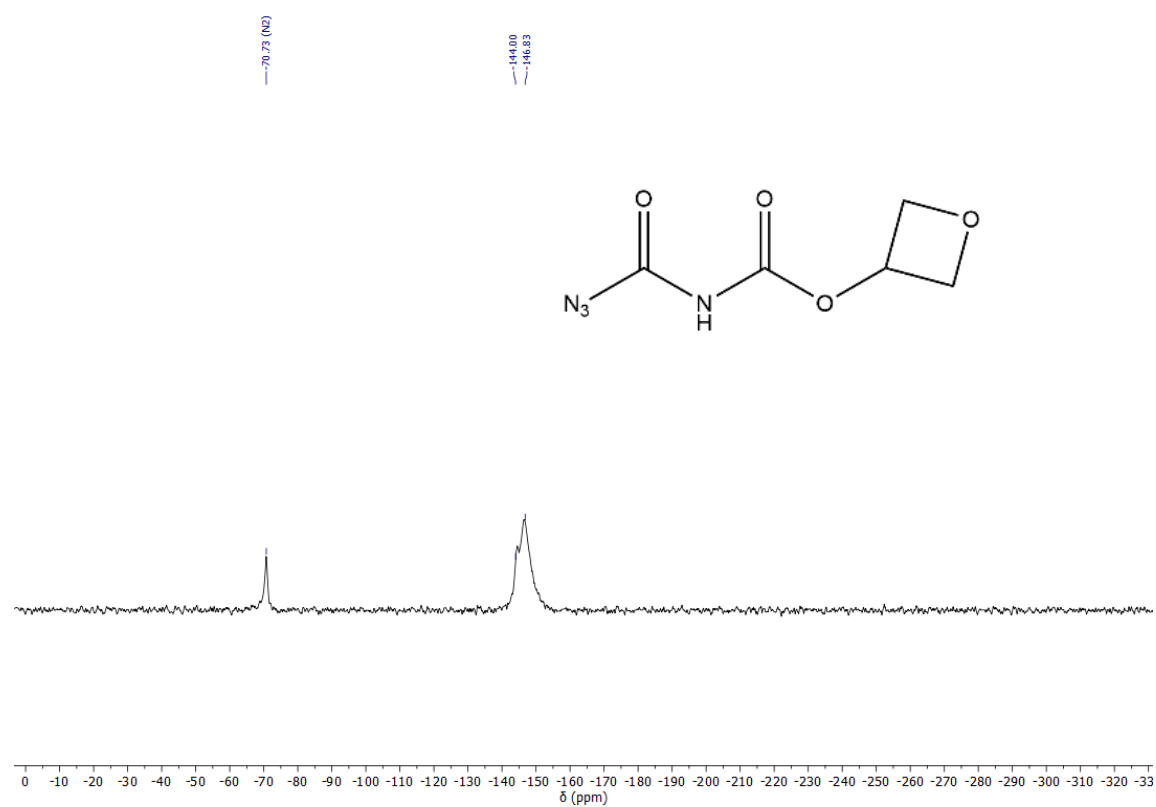


Figure 18. ^{14}N NMR spectrum of oxetan-3-yl-*N*-azidocarbonyl-carbamate (5).

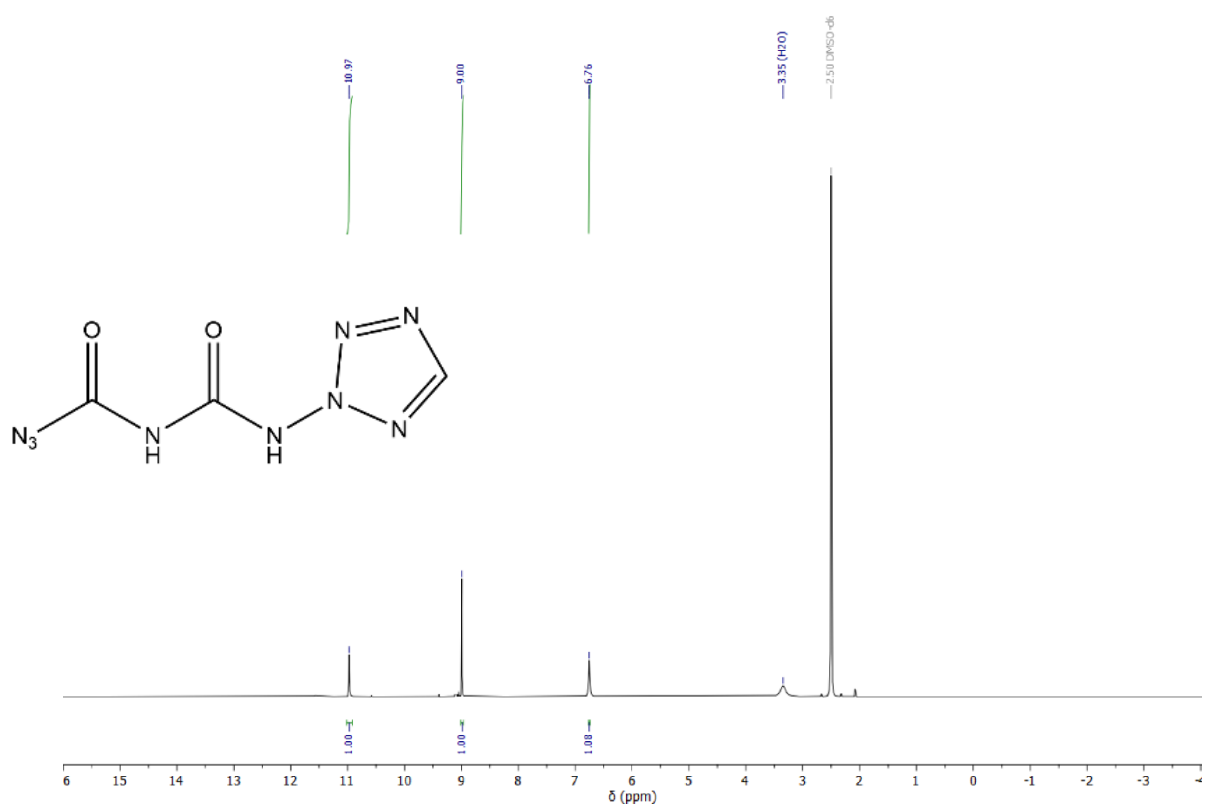


Figure 19. ^1H NMR spectrum of *N*-azidocarbonyl-*N'*-(2*H*-tetrazol-2-yl)-urea (6).

5 Carbonylazides

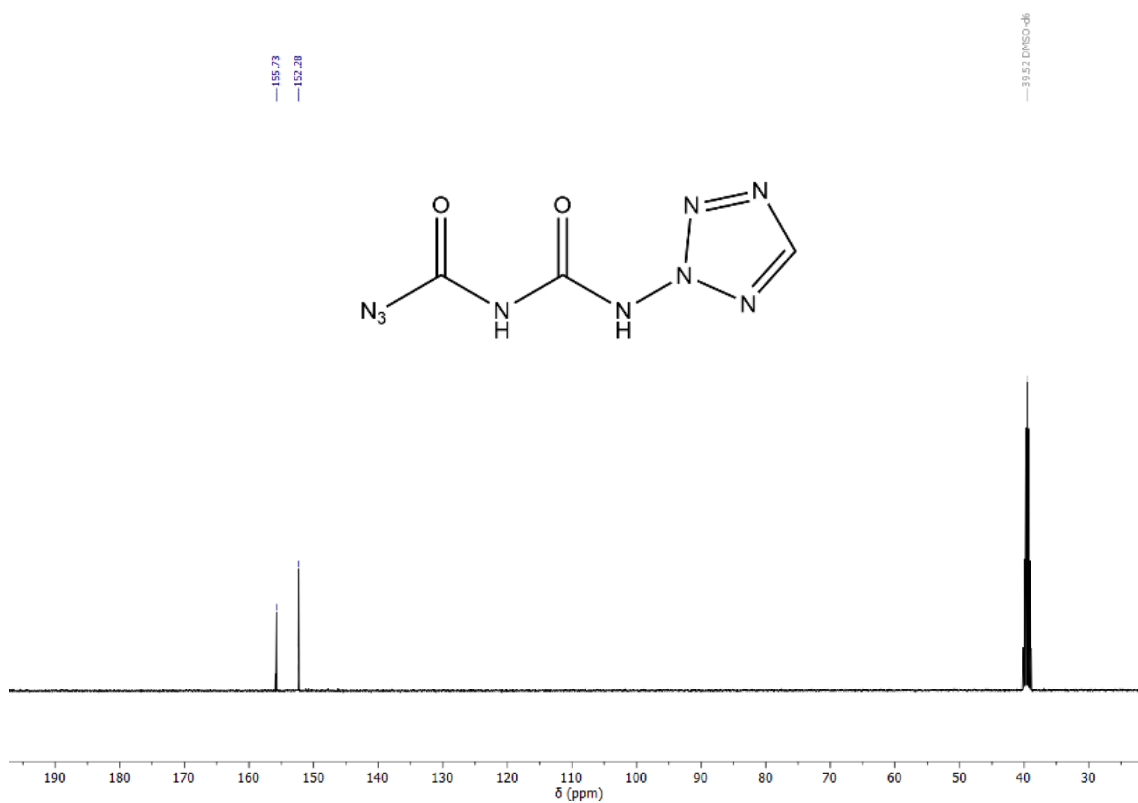


Figure 20. $^{13}\text{C}\{^1\text{H}\}$ -NMR spectrum of N-azidocarbonyl-N'-(2H-tetrazol-2-yl)-urea (6).

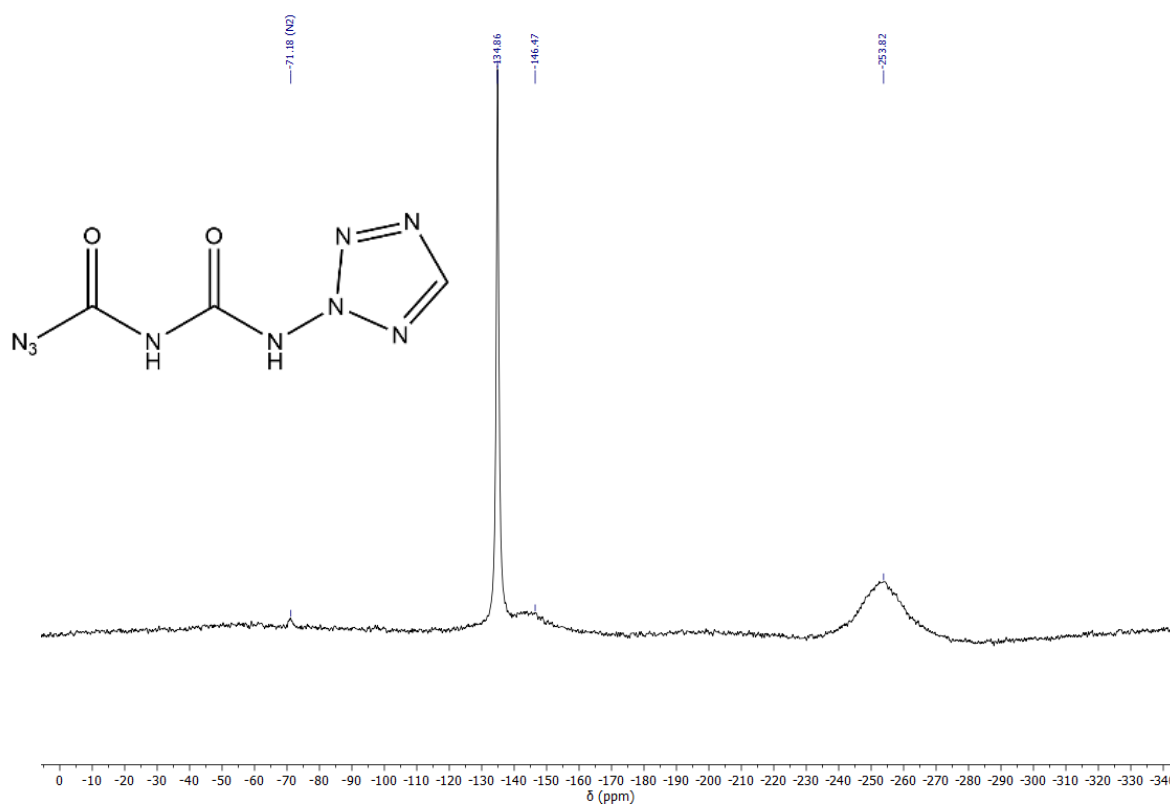


Figure 21. ^{14}N NMR spectrum of N-azidocarbonyl-N'-(2H-tetrazol-2-yl)-urea (6).

5.5.3 IR Spectroscopy of Carbamoyl azide (2)

IR spectrum of solid carbamoyl azide (**2**) was recorded using an FTIR-ATR (attenuated total reflectance) Bruker 70V spectrometer at a resolution of 2 cm^{-1} . Gas-phase IR spectra were measured in a KBr gas cell on an INSA OPTICS FT-IR spectrometer (FOLI10-R) at a resolution of 2 cm^{-1} . Raman spectrum were recorded on a HR800 spectrometer at a resolution of 2 cm^{-1} . Matrix IR spectra were recorded on an FTIR Bruker 70V spectrometer in a reflectance mode using a transfer optic, and a KBr beam splitter and liquid nitrogen cooled mercury cadmium telluride (MCT) detector were used in the mid-IR region ($4000\text{--}500\text{ cm}^{-1}$) at a resolution of 0.5 cm^{-1} . The gaseous sample was mixed by passing a flow of Ne gas through a U-trap ($25\text{ }^\circ\text{C}$) containing ca. 10 mg of the azide. Then the mixture (sample/matrix gas $\approx 1 : 1000$ estimated) was deposited (2 mmol h^{-1}) onto the Rh-plated copper block matrix support (3 K) in a dynamic vacuum ($\sim 10^{-4}\text{ Pa}$).

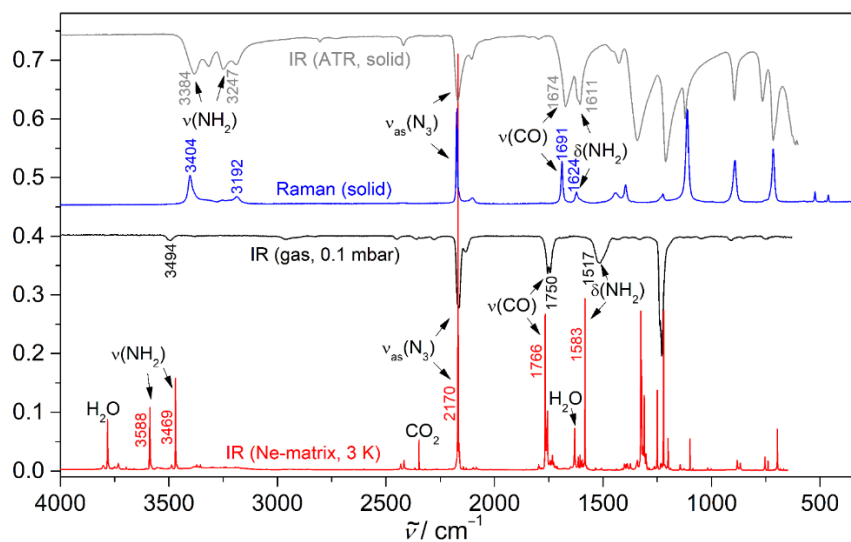


Figure 22. IR and Raman spectra of carbamoyl azide (**2**).

The FT-IR spectrum of pure, solid **2** shows two medium intensity bands at 3384 and 3247 cm^{-1} which correspond to the amino group, and a strong band at 1674 cm^{-1} for the carbonyl group. In the Ne-matrix and gas phase IR spectra, the stretching modes of the amino group are observed at 3588 and 3470 cm^{-1} , which are dramatically blue-shifted in relation to the IR spectrum of the pure solid. In contrast, the CO stretching mode occurs at 1766 cm^{-1} in the matrix IR spectrum, and at 1750 cm^{-1} in the gas phase spectrum, and is therefore significantly red-shifted in the solid state spectrum where it is observed at 1674 cm^{-1} . Clearly, these large shifts are due to strong intermolecular hydrogen bonds between the amino and carbonyl groups in the solid state. In contrast, the bands for the asymmetric stretching mode of the azido moiety in the IR (gas, solid, and Ne-matrix) and Raman (solid) spectra remain almost unchanged at around 2170 cm^{-1} .

5.5.4 X-ray Diffraction and Hirshfeld Analysis

Crystal structure data were obtained from an Oxford Xcalibur3 diffractometer with a Spellman generator (voltage 50kV, current 40mA) and a Kappa CCD area for data collection using Mo-K α radiation ($\lambda=0.71073\text{\AA}$) or a Bruker D8 Venture TXS diffractometer equipped with a multilayer monochromator, a Photon 2 detector and a rotation-anode generator (Mo-K α radiation). The data collection was performed using the CRYSTALIS RED software.^[32] The solution of the structure was performed by direct methods and refined by full-matrix least-squares on F² (SHELXT)^[33] implemented in the OLEX2^[34] software suite. The non-hydrogen atoms were refined anisotropically and the hydrogen atoms were located and freely refined. The absorption correction was carried out by a SCALE3 ABSPACK multiscan method.^[35] The DIAMOND2 plots shown with thermal ellipsoids at the 50% probability level and hydrogen atoms are shown as small spheres of arbitrary radius. The SADABS program embedded in the Bruker APEX3 software was used for multi-scan absorption corrections in all structures.^[36]

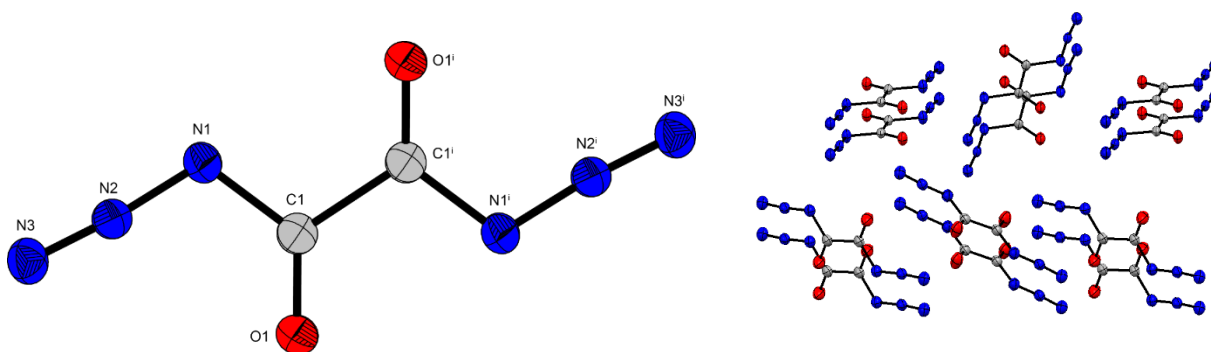


Figure 23. Crystal structure of oxalyl diazide (**1**). Thermal ellipsoids are drawn at the 50 % probability level. Oxalyl diazide forms alternating pairs in the crystal.

Oxalyl diazide (**1**) crystallizes in the monoclinic space group $P2_1/c$ with 4 molecules in the unit cell and a density of 1.751 g cm^{-3} at 102 K. The bond lengths are in good accordance with the standard bond lengths expected. The C1 shows a nearly trigonal planar arrangement, also the azide moiety is slightly bent with an N1-N2-N3 angle of 174.4° . The molecule itself is planar. Oxalyl diazide forms pairs in the crystal and these pairs are arranged alternately. Hirshfeld analysis showed only the presence of destabilizing and repulsive short contacts in the molecule. The short contacts consist of N...O (45.6 %), N...N (31.9 %), C...N (15.3 %) and O...O (6.8 %) interactions. The distance for all contacts is large and at least 3.0 \AA . The repulsive interactions cause the molecule to be highly rigid with respect to lattice deformation and mechanical stimuli.^[37–39] Since there are no stabilizing interactions between the oxalyl diazide molecules, it can be assumed that the

5 Carbonylazides

compound is extremely unstable, with very high sensitivity towards external stimuli, and very low thermal stability.

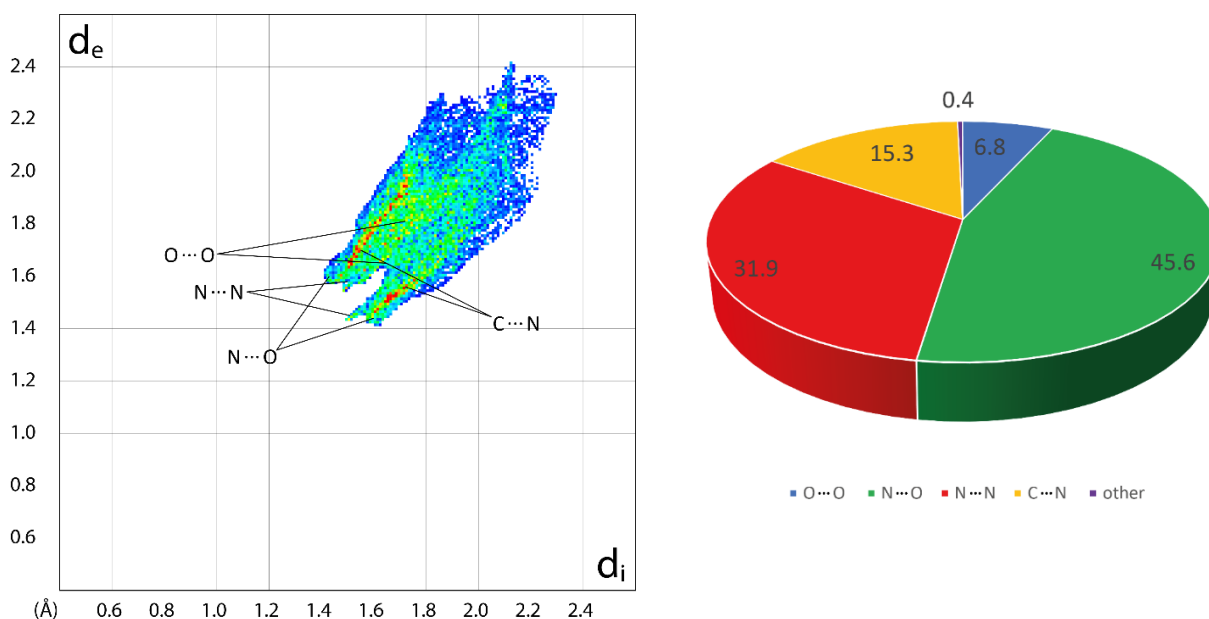


Figure 24. Two-dimensional Hirshfeld fingerprint plot of oxalyl diazide (**1**). Close contact distribution of compound **1**.

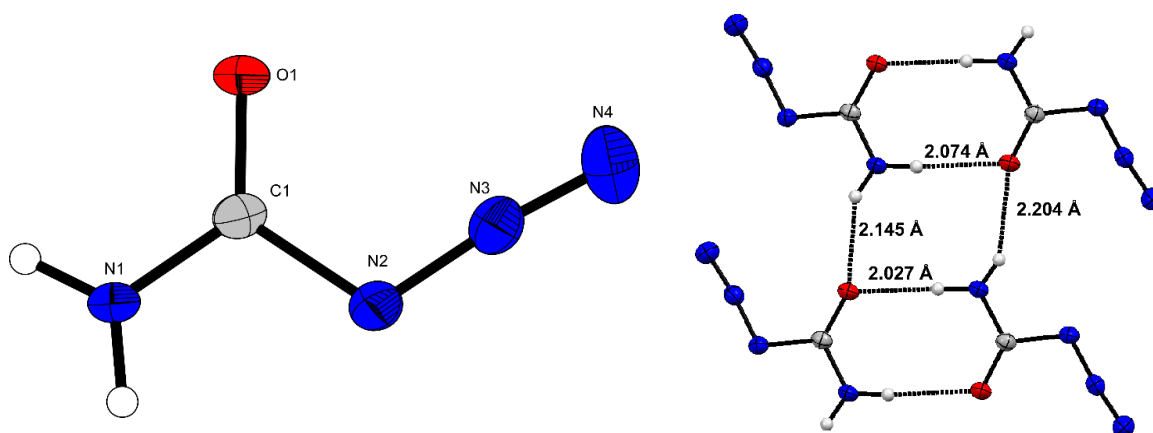


Figure 25. Crystal structure of carbamoyl azide (**2**). Thermal ellipsoids are drawn at the 50 % probability level. The carbamoyl azide (**2**) has strong hydrogen bonds with a distance of about 2 Å.

Carbamoyl azide (**2**) crystallizes in the monoclinic space group $P2_1/n$ with eight formula units in the unit cell and a density of 1.611 g cm^{-3} at 101 K. All bond lengths were found to be in the range of those expected for standard bond lengths. The arrangement around the C1 should be trigonal planar, but the angle at N2-C1-N1 (111.2°) deviates considerably from the expected 120° . The azide moiety is only slightly bent (174.2°) and is oriented *syn* with respect to the carbonyl group.

5 Carbonylazides

The molecule itself is planar. There are strong hydrogen bonds between the molecules with distances of 2.027 Å to 2.204 Å. A Hirshfeld analysis confirmed strong O...H (20.4 %) contacts with a distance of around 2 Å. Further, quite strong N...H (27.8 %) interactions are found with a distance of 3 Å. Some destabilizing interactions are also found, in particular, N...N (28.1 %), N...O (9.4 %) and H...H (6.2 %).^[37–39] A summary of the Hirshfeld analysis concludes that the destabilizing close contacts are fairly well counterbalanced by the stabilizing interactions, and it is assumed that the molecule is quite thermally stable and not that sensitive towards external stimuli such as friction or impact.

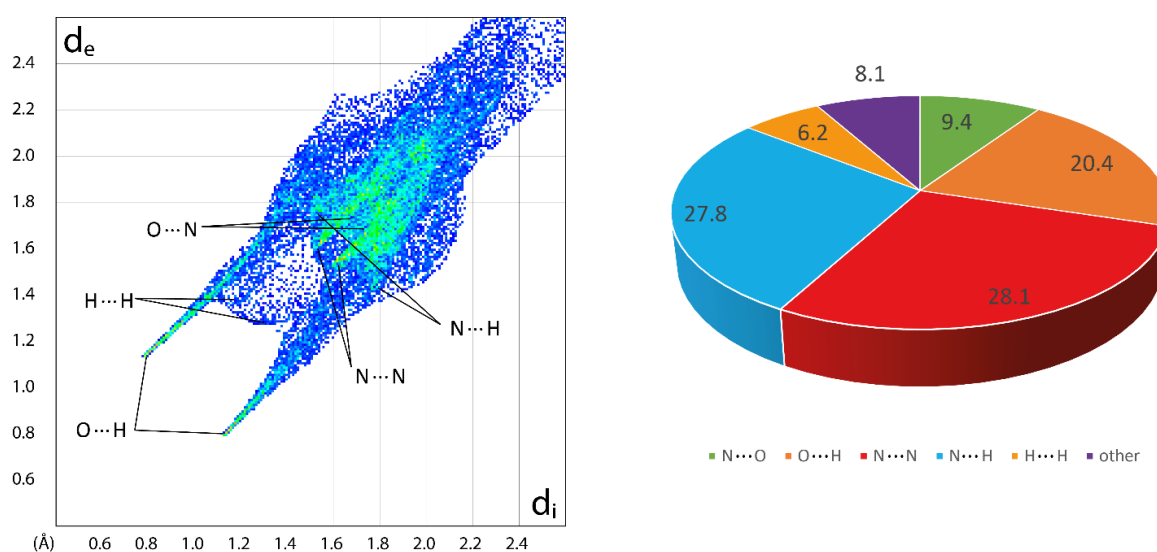


Figure 26. Two-dimensional Hirshfeld fingerprint plot of carbamoyl azide (**2**). Close contact distribution of compound **2**.

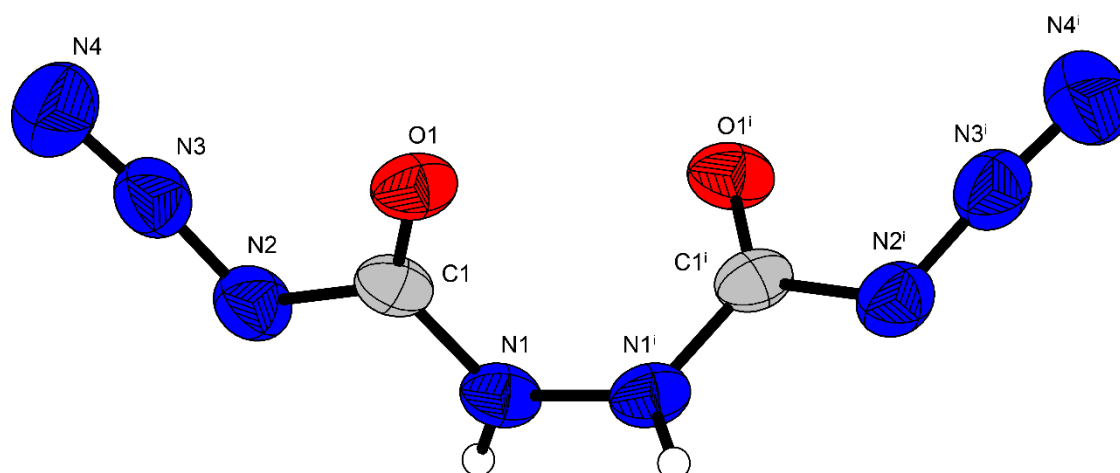


Figure 27. Crystal structure of *N,N'*-bis(azidocarbonyl)hydrazine (**3**). Thermal ellipsoids are drawn at the 50 % probability level.

5 Carbonylazides

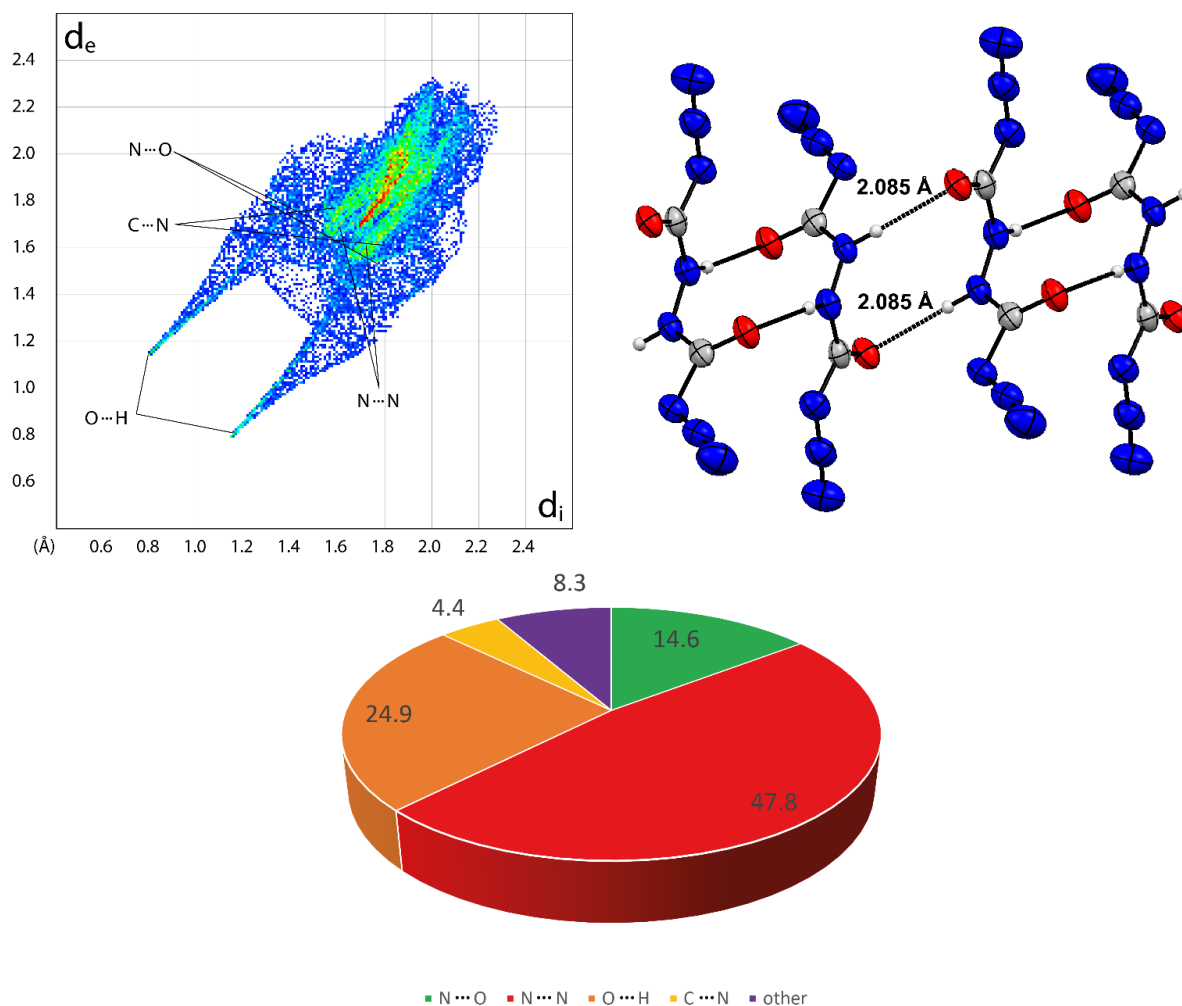


Figure 28. Two-dimensional Hirshfeld fingerprint plot of *N,N'*-bis(azidocarbonyl)hydrazine (**3**). Network of hydrogen bonds in the crystal of **3** with a distance of about 2 Å. Close contact distribution of compound **3**.

N,N'-bis(azidocarbonyl)hydrazine (**3**) crystallizes in the monoclinic space group *C2/c* with 4 molecules in the unit cell and a density of 1.697 g cm⁻³ at 173 K. The bond lengths correspond to those expected for standard bond lengths. The C1 atom shows distortion from a trigonal planar arrangement, since the O1-C1-N2 (125.8°) as well as at N1-C1-O1 (124.9°) angles are larger than 120°, while the N1-C1-N2 angle (109.2°) is smaller. The azido groups have an angle of 173.7°. As described before, the azide moiety is arranged *syn* relative to the carbonyl groups. The molecule possesses a center of symmetry between the nitrogen atoms of the hydrazine bridge with both sides of the symmetry point being planar. The molecule is twisted at the hydrazine bridge with a torsion angle of 72.2°. Compound **3** possesses very strong intermolecular hydrogen bonds with distances of 2.085 Å, resulting in the formation of a network. A Hirshfeld analysis showed strong O...H (24.9 %) close contacts with a distance of around 2 Å. A high percentage of N...N (47.8 %)

5 Carbonylazides

contacts are found, which indicates compound **3** should show high sensitivity, due to the strong repulsive interactions which should occur upon crystal lattice deformation such those resulting from mechanical stimuli.^[37–39] Moreover, repulsive N...O (14.6 %) interactions are also found in the molecule. In summary, a lot of repulsive close contacts are found in **3**, but these are largely counterbalanced by the strong hydrogen bonds which are present. Compound **3** should be more sensitive towards mechanical stimuli than **2**, but less sensitive than **1**. *N,N'*-bis(azidocarbonyl)hydrazine (**3**) should show thermal stability similar to that as **2**.

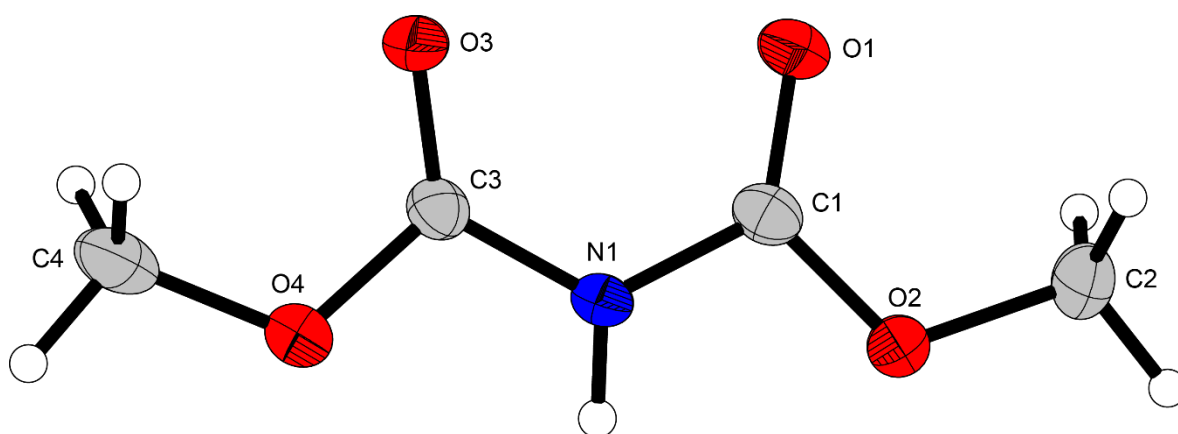


Figure 29. Crystal structure of dimethyl iminodicarbonate (**4**). Thermal ellipsoids are drawn at the 50 % probability level.

Dimethyl iminodicarbonate (**4**) crystallizes in the monoclinic space group $P2_1/c$ with four molecules in the unit cell and a density of 1.448 g cm^{-3} at 104 K. All bonds lengths correspond with those in the range of the expected standard bond lengths. The O1-C1-O2 and O1-C1-N1 angles are slightly larger (127.0° and 124.8° respectively) than those expected for a trigonal planar arrangement. The N1-C1-O2 angle (108.2°) is more similar to that observed for a tetrahedral arrangement. The C1-N1-C3 angle is 124.9° . The same situation concerning the angles is on the other side of the symmetry axis of the molecule. Compound **4** is completely planar with no twists nor torsions. A strong hydrogen bond is found in this molecule with a distance of 2.037 \AA from the H1 of N1 to O3.

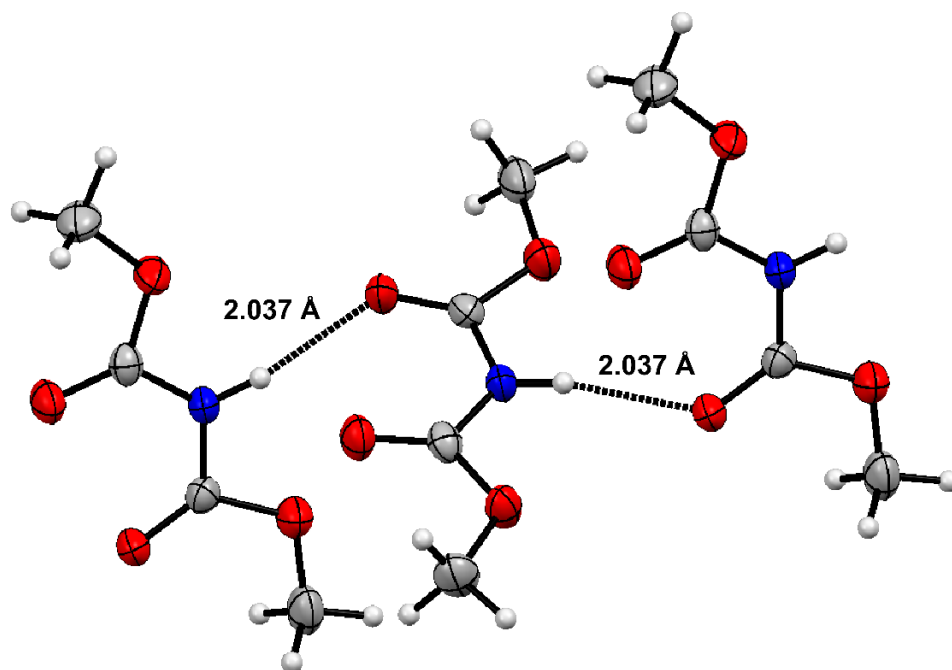


Figure 30. Dimethyl iminodicarbonate (**4**) forms a network in the crystal due to the formation of hydrogen bonds with a distance of 2.037 Å.

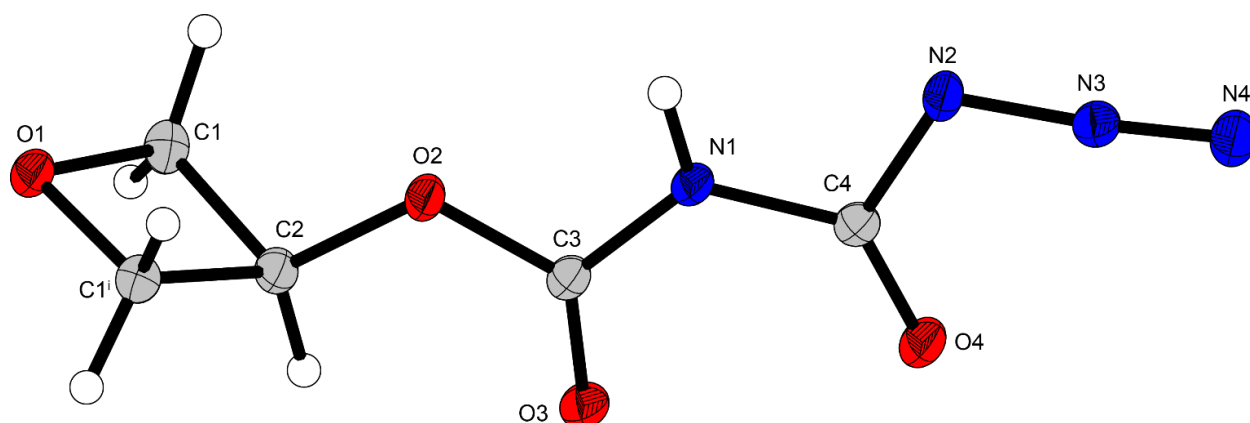


Figure 31. Crystal structure of oxetan-3-yl-*N*-azidocarbonyl-carbamate (**5**). Thermal ellipsoids are drawn at the 50 % probability level.

Oxetan-3-yl-*N*-azidocarbonyl-carbamate crystallizes in the monoclinic space group $C2/m$ with 4 formula units in the unit cell and a density of 1.651 g cm^{-3} at 101 K. All bond lengths are in the range expected for standard bond lengths. The angles in the oxetane ring are 90.9° (C1-O1-C1'), 91.3° (O1-C1-C2 and O1-C1'-C2), and 86.0° (C1-C2-C1'). Two angles centered at atoms C3 and C4 are slightly larger than the expected 120° , namely, $O3-C3-O2$ is 126.1° , $O3-C3-N1$ is 127.2° , while $O2-C3-N1$ is 106.6° , which is significantly smaller than a trigonal planar angle and also smaller than a tetrahedral angle. Also, $N1-C4-N2$ (107.0°) is smaller than a trigonal planar angle and a tetrahedral angle. The other two are larger than a trigonal planar angle with 128.4° ($N1-C4-O4$)

and 124.6° (O4-C4-N2). The azide moiety is only slightly bent with an angle of 174.9° . The usually planar oxetane group has a torsion angle of 5.3° and is twisted 132.2° with respect to the rest of the molecule which is planar. Compound **5** has strong intermolecular hydrogen bonds from H1 at N1 to O1 of the oxetane ring with a distance of 1.938 \AA . Two molecules form pairs in the crystal through two symmetrical hydrogen bonds of the same distance.

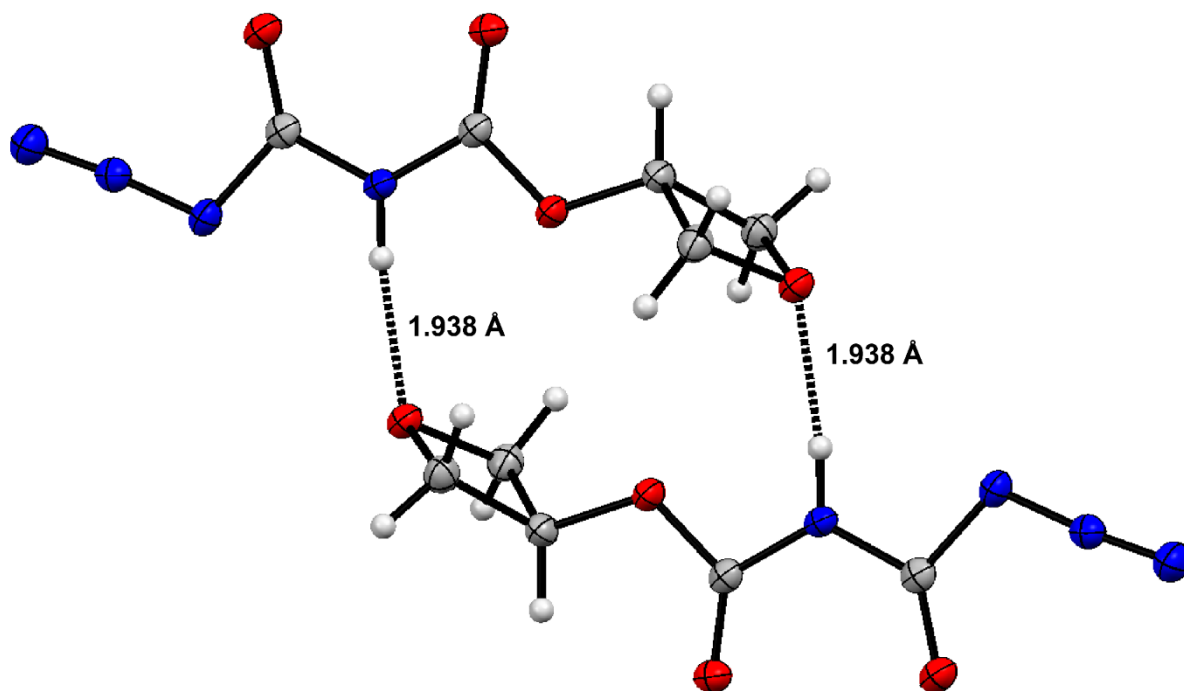


Figure 32. Two molecules of oxetan-3-yl-*N*-azidocarbonyl-carbamate (**5**) form pairs via two hydrogen bonds with a distance of 1.938 \AA .

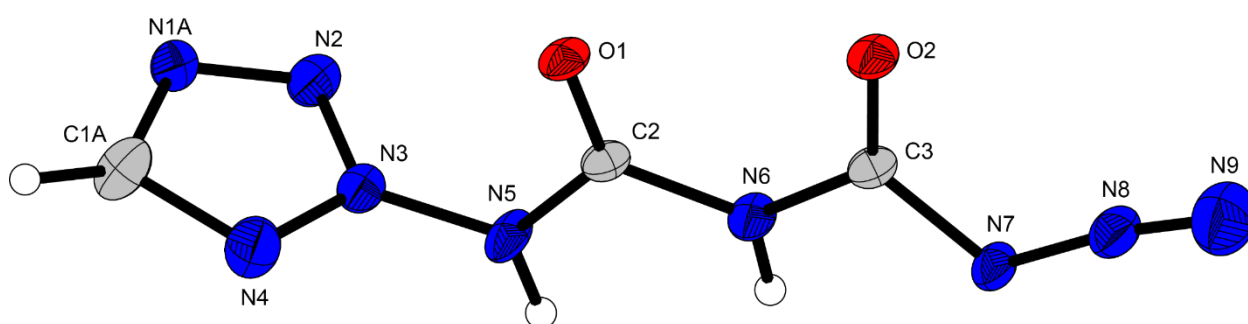


Figure 33. Crystal structure of *N*-azidocarbonyl-*N'*-(2*H*-tetrazol-2-yl)-urea (**6**). Thermal ellipsoids are drawn at the 50 % probability level.

N-azidocarbonyl-*N'*-(2*H*-tetrazol-2-yl)-urea (**6**) crystallizes in the monoclinic space group $P2_1/c$ with four molecules in the unit cell and a density of 1.727 g cm^{-3} at 102 K. The bond lengths are in good agreement with standard bond lengths. As described for the previous molecule (**5**), the

5 Carbonylazides

N5-C2-O1 (123.0°) and O1-C2-N6 (125.0°) angles are slightly larger than the expected values of 120°. The N5-C2-N6 (112.1°) angle is significantly smaller than a trigonal planar angle, but larger than a tetrahedral angle. The two angles, N6-C3-O2 and O2-C3-N7, are both 126.3°, which is also larger than that expected for a trigonal planar angle. The N6-C3-N7 angle is only 107.5°, which is smaller than both a trigonal planar and tetrahedral angle. The azido group N7-N8-N9 is bent with an angle of 171.7°. The usually planar tetrazole motif has a small torsion angle of about 4°, and is twisted by about 90° with respect to the rest of the molecule. The rest of the molecule is nearly planar, only O2-C3-N6-C2 is twisted by 9.8°. Compound 6 forms a network, in which one molecule forms three strong hydrogen bonds to the neighboring molecule. The H6-O1 distance is 2.006 Å, H5-O1 is 2.099 Å and H5-O2 is 2.201 Å.

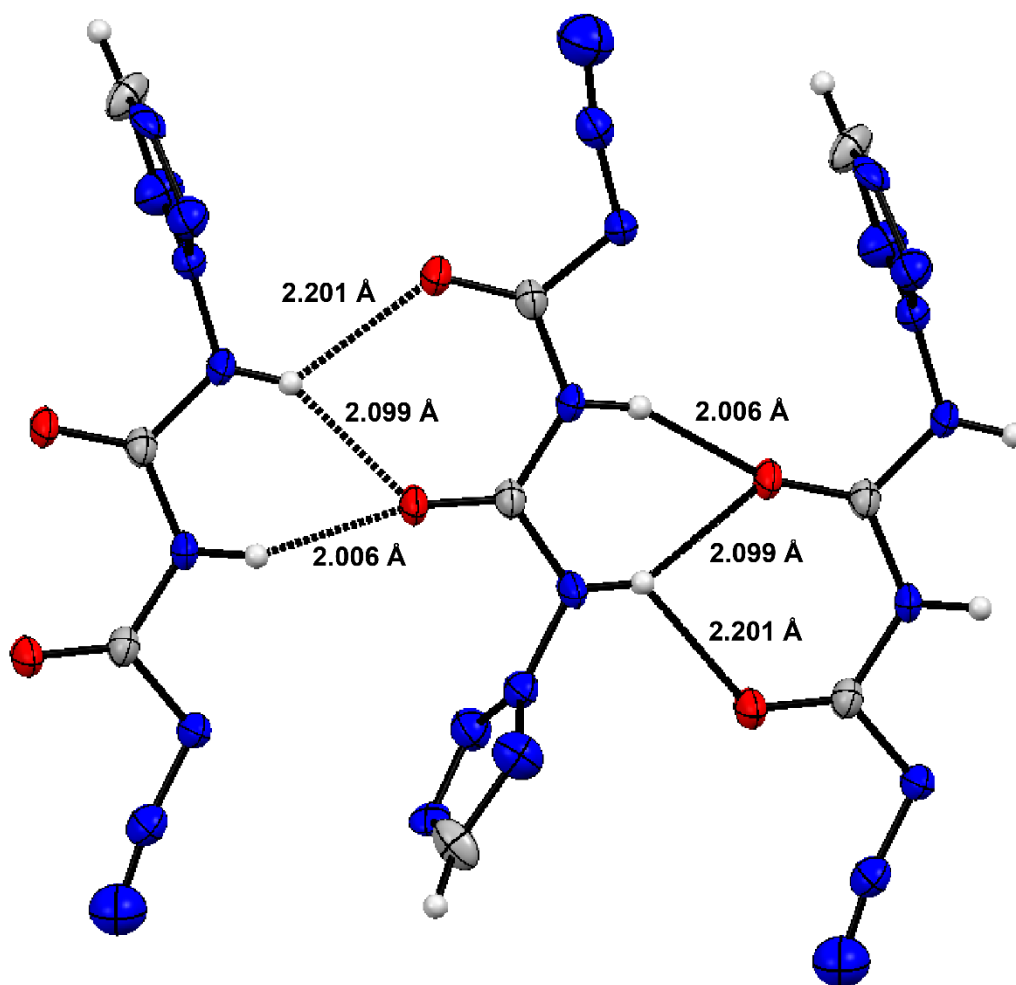


Figure 34. Network of *N*-azidocarbonyl-*N'*-(2*H*-tetrazol-2-yl)-urea (**6**) forming three hydrogen bonds between the molecules with a distance of about 2 Å.

Table 2. Crystallographic data and structure refinement details for the prepared compounds **1** – **3**.aaaa

	Oxalyl diazide (1)	Carbamoyl azide (2)	<i>N,N'</i> -bis(azidocarbonyl)hydrazine (3)
Formula	C ₂ N ₆ O ₂	CH ₂ N ₄ O	C ₂ H ₂ N ₈ O ₂
FW [g mol ⁻¹]	140.08	86.07	170.12
Crystal system	monoclinic	monoclinic	monoclinic
Space group	<i>P2</i> ₁ / <i>c</i> (No. 14)	<i>P2</i> ₁ / <i>n</i> (No. 14)	<i>C2</i> / <i>c</i> (No. 15)
Color / Habit	colorless platelet	colorless rod	colorless platelet
Size [mm]	0.08 x 0.35 x 0.50	0.048 x 0.182 x 0.744	0.01 x 0.03 x 0.04
a [Å]	9.9766(15)	5.1411(6)	20.9800(14)
b [Å]	5.1435(5)	22.5003(19)	4.6103(3)
c [Å]	11.0086(15)	6.5540(10)	7.1227(4)
α [°]	90	90	90
β [°]	109.822(16)	110.632(14)	104.894(2)
γ [°]	90	90	90
V [Å ³]	531.43(13)	709.52(16)	665.79(7)
Z	4	8	4
ρ _{calc.} [g cm ⁻³]	1.751	1.611	1.697
μ [mm ⁻¹]	0.155	0.139	0.148
F(000)	280	352	344
λ _{MoKα} [Å]	0.71073	0.71073	0.71073
T [K]	102	101	173
θ Min-Max [°]	2.2, 25.3	3.4, 26.4	4.0, 26.4
Dataset	-12: 10 ; -4: 6 ; -13: 12	-6: 6 ; -26: 28 ; -8: 6	-26: 26 ; -5: 5 ; -8: 8
Reflections collected	3015	5528	5226
Independent refl.	975	1458	667
R _{int}	0.037	0.036	0.029
Observed reflections	756	1135	580
Parameters	91	125	59
R ₁ (obs) ^[a]	0.0460	0.0352	0.0345
wR ₂ (all data) ^[b]	0.1314	0.0828	0.0841
S ^[c]	1.08	1.07	1.14
Resd. dens [e Å ⁻³]	-0.31, 0.32	-0.18, 0.16	-0.11, 0.11
Device type	Oxford Xcalibur3	Oxford Xcalibur3	Bruker D8 Venture TXS
Solution	SHELXT	SHELXT	SHELXT
Refinement	SHELXL-2018	SHELXL-2018	SHELXL-2018
Absorption correction	multi-scan	multi-scan	multi-scan
CCDC	2077536	2077537	2077539

[a] $R_1 = \frac{\sum ||F_0| - |F_c||}{\sum |F_0|}$; [b] $wR_2 = \frac{[\sum [w(F_0 - F_c)^2]]^{1/2}}{[\sum w(F_0)^2]^{1/2}}$; $w = \frac{[\sigma^2(F_0) + (xP)^2 + yP] - 1}{P}$ and $P = (F_0^2 + 2F_c^2)/3$; [c] $S = \frac{[\sum [w(F_0 - F_c)^2]]^{1/2}}{(n-p)}$ (n = number of reflections; p = total number of parameters).

Table 3. Crystallographic data and structure refinement details for the prepared compounds **4** – **6**.aaaa

	Dimethyl iminodicarbonate (4)	Oxetan-3-yl- <i>N</i> - azidocarbonyl-carbamate (5)	<i>N</i> -Azidocarbonyl- <i>N'</i> -(2 <i>H</i> - tetrazol-2-yl)-urea (6)
Formula	C ₄ H ₇ NO ₄	C ₅ H ₆ N ₄ O ₄	C ₃ H ₃ N ₉ O ₂
FW [g mol ⁻¹]	133.11	186.14	197.14
Crystal system	monoclinic	monoclinic	monoclinic
Space group	<i>P</i> 2 ₁ / <i>c</i> (No. 14)	<i>C</i> 2/ <i>m</i> (No. 12)	<i>P</i> 2 ₁ / <i>c</i> (No. 14)
Color / Habit	colorless needle	colorless prism	colorless platelet
Size [mm]	0.02 x 0.08 x 0.50	0.01 x 0.25 x 0.50	0.15 x 0.25 x 0.48
<i>a</i> [Å]	12.7890(18)	16.3279(17)	8.8833(12)
<i>b</i> [Å]	5.8869(7)	5.8786(7)	8.9823(7)
<i>c</i> [Å]	8.2990(9)	7.8026(7)	10.0444(12)
α [°]	90	90	90
β [°]	102.200(12)	90.113(8)	108.873(13)
γ [°]	90	90	90
<i>V</i> [Å ³]	610.70(13)	748.93(14)	758.38(16)
<i>Z</i>	4	4	4
ρ _{calc.} [g cm ⁻³]	1.448	1.651	1.727
μ [mm ⁻¹]	0.131	0.144	0.147
<i>F</i> (000)	280	384	400
λ _{MoKα} [Å]	0.71073	0.71073	0.71073
<i>T</i> [K]	104	101	102
θ Min-Max [°]	1.6, 26.4	2.5, 26.4	2.4, 26.4
Dataset	-15: 15 ; -7: 7 ; -10: 8	-20: 15 ; -7: 7 ; -9: 8	-9: 11 ; -11: 11 ; -12: 11
Reflections collected	3774	2471	4769
Independent refl.	1253	830	1546
<i>R</i> _{int}	0.049	0.022	0.031
Observed reflections	787	731	1160
Parameters	88	90	146
<i>R</i> ₁ (obs) ^[a]	0.0664	0.0260	0.0451
<i>wR</i> ₂ (all data) ^[b]	0.1769	0.0672	0.1297
<i>S</i> [c]	1.04	1.05	1.05
Resd. dens [e Å ⁻³]	-0.22, 0.89	-0.17, 0.21	-0.32, 0.23
Device type	Oxford Xcalibur3	Oxford Xcalibur3	Oxford Xcalibur3
Solution	SHELXT	SHELXT	SHELXT
Refinement	SHELXL-2018	SHELXL-2018	SHELXL-2018
Absorption correction	multi-scan	multi-scan	multi-scan
CCDC	2077540	2077535	2077538

[a] $R_1 = \sum ||F_0| - |F_c|| / \sum |F_0|$; [b] $wR_2 = [\sum [w(F_0 - F_c)^2] / \sum [w(F_0)^2]]^{1/2}$; $w = [\sigma^2(F_0) + (xP)^2 + yP]^{-1}$ and $P = (F_0^2 + 2F_c^2) / 3$; [c] $S = \{\sum [w(F_0 - F_c)^2] / (n - p)\}^{1/2}$ (n = number of reflections; p = total number of parameters).

5.5.5 Thermal Analysis

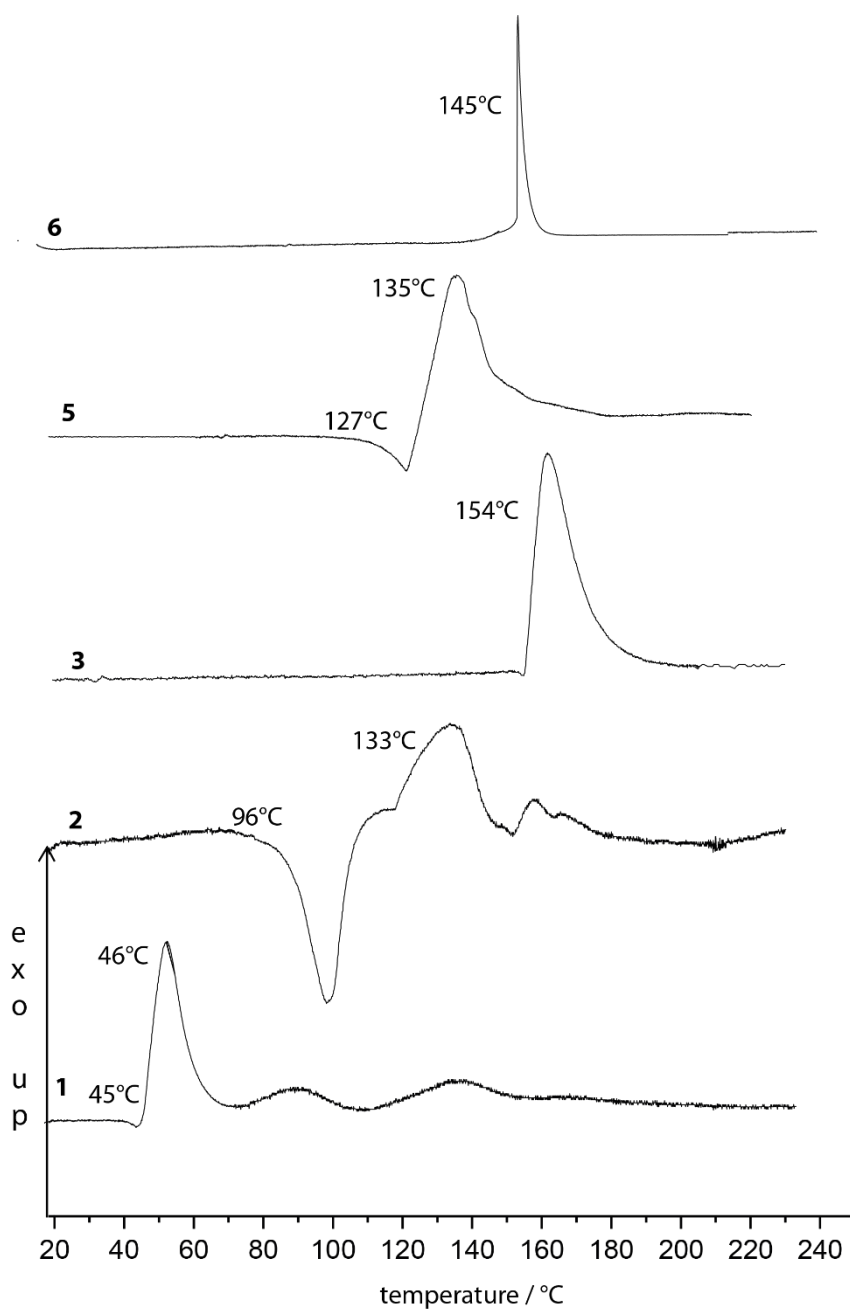


Figure 35. Differential thermal analysis plots of compound 1–3, 5 and 6.

DTA plots of compounds **1**, **2** and **5** showed melting point of 45°C, 96°C and 127°C for the respective compound. All synthesized carbonyl azide derivatives have a decomposition temperature of higher than 100°C, up to 154°C for **3**, except oxalyl diazide (**1**) which is rather unstable and decomposes at 46°C.

5.5.6 Computation

The atomization was used to determine the heat of formation of **1–3** using the atom energies in **Table 4**.

$$\Delta_f H^\circ_{(g, M, 298)} = H_{(molecule, 298)} - \sum H^\circ_{(atoms, 298)} + \sum \Delta_f H^\circ_{(atoms, 298)}$$

Table 4. CBS-4M electronic enthalpies for atoms C, H, N and O and their literature values.

	$-H^{298} / \text{a.u.}$	$\Delta_f H^\circ_{\text{gas}}^{[40]}$
H	0.500991	217.998
C	37.786156	716.68
N	54.522462	472.68
O	74.991202	249.18

The Gaussian16 program package was used to calculate room temperature enthalpies on the CBS-4M level of theory.^[41] In order to obtain the energy of formation for the solid phase of **1**, the Trouton's Rule has to be applied ($\Delta H_{\text{sub}} = 188 \cdot T_m$).

Table 5. Heat of formation calculation results for compounds **1–3**, **5**, **6**.

M	$-H^{298}$ [a] [a.u.]	$\Delta_f H^\circ(g, M)$ [b] [kJ mol ⁻¹]	$\Delta_{\text{sub}} H^\circ (M)$ [c] [kJ mol ⁻¹]	$\Delta_f H^\circ(s)$ [d] [kJ mol ⁻¹]	Δn	$\Delta_f U(s)$ [e] [kJ kg ⁻¹]
1	554.357072	389.6	59.8122	329.7	-4.0	2425.1
2	333.080962	-111.1	69.4002	41.7	-3.5	585.0
3	664.930052	389.7	80.3042	309.3	-6.0	1906.2
5	713.055212	-265.3	75.2282	-340.5	-7.0	-1736.1
6	758.261604	426.7	78.6122	348.1	-7.0	1854.0

[a] CBS-4M electronic enthalpy; [b] gas phase enthalpy of formation; [c] sublimation enthalpy; [d] standard solid state enthalpy of formation; [e] solid state energy of formation.

To obtain insight into whether a closed tetrazolone or iminol form exist, we calculated six different possible tautomers using the G09W code.^[41] The energies were calculated at the CBS-4M level. The CBS-4M results suggested the presence of the mono- (**C**) and di-tetrazolone (**E**) forms relative to the amide (**A**). However, we were not able to experimentally verify the two more energetically favorable forms.

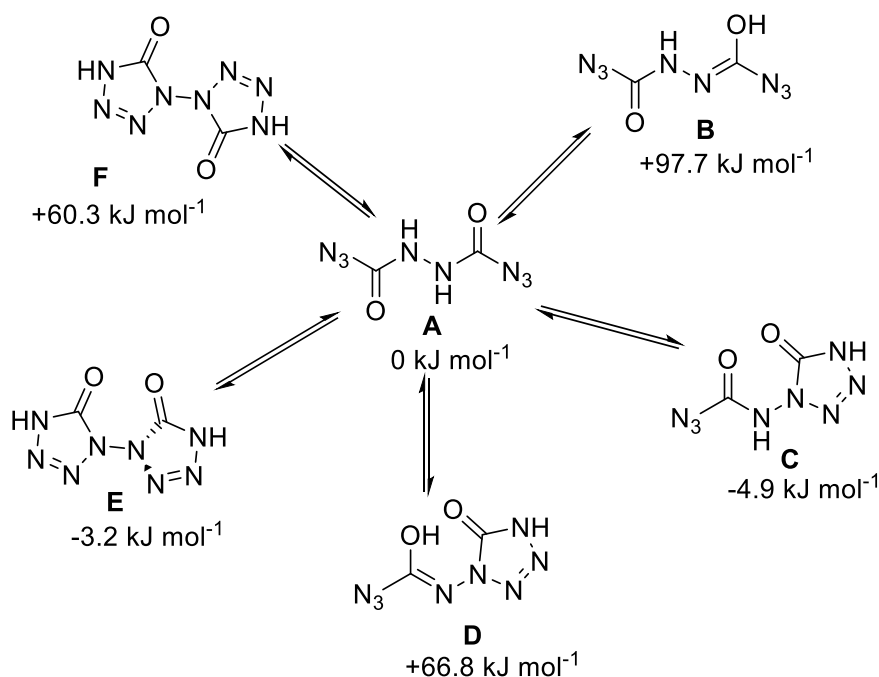


Figure 36. Six different tautomers of *N,N'*-bis(azidocarbonyl)hydrazine (**3**) and their respective energies on the CBS-4M level relative to that of **A**.

In order to obtain more reliable energies for molecules **A**, **C** and **E** in solution, we carried out MP2 calculations with a cc-pVDZ basis set using the Polarizable Continuum Model. The Polarizable Continuum Model (PCM) is a widely used implicit solvation model. Implicit solvation models place the molecule of interest inside a cavity in a continuous homogenous dielectric medium that represents the solvent. As the solvent we used water and acetone with dielectric constants of $\epsilon(\text{H}_2\text{O}) = 78.39$ and $\epsilon(\text{acetone}) = 20.7$. The results are summarized in table 4. The results of the PCM model calculation indicate that the mono-tetrazolone (**C**) form is unfavored in relation to **A** in the solvents water and acetone with energies of +12.6 kJ mol⁻¹ and +13.0 kJ mol⁻¹, respectively. Furthermore, the di-tetrazolone (**E**) form is strongly unfavored relative to **A** with energies of +41.0 kJ mol⁻¹ in water and +42.3 kJ mol⁻¹ in acetone.

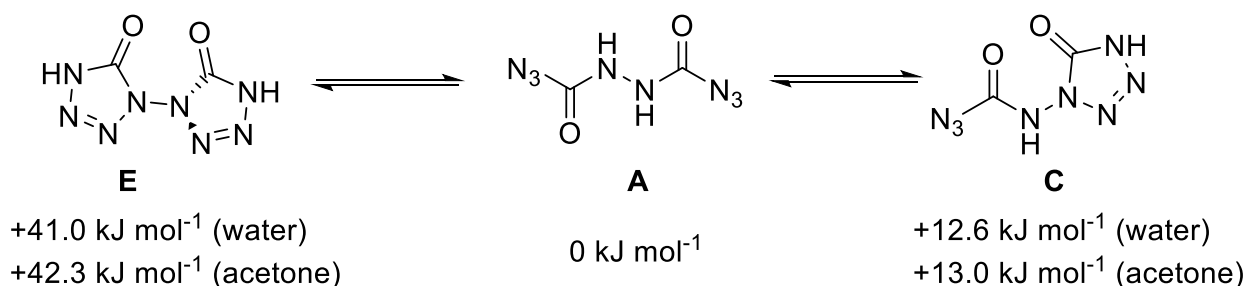


Figure 37. Three tautomers of *N,N'*-bis(azidocarbonyl)hydrazine (**3**) and their respective energies on the MP2/cc-pVDZ level (PCM model) relative to **A** with water or acetone as the solvents.

Table 6. Energy differences for the six tautomers of compound **3** and additionally PCM calculations with solvents being water and acetone for **A, C, E**.

	A	B	C	D	E	F*
Symmetry	C ₂		C ₁		C ₂	
CBS-4M						
-E / a. u.	664.93005 2	664.89283 0	664.93192 6	664.90461 1	664.93127 1	664.90708 1
ΔH°_f (g) / kJ mol ⁻¹	+389.7	+487.4	+384.8	+465.5	+386.5	+450.0
ΔE / kJ mol ⁻¹	0.0	+97.7	-4.9	+66.8	-3.6	+60.3
MP2/cc-pVDZsolvent = water (PCM model)						
-E / a. u.	664.06313 1	-	664.05835 3	-	664.04745 0	-
ΔE / kJ mol ⁻¹	0.0	-	+12.5604	-	+41.03064	-
MP2/cc-pVDZ solvent = acetone (PCM model)						
-E / a. u.	664.06259 9	-	664.05753 1	-	664.04651 8	-
ΔE / kJ mol ⁻¹	0.0	-	+12.97908	-	+42.28668	-

* transition state

5.6 References

- [1] T. Curtius, *Ber. Dtsch. Chem. Ges.* **1894**, 27, 778 – 781.
- [2] J. Thiele, O. Stange, *Liebigs Ann. Chem.* **1894**, 283, 1 – 46.
- [3] S. Bräse, C. Gil, *Angew. Chem., Int. Ed.* **2005**, 44, 5188 – 5240.
- [4] Q. J. Axthammer, T. M. Klapötke, B. Krumm, R. Scharf, C. C. Unger, *Dalton Trans.* **2016**, 45, 18909 – 18920.
- [5] Y. Ling, J. Guo, Q. Yang, P. Zhu, J. Miao, W. Hao, Y. Peng, J. Yang, K. Xu, B. Xiong, G. Liu, J. Tao, J. Luo, Q. Zhu, Y. Zhang, *Eur. J. Med. Chem.* **2018**, 144, 398 – 409.
- [6] R. Ikeda, T. Kimura, T. Tsutsumi, S. Tamura, N. Sakai, T. Konakahara, *Bioorg. Med. Chem. Lett.* **2012**, 22, 3506 – 3515.
- [7] H.-G. Mack, C. O. Della Védova, H. Willner, *J. Mol. Struct.* **1993**, 291, 197 – 209.
- [8] X. Zeng, M. Gerken, H. Beckers, H. Willner, *Inorg. Chem.* **2010**, 49, 9694 – 9699.
- [9] K. Banert, C. Berndt, M. Hagedorn, H. Liu, T. Anacker, J. Friedrich, G. Rauhut, *Angew. Chem., Int. Ed.* **2012**, 51, 4718 – 4721.
- [10] X. Zeng, E. Bernhardt, H. Beckers, K. Banert, M. Hagedorn, H. Liu, *Angew. Chem., Int. Ed.* **2013**, 52, 3503 – 3506.
- [11] T. Curtius, K. Heidenreich, *J. prakt. Chem.* **1895**, 52(1), 454 – 489.
- [12] X. Zeng, H. Beckers, H. Willner, J. F. Stanton, *Eur. J. Inorg. Chem.* **2012**, 21, 3403 – 3409.

5 Carbonylazides

- [13] H. Wan, H. Li, J. Xu, Z. Wu, Q. Liu, X. Chu, M. Abe, D. Bégué, X. Zeng, *Org. Chem. Front.* **2017**, *4*, 1839 – 1848.
- [14] Q. Liu, H. Wan, Y. Lu, B. Lu, X. Zeng, *Eur. J. Org. Chem.* **2019**, *2–3*, 401 – 411.
- [15] M. Benz, T. M. Klapötke, B. Krumm, M. Lommel, J. Stierstofer, *J. Am. Chem. Soc.* **2021**, *143*, 1323 – 1327.
- [16] H. W. Roesky, O. Glemser, *Chem Ber.* **1964**, *97*, 1710 – 1712.
- [17] T. M. Klapötke, B. Krumm, R. Scharf, *Eur. J. Inorg. Chem.* **2016**, *19*, 3086 – 3093.
- [18] S. Mohan, K. S. P. Durairaj, S. P. Jose, *Spectrochim. Acta, Part A* **2003**, *59*, 1697 – 1704.
- [19] J. M. Harris, R. McDonald, J. C. Vederas, *J. Chem. Soc., Perkin Trans. 1* **1996**, 2669 – 2674.
- [20] M. Figlus, A. C. Tarruella, A. Messer, S. L. Sollis, R. C. Hartley, *Chem. Comm.* **2010**, *46*, 4405 – 4407.
- [21] I.-H. Kim, C. Morisseau, T. Watanabe, B. D. Hammock, *J. Med. Chem.* **2004**, *47*, 2110 – 2122.
- [22] Z. Jaman, T. J. P. Sobreira, A. Mufti, C. R. Ferreira, R. G. Cooks, D. H. Thompson, *Org. Process Res. Dev.* **2019**, *23*, 334 – 341.
- [23] L. A. Ramos, X. Zeng, S. E. Ulic, H. Beckers, H. Willner, C. O. Della Védona, *J. Org. Chem.* **2012**, *77*, 6456 – 6462.
- [24] A. Baumann, A. Erbacher, C. Evangelisti, T. M. Klapötke, B. Krumm, S. F. Rest, M. Reynders, V. Sproll, *Chem. – Eur. J.* **2013**, *19*, 15627 – 15638.
- [25] <http://www.bam.de>
- [26] NATO Standardization Agreement (STANAG) on Explosives, *Impact Sensitivity Tests*, no. 4489, 1st ed., September 17, **1999**.
- [27] WIWEB-Standardarbeitsanweisung 4-5.1.02, Ermittlung der Explosionsgefährlichkeit, hier der Schlagempfindlichkeit mit dem Fallhammer, November 8, **2002**.
- [28] NATO Standardization Agreement (STANAG) on Explosives, *Friction Sensitivity Tests*, no. 4487, 1st ed., August 22, **2002**.
- [29] WIWEB-Standardarbeitsanweisung 4-5.1.03, Ermittlung der Explosionsgefährlichkeit oder der Reibeempfindlichkeit mit dem Reibeapparat, November 8, **2002**.
- [30] Impact: Insensitive >40 J, less sensitive ≤35 J, sensitive ≤4 J, very sensitive ≤3 J; friction: Insensitive >360 N, less sensitive=360 N, sensitive 80 N, very sensitive ≤80 N, extreme sensitive ≤10 N; According to the UN Recommendations on the Transport of Dangerous Goods (+) indicates: not safe for transport.
- [31] K. Banert, Y.-H. Joo, T. Rüffer, B. Walfort, H. Lang, *Angew. Chem. Int. Ed.* **2007**, *46*, 1168–1171.
- [32] CrysAlisPro, Oxford Diffraction Ltd., *version 171.33.41*, **2009**.
- [33] G. M. Sheldrick, *Acta Cryst.* **2015**, *A71*, 3 – 8.
- [34] O. V. Dolomanov, L. J. Bourhis, R. J. Gildea, J. A. K. Howard, H. Puschmann, *J. Appl. Cryst.* **2009**, *42*, 339 – 341.

5 Carbonylazides

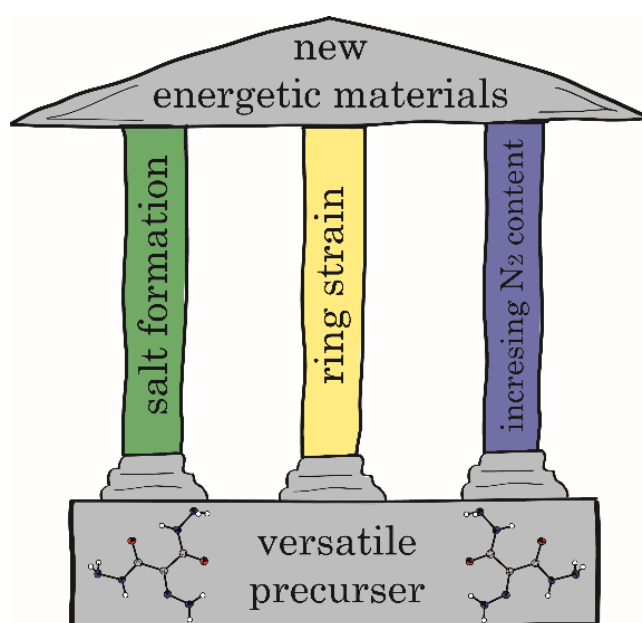
- [35] *SCALE3 ABSPACK—An Oxford Diffraction program* (1.0.4, gui: 1.0.3), Oxford Diffraction Ltd., **2005**.
- [36] *APEX3*. Bruker AXS Inc., Madison, Wisconsin, USA.
- [37] D. E. Dosch, M. Reichel, M. Born, T. M. Klapötke, K. Karaghiosoff, *Cryst. Growth Des.* **2021**, *21*(1), 243 – 248.
- [38] Y. Ma, A. Zhang, X. Xue, D. Jiang, Y. Zhu, C. Zhang, *Cryst. Growth Des.* **2014**, *14*, 6101 – 6114.
- [39] M. A. Spackman, D. Jayatilaka, *CrystEngComm* **2009**, *11*, 19 – 32.
- [40] M. W. Chase Jr., NIST-JANAF Thermochemical Tables, Fourth Edition, *J. Phys. Chem. Ref. Data, Monograph 9* **1998**, 1 – 1951.
- [41] M. J. Frisch, G. W. Trucks, H. B. Schlegel, G. E. Scuseria, M. A. Robb, J. R. Cheeseman, G. Scalmani, V. Barone, G. A. Petersson, H. Nakatsuji, X. Li, M. Caricato, A. V. Marenich, J. Bloino, B. G. Janesko, R. Gomperts, B. Mennucci, H. P. Hratchian, J. V. Ortiz, A. F. Izmaylov, J. L. Sonnenberg, D. Williams-Young, F. Ding, F. Lipparini, F. Egidi, J. Goings, B. Peng, A. Petrone, T. Henderson, D. Ranasinghe, V. G. Zakrzewski, J. Gao, N. Rega, G. Zheng, W. Liang, M. Hada, M. Ehara, K. Toyota, R. Fukuda, J. Hasegawa, M. Ishida, T. Nakajima, Y. Honda, O. Kitao, H. Nakai, T. Vreven, K. Throssell, J. A. Montgomery, Jr., J. E. Peralta, F. Ogliaro, M. J. Bearpark, J. J. Heyd, E. N. Brothers, K. N. Kudin, V. N. Staroverov, T. A. Keith, R. Kobayashi, J. Normand, K. Raghavachari, A. P. Rendell, J. C. Burant, S. S. Iyengar, J. Tomasi, M. Cossi, J. M. Millam, M. Klene, C. Adamo, R. Cammi, J. W. Ochterski, R. L. Martin, K. Morokuma, O. Farkas, J. B. Foresman, D. J. Fox, *Gaussian16*, Gaussian, Inc., Wallingford, CT, USA, **2016**.

2-Hydrazonyl-Propandihydrazide – A Versatile Precursor for High-Energy Materials

Alexander G. Harter, Thomas M. Klapötke, Christian Riedelsheimer, Jörg Stierstorfer, Sebastian M. Strobel, Michael Voggenreiter

As published in *European Journal of Inorganic Chemistry* **2022**, e202200100.

DOI: 10.1002/ejic.202200100



6.1 Abstract

In this work, 2-hydrazone-malonohydrazide (**2**), a new precursor for energetic materials based on diethyl 2,2-diazidomalonate (**1**) was investigated. Therefore, its versatility was shown by various secondary reactions, including formation of the energetic salts (**3–5**), the synthesis of a nitrogen rich bistriazole (**10**) and the highly instable diazido derivative (**6**). In addition, a *Curtius* degradation could be observed in detail. When possible, the compounds were analyzed by low temperature X-ray diffraction. All measurable compounds were analyzed by ^1H and ^{13}C NMR spectroscopy, elemental analysis, differential thermal analysis (DTA) and regarding their sensitivity towards impact and friction according to BAM standard techniques. All promising compounds were evaluated regarding their energetic behavior using the EXPLO5 code (V6.05) and compared to RDX and CL-20. In addition, compound **2** was investigated towards its aquatic toxicity, using the bioluminescent bacteria *vibrio fischeri*.

6.2 Introduction

Due to the wide spread use of energetic materials in both civilian and military applications, there is a constant need for improvement of known compounds, as well as the development of new energetic materials, exceeding their predecessors in regard to their performance, cost effectiveness and eco-friendliness.^[1-3] Countless discoveries of the last decade have proven nitrogen rich heterocycles like oxadiazoles, triazoles and tetrazoles to be promising backbones in high-energy material (HEM) synthesis.^[4-6] Compounds based on these systems often possess the desired properties like high density and detonation performance, good thermal stabilities and low sensitivities.^[7,8] By the formation of nitrogen rich salts these properties can be further improved.^[9] One of the most prominent examples for this class of molecules is TKX-50, surpassing commonly used energetic materials like RDX in almost all relevant properties.^[10-12] It is synthesized from glyoxal, which is an excellent example for a versatile precursor in the field of HEMs. Numerous compounds including K₂DNABT, CL-20, TKX-50, bisfuroxanes and furazanes can be prepared starting from glyoxal.^[13-15] Another well known example is nitroacetonitrile, which is commonly used to synthesize annulated 1,2,4-triazines.^[16] Some examples for energetic precursors are summarized in **Figure 1**. But the way to these promising energetic compounds often consists of long synthetic routes including numerous steps and complicated reaction paths, some of examples of these are shown in **Figure 2**. It is therefore of high importance to develop new precursor molecules, which are cheap and easy to synthesize and provide various

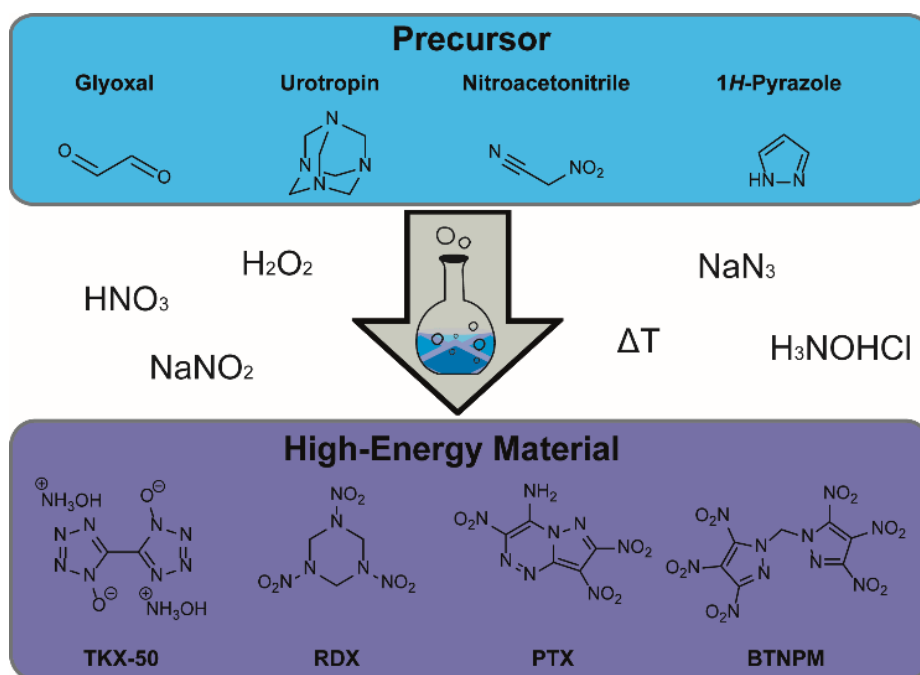


Figure 1. A selection of commonly used precursor molecules and their respective HEMs.

possibilities for functionalization in order to obtain HEMs. In addition, it would be ideal if they possess low sensitivities and no toxicity. Therefore, this work focuses on the synthesis of energetic materials, based on 2-hydrazone-malonohydrazide (**2**), a new energetic precursor. Those new compounds are extensively characterized in regard to their energetic and structural properties.

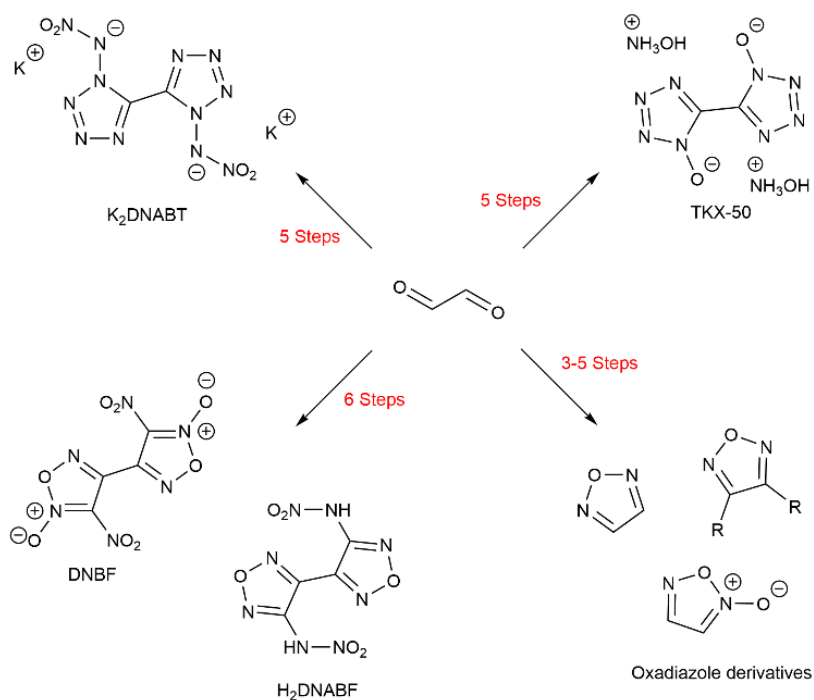
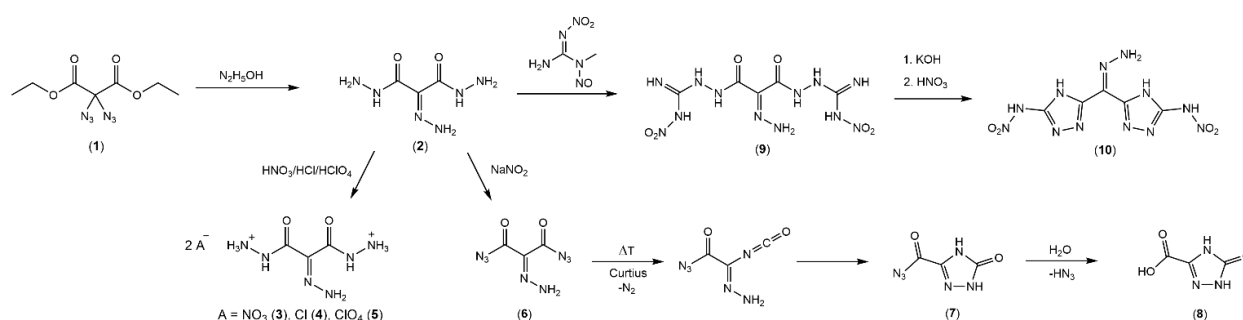


Figure 2. Glyoxal as a precursor for various energetic materials like K_2DNABT , TKX-50, furazane and furoxane derivatives

6.3 Results and Discussion

6.3.1 Synthesis

Diethyl 2,2-diazidomalonate (**1**) was synthesized according to literature procedure.^[17] 2-Hydrazonemalonohydrazide (**2**) was obtained by substitution of the azide groups and the ethoxy groups using an excess of hydrazinium hydroxide. Two ethanol molecules are cleaved by the nucleophilic attack of the hydrazine on the carboxyl carbon atom. The ionic compounds **3–5** are synthesized by *Brønsted* acid-base chemistry when reacting compound **2** with nitric, hydrochloric and perchloric acid, respectively. Hereby, compound **2** is protonated twice and the double salts of the 2-hydrazonemalonohydrazinium cation are formed. After diazotation of compound **2** a *Curtius* degradation starting from compound **6** can be observed. Hereby, 3-carbonylazido-1*H*-1,2,4-triazol-5-one (**7**) is formed almost instantly over the isocyanate intermediate, which reacts further to compound **8**, when exposed to ambient humidity. Additionally, compound **2** was reacted with *N*-methyl-*N*-nitroso-*N'*-nitroguanidine in order to form compound **9**, which was followed by a triazole ring closure, performed under basic conditions and subsequent acidification yielding the neutral compound **10** (Scheme 1). All compounds were fully characterized by IR and multinuclear NMR spectroscopy, mass spectrometry and differential thermal analysis. Further, selected compounds were analyzed using low-temperature single-crystal X-ray measurements.



Scheme 1. Synthesis of compound **2** as a versatile precursor for energetic compounds **3**, **4**, **5**, **9** and **10**, as well as the Curtius degradation from compound **6** to **8**.

6.3.2 Crystal Structures

Measurable crystals could be obtained for the compounds **2–5**, **7** and **8**, either directly from the reaction mixture (**7**, **8**) or by recrystallization from water (**2–5**). General information on the X-ray measurements and refinements are given in the SI. Structures were deposited with the CCDC

6 Hydrazonyl-Propandihydrazide

database under the following numbers (**2**: 2149590, **3**: 2149591, **4**: 2149592, **5**: 2149593, **7**: 2149594, **8**: 2149595). For all structure, thermal ellipsoids are drawn at the 50% probability level.

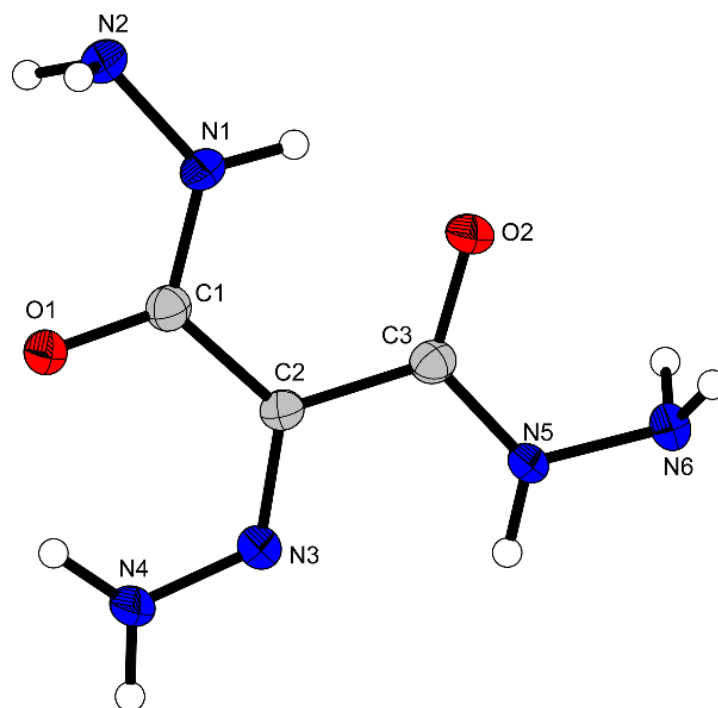


Figure 3. Molecular unit of 2-hydranonemalonohydrazide (**2**).

2-Hydranonemalonohydrazide (**2**) crystallizes in the monoclinic space group $P2_1/c$ with a density of 1.601 g/cm^3 at 113 K (**Figure 3**). The cell volume is $664.35(9) \text{ \AA}^3$ with four formula units per cell. The molecule is highly planar, shown by the torsion angles, which are very close to 0° or 180° . ($N6-N5-C3-C2$ 173.8° , $N4-N3-C2-C1$ 0.3° , $N2-N1-C1-C2$ 178.9°). Both, intramolecular and intermolecular hydrogen bonds can be observed. ($N4-H4B \cdots O1$, $N5-H5 \cdots N3$, $N1-H1 \cdots O2$, $N2-H2A \cdots O1$, $N4-H4B \cdots O2$). The bond lengths confirm the mesomeric system, with values between single and double bonds for $C1-N1$ (1.333 \AA), $C2-N3$ (1.314 \AA), $N3-N4$ (1.309 \AA) and $C3-N5$ (1.336 \AA).^[18,19]

2-Hydranonemalonohydrazinium dinitrate $\cdot 0.25 \text{ H}_2\text{O}$ (**3**) crystallizes in the monoclinic space group $P2_1/c$ with a density of 1.743 g/cm^3 at 107 K (**Figure 4**). The cell volume is $1107.53(10) \text{ \AA}^3$ with one formula unit per cell. The torsion angles show a planar molecule, similar to compound **2** ($N6-N5-C3-C2$ -174.9° , $N4-N3-C2-C1$ 0.7° , $N2-N1-C1-C2$ 176.4°). The compound crystallizes with one water per four product molecules.

6 Hydrazyl-Propandihyrazide

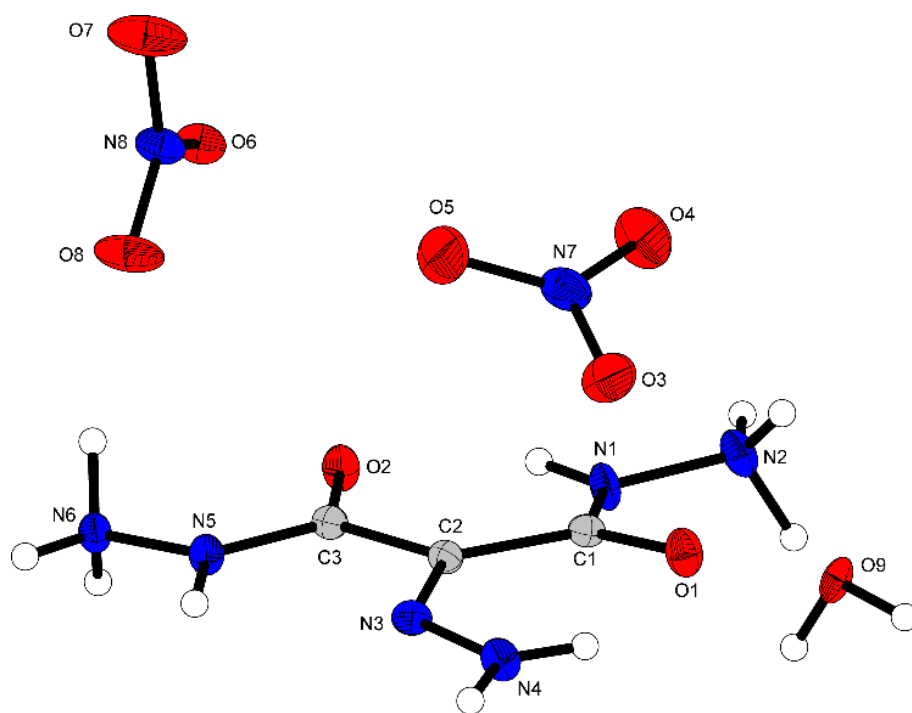


Figure 4. Molecular unit of 2-hyazonemalonohydrazinium dinitrate · 0.25 H₂O (**3**).

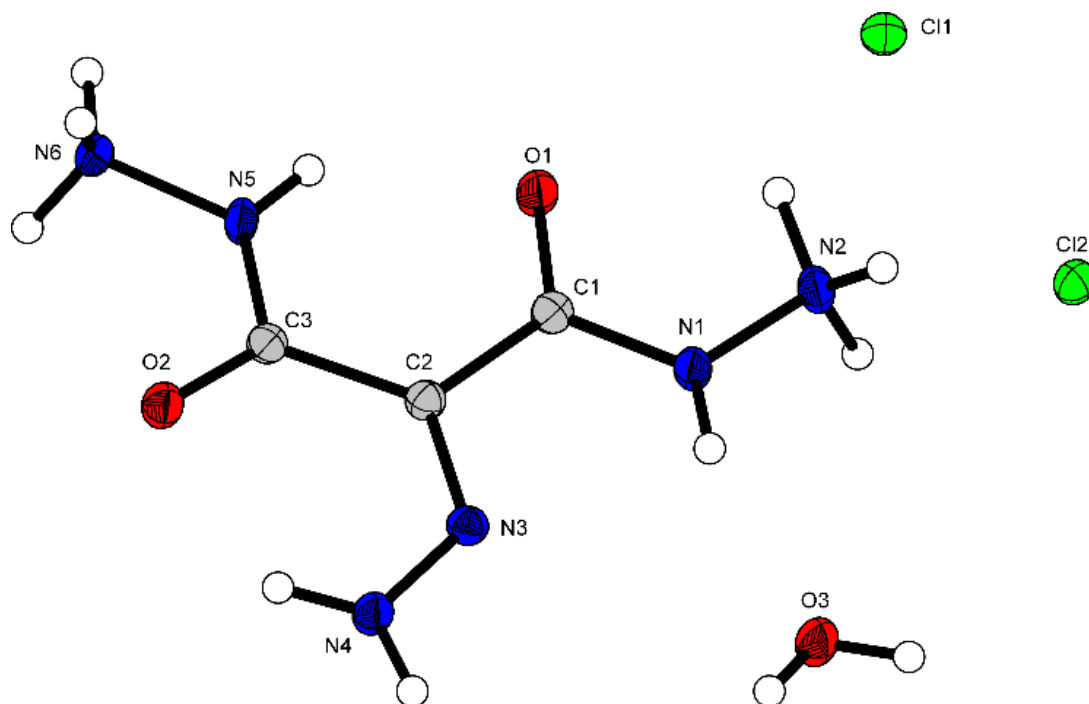


Figure 5. Molecular unit of 2-hyazonemalonohydrazinium dichloride monohydrate (**4**).

Compound **4** crystallizes in the triclinic space group *P*-1 with a density of 1.657 g cm⁻³ at 100 K and two formula units per unit cell (**Figure 5**). The cell volume is 503.15(6) Å³. The structure shows high similarities to the previously described compounds **2** and **3** in regard to its planarity (N6–N5–C3–C2 -172.7°, N4–N3–C2–C1 176.2°, N2–N1–C1–C2 178.3°). The crystal structure contains one water per unit cell. All bond lengths comply with the described values for compound **2**.

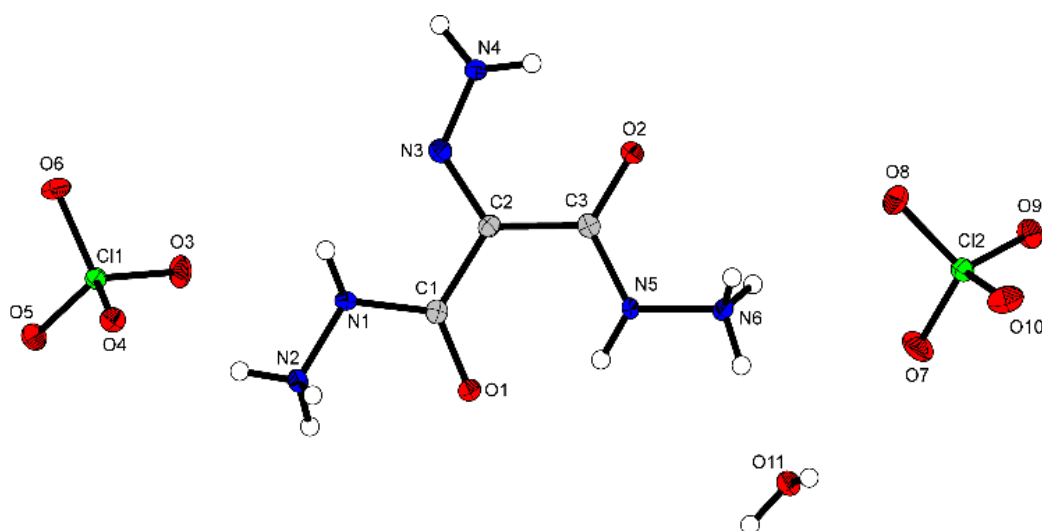


Figure 6. Molecular unit of 2-hydrazonemalonohydrazinium diperchlorate monohydrate (**5**).

Compound **5** crystallizes in the monoclinic space group $P2_1/n$ with a density of 1.991 g cm^{-3} at 105 K and four formula units per unit cell (**Figure 6**). The cell volume is $1264.94(13) \text{ \AA}^3$. The structure fits the expectations in regard to the torsion angles, being slightly less planar than the previous described structures ($\text{N6-N5-C3-C2} -171.0^\circ$, $\text{N4-N3-C2-C1} 178.5^\circ$, $\text{N2-N1-C1-C2} -168.8^\circ$). The crystal structure contains one water per unit cell. All bond lengths comply with the expected values for C–C, C–N, C–O and N–N single and double bonds.^[18,19]

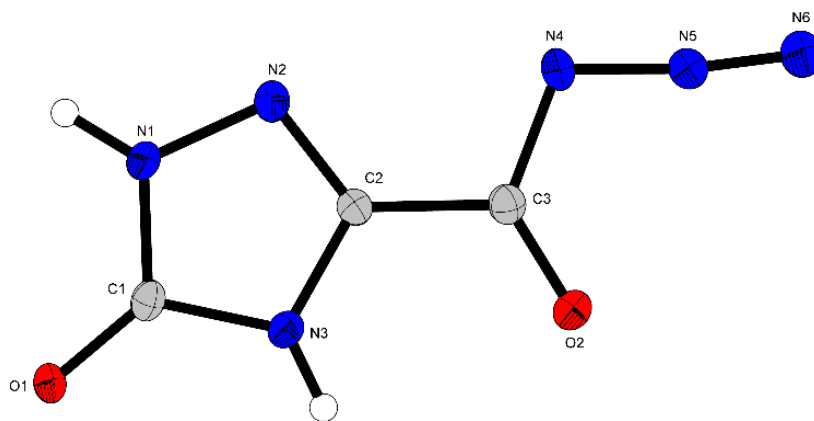


Figure 7. Molecular unit of 3-carbonylazido-1H-1,2,4-triazol-5-one (**7**).

Compound **7** crystallizes in the monoclinic space group $P2_1/c$ with a density of 1.797 g cm^{-3} at 105 K and four formula units per unit cell (**Figure 7**). The cell volume is $569.48(17) \text{ \AA}^3$. Based on the torsion angles the structure can also be described as planar ($\text{C1-N1-N2-C2} -0.4^\circ$, $\text{N2-C2-C3-N4} 2.7^\circ$, $\text{N5-N4-C3-O2} 2.3^\circ$). All bond lengths comply with the expected values for C–C, C–N, C–O and N–N single and double bonds ($\text{C2-C3} 1.49 \text{ \AA}$, $\text{N1-N2} 1.38 \text{ \AA}$, $\text{N4-C3} 1.40 \text{ \AA}$, $\text{C1-O1} 1.25 \text{ \AA}$).^[18,19]

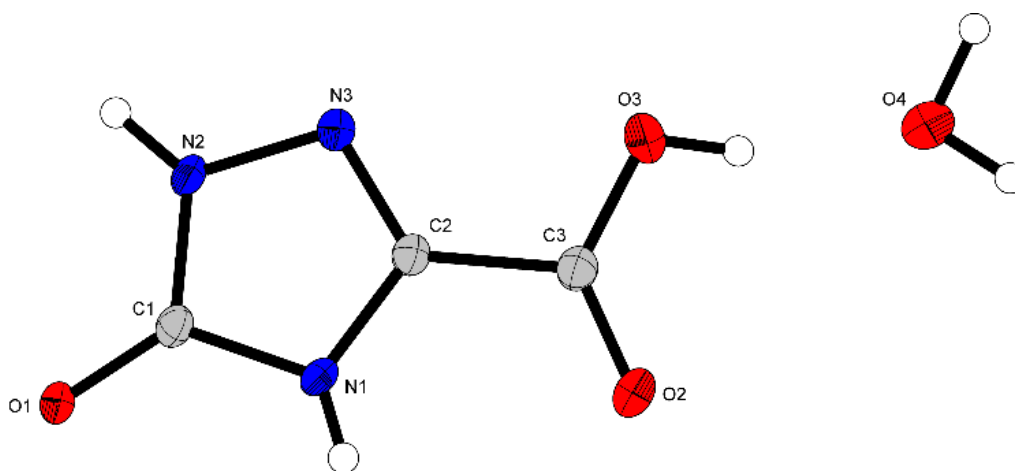


Figure 8. Molecular unit of 3-Carboxyl-1H-1,2,4-triazol-5-one monohydrate (**8**).

Compound **8** crystallizes in the monoclinic space group $P2_1/c$ with a density of 1.766 g cm^{-3} at 102 K and four formula units per unit cell (**Figure 8**). The cell volume is $553.20(4) \text{ \AA}^3$. Similar to compound **7** the torsion angles describe a planar structure (C2-N1-C1-N2 -0.4° , N1-C2-C3-O3 0.8° , N3-N2-C1-O1 -177.6°). The compound crystallizes with one water molecule per unit cell. All bond lengths comply with the expected values for C–C, C–N, C–O and N–N single and double bonds (C2-C3 1.49 \AA , N2-N3 1.37 \AA , N3-C2 1.30 \AA , C1-O1 1.25 \AA).^[18,19]

6.3.3 NMR and Vibrational Spectroscopy

All ^1H and ^{13}C NMR measurements were performed in DMSO-d_6 . The proton NMR of compound **2** shows five signals. This is due to the *E/Z*-isomerism caused by the inflexible hydrazone moiety, building intramolecular hydrogen bridges with one side of the otherwise symmetrical molecule. The two signals at 4.26 and 4.46 ppm belong to the NH_2 - groups of the hydrazides. The two signals at 8.88 and 10.20 ppm are the NH groups, which are shifted more due to a higher influence of the described effect on those protons. The same effect can be observed in the corresponding ^{13}C spectrum, which shows three signals. The two signals at 162.9 and 164.9 ppm belong to the unsymmetrically carbohydrazides and the signal at 119.0 ppm represents the hydrazone group. Compound **3**, **5** and **9** behave in a similar manner, as it would be expected. Although compound **10** also has the intermediate hydrazone group, it shows symmetric signals in the ^1H and ^{13}C spectra, which are caused by the mesomerism of the ring system. The IR spectrum of **6** was measured in chloroform, since this compound decomposes as soon as it is isolated. The hydrazone moiety can be identified by the two broad bands at 3313 and 3163 cm^{-1} , as well as the

band at 1574 cm^{-1} . The band at 2129 cm^{-1} corresponds to the azide groups and the carbonyl vibration is found at 1675 cm^{-1} .^[20,21]

6.3.4 Physicochemical Properties

All energetic compounds were characterized regarding their physicochemical properties. This includes their sensitivities towards impact, friction and electrostatic discharge, the thermal behavior and detonation parameters. Those were determined experimentally or computationally and compared to RDX, being the state-of-the-art secondary explosive in industrial use, and CL-20, which is one of the best performing compounds in terms of detonation properties shown in **Table 1**. The sensitivity values towards impact and friction were determined according to the BAM standards.^[22] When looking at compound **2** and the energetic salts **3** and **5**, it was observed, that they are insensitive towards friction, with values above 360 N. In regard to the impact values only compound **3** shows a slight sensitivity of 30 J. For compound **3** and **5** the insensitivity can be explained by the crystal water, generally reducing those values. Compound **9** also shows no sensitivity towards impact and friction with values of above 40 J and 360 N. Compound **10** exhibits interesting properties, possessing a high impact sensitivity of 2.5 J, which is close to the range of primary explosives, while at the same time being almost insensitive towards friction stimuli with a value of 360 N. When compared to RDX and CL-20, all compounds are less sensitive, with the exception of compound **10** showing a higher impact sensitivity. It was attempted to measure the friction sensitivity of compound **6** directly after separating it from the reaction mixture, which resulted in positive tests at 1 N. But it has to be mentioned that the *Curtius* degradation visibly took place, as the product turned yellow during the measurement and therefore no certain values could be obtained. The thermal properties of all compounds were determined by differential thermal analysis. None of the measured compounds show endothermic events, which could be assigned to melting points. In terms of decomposition temperatures, the range starts at a rather low value $124\text{ }^{\circ}\text{C}$ for the perchlorate salt **5** and ends at $209\text{ }^{\circ}\text{C}$ for compound **9**. The remaining three compounds **2**, **3** and **10** show decent decomposition temperatures slightly below $180\text{ }^{\circ}\text{C}$. The DTA plots of compound **2**, **9** and **10** is depicted in **Figure 9**. With the exception of compound **9**, all measured compounds are less stable towards thermal influences than RDX. The investigated compounds exhibit very high combined nitrogen and oxygen contents up to 84 % for compound **3**. Based on the densities, obtained by gas pycnometry or from the crystal structures the energetic properties were calculated with EXPLO5 (V6.05).^[23]

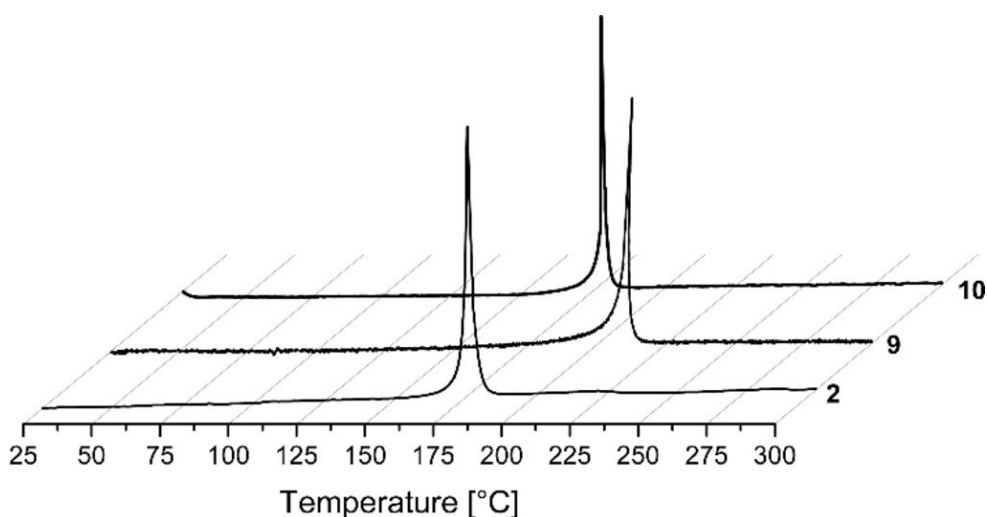


Figure 9. DTA plot of compounds **2**, **9** and **10** measured with a heating rate of $5 \text{ K}\cdot\text{min}^{-1}$

The heats of formation were obtained by CBS-4 M calculations. The densities of compound **2** and its salts **3** and **5** range from 1.56 g cm^{-3} to 1.94 g cm^{-3} with the neutral compound showing the lowest value, the perchlorate salt the highest value and the nitrate salt a moderate value of 1.70 g cm^{-3} , which is in line with the expectations. The densities of compounds **9** and **10** were determined by gas pycnometry, since no crystal structures could be obtained. Compound **9** shows a lower density of 1.73 g cm^{-3} , when compared to compound **10**, which was to be expected due to the large size of the molecule. With 1.81 g cm^{-3} compound **10** is in the same density range of RDX, which is a promising starting condition for the detonation properties. When looking at the detonation velocities and pressures, the values of the measured compounds range from $7610 \text{ m}\cdot\text{s}^{-1}$ and 19.3 GPa for compound **2**, up to $9082 \text{ m}\cdot\text{s}^{-1}$ and 36.9 GPa for compound **5**. Therefore, compounds **3** and **5** are able to surpass RDX in terms of their detonation properties, exhibiting detonation velocities around $9000 \text{ m}\cdot\text{s}^{-1}$. Compound **10** still shows decent values which are only slightly below RDX with a detonation velocity of $8654 \text{ m}\cdot\text{s}^{-1}$ and a pressure of 31.0 GPa . It was expected, that compounds **2** and **9** are the least well performing, since they lack structural energetic properties. This was confirmed by the calculations, with values of $7610 \text{ m}\cdot\text{s}^{-1}$ and 19.3 GPa for compound **2** and $8228 \text{ m}\cdot\text{s}^{-1}$ and 25.9 GPa for compound **9**. CL-20 surpasses all synthesized compounds in terms of thermal stability and detonation performance, which was to be expected. But due to much simpler and more cost-efficient syntheses, as well as lower sensitivities, the presented compounds are still a valuable addition to the roster of secondary explosives and prove the worth of compound **2** as an energetic precursor.

6 Hydrazonyl-Propandihydrazide

Table 1. Physiochemical properties of compounds **2**, **3**, **5**, **9**, **10** and RDX and CL-20^[24].

	2	3	5	9	10	RDX	CL-20
Formula	C ₃ H ₈ N ₆ O ₂	C ₃ H _{10.5} N ₈ O _{8.25}	C ₃ H ₁₂ N ₆ O ₁₁ Cl ₂	C ₅ H ₁₀ N ₁₂ O ₆	C ₅ H ₆ N ₁₂ O ₄	C ₃ H ₆ N ₆ O ₆	C ₆ N ₁₂ H ₆ O ₁₂
<i>M</i> [g·mol ⁻¹]	160.14	290.56	379.06	334.21	298.18	222.12	438.19
<i>IS</i> ^[a] [J]	>40	30	>40	>40	2.5	7.5	3
<i>FS</i> ^[b] [N]	>360	>360	>360	>360	360	120	96
<i>N+O</i> ^[c] [%]	72.46	83.89	68.60	79.01	77.83	81.06	82.17
Ω_{CO_2} ^[d] [%]	-80	-17	0	-43	-34	-22	-11
<i>T</i> _{endo} ^[e] / <i>T</i> _{exo} ^[f] [°C]	-/178	-/167	-/124	-/209	-/177	203/208	-/224
ρ ^[g] [g·cm ⁻³]	1.56	1.70	1.94	1.73	1.81	1.82	2.08
$\Delta_f H^\circ$ ^[h] [kJ·mol ⁻¹]	-21	224	-239	184	541	87	365
EXPLO5 V6.05							
$-\Delta_E U^\circ$ ^[i] [kJ·kg ⁻¹]	2851	6552	5993	4327	5137	5807	6160
<i>T</i> _{C-J} ^[j] [K]	2096	4073	4080	3023	3624	3800	4071
$\rho_{\text{C-J}}$ ^[k] [GPa]	19.3	34.2	36.9	25.9	31.0	34.0	44.5
<i>D</i> _{C-J} ^[l] [m·s ⁻¹]	7610	8920	9082	8228	8654	8882	9778
<i>V</i> ₀ ^[m] [dm ³ ·kg ⁻¹]	885	859	837	829	766	793	720

[a] Impact sensitivity (BAM drophammer, method 1 of 6); [b] friction sensitivity (BAM friction tester, method 1 of 6); [c] combined nitrogen and oxygen content; [d] oxygen balance toward carbon dioxide ($\Omega_{\text{CO}_2} = (n\text{O} - 2x\text{C} - y\text{H}/2)(1600/\text{M})$); [e] endothermic peak (DTA, $\beta = 5 \text{ }^\circ\text{C}\cdot\text{min}^{-1}$); [f] temperature of decomposition (DTA, $\beta = 5 \text{ }^\circ\text{C}\cdot\text{min}^{-1}$); [g] density at 298 K, for compound **9** and **10** determined by gas pycnometry; [h] standard molar enthalpy of formation; [i] detonation energy; [j] detonation temperature; [k] detonation velocity; [l] detonation pressure; [m] volume of detonation gases at standard temperature and pressure conditions.

6.3.4 Toxicity Assessment

In order to determine the ecotoxicological impact of the presented precursor, EC₅₀ measurements based on the bioluminescent *vibrio fischeri* NRRL-B-11177 marine bacteria strain were performed. Therefore, the EC₅₀ values of compound **2** were measured after 15 and 30 minutes and compared to the measured values of glyoxal, which is one of the most common precursors in energetic synthesis. The EC₅₀ value refers to the concentration of a toxicant which induces a response of 50 % after a specific exposure time. In this case the EC₅₀ value is determined by inhibition of the luminescence by 50 %, when exposed to the toxicant.^[25] Based on the resulting effective concentration the measured substances were classified as nontoxic (>1.00 g·L⁻¹), toxic (0.10–1.00 g·L⁻¹), and very toxic (<0.10 g·L⁻¹).^[26] The measured values are shown in **Table 2**. Compound **2** can be described as nontoxic, since its EC₅₀ value is above 1 g·L⁻¹. Glyoxal is classified as toxic with values of 0.43 g·L⁻¹ and 0.33 g·L⁻¹ after 15 min and 30 min, respectively. Therefore, compound **2** can be described as an ecofriendly precursor for energetic material synthesis.

Table 2. EC50 values of **2** and glyoxal.

Incubation	2	Glyoxal
15 min	4.62	0.43
30 min	2.61	0.33

6.4 Conclusion

In this work, we present 2-hydrizonemalonohydrazide (**2**) as a new precursor in energetic material synthesis. Therefore, the energetic salts **3** and **5**, as well as a bridged nitraminobistriazole (**10**) were synthesized deriving from compound **2** by straightforward and short methods. Additionally, a *Curtius* degradation of 2-hydrizonemalonyldiazide (**6**) was observed including the intermediate (**7**) and final product (**8**). Crystal structures of compounds **2–5**, **7** and **8** were determined. The densities range from 1.56 g·cm⁻³ of the precursor (**2**) to 1.94 g·cm⁻³ of the perchlorate salt (**5**). All compounds were characterized via NMR, and IR as well as regarding their physiochemical properties, including thermal behavior and sensitivity towards impact and friction. Due to its very unstable character towards various stimuli, compound **6** was only analyzed by IR spectroscopy. For compound **7**, only the crystal structure could be obtained

due to the short lifespan of this intermediate at standard conditions. The compounds investigated towards their energetic behavior show almost no friction and impact sensitivities, with the exception of compound **10** (3 J, 360 N) and compound **3** (30 J, >360 N). The compounds **2**, **3**, **5**, **9**, and **10** were investigated in regard to their detonation parameters, which were calculated with the EXPLO5 code. Compounds **3** and **5** exceed RDX in terms of all calculated values with detonation velocities of 8920 m s^{-1} and 9082 m s^{-1} , respectively. Compounds **9** and **10** are still in the same range of RDX with values of 8228 m s^{-1} and 8654 m s^{-1} . Finally, the new precursor was evaluated by the luminous bacteria inhibition test in order to investigate its ecotoxicological impact. It was compared to glyoxal to provide a well-known precursor as reference. 2-Hydrazone-malonohydrazide (**2**) is categorized as nontoxic, while the measurements show a toxic classification for glyoxal towards aqueous organisms.

Financial support of this work by the Ludwig-Maximilians University of Munich (LMU), the Office of Naval Research (ONR) under grant no. ONR N00014-19-1-2078 and the Strategic Environmental Research and Development Program (SERDP) under contract no. W912HQ19C0033 is gratefully acknowledged. The authors thank Stefan Huber for his help with the sensitivity measurement and Jasmin Lechner for graphical support.

6.5 Supporting Information

6.5.1 Experimental Procedures

Caution! Geminal diazides are energetic materials with high sensitivities towards shock and friction. Therefore, proper security precautions (safety glass, face shield, earthened equipment and shoes, Kevlar gloves and ear plugs) have to be applied while synthesizing and handling the described compounds.

Chemicals and solvents were employed as received (Sigma-Aldrich, Acros, TCI, Spirochem AG). Compound (**1**) and N-methyl-N-nitroso-N'-nitroguanidine were synthesized according to literature procedures.^[17,27] ^1H , ^{13}C and ^{14}N spectra were recorded using a Bruker AMX 400 instrument. The chemical shifts quoted in ppm refer to tetramethylsilane (^1H , ^{13}C) and nitromethane (^{14}N). Decomposition temperatures were determined on a Mettler Toledo DSC822e at a heating rate of $5 \text{ }^\circ\text{C min}^{-1}$ using $40 \mu\text{L}$ aluminum crucibles and nitrogen purge gas at a flow rate of 30 mL min^{-1} . Evaluations of thermal behavior were performed using the STAR^e Software Version 16.20. Infrared (IR) spectra were recorded using a Perkin-Elmer Spektrum One

6 Hydrazonyl-Propandihydrazide

FT-IR instrument. Raman spectra were obtained using a Bruker MultiRam FT Raman spectrometer and a neodymium-doped yttrium aluminum garnet (Nd:YAG) laser ($\lambda = 1064$ nm, 1074 mW). Elemental analyses were performed with an Elementar Vario el by pyrolysis of the sample and subsequent analysis of formed gases (standard deviation liquids: $\pm 0.5\%$). The sensitivity data were collected using a BAM (Bundesanstalt für Materialforschung) drophammer^[28] according to STANAG 4489^[29] modified instruction^[30] and a BAM friction tester^[31] according to STANAG 4487^[32] modified instruction. The classification of the tested compounds results from the 'UN Recommendations on the Transport of Dangerous Goods'.^[33]

2-Hydrazonemalonohydrazide (2)

Diethyl 2,2-diazidomalonate (**1**) (1.00 g, 4.13 mmol, 1.0 eq) was dissolved in water (5 mL) and hydrazine hydrate (1.2 mL, 24.77 mmol, 6.0 eq) was added. Afterwards it was stirred for 24 h at room temperature. The precipitate was filtered and washed with cold water. The filtrate was concentrated in vacuo in order to obtain an additional amount of product. Compound (**2**) was obtained as colorless solid (452 mg, 2.82 mmol, 68 %).

¹H-NMR (400 MHz, DMSO-d₆) δ (ppm) = 10.52 (s, 2H, NH₂), 10.20 (s, 1H, NH), 8.88 (s, 1H, NH), 4.47 (s, 2H, NH₂), 4.24 (s, 2H, NH₂); ¹³C-NMR (101 MHz, DMSO-d₆) δ (ppm) = 165.4, 163.3, 119.5; IR (ATR, rel. int.): $\tilde{\nu}$ (cm⁻¹) = 3386 (m), 3305 (m), 3195 (m), 2170 (w), 2137 (w), 2007 (w), 1992 (w), 1635 (m), 1601 (m), 1552 (m), 1488 (s), 1325 (m), 1279 (m), 1219 (m), 1137 (m), 1090 (m), 990 (m), 962 (s), 815 (m), 794 (m), 721 (s), 633 (m), 555 (s), 488 (m), 407 (s); **Elemental analysis:** calcd. (%) for C₃H₈N₆O₂ (M = 160,14 g mol⁻¹): C 22.50, H 5.04, N 52.48; found: C 22.62, H 5.08, N 52.16; **Sensitivities** (grain size: 100 – 500 μ m): BAM impact: >40 J, BAM friction: >360 N; **DTA** (5 °C min⁻¹): T_{exo} = 178 °C.

2-Hydrazonemalonohydrazinium dinitrate · 0.25 H₂O (3)

2-Hydrazineylidenemalonohydrazide (**2**) (250 mg, 1.56 mmol, 1.0 eq.) was mixed with nitric acid (5 ml, 65 %) and stirred at 50 °C for 1 h. Compound (**3**) (310 mg, 1.08 mmol, 69 %) was obtained as pale-yellow crystals.

¹H NMR (400 MHz, DMSO-d₆): δ (ppm) = 11.5 – 9.0 (broad), 10.53; ¹³C NMR (101 MHz, DMSO-d₆): δ (ppm) = 164.7, 161.3, 115.4; ¹⁴N NMR (27 MHz, DMSO-d₆): δ (ppm) = -4, -359; IR (ATR, rel. int.): $\tilde{\nu}$ (cm⁻¹) = 3230 (m), 2151 (m), 2010 (w), 1997 (w), 1891 (w), 1646 (m), 1550 (m), 1495 (m), 1417 (m), 1309 (s), 1272 (s), 1186 (s), 1157 (s), 1104 (m), 1043 (m), 1010 (m), 985 (m), 824 (m), 788

6 Hydrazonyl-Propandihydrazide

(m), 688 (s), 577 (s), 491 (s), 471 (s), 436 (s), 425 (s), 410 (s), 401 (s); **Elemental analysis**: calcd. (%) for $C_3H_{10}N_8O_8 \cdot 0.25 H_2O$ ($290.56 \text{ g mol}^{-1}$): C 12.40, H 3.64, N 38.55; found: C 12.05, H 3.40, N 38.29; **Sensitivities** (grain size: 100 - 300 μm): BAM impact: 30 J, BAM friction: >360 N; **DTA** ($5 \text{ }^\circ\text{C min}^{-1}$): $T_{\text{exo}} = 167 \text{ }^\circ\text{C}$.

2-Hydrazonemalonohydrazinium dichloride monohydrate (4)

2-Hydrazineylidenemalonohydrazide (**1**) (250 mg, 1.56 mmol, 1.0 eq.) was mixed with hydrochloric acid (5 ml, 30 %) and 5 ml water and stirred at room temperature for 1 h. Compound (**4**) (360 mg, 1.54 mmol, 99 %) was obtained as pale-yellow crystals.

$^1\text{H NMR}$ (400 MHz, DMSO- d_6): δ (ppm) = 12.0 – 9.5 (broad), 10.64, 10.56; **$^{13}\text{C NMR}$** (101 MHz, DMSO- d_6): δ = 164.6, 161.2, 115.2; **IR** (ATR, rel. int.): $\tilde{\nu}$ (cm^{-1}) = 3338 (w), 3185 (w), 2758 (w), 2669 (w), 1983 (w), 1948 (w), 1670 (w), 1648 (w), 1616 (w), 1470 (m), 1335 (w), 1296 (w), 1253 (w), 1213 (w), 1175 (w), 1136 (m), 1066 (w), 1009 (w), 879 (w), 806 (w), 738 (w), 681 (w), 590 (m), 529 (m), 478 (w), 420 (m); **Elemental analysis**: calcd. (%) for $C_3H_{10}Cl_2N_6O_2 \cdot H_2O$ ($251.06 \text{ g mol}^{-1}$): C 14.35, H 4.82, N 33.47; found: C 14.40, H 4.57, N 33.65; **Sensitivities** (grain size: 100 - 300 μm): BAM impact: >40 J, BAM friction: >360 N; **DTA** ($5 \text{ }^\circ\text{C min}^{-1}$): $T_{\text{exo}} = 191 \text{ }^\circ\text{C}$.

2-Hydrazonemalonohydrazinium diperchlorate monohydrate (5)

2-Hydrazineylidenemalonohydrazide (**2**) (250 mg, 1.56 mmol, 1.0 eq.) was mixed with perchloric acid (0.5 ml, 60 %) and 5 ml water and stirred at room temperature for 1 h. Compound (**5**) (130 mg, 0.36 mmol, 23 %) was obtained as pale-yellow crystals.

$^1\text{H NMR}$ (400 MHz, DMSO- d_6): δ (ppm) = 10.63, 10.59, 4.98, 4.63; **$^{13}\text{C NMR}$** (101 MHz, DMSO- d_6): δ (ppm) = 164.7, 161.3, 115.2; **IR** (ATR, rel. int.): $\tilde{\nu}$ (cm^{-1}) = 3543 (w), 3423 (w), 3149 (w), 1676 (w), 1580 (w), 1494 (m), 1310 (w), 1109 (m), 1041 (m), 929 (w), 807 (w), 619 (m), 585 (m), 484 (m), 417 (m); **Elemental analysis**: calcd. (%) for $C_3H_{10}N_6O_{10}Cl_2 \cdot H_2O$ ($379.06 \text{ g mol}^{-1}$): C 9.51, H 3.19, N 22.17; found: C 9.46, H 3.00, N 21.99; **Sensitivities** (grain size: 100 – 500 μm): BAM impact: >40 J, BAM friction: >360 N; **DTA** ($5 \text{ }^\circ\text{C min}^{-1}$): $T_{\text{exo}} = 124 \text{ }^\circ\text{C}$.

2-Hydrazonemalonyldiazide (6)

2-Hydrazineylidenemalonohydrazide (**2**) (500 mg, 3.12 mmol, 1.0 eq.) was dissolved in concentrated hydrochloric acid (10 ml, 32 %). Chloroform (40 mL) was added and the solution was cooled below $0 \text{ }^\circ\text{C}$. Sodium nitrite (450 mg, 6.52 mmol, 2.1 eq.), dissolved in water (2 mL),

6 Hydrazonyl-Propandihydrazide

was added dropwise under heavy stirring, while the temperature was kept below 0 °C. The organic phase was washed with ice water and filtered through a magnesium sulfate layer into a crystallizing bowl. The residue was left for crystallization and compound (**5**) was obtained as colorless highly hygroscopic crystals (290 mg, 1.59 mmol, 51 %).

IR (ATR, rel. int.): $\tilde{\nu}$ (cm⁻¹) = 3312 (w), 3162 (w), 2985 (w), 2128 (w), 1978 (w), 1756 (w), 1674 (w), 1573 (w), 1467 (w), 1297 (w), 1235 (w), 1154 (w), 1046 (w), 960 (w), 854 (w), 828 (w), 753 (w), 669 (w), 588 (w), 548 (w), 470 (w), 416 (w).

3-Carbonylazido-1H-1,2,4-triazol-5-one (**7**)

2-Hydrazonemalonyldiazide (**6**) was stored in the freezer for 2 days at -20 °C. Colorless crystals were obtained from the stored compound, which turned out to be 3-carbonylazido-1H-1,2,4-triazol-5-one (**6**), shown by x-ray measurements.

3-Carboxyl-1H-1,2,4-triazol-5-one monohydrate (**8**)

2-Hydrazonemalonyldiazide (**6**) was stored in the refrigerator for 7 days at 3 °C. Yellow crystals were obtained from the stored compound, which turned out to be 3-carboxyl-1H-1,2,4-triazol-5-one (**7**), shown by x-ray measurements.

¹H NMR (400 MHz, DMSO-d₆): δ (ppm) = 12.54 (s, 1H), 12.43 (s, 1H); **¹³C NMR** (101 MHz, DMSO-d₆): δ (ppm) = 162.5, 155.8, 139.5.

Bis(nitroguanidinyl)-2-hydrazonemalonohydrazide (**9**)

2-Hydrazineylidenemalonohydrazide (**2**) (725 mg, 4.53 mmol, 1.0 eq.) was dissolved in H₂O (15 ml) and N-methyl-N-nitroso-N'-nitroguanidine (1.33 g, 9.05 mmol, 2.0 eq.) dissolved in H₂O (50 ml) was added. The reaction mixture was stirred for 50 min at 95 °C. The precipitate was collected by filtration, washed with cold H₂O and cold EtOH and dried at rt to yield compound **8** (1.32 g, 3.95 mmol, 87 %) as a yellow solid.

¹H NMR (400 MHz, DMSO-d₆): δ (ppm) = 10.70, 10.40, 9.90, 9.84-9.48, 8.66, 7.99; **¹³C NMR** (101 MHz, DMSO-d₆): δ (ppm) = 165.5, 163.2, 161.4, 161.2, 118.5; **IR** (ATR, rel. int.): $\tilde{\nu}$ (cm⁻¹) = 3387 (vw), 3293 (vw), 3191 (w), 2971 (vw), 1739 (s), 1669 (vw), 1652 (vw), 1610 (m), 1567 (s), 1505 (m), 1476 (w), 1429 (s), 1376 (s), 1345 (s), 1261 (s), 1230 (vs), 1217 (vs), 1189 (vs), 1116 (m), 1058 (s), 954 (vw), 923 (vw), 836 (vw), 779 (vw), 739 (vw), 563 (vs), 517 (vs), 486 (vs), 473 (vs), 412 (vs);

Elemental analysis: calcd. (%) for $C_5H_{10}N_{12}O_6$ ($334.21 \text{ g mol}^{-1}$): C 17.97, H 3.02, N 50.29; found: C 18.08, H 3.04, N 50.43; **Sensitivities** (grain size: 100–500 μm): BAM impact: >40 J, BAM friction: >360 N; **DTA** ($5 \text{ }^\circ\text{C min}^{-1}$): $T_{\text{exo}} = 209 \text{ }^\circ\text{C}$.

2,2-Methylhydrazone-5,5-dinitramino-1H-1,3,4-bistriazole (10)

Bis(nitroguanidinyl)-2-hydrasonemalonohydrazide (**9**) (3.40 g, 10.2 mmol, 1.0 eq.) was dissolved in H_2O (80 ml) and KOH (1.71 g, 30.5 mmol, 3.0 eq.) dissolved in H_2O (65 ml) was added. The reaction mixture was stirred over night at $80 \text{ }^\circ\text{C}$, cooled to $50 \text{ }^\circ\text{C}$ and conc. HNO_3 (65 %) was added until pH = 3. The precipitate was collected by filtration, washed with cold H_2O and dried for two days at $100 \text{ }^\circ\text{C}$ to yield compound **10** (1.53 g, 5.13 mmol, 50 %) as a beige solid.

1H NMR (400 MHz, $DMSO-d_6$): δ (ppm) = 14.17 (bs, 2H, ring-NH), 10.30–9.00 (m, 4H, N-NH₂, NH); **^{13}C NMR** (101 MHz, $DMSO-d_6$): δ (ppm) = 152.79, 152.11, 112.03; **MS:** m/z (ESI⁻) = 297.1 [$C_5H_6N_{12}O_4$]; **IR** (ATR): $\tilde{\nu} = 3181$ (vw), 1560 (m), 1483 (w), 1401 (w), 1225 (s), 1144 (m), 1044 (m), 988 (m), 913 (m), 871 (m), 771 (s), 731 (s), 707 (s), 614 (s), 492 (vs), 419 (vs); **Elemental analysis** : calcd. (%) for $C_5H_6N_{12}O_4$: C 20.14, H 2.03, N 56.37 found: C 19.79, H 2.23, N 53.88; **Sensitivities** (grain size: 300–1000 μm): BAM impact: 2.5 J, BAM friction: 360 N; **DTA** (onset, $5 \text{ }^\circ\text{C min}^{-1}$): $T_{\text{exo}} = 177 \text{ }^\circ\text{C}$.

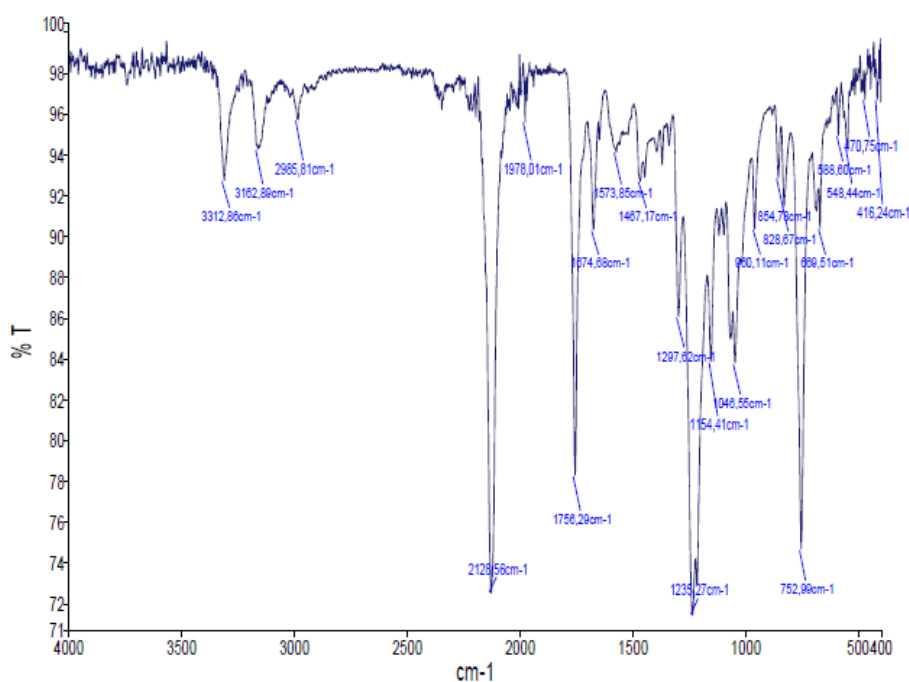


Figure 10. IR Spektrum of compound **6** measured in chloroform.

6.5.2 X-ray Diffraction

Crystal structure data were obtained by measurements on an Oxford Xcalibur3 diffractometer with a Spellman generator (voltage 50 kV, current 40 mA) and a Kappa CCD area for data collection using Mo-K α radiation ($\lambda = 0.71073 \text{ \AA}$) or a Bruker D8 Venture TXS diffractometer equipped with a multilayer monochromator, a Photon 2 detector and a rotation-anode generator (Mo-K α radiation). The data collection was performed using the CRYSTALIS RED software.^[34] The solution of the structure was performed by direct methods and refined by full-matrix least-squares on F2 (SHELXT)^[35] implemented in the OLEX2^[36] software suite. The non-hydrogen atoms were refined anisotropically and the hydrogen atoms were located and freely refined. The absorption correction was carried out by a SCALE3ABSPACK multiscan method.^[37] The DIAMOND2 plots shown with thermal ellipsoids at the 50% probability level and hydrogen atoms are shown as small spheres of arbitrary radius. The SADABS program embedded in the Bruker APEX3 software was used for multi-scan absorption corrections in all structures.^[38]

Table 3 Crystallographic data and structure refinement details for the prepared compounds **2** and **3**.

	2-Hydrazonemalonohydrazide (2)	2-Hydrazonemalonohydrazinium dinitrate · 0.25 H ₂ O (3)
Formula	C ₃ H ₈ N ₆ O ₂	4(C ₃ H ₁₀ N ₆ O ₂), 8(N O ₃), H ₂ O
FW [g mol ⁻¹]	160.15	1162.77
Crystal system	monoclinic	monoclinic
Space group	P21/c (No. 14)	P21/c (No. 14)
Color / Habit	yellow plate	colorless block
Size [mm]	0.07 x 0.11 x 0.31	0.02 x 0.04 x 0.04
a [Å]	6.2858(5)	7.3700(4)
b [Å]	15.5408(11)	16.8814(9)
c [Å]	6.9831(5)	9.5319(5)
α [°]	90	90
β [°]	103.118(7)	110.949(2)
γ [°]	90	90
V [Å ³]	664.35(9)	1107.53(10)
Z	4	1
ρ _{calc.} [g cm ⁻³]	1.601	1.743
μ [mm ⁻¹]	0.134	0.168
F(000)	336	602
λ _{MoKα} [Å]	0.71073	0.71073
T [K]	113	107
θ Min-Max [°]	3.3, 26.4	2.6, 26.4
Dataset	-7: 7 ; -16: 19 ; -8: 7	-9: 9 ; -21: 21 ; -11: 11
Reflections collected	4967	18977
Independent refl.	1354	2259
R _{int}	0.039	0.041
Observed reflections	1029	1931
Parameters	132	224
R ₁ (obs) ^[a]	0.0396	0.0441
wR ₂ (all data) ^[b]	0.0916	0.1209
S ^[c]	1.02	1.08
Resd. dens [e Å ⁻³]	-0.17, 0.27	-0.39, 0.56
Device type	Xcalibur Sapphire3	Bruker D8 Venture
Solution	SIR-92	SIR-92
Refinement	SHELXL-2018	SHELXL-2018
Absorption correction	Multi-Scan	Multi-Scan
CCDC	2149590	2149591

^[a] $R_1 = \sum ||F_o| - |F_c|| / \sum |F_o|$; ^[b] $wR_2 = [\sum [w(F_o^2 - F_c^2)^2] / \sum [w(F_o^2)]]^{1/2}$; $w = [\sigma^2(F_o^2) + (xP)^2 + yP]^{-1}$ and $P = (F_o^2 + 2F_c^2) / 3$;
^[c] $S = \{\sum [w(F_o^2 - F_c^2)^2] / (n-p)\}^{1/2}$ (n = number of reflections; p = total number of parameters).

Table 4. Crystallographic data and structure refinement details for the prepared compounds **4** and **5**.

	2-Hydrasonemalonohydrazinium dichloride monohydrate (4)	2-Hydrasonemalonohydrazinium diperchlorate monohydrate (5)
Formula	C ₃ H ₁₂ N ₆ O ₃ Cl ₂	C ₃ H ₁₂ N ₆ O ₁₁ Cl ₂
FW [g mol ⁻¹]	251.09	379.09
Crystal system	triclinic	monoclinic
Space group	P-1 (No. 2)	P21/n (No. 14)
Color / Habit	colorless block	colorless block
Size [mm]	0.26 x 0.29 x 0.46	0.33 x 0.44 x 0.73
a [Å]	7.1408(5)	7.5892(5)
b [Å]	8.0780(6)	9.0429(5)
c [Å]	9.1789(6)	18.7124(10)
α [°]	106.400(6)	90
β [°]	91.970(6)	99.935(6)
γ [°]	96.736(6)	90
V [Å ³]	503.15(6)	1264.94(13)
Z	2	4
ρ _{calc.} [g cm ⁻³]	1.657	1.991
μ [mm ⁻¹]	0.641	0.592
F(000)	260	776
λ _{MoKα} [Å]	0.71073	0.71073
T [K]	100	105
θ Min-Max [°]	2.3, 26.4	2.2, 26.4
Dataset	-6: 8 ; -7: 10 ; -10: 11	-9: 9 ; -5: 11 ; -23: 13
Reflections collected	3011	4478
Independent refl.	2053	2585
R _{int}	0.015	0.022
Observed reflections	1865	2159
Parameters	175	229
R ₁ (obs) ^[a]	0.0278	0.0347
wR ₂ (all data) ^[b]	0.0719	0.0873
S ^[c]	1.07	1.06
Resd. dens [e Å ⁻³]	-0.33, 0.35	-0.41, 0.41
Device type	Xcalibur Sapphire3	Xcalibur Sapphire3
Solution	SIR-92	SIR-92
Refinement	SHELXL-2018	SHELXL-2018
Absorption correction	Multi-Scan	Multi-Scan
CCDC	2149591	2149591

^[a]R₁ = Σ ||F₀ - |F_c|| / Σ |F₀|; ^[b]wR₂ = [Σ[w(F₀² - F_c²)²] / Σ[w(F₀²)]^{1/2}; w = [σ²(F₀²) + (xP)² + yP]⁻¹ and P = (F₀² + 2F_c²) / 3; ^[c]S = {Σ[w(F₀² - F_c²)²] / (n - p)}^{1/2} (n = number of reflections; p = total number of parameters).

Table 4. Crystallographic data and structure refinement details for the prepared compounds **7** and **8**.

	3-Carbonylazido-1 <i>H</i> -1,2,4-triazol-5-one (7)	3-Carboxyl-1 <i>H</i> -1,2,4-triazol-5-one monohydrate (8)
Formula	C ₃ H ₂ N ₆ O ₂	C ₃ H ₅ N ₃ O ₄
FW [g mol ⁻¹]	154.11	147.10
Crystal system	monoclinic	monoclinic
Space group	P21/c (No. 14)	P21/c (No. 14)
Color / Habit	yellow needle	colorless block
Size [mm]	0.07 x 0.13 x 0.50	0.04 x 0.05 x 0.06
a [Å]	8.9958(18)	8.6849(4)
b [Å]	4.9646(8)	4.9774(2)
c [Å]	12.909(2)	12.8833(5)
α [°]	90	90
β [°]	98.963(16)	96.624(1)
γ [°]	90	90
V [Å ³]	569.48(17)	553.20(4)
Z	4	4
ρ _{calc.} [g cm ⁻³]	1.797	1.766
μ [mm ⁻¹]	0.153	0.164
F(000)	312	304
λ _{MoKα} [Å]	0.71073	0.71073
T [K]	105	102
θ Min-Max [°]	2.3, 26.4	3.2, 26.4
Dataset	-4: 11 ; -6: 6 ; -16: 14	-10: 10 ; -6: 6 ; -16: 16
Reflections collected	2051	8781
Independent refl.	1161	1130
R _{int}	0.024	0.030
Observed reflections	847	998
Parameters	108	108
R ₁ (obs) ^[a]	0.0431	0.0429
wR ₂ (all data) ^[b]	0.1085	0.1169
S ^[c]	1.05	1.09
Resd. dens [e Å ⁻³]	-0.22, 0.25	-0.22, 0.93
Device type	Xcalibur Sapphire3	Bruker D8 Venture
Solution	SIR-92	SIR-92
Refinement	SHELXL-2018	SHELXL-2018
Absorption correction	Multi-Scan	Multi-Scan
CCDC	2149591	2149591

^[a]R₁ = Σ ||F_o| - |F_c|| / Σ |F_o|; ^[b]wR₂ = [Σ[w(F_o² - F_c²)²] / Σ[w(F_o²)]^{1/2}; w = [σ²(F_o²) + (xP)² + yP]⁻¹ and P = (F_o² + 2F_c²) / 3;
^[c]S = {Σ[w(F_o² - F_c²)²] / (n - p)}^{1/2} (n = number of reflections; p = total number of parameters).

6.5.3 Heat of Formation Calculation

The atomization was used to determine the heat of formation of **1–3** using the atom energies in **Table 5**.

$$\Delta_f H^\circ_{(g, M, 298)} = H_{(\text{molecule}, 298)} - \sum H^\circ_{(\text{atoms}, 298)} + \sum \Delta_f H^\circ_{(\text{atoms}, 298)}$$

Table 5. CBS-4M electronic enthalpies for atoms C, H, N and O and their literature values.

	$-H^{298} / \text{a.u.}$	$\Delta_f H^\circ_{\text{gas}}^{[39]}$
H	0.500991	217.998
C	37.786156	716.68
N	54.522462	472.68
O	74.991202	249.18

The Gaussian16 program package was used to calculate room temperature enthalpies on the CBS-4M level of theory.^[4] In order to obtain the energy of formation for the solid phase of **1**, the Trouton's Rule has to be applied ($\Delta H_{\text{sub}} = 188 \cdot T_m$).

Table 6. Heat of formation calculation results for compounds **2, 3, 5, 9** and **10**.

M	$-H^{298} \text{ [a] [a.u.]}$	$\Delta_f H^\circ(\text{g}, \text{M}) \text{ [b] [kJ mol}^{-1}\text{]}$	$\Delta_f H^\circ(\text{s}) \text{ [d] [kJ mol}^{-1}\text{]}$	Δn	$\Delta_f U(\text{s}) \text{ [e] [kJ kg}^{-1}\text{]}$
2	597.21415	-59.3	-29.6	-8.0	-61.1
3	597.21415	1641.3	224.2	-13.0	896.0
5	597.21415	1641.3	-239.2	-14.0	-566.3
9	1302.977801	274.8	184.1	-14.0	654.8
10	1150.335969	625.4	540.7	-11.0	1904.9

[a] CBS-4M electronic enthalpy; [b] gas phase enthalpy of formation; [c] sublimation enthalpy; [d] standard solid state enthalpy of formation; [e] solid state energy of formation.

6.6 References

- [1] D. M. Badgular, M. B. Talawar, S. N. Asthana, P. P. Mahulikar, *J. Hazard. Mat.* **2008**, *151*, 289.
- [2] M. B. Talawar, R. Sivabalan, T. Mukundan, H. Muthurajan, A. K. Sikder, B. R. Gandhe, A. S. Rao, *J. Hazard. Mat.*, **2009**, *161*, 589.
- [3] P. F. Pagoria, G. S. Lee, A. R. Mitchell, R. D. Schmidt, *Thermochimica Acta*, **2002**, *384*, 187–204.
- [4] L. Kukuljan, K. Kranjc, *Tetrahedron Lett.*, **2019**, *60*, 207–209.
- [5] V. Thottempudi, H. Gao, and J. M. Shreeve, *J. Am. Chem. Soc.* **2011**, *133*, *16*, 6464–6471.
- [6] T. M. Klapötke, M. Leroux, P. C. Schmid, J. Stierstorfer, *Chem. Asian J.* **2016**, *11*, 844.
- [7] T. M. Klapötke, *Chemistry of High-Energy Materials*, De Gruyter, Boston, Berlin, **2017**.
- [8] Z. Xu, G. Cheng, H. Yang, X. Ju, P. Yin, J. Zhang, J. M. Shreeve, *Angew. Chem. Int. Ed.* **2017**, *56*, 5877.
- [9] C. He, G. H. Imler, D. A. Parrish, J. M. Shreeve, *J. Mater. Chem. A*, **2018**, *6*, 16833-16837.
- [10] N. Fischer, D. Fischer, T. M. Klapötke, D. G. Piercey, J. Stierstorfer, *J. Mater. Chem.*, **2012**, *22*, 20418-20422.
- [11] G. Zhao, C. He, P. Yin, G. H. Imler, D. A. Parrish, J. M. Shreeve, *J. Am. Chem. Soc.* **2018**, *140*, 3560–3563.
- [12] Y. F. Golenko, M. A. Topchiy, A. F. Asachenko, M. S. Nechaev, D. V. Pleshakov, *Chin. J. Chem.* **2017**, *35*, 98–102.
- [13] D. Fischer, T. M. Klapötke, J. Stierstorfer, *Angew. Chem. Int. Ed.*, **2014**, *53*, 8172-8175.
- [14] D. Fischer, T. M. Klapötke, J. Stierstorfer, *Eur. J. Inorg. Chem.*, **2014**: 5808-5811.
- [15] M. D. Coburn, *J. Label. Compd. Rad.*, **1985**, *22* (2), 183-187.
- [16] S. E. Creegan, D. G. Piercey, *RSC Adv.*, **2020**, *10*, 39478.
- [17] H. Erhardt, A. P. Häring, A. Kotthaus, M. Roggel, M. L. Tong, P. Biallas, M. Jübermann, F. Mohr, S. F. Kirsch, *J. Org. Chem.*, **2015**, *80* (24), 12460-12469.
- [18] A. F. Hollemann, E. Wiberg, N. Wiberg, *Lehrbuch der anorganischen Chemie*, de Gruyter: New York, **2007**.
- [19] F. H. Allen, O. Kennard, D. G. Watson, L. Brammer, A. G. Orpen, R. Taylor, *J. Chem. Soc.* **1987**, 1–19.
- [20] A. G. Harter, T. M. Klapötke, J. Stierstorfer, M. Voggenreiter, X. Zeng, *ChemPlusChem*, **2021**, *86*, 870.
- [21] A. G. Harter, T. M. Klapötke, C. Riedelsheimer, J. Stierstorfer, M. Voggenreiter, *Eur. J. Inorg. Chem.* **2021**, *23*, 2241.
- [22] Test Methods According to the UN Recommendations on the Transport of Dangerous Goods, Manual of Test and Criteria, Fourth Revised Edition, United Nations Publication, New York

6 Hydrazonyl-Propandihydrazide

and Geneva, 2003, ISBN 92–1-139087 7, Sales No. E.03.VIII. 2; 13.4.2 Test 3a (ii) BAM Fallhammer.

- [23] M. Suceška, EXPLO5 program, Zagreb, Croatia, **2018**.
- [24] M. Härtel, **2017**: Studies towards the gas-phase detection of hazardous materials by vapor pressure measurements with the transpiration method in combination with vacuum outlet GC/MS. Dissertation, LMU München: Fakultät für Chemie und Pharmazie.
- [25] Drzyzga, O., Gorontzy, T., Schmidt, A. *et al.* Toxicity of explosives and related compounds to the luminescent bacterium *Vibrio fischeri* NRRL-B-11177. *Arch. Environ. Contam. Toxicol.* **28**, 229–235 (1995).
- [26] C. J. Cao, M. S. Johnson, M. M. Hurley, T. M. Klapötke, J. *Propuls. Energet.*, **2012**, 5, 41–51.
- [27] A. McKay, G. F. Wright, *J. Am. Chem. Soc.*, **1947**, 69, 3028–3030.
- [28] <http://www.bam.de>
- [29] NATO Standardization Agreement (STANAG) on Explosives, *Impact Sensitivity Tests*, no. 4489, 1st ed., September 17, **1999**.
- [30] WIWEB-Standardarbeitsanweisung 4-5.1.02, Ermittlung der Explosionsgefährlichkeit, hier der Schlagempfindlichkeit mit dem Fallhammer, November 8, **2002**.
- [31] NATO Standardization Agreement (STANAG) on Explosives, *Friction Sensitivity Tests*, no. 4487, 1st ed., August 22, **2002**.
- [32] WIWEB-Standardarbeitsanweisung 4-5.1.03, Ermittlung der Explosionsgefährlichkeit oder der Reibeempfindlichkeit mit dem Reibeapparat, November 8, **2002**.
- [33] Impact: Insensitive >40 J, less sensitive ≤35 J, sensitive ≤4 J, very sensitive ≤3 J; friction: Insensitive >360 N, less sensitive=360 N, sensitive 80 N, very sensitive ≤80 N, extreme sensitive ≤10 N; According to the UN Recommendations on the Transport of Dangerous Goods (+) indicates: not safe for transport.
- [34] CrysAlisPro, Oxford Diffraction Ltd. version 171.33.41, **2009**.
- [35] G. M. Sheldrick, *Acta Cryst.*, **2015**, A71, 3–8.
- [36] Dolomanov, O. V., Bourhis, L. J., Gildea, R. J., Howard, J. A. K. & Puschmann, H. J., *Appl. Cryst.*, **2009**, 42, 339–341.
- [37] SCALE3 ABSPACK – An Oxford Diffraction program (1.0.4, gui: 1.0.3), Oxford Diffraction Ltd., **2005**.
- [38] APEX3. Bruker AXS Inc., Madison, Wisconsin, USA.
- [39] M. W. Chase Jr., NIST-JANAF Thermochemical Tables, Fourth Edition, *J. Phys. Chem. Ref. Data, Monograph 9*, **1998**, 1 – 1951.
- [40] M. J. Frisch, G. W. Trucks, H. B. Schlegel, G. E. Scuseria, M. A. Robb, J. R. Cheeseman, G. Scalmani, V. Barone, G. A. Petersson, H. Nakatsuji, X. Li, M. Caricato, A. V. Marenich, J. Bloino,

6 Hydrazonyl-Propandihydrazide

B. G. Janesko, R. Gomperts, B. Mennucci, H. P. Hratchian, J. V. Ortiz, A. F. Izmaylov, J. L. Sonnenberg, D. Williams-Young, F. Ding, F. Lipparini, F. Egidi, J. Goings, B. Peng, A. Petrone, T. Henderson, D. Ranasinghe, V. G. Zakrzewski, J. Gao, N. Rega, G. Zheng, W. Liang, M. Hada, M. Ehara, K. Toyota, R. Fukuda, J. Hasegawa, M. Ishida, T. Nakajima, Y. Honda, O. Kitao, H. Nakai, T. Vreven, K. Throssell, J. A. Montgomery, Jr., J. E. Peralta, F. Ogliaro, M. J. Bearpark, J. J. Heyd, E. N. Brothers, K. N. Kudin, V. N. Staroverov, T. A. Keith, R. Kobayashi, J. Normand, K. Raghavachari, A. P. Rendell, J. C. Burant, S. S. Iyengar, J. Tomasi, M. Cossi, J. M. Millam, M. Klene, C. Adamo, R. Cammi, J. W. Ochterski, R. L. Martin, K. Morokuma, O. Farkas, J. B. Foresman, and D. J. Fox, Gaussian16 ,Gaussian, Inc., Wallingford, CT, USA, **2016**.

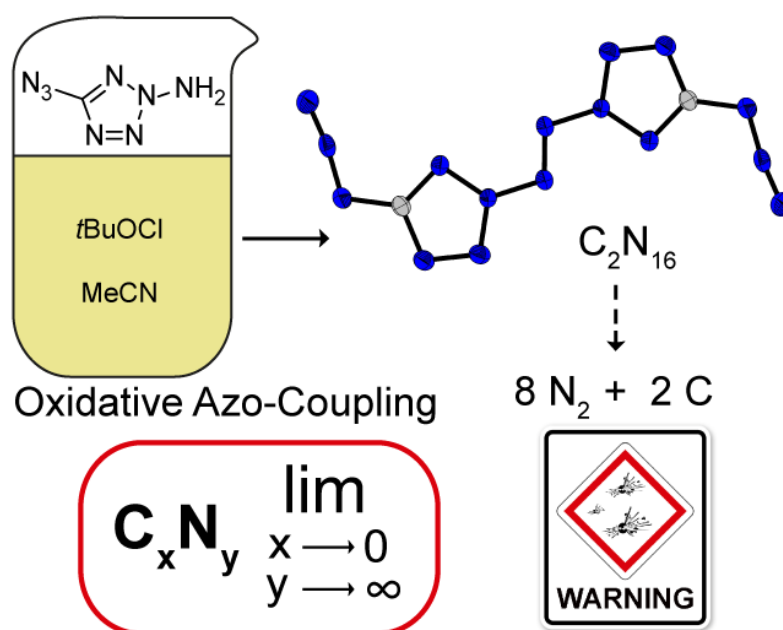
7 Binary 2,2'-Azobis-5-Azidotetrazole

Synthesis and Characterization of Binary, Highly Endothermic and Extremely Sensitive 2,2'-Azobis-5-Azidotetrazole (C_2N_{16})

Maximilian Benz, Thomas M. Klapötke, Jörg Stierstorfer and Michael Voggenreiter

As published in *Journal of the American Chemical Society* **2022**, *144*(14), 6143–6147.

DOI: 10.1021/jacs.2c00995



7.1 Abstract

C_2N_{16} (2,2'-azobis-(5-azidotetrazole)) (**3**), a highly energetic nitrogen-rich binary CN compound was obtained in a three-step synthesis through the formation of 5-azidotetrazole (**1**), the subsequent amination using THA and by oxidative azo-coupling of the obtained 2-amino-5-azidotetrazole (**2**) with *t*BuOCl as an oxidant in MeCN. A nitrogen-carbon ratio of 8:1, eight nitrogen atoms in a row as well as a nitrogen content of over 90% was unknown for a binary heterocyclic compound up to now. The successful isolation was confirmed through X-ray diffraction as well as by vibrational and ^{13}C NMR spectroscopy. C_2N_{16} can explode instantly and shows mechanical sensitivities far higher than quantitatively measurable. Nevertheless, it features interesting energetic performances which were calculated using different quantum chemical methods

7.2 Introduction

Binary CN compounds aroused enormous interest even in the early days of chemistry. Generations of chemists have paid great attention to this class of substances because of the complexity of their synthesis. This is mainly due to the fact, that with a raise of the nitrogen content, the sensitivity of the compounds is drastically increased.^[1] With the improvement of the nitrogen content, other properties relevant for the energetic materials research are evoking similarly including mainly the high energy of formation and the formation of almost exclusively gaseous reaction products.^[2] Ideal improvement of these energetic parameters would be obtained by compounds that are composed exclusively of nitrogen (e.g. cubic gauche nitrogen (cg-N)^[3], $(N_5^+)(N_3^-)$ ^[4, 5], N_5^- derivatives^[6]). However, since their elaborate synthesis and partly instability, research on new CN substances is just as promising, since these compounds can fulfill the above-mentioned properties comparably well. Some examples of nitrogen-rich CN compounds are listed in **Figure 1**.

While cyanogen $((CN)_2)$ is a stable gas^[7, 8], γ - C_3N_4 is a solid that is predicted to have extreme hardness properties^[9], the valuable synthetic building block cyanogen azide (with a CN ratio of 1:4), first described by *Darzens* in 1912, already tends to detonate spontaneously in the dry state. Examples of further high-nitrogen CN compounds are based on azide substituted heterocycles especially triazines^[10, 11], tetrazines^[12-14] and tetrazoles^[1]. In 2007, Banert *et al* succeeded in preparing and fully characterizing the binary CN derivative tetraazido-methane $(C(N_3)_4)$ ^[15]. It is to

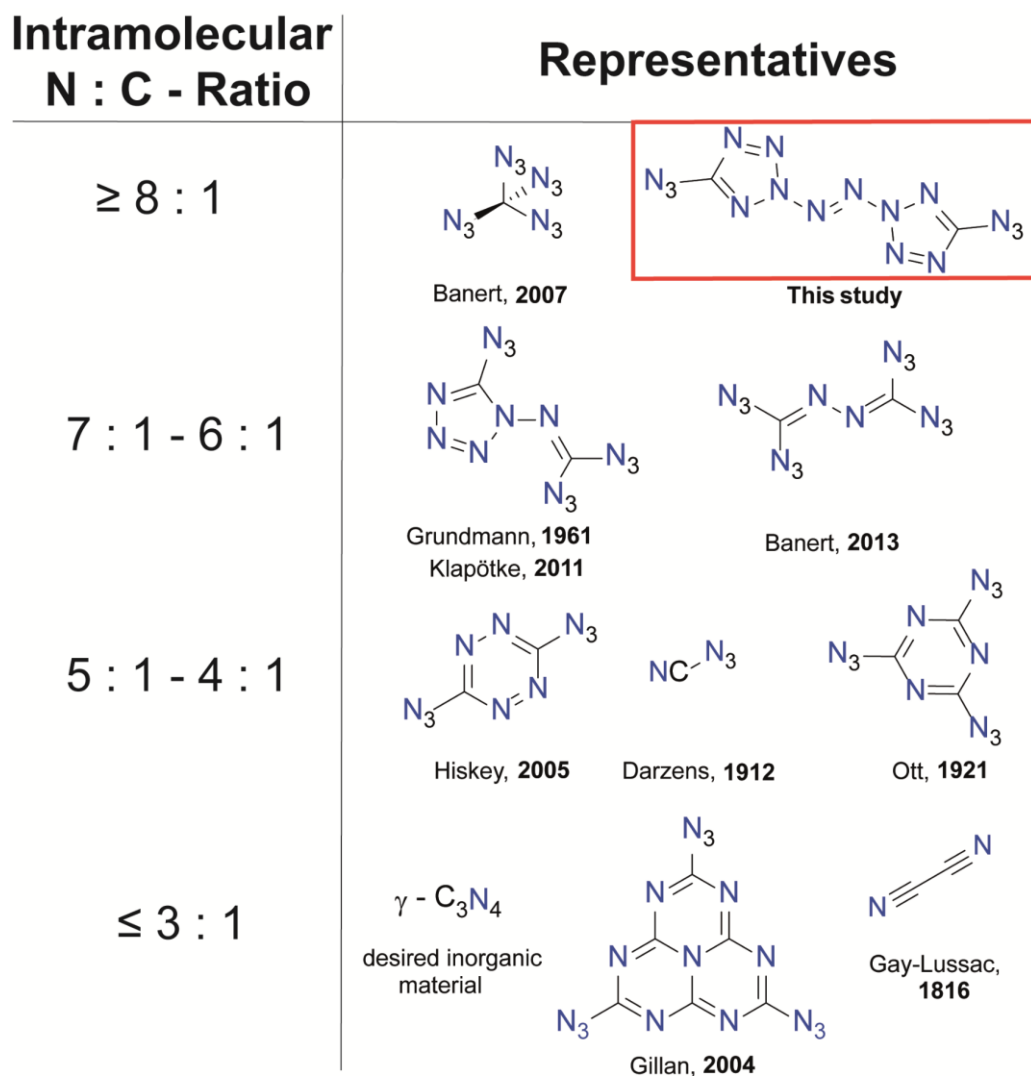


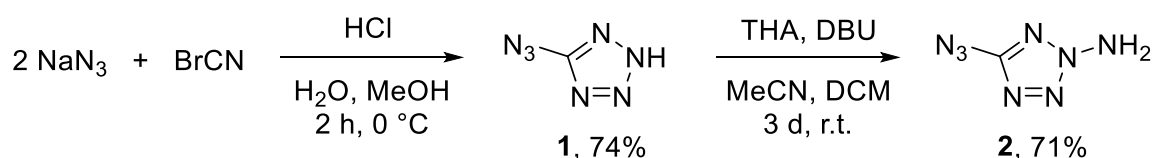
Figure 1. Representation of binary CN compounds, ranked according to their increasing nitrogen-carbon ratio.

date the compound with the highest CN ratio and at the same time one of the formally simplest CN derivatives. However, tetraazidomethane is a highly sensitive liquid, which has not been structurally characterized but by detection of consecutive reaction or decomposition products. More recently, work on C₂N₁₄, among others, has caused a great interest throughout the scientific community. This research revealed the existence of C₂N₁₄ in "open-chained" form as liquid isocyanogen tetraazide^[16] and in "closed" form as solid 1-diazidocarbamoyl-5-azidotetrazole^[1, 17], whereas the open form can be isomerized into the closed form at elevated temperatures.^[16] However, what they have in common is their extremely sensitivity to external influences. Based on the insights gained from the study of C₂N₁₄, we succeeded in increasing the C:N ratio again by applying the use of a tetrazole backbone with azide functions and additionally introduction an azo bridge.^[18, 19]

C₂N₁₆, presented in this study, is not only the compound with the highest CN ratio for binary, heterocyclic molecules, but also features a chain of eight catenated nitrogen atoms, setting a new benchmark for CN compounds.

7.3 Results and Discussion

Our synthetic procedure starts with the formation of 5-azidotetrazole from sodium azide and cyanogen bromide, using a literature procedure.^[20, 21] The following *N*-amination of **1** was carried out in acetonitrile with one equivalent of base (DBU) and THA (*O*-tosylhydroxylamine) as amination agent. This reaction yielded **2** as the only product. Electron withdrawing groups at the tetrazole carbon atom usually direct electrophilic substituents toward the 2-position. (**Scheme 1**).^[22, 23] Since compound **2** is a new and also potential starting material for further



Scheme 1. Synthesis of 5-azidotetrazole from sodium azide and cyanogen bromide and subsequent amination using THA toward 2-amino-5-azidotetrazole (**2**).

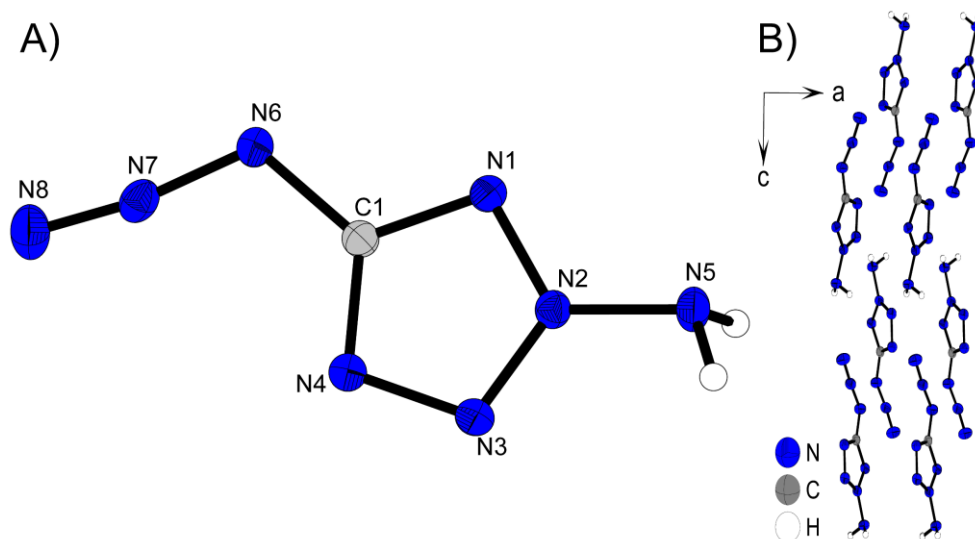
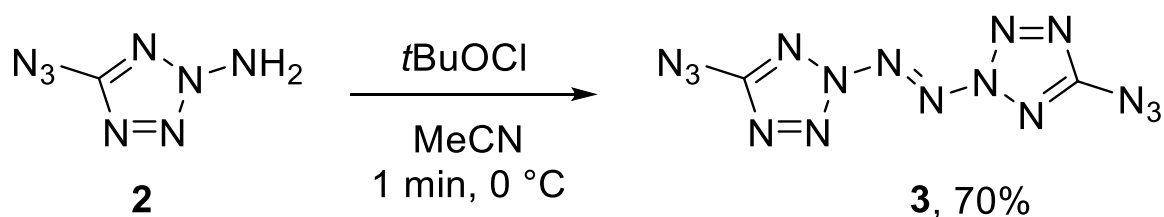


Figure 2 **A)** Molecular structure of **2** as determined by low-temperature X-ray diffraction with thermal ellipsoids drawn at the 50% probability level; **B)** view on the packing of **2** along the *b* axis. Selected bond lengths [Å]: N2-N5 1.393(2), C1-N6 1.395(2); Selected hydrogen bonds: N5-H5A...N1: N5-H5A 0.88(3) Å, H5A...N1 2.42(2) Å, N5...N1 3.238(2) Å, N5-H5A-N1 156(2) °; N5-H5B...N3: N5-H5B 0.88(3) Å, H5B...N3 2.34(3) Å, N5...N3 3.201(2) Å, N5-H5B-N3 167(2) °; N5-H5A...N8: N5-H5A 0.88(3) Å, H5A...N8 2.69(2) Å, N5...N8 3.028(2) Å, N5-H5A-N8 104.8(2) °.

energetic derivatizations, it was characterized as well. Crystalline **2**, which was obtained from slow evaporation of MeOH, crystallized in the orthorhombic space group $P2_12_12_1$ with four molecular units per unit cell (**Figure 2A**). The density is 1.769 g cm^{-3} at 173 K and therefore higher than for the respective 1-amino-5-azidotetrazole.^[24] As depicted in **Figure 2B**, **2** forms a chain like motive along c which is mainly stabilized through moderately strong hydrogen bridged between the protons and the ring or the N_γ of the azide function. The NMR data for **2** displays a broad signal at 6.65 ppm representing the amino protons and a ^{13}C resonance at 160.6 ppm. **2** shows a smooth melting in DTA experiments at 62 °C followed by a sharp decomposition at a temperature of 142 °C.

The key step of our study, the oxidative azo coupling of **2**, was very challenging. The established synthetic protocols for oxidative azo coupling of N -amines using sodium dichloroisocyanuric acid or trichloroisocyanuric acid^[25–27] could also be successfully applied to our reaction. However, consequent spontaneous detonations appeared as a result of precipitation of the substance during the reaction. To avoid this, we tried to keep **3** in solution as long as possible during the reaction and to minimize the shock possibilities within the reaction vessel (no stirring bar, soft plastic reaction vessel), without success. Finally, we decided to use $t\text{BuOCl}$, which is widely used in similar oxidation reactions,^[28–30] as the oxidant because of the advantageous solvent mixture during the reaction (**Scheme 2**). In contrast to the oxidations with derivatives of isocyanuric acid,



Scheme 2. Synthesis of 2,2'-azobis-(5-azidotetrazole) (ABAT) (**3**) through oxidation of **2** using $t\text{BuOCl}$.

the method we have chosen uses and produces only volatile reactants (MeCN, $t\text{BuOH}$), which can be evaporated carefully. From this mixture, **3** crystallized in the form of slightly yellow-greenish blocks. Because of the risk of spontaneous and mechanically caused explosions during the isolation, only very small batches (50 mg of starting material) were performed. Through this method, a sufficient amount of **3** could be gathered over several batches to allow all possible analyses to be performed. In addition, **3** is not stable long-term^[31,32] and decomposes slowly in solution with evolution of nitrogen. During the investigation of **3**, several detonative events were

observed (**Figure 4D**)) and plastic as well as glass fragments of different sizes (nano to macro) were obtained. It should be pointed out that **3** is one of the most sensitive materials we have ever handled. As mentioned above, **3** was obtained in the form of slightly yellow-greenish blocks suitable for X-ray diffraction. The stated color was proven by UV-vis calculations (see the Supporting Information). It crystallizes in the triclinic space group $P-1$ with a density of 1.803 g cm^{-3} at 298 K, which is the highest one reported for a binary CN compound. The structure features an inversion center located directly on the azo bridge (**Figure 3**). The molecule itself is arranged in an almost planar fashion. The presence of a conjugated π system is one of the reasons for its very high density. The values of the bond distances (**Figure 3**) and angles for the *N*-azo bridge and the azide moieties show no peculiarities and are similar to those observed for known related compounds.^[20,27]

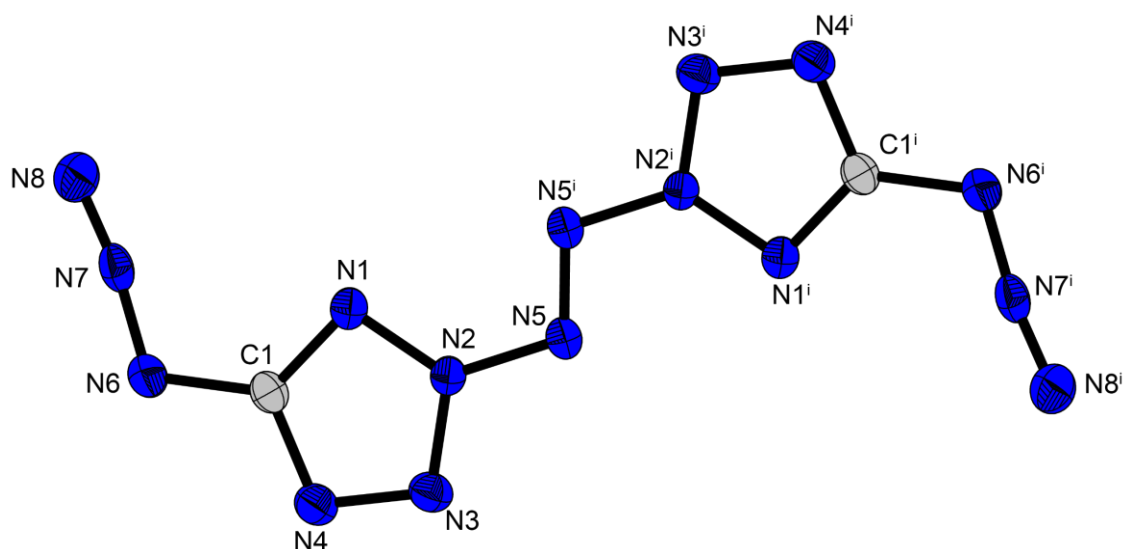
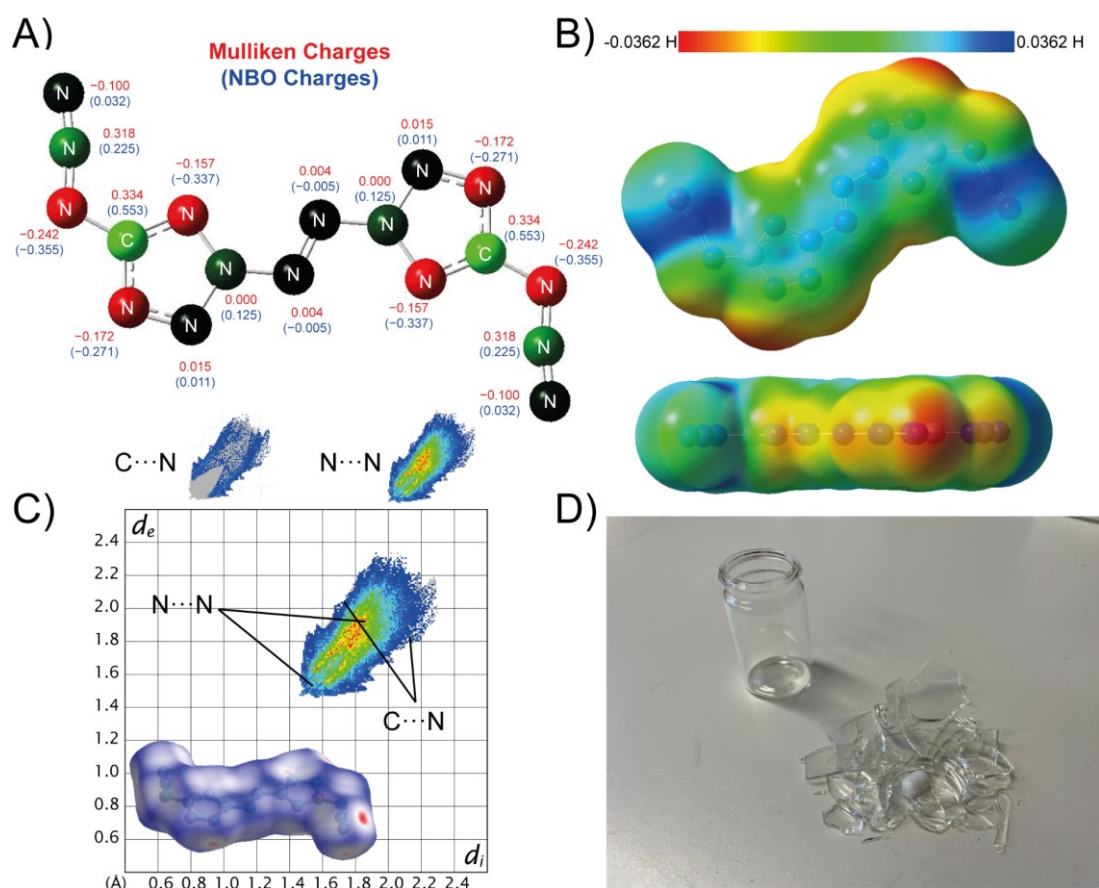


Figure 3. Molecular unit of **3** determined by low-temperature X-ray diffraction with thermal ellipsoids drawn at 50% probability level. Selected bond distances [Å]: N6-N7 1.264(3), N7-N8 1.111(3), N2-N5 1.374(2), N5-N5ⁱ 1.252(3) and angles [°] N2-N5-N5ⁱ 109.5(2), N1-C1-N6 126.7(2), N1-C1-N6-N7 3.4(2), N3-N2-N5-N5ⁱ 0.1(2).

The 2D structure of **3** is almost completely determined by the formation of electrostatic interactions between nitrogen atoms due to the absence of hydrogen atoms and the resulting unavailability of hydrogen bridges. A coplanar layer of molecular units is formed in the *bc* plane; they are not arranged in a coplanar fashion but are twisted against each other. The pattern along the space diagonal appears to behave like a zigzag structure. The shortest intramolecular contacts can be found between N_β of the azide function and nitrogen atoms N1 and N4 of the tetrazole ring (N7-N9 3.154(2) Å, N4-N15 3.100(3) Å). The observed crystal structure is formed

and stabilized solely by the interactions between electron pairs and positively polarized nitrogen atoms. The calculated Mulliken charges and the electrostatic potential (ESP) show a clear charge separation within the molecule (**Figure 4**). Here the strongest positively polarized atoms are C1 and N $_{\beta}$, and the strongest negatively polarized atoms are N $_{\alpha}$, N1, and N4. Through the analysis of the Hirshfeld surfaces^[33] (**Figure 4C**), an extremely high sensitivity can be assumed, since only few and very weak interactions are demonstrated. This creates an unstable crystal packing in which the molecules can easily be displaced against each other, thus leading to decomposition.^[34] The closest near contacts (N \cdots N) are in the range of 3 Å. In addition to the crystal structure, we were able to perform only NMR and IR spectroscopy. For compound **3**, the carbon resonance was observed at 164.1 ppm, in the typical range for 2-substituted 5-azidotetrazoles.



2150 cm⁻¹. Compared with the spectrum of **2**, the disappearance of the proton vibrations at around 3300 cm⁻¹ is additional evidence for the formation of **3**. The theoretical vibrational frequencies were calculated at the BLYP/6-31G(d) level of theory (point group *C_{2h}* for the gas phase). They are in good accordance with the measured values and can be found in the Supporting Information along with more details about the calculation.

The sensitivity values for **2** and **3** are clearly in the range for extremely sensitive compounds, but the two compounds differ significantly in their handling. **2** can be classified as a primary explosive (impact sensitivity (IS) < 1 J, friction sensitivity (FS) = 2 N) but can be handled without hesitation if all safety precautions (plastic equipment, earthed equipment, etc.) are obeyed. The scenario is entirely different for **3**. Its IS and FS are way below our devices' measuring capabilities (**Table 1**). **3** decomposes detonatively under any kind of stress, whether thermal or mechanical, as well as spontaneously in the absence of light and without any noticeable external influence. **3** is thermally stable up to 114 °C, which is surprisingly high since only a few intramolecular interactions result from the crystal structure.

Table 1. Physico-chemical properties of **2** and **3** as well as for C₂N₁₄ (1-diazidocarbamoyl-5-azidotetrazole) and Lead Azide.

	2	3	C ₂ N ₁₄ ^[1]	Pb(N ₃) ₂ (RD-1333)
Formula	CH ₂ N ₈	C ₂ N ₁₆	C ₂ N ₁₄	PbN ₆
IS [J] ^[a]	<1	<<<0.25	<0.25	4
FS [N] ^[b]	2	<<<0.1	<5	<0.1
ρ [g cm ⁻³] ^[c]	1.736	1.803	1.679	4.8
N [%] ^[d]	88.9	90.3	89.1	28.9
T _{melt} /T _{dec} ^[e]	62/142	-/114	78/124	315
Δ _f H° [kJ mol ⁻¹] ^[f]	703.7 (668.8)	1700.7 (1664.9)	1495.0	450.1
-Δ _{Ex} U° [kJ kg ⁻¹] ^[g]	5672 (5401)	6705 (6561)	6632	1560
P _{CJ} [kbar] ^[h]	343 (334)	366 (362)	300	357
V _{det} [ms ⁻¹] ^[i]	9472 (9384)	9515 (9476)	8853	6187

[a] Impact sensitivity (BAM drophammer (1 of 6)). [b] Friction sensitivity (BAM friction tester (1 of 6)). [c] Density from X-ray diffraction analysis recalculated to 298 K ($d_{298K} = \frac{d_T}{1 + \alpha_V(298 - T_0)}$; $\alpha_V = 1.6 \cdot 10^{-4} \text{ K}^{-1}$)³⁵ [d] Nitrogen content. [e] Melting/Decomposition temperature (DTA; β = 5 °C min⁻¹). [f] Calculated enthalpy of formation CBS-4M (CBS-QB3). EXPLO5_V6.05.02: [g] Energy of explosion. [h] Detonation pressure at Chapman-Jouguet point. [i] Detonation velocity.

The calculated enthalpies of formation (values from CBS-4M calculations) again illustrate the enormously high endothermic character of **2** (Δ_fH° = 703.7 kJ mol⁻¹) and **3** (Δ_fH° = 1700.7 kJ mol⁻¹). Through the high crystallographic densities paired with the extremely

high energies of formation, the detonation velocities are calculated to be around 9500 m s^{-1} using the EXPLO5 code.

7.4 Conclusion

In conclusion, we obtained 2,2'-azobis(5-azidotetrazole) (**3**) through straightforward synthesis involving amination of 5-azidotetrazole to obtain 2-amino-5-azidotetrazole (**2**) followed by oxidative azo coupling of **2** using *t*BuOCl. The sensitivities of **3** are far below the measurement limits of our equipment. The nitrogen contents, crystallographic densities, and calculated enthalpies of formation for **3** and its precursor **2** are remarkably high, resulting in impressive theoretical values for the detonation velocity and energy. The synthesis of **3** sets a new benchmark for a binary heterocyclic CN compound with a nitrogen:carbon ratio of 8:1 and should inspire the community to continue the quest for all-nitrogen compounds.

Financial support of this work by Ludwig-Maximilian University (LMU), the Office of Naval Research (ONR) under Grant ONR N00014-19-1-2078, and the Strategic Environmental Research and Development Program (SERDP) under Contract W912HQ19C0033 is gratefully acknowledged. We thank Mr. Marcus Lommel (LMU Munich) for X-ray diffraction experiments and Ms. Jasmin Lechner (LMU Munich) for DSC measurements and assistance with graphical illustrations.

7.5 Supporting Information

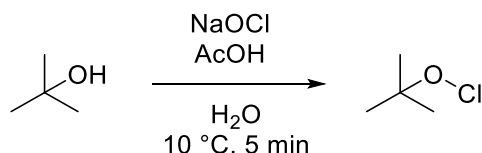
7.5.1 Experimental Procedures

CAUTION! *All investigated compounds are potentially explosive materials. In particular the title compound, ABAT (**3**), is extremely sensitive and tends to explode in dry state and even spontaneously without the influence of any kind of external stimuli. Safety precautions and equipment (such as wearing leather coat, face shield, Kevlar sleeves, Kevlar gloves, earthed equipment and ear plugs) must be used during all manipulations.*

^1H , ^{13}C , ^{14}N and ^{15}N NMR spectra were recorded on *BRUKER AMX 400* instruments. Chemical shifts are referenced with respect to tetramethylsilane ($^1\text{H}/^{13}\text{C}$) and nitromethane ($^{14}\text{N}/^{15}\text{N}$). Infrared spectra (IR) were recorded in the region $4000\text{-}400 \text{ cm}^{-1}$ on a *PERKIN ELMER Spectrum BX-59343* instrument with a *SMITHS DETECTION DuraSamplIR II Diamond ATR* sensor. The

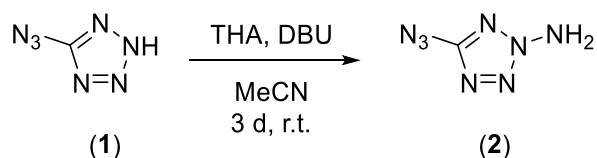
absorption bands are reported in wavenumbers (cm^{-1}). Decomposition temperatures were measured via differential thermal analysis (DTA) with an *OZM Research DTA 552-Ex* instrument or differential scanning calorimetry (DSC) using a *Linseis PT10 DSC* device at a heating rate of $5\text{ }^{\circ}\text{C}/\text{min}$ and in a range of room temperature to $400\text{ }^{\circ}\text{C}$. All sensitivities toward impact (IS) and friction (FS) were determined according to BAM (Bundesanstalt für Materialforschung und Prüfung) standards using a BAM drop hammer and a BAM friction apparatus by applying the 1 of 6 method.^[36] **2** was tested for sensitivity towards electrical discharge using an *Electric Spark Tester ESD 2010 EN* from OZM. Energetic properties have been calculated with the EXPLO5 6.02 computer ^[37] code using the RT converted X-ray density and calculated solid state heats of formation.

Tert-butyl hypochlorite



Tert-butyl hypochlorite was synthesized according to a literature known procedure.^[38] NaOCl solution (13% active chlorine, 500 mL) was placed in a round bottom flask and cooled to below $10\text{ }^{\circ}\text{C}$ with an ice bath. A mixture of *tert*-butanol (37.0 mL, 390 mmol) and acetic acid (24.5 mL, 430 mmol) was added in one portion and the solution was stirred vigorously for 5 min. Afterward, the aqueous layer was discarded and the yellow organic phase was washed with sodium carbonate solution (10%, 100 mL) and water (100 mL). The product can then be stored over CaCl_2 in the fridge at $8\text{ }^{\circ}\text{C}$. The yield is 80%. The purity was checked by ^1H NMR.

2-Amino-5-azidotetrazole (2)



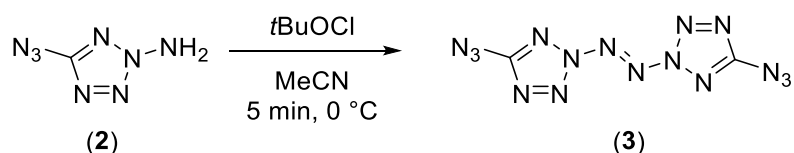
Amination reaction was performed according to a literature known protocol for amination of azoles using THA.^[39] Freshly prepared ethyl *O*-*p*-tosylsulphonylacetohydroxamate (1.71 g, 6.52 mmol, 1.5 eq) was added in portions to perchloric acid (60%, 10 mL) and the mixture was stirred for 3 h. The now-free tosylhydroxylamine (THA) suspension was quenched on ice water (60 mL) and after the ice melted it was extracted with dichloromethane (5 x 30 mL). The

7 Binary 2,2'-Azobis-5-Azidotetrazole

combined organic phases were dried over anhydrous sodium sulfate and added in one portion to an ice cooled solution of 5-azido-2*H*-tetrazole (0.48 g, 4.34 mmol, 1.0 eq) and 1,8-diazabicyclo(5.4.0)undec-7-ene (DBU) (0.66 mL, 4.34 mmol, 1.0 eq) in acetonitrile (70 mL). The solution was stirred for three days at room temperature. The slightly cloudy solution was evaporated under reduced pressure and purified using column chromatography (*i*Hex/EtOAc: 4:1; $R_f = 0.18$) to yield **2** as colorless crystalline solid (0.39 g, 3.08 mmol, 71%).

DTA (5 °C min⁻¹): 62 °C (endo), 142 °C (exo). **Sensitivities**: BAM drop hammer: <1 J, friction tester: 2 N, ESD: 45 mJ. **IR** (ATR) $\tilde{\nu}$ (cm⁻¹) = 3325(s), 3260(m), 3197(m), 2918(w), 2178(s), 2150(vs), 1611(w), 1505(s), 1423(s), 1391(s), 1355(s), 1303(m), 1223(s), 1195(vs), 1177(s), 1046(w), 1030(s), 990(m), 906(vs), 795(m), 740(s), 725(s), 686(m), 678(m), 661(m), 542(s), 523(s), 493(m), 464(w), 457(w), 444(m), 432(m), 419(m), 412(m), 403(s). **Elem. Anal.** (CH₂N₈O₆, 126.08 g mol⁻¹) calcd.: C 9.53, H 1.60, N 88.87 %. Found: C 9.21, H 1.90, N 86.43%; **¹H NMR** (CD₃-CN, 400 MHz, ppm) $\delta = 6.65$ (s, 2H). **¹³C NMR** (CD₃-CN, 101 MHz, ppm) $\delta = 160.6$ **¹⁴N NMR** (DMSO-D₆, 29 MHz, ppm) $\delta = -144, -303$. **¹⁵N NMR** (CD₃OD, 42 MHz, ppm) $\delta = -9.9, -79.7, -95.1, -102.5, -144.4, -145.2, -292.3, -301.4$. **HRMS** (ESI) m/z : [M⁺] Calcd for CH₃N₈ 127.0475, found: 127.0473.

2,2'-Azobis-(5-azidotetrazole)



2-Amino-5-azidotetrazole (46 mg, 0.36 mmol, 1.0 eq) was dissolved in MeCN (1.5 mL) in a plastic beaker and cooled to 0 °C using an ice bath. Freshly prepared *t*BuOCl (71 mg, 0.66 mmol, 1.8 eq.) was added dropwise and the mixture was allowed to stand for 60 seconds. The solution was transferred in a plastic bowl and the solvent was evaporated behind a face shield. Due to the high sensitivity of the **3** the yield could not be determined exactly but was measured to be around 70%.

DSC (5 °C min⁻¹): 113 °C (exo). **Sensitivities**: BAM drop hammer: <<1 J, friction tester: <<0.1 N, ESD: too sensitive for measurement. **IR** (ATR) $\tilde{\nu}$ (cm⁻¹) = 2150 (vs), 1608 (w), 1505 (s), 1411 (w), 1377 (m), 1221 (w), 1184 (w), 1090 (w), 1024 (w), 942 (m), 883 (m), 819 (w), 798 (w), 737 (m), 682 (w), 527 (w), 496 (w). **Elem. Anal.** (C₂N₁₆, 248.13 g mol⁻¹) calcd.: C 9.68, N 90.32 %. Found: too sensitive for measurement. **¹H NMR** (CD₃-CN, 400 MHz, ppm) $\delta = -$. **¹³C NMR** (CD₃-CN, 101 MHz, ppm) $\delta = 164.1$.

7.5.2. X-ray Diffraction and Hirshfeld Analysis

Crystal structure data were obtained from a Bruker D8 Venture TXS diffractometer equipped with a multilayer monochromator, a Photon 2 detector and a rotation-anode generator (Mo- K_{α} radiation). The data collection was performed using the CRYSTALIS RED software.^[40] The solution of the structure was performed by direct methods and refined by full-matrix least-squares on F2 (SHELXT)^[41] implemented in the OLEX2^[42] software suite. The non-hydrogen atoms were refined anisotropically and the hydrogen atoms were located and freely refined. The absorption correction was carried out by a SCALE3 ABSPACK multiscan method.^[43] The DIAMOND2 plots shown with thermal ellipsoids at the 50% probability level and hydrogen atoms are shown as small spheres of arbitrary radius. The SADABS program embedded in the Bruker APEX3 software was used for multi-scan absorption corrections in all structures.^[44]

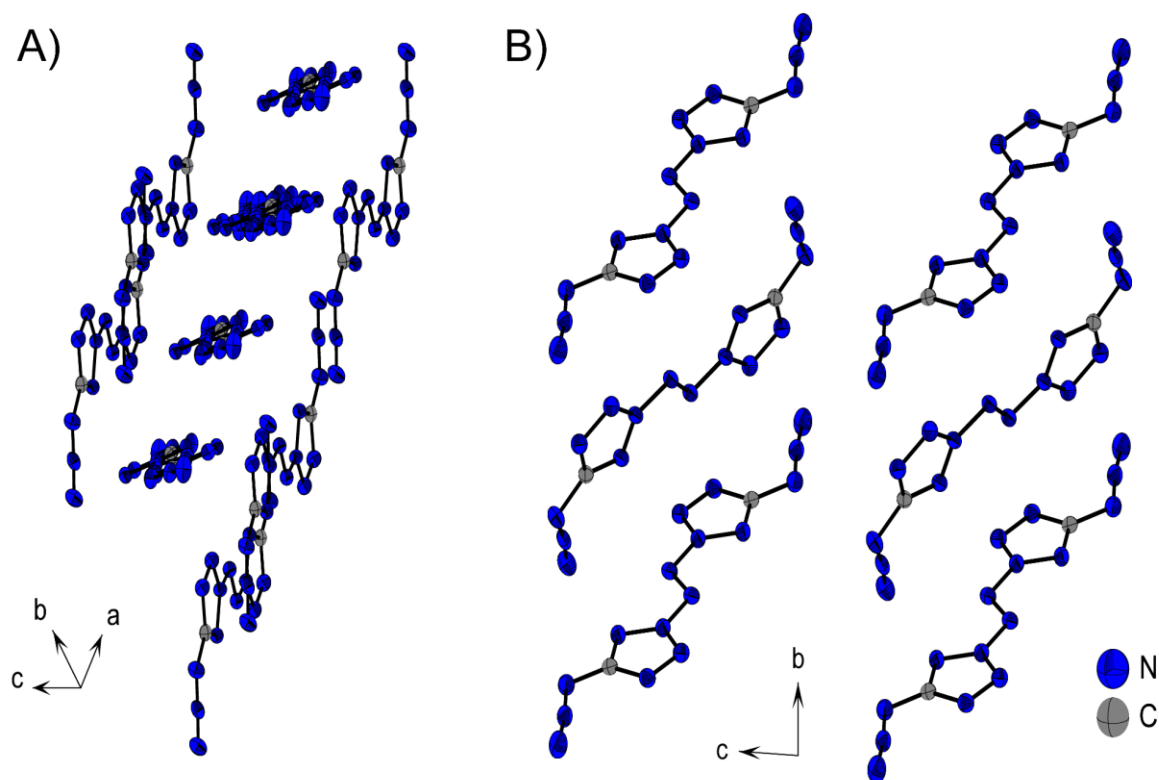


Figure 5. Illustration of the three-dimensional arrangement of **3**. **A)** along an arbitrary viewing direction, **B)** along the *a* axis.

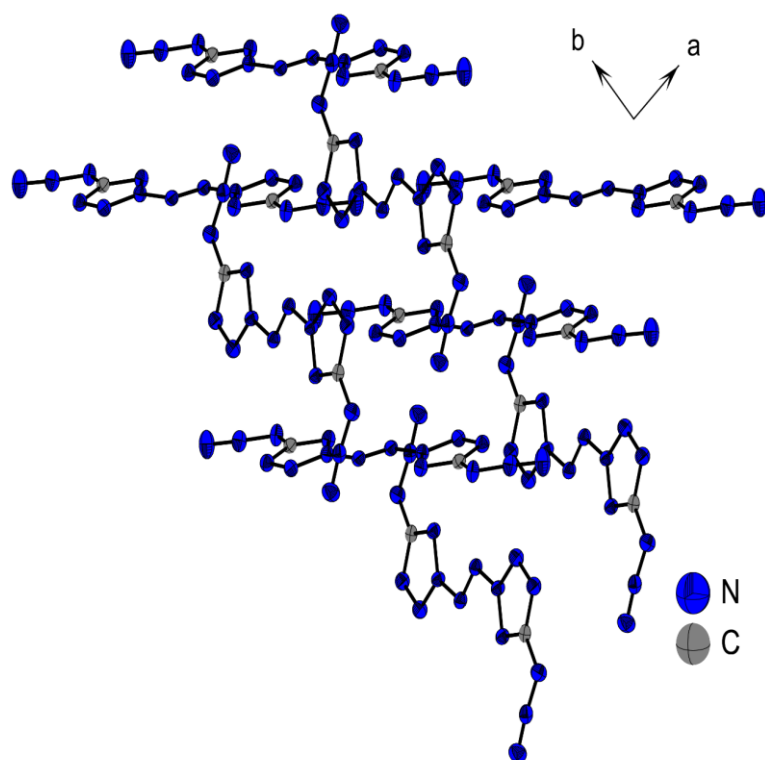


Figure 6. Representation of the pattern along *c*.

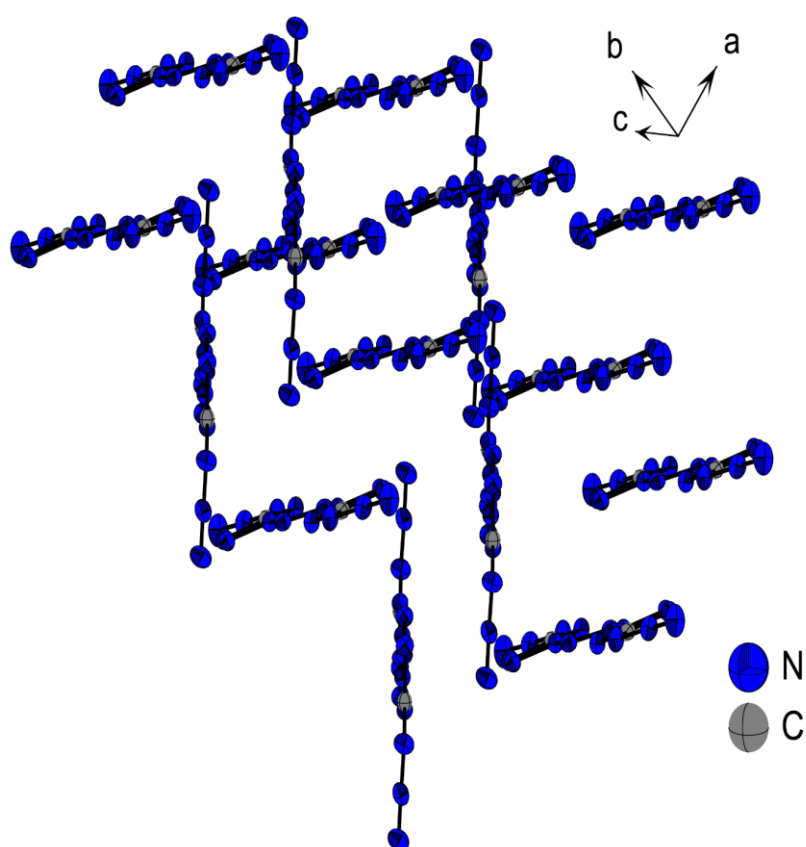


Figure 7. Representation of the zigzag pattern along the stated room direction.

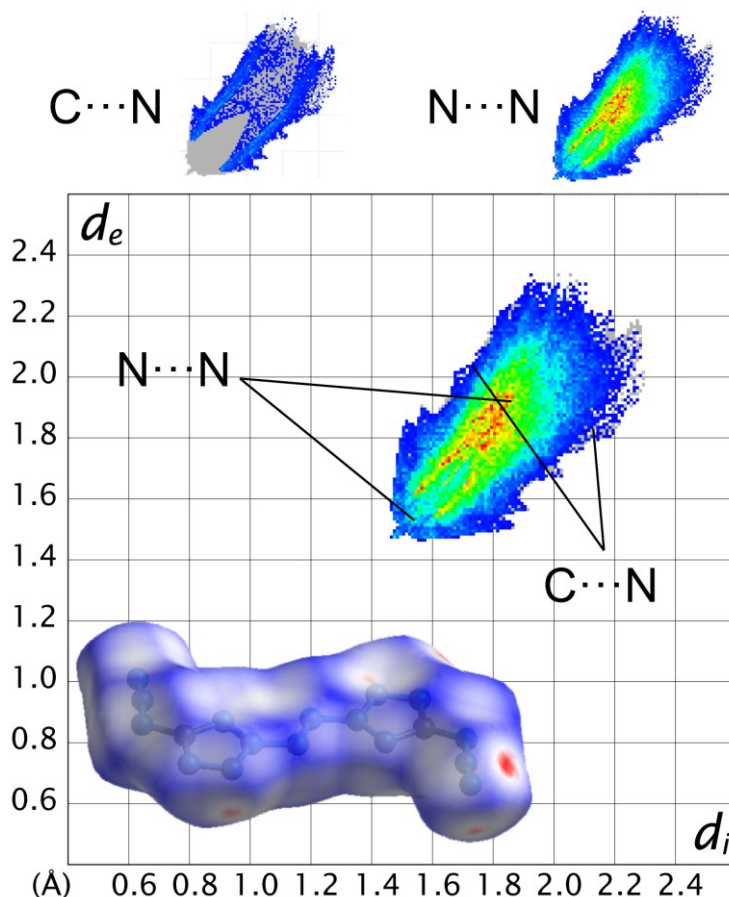


Figure 8. Representation of the Hirshfeld surface of **3** and the thereof calculated 2D fingerprint plot.

Hirshfeld surfaces are based on the respective crystal structure of the investigated compound and can therefore be calculated using the respective cif file.^[45] The Hirshfeld surface shows the next close contacts (red color) within the crystal pattern. The thereof generated 2D fingerprint plot indicates the distance and type of interaction toward the surrounding atoms in the crystal layering structure (d_e : distance of the Hirshfeld surface to the nearest exterior atom, d_i : distance of the Hirshfeld surface to the nearest interior atom).^[45] The 2D fingerprint plot shows only weak interactions of N...N (93.4%) in the area of $d_e + d_i > 3 \text{ \AA}$ and C...N (6.6%) in the area of $d_e + d_i > 3.3 \text{ \AA}$. From the Hirshfeld analysis only a few weak repulsive interactions (N...N) and no attractive polar interactions result.

Table 2. Crystallographic data and structure refinement details for **2** and **3**.

	2	3
Formula	CH ₂ N ₈	C ₂ N ₁₆
FW [g mol ⁻¹]	126.11	248.18
Crystal system	orthorhombic	triclinic
Space group	<i>P</i> 2 ₁ 2 ₁ 2 ₁ (No. 19)	<i>P</i> -1 (No. 2)
Color / Habit	colorless block	green block
Size [mm]	0.10 x 0.13 x 0.14	0.02 x 0.08 x 0.18
a [Å]	3.5082(2)	5.0759(3)
b [Å]	7.0952(4)	9.4232(5)
c [Å]	19.0265(9)	9.4790(5)
α [°]	90	86.025(2)
β [°]	90	83.192(2)
γ [°]	90	86.782(2)
V [Å ³]	473.60(4)	448.59(4)
Z	4	2
ρ _{calc.} [g cm ⁻³]	1.769	1.837
μ [mm ⁻¹]	0.143	0.150
F(000)	256	248
λ _{MoKα} [Å]	0.71073	0.71073
T [K]	173	173
θ Min-Max [°]	3.1, 28.3	2.2, 27.2
Dataset	-4: 4 ; -9: 9 ; -24: 25	-6: 6 ; -11: 12 ; -12: 12
Reflections collected	8830	7911
Independent refl.	1183	2000
<i>R</i> _{int}	0.026	0.038
Observed reflections	1163	1603
Parameters	91	163
<i>R</i> ₁ (obs) ^[a]	0.0274	0.0491
w <i>R</i> ₂ (all data) ^[b]	0.0668	0.0978
<i>S</i> ^[c]	1.17	1.14
Resd. dens [e Å ⁻³]	-0.20, 0.15	-0.24, 0.24
Device type	Bruker D8 Venture	Bruker D8 Venture
Solution	SIR-92	SIR-92
Refinement	SHELXL-2013	SHELXL-2013
Absorption correction	multi-scan	multi-scan
CCDC	2142885	2142884

^[a] $R_1 = \sum ||F_o| - |F_c|| / \sum |F_o|$; ^[b] $wR_2 = [\sum [w(F_o^2 - F_c^2)^2] / \sum [w(F_o^2)]]^{1/2}$; $w = [\sigma^2(F_o^2) + (xP)^2 + yP]^{-1}$ and $P = (F_o^2 + 2F_c^2) / 3$;

^[c] $S = \{\sum [w(F_o^2 - F_c^2)^2] / (n-p)\}^{1/2}$ (n = number of reflections; p = total number of parameters).

7.5.3 Computations and Heat of Formation Calculation

All quantum chemical calculations were carried out using the Gaussian G09 program package.^[46] The enthalpies (H) and free energies (G) were calculated using the complete basis set (CBS) method of Petersson and co-workers in order to obtain very accurate energies. The CBS models are using the known asymptotic convergence of pair natural orbital expressions to extrapolate from calculations using a finite basis set to the estimated CBS limit. CBS-4 starts with an HF/3-21G(d) geometry optimization; the zero-point energy is computed at the same level. It then uses a large basis set SCF calculation as a base energy, and an MP2/6-31+G calculation with a CBS extrapolation to correct the energy through second order. A MP4(SDQ)/6-31+ (d,p) calculation is used to approximate higher order contributions. In this study, we applied the modified CBS-4M.^[47,48] The CBS-QB3 has been modified by the inclusion of diffuse functions in the geometry optimization step to give CBS-QB3.^[49] The five-step CBS-QB3 series of calculations starts with a geometry optimization at the B3LYP level, followed by a frequency calculation to obtain thermal corrections, zero-point vibrational energy, and entropic information. The next three computations are single-point calculations (SPCs) at the CCSD(T), MP4SDQ, and MP2 levels. The CBS extrapolation then computes the final energies.^[50] The standard molar enthalpy of formation of solids **2** and **3** was calculated using $\Delta_f H^\circ(g)$ subtracting the enthalpy of sublimation estimated by applying *Trouton's rule* ^[51]. ($\Delta H_{\text{sub}} = 188 \cdot T_m$). Since no melting point was observed for **3**, its decomposition temperature has been used. (**2**: T_m 62 °C, $\Delta H_{\text{sub}} = 63.0 \text{ kJ mol}^{-1}$, **3**: T_{dec} 114 °C, $\Delta H_{\text{sub}} = 72.8 \text{ kJ mol}^{-1}$). The calculation results are summarized in **Table 3**.

Table 3. Heat of Formation calculation results based on CBS-4M and CBS-QB3.

	$-H^{298}$ [a] [a.u.] CBS-4M	$\Delta_f H^\circ(g,M)$ [kJ mol ⁻¹] [b]	$\Delta_f H^\circ(s)$ [c] [kJ mol ⁻¹]	$-H^{298}$ [d] [a.u.] CBS-QB3	$\Delta_f H^\circ(g,M)$ [kJ mol ⁻¹] [e]	$\Delta_f H^\circ(s)$ [f] [kJ mol ⁻¹]
2	476.555101	766.8	703.7	476.555101	766.8	703.7
3	950.682697	1773.5	1700.7	950.682697	1773.5	1700.7

[a] CBS-4M electronic enthalpy; [b] gas phase enthalpy of formation based on CBS-4M; [c] standard solid state enthalpy of formation based on CBS-4M; [d] CBS-QB3 electronic enthalpy; [e] gas phase enthalpy of formation based on CBS-QB3; [f] standard solid state enthalpy of formation based on CBS-QB3;

Table 4. IR frequencies and intensities calculated at the BLYP/6-31G(d) level of theory. The frequencies were fitted with a scaling factor of 0.9940 according to *Witek et al.*^[52] Frequencies highlighted in gray with an intensity of 0 do not result in real measured frequencies due to the symmetry present in the molecule.

IR Frequencies	IR Frequencies (fitted)	IR Intensities
-	20	0.35
-	46	1.36
-	60	0.75
	77	0.00
	90	0.00
-	101	0.45
	129	0.00
-	138	1.84
	215	0.00
	248	0.00
-	277	0.09
	314	0.00
	370	0.00
-	386	3.14
-	419	1.65
	444	0.00
	495	0.00
496	496	12.88
-	502	44.57
	524	0.00
527	543	97.66
	602	0.00
-	611	3.26
682	681	56.53
	706	0.00
737	707	12.37
	746	0.00
798	790	62.52
	862	0.00
883	877	536.97
	938	0.00
	1017	0.00
1024	1019	10.73
1090	1064	112.05
	1083	0.00
1184	1173	631.61
	1188	0.00
	1191	0.00
	1199	0.00
	1253	0.00
1221	1264	96.79
	1349	0.00
1377	1360	134.60

	1400	0.00
1505	1473	1058.83
	1482	0.00
2150	2162	1251.06
	2166	0.00

-0.0362 H  0.0362 H

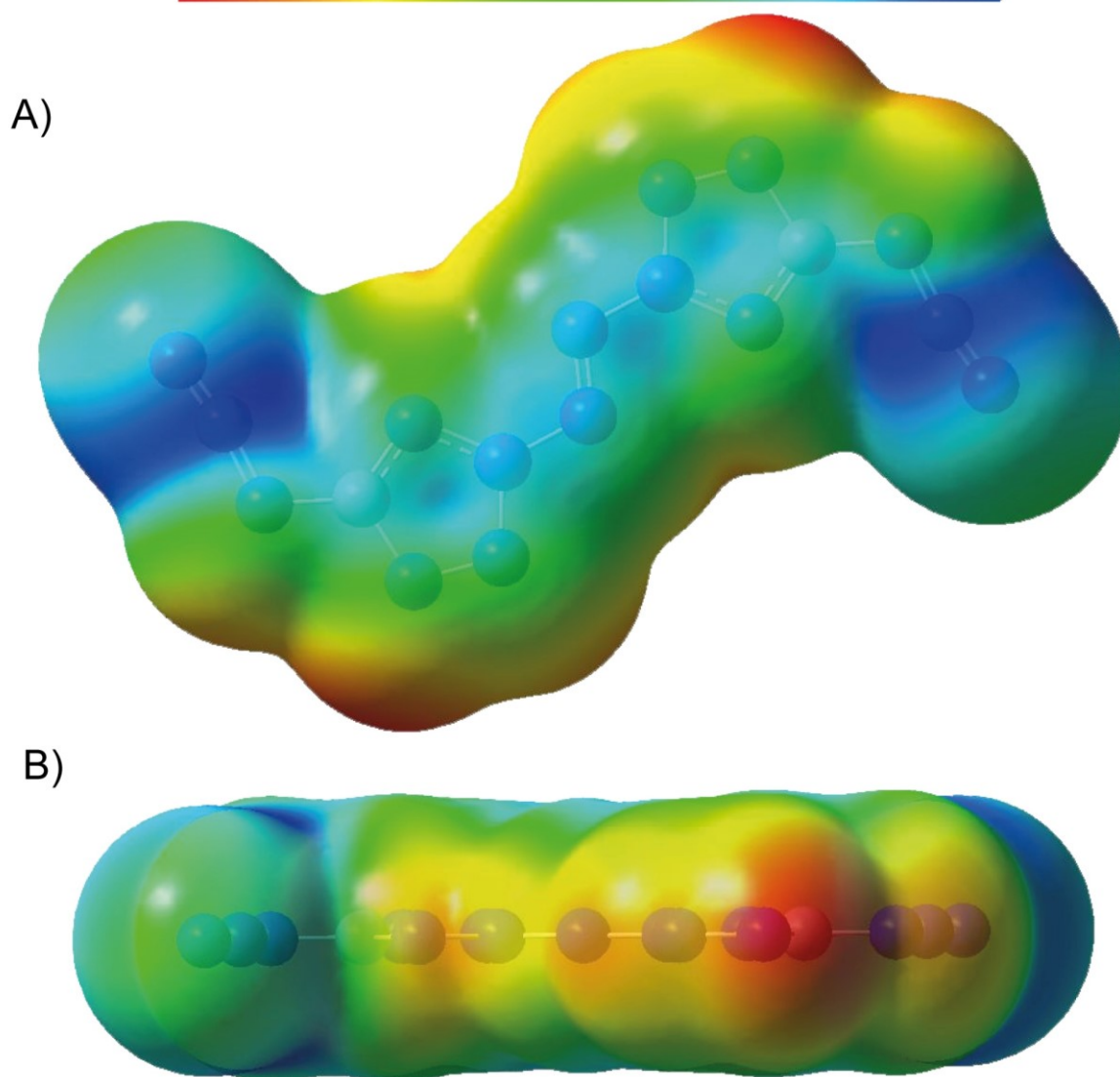


Figure 9. Representation of the molecular electrostatic potential of **3** in the $0.001 \text{ e bohr}^{-3}$ isosurface computed at the B3LYP/6-31G(d,p) level with the color range from -0.036 to 0.036 H . Red color represent electron-rich and blue color electron-deficient regions. A) top view, B) side view.

To get a better insight of the electronic situation of **3** its electrostatic potential (ESP) was calculated at the B3LYP/6-21G(d,p) level of theory in the gas phase structure (C_{2h}). The output of the calculation of the ESP can be found in **Figure 9**. There, the highest electron density can be detected to be on the double-bonded nitrogen atoms N1, N3 and N4 of the tetrazole. A lack of

electrons is determined at the N_β of the azide function as well as for the planar 2,2'-azobistetrazole system. The consideration of the electrostatic potential of **3** results in the observable bond characteristics in the crystal, which occur between positively and negatively polarized regions.

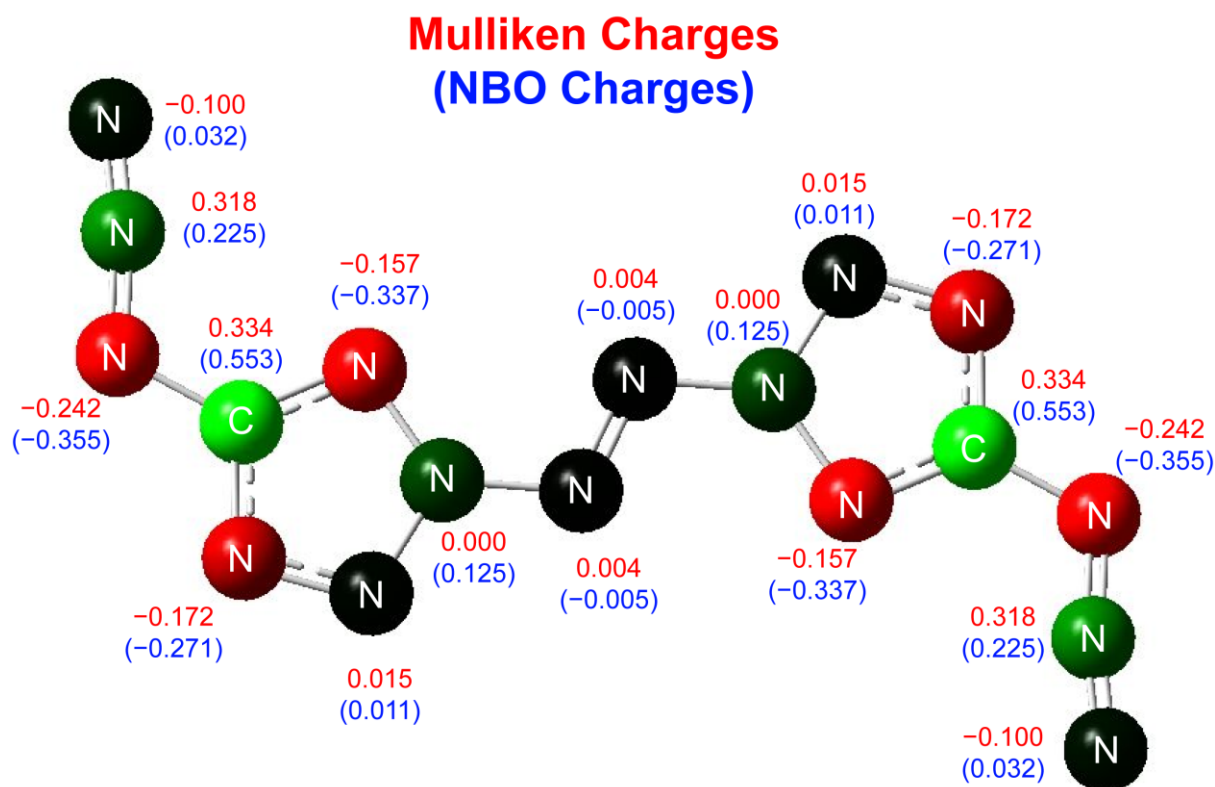


Figure 10. Representation of the natural bond orbital (NBO) and Mulliken charges of **3** calculated based on the B3LYP/cc-pVDZ level of theory.

Since we assumed kind of a charge separation within the molecule, NBOs (natural bond orbitals) as well as Mulliken charges of 2,2'-azobis-(5-azidotetrazole) (**3**) were calculated on the B3LYP/cc-pVDZ level of theory using the gas phase structure (C_{2h}). The values for the NBO and Mulliken calculation differ slightly but show the same trend. For both methods, the highest positively charged atom is the carbon, consisting of three neighbor atoms with a higher electronegativity. Moreover, N_β is also positively polarized, which is illustrated by the Lewis structure of covalent azides, in which it is always partially positively charged. N_α , N1 and N4 are strongly negatively polarized, with N_α having the highest negative polarization for both calculation methods. The azo bridge does not show any polarization and, as already shown in the ESP and the crystal structure, does not participate in intermolecular interactions.

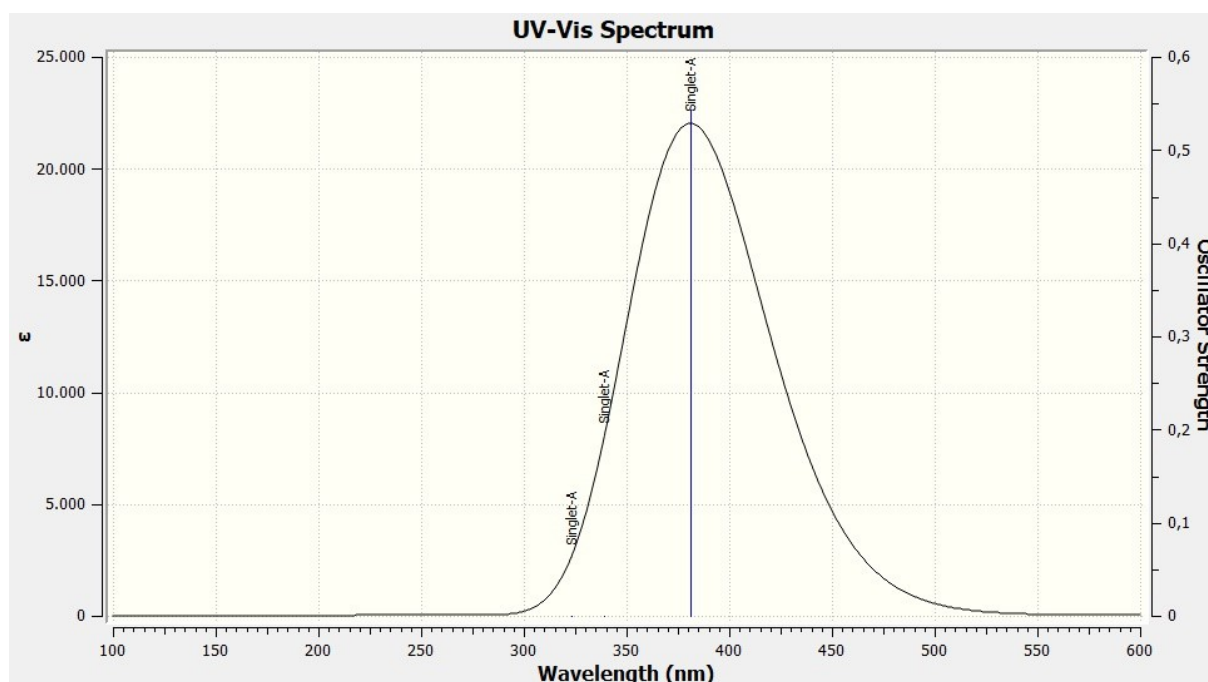


Figure 11. Calculated UV/Vis spectrum of compound **3**.

The calculation was performed using TD-SCF DFT calculations applying method B3LYP with a basis set of 6-311G. The results of the calculation is depicted in **Figure 11**. For compound **3**, an absorption maximum at 381 nm is observed. Therefore, the compound should appear in a yellowish color.

7.5.4 Spectroscopy

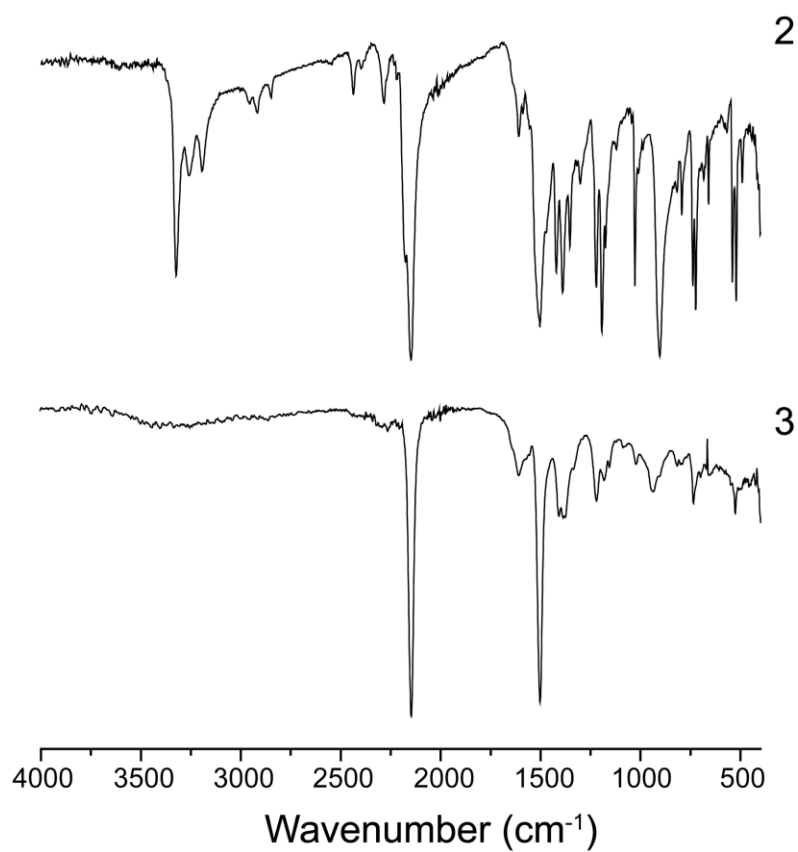
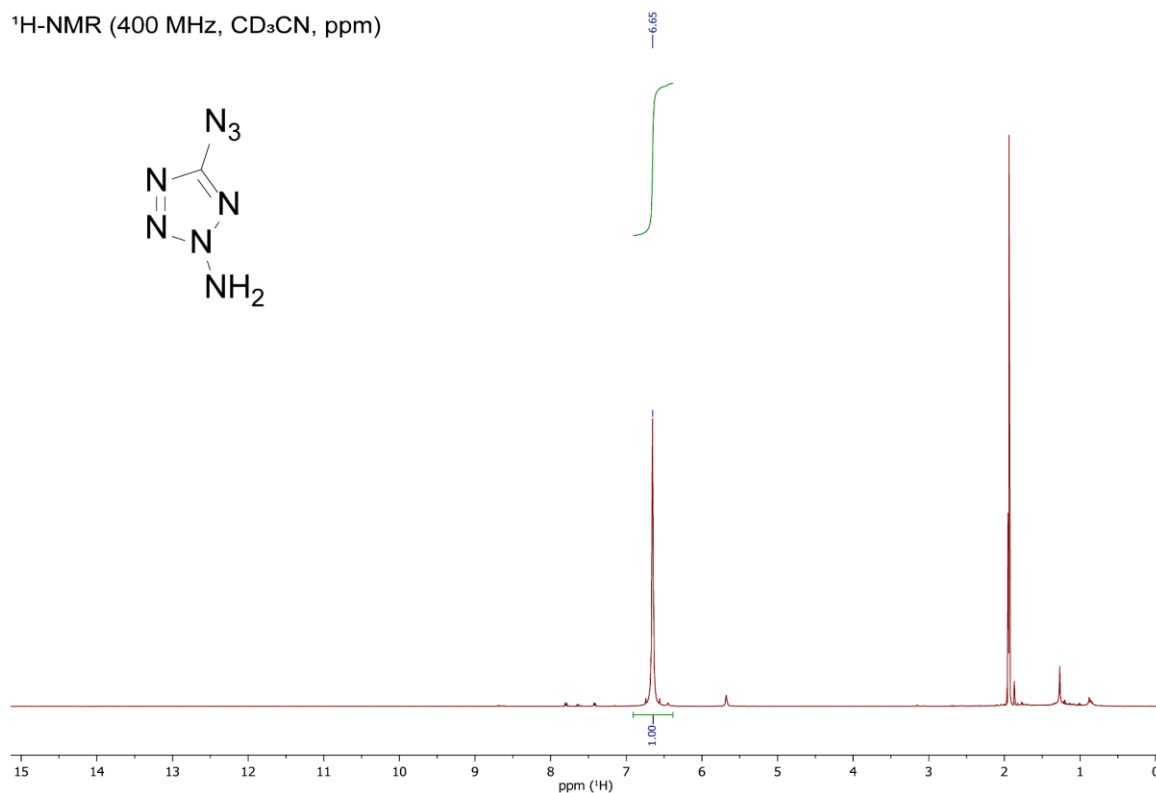


Figure 12. IR spectra of compounds 2 and 3.

¹H-NMR (400 MHz, CD₃CN, ppm)Figure 13. ¹H NMR spectrum of 2.

7 Binary 2,2'-Azobis-5-Azidotetrazole

^{13}C -NMR (101 MHz, CD_3CN , ppm)

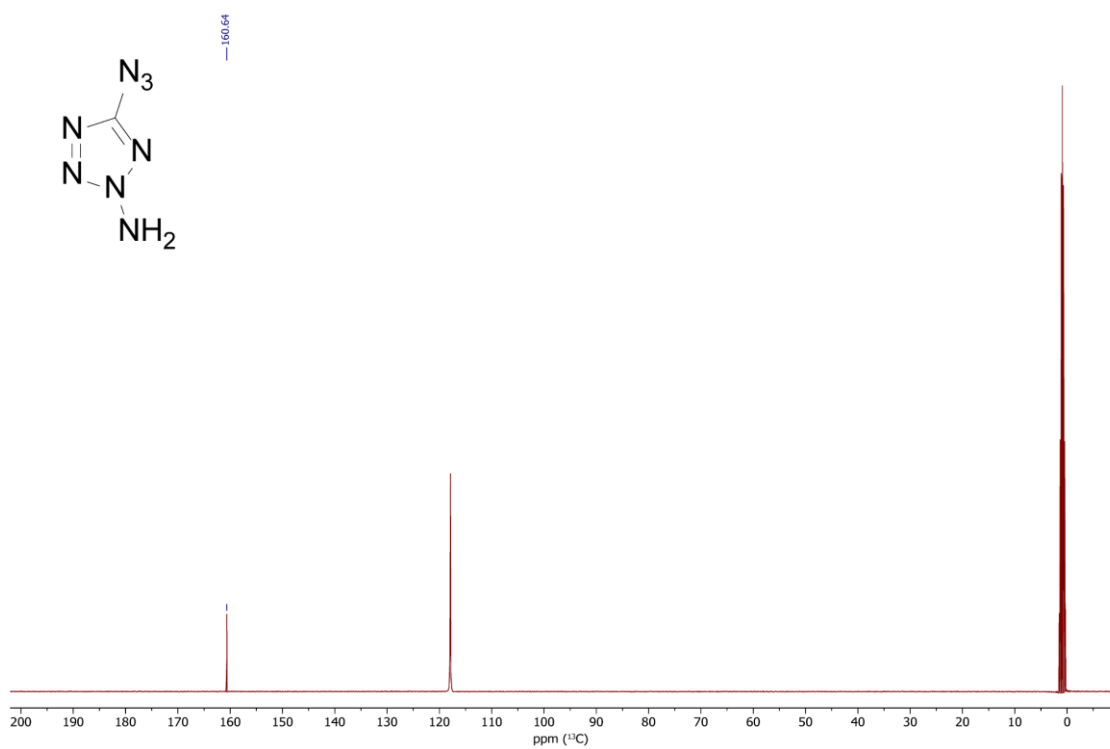


Figure 14. ^{13}C NMR spectrum of 2.

^{15}N -NMR (41 MHz, CD_3OD , ppm)

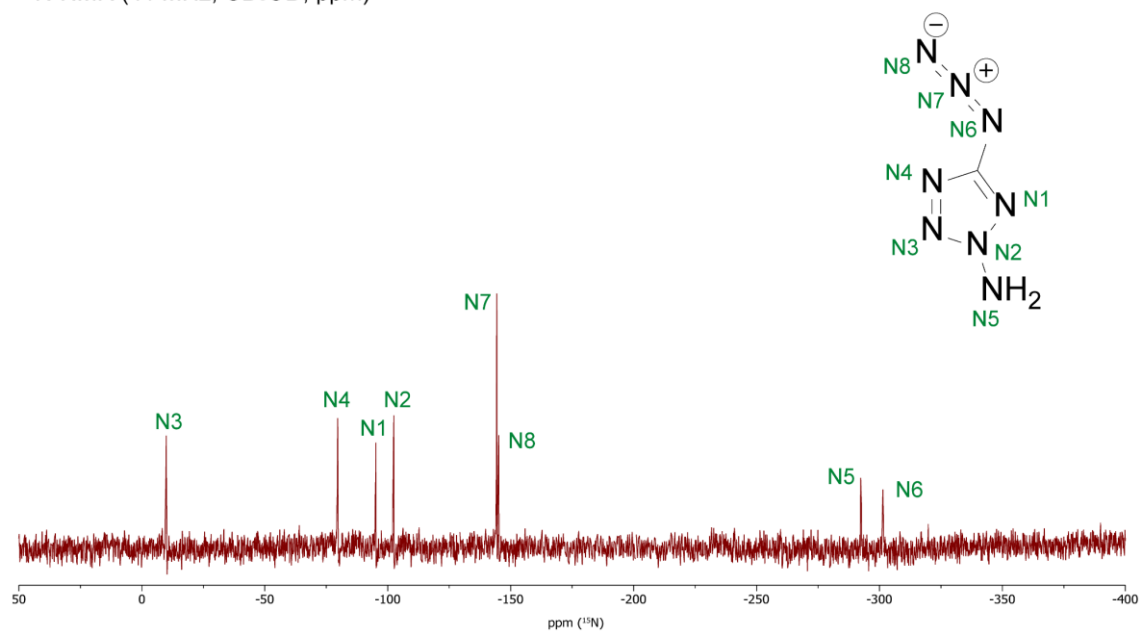


Figure 15. ^{15}N NMR spectrum of 2.

7 Binary 2,2'-Azobis-5-Azidotetrazole

^{13}C -NMR (101 MHz, CD_3CN , ppm)

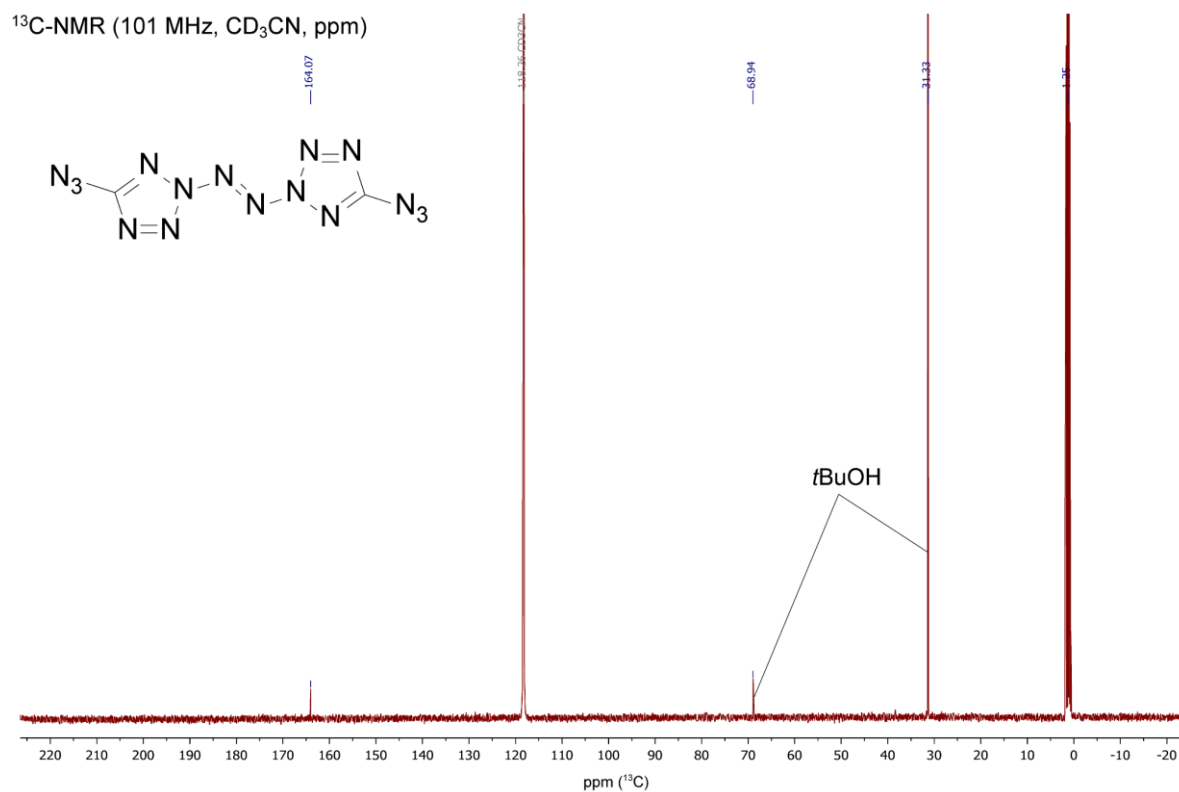


Figure 16. ^{13}C NMR spectrum of **3**.

7.5.5 Thermal Analysis

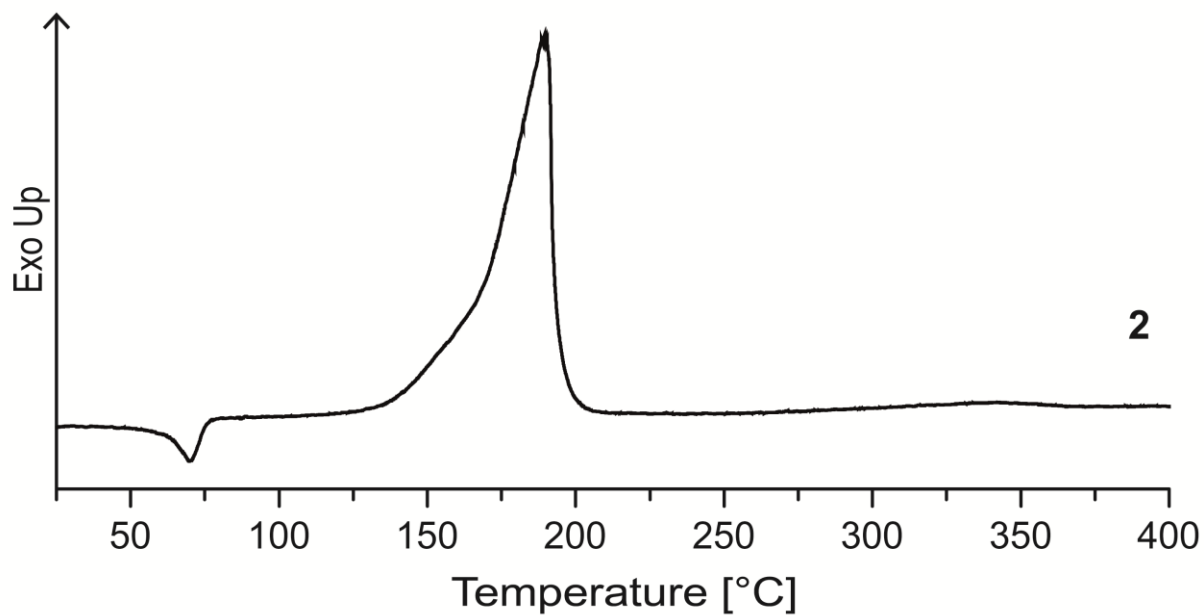


Figure 17. DTA plot of compound **2** with a heating rate of $5\text{ }^{\circ}\text{C min}^{-1}$.

7.6 References

- [1] Klapötke, T. M.; Martin, F. A.; Stierstorfer, J., C₂N₁₄: An Energetic and Highly Sensitive Binary Azidotetrazole. *Angew. Chem. Int. Ed.* **2011**, *50* (18), 4227-4229.
- [2] O'Sullivan, O. T.; Zdilla, M. J., Properties and Promise of Catenated Nitrogen Systems As High-Energy-Density Materials. *Chem. Rev.* **2020**, *120* (12), 5682-5744.
- [3] Eremets, M. I.; Gavriluk, A. G.; Trojan, I. A.; Dzivenko, D. A.; Boehler, R., Single-bonded cubic form of nitrogen. *Nat. Mater.* **2004**, *3* (8), 558-563.
- [4] Christe, K. O.; Wilson, W. W.; Sheehy, J. A.; Boatz, J. A., N₅⁺: A Novel Homoleptic Polynitrogen Ion as a High Energy Density Material. *Angew. Chem. Int. Ed.* **1999**, *38* (13-14), 2004-2009.
- [5] Dixon, D. A.; Feller, D.; Christe, K. O.; Wilson, W. W.; Vij, A.; Vij, V.; Jenkins, H. D. B.; Olson, R. M.; Gordon, M. S., Enthalpies of Formation of Gas-Phase N₃, N₃⁻, N₅⁺, and N₅⁻ from Ab Initio Molecular Orbital Theory, Stability Predictions for N₅⁺N₃⁻ and N₅⁺N₅⁻, and Experimental Evidence for the Instability of N₅+N₃. *J. Am. Chem. Soc.* **2004**, *126* (3), 834-843.
- [6] Zhang, C.; Sun, C.; Hu, B.; Yu, C.; Lu, M., Synthesis and characterization of the pentazolate anion cyclo-N₅⁻ in (N₅)₆(H₃O)₃(NH₄)₄Cl. *Science* **2017**, *355* (6323), 374-376.
- [7] Kesting, W., Über das Hydrazidcarbonazid und seine Entstehung als Nebenprodukt bei der Diazotierung von Carbohydrazid. *Ber. Dtsch. Chem. Ges.* **1924**, *57* (8), 1321-1324.
- [8] Gay-Lussac, J. L., Untersuchungen über die Blausäure. *Ann. Phys.* **1816**, *53*, 139-183.
- [9] Schnick, W., Carbon(IV) Nitride C₃N₄— A New Material Harder Than Diamond? *Angew. Chem. Int. Ed.* **1993**, *32* (11), 1580-1581.
- [10] Ott, E.; Ohse, E., Zur Kenntnis einfacher Cyan- und Cyanurverbindungen. II. Über das Cyanurtriazid, (C₃N₁₂). *Ber. Dtsch. Chem. Ges.* **1921**, *54* (2), 179-186.
- [11] Miller, D. R.; Swenson, D. C.; Gillan, E. G., Synthesis and Structure of 2,5,8-Triazido-s-Heptazine: An Energetic and Luminescent Precursor to Nitrogen-Rich Carbon Nitrides. *J. Am. Chem. Soc.* **2004**, *126* (17), 5372-5373.
- [12] Chen, D.; Yang, H.; Yi, Z.; Xiong, H.; Zhang, L.; Zhu, S.; Cheng, G., C₈N₂₆H₄: An Environmentally Friendly Primary Explosive with High Heat of Formation. *Angew. Chem. Int. Ed.* **2018**, *57* (8), 2081-2084.
- [13] Huynh, M. H. V.; Hiskey, M. A.; Chavez, D. E.; Naud, D. L.; Gilardi, R. D., Synthesis, Characterization, and Energetic Properties of Diazido Heteroaromatic High-Nitrogen C–N Compound. *J. Am. Chem. Soc.* **2005**, *127* (36), 12537-12543.
- [14] Huynh, M. H. V.; Hiskey, M. A.; Archuleta, J. G.; Roemer, E. L.; Gilardi, R., 3,6-Di(azido)-1,2,4,5-Tetrazine: A Precursor for the Preparation of Carbon Nanospheres and Nitrogen-Rich Carbon Nitrides. *Angew. Chem. Int. Ed.* **2004**, *43* (42), 5658-5661.

- [15] Banert, K.; Joo, Y.-H.; Ruffer, T.; Walfort, B.; Lang, H., The Exciting Chemistry of Tetraazidomethane. *Angew. Chem. Int. Ed.* **2007**, *46* (7), 1168-1171.
- [16] Banert, K.; Richter, S.; Schaarschmidt, D.; Lang, H., Well Known or New? Synthesis and Structure Assignment of Binary C₂N₁₄ Compounds Reinvestigated. *Angew. Chem. Int. Ed.* **2013**, *52* (12), 3499-3502.
- [17] Grundmann, C. J.; Schnabel (O.M.C. Corp.), W. J. C. J. Gundmann, W. J. Schnabel (O.M.C. Corp.), US 2290412, **1961**.
- [18] Zhang, Q.; Shreeve, J. M., Growing Catenated Nitrogen Atom Chains. *Angew. Chem. Int. Ed.* **2013**, *52* (34), 8792-8794.
- [19] Tang, Y.; Yang, H.; Wu, B.; Ju, X.; Lu, C.; Cheng, G., Synthesis and Characterization of a Stable, Catenated N11 Energetic Salt. *Angew. Chem. Int. Ed.* **2013**, *52* (18), 4875-4877.
- [20] Klapötke, T. M.; Stierstorfer, J., The CN₇⁻ Anion. *J. Am. Chem. Soc.* **2009**, *131* (3), 1122-1134.
- [21] Stierstorfer, J.; Klapötke, T. M.; Hammerl, A.; Chapman, R. D., 5-Azido-1H-tetrazole – Improved Synthesis, Crystal Structure and Sensitivity Data. *Z. Anorg. Allg. Chem.* **2008**, *634* (6-7), 1051-1057.
- [22] Klapötke, T. M.; Piercey, D. G.; Stierstorfer, J., The Taming of CN₇⁻: The Azidotetrazolate 2-Oxide Anion. *Chem. Eur. J.* **2011**, *17* (46), 13068-13077.
- [23] Klapötke, T. M.; Piercey, D. G.; Stierstorfer, J., Amination of energetic anions: high-performing energetic materials. *Dalton Trans.* **2012**, *41* (31), 9451-9459.
- [24] Klapötke, T. M.; Krumm, B.; Martin, F. A.; Stierstorfer, J., New Azidotetrazoles: Structurally Interesting and Extremely Sensitive. *Chem. Asian J.* **2012**, *7* (1), 214-224.
- [25] Li, F.; Cong, X.; Du, Z.; He, C.; Zhao, L.; Meng, L., 1,1'-Diamino-5,5'-azotetrazole: a nitrogen rich compound. *New J. Chem.* **2012**, *36* (10), 1953-1956.
- [26] Tang, Y.; Yang, H.; Shen, J.; Wu, B.; Ju, X.; Lu, C.; Cheng, G., Synthesis and characterization of 1,1'-azobis(5-methyltetrazole). *New J. Chem.* **2012**, *36* (12), 2447-2450.
- [27] Klapötke, T. M.; Piercey, D. G., 1,1'-Azobis(tetrazole): A Highly Energetic Nitrogen-Rich Compound with a N10 Chain. *Inorg. Chem.* **2011**, *50* (7), 2732-2734.
- [28] Chavez, D. E.; Bottaro, J. C.; Petrie, M.; Parrish, D. A., Synthesis and Thermal Behavior of a Fused, Tricyclic 1,2,3,4-Tetrazine Ring System. *Angew. Chem. Int. Ed.* **2015**, *54* (44), 12973-12975.
- [29] Tang, Y.; Kumar, D.; Shreeve, J. M., Balancing Excellent Performance and High Thermal Stability in a Dinitropyrazole Fused 1,2,3,4-Tetrazine. *J. Am. Chem. Soc.* **2017**, *139* (39), 13684-13687.
- [30] Tang, Y.; He, C.; Yin, P.; Imler, G. H.; Parrish, D. A.; Shreeve, J. M., Energetic Functionalized Azido/Nitro Imidazole Fused 1,2,3,4-Tetrazine. *Eur. J. Org. Chem.* **2018**, *2018* (19), 2273-2276.

- [31] Gorn, M. V.; Gritsan, N. P.; Goldsmith, C. F.; Kiselev, V. G., Thermal Stability of Bis-Tetrazole and Bis-Triazole Derivatives with Long Catenated Nitrogen Chains: Quantitative Insights from High-Level Quantum Chemical Calculations. *J. Phys. Chem. A* **2020**, *124* (38), 7665-7677.
- [32] Zhao, X.; Qi, C.; Zhang, R.; Zhang, S.; Li, S.; Pang, S., The stability and decomposition mechanism of the catenated nitrogen compounds. *J. Mol. Model.* **2015**, *21* (9), 223.
- [33] Spackman, P. R.; Turner, M. J.; McKinnon, J. J.; Wolff, S. K.; Grimwood, D. J.; Jayatilaka, D.; Spackman, M. A., CrystalExplorer: a program for Hirshfeld surface analysis, visualization and quantitative analysis of molecular crystals. *J. Appl. Crystallogr.* **2021**, *54* (3), 1006-1011.
- [34] Reichel, M.; Dosch, D.; Klapötke, T.; Karaghiosoff, K., Correlation between Structure and Energetic Properties of Three Nitroaromatic Compounds: Bis(2,4-dinitrophenyl) Ether, Bis(2,4,6-trinitrophenyl) Ether, and Bis(2,4,6-trinitrophenyl) Thioether. *J. Am. Chem. Soc.* **2019**, *141* (50), 19911-19916.
- [35] Klapötke, T. M., *Chemistry of High-Energy Materials*. De Gruyter: Boston, Berlin, **2019**.
- [36] a) Reichel & Partner GmbH, <http://www.reichelt-partner.de>; b) Test methods according to the UN Recommendations on the Transport of Dangerous Goods, *Manual of Test and Criteria*, fourth revised edition, United Nations Publication, New York and Geneva, **2003**, ISBN 92-1-139087-7, Sales No. E.03.VIII.2; 13.4.2 Test 3 a (ii) BAM Fallhammer.
- [37] Sućeska, M., EXPLO5 V6.02 program, Brodarski Institute, Zagreb, Croatia, **2014**.
- [38] Mintz, M. J.; Walling, C., t-Butyl hypochlorite. *Org. Synth.* **2003**, *49*, 9.
- [39] a) Klapötke, T. M.; Piercey, D. G.; Stierstorfer, J., Amination of energetic anions: high-performing energetic materials. *Dalton Trans.* **2012**, *41*, 9451-9459, b) Glover, E. E.; Rowbottom, K. T., N-amination and subsequent oxidation of some fused imidazoles and triazoles. *J. Chem. Soc., Perkin Trans. 1* **1976**, 367-371.
- [40] *CrysAlisPro*, Oxford Diffraction Ltd. version 171.33.41, **2009**.
- [41] Sheldrick, G.M., *Acta Cryst.* **2015**, *A71*, 3-8.
- [42] Dolomanov, O. V.; Bourhis, L. J.; Gildea, R. J.; Howard, J. A. K.; Puschmann, H., OLEX2: A complete structure solution, refinement and analysis program. *J. Appl. Cryst.* **2009**, *42*, 339-341.
- [43] *SCALE3 ABSPACK – An Oxford Diffraction program* (1.0.4, gui: 1.0.3), Oxford Diffraction Ltd., **2005**.
- [44] *APEX3*. Bruker AXS Inc., Madison, Wisconsin, USA.
- [45] a) Spackman, P. R.; Turner, M. J.; McKinnon, J. J.; Wolff, S. K.; Grimwood, D. J.; Jayatilaka, D.; Spackman, M. A., CrystalExplorer: a program for Hirshfeld surface analysis, visualization and quantitative analysis of molecular crystals. *J. Appl. Crystallogr.* **2021**, *54* (3), 1006-1011; b) Bauer, L.; Benz, M.; Klapötke, T. M.; Lenz, T.; Stierstorfer, J., Polyazido-methyl Derivatives of Prominent Oxadiazole and Isoxazole Scaffolds: Synthesis, Explosive properties, and Evaluation. *J. Org. Chem.* **2021**, *86*, 9, 6371-6380.

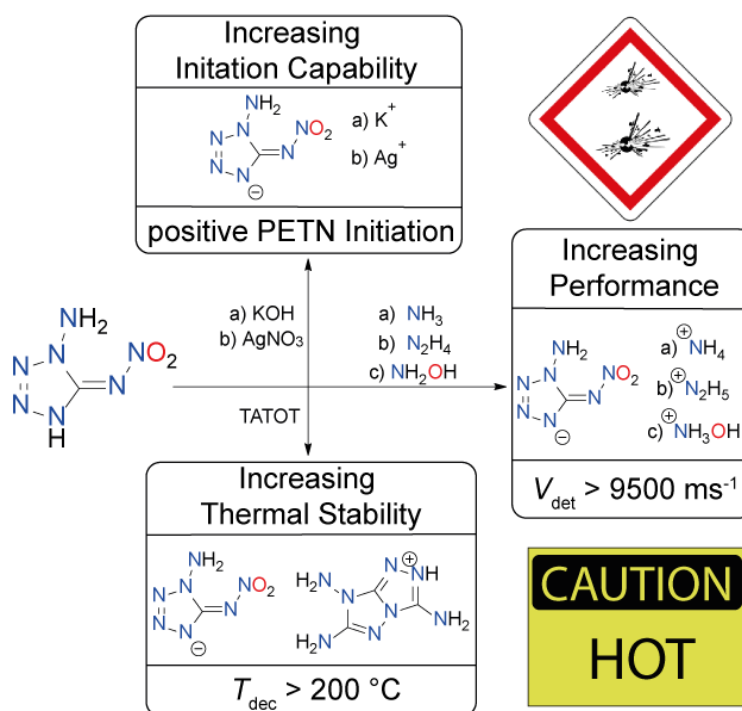
- [46] Frisch, M. J.; Trucks, G. W.; Schlegel, H. B.; Scuseria, G. E.; Robb, M. A.; Cheeseman, J. R.; Scalmani, G.; Barone, V.; Petersson, G. A.; Nakatsuji, H.; Li, X.; Caricato, M.; Marenich, A. V.; Bloino, J.; Janesko, B. G.; Gomperts, R.; Mennucci, B.; Hratchian, H. P.; Ortiz, J. V.; Izmaylov, A. F.; Sonnenberg, J. L.; Williams-Young, D.; Ding, F.; Lipparini, F.; Egidi, F.; Goings, J.; Peng, B.; Petrone, A.; Henderson, T.; Ranasinghe, D.; Zakrzewski, V. G.; Gao, J.; Rega, N.; Zheng, G.; Liang, W.; Hada, M.; Ehara, M.; Toyota, K.; Fukuda, R.; Hasegawa, J.; Ishida, M.; Nakajima, T.; Honda, Y.; Kitao, O.; Nakai, H.; Vreven, T.; Throssell, K.; Montgomery, J. A., Jr.; Peralta, J. E.; Ogliaro, F.; Bearpark, M. J.; Heyd, J. J.; Brothers, E. N.; Kudin, K. N.; Staroverov, V. N.; Keith, T. A.; Kobayashi, R.; Normand, J.; Raghavachari, K.; Rendell, A. P.; Burant, J. C.; Iyengar, S. S.; Tomasi, J.; Cossi, M.; Millam, J. M.; Klene, M.; Adamo, C.; Cammi, R.; Ochterski, J. W.; Martin, R. L.; Morokuma, K.; Farkas, O.; Foresman, J. B.; Fox, D. J., Gaussian 09 A.02, Gaussian, Inc., Wallingford, CT, USA, **2009**.
- [47] Ochterski, J. W.; Petersson, G. A.; Montgomery Jr., J. A., A complete basis set model chemistry. V. Extensions to six or more heavy atoms, *J. Chem. Phys.* **1996**, *104*, 2598–2619; b) Montgomery Jr., J. A.; Frisch, M. J.; Ochterski, J. W.; Petersson, G. A., A complete basis set model chemistry. VII. Use of the minimum population localization method, *J. Chem. Phys.* **2000**, *112*, 6532–6542.
- [48] a) Curtiss, L. A.; Raghavachari, K.; Redfern, P. C.; Pople, J. A., Assignment of Gaussian-2 and density functional theories for the computation of enthalpies of formation, *J. Chem. Phys.* **1997**, *106*, 1063–1079; b) Byrd, E. F. C.; Rice, B. M., Improved prediction of heats of formation of energetic materials using quantum mechanical calculations, *J. Phys. Chem. A* **2006**, *110*, 1005–1013; c) Rice, B. M.; Pai, S. V.; Hare, J., Predicting heats of formation of energetic materials using quantum mechanical calculations, *Comb. Flame* **1999**, *118*, 445–458.
- [49] Montgomery, J. A. Jr.; Frisch, M. J.; Ochterski, J. W.; Petersson, G. A. A complete basis set model chemistry. VII. Use of the minimum population localization method. *J. Chem. Phys.* **2000**, *112*, 6532–6542.
- [50] Pickard, F. C. IV; Pokon, E. K.; Liptak, M. D.; Shields, G. C. Comparison of CBS-QB3, CBS-APNO, G2, and G3 thermochemical predictions with experiment for formation of ionic clusters of hydronium and hydroxide ions complexed with water. *J. Chem. Phys.* **2005**, *122*, 24302–24307.
- [51] Westwell, M. S.; Searle, M. S.; Wales, D. J.; Williams, D. H., Empirical correlations between thermodynamic properties and intermolecular forces. *J. Am. Chem. Soc.* **1995**, *117*, 5013–5015; b) Trouton, F., IV. On molecular latent heat, *Philos. Mag.* **1884**, *18*, 54–57.
- [52] Witek, H. A.; Keiji, M., Systematic study of vibrational frequencies calculated with the self-consistent charge density functional tight-binding method. *J. Comp. Chem. THEOCHEM* **2004**, *25*, 1858–1864.

8 1-Amino-5-nitriminotetrazole

1-Amino-5-nitriminotetrazolate: High Performing Energetic Anion

Maximilian Benz, Thomas M. Klapötke, Jörg Stierstorfer and Michael Voggenreiter

Unpublished Manuscript



8.1 Abstract

1-Amino-5-nitriminotetrazole (HANIT) is synthesized via protection of 1,5-diaminotetrazole with acetone followed by aprotic nitration using N_2O_5 and in situ deprotection. The salts of 1-amino-5-nitriminotetrazolate are synthesized by addition of the corresponding bases. Especially the nitrogen rich derivatives show insane explosive properties and compete with the most powerful, CHNO-based, non-nuclear explosives. The initiation test showed the initiation capability of the potassium and silver salt, which were able to initiate PETN. The TATOT salt is a promising secondary explosive, since it combines the high performance of the anion with insensitivity and thermal stability of the cationic moiety. The compounds were studied by X-ray diffraction, spectroscopic analysis (NMR and IR) and DTA. The sensitivities towards external stimuli were determined and the energetic performances were calculated by the EXPLO5 using the heats of formation obtained by CBS-4M calculation.

8.2 Introduction

The search for new energetic materials, especially in the field of tetrazoles, continues unabated. Tetrazoles exhibit a high heat of formation, which can be further enhanced by the introduction of energetic groups.^[1] For example, 5-azidotetrazole and 5-nitrotetrazole feature high heats of formation but various drawbacks as neutral compounds, such as high sensitivity or low thermal stability.^[2–5] A good equity is 5-nitriminotetrazole which offers a good combination of heat of formation, stability, sensitivity and energetic performance as neutral compound.^[6,7] Over the years, 5-nitriminotetrazole was studied and further functionalized in the 1-position.^[8,9] It was possible to obtain alkylated species, in particular the 1-methyl-5-nitriminotetrazole, which has less energetic properties than the parent compound but is also much less sensitive towards impact and friction.^[7] The salts of 1-hydroxy-5-nitriminotetrazole feature very good properties but on the other hand, no values for the neutral compound are available.^[10] *Fischer et al.* succeeded in the preparation of 1,5-di(nitramino)tetrazole which has an incredibly detonation velocity of nearly $10\,000\text{ m s}^{-1}$ but also extreme sensitivities.^[11] Another remarkable compound is the 1-nitramino-5-aminotetrazole which is extremely sensitive and less thermally stable but has good detonative properties.^[12] The constitutional isomer, namely 1-amino-5-nitriminotetrazole, which has comparable energetic properties with far greater thermal and mechanical stability. This compound was also prepared by *Fischer* in a six-step synthesis starting from CS_2 .^[13] However, we have successfully developed a new and attractive route with better yield to the target molecule.

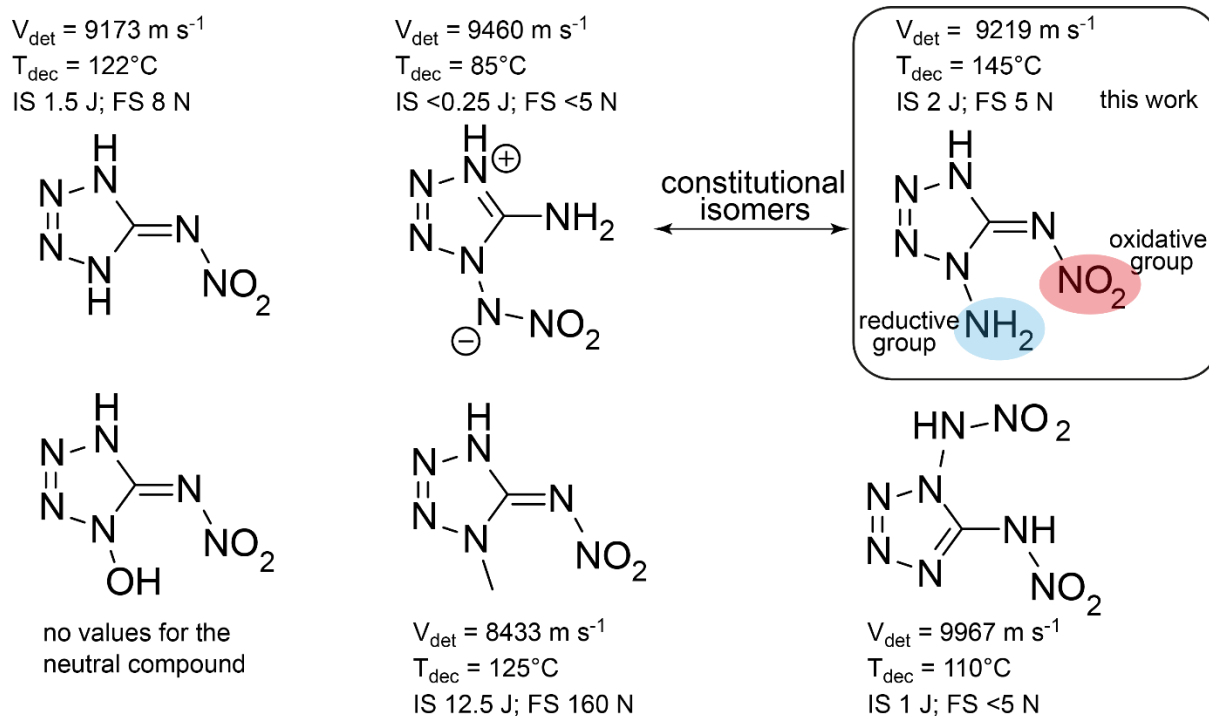
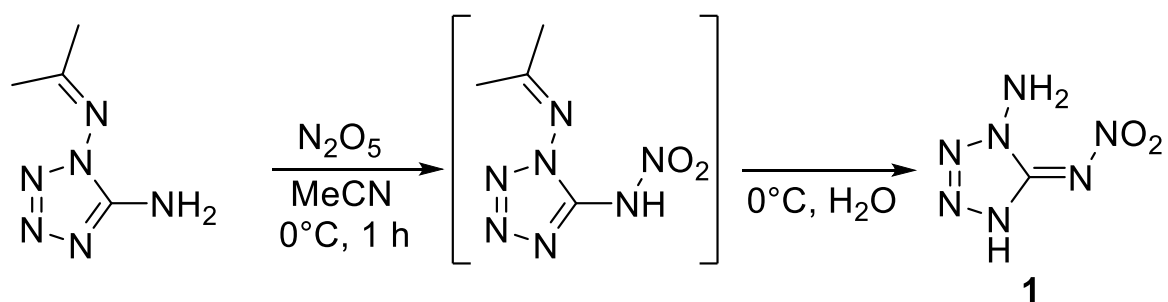


Figure 1. Comparison of different nitriminotetrazoles with emphasis on the constitutional isomers 1-nitramino-5-aminotetrazole and 1-amino-5-nitriminotetrazole, which was synthesized in this work.^[7–10]

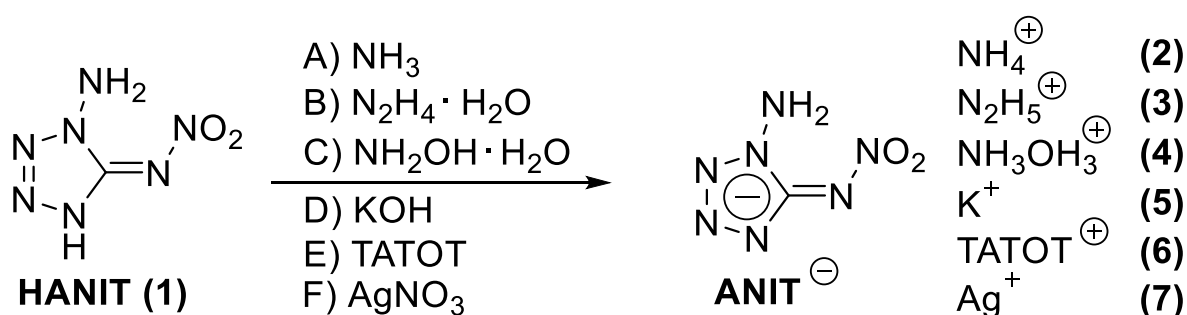
In this work, we report on the facile synthesis of 1-amino-5-nitrimino-tetrazole and six different energetic salts, all of which exhibit excellent energetic properties.

8.3 Results and Discussion

1,5-Diaminotetrazole and 1-isopropylideneamino-5-aminotetrazole were synthesized according to literature procedures.^[14–16] The main challenge was to nitrate only the 5-position without the simultaneous nitration of the 1-position to end up with 1,5-dinitraminotetrazole. It was necessary to use a protection group at the 1-position and aprotic nitration conditions. An exact stoichiometric amount of dinitrogen pentoxide was used to obtain 1-isopropylideneamino-5-nitraminotetrazole. Upon quenching with ice-water, the residual nitrate anion of dinitrogen pentoxide forms nitric acid which splits off the protection group at the 1-position to form the target molecule 1-amino-5-nitriminotetrazole (**HANIT, 1**). (**Scheme 1**) The extraction had to be done rapidly in the cold because of the water solubility of **1** at room temperature, yet **1** was then obtained as a yellow crystalline solid in 70% yield. The ammonium salt (**2**) as well as the potassium salt (**5**) were obtained by the use of an ethanolic solution of ammonia and potassium hydroxide, respectively. For all other salts, an aqueous solution of the corresponding base was used.



Scheme 1. Direct nitration of 1-isopropylideneamino-tetrazole-5-amine with dinitrogen pentoxide which cleaves the protection group upon quenching with water to yield 1-amino-5-nitriminotetrazole (**HANIT**, **1**).



TATOT = 3,6,7-triamino-[1,2,4]triazole[4,3-b][1,2,4]triazole

Scheme 2. Salt formation of ANIT with different cations **2–7**.

Single crystals suitable for X-ray diffraction were obtained by recrystallization from common organic solvents or water. Details on the measurement and refinement data for every compound can be found in the Supporting Information. The data were uploaded to the CSD database with the [CCDC numbers](#)

HANIT (1) crystallizes in the monoclinic space group $P2_1/n$ with 8 molecules in the unit cell and a density of 1.779 g cm^{-3} at 173 K. (**Figure 2A**) The amino-function stabilizes the nitro group intermolecularly with a distance of 2.140 \AA . **Figure 2B** depicts the arrangement in the crystal along the a axis with alternating layers, having an angle of 61.26° to each other.

The TATOT salt of ANIT (**6**) crystallizes in the monoclinic space group $P2_1/c$ with 4 molecules in the unit cell and a density of 1.837 g cm^{-3} at 173 K which is slightly higher than the density of the parent compound **1**. (**Figure 4A**) The TATOT cation forms a hydrogen bridge to the ANIT anion with a distance of 1.971 \AA . The molecules arrange in slightly distorted sheets along the c axis, forming alternating crosses as shown in **Figure 4B**.

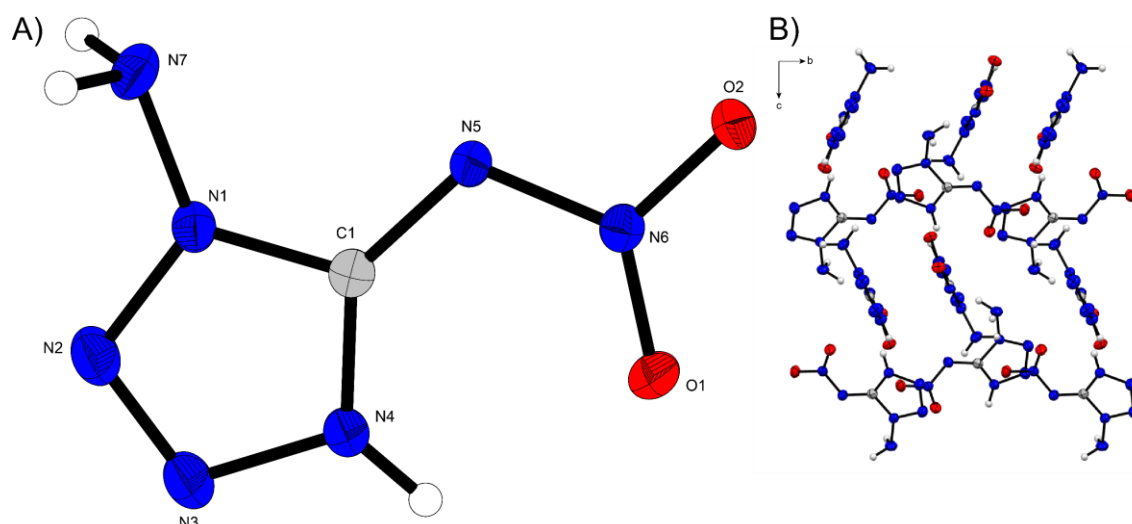


Figure 2. A) Crystal structure of **1**. B) View along the *a* axis with different alternating layers of HANIT.

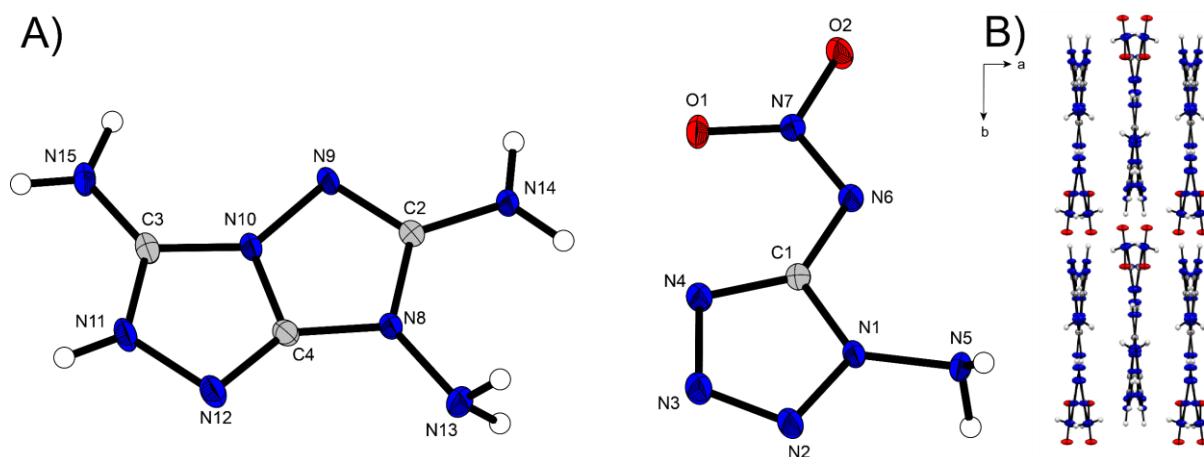


Figure 4. A) Molecular structure of **6**. B) Alternating cross-shaped arrangement of **6** consisting of 1-amino-5-nitriminotetrazolate units facing the TATOT moieties.

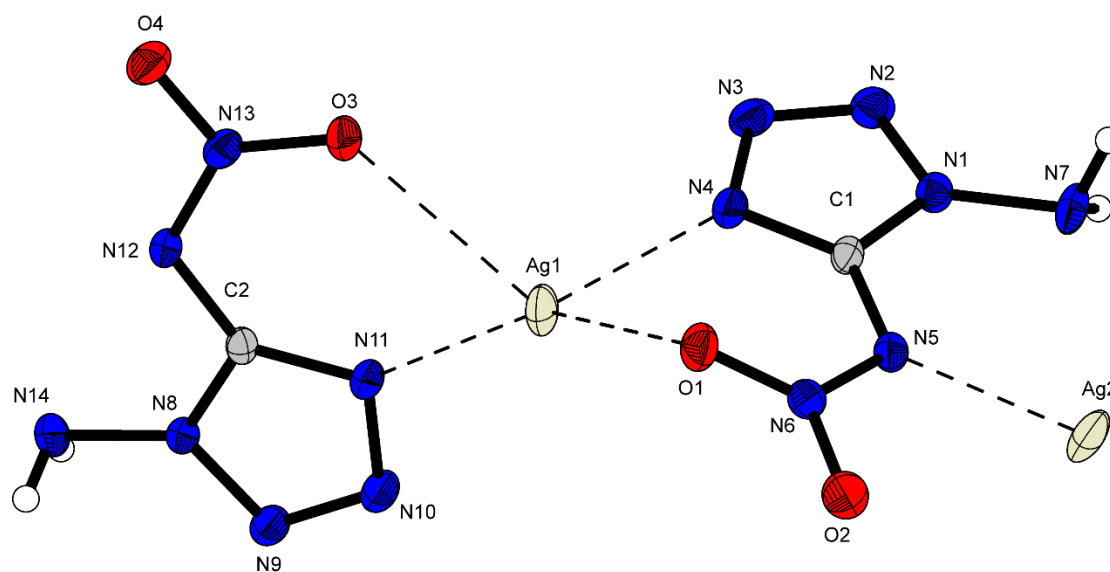


Figure 5. X-ray structure of silver ANIT (**7**). The silver cation is tetrahedrally coordinated by two 1-amino-5-nitriminotetrazolates.

AgANIT (7) crystallizes in the orthorhombic space group *Pbca* with 8 formula units in the unit cell and a density of 2.988 g cm^{-3} at room temperature. (**Figure 5**) The silver cation is in between two 1-amino-5-nitriminotetrazolate anion and is tetrahedrally coordinated which forms a macrostructure of bridging silver atoms. Proton NMR spectroscopy revealed the amino function of all salts as singlet signal at around 6.20 ppm except for **7** which is shifted downfield to 6.54 ppm. Further, the carbon spectrum showed one signal for the tetrazole carbon of the **ANIT** anion at about 155 ppm which is slightly shifted downfield compared to the parent compound (149 ppm). The nitrimine group can be observed in the ^{14}N -NMR between -4 to -20 ppm for all compounds. Differential thermal analysis (DTA) for **2** and **4** showed melting points at 170°C and 155°C . Compounds **5**, **6** and **7** have comparably high decomposition temperatures of 244°C , 215°C and 218°C without prior melting. In relation to the parent compound **1** (145°C), the thermal stability increases for all synthesized salts. All compounds were analyzed regarding their sensitivity according to BAM standards. **HANIT** has an impact sensitivity of 2 J and a friction sensitivity of 5 N, which is in the range of primary explosives, but the neutral compound can be handled safely if all precautions such as plastic and grounded equipment are obeyed. All tested salts are sensitive towards impact with sensitivities of 1–2 J except **6** which is rather insensitive towards external stimuli (IS = 20 J, FS = 240 N). The potassium salt **5** is just as sensitive to friction as the neutral compound **1** with detonative decomposition at 5 N and the silver salts **7** is extremely sensitive with values below our measuring limit. The others salts can be classified as friction sensitive with a detonation occurring at 15–20 N. The heat of formation of the respective compounds were calculated on the CBS-4M level of theory using the atomization method. All compounds have highly positive calculated enthalpies of formation (**1**: $+416.1 \text{ kJ mol}^{-1}$; **6**: $+898.1 \text{ kJ mol}^{-1}$). Together with the crystallographic densities recalculated to room temperature, the energetic performances were calculated with EXPLO5 code.^[17] (**Table 1**) All synthesized compounds have detonation velocities of over 9000 m s^{-1} , the hydrazinium (**3**) and hydroxylammonium (**4**) salt even reach almost $10\,000 \text{ m s}^{-1}$. Calculated detonation velocities easily outperform RDX and especially **3** and **4** even surpass TKX-50. The detonation pressure of **1** is 343 kbar, which is close to the value of RDX (380 kbar) but not near the detonation pressure of TKX-50 (424 kbar). To get a better insight into the high sensitivities of the neutral compound **1** despite the stabilizing amino-nitro push-pull system, a natural bond orbital (NBO) calculation was performed. (**Figure 6A**). The most positively polarized atoms are N6 next to the oxygen atoms

Table 2. Comparison of **1–7** with TKX-50^[18] and RDX^[18].

	1	2	3	4	5	6	7	TKX-50 ^[18]	RDX ^[18]
Formula	CH ₃ N ₇ O ₂	CH ₆ N ₈ O ₂	CH ₇ N ₉ O ₂	CH ₆ N ₈ O ₃	CH ₂ N ₇ O ₂ K	C ₄ H ₁₁ N ₁₅ O ₂	CH ₂ N ₇ O ₂ Ag	C ₂ H ₈ N ₁₀ O ₄	C ₃ H ₆ N ₆ O ₆
IS [J] ^[a]	2	1	2	2	<1	20	<1	20	7.5
FS [N] ^[b]	5	20	15	20	5	240	<1	120	120
ρ_{298K} [g cm ⁻³] ^[c]	1.746	1.731	1.725	1.807	1.98 ^[j]	1.803	2.988	1.877	1.806
N+O [%] ^[d]	89.64	88.89	89.23	89.86	71.00	80.37	51.62	86.41	81.06
T _{melt} / T _{dec} [°C] ^[e]	-/145	170/185	-/175	155/170	-/244	-/215	-/218	-/221	205/210
$\Delta_f H^\circ$ [kJ mol ⁻¹] ^[f]	416.1	377.6	528.9	436.1	-165.5	898.1	-	446.6	86.3
$-\Delta_E U^\circ$ [kJ kg ⁻¹] ^[g]	5793	5400	5899	6343	2966	4595	-	6025	6190
V _{det} [m s ⁻¹] ^[h]	9219	9557	9849	9915	7789	9312	-	9698	8983
p _{C-J} [kbar] ^[i]	343	347	370	402	235	324	-	424	380

[a] Impact sensitivity (BAM drophammer, 1 of 6). [b] Friction sensitivity (BAM friction tester, 1 of 6). [c] Density from X-ray diffraction analysis recalculated to 298 K: $\rho_{298K} = \rho_T / [1 + \alpha_V(298\text{ K} - T)]$ where $\alpha_V = 1.6 \times 10^{-4} \text{ K}^{-1}$.^[1] [d] Combined nitrogen and oxygen content. [e] Melting/decomposition temperature (DTA, $\beta = 5 \text{ }^\circ\text{C min}^{-1}$). [f] Calculated enthalpy of formation, CBS-4M. [g] Energy of explosion (EXPLO5, ver. 6.05.02).^[17] [h] Detonation velocity (EXPLO5, ver. 6.05.02).^[17] [i] Detonation pressure at the Chapman–Jouguet point (EXPLO5, ver. 6.05.02).^[17] [j] Gas pycnometer at 298 K.

and the tetrazole carbon atom. The strongest negatively charged atoms are N7, followed by N5 and the two oxygen atoms. It implies that there is no unusual charge distribution in the neutral molecule. Potassium and silver salt **5** and **7**, unlike the other compounds, showed detonation when heated, therefore we performed an initiation test to investigate whether **5** is suitable as a primary explosive. The setup consists of 200 mg pressed PETN (10 tons, 3 seconds) in a copper tube and 50 mg of unpressed **5** on top. The charge is ignited by a commercial igniter. A hole or dent in the copper base plate suggests a positive initiation test. It can be concluded that potassium salt **5** is capable of detonating PETN. (**Figure 6B**) A hot plate test was performed to visualize the different thermal behavior and decomposition of **1** and **5**. As depicted in **Figure 6C–D**, the neutral compound **1** only deflagrates violently, whereas **KANIT (5)** detonates with a dull bang and a smoke cloud.

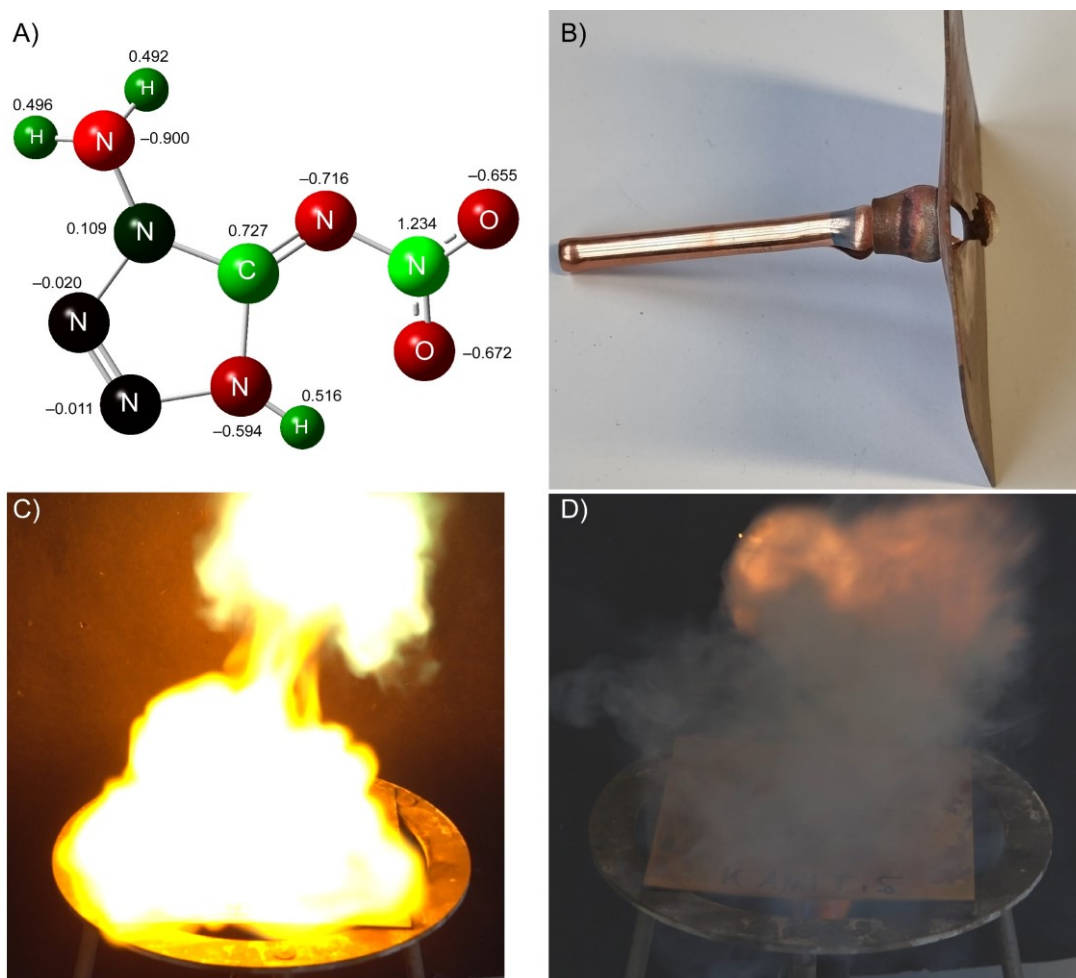


Figure 6. A) Charge distribution as NBO calculation result of the neutral compound **1**. B) Positive initiation test of the potassium salt **5**. C) Deflagration of **HANIT (1)** on the hot plate test. D) Detonation of **KANIT (5)** on the hot plate test.

8.4 Conclusion

We conclude that 1-amino-5-nitriminotetrazole and its salts are very powerful energetic materials. All offer higher thermal stability, higher energetic performance at comparable sensitivities with respect to other nitriminotetrazole derivatives. Hydroxylammonium 1-amino-5-nitriminotetrazolate (**4**), with a detonation velocity of 9915 m s^{-1} , competes with the most powerful non-nuclear explosives but is rather sensitive. The TATOT salt **6** is the most promising for use as secondary explosive due to its relative insensitivity (IS 20 J, FS 240 N) combined with a high detonation velocity of higher than 9300 m s^{-1} and a thermal stability of 215°C . With this rather simple synthesis, we fill a gap in the synthetic world of high-performing energetic tetrazoles.

Financial support of this work by Ludwig-Maximilians University (LMU), the Office of Naval Research (ONR) under Grant ONR N00014-19-1-2078, and the Strategic Environmental Research and Development Program (SERDP) under Contract W912HQ19C0033 is gratefully acknowledged.

8.5 Supporting Information

8.5.1 Experimental Procedures

CAUTION! All described compounds are powerful energetic materials with high sensitivities towards shock and friction. Therefore, proper security precautions (safety glass, face shield, earthed equipment and shoes, Kevlar gloves and ear plugs) have to be applied all time while synthesizing and handling the described compounds. Especially KANIT (**5**) and AgANIT (**7**) are extremely sensitive. Chemicals and solvents were employed as received (Sigma-Aldrich, Acros, TCI). ^1H , ^{13}C and ^{14}N spectra were recorded using a Bruker AMX 400 instrument. The chemical shifts quoted in ppm refer to tetramethylsilane (^1H , ^{13}C) and nitromethane (^{14}N). Decomposition temperatures were determined on an OZM Research DTA 552–Ex instrument with a heating rate of 5°C min^{-1} . Infrared (IR) spectra were recorded using a Perkin-Elmer Spektrum One FT–IR instrument. Elemental analyses were performed with an Elementar Vario el by pyrolysis of the sample and subsequent analysis of formed gases. The sensitivity data were collected using a BAM (Bundesanstalt für Materialforschung) drophammer^[19] according to STANAG 4489^[20] modified instruction^[21] and a BAM friction tester^[22] according to STANAG 4487^[23] modified instruction.^[24]

The classification of the tested compounds results from the 'UN Recommendations on the Transport of Dangerous Goods'. [25]

1-Amino-5-nitriminotetrazole (1)

1-(Propan-2-ylideneamino)-1*H*-tetrazol-5-amine (1.00 g, 7.14 mmol, 1.0 eq.) was suspended in MeCN (5 mL), cooled to 0°C and then dinitrogen pentoxide (0.77 g, 7.14 mmol, 1.0 eq.) in MeCN (15 mL) was added at 0°C. The mixture dissolved while turning yellow and was stirred for 45 minutes. The solution was poured onto ice (70 g) and extracted with cold ethyl acetate (3 x 25 mL). The combined organic layers were washed with cold brine solution (1 x 25 mL) prior to drying. The solvent was removed to yield 0.72 g (4.96 mmol, 70%) of 1-amino-5-nitriminotetrazole as yellow crystals.

DTA (5 °C min⁻¹): 145 °C (exo, dec.); **Sensitivities** (≤500 μm): **BAM drop hammer**: 2 J, **friction tester**: 5 N, **ESD**: 40 mJ; **IR** (ATR) $\tilde{\nu}$ (cm⁻¹) = 3320(m), 3250(m), 3204(m), 3142(m), 1710(m), 1579(s), 1480(m), 1435(s), 1300(s), 1238(vs), 1034(s), 991(s), 950(s), 872(s), 776(s), 753(s), 712(s), 699(s), 643(s), 570(s), 522(s), 463(s), 433(s), 424(s), 409(s); **Elem. Anal.** (CH₃N₇O₂, 145.08 g mol⁻¹) calcd.: C 8.28, H 2.08, N 67.58 %. Found: C 7.83, H 2.54, N 66.74 %; **¹H NMR** (DMSO-d₆, 400 MHz, ppm) δ = 8.86 (br s, 3H); **¹³C NMR** (DMSO-d₆, 101 MHz, ppm) δ = 149.0; **¹⁴N NMR** (DMSO-d₆, 29 MHz, ppm) δ = -8.

Ammonium 1-amino-5-nitriminotetrazolate (2)

1-Amino-5-nitriminotetrazole (0.30 g, 2.07 mmol, 1.0 eq.) was dissolved in ethanol (10 mL) and ammonia solution (2 M in EtOH, 1.04 mL, 2.07 mmol, 1.0 eq) was added. The solution was stirred for 10 min at 50 °C and the solvent was evaporated. Ammonium 1-amino-5-nitriminotetrazolate (0.29 g, 1.80 mmol, 87%) was obtained after recrystallization from EtOAc/EtOH as orange crystalline powder.

DTA (5 °C min⁻¹): 170 °C (endo, melt.) followed by 185 °C (exo, dec.); **Sensitivities** (≤500 μm): **BAM drop hammer**: 1 J, **friction tester**: 20 N; **IR** (ATR) $\tilde{\nu}$ (cm⁻¹) = 3324(m), 3304(w), 3254(m), 3192(s), 3034(m), 2845(m), 1611(w), 1507(s), 1440(s), 1385(m), 1362(s), 1282(vs), 1188(s), 1101(s), 1029(s), 991(m), 933(s), 892(s), 775(m), 758(m), 736(m), 709(m), 684(m), 668(w), 532(m), 469(m), 455(m), 448(m), 440(m), 422(w), 415(w), 403(m); **Elem. Anal.** (CH₆N₈O₂, 162.11 g mol⁻¹) calcd.: C 7.41, H 3.73, N 69.12 %. Found: C 7.21, H 3.63, N 68.09 %; **¹H NMR** (DMSO-d₆, 400 MHz, ppm) δ = 7.14 (m, 4H), 6.20 (s, 2H); **¹³C NMR** (DMSO-d₆, 101 MHz, ppm) δ = 155.0; **¹⁴N NMR** (DMSO-d₆, 29 MHz, ppm) δ = -14, -358.

Hydrazinium 1-amino-5-nitriminotetrazolate (3)

1-Amino-5-nitriminotetrazole (0.25 g, 1.72 mmol, 1.0 eq.) was dissolved in ethanol (10 mL) and hydrazinium hydroxide (83 μ L, 1.72 mmol, 1.0 eq) was added. The solution was stirred for 10 min at 50 °C and the solvent was evaporated. Hydrazinium 1-amino-5-nitriminotetrazolate (0.24 g, 1.33 mmol, 77%) was obtained after recrystallization from EtOAc/EtOH as yellowish powder.

DTA (5 °C min⁻¹): 175 °C (exo, dec.); **Sensitivities** (\leq 500 μ m): **BAM drop hammer**: 2 J, **friction tester**: 15 N; **IR** (ATR) $\tilde{\nu}$ (cm⁻¹) = 3290(s), 3121(s), 2942(m), 2633(m), 1657(m), 1538(m), 1510(s), 1461(m), 1450(m), 1358(s), 1318(vs), 1152(m), 1129(s), 1090(vs), 1020(s), 1007(s), 976(s), 965(s), 880(m), 768(s), 753(s), 735(s), 706(s), 699(s), 686(m), 645(m), 532(s), 475(s), 403(s); **Elem. Anal.** (CH₇N₉O₂, 177.13 g mol⁻¹) calcd.: C 6.78, H 3.98, N 71.17 %. Found: C 7.00, H 4.22, N 69.86 %; **¹H NMR** (DMSO-d₆, 400 MHz, ppm) δ = 7.10 (s, 5H), 6.19 (s, 2H); **¹³C NMR** (DMSO-d₆, 101 MHz, ppm) δ = 155.5; **¹⁴N NMR** (DMSO-d₆, 29 MHz, ppm) δ = -15.

Hydroxylammonium 1-amino-5-nitriminotetrazolate (4)

1-Amino-5-nitriminotetrazole (0.24 g, 1.66 mmol, 1.0 eq.) was dissolved in ethanol (10 mL) and aqueous hydroxylamine solution (50 wt%, 0.11 mL, 1.66 mmol, 1.0 eq) was added. The solution was stirred for 10 min at 50 °C. After cooling to room temperature, hydroxylammonium 1-amino-5-nitriminotetrazolate (0.24 g, 1.38 mmol, 81%) was precipitated by the addition of Et₂O (100 mL) to the intensively stirring solution as a slightly yellow powder.

DTA (5 °C min⁻¹): 155 °C (endo, melt.) followed by 170 °C (exo, dec.); **Sensitivities** (\leq 500 μ m): **BAM drop hammer**: 2 J, **friction tester**: 20 N; **IR** (ATR) $\tilde{\nu}$ (cm⁻¹) = 3325(m), 3213(m), 3063(m), 2852(m), 2772(m), 2674(m), 1633(m), 1516(s), 1464(s), 1419(m), 1352(s), 1307(vs), 1288(vs), 1259(s), 1187(vs), 1168(vs), 1116(s), 1039(s), 998(s), 949(s), 893(s), 776(s), 766(s), 735(vs), 705(vs), 686(s), 667(s), 519(m), 467(m); **Elem. Anal.** (CH₆N₈O₃, 178.11 g mol⁻¹) calcd.: C 6.74, H 3.40, N 62.91 %. Found: C 6.88, H 3.65, N 61.37 %; **¹H NMR** (DMSO-d₆, 400 MHz, ppm) δ = 9.88 (br s, 4H), 6.19 (s, 2H); **¹³C NMR** (DMSO-d₆, 101 MHz, ppm) δ = 155.6; **¹⁴N NMR** (DMSO-d₆, 29 MHz, ppm) δ = -15, -359.

Potassium 1-amino-5-nitriminotetrazolate (5)

1-Amino-5-nitriminotetrazole (0.42 g, 2.86 mmol, 1.0 eq.) was dissolved in ethanol (10 mL) and potassium hydroxide (0.16 g, 2.86 mmol, 1.0 eq) dissolved in ethanol (5 mL) was added. Potassium 1-amino-5-nitriminotetrazolate precipitated instantly as yellow amorphous powder which was filtered, washed with diethyl ether and dried. Potassium 1-amino-5-

8 1-Amino-5-nitriminotetrazole

nitriminotetrazolate (0.49 g, 2.65 mmol, 93%) was obtained after recrystallization from a methanol/water mixture as dark yellowish to brownish solid.

DTA (5 °C min⁻¹): 244 °C (exo, dec.); **Sensitivities** (≤500 μm): **BAM drop hammer**: <1 J, **friction tester**: 5 N; **IR** (ATR) $\tilde{\nu}$ (cm⁻¹) = 3318(m), 3204(m), 1627(m), 1504(s), 1308(vs), 1282(vs), 1101(s), 1030(s), 886(m), 830(m), 777(s), 735(m), 686(m), 419(s); **Elem. Anal.** (CH₂N₇O₂K, 183.17 g mol⁻¹) calcd.: C 6.56, H 1.10, N 53.53 %. Found: too sensitive for measurement; **¹H NMR** (DMSO-d₆, 400 MHz, ppm) δ = 6.20 (s, 2H); **¹³C NMR** (DMSO-d₆, 101 MHz, ppm) δ = 155.0; **¹⁴N NMR** (DMSO-d₆, 29 MHz, ppm) δ = -14.

3,6,7-Triamino-[1,2,4]triazole[4,3-b][1,2,4]triazolium 1-amino-5-nitriminotetrazolate (6)

1-Amino-5-nitriminotetrazole (0.12 g, 0.83 mmol, 1.0 eq.) was dissolved in water (10 mL) and 3,6,7-triamino-[1,2,4]triazole[4,3-b][1,2,4]triazole (TATOT) (0.13 g, 0.83 mmol, 1.0 eq) was added. The solution was heated to 60 °C with the aid of an oil bath and stirred for 30 min at this temperature. After filtration, the solution was left for crystallization to yield 3,6,7-triamino-[1,2,4]triazole[4,3-b][1,2,4]triazolium 1-amino-5-nitriminotetrazolate (0.23 g, 0.76 mmol, 92%) as slightly beige crystalline solid.

DTA (5 °C min⁻¹): 215 °C (exo, dec.); **Sensitivities** (≤500 μm): **BAM drop hammer**: 20 J, **friction tester**: 240 N; **IR** (ATR) $\tilde{\nu}$ (cm⁻¹) = 3290(m), 3114(m), 3006(m), 1683(s), 1669(s), 1651(s), 1645(s), 1509(m), 1464(m), 1399(m), 1305(s), 1257(s), 1167(m), 1107(m), 1077(m), 1046(m), 1028(s), 1014(s), 974(m), 914(s), 837(m), 755(s), 707(s), 694(s), 619(s), 600(s), 521(vs), 460(s), 420(s), 413(s), 404(s); **Elem. Anal.** (C₄H₉N₁₅O₂, 299.22 g mol⁻¹) calcd.: C 16.06, H 3.03, N 70.22 %. Found: C 15.94, H 2.99, N 69.62 %; **¹H NMR** (DMSO-d₆, 400 MHz, ppm) δ = 13.33 (br s, 1H), 8.10 (s, 2H), 7.20 (s, 2H), 6.17 (br s, 2H), 5.76 (s, 2H); **¹³C NMR** (DMSO-d₆, 101 MHz, ppm) δ = 160.6, 155.6, 148.0, 141.7; **¹⁴N NMR** (DMSO-d₆, 29 MHz, ppm) δ = -15.

Silver 1-amino-5-nitriminotetrazolate (7)

1-Amino-5-nitriminotetrazole (0.30 g, 2.07 mmol, 1.0 eq.) was dissolved in water (5 mL) and silver nitrate (0.351 g, 2.07 mmol, 1.0 eq) dissolved in water (5 mL) was added. Silver 1-amino-5-nitriminotetrazolate precipitated instantly as dark greyish amorphous powder which was filtered, washed with water and dried. Silver 1-amino-5-nitriminotetrazolate (0.47 g, 1.87 mmol, 90%) was obtained after recrystallization from 2 M ammonia (10 mL) as greyish to colorless crystals.

DTA (5 °C min⁻¹): 218 °C (exo, dec.); **Sensitivities** (≤500 μm): **BAM drop hammer**: <1 J, **friction tester**: <1 N; **IR** (ATR) $\tilde{\nu}$ (cm⁻¹) = 3203 (w), 2154 (w), 2015 (w), 1506 (m), 1465 (m), 1411 (m), 1370

(m), 1330 (s), 1263 (s), 1139 (m), 1090 (m), 1011 (m), 926 (m), 831 (m), 802 (m), 758 (m), 722 (m), 677 (m), 441 (m); **Elem. Anal.** ($\text{CH}_2\text{N}_7\text{O}_2\text{Ag}$, $251.94 \text{ g mol}^{-1}$) calcd.: C 4.77, H 0.80, N 38.92 %. Found: too sensitive for measurement; $^1\text{H NMR}$ (DMSO-d_6 , 400 MHz, ppm) $\delta = 6.53$ (s, 2H); $^{14}\text{N NMR}$ (DMSO-d_6 , 29 MHz, ppm) $\delta = -4$.

8.5.2 Crystallographic Detail

Crystal structure data were obtained from an Oxford Xcalibur3 diffractometer with a Spellman generator (voltage 50 kV, current 40 mA) and a Kappa CCD area for data collection using Mo-K α radiation ($\lambda=0.71073\text{\AA}$) or a Bruker D8 Venture TXS diffractometer equipped with a multilayer monochromator, a Photon 2 detector and a rotation-anode generator (Mo-K α radiation). The data collection was performed using the CRYSTALIS RED software.^[25] The solution of the structure was performed by direct methods and refined by fullmatrix least-squares on F² (SHELXT)^[26] implemented in the OLEX2^[27] software suite. The non-hydrogen atoms were refined anisotropically and the hydrogen atoms were located and freely refined. The absorption correction was carried out by a SCALE3 ABSPACK multiscan method.^[28] The DIAMOND2 plots shown with thermal ellipsoids at the 50% probability level and hydrogen atoms are shown as small spheres of arbitrary radius. The SADABS program embedded in the Bruker APEX3 software was used for multi-scan absorption corrections in all structures.^[29]

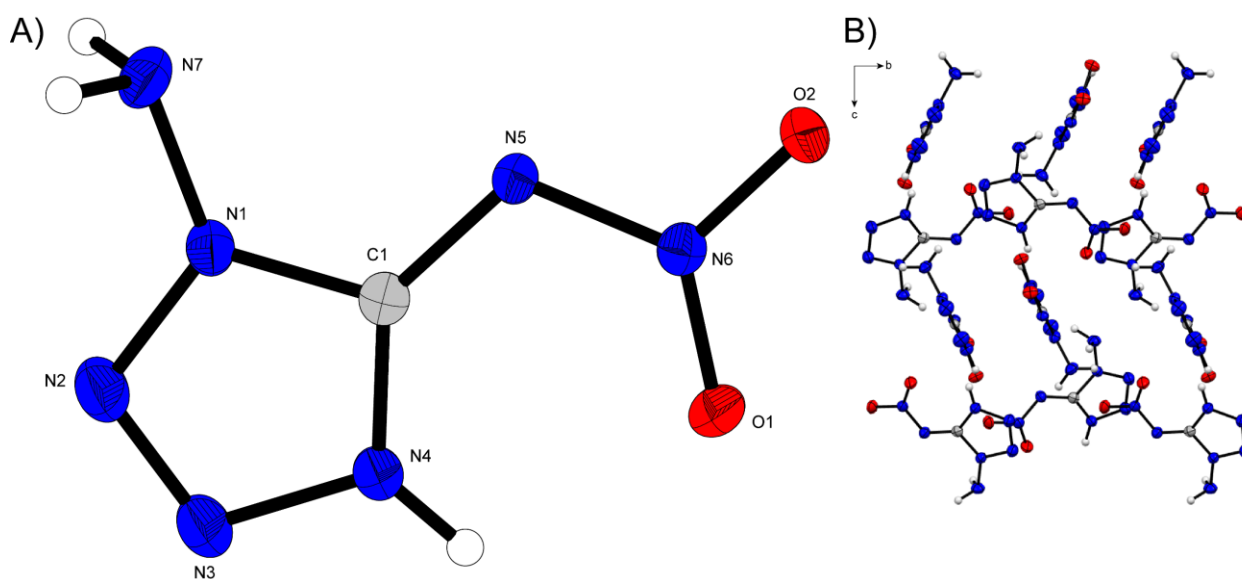


Figure 7. A) Crystal structure of HANIT 1. Thermal ellipsoids are drawn at the 50% probability level. B) Layers of HANIT.

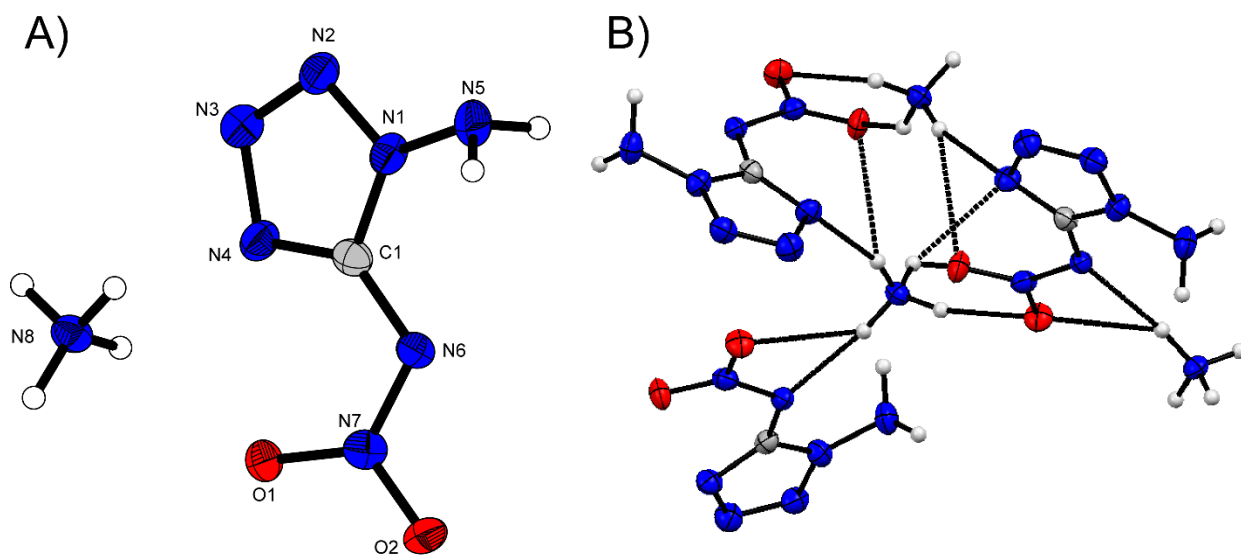


Figure 8. A) Structure of ammonium ANIT (**2**). Thermal ellipsoids are drawn at the 50% probability level. **B)** Central ammonium cation bridges three 1-amino-5-nitriminotetrazolates.

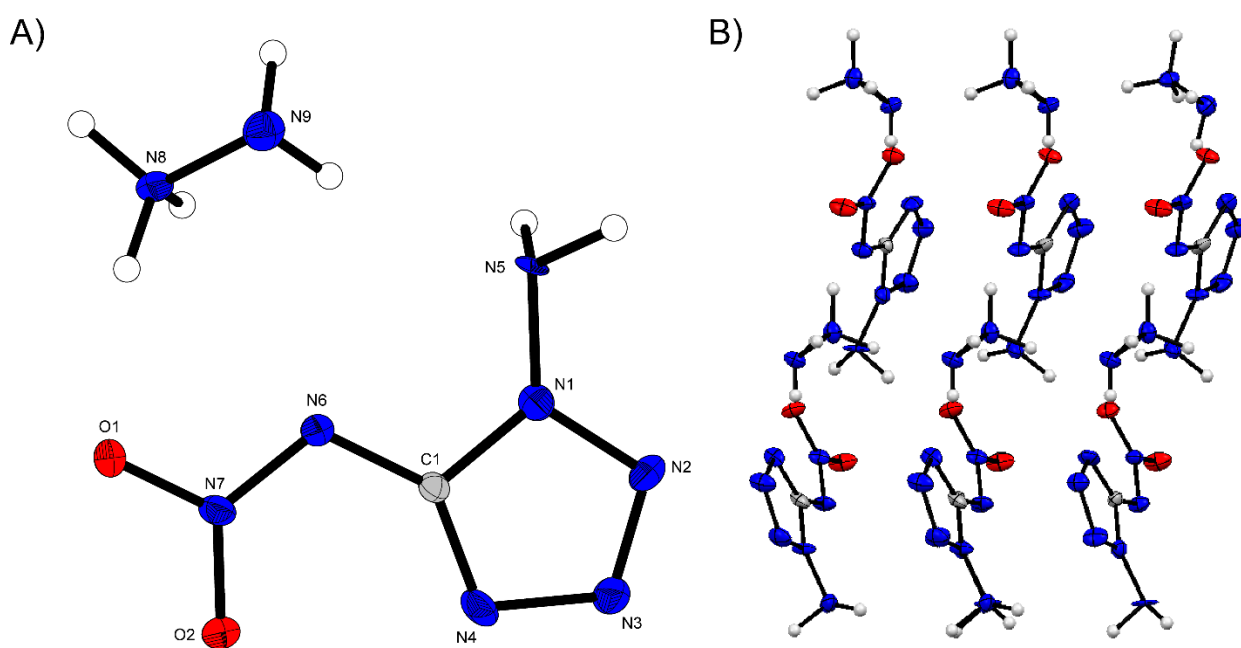


Figure 9. A) Crystal structure of **3**. Thermal ellipsoids are drawn at the 50% probability level. **B)** Layers of hydrazinium ANIT (**3**).

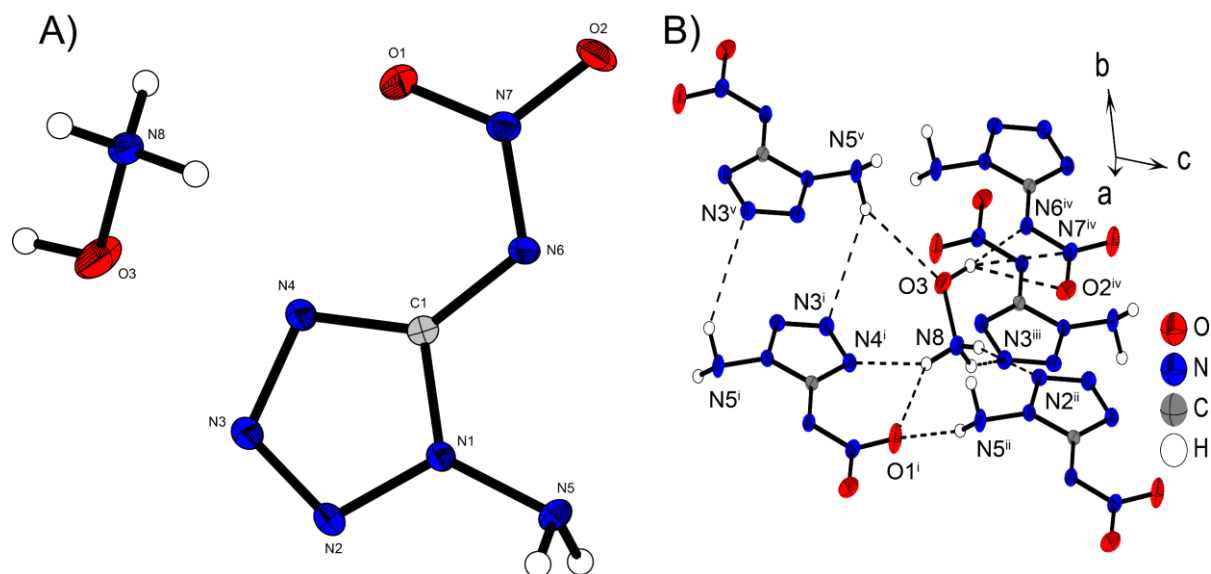


Figure 10. A) Hydroxylammonium ANIT **4**. Thermal ellipsoids are drawn at the 50% probability level. B) Molecular hydrogen interactions of the hydroxylammonium cation with 5 different ANIT anions.

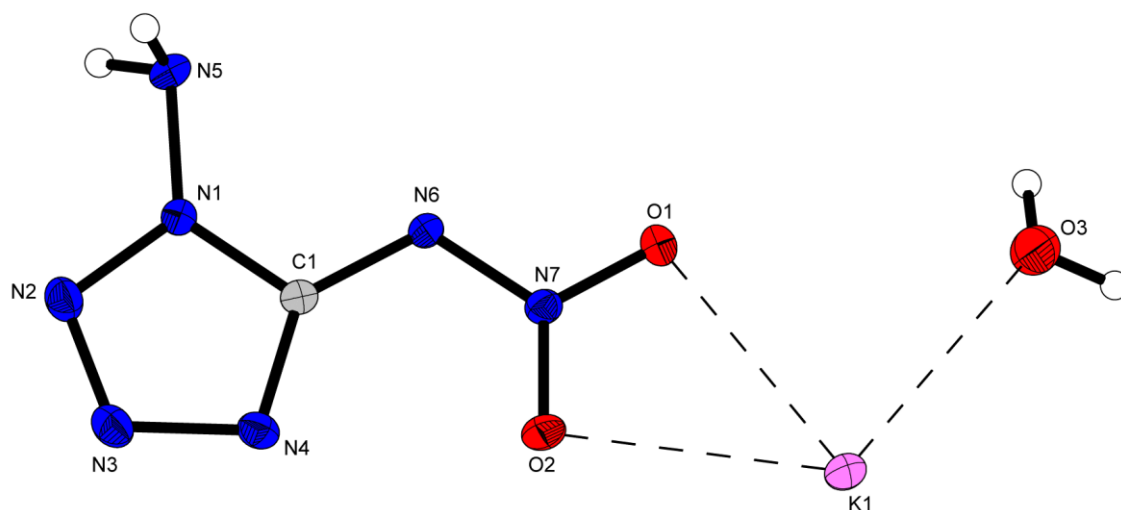


Figure 11. Crystal structure of KANIT **5**. Thermal ellipsoids are drawn at the 50% probability level.

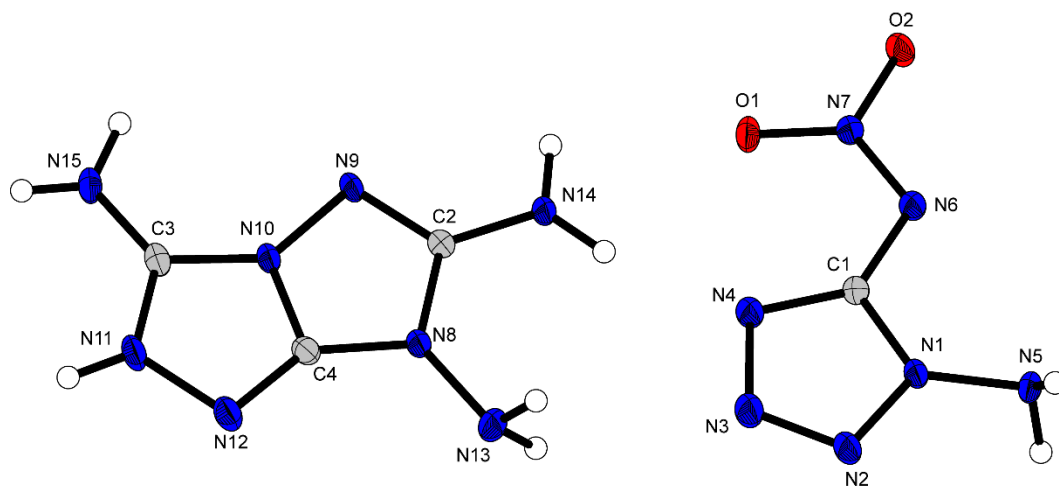


Figure 12. Crystal structure of **6**. Thermal ellipsoids are drawn at the 50% probability level.

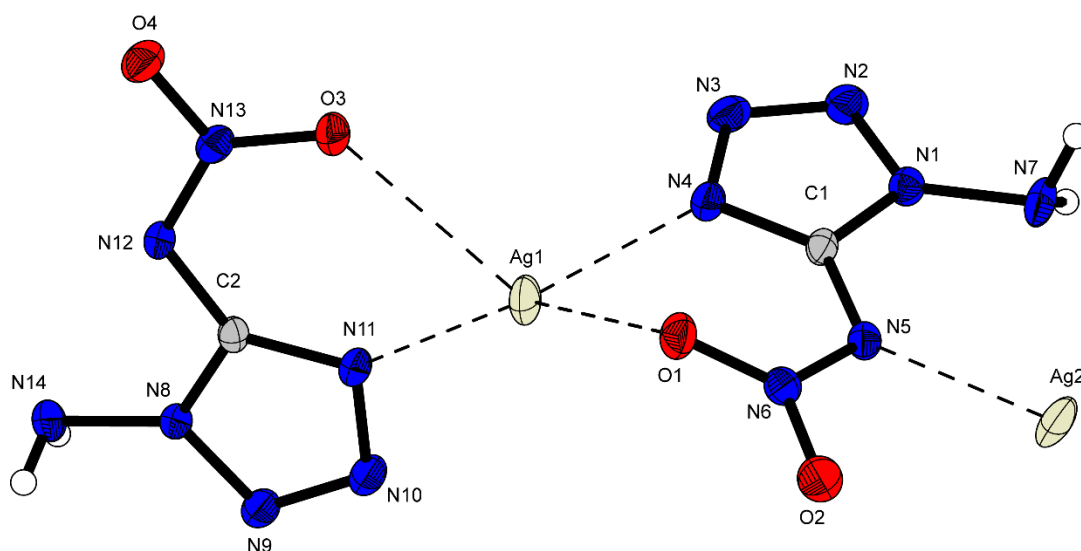


Figure 13. Crystal structure of AgANIT **7**. Thermal ellipsoids are drawn at the 50% probability level. The silver atom is tetrahedrally coordinated.

Table 2. Crystallographic data and structure refinement details for the prepared compounds.

	1	2	3
Formula	CH ₃ N ₇ O ₂	CH ₆ N ₈ O ₂	CH ₇ N ₉ O ₂
FW [g mol ⁻¹]	145.10	162.14	177.16
Crystal system	monoclinic	orthorhombic	monoclinic
Space group	<i>P</i> 2 ₁ / <i>n</i> (No. 14)	<i>P</i> 2 ₁ 2 ₁ 2 ₁ (No. 19)	<i>P</i> 2 ₁ (No. 4)
Color / Habit	colorless block	colorless block	colorless rod
Size [mm]	0.06 x 0.10 x 0.18	0.10 x 0.25 x 0.25	0.02 x 0.03 x 0.15
<i>a</i> [Å]	8.6883(4)	5.5868(8)	3.5756(3)
<i>b</i> [Å]	8.6632(4)	9.8955(17)	11.4593(9)
<i>c</i> [Å]	14.8335(6)	10.9316(16)	16.4406(13)
α [°]	90		90
β [°]	103.976(2)		96.238(3)
γ [°]	90		90
<i>V</i> [Å ³]	1083.44(8)	604.35(16)	669.65(9)
<i>Z</i>	8	4	4
ρ_{calc} [g cm ⁻³]	1.779	1.782	1.757
μ [mm ⁻¹]	0.159	0.157	0.154
<i>F</i> (000)	592	336	368
$\lambda_{\text{MoK}\alpha}$ [Å]	0.71073	0.71073	0.71073
<i>T</i> [K]	173	101	173
θ Min-Max [°]	2.8, 27.6	2.8, 26.3	3.6, 27.5
Dataset	-11: 11 ; -11: 11 ; -19: 19	-6: 6 ; -12: 8 ; -13: 7	-4: 4 ; -13: 14 ; -21: 21
Reflections collected	25821	2016	8394
Independent refl.	2487	1234	2757
Rint	0.043	0.044	0.036
Observed reflections	2140	859	1953
Parameters	205	124	218

8 1-Amino-5-nitriminotetrazole

R1 (obs)[a]	0.0313		0.0586	0.0312
wR2 (all data)[b]	0.0817		0.1089	0.0785
S [c]	1.09		1.00	1.01
Resd. dens [e Å ⁻³]	-0.22, 0.21		-0.26, 0.32	-0.17, 0.19
Device type	Bruker D8 Venture TXS		Oxford Xcalibur3	Bruker D8 Venture TXS
Solution	SIR-92		SHELXT	SIR-92
Refinement	SHELXL-2018		SHELXL-2018	SHELXL-2018
Absorption correction	multi-scan		multi-scan	multi-scan
CCDC				
	4	5	6	7
Formula	CH ₆ N ₈ O ₂	CH ₄ KN ₇ O ₃	C ₄ H ₉ N ₁₅ O ₂	C ₂ H ₄ Ag ₂ N ₁₄ O ₄
FW [g mol ⁻¹]	178.14	201.21	299.26	503.93
Crystal system	triclinic	monoclinic	monoclinic	orthorhombic
Space group	<i>P</i> -1 (No. 2)	<i>C</i> 2/ <i>c</i> (No. 15)	<i>P</i> 2 ₁ / <i>c</i> (No. 14)	<i>Pbca</i> (No. 61)
Color / Habit	colorless block	yellow block	colorless block	colorless block
Size [mm]	0.10 x 0.12 x 0.20	0.04 x 0.06 x 0.20	0.04 x 0.08 x 0.10	0.04 x 0.04 x 0.08
a [Å]	7.3477(4)	13.4126(7)	12.0270(5)	7.9795(3)
b [Å]	7.3488(4)	11.8979(6)	6.2786(2)	12.2372(4)
c [Å]	7.4546(4)	9.8337(5)	14.6649(6)	22.9422(7)
α [°]	103.712(2)	90	90	
β [°]	110.124(2)	116.801(2)	102.224(1)	
γ [°]	111.085(2)	90	90	
V [Å ³]	321.35(3)	1400.70(13)	1082.28(7)	2240.23(13)
Z	2	8	4	8
ρ _{calc.} [g cm ⁻³]	1.841	1.908	1.837	2.988
μ [mm ⁻¹]	0.168	0.742	0.152	3.553
F(000)	184	816	616	1920
λMoKα [Å]	0.71073	0.71073	0.71073	0.71073
T [K]	173	173	173	299
θ Min-Max [°]	3.4, 26.4	3.4, 33.2	2.8, 27.5	3.1, 26.4
Dataset	-9: 9 ; -9: 9 ; -9: 9	-20: 20 ; -18: 18 ; -15: 15	-15: 15 ; -8: 8 ; -19: 18	-9: 9 ; -15: 15 ; -28: 28
Reflections collected	5393	19444	26602	34160
Independent refl.	1281	2690	2481	2284
R _{int}	0.023	0.035	0.034	0.029
Observed reflections	1198	2372	2198	2082
Parameters	133	125	226	207
R1 (obs)[a]	0.0318	0.0316	0.0392	0.0321
wR2 (all data)[b]	0.0822	0.0837	0.1061	0.0819
S [c]	1.06	1.06	1.10	1.13
Resd. dens [e Å ⁻³]	-0.19, 0.27	-0.50, 0.69	-0.27, 0.27	-0.96, 1.18
Device type	Bruker D8 Venture TXS	Bruker D8 Venture TXS	Bruker D8 Venture TXS	Bruker D8 Venture TXS

Solution	SIR-92	SHELXT	SIR-92	SIR-92
Refinement	SHELXL-2018	SHELXL-2018	SHELXL-2018	SHELXL-2018
Absorption correction	multi-scan	multi-scan	multi-scan	multi-scan
CCDC				

[a] $R1 = \sum ||F0| - |Fc|| / \sum |F0|$; [b] $wR2 = [\sum [w(F02 - Fc2)^2] / \sum [w(F0)^2]]^{1/2}$; $w = [\sigma^2(F02) + (xP)^2 + yP]^{-1}$ and $P = (F02 + 2Fc2) / 3$; [c] $S = \{\sum [w(F02 - Fc2)^2] / (n - p)\}^{1/2}$ (n = number of reflections; p = total number of parameters).

8.5.3 Computational Details

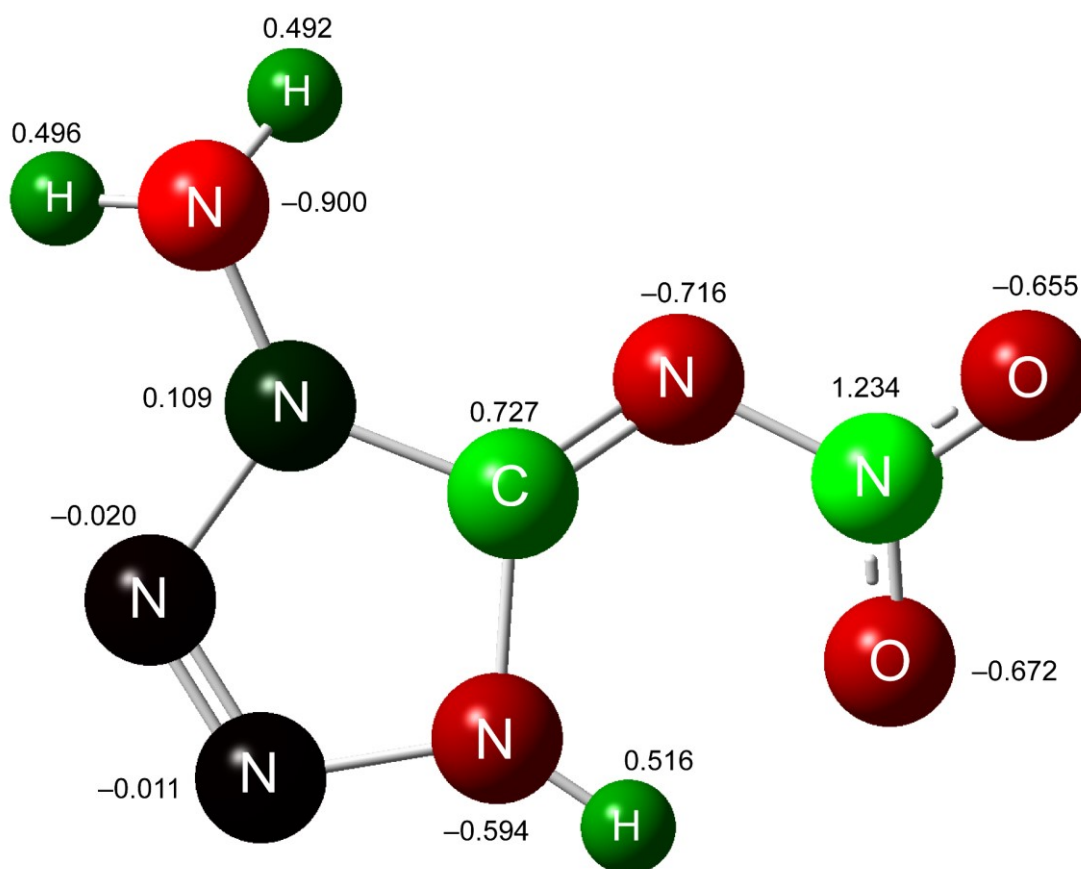


Figure 14. Representation of the natural bond orbital (NBO) of HANIT **1** based on the B3LYP/cc-pVDZ level of theory.

Since we assumed kind of a charge separation within the molecule, NBOs (natural bond orbitals) of HANIT (**1**) were calculated on the B3LYP/cc-pVDZ level of theory using the gas phase structure. The highest positively charged atom is the nitrogen atom of the nitro group, consisting of two neighbor atoms with a higher electronegativity and one neighbor atom with the same electronegativity. Further, the carbon atom in the molecules is positively polarized. The strongest negatively charged atoms are N7, followed by N5 and the two oxygen atoms.

The atomization was used to determine the heat of formation of **1–3** using the atom energies in

Table 3.

$$\Delta_f H^\circ_{(g, M, 298)} = H_{(molecule, 298)} - \sum H^\circ_{(atoms, 298)} + \sum \Delta_f H^\circ_{(atoms, 298)}$$

Table 3. CBS-4M electronic enthalpies for atoms C, H, N and O and their literature values.

	$-H^{298} / \text{a.u.}$	$\Delta_f H^\circ_{\text{gas}}^{[30]}$
H	0.500991	217.998
C	37.786156	716.68
N	54.522462	472.68
O	74.991202	249.18
K	-599.187712	89

The Gaussian16 program package was used to calculate room temperature enthalpies on the CBS-4M level of theory.^[31] In order to obtain the energy of formation for the solid phase of **1**, the Trouton's Rule has to be applied ($\Delta H_{\text{sub}} = 188 \cdot T_m$).

Table 4. Heat of formation calculation results for compounds **1–6**.

M	$-H^{298} [a] [\text{a.u.}]$	$\Delta_f H^\circ(g, M) [b] [\text{kJ mol}^{-1}]$	$\Delta_f H^\circ(s) [d] [\text{kJ mol}^{-1}]$	Δn	$\Delta_f U(s) [e] [\text{kJ kg}^{-1}]$
1	572.712468	416.1	494.7	-6.0	2970.4
2	629.004042	922.6	377.6	-8.0	2451.8
3	684.237957	1060.7	528.9	-9.0	3111.9
4	704.070683	973.7	436.1	-8.5	2566.8
5	1171.39515	376.3	-165.5	-5.5	-1053.9
6	1127.68157	1367.3	898.1	-13.0	3109.3

[a] CBS-4M electronic enthalpy; [b] gas phase enthalpy of formation; [c] sublimation enthalpy; [d] standard solid state enthalpy of formation; [e] solid state energy of formation. [

8.6 References

- [1] T. M. Klapötke, *Chemistry of High-Energy Materials* **2019**, Berlin, Boston: de Gruyter.
- [2] T. M. Klapötke, J. Stierstorfer, *J. Am. Chem. Soc.* **2009**, *131*, 1122–1134.
- [3] J. Stierstorfer, T. M. Klapötke, A. Hammerl, R. D. Chapman, *Z. Anorg. Allg. Chem.* **2008**, *634*, 1051–1057.
- [4] T. M. Klapötke, D. G. Piercey, N. Mehta, K. D. Oyler, M. Jorgensen, S. Lenahan, J. S. Salan, J. W. Fronaberger, M. D. Williams, *Z. anorg. allg. Chem.* **2013**, *639*, 681–688.
- [5] T. M. Klapötke, C. M. Sabaté, J. Stierstorfer, *New J. Chem.* **2009**, *33*, 136–147.
- [6] J. A. Garrison, R. M. Herbst, *J. Org. Chem.* **1957**, *22(3)*, 278–283.
- [7] T. M. Klapötke, J. Stierstorfer, *Helv. Chim. Acta* **2007**, *90*, 2132–2150.

- [8] Y.-H. Joo, J. M. Shreeve, *Angew. Chem. Int. Ed.* **2010**, *49*, 7320–7323; *Angew. Chem* **2010**, *122*, 7478–7481.
- [9] Y.-H. Joo, J. M. Shreeve, *Angew. Chem. Int. Ed.* **2009**, *48*, 564–567; *Angew. Chem* **2009**, *121*, 572–575.
- [10] D. Fischer, T. M. Klapötke, J. Stierstorfer, *Eur. J. Inorg. Chem.* **2015**, 4628–4632.
- [11] D. Fischer, T. M. Klapötke, J. Stierstorfer, *Angew. Chem. Int. Ed.* **2015**, *54*, 10299–10302; *Angew. Chem.* **2015**, *127*, 10438–10441.
- [12] T. M. Klapötke, F. A. Martin, J. Stierstorfer, *Chem. Eur. J.* **2012**, *18*, 1487–1501.
- [13] D. Fischer, T. M. Klapötke, J. Stierstorfer, *15th New Trends in Research of Energetic Materials Seminar, Pardubice, Czech*, **2012**, 115–127.
- [14] Y.-H. Joo, B. Twamley, S. Garg, J. M. Shreeve, *Angew. Chem. Int. Ed.* **2008**, *47*, 6236–6239; *Angew. Chem.* **2008**, *120*, 6332–6335.
- [15] P. N. Gaponik, V. P. Karavai, *Chem. Heterocycl. Compd.* **1984**, *20*, 1388–1391.
- [16] F. Li, Y. Cong, Z. Du, C. He, L. Zhao, L. Meng, *New J. Chem.* **2012**, *36*, 1953–1956.
- [17] M. Suceska, EXPLO5 program, Zagreb, Croatia, **2018**.
- [18] N. Fischer, D. Fischer, T. M. Klapötke, D. G. Piercey, J. Stierstorfer, *J. Mater. Chem.* **2012**, *22*, 20418–20422.
- [19] <http://www.bam.de>
- [20] NATO Standardization Agreement (STANAG) on Explosives, *Impact Sensitivity Tests*, no. 4489, 1st ed., September 17, **1999**.
- [21] WIWEB-Standardarbeitsanweisung 4-5.1.02, Ermittlung der Explosionsgefährlichkeit, hier der Schlagempfindlichkeit mit dem Fallhammer, November 8, **2002**.
- [22] NATO Standardization Agreement (STANAG) on Explosives, *Friction Sensitivity Tests*, no. 4487, 1st ed., August 22, **2002**.
- [23] WIWEB-Standardarbeitsanweisung 4-5.1.03, Ermittlung der Explosionsgefährlichkeit oder der Reibeempfindlichkeit mit dem Reibeapparat, November 8, **2002**.
- [24] Impact: Insensitive >40 J, less sensitive ≤35 J, sensitive ≤4 J, very sensitive ≤3 J; friction: Insensitive >360 N, less sensitive=360 N, sensitive 80 N, very sensitive ≤80 N, extreme sensitive ≤10 N; According to the UN Recommendations on the Transport of Dangerous Goods (+) indicates: not safe for transport.
- [25] CrysAlisPro, Oxford Diffraction Ltd., *version 171.33.41*, **2009**.
- [26] G. M. Sheldrick, *Acta Cryst.* **2015**, *A71*, 3 – 8.

- [27] O. V. Dolomanov, L. J. Bourhis, R. J. Gildea, J. A. K. Howard, H. Puschmann, *J. Appl. Cryst.* **2009**, *42*, 339 – 341.
- [28] *SCALE3 ABSPACK – An Oxford Diffraction program (1.0.4, gui: 1.0.3)*, Oxford Diffraction Ltd., **2005**.
- [29] *APEX3*. Bruker AXS Inc., Madison, Wisconsin, USA.
- [30] M. W. Chase Jr., NIST-JANAF Thermochemical Tables, Fourth Edition, *J. Phys. Chem. Red. Data, Monograph 9* **1998**, 1 – 1951.
- [31] M. J. Frisch, G. W. Trucks, H. B. Schlegel, G. E. Scuseria, M. A. Robb, J. R. Cheeseman, G. Scalmani, V. Barone, G. A. Petersson, H. Nakatsuji, X. Li, M. Caricato, A. V. Marenich, J. Bloino, B. G. Janesko, R. Gomperts, B. Mennucci, H. P. Hratchian, J. V. Ortiz, A. F. Izmaylov, J. L. Sonnenberg, D. Williams-Young, F. Ding, F. Lipparini, F. Egidi, J. Goings, B. Peng, A. Petrone, T. Henderson, D. Ranasinghe, V. G. Zakrzewski, J. Gao, N. Rega, G. Zheng, W. Liang, M. Hada, M. Ehara, K. Toyota, R. Fukuda, J. Hasegawa, M. Ishida, T. Nakajima, Y. Honda, O. Kitao, H. Nakai, T. Vreven, K. Throssell, J. A. Montgomery, Jr., J. E. Peralta, F. Ogliaro, M. J. Bearpark, J. J. Heyd, E. N. Brothers, K. N. Kudin, V. N. Staroverov, T. A. Keith, R. Kobayashi, J. Normand, K. Raghavachari, A. P. Rendell, J. C. Burant, S. S. Iyengar, J. Tomasi, M. Cossi, J. M. Millam, M. Klene, C. Adamo, R. Cammi, J. W. Ochterski, R. L. Martin, K. Morokuma, O. Farkas, J. B. Foresman, D. J. Fox, Gaussian16, Gaussian, Inc., Wallingford, CT, USA, **2016**.